EUROPEAN RESEARCH REACTOR CONFERENCE 2022

Budapest, 6 – 10 June 2022

Radisson Blu Béke Hotel

PROCEEDINGS

A SUMMARY OF THE INNOVATIVE FUEL ASSEMBLY DEVELOPMENT WORK PERFORMED IN THE FRAME OF THE LEU-FOREvER PROJECT FOR THE 4EVERTEST IRRADIATION

Vincenzo Romanello[a], Antonio Dambrosio[a], Jaroslav Ernest[a], Milos Kyncl[a], Miroslav Hrehor[a]

François Huet[b], Michel Boyard[b], Jeremy Koubbi[b], Romain Duperray[b]

Betrand Stepnik[c], Cyrille Rontard[c]

[a]Research Centre Rez (CVR) - 26068 Husinec-Rez 130 - Czech Republic

[b]*TechnicAtome - 1100 Avenue Jean-René Guillibert Gautier de la Lauzière, CS 50497, 13593 Aix en Provence – France*

[c]*Framatome - ZI les bérauds BP 1114 26104 Romans-sur-Isere - France*

Abstract

Project LEU-FOREvER put together a consortium of 9 European stakeholders, including research centers, designers and fuel manufacturers, with the specific aim to secure the nuclear fuel supply for European research reactors. One of the shortage risks has been addressed by the project with the definition of a second supply chain for the fuel of the medium power research reactors (MPRRs) originally manufactured with the Soviet technology; this aspect became rather critical in the last months given the geopolitical events. For this reason, one activity was the definition of a core which could accommodate both the original Russian technology (uranium oxide extruded fuel meat) and new European designed fuel elements (uranium silicide dispersed fuel meat) that are being developed, licensed and qualified in the frame of the 4EVERTEST within LEU-FOREvER project. The Czech reactor LVR-15 was selected for performing the developed assembly irradiation test, which will be followed by a basic post irradiation inspection for a basic assessment of the irradiation performance. For this reason, the project proceeded through various logical and operative steps. They are briefly summarized in the present work, starting with the collection of the relevant information about reactor characteristics by fuel designer, then the design phase performed in parallel by the designer and reactor operator in order to tune the codes and data coherently, followed by the detailed safety analysis study to be submitted to national regulator in order to get the irradiation license approval. The fuel assembly prototype is currently irradiated in the LVR-15 reactor together with its usual fuel.

Introduction

Nuclear and radiation technology is today very useful for various applications, ranging from medical uses with productions of various radioisotopes (Mo-99 is one of the most common, but also many others [1]), technology development (neutron and materials science, imaging, activation analysis) and education of new specialists in these fields [2]. It must be kept in mind in fact that although key medical isotopes supplies are stable, some critical vulnerabilities remain [3].

One of the biggest challenges for the European research reactors today is to secure a stable and reliable supply of their nuclear fuel. Two main factors have been identified in this regard: (i) the ongoing conversion of High-Performance Research Reactors (HPRRs) from High (HEU) to Low Enriched Uranium fuels (LEU), and (ii) the needed diversification of the supply chain for the fuel assemblies of the European Medium Power Research Reactors (MPRRs), reactors designed and provided by Soviet Union. In order to fulfill these goals, a multidisciplinary consortium composed by fuel and core designers, operators, research centers and a fuel manufacturer has been established in order to tackle both issues in the framework of the H2020 Euratom LEU-FOREvER (Low Enriched Uranium - Fuels fOR REsEarch Reactors) project [4] [5].

For European MPRRs, a new ‘mixed’ core design is going to be tested with both the original ROSATOM and new European fuel element [6] which was developed and which was licensed for the irradiation test (“4EVERTEST”) within LEU-FOREvER. The LVR-15 research reactor in the Czech Republic, operated by the

Research Centre Rez (CVR), will serve as a case study. For this scope, effective steps were established and followed with a useful and close cooperation between the reactor operator, the fuel designer (TechnicAtome) and the manufacturer (Framatome-CERCA).

This action has benefited from the feedback of the MARIA reactor and its current two supply chains. The first one is the original supply chain from the reactor designer of MARIA reactor, based on extrusion manufacturing process for the UO_2 fuel meat. The second one is based on U_3Si_2 fuel meat (rolled plate).

The first step is the complete and careful collection of necessary information about the reactor systems and its characteristics by the fuel assembly designer. The outcome was a data gathering matrix document in which proper detail core characteristics, such as fuel components (geometry and materials), reflector, experimental devices, interfaces (in particular concerning the core grid and shutdown systems), cooling systems, performances concerning fuel consumption and core lifecycle, safety criteria, transients requirements and fuel compliance strategy are described. The end of the first step was the definition of the fuel development strategy compliant with IAEA Guideline on Research Reactors Fuel Qualification [7], according to which no impact on existing reactor core and interfaces should be guaranteed, the new designed fuel should present a similar heating surface and flow section of the original assembly, the fuel meat was already qualified (according to NUREG-1313 [8]) and, finally, a fuel assembly design similar to those of other reactors already qualified was selected. The choice of the design was based on this strategy, although the authors are aware it was not the best technical possible option to adopt.

The second step consisted in the design activity. During this phase, two calculation schemes have been compared: the calculation scheme used by the fuel designer and the calculation scheme used by the operator for the licensing process. In particular, the neutronic models were compared both concerning the prototype FA and the full core. Maximum discrepancy was of the order of ca. 50 pcm, proving a good models' agreement and well-tuned solver options, energy multi-groups libraries and calculation procedures. Two sample core configurations were checked as well, one fully composed of Russian design (IRT-4M) fuel and the other one with European design (FPFA, Flat Plate Fuel Assembly), in particular concerning the reactivity excess, total rod worth, effective delayed neutron fraction and power peaking factor. Finally, thermal and fast flux maps were compared, showing the same shape and very close absolute values.

The fuel designer made also a thermohydraulic detailed sensitivity analysis concerning various parameters like thermal conditions and manufacturing tolerances and physical uncertainties in order to integrate them in the assessment of the final FA performance.

Finally, the fuel designer prescribed, in detailed requirements, the hydraulic test to be performed on a dedicated fuel mockup. The technical drawings have been discussed between fuel designer and fuel manufacturer and then checked and approved by the reactor operator.

The next step was the fabrication of the fuel mockup and delivery to the reactor operator, which performed a hydraulic test according to the designer prescription, in particular, in order to assess the pressure losses of the fuel assemblies experimentally. It is mandatory that the new fuel presents a pressure loss vs. coolant flow consistent with the safety analysis report (Russian IRT-4M fuel assemblies), otherwise a dangerous coolant flow unbalance could consequently cause an unsatisfactory cooling of some elements and locally increase the power peaking factor.

Afterwards, neutronic calculations, the hydraulic test and the safety thermohydraulic calculations were put together in a safety report amendment (in particular, chapter 16) which was submitted to national regulator (SUJB, State Office for Nuclear Safety in Czech Republic) in order to get the irradiation license approval.

The next was step was the irradiation of the fuel assembly into the reactor (which is currently ongoing) and then, after the minimum required cooling time, a basic post irradiation inspection (PII), to be reported in detail in the planned project deliverables. The described steps and their logic flow are summarized in Fig.1.

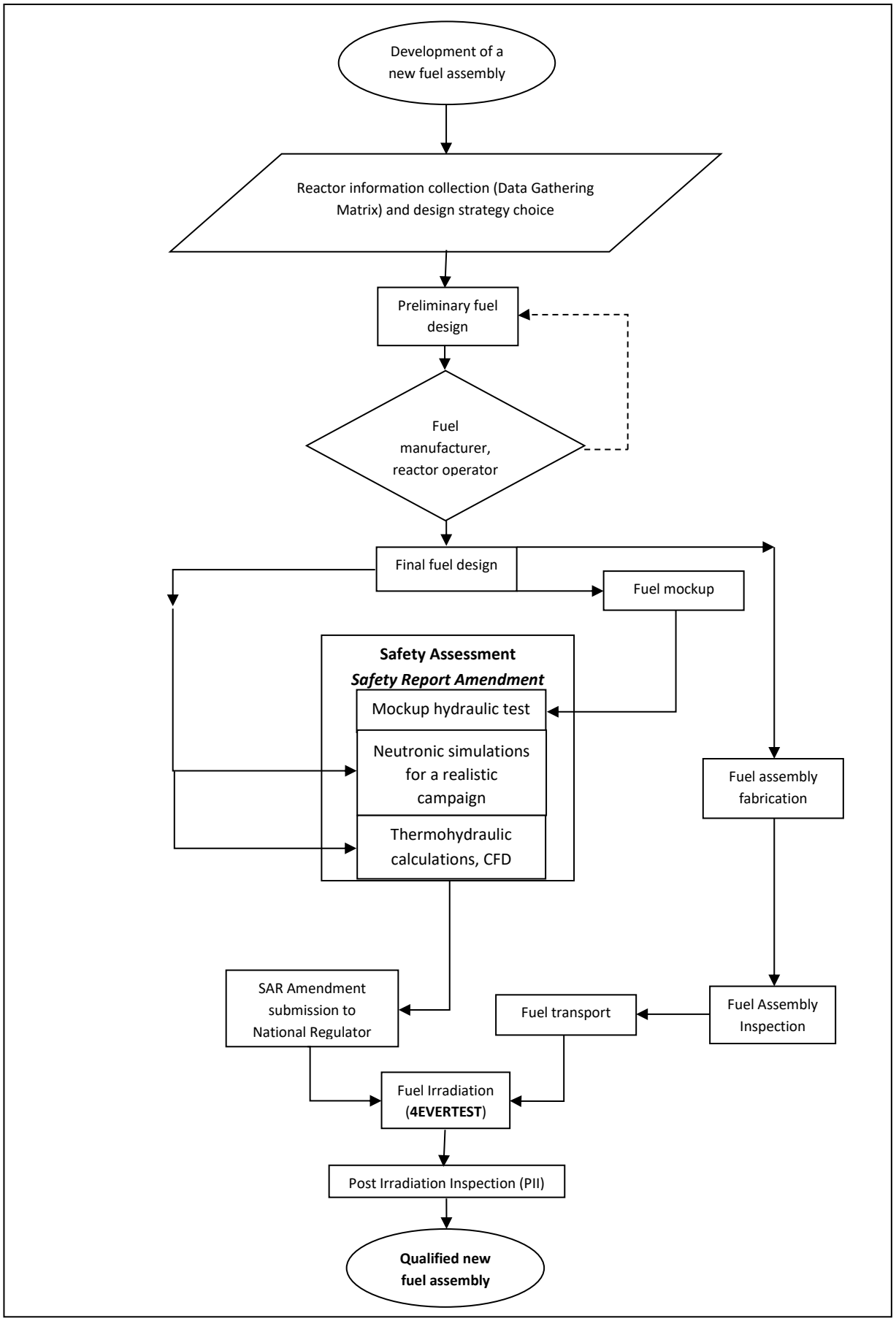

Fig.1 - Operational steps followed for the development of the MPRR test assembly for the LEU-FOREvER 4EVERTEST

Preliminary fuel design

The approach adopted in the fuel design process in the frame of LEU-FOREvER project was to provide a new kind of fuel without new constraints for the operator: no changes needed in the reactivity control system and in the cooling system even in the mixed core case. It means that the current absorbers and their associated guide tubes and drive mechanisms would not be changed due to the new fuel adoption. It also means that the new fuel keeps the same FAs external water channel.

The two types of Standard Fuel Assemblies (SFAs) designs are rather different due to different manufacturer technologies (UO_2 extrusion technology in one case and U_3Si_2 rolled plate in the other one). Then, IRT-4M is based on concentric squared tubes while FPFA design is based on parallel flat plate. Flat plate thickness is another significant difference in FAs characteristics: IRT-4M has higher thicknesses for fuel meat (+37%) and cladding (+18%) compared to FPFA ones. Concerning fuel meat, IRT-4M density is almost 80% lower than FPFA one, therefore U-235 mass per FA in IRT-4M is 28% lower than in FPFA one; IRT-4M water channels are 7% smaller than FPFA ones.

In Fig.2 the IRT-4M and the FPFA fuel element designed in the frame of the project are represented. Further details are reported in [9].

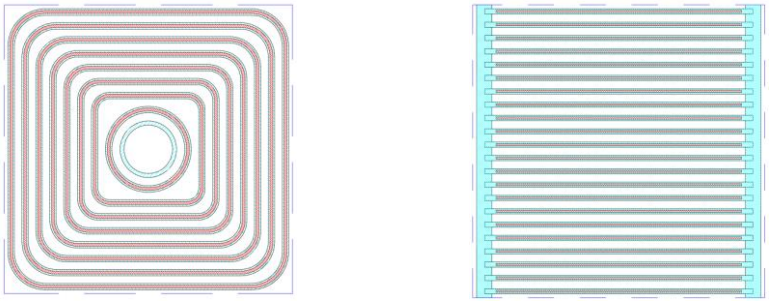

Fig 2. SFAs cross sections - Left: IRT-4M – Right: FPFA

Preliminary neutronics calculation

The two main objectives of this step were to:

- Compare the neutron characteristics of the different fuel assemblies
- Check the agreement between the neutronic calculation schemes used by the fuel designer and the reactor operator (benchmark) in order to prepare the safety assessment.

Through this process, the main differences between the different fuel assemblies have been analyzed and a quantification of models and calculation codes biases was achieved and level of confidence in further calculations was evaluated. In order to do it, a dedicated validation methodology was developed. The aim was to acquire the highest level of confidence in calculations to limit potential issues during successive fuel studies, namely during support studies to obtain a new operational license from the safety regulatory body in Czech Republic (SUJB).

In order to create a reference point, LVR-15 core calculations with its current fuel based on IRT-4M assemblies, on a specific configuration were done. For benchmarking purposes, these calculations were

performed in parallel by the designer with its neutronic calculation scheme, COCONEUT [10] and by reactor operator with SERPENT-2 [11] and SCALE [12] codes.

Then performances assessment of a core completely fuelled with the new fuel assemblies designed in the frame of the project was achieved as well. These cores were created for codes benchmarking and efficient data exchange purposes only (a realistic core was designed in the successive step).

Finally, performances comparisons between results obtained by the designer and the reactor operator on these two cores were carried out on a set of neutronic parameters of interest.

This work gave an insight of performances reachable for LVR-15 core fueled with a LEU silicide dispersed fuel.

These comparisons allowed us to conclude that developed models and used codes:

• provide consistent results

• could be enforced at core level

For this purpose, two sample configurations (fully theoretical, just for comparison purposes) were established, one IRT-4M based and the other one entirely FPFA based.

In order to compare and analyse the impact of FA modifications, the designer and reactor operator calculated the same core configuration ([9]) for both types of FAs (including aluminum alloy):

• 20 SFAs and 12 CFAs
• No experimental devices to avoid induced disturbance.

considering reactivity excess, β_{eff}, total rod worth and power peaking factor (PPF) at core level, calculated both by the designer and reactor operator, including a numerical comparison of the results.

It showed a good agreement between deterministic and probabilistic results. Indeed, FPFA core compared to IRT-4M one exhibits:

• Reactivity Excess decrease of about 17% (due to the inefficient layout of the controlled assemblies)

• PPF (Peaking Power Factors) rise from 5% to 10%

• similar β_{eff}

• consistent total rod worth, except for Apollo-2 code *(2D full core calculations are not relevant for assessing 3D effects).*

Part of these results are explained by a higher U-235 mass and wider water channels in FPFA assemblies.

Figs. 3 and 4 present respectively IRT-4M and FPFA core thermal fluxes maps obtained with the different codes used.

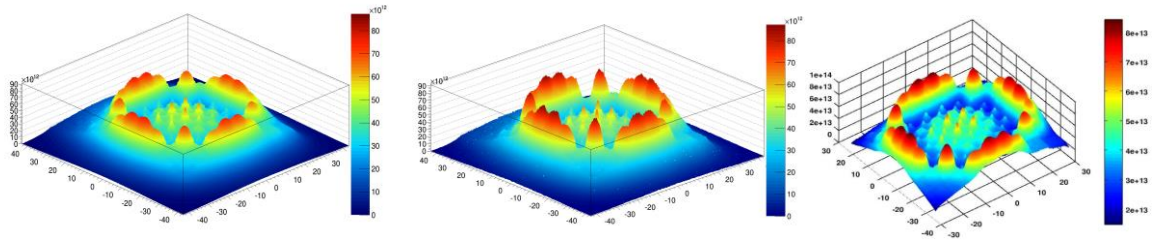

Fig.3 - Thermal flux map of the IRT-4M Core (n·cm^{-2}·s^{-1}): from left, Apollo-2 (TA), Tripoli-4 (TA) and Serpent-2 (CVR)

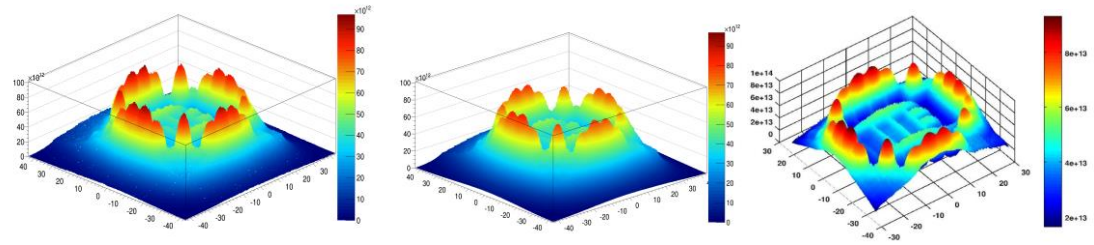

Fig.4 - Thermal flux map of the FPFA Core (n·cm^{-2}·s^{-1}): from left, Apollo-2 (TA), Tripoli-4 (TA) and Serpent-2 (CVR)

These maps show the same shape and close absolute values. Concerning Apollo-2 and Tripoli-4 results, discrepancies are in the range -1% < ε < 3%. As thermal fluxes maps are in a good agreement, it can be assumed that all reaction rates are calculated properly at core level.

One of the first steps of the fuel diversification is to check the alignment between calculations codes used. This step gives to stakeholders a good level of confidence in calculation tools used for the project. Fuel assemblies and fresh core calculations led to consistent results in this phase of the project, opening the door to successive steps.

Further details can be found in [9].

Mockup and fuel assembly R&D and manufacture aspects

Framatome-CERCA is the European manufacturer of nuclear research reactor fuels and has a sixty years proven track record. The LVR-15 fuel assembly concept have been developed from scratch. The manufacturing methodology is shortly described in this paragraph.

First, the best fuel option suitable for LVR-15 was chosen using Technological Readiness Levels (TRLs) and their Manufacturing Readiness Levels (MRLs) assessments. The methodology used for the TRL analysis is an adaptation of the European Commission work programme definition of the TRLs and the European Cooperation for Space Standardization (ECSS) adaptation of the international ISO 16290 - 2013 standard [13], [14]. The analysis of existing Research Reactor (RR) fuel systems was performed as well as an assessment of the fuel options already existing or currently under development. The main parameters considered for the assessment were fuel technology maturity, robustness, economic impact, consumption, fabricability and uranium density. It is important to note that the sustainability of a specific fuel system is considered reactor-dependent. The solution adopted therefore is specific for the LVR-15 reactor and cannot be generalized. The

selected fuel system was U_3Si_2 with 4.8 gU/cc loading in a square assembly with flat plates. The experience and fabrication status of U_3Si_2 fuel system is explained in greater detail in [15] and [16]. Then the external geometry of the fuel assembly has been adapted to the LVR-15 geometry, and the fuel plate design optimized considering space, irradiation and economic performance. This fuel type has been manufactured by Framatome since the 80's, with a well-established manufacturing process, thus adopting a high manufacturing and technology readiness level (TRL-9). The silicide fuel at this loading is fully qualified under irradiation and is currently used for the fuel of the HFR reactor (The Netherlands), the OPAL reactor (Australia), and many other research reactors around the world.

Second, this fuel option design was confirmed after performing proper numerical simulations. This is explained in the previous chapter of this paper.

Third, manufacturing tests and measurements were made using depleted uranium at several stages of the LVR-15 mockup to prototype some manufacturing steps and to refine the manufacturing program.

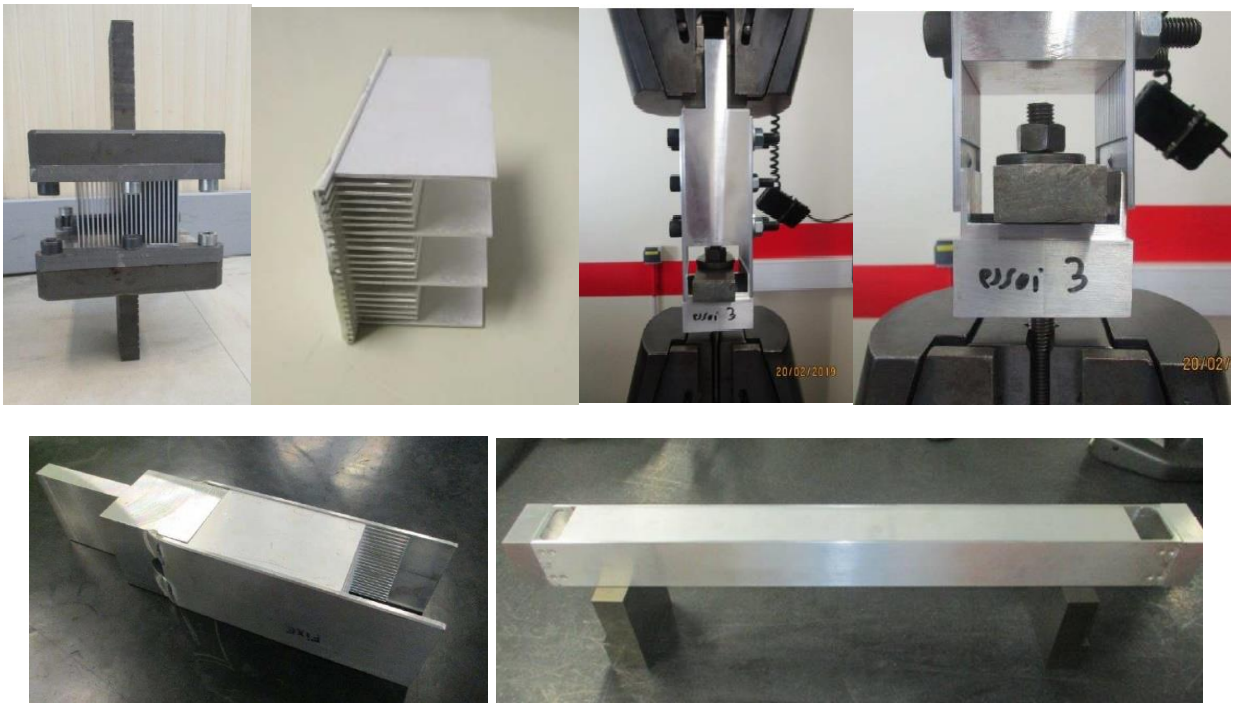

Fig.5 – Some of the tests performed on LVR-15 assembly mockup to ensure the fabricability

Figure 5 presents the mechanical, swedging and riveting tests performed on the assembly to the side-plates and nozzle. Height tests were made and about 14 mock-ups were manufactured and tested. The mechanical behaviours of the assembly are very important for handling and safety purpose. The geometry preservation shall be guaranteed under irradiation together with the mechanical resistance of each attached part.

Then, the plate itself was developed. For that purpose, 10 fuel plates with depleted uranium were produced to select the best manufacturing set of parameters and to verify each quality or safety criteria. Figure 6 presents the fabrication route for U_3Si_2 plate manufacturing. Figure 7 shows specific measurements of the uranium parts to illustrate the main safety criteria. The plate cladding is the first safety barrier of the fuel. Its integrity is measured in order to ensure a minimum cladding thickness value. The uranium distribution in the plate is also measured to be sure that no uranium accumulation occurs, potentially leading to hot points and local fusion in the core.

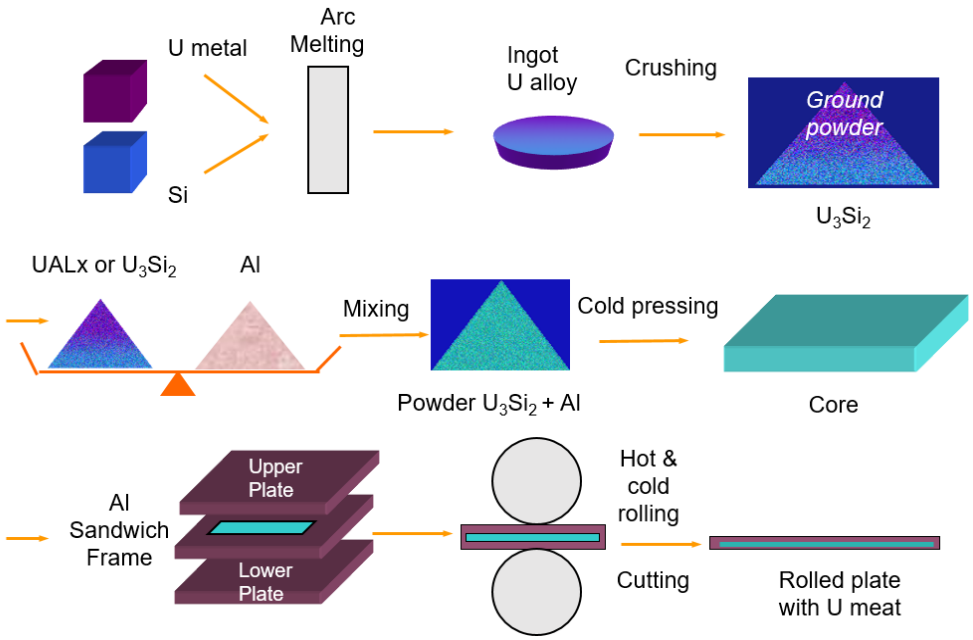

Fig.6 – Fabrication route of U_3Si_2 fuel plates [17]

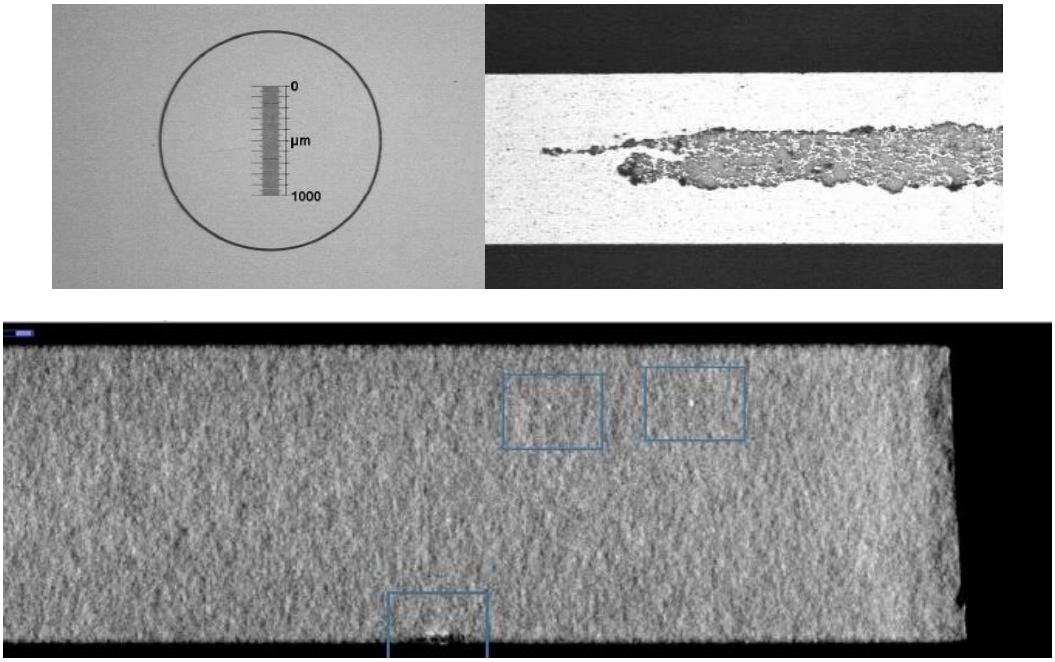

Fig.7 – Cross sections of LVR-15 plates (top) – X-ray picture of LVR-15 plate to measure the uranium homogeneity [18]

Finally, the LEU fuel assembly was produced using the fuel option selected, the design was established upon agreement between the designers, the reactor operator and the manufacturer, and the manufacturing program tested and optimized the best option for the LVR-15 reactor. Picture 8 presents the final LVR-15 assembly obtained.

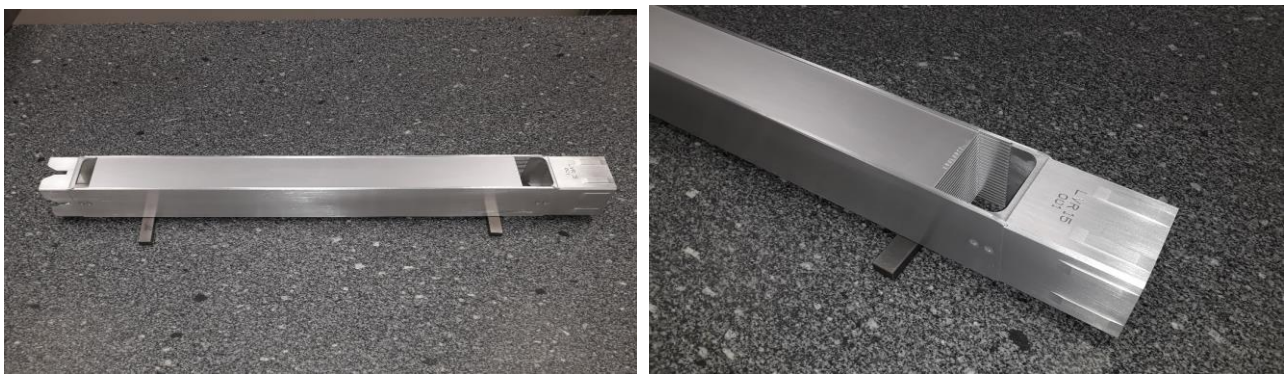

Fig.8 – LVR-15 R&D fuel assembly

The Hydraulic Test and the Fuel Inspection

After the preliminary calculation phase, a draft design and the technical drawings were issued by the designer. They were sent to the fuel manufacturer and reactor operator for a check and final remarks, which were finally implemented in the final design. After this phase the fuel manufacturer, Framatome-CERCA, fabricated the fuel mockup (with no fuel) and sent it to the reactor operator for hydraulic testing and the check for interfaces compatibility (e.g. with fuel manipulators) (Fig.9).

Fig.9 – The FPFA mockup manufactured by Framatome CERCA

The goals and the technical requirements of the hydraulic test were established by the designer, through a dedicated project deliverable.

The defined main goals were:

- Building a database of pressure drops as function of the FA liquid flow within the defined range (using an isothermal hydraulic test);
- Building the hydraulic characteristic with appropriate achievable uncertainties;

In order to achieve these purposes, the designer recommended to:

- Perform a complete metrological control of the dummy FA and of the test section;
- Accurately regulate the thermal hydraulic conditions within the loop;
- Accurately measure the thermal hydraulic conditions within the FA.

The proper liquid flow range together with estimated FA pressure drops, temperature range, pressure range and corresponding Reynolds number in the mean channels was clearly established, based on thermohydraulic preliminary calculations. The reactor bottom grid was simulated as well.

Strict measurement accuracy requirements were clearly fixed by the designer: 1% for mass flow, 1°C for temperature and 1% for pressure. It was recommended to have at least 2 pressure sensors upstream and 2 downstream of the mockup in order to measure the pressure drop reliably; they must be located in steady-state flow zones: it was suggested to place inlet sensors at a distance at least 10 times the FA mean channel hydraulic diameter, 25 times for the downstream one. The fluid viscosity heavily varies with temperature, so its accurate control represents a key factor to ensure the Reynolds similitude. It was also recommended to control and measure the eccentricity of the mockup within the test slot.

The tested mass flow range shall be representative of the different reactor conditions both in normal and accidental situations. Finally, it was proposed a possible solution for the test loop scheme (Fig.10).

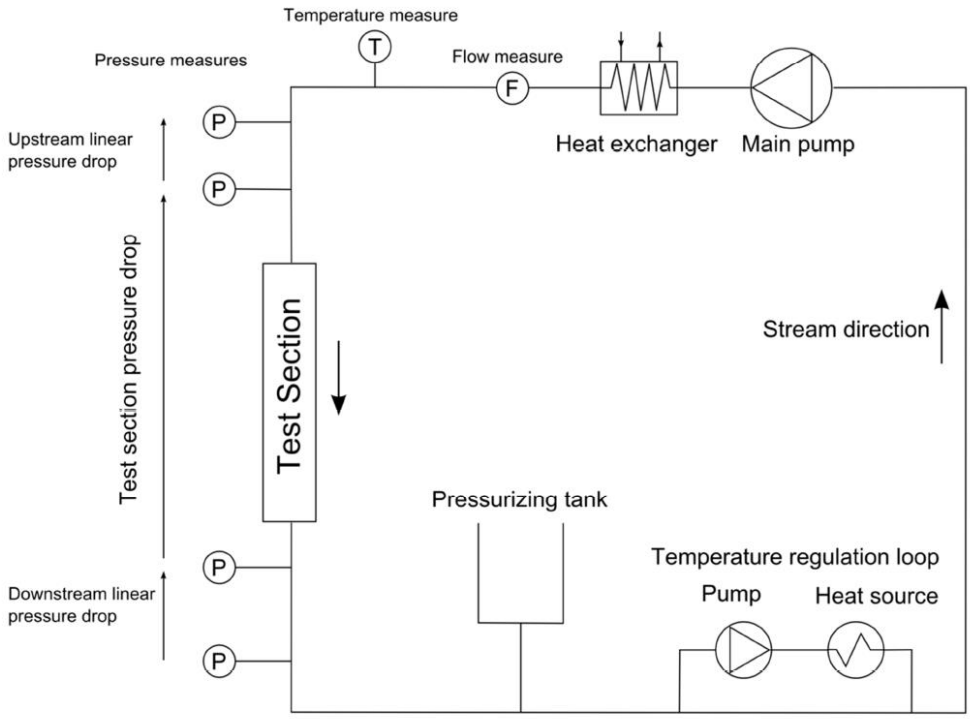

Fig. 10- Test loop for the pressure drop measurement

The execution of the hydraulic test was performed by an external specialized company.

Given the importance of the temperature measurement, two thermocouples were used, one just before the test section and one just after it. The reading of these two thermocouples is supposed to be very close in order to confirm the isothermal measurement, as required by the designer. The reason for placing the

thermocouples in these locations is that unlike the pressure measurement, they can potentially disturb the flow as they have to be placed in the flow stream.

In order to maintain a high water purity and avoid any possibility of corrosion, the entire loop was constructed from plastic materials. An Intermediate Bulk Container (IBC) of 1 m^3 was used as a pressurizer as well as the water supply tank. Given the water mass used, its temperature in the main loop was very stable and the regulation down to 0.1°C was possible. Three 10-liters accumulation heaters were used to heat up the water in the supply tank; the power of each heater was 2.4 kW. The water for the test section was produced by a reverse osmosis device able to produce water of laboratory quality. The minimum time of the single measurement was 90 seconds with data sampling every second. Every measurement was performed increasing the flow rate at a fixed temperature gradually and then reducing it to the original value, in order to check the repeatability of the measurement (a pump oil leak, for example, would potentially affect the accuracy of the measurement). Obtained data were carefully checked for a proper statistical relevance: the standard deviation was an order of magnitude smaller than the error of the measuring device. This means that the number of measured points was sufficient to get good statistics, the experiment was well stabilized with respect to the possibilities of the measurement devices, the probability of the measured points lying within the interval of the error was at least 99.73% and most importantly no significant fluctuations were observed regardless the fact that the pressure measurement was located close to the mockup.

The result of the measurement at various temperatures (between 40 °C and 50 °C) is reported in Fig.11.

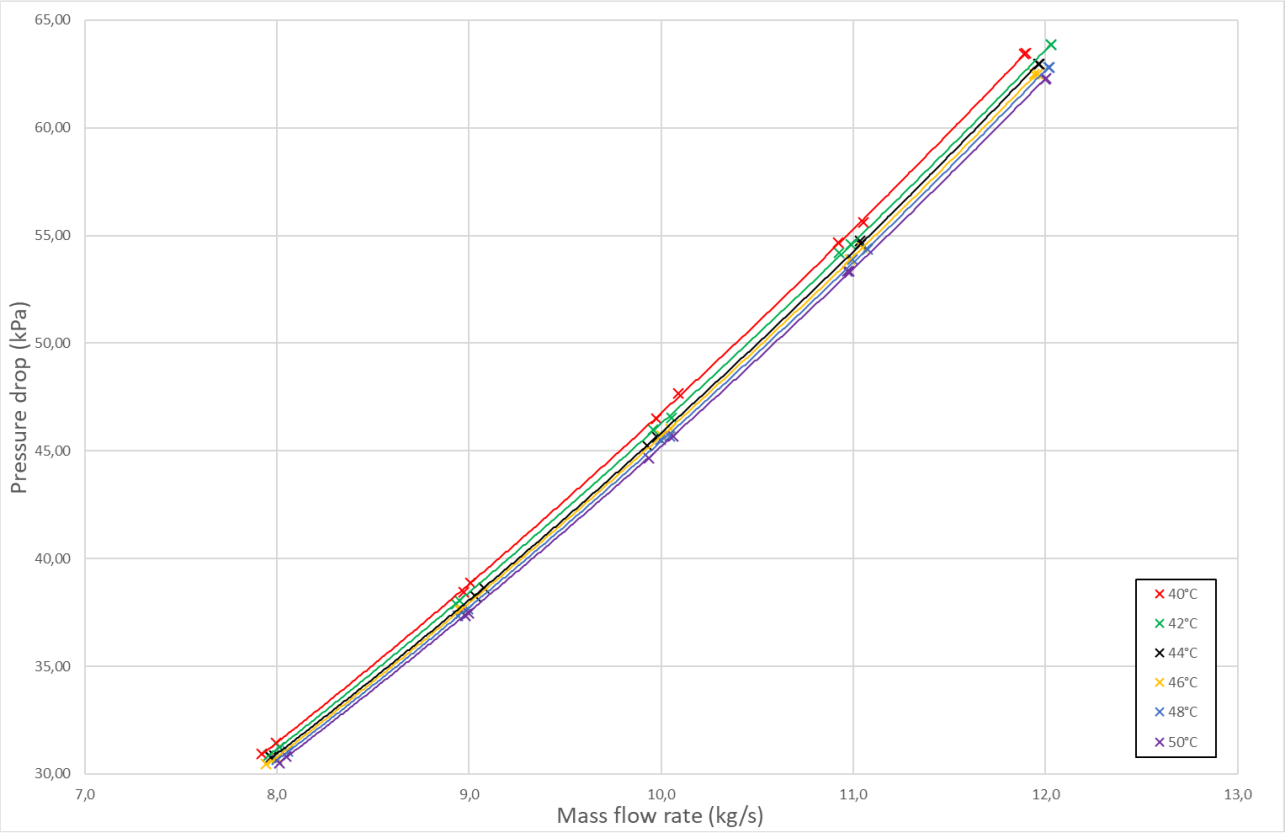

Fig. 11 – FPFA mockup pressure drop vs. flow rate

The pressure drop test proved that the calculations of the designer were accurate within a discrepancy of the order of 2%.

Later on, another test was performed on the same assembly but oriented to check low flow rates. For this purpose, the test section was modified taking into account the final shape of the top and bottom nozzles, which include windows. Therefore, a transition into a rectangular channel was manufactured and the square channel cage made of plexiglass was used. In this case the effect of the windows on the pressure drop could be evaluated when compared to the previous measurement (they can be seen in Fig.12 at a mass flow point of 8.0 kg/s, the discrepancy is 1.4 kPa for both 40°C and 50°C).

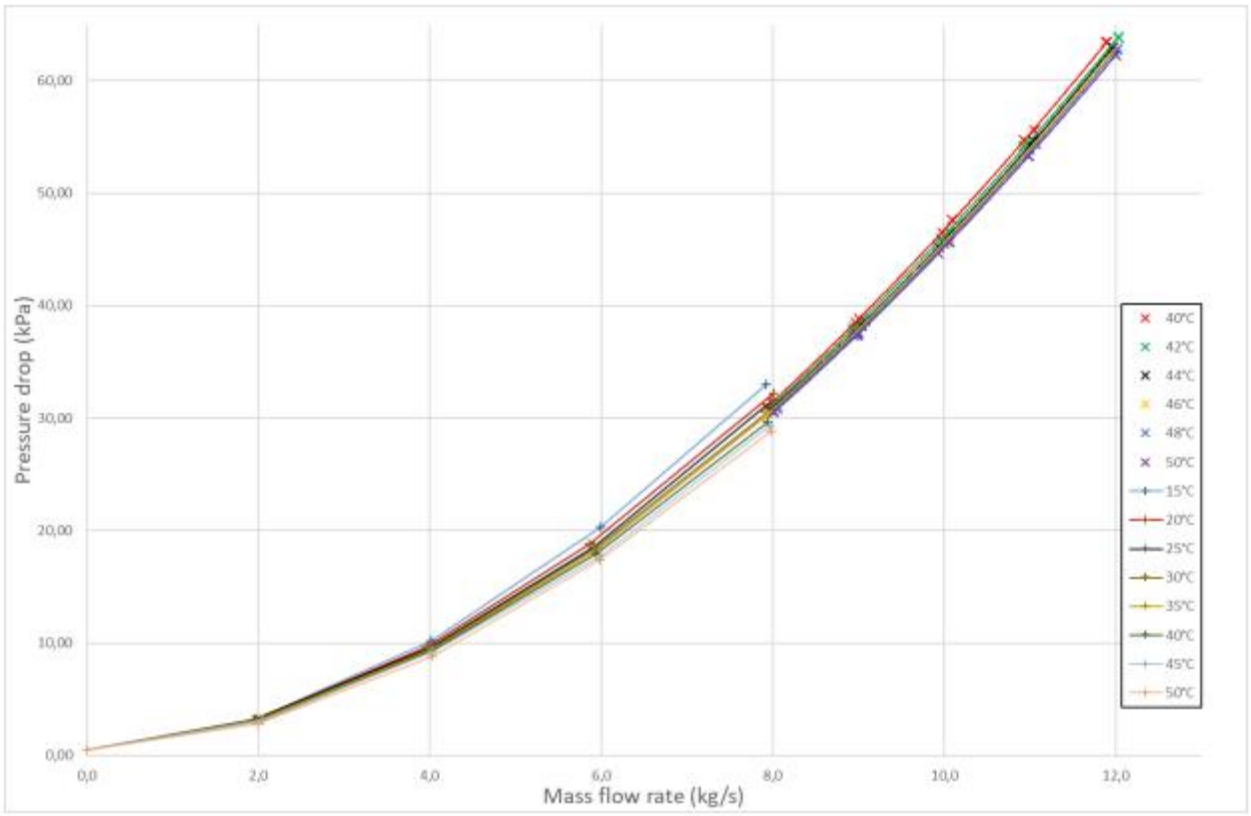

Fig.12 – FPFA mockup pressure drop trend vs. mass flow rate (low flow rates oriented measurement)

The Fuel Safety Assessment Procedure

The main objective of the fuel safety assessment procedure performed by the reactor operator was to identify and assess a possible LVR-15 prototype realistic campaign for the new designed FPFA fuel, characterize it during normal operation, identify some critical accidental scenarios mentioned in the Safety Assessment Report (SAR) submitted to the Czech nuclear regulator (SUJB) and perform a preliminary evaluation of the consequences from the nuclear safety point of view.

The identified campaign for the irradiation of the FPFA fuel was the K-216 modified; two positions were considered (for the full campaign), i.e., B-6 and B-4 (Fig.13), both at the periphery of the core, due to the prototype test irradiation purpose. For a preliminary estimate, the position B-4 was chosen to assess from the neutronic point of view, due to its higher average power vs. time (as clearly shown by NODER calculations [19]). The campaign is subdivided in 12 phases and 117 steps, with a maximum assembly power of 506.7 kW and an average of 376.6 kW in B-4 position; total irradiation time is 34.21 days. No external devices are considered, in order to avoid any possible disturbance. Reflector is composed mainly by full beryllium blocks.

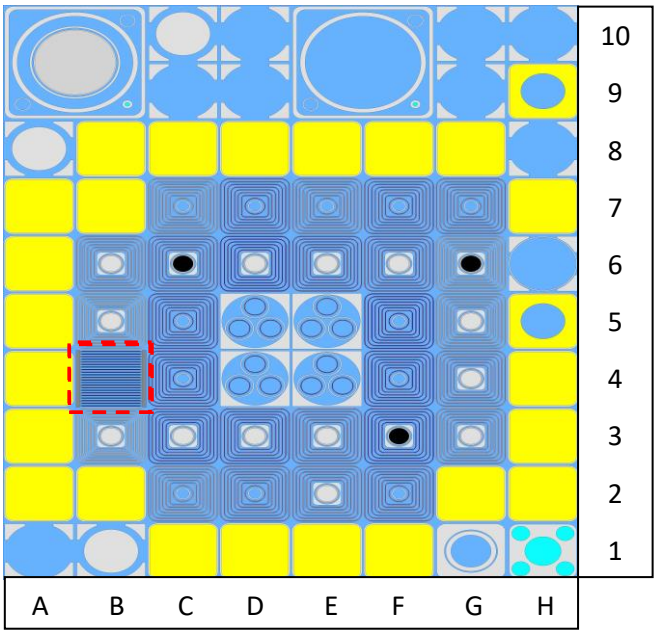

Fig. 13 – Example scheme of the LVR-15 core during the K-216 campaign *(in the red box the FPFA test fuel assembly in B-4 position)*

The nominal power of the reactor during the steady state operation is 9.7 MW_{th}. The configuration is modified at every step such as the position of the control rods. The whole reactor campaign was calculated with the NODER code, currently used by the LVR-15 reactor team. For the purpose of the Monte Carlo calculation, it was chosen step 64, in the middle of the campaign and distant from any Xe transient. The input in SERPENT code was prepared considering a different material composition for every different assembly based on its burnup (NODER code provided the burnup and then composition was obtained from an interpolated matrix enclosing the assembly composition vs. burnup in an infinite lattice), further subdivided in 5 different axial compositions (5 chunks, 12 cm high each).

In the adopted scheme control rods are fully extracted, except for positions C-6 and G-6, where they are fully inserted, while control rods in positions F-3 and G-3 are partially inserted (5 and 35 cm, respectively, from the bottom of the active core quote). The scheme of the core is reported in Fig. 13. In Fig. 14 the thermal neutron flux map averaged on the full assembly's height (i.e. 60 cm) is shown, together with the map of the relative values. Maximum flux values are located in the center of the core, in the moly targets positions, as expected (the axial shape and composition of the targets is not uniform).

The fission power was evaluated as well and is presented in Fig. 15: the maximum values are reached in the assemblies in positions C-4 and B-4, with 490 and 470 kW, respectively.

Further details are discussed in [19].

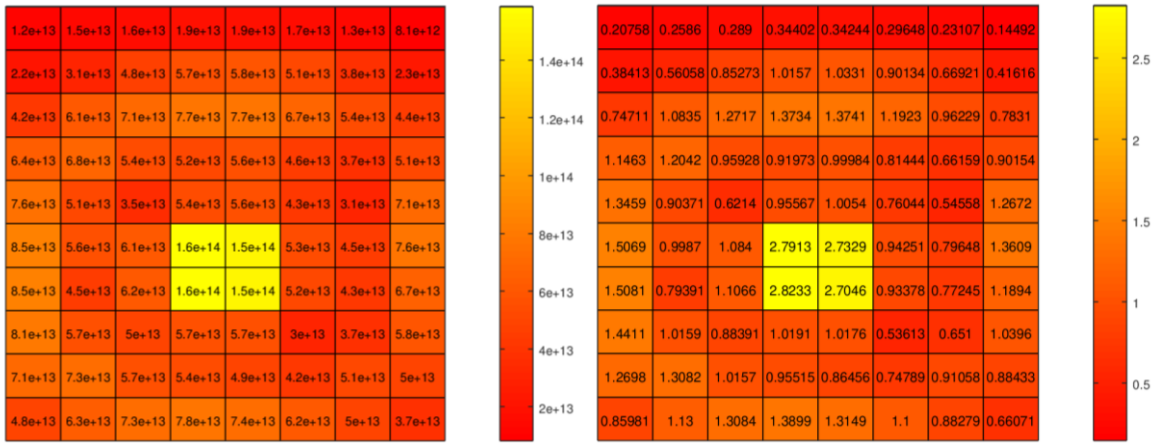

Fig. 14 – Thermal neutrons flux (n/cm^{2}s) maps (from above: absolute and relative) at the center of the core (central chunk) for each assembly

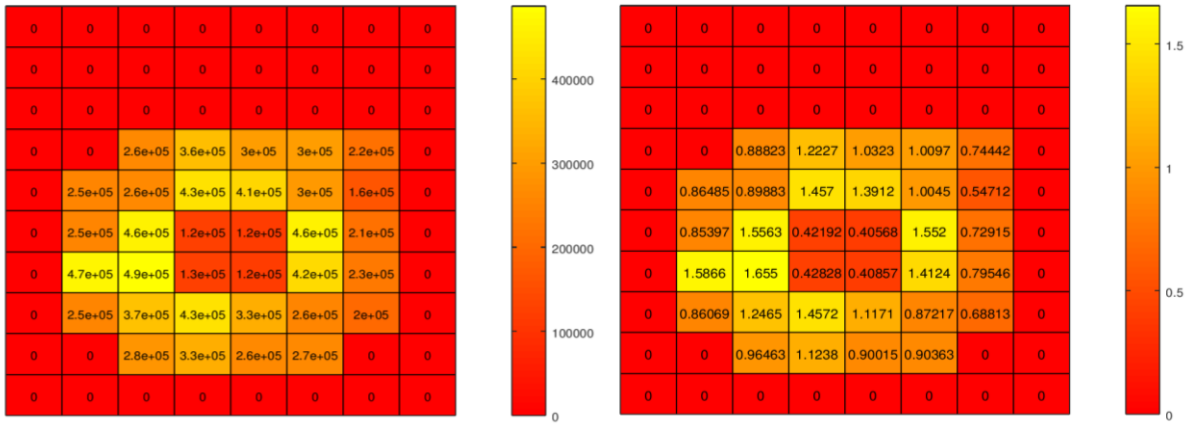

Fig. 15 – Power map (W) at step 64 at the center of the core and its relative values

Thermohydraulic calculations for the Safety Assessment to be Submitted to the National Regulator

In order to prepare an amendment for the LVR-15 reactor Safety Report for the national regulator, several analyses including different accidental scenarios were run using RELAP-5 code. In order to increase the safety margins, the reactor power was set to 10 MW_{th} (instead of 9.7), the water flow was set to 1350 m^3/h (instead of 1500 m^3/h, which is the nominal value), respectively 3% higher and 10% less than the values used for the neutronic analyses. The maximum assembly power historically achieved during all the campaigns with the IRT-4M was selected as well: the hottest IRT-4M 8-tubes and 6-tubes assembly power were assumed, respectively 565.10 kW and 514.24 kW; for the FPFA, the maximum power of 506.74 kW was used. Of course, the analysis took into account also surface and volumetric densities.

The postulated initiating events that are taken into consideration include various scenarios such as Reactivity Initiated Accidents (RIA), Loss Of Operative Power (LOOP) and Loss Of Flow Accidents (LOFA). They are divided into categories:

- Category I: normal operations and operational transients
- Category II: abnormal operation, high frequency events
- Category III: Design Basis Accidents (DBA) with medium to low frequency

- Category IV: Design Extended Conditions (DEC A), accidents without serious fuel failure and very low frequency

One scenario per each category was described in detail: a LOOP with failure of RCP-1 (Cat II – chapter 16.2.2.2 of the safety report), an uncontrolled removal of the control rod which leads to a reactivity insertion of 2.8 β / 30 sec (Cat III – chapter 16.2.3.2 of the safety report) and a LOOP with failure of all pumps (Cat IV – chapter 16.2.2.4 of the safety report). The trend of the cladding temperatures in the three scenarios mentioned above are reported in Fig.s 16-18.

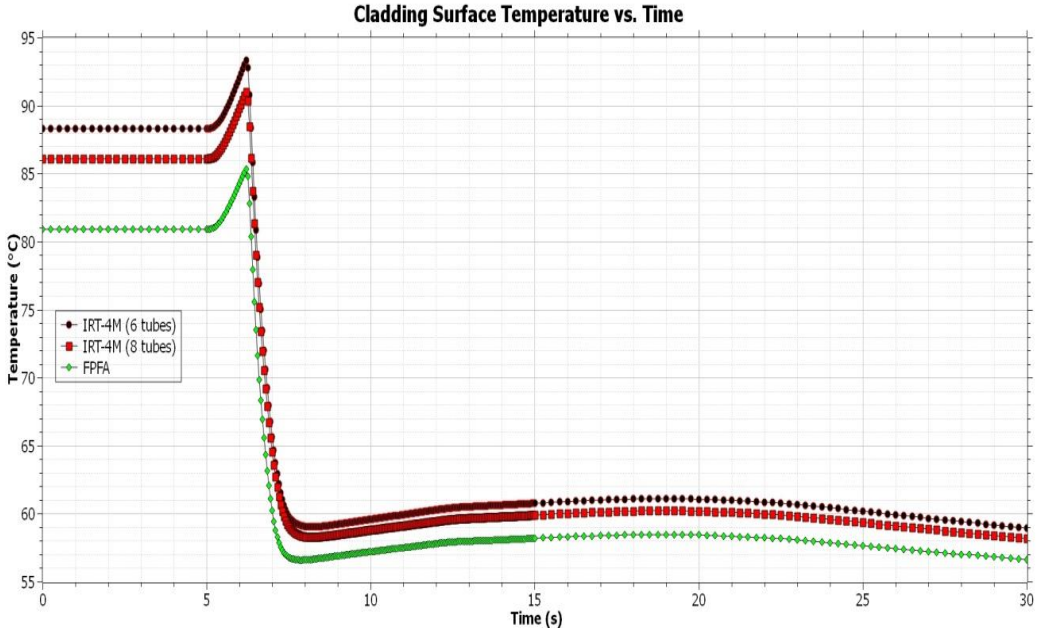

Fig. 16: Loss of working power supplies – RCP 1 start-up failure: IRT-4M and FPFA test assembly fuel elements maximum surface temperature

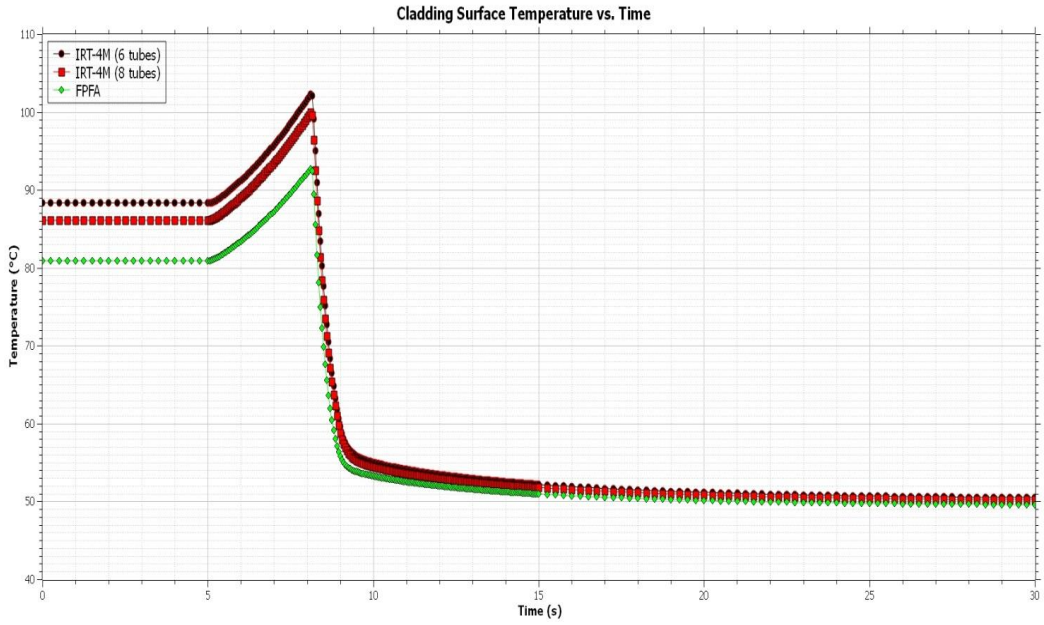

Fig. 17: Uncontrolled removal of the absorption rod with the action of emergency protection – reactivity input 2.8 β / 30 sec: IRT-4M and FPFA test assembly fuel elements maximum surface temperature

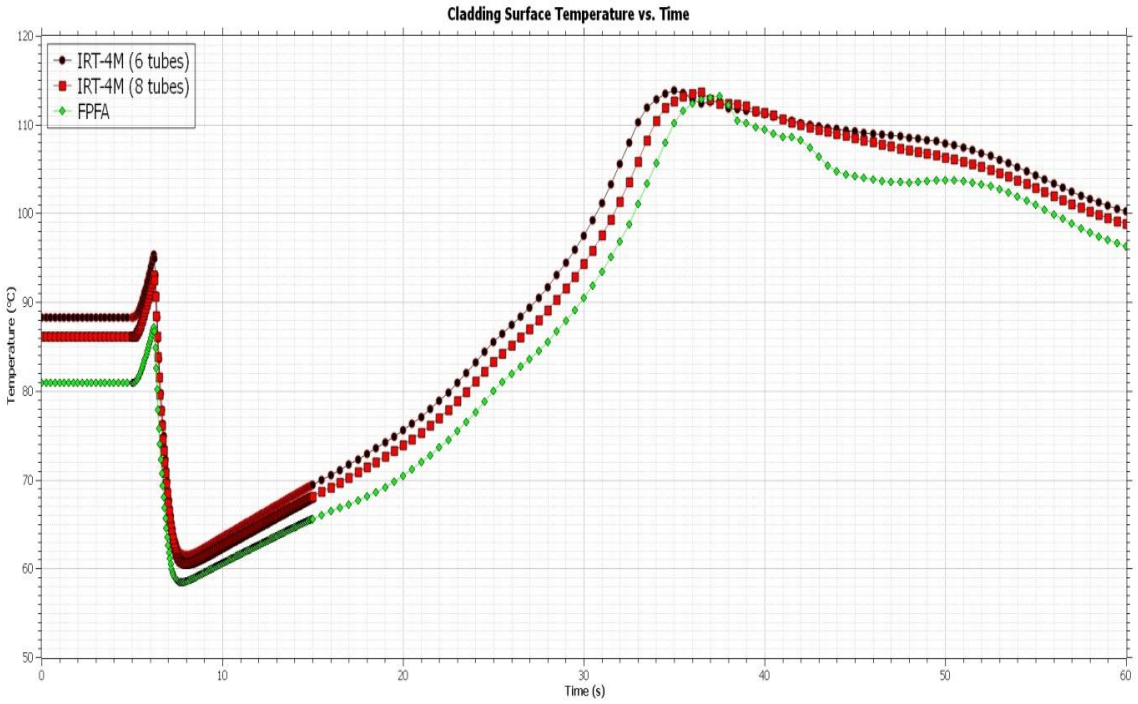

Fig. 18: Loss of working power supplies – RCP 1 start-up failure and emergency feedwater pump failure: IRT-4M and FPFA fuel elements maximum surface temperature

The analysis proved that the fuel irradiation is safe under every scenario. Further details can be found in [20].

Manufacturing of the Fuel Assembly and Irradiation Start

In accordance with [7], thanks to the proven design technology of the uranium silicide flat plate [8] and the characteristics of the LVR-15 core, no lead test assemblies are needed. Then, in parallel to the safety assessment, in order to prepare the next step, just one new standard fuel assembly has been manufactured.

The fuel assembly has been manufactured by Framatome-CERCA, which has a many decades experience with U_3Si_2 fuel manufacturing. The fuel assembly inspection was performed online (due to the COVID-19 emergency), in presence of the reactor operator, the fuel designer and the nuclear safety authority. Various checks were performed: critical dimensions of the fuel assembly (external sizes important for the assembly coupling with reactor elements and the gaps size), composition of the fuel, contamination of the surfaces, distribution of eventual stray particles in fuel and presence and extension of the eventual 'dog-bone' areas (those with reduced cladding thickness due to the fabrication process, resembling the shape of a dog bone in fact) with x-rays radiographs, nozzles dimensions compliance and finally, the results on the nozzles pull test. The fuel manufacturer recorded questions received during the inspection and issued a detailed written answer. The test fuel assembly was afterwards transported to Czech Republic based on a permission from the Czech regulator after evaluating a number of documents specified in the Act No. 263/2016 Coll. (Atomic Act), in particular:

- Instructions for the transport of non-irradiated fuel assemblies in the Czech Republic
- Programme for ensuring radiation protection during transport of a prototype standard fuel assembly of the FPFA plate type in the territory of the Czech Republic
- Plan for the provision of physical protection for transport
- Analysis and assessment of a radiation emergency (contained in the document of Risk assessment for the transport of a non-irradiated fuel cluster on the territory of the Czech Republic)

- Emergency Plan for the transport of non-irradiated fuel assemblies in the territory of the Czech Republic
- Management System Programme for the transport of a prototype standard FPFA plate-type fuel assemblies in the territory of the Czech Republic.

The irradiation in the LVR-15 core started around half of March 2022.

Conclusions

The project LEU-FOREvER, collecting 9 stakeholders among fuel designers and manufacturers, reactor operators and research centers, was started in October 2017 with the main aim to secure the nuclear fuel supply to European research reactors. The project's goal was to address two main issues: the conversion of the High-Performance Research Reactors from high to low enriched fuels and establish a European alternative for fuel manufacturing for the Medium Power Research Reactors. For the last goal achievement, a new fuel assembly was designed, manufactured and it is tested in the Czech reactor LVR-15. For this purpose, first main technical characteristics information of the reactor was collected by the designer. The next step consisted in the design of a new fuel assembly concept, based on flat plates and with a uranium silicide meat based technology, which allowed to sensibly improve the specific uranium content with respect to the volume unit. The design was reviewed and approved by the reactor operator and fuel manufacturer. Then, a fuel mockup was manufactured and delivered to the operator for checking interfaces compatibility (e.g. with fuel manipulators) and, more important, in order to perform an accurate hydraulic test (the specification of which was provided by the designer). In parallel, the reactor operator performed the necessary neutronic and thermohydraulic safety assessment calculations and submitted the report to the national regulatory body for the irradiation license approval: the irradiation license from the regulator was obtained in less than 3 months from submission. The assembly is now under irradiation in the reactor, slightly less than 4.5 years after the project start. The final step of the program will be a basic post-irradiation inspection for a preliminarily assessment of the fuel performance.

The various steps of the project described in detail in the present paper presented various practical difficulties which had to be solved step by step and just in time, with the cooperation of all the project partners involved. The scope of the present work is to indicate a clear methodology for the development of an innovative fuel for research reactors starting from scratch, with a detailed description of the needed steps and their logical sequence for a fruitful and smooth implementation of the project.

A follow-up of the present work will be issued as soon as the irradiation report and the post-irradiation inspection reports of the tested fuel assembly will be issued.

Acknowledgements

The authors are grateful to Mr. Pavel Jíška for reviewing this text and for his valuable hints, in particular concerning the neutronic calculations section. They wish to thank also Euratom for the financial support to LEU-FOREvER project, which has received funding from the research and training programme 2016-2017 under grant agreement No. 754378. The presented work has also been realized within Institutional Support by Ministry of Industry and Trade of the Czech Republic.

The fuel assembly manufacturing has been performed in partnership with Framatome-CERCA in LEU-FOREvER project.

References

[1] IAEA, “Manual for reactor produced radioisotopes,” IAEA-TECDOC-1340, Vienna (Austria), 2003.

[2] A. Hawari, "Importance of Research Reactors in Human Capacity Building in Nuclear Science and Engineering," IAEA, Rabat (Morocco), 2011.

[3] N. Jawerth, "Supplies of Key Medical Isotopes Stable, but Vulnerabilities Remain," 22 Sep 2017. [Online]. Available: https://www.iaea.org/newscenter/news/supplies-of-key-medical-isotopes-stable-but-vulnerabilities-remain. [Accessed 04 06 2021].

[4] EC, "Low Enriched Uranium Fuels fOR REsEarch Reactors," European Commission, 1 October 2017. [Online]. Available: https://cordis.europa.eu/project/id/754378. [Accessed 08 06 2021].

[5] S. Valance, «The European Project Fuel fOr Reactors - FOREvER: LEU fuels for medium and high power research reactors in Europe,» in *RRFM-2018*, Munich (Germany), 2018.

[6] M. Boyard, «Fuel Assembly Design For An Irradiation in A European Medium Power Research Reactor,» in *RRFM-IGORR-2019*, Dead Sea (Jordan), 2019.

[7] I. (. A. E. Agency), "Good pratices for qualification of high density low enriched uranium research reactor fuels," Vienna, 2009.

[8] U. N. R. C. -. O. o. N. R. Regulation, "Safety Evaluation Report related to the Evaluation of Low-Enriched Uranium Silicide-Aluminum Dispersion Fuel for Use in Non-Power Reactors," *NUREG-1313,* July 1988.

[9] J. Koubbi, «FOREvER Project: Preliminary Neutronic Calculations Status,» in *RRFM-IGORR-2019*, Dead Sea (Jordan), 2019.

[10] J.-G. Lacombe&al., «COCONEUT: Enhancing Neutronic Design for Research Reactors,» in *RRFM-IGORR*, Berlin, 2016.

[11] J. e. a. Leppänen, «The Serpent Monte Carlo code: status, development and applications in 2013,» *Ann. Nucl. En.,* vol. 82, pp. 142-150, 2015.

[12] O. R. N. Laboratory, «A Comprehensive Modeling and Simulation Suite for Nuclear Safety Analysis and Design,» 2011.

[13] «ECSS-E-AS-11C – Adoption Notice of ISO 16290, Space systems».

[14] «ISO 16290:2013, Space systems — Definition of the Technology Readiness Levels (TRLs) and their criteria of assessment,» [Online]. Available: https://www.iso.org/standard/56064.html.

[15] S. P. Y. G. D. G. B. Stepnik, «Proceeding of RERTR 2018 – 39TH International Meeting on Reduced Enrichment for Research and Test Reactors,» in *RERTR-2018*, Edinburgh (Scotland), 2018.

[16] B. Stepnik, "Report on existing process on U3Si2," LEU-FOREVER Deliverable D2.1, 2020.

[17] J. Allenou, "Report in existing process on U3Si2," LEU-FOREVER deliverable D2.1.1.

[18] B. Stepnik, "Fabrication report of LVR-15 LEU LTA (standard element)," LEU-FOREVER deliverable D5.8.

[19] A. D. M. K. M. H. V. Romanello, «Thermohydraulic Safety Criteria Assessment for the 4EVERTEST Innovative Fuel Assembly Irradiation in the Frame of the LEU-FOREvER Project,» in *RRFM-2021*, Helsinki (Finland), 2021.

[20] A. D. J. E. M. Z. M. H. M. B. f. H. V. ROMANELLO, "PRELIMINARY ASSESSMENT OF THE SAFETY CRITERIA FOR THE 4EVERTEST FUEL ASSEMBLY IRRADIATION IN THE FRAME OF THE LEU-FOREVER PROJECT," in *RRFM-2021*, Online, 2021.

[21] V. B. e. al, «Conversion of Reactor LVR-15 in Czech Republic from HEU to LEU Fuel,» in *RRFM Conference*, Rome, 2011.

[22] D. A. e. alii, «Neutronic analysis of the LVR-15 research reactor using the PARCS code,» *Ann. Nucl. En.,* vol. 117, pp. 145-154, 2018.

[23] B. a. alii, «Conversion of Reactor LVR-15 in Czech Republic from HEU to LEU Fuel,» in *RRFM*, Rome, 2011.

[24] K. T. S. P. V. U. A. Kecek, «Development of M5 Cladding Material Correlations in the TRANSURANUS Code,» JRC, Karlsruhe, 2016.

SIMULATION OF THE CROCUS REACTOR IN THE FRAMEWORK OF THE H2020 CORTEX (CORE *monitoring Techniques and EXperimental validation and demonstration*) PROJECT

T. BARRACHINA, N. OLMO, R. MIRÓ, A. VIVANCOS, S. GALLARDO, G. VERDÚ
Institute for Industrial, Radiophysical and Environmental Safety
Universitat Politècnica de València
Camí de Vera, s/n
46022 València (Spain)

ABSTRACT

The CROCUS reactor is a light water moderated reactor located on the campus of the École Polytechnique Federal de Laussane (EPFL) in Switzerland. It is operated by EPFL's Laboratory for Reactor Physics and System Behaviour (LRS). The power of the reactor is limited with an upper limit of 100 W, it is classified as a zero power reactor. It reaches approximately 2.5 x 10^7 neutrons per square cm and second in the centre of the core for a reactor power of 1 W. The CROCUS reactor has a quasi-cylindrical shape with a diameter of approximately 58 cm and a height of 100 cm. Its main characteristic is that inside it has two differentiated radial zones that in turn have different cell sizes. It has two types of fuel elements.
The goal of this work is to simulate a steady state case in the CROCUS reactor with two neutronic deterministic codes: PARCS and VALKIN-FVM-Sn.
To perform the simulations, both codes are fed with kinetic parameters and cross-sections. The set of cross-sections have been obtained with the Monte Carlo code SERPENT.
The comparison of the results shows a good agreement between both codes. This work serves to assess the capabilities of the VALKIN-FVM-Sn code to deal with this kind of simulations.

1. Introduction

The main challenge of the H2020 CORTEX (Core monitoring Techniques and Experimental validation and demonstration) project is the development of neutron noise monitoring techniques [1] for implementation in commercial nuclear reactors, thus allowing early detection of anomalies and their characterization.
For this, the development of new tools and methodologies is required to improve the current understanding of the phenomenology of neutron noise. As well as the validation of these techniques against real transients, allowing both the demonstration of their capabilities and the bounding and overcoming of their limitations.
In this context, and within the framework of the collaboration of the Universitat Politècnica de València in the CORTEX project, the reproduction of the experiment carried out in the CROCUS experimental reactor is proposed. In it, the neutron noise corresponding to the vibration introduced by a group of fuel rods in the periphery of the core has been simulated and recorded.
In this way, the purpose of the work developed is the reproduction of these experiments using the PARCSv3.2 code [2] and the VALKIN-FVM-Sn Code [3].
The PARCS code is a three-dimensional reactor core simulator originally developed at Purdue University (Indiana, USA), and actually at Michigan University, while distributed by the Nuclear Regulatory Commission (NRC), for conducting core analysis of commercial reactors. It has different approximations to solve the neutron transport equation: diffusion and SP_3.
VALKIN-FVM-Sn is a neutronic code developed by Senubio group of Institute for Industrial, Radiophysical and Environmental Safety in Universitat Politècnica de València. It solves the neutron transport equation with the Finite Volume Method for the space dominion and the Discrete Ordinates for the angular, for any number of energy groups. The major advantage of

this method is that it can deal with any complex geometry, calculating several modes on unstructured meshes. In addition, it uses the SLEPc library for solving the eigenvalue problem and the time-dependent ordinary differential equation and the PETSc library for solving vector and matrix operations, as well as linear systems. VALKIN-FVM-Sn can perform the different operations in parallel computers (MPI).
The set of cross-sections used in VALKIN-FVM-Sn comes from the same case in Serpent [4].
The work presented in this paper is the first step in the simulation of the transient in the CROCUS reactor presented in the COLIBRI (*CROCUS Oscillator for Lateral Increase Between u-metal Rods and Inner zone*) program [5].
We present the comparison between PARCS and VALKIN-FVM-Sn in the steady-state case. This required first step is very important to assess the cross-sections obtained with Serpent in both codes, and also to assess the results from both codes before simulating the transient.
The paper is structured as follows: section 2 explains the geometry and materials of the CROCUS reactor. Section 3 is devoted to explain the model of the CROCUS reactor in PARCS and in VALKIN-FVM-Sn. The results are showed in Section 4 and finally, the main conclusions and further works are summarized in Section 5.

2. The CROCUS reactor

The work developed is based on the reproduction of the experiments carried out in the CROCUS experimental reactor within the framework of the H2020 CORTEX program. Unlike the transients that could be collected from a commercial reactor, since the CROCUS reactor is an experimental reactor, the description of its main characteristics is of great interest. As well as the transient objects of study, which will make use of the COLIBRI oscillator.
The CROCUS reactor [6] is a light water moderated reactor located on the campus of the École Polytechnique Federal de Laussane (EPFL) in Switzerland. It is operated by EPFL's Laboratory for Reactor Physics and System Behaviour (LRS). The power of the reactor is limited with an upper limit of 100 W, so it produces hardly any heat allowing it to be classified as a zero power reactor. To provide an order of magnitude with respect to its neutron flux, it reaches approximately 2.5 x 10^7 neutrons per square cm and second in the centre of the core for a reactor power of 1 W.
Like most reactors, the CROCUS reactor has a quasi-cylindrical shape with a diameter of approximately 58 cm and a height of 100 cm. Its main characteristic is that in its interior it has two differentiated radial zones that in turn have different cell sizes, as can be seen in Figure 1 [5].
The reactivity of the core is controlled by varying the level of water in the reactor, for which there is a reactivity equivalence of ±0.4 pcm for every ±0.1 mm; or by means of two control rods that are symmetrically located near the periphery, as can be seen in Figure 1b (highlighted in yellow).

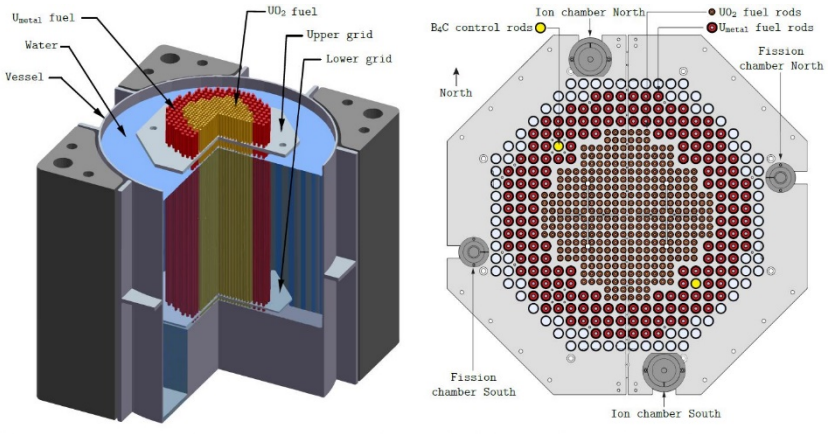

(a) Core structure and internals: isometric view (b) Upper grid and fuel lattices: top view

Fig 1. The CROCUS research reactor.

The neutron moderator used is water. There is also an outer zone of the nucleus surrounded by water as a neutron reflector, which covers a circumference of 130 cm in diameter. In turn, the core plus reflector assembly is surrounded by an aluminium tank with a continuous thickness of 1.2 cm. Likewise, the temperature of the moderator is fixed at approximately 20ºC by means of a refrigeration circuit.
In turn, the reactor has 6 independent stop mechanisms that allow the reactor to be brought to a subcritical state in less than a second. In this way, there are two cruciform Cadmium blades in the centre of the core and four tanks regulated by a system of valves that allow the level of the moderator to be regulated.
Due to the low power generated in the CROCUS reactor, the behaviour of the neutron population inside the core is barely influenced by its thermal effects. In addition, there is an additional advantage because the neutron flux being low, the effects of fuel burnup can be neglected. In this way, neutron phenomena can be treated in isolation, providing a powerful and optimal stationary validation tool for neutron codes.
The CROCUS reactor has two clearly differentiated types of fuel elements. The inner part of the core is made up of 336 rods of uranium oxide (UO_2), enriched to 1.806 percent by weight and with a cell size (the rod plus the surrounding moderator area) of a square area of 1.837 cm, each side. The region peripheral to the written region is, in turn, made up of 176 metallic uranium rods, enriched to 0.947 percent by weight, comprising a square area of 2.917 cm on each side, for each cell. The versatility of the reactor allows the loading of other different arrangements, but the one described will be the one used throughout the experimentation under study.

3. The model of the CROCUS reactor

In this section, the models developed for Serpent, PARCS and VALKIN-FVM-Sn of the CROCUS reactor are described. The original models for Serpent and PARCS were the subject of a thesis at the EFPL [5]. The inputs for these both codes were provided to the participants of the H2020 CORTEX project, among whom this work is framed, and will be the starting point of the work to simulate the transient, which is the final goal of this work.
From Serpent, the set of homogenized cross-sections and collapsed for two energy groups are obtained to feed PARCS and VALKIN-FVM-Sn.
The Serpent version used in this work is 2.1.31 with the JEFF-3.1.1 neutron libraries. In order to reach an estimate of the first eigenvalue (k-effective) with an uncertainty lower than ±0.7 pcm (±0.7·10-5), 10,000 cycles of one million particles in each one are simulated. Given the realistic modelling of the core and the large number of cycles and particles considered, the simulation of each case requires a high computational cost of more than 4300 hours/core.
The original model contemplates the existence of 7 regions for the homogenization of the neutron properties.
Once the simulation is done, the sets of cross-sections can be processed to serve as input to PARCS and VALKIN-FVM-Sn. In this way, the Serpent output is read and written in another format which is different in both codes
The simulation of the transient generated in the CROCUS reactor with the COLIBRI incore device represents a challenge for different reasons. On one hand, the dimensional and material characteristics of the CROCUS reactor with a high probability of neutron leaks in the reactor due to its small size, the presence of regions with a large neutron absorption (cadmium layers) and the inconsistency between the two cell sizes, corresponding to the inner and peripheral regions. And on the other hand, the difficulty in defining the real perturbations in the two codes.
In this paper, we present the work meant to analyse in both codes the influence of the mesh in the steady-state results. From these results, then we proceed with the simulation of the transient.

3.1 The model in PARCS

To solve the drawback of the different cell size in the reactor, two geometric models were defined in PARCS: the first has the cell size of the ceramic uranium region (located in the inner part of the reactor, 1,837 cm) and the second has the cell size of the metallic uranium region (located at the periphery of the reactor, 2,917 cm). Although this choice implies that there is no available model capable of faithfully and simultaneously reproducing the neutrons in both parts of the reactor, the lack of a common factor between both cell sizes (2.917/1.837 = 1.5879…) forces us to the consideration of both models.
The number of cells in each mesh is 44 x 44 and 72 x72 cells with 2.917 and 1.837 cm for the cell size, respectively. Regarding the number of axial planes, in both meshes, the height of the reactor is divided into a total of 53 cells, which correspond to the part of the core covered by the moderator, with a cell size of 1.7871.
In addition, the calculation with PARCS has been performed using the FDM solver.
The control rods are defined in the PARCS model with its cross-section generated by Serpent.

3.2 The model in VALKIN-FVM-Sn

The method implemented in VALKIN-FVM-Sn is structured in three steps. First, the discretization of the geometry with a mesh generator. Second, the discretization of the steady state of the Neutron Transport Equation with the Discrete Ordinate Method and the Finite Volume Method. Third, the solution of the eigenvalue problem.
The geometry discretization is performed with the Gmsh mesh generator [7]. This code was selected because it is free and easy to use. Several eigenvalues and eigenvectors can be calculated with SLEPc library. VALKIN-FVM-Sn is written in the FORTRAN language and can be run in parallel.
The final eigenvalue problem is composed of the system of equations composed of Transport Equation, for each direction, cell and energy group. The eigenvector is composed of the mean values of the angular flux of neutrons of energy group g and direction Ωm in each cell of the geometry (ψ_g,m,i). Regarding the mean face values, they are calculated from the mean cell values, using interpolation schemes. Two different methods have been used, one for internal faces and one for boundary faces.

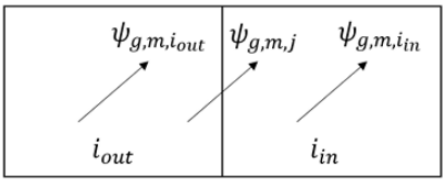

Fig 2. Definition of cells i_{in} and i_{out}.

For the internal faces, the linear-step method is used, which combines the linear and step methods, with the aim of obtaining the advantages of both methods. This combination is based on obtaining the values for each of the methods and averaging them with a δ factor:

$$\psi_{g,m,j} = \delta\psi_{g,m,j} + (1-\delta)\psi_{g,m,j} = \frac{(1-\delta)r_{i_{out},j}}{r_{i_{in},j}+r_{i_{out},j}}\psi_{g,m,i_{in}} + \frac{r_{i_{in},j}+\delta r_{i_{out},j}}{r_{i_{in},j}+r_{i_{out},j}}\psi_{g,m,i_{out}} \quad (1)$$

If δ=0, the method is equivalent to the linear method; if δ=1, the method is equivalent to the step method. The step method is equivalent to the Upwind scheme of the Finite Volumes Method, which estimates the value of the face as if it were the same as that of the cell. Its main

advantages are simplicity, stability, convergence and the guarantee that the value is always positive. The main drawback is its accuracy, since it is of the first order and overestimates the value of leaks. The linear method is equivalent to the Central Difference interpolation scheme of the Finite Volume Method. This scheme assumes that the flux has a linear distribution between the two cells adjacent to the face, to calculate the value of the flux in the face. The main advantage is its precision, since it is second order. The main drawbacks are convergence, instability and the possibility of obtaining negative values. On the other hand, the main drawback of the linear-step method is finding the optimal value of δ. Initially, values close to 0 must be used, so that the method has the precision of the linear method. But these values have to be slightly higher than 0, to avoid solutions with negative flows. Therefore, a sensitivity analysis must be performed to determine the value of this parameter for each case.
As in the PARCS model, the reactor is divided into 44x44 radial cells and 53 axial cells. The size of the radial cells is 2.917 cm and the axial cells 1.787 cm.
In this work, different meshes have been obtained with gmsh to analyse the influence of the mesh size in the results. These meshes are structured meshes with different divisions of the radial and axial cells as shown in Table 1.

Tab 1: Meshes used in VALKIN-FVM-Sn.

Mesh	Divisions in x	Divisions in y	Divisions in z
1	1	1	1
2	2	2	1
3	2	2	2
4	3	3	3

4. Analyses of the Results

The parameters used to compare the results are k-effective, the axial power profile and the radial power profile.
The k-effective is compared with the value obtained with Serpent. The values and the corresponding errors are shown in Table 2.

Tab 2: Comparison of k-effective.

Serpent	VALKIN-FVM-Sn				PARCS	
	Mesh 1	Mesh 2	Mesh 3	Mesh 4	Mesh 1	Mesh 2
1.00167	1.00168	1.00165	1.00169	1.00165	0.996938	0.994298
Error (pcm)	1.0	2.0	2.0	2.0	473.2	737.2

The comparison of the results is made between analogous meshes, that is, between VALKIN-FVM-Sn with Mesh 2 and PARCS with Mesh 1. The RMS of the errors between PARCS and VALKIN-FVM-Sn is 0.52%.

The radial power profiles are shown in the Figures 3 and 4. The RMS of the errors in the radial power profiles is 2.57%.

As it can be observed, there is a good agreement between all the results.

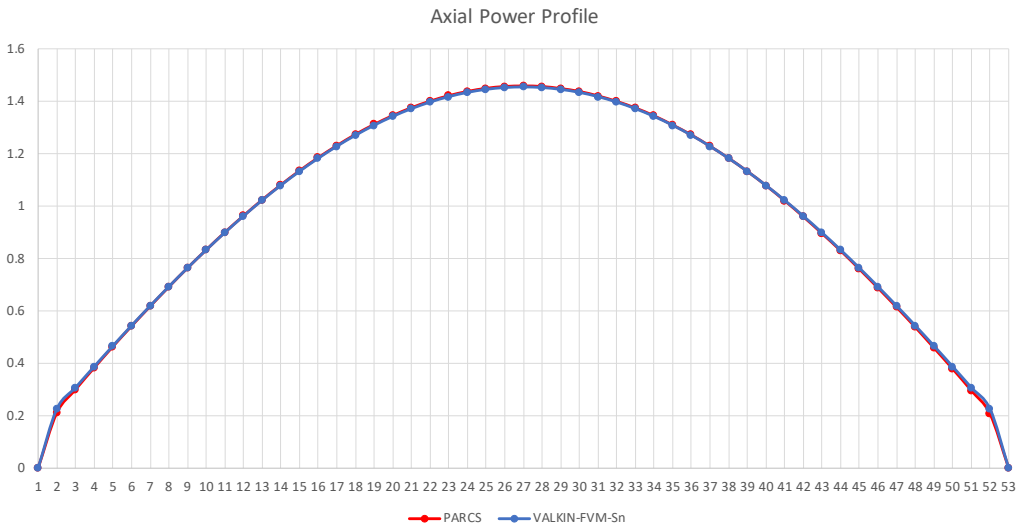

Fig 2. Comparison of the axial power profile

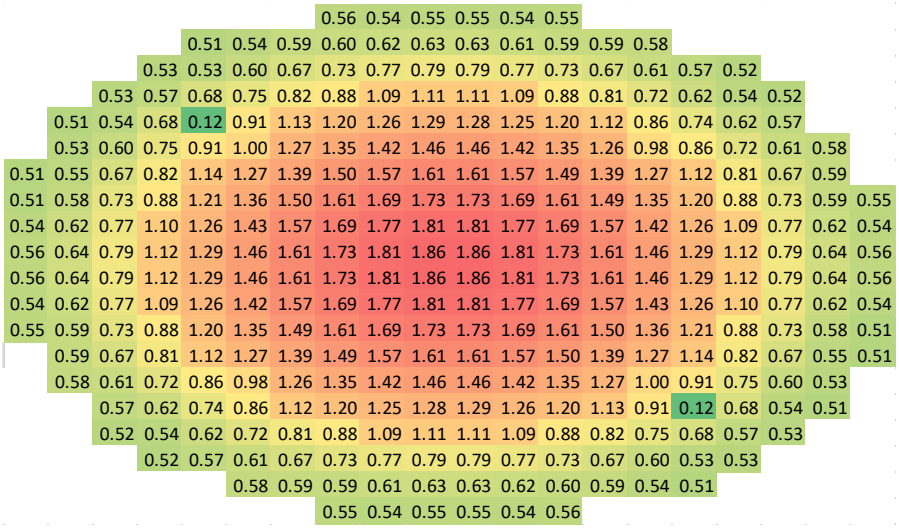

Fig 3. PARCS radial power profile

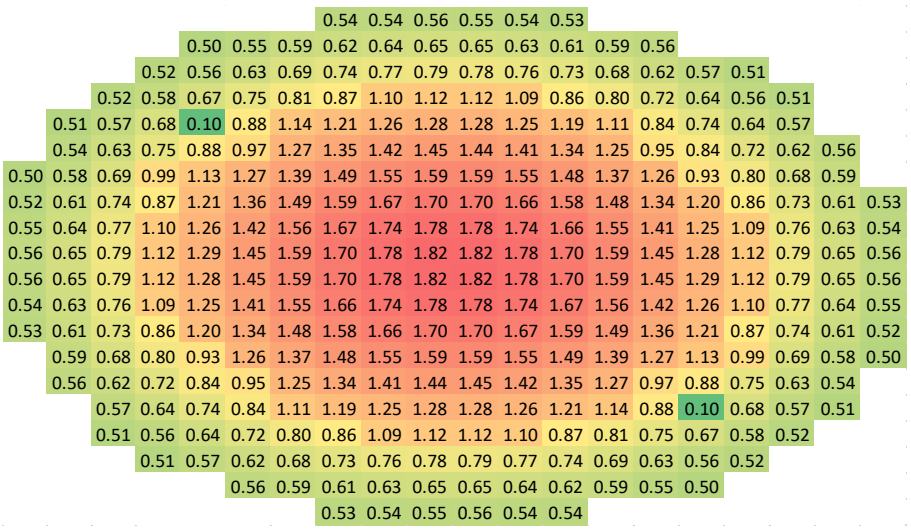

Fig 4. VALKIN-FVM-Sn radial power profile.

5. Conclusions and further work

In this paper, the simulation of the CROCUS Reactor has been performed with PARCS and VALKIN-FVM-Sn, using the cross-sections from Serpent.
The results from the steady-state case show a very high agreement between both codes. However, a more in-depth analysis is necessary to carry out to investigate which is the value of the parameter δ suitable for the different reactors based on the mesh size.
Future works will continue with the simulation of the transient introducing the perturbations induced with the COLIBRI device in both codes PARCS and VALKIN-FVM-Sn.
The main goal is to assess the capabilities of the VALKIN-FVM-Sn code to deal with this kind of simulations.

6. References

[1] Demazière, C., Vinai, P., Hursin, M., Kollias, S., & Herb, J. (2018). Overview of the CORTEX project. *Int. Conf. Physics of Reactors – Reactor Physics Paving the Way towards More Efficient Systems (PHYSOR2018) Cancun, Mexico, April 22-26, 2018.*

[2] Downar, T., Xu, Y., Seker, Y., & Hudson, N. (2012). *Theory Manual for the PARCS Kinetics Core Simulator Module*.

[3] Bernal García, Á. (2018). *Development of a 3D Modal Neutron Code with the Finite Volume Method for the Diffusion and Discrete Ordinates Transport Equations. Application to Nuclear Safety Analyses*. Universitat Politècnica de València. https://doi.org/10.4995/Thesis/10251/112422

[4] Leppänen, J., Pusa, M., Viitanen, T., Valtavirta, V., & Kaltiaisenaho, T. (2015). The Serpent Monte Carlo code: Status, development and applications in 2013. Annals of Nuclear Energy, 82, 142–150. https://doi.org/10.1016/j.anucene.2014.08.024

[5] Lamirand, V., Pakari, O., & Laureau, A. (2018). *Experimental report of the 1st campaign at AKR-2 and CROCUS*. Laussane, Switzerland.

[6] Rais, A. (2018). *Performance assessment of a 3-D steady-state and spatial kinetics model for the CROCUS reactor*. 169. Retrieved from https://infoscience.epfl.ch/record/255084?ln=en

[7] Geuzaine, Christophe and Jean-François Remacle (2009). *Gmsh: A 3-D finite element mesh generator with built-in pre-and post-processing facilities*. In: International journal for numerical methods in engineering 79.11, pp. 1309–1331 (cit. on pp. 25, 48).

FRM II: COLD SOURCE ISSUES, DIAGNOSIS, REMOVAL, OUTLOOK

A. PICHLMAIER, V. HUTANU, F. JESCHKE, R. SCHÄTZLEIN

Technical University Of Munich, ZWE FRM II
Lichtenbergstr. 1, 85748 Garching, Germany

ABSTRACT

The Cold Neutron Source is arguably the most important of the secondary sources of FRM II. When its damage was diagnosed and confirmed, it had to be pulled from the rector in order to allow for continuation of the reactor operation. This paper describes the most important steps of this process.

1 Introduction

The Technical University of Munich (TUM) operates the FRM II, a heavy-water moderated and light-water cooled pool-type research reactor with 20 MW thermal power. It uses one single fuel element which is usable for 60 full power days. The FRM II is mainly used as a beam tube reactor for neutron scattering experiments. However, it also has a dedicated neutron activation analysis beamline, a tomography facility, a beamline of slow positrons and one primarily for medical purposes. It is also used for radioisotope production and silicon doping. Criticality was reached for the first time in 2004, routine operation started in 2005.

2 The CNS at FRM II

The cold neutron source (CNS) at FRM II is a so called experimental facility or secondary source. Among the secondary sources it is the most intensively used one: every beam line in the neutron guide hall west and two more in the experimental hall uses cold neutrons from the cold source. In fact, the CNS needs to be operational and in cooled-down status for every increase of reactor power above 400 kW to protect the delicate setup from damage due to radiation induced heating. Alternatively, the FRM II parameter space allows for operation with completely removed CNS. Because of the well-known challenges of the removal operation and the obvious limitations of the scientific applications for operation without the CNS this possibility was reviewed as purely academic and never considered as a real option until summer 2021. When the decision was taken to remove the CNS and to run FRM II for the time it would take to procure a new one it was clear that only after detailed investigation of the situation this could be transformed into a success story.

Operationally, the CNS uses the thermal siphon principle. The double walled vessel of liquid deuterium is located in close vicinity to the reactor core (about 30 cm). The inner vessel is made from Al-6061, the outer one made from zircalloy. Both are separated by some millimeters of vacuum insulation. The volume of the liquid deuterium containing part is about 25 dm^3. Due to radiation heating the deuterium is constantly boiling and evaporates. It is condensed back into the liquid state at a helium-driven heat exchanger at a temperature of about 20 K. The liquid flows or drops back into the reservoir due to gravity. Because of the usage of a displacer, the total volume of liquid deuterium is only about 12 to 14 dm^3. Inside the thermal siphon is a beam tube initially intended for usage as source for ultra-cold neutrons (UCN). However, the UCN facility at FRM II has never been realized and at the current state this tube represents little more than an additional heat load. The He/D2-heat exchanger is shielded against the beam tube by a Cd-tube (made from soldered individual sheet metal pieces) and from the bottom by several blocks of borated aluminum. Due to space constraints the whole setup is tilted about 9 degrees. Details are shown in Figure 1.

To keep the deuterium liquid at nominal reactor power, about 7 kW of cooling power at 20 K are needed. Production of the cold is done in a room adjacent to the reactor hall by expansion of compressed Helium gas at room temperature. The compression in turn takes place in a different building hence avoiding any nuisance related to heat, noise and vibrations caused by the compressor.

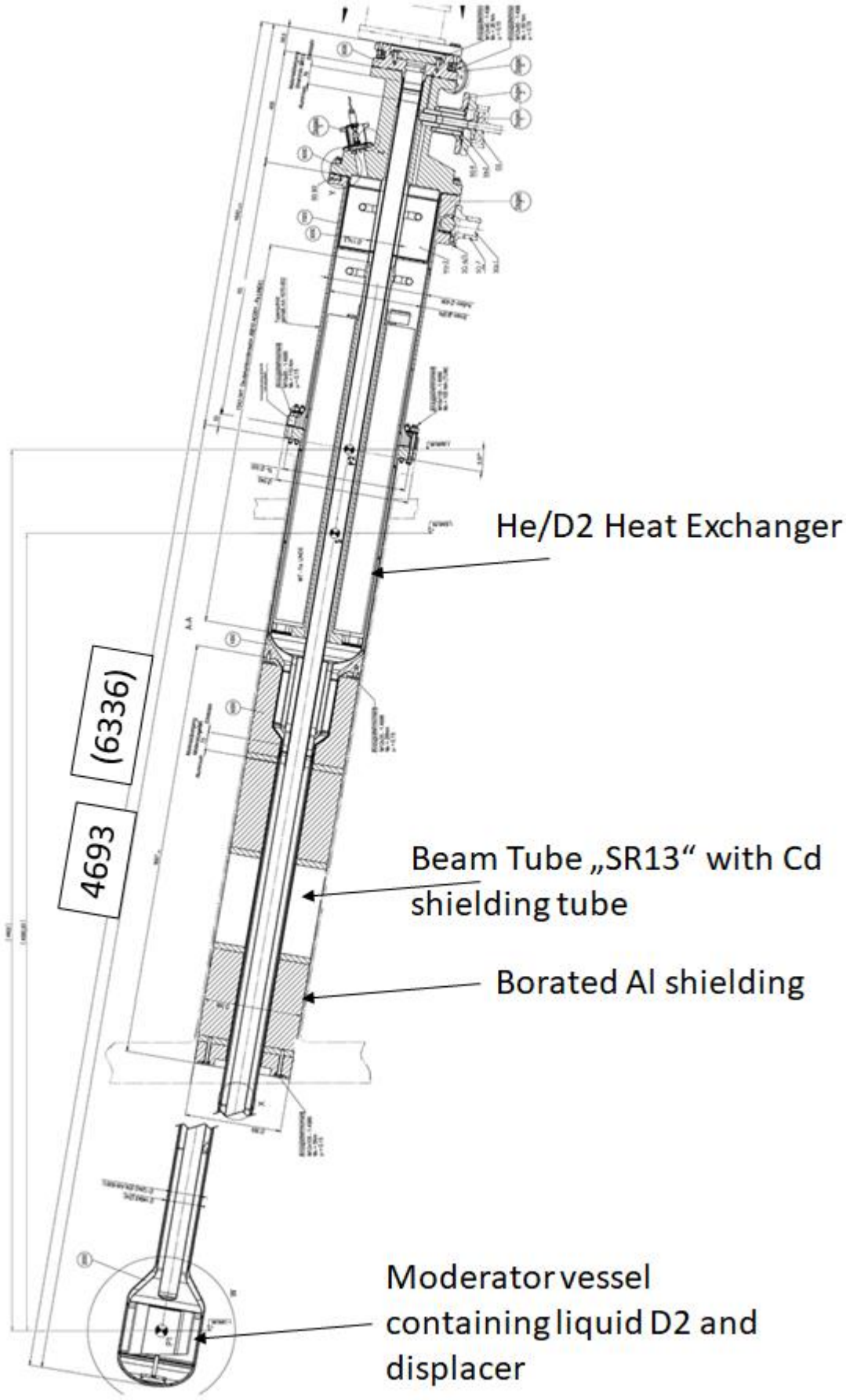

Figure 1: Overview Cold Neutron Source (CNS).

3 Events in the years 2021/2022

During the start-up of the reactor in 2021, an increase in the D2-gas pressure triggered an automatic SCRAM as foreseen in such cases. All systems related to the SCRAM worked as specified. Detailed investigation showed an additional heat load in the displacer that could be identified as Cadmium from the shielding tube. No repair of the Inpile part of the CNS is possible, therefore the decision was taken to remove the cold soure. Details are published, e. g. in [1].

The decision for removal of the CNS triggered a wide array of activities in practically all of the technical and scientific groups at FRM II. A detailed plan was put together what to do and in which order to actually remove the source from the moderator vessel. Scientists explored experimental possibilities with modified neutron spectrum. The most important milestones from the operator's point of view were:

- Get all the paperwork straightened out and organize the necessary inspections with the technical support organization (TSO).
- Empty and dry the heavy water filled reactor moderator vessel.
- Check the availability of the suite of required tools, do the required inspections of the tools and organize the necessary presence of the TSO.
- Design and build the components necessary for reactor operation without the cold source.
- Set up the plan and organize the resources in terms of manpower for the operation.
- Have the dose estimates checked by calculation.
- Explain the plan and options to the stake holders.
- Start to organize scientific usage of the FRM II without the CNS.
- Reinforce activities to reconstruct the new CNS.

While every step implies challenges of its own, from the technical point of view especially demanding is the sheer fact of moving the CNS within the given space restrictions in the FRM II moderator vessel. On the left of Figure 2 a schematic cut through the moderator vessel of FRM II reactor is shown. Red in the center is the fuel assembly (one single fuel element, diameter about 250 mm for scale (denoted by 1 in the figure). Around it the five shut-down rods are visible (2) and the tips of the thermal neutron beam tubes (3), all about 25 cm from the fuel assembly, where the highest density of thermal neutrons is located. Also at this distance from the fuel assembly, the hot source (4 in the picture) and the CNS (5), both cut-open shown, are placed. Cold neutron beam tubes (6) point to the center of CNS. On the right of Figure 2 a photograph of the cold source taken in the moderator tank in 2021 is shown. It is snug tight with the adjacent beam tubes and even after sixteen years of reactor operation bright and shiny. Even the reflections of the beam tubes are clearly visible on the surface of the zircalloy vessel.

A special contraption vaguely reminiscent of a rocket launcher (officially called "MDV") is required to precisely pull on the CNS and guide it without risking any damage to the adjacent beam tubes. In order to do so, this setup is precisely adjusted to guide the CNS, which in term is mounted by way of a specially designed slider to the MDV. The actual movement is done with the help of the main crane and – for the first and most delicate movement – using a manually operated pulley. With all the preparations finally completed, the operation itself did not take more than a day.

This maneuver in toto is so unique that it made it to the front page of the FRM II 2021 annual report (Figure 3).

The Figure **4** shows the reactor pool with the CNS removed and replaced by a dummy used to hold all the supply lines at their proper place. This is done to maintain these delicate lines in operational condition awaiting the time when they will supply again the required media to the new CNS. While the untrained observer barely notices the difference between the situations "CNS mounted" and "CNS removed and replaced by a dummy" the impact for the scientific versatility of FRM II however is not to be underestimated.

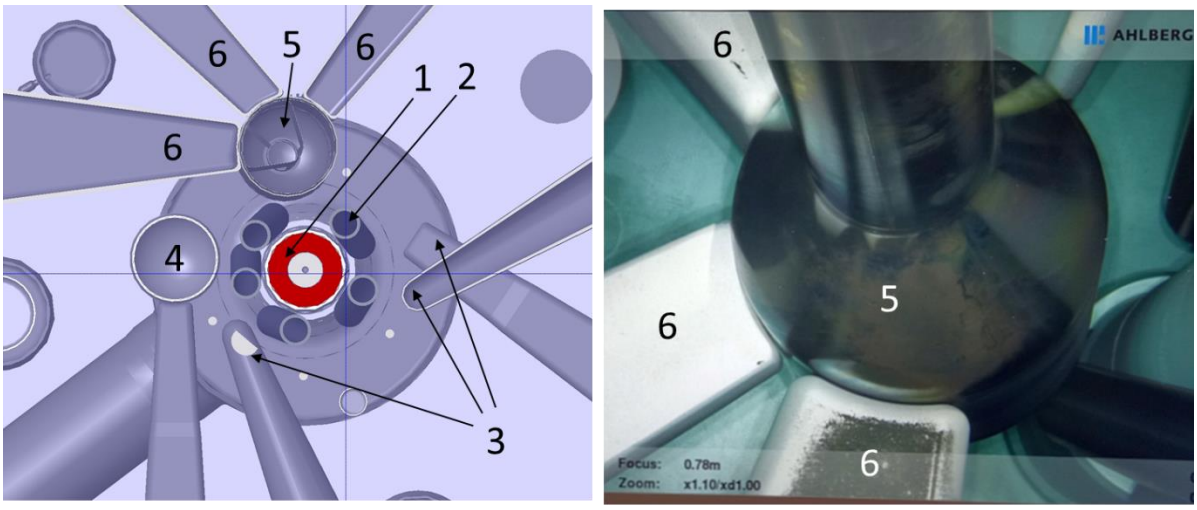

Figure 2: Left) A cut through the heavy water tank of the FRM II reactor: 1) in the center is fuel element, 2) shut-down rods, 3) thermal neutron beam tubes, 4) hot neutron source, 5) cold neutron source moderator vessel, 6) cold neutron beam tubes. Right) A photograph of the CNS moderator vessel taken after sixteen years of operation. Note the reflections of the beam tubes on the moderator vessel surface. Numbering same as left.

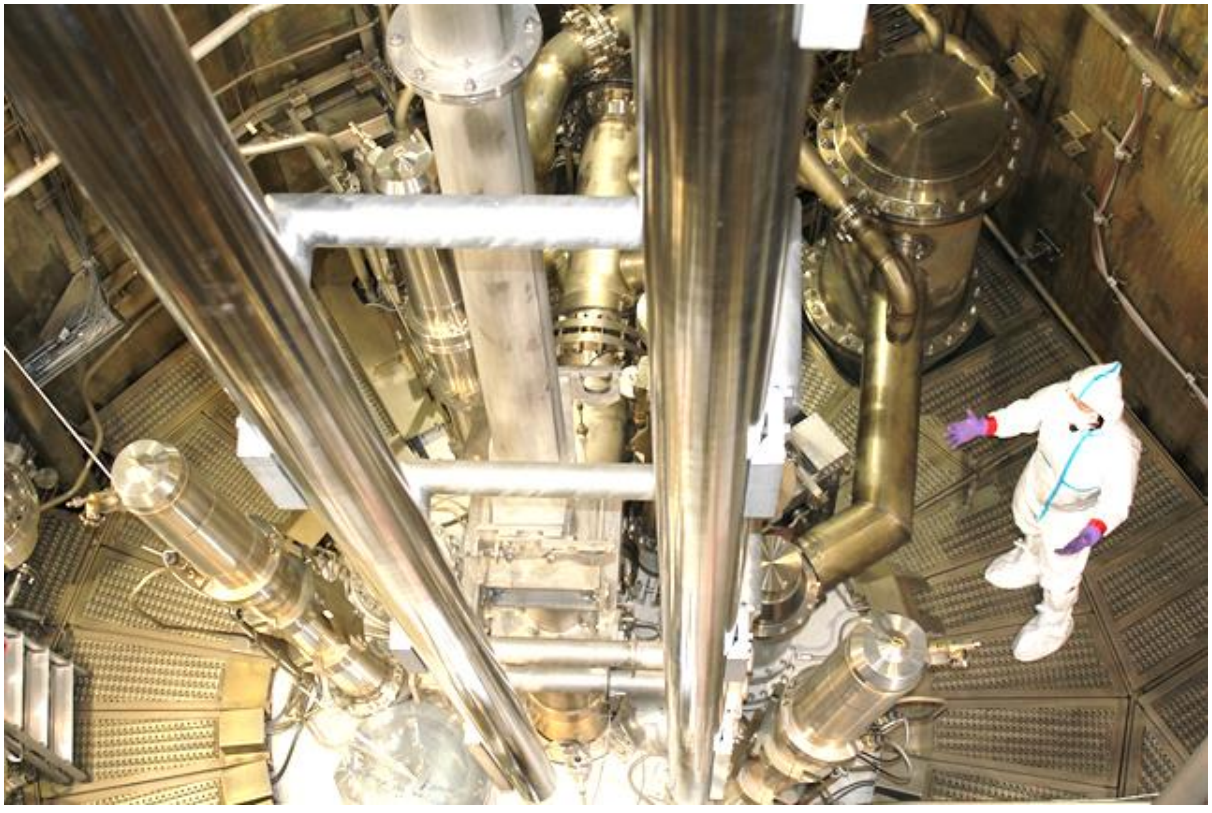

Figure 3: Excerpt from the FRM II 2021 annual report front page: The MDV mounted in the reactor pool.

Figure 4: The dummy mounted at the place of the CNS (encircled in red). Prominent to the right is one of the shut-down rods, another one barely visible on the bottom left. The thicker flexible lines in the back were and will be used to supply vacuum and liquid deuterium. The medium one on the left is a helium supply line (the other one hidden behind the shut-down rod). The bellows in front hoses electric lines for instrumentation.

4 Conclusion and Outlook

The CNS is arguably the most important component for the scientific usage of FRM II. Its failure during startup of the reactor in 2021 was a severe drawback for the user community. From the operator's point of view, removal of the CNS is an extremely delicate operation where a lot can possibly go wrong. This operation could be successfully completed. A new CNS is already under construction. Due to the vicinity to the reactor core it needs to meet highest quality standards and will take some time still to be completed. In the meantime, we will finalize all the necessary steps both technical and from an administrative point of view, to operate the FRM II without its CNS.

5 Acknowledgements

The authors would like to thank for fruitful discussions and valuable hands-on work the operational groups at FRM II. Especially E. Ernst, P. Jüttner, M. Kreß, V. Zill (engineering), M. Fuß (CNS), K. Höglauer (reactor operations), E. Krapf (health physics), J. Favoli (occupational safety), B. Pollom (change request management, documentation), A. Röhrmoser (neutronics and activation calculations), N. Wiegner (reactor pool operations). Former colleagues, in theory already enjoying retirement, did not hesitate to contribute with knowledge and experience, first and foremost D. Päthe and A. Schölderle. Last but not least, we would like to acknowledge the patience and continued support for the FRM II by all its stake holders, especially the scientific user community and the TUM Board of Management.

6 References

[1] CARBON-14, COLD SOURCE, CYCLE OF FUEL AND THE CORONA PANDEMIC − FRM II OPERATOR'S CHALLENGES IN THE YEARS 2020/21
A. Pichlmaier, A. Backs, F. Jeschke, P. Link, C. Reiter, Z. Revay, A. Röhrmoser, R. Schätzlein, B. Schillinger, M. Schulz, S. Sebold, C. Stieghorst, T. Neuwirth, A. Wirtz
RRFM 2021 Helsinki, https://www.euronuclear.org/scientific-resources/conference-proceedings/

Dynamics and influence of beryllium reflector poisoning on the reactivity of the WWR-K reactor core

D. SAIRANBAYEV, A. SHAIMERDENOV,
Sh. GIZATULIN, A. MARTYUSHOV
The Institute of Nuclear Physics
1 Ibragimov st., 050032 Almaty, Kazakhstan

ABSTRACT

The interaction of neutrons with beryllium leads to the formation of ^{3}H and strong neutron absorbers ^{3}He and ^{6}Li in the reflector (the so-called beryllium poisoning). After the reactor is shut down, the concentration of ^{3}He increases in time due to the decay of tritium. This article shows the effect of the accumulation of neutron absorber nuclides in a beryllium reflector on the reactivity of the WWR-K research reactor. The results were based on Monte Carlo MCNP calculations and solutions of differential equations that describe time-dependent absorber concentrations as a function of reactor operating time and shutdown periods. To determine the values of the nuclear concentrations of parasitic isotopes, the entire history of the reactor was taken into account. It was found that the accumulation of ^{3}He and ^{6}Li in beryllium reflectors during actual operation reduced the operating reactivity margin by about 7%.

Introduction

Beryllium is widely used as a neutron reflector in nuclear reactors due to its good reflective properties, the contribution of additional neutrons and a unique combination of structural, chemical characteristics, atomic number and neutron absorption cross-section characteristics. In addition, it has the advantage that it reduces the critical mass [1]. Beryllium has a different type of reactions with gamma radiation, such as the (g, n) reaction with the formation of photoneutrons. However, when used, it has a disadvantage, since the residual power after shutdown is slightly higher, and the power decay time is also slightly longer than in conventional water-water reactors without beryllium [2]. The collision of fast neutrons with beryllium atoms leads to the transfer of energy from neutrons to atoms and causes the displacement of atoms, which, in turn, destroys the crystal lattice and thereby changes the properties of beryllium [3].

The main reaction between fast neutrons and beryllium atoms is (n,2n), while the reaction (n,a) is also significant, its contribution is about 10%. Gases ^{4}He, ^{3}He and ^{3}H formed in this reaction will accumulate as the burnout increases. This can cause certain hazards, such as bloating, hardening, or breakage. At the same time, the accumulation of reaction products ^{6}Li and ^{3}He will increase neutron poisoning, thus reactivity will gradually decrease and outweigh the advantages associated with (n,2n) and (g,n) reactions [4]. In this regard, it is important to assess beryllium poisoning in the beryllium reflectors of the WWR-K reactor and, due to the lack of an experimental method, numerical methods are used to determine it.

Calculation of nuclear concentrations of He-3 and Li-6 in a beryllium reflector

In order to assess beryllium poisoning, the output of lithium-6, tritium and helium-3 was determined for each block by calculating the corresponding reaction rates for beryllium, taking into account the time spent by the block in the core. Numerical prediction of beryllium poisoning is necessary due to the lack of experimental methods for its determination.

The process of beryllium poisoning begins when beryllium is irradiated with neutrons. Reaction (n, α) with a threshold energy of about 0.7 MeV leads to many reactions (without taking into account all reactions that do not lead to the accumulation of ^{6}Li and ^{3}He) [5].

$$^{9}_{4}Be\ (n,\alpha)\ ^{6}_{2}He,$$

$$
\begin{aligned}
&{}^{6}_{2}He \xrightarrow{\beta-} {}^{6}_{3}Li, \quad T_{1/2}=0.8 \text{ sec}\\
&{}^{6}_{3}Li\ (n,\alpha)\ {}^{3}_{1}H\\
&{}^{3}_{1}He \xrightarrow{\beta-} {}^{3}_{2}He, \quad T_{1/2}=12.33 \text{ years}\\
&{}^{3}_{2}He\ (n,p)\ {}^{3}_{1}H.
\end{aligned}
\tag{1}
$$

The exact history of the WWR-K reactor at nominal power, shown in Figure 1, namely the time from the first power start of the reactor with LEU fuel until April 2021, was used in the analysis to predict reliable beryllium poisoning values. Figure 23 shows that the accumulation of ^{3}He and ^{6}Li in beryllium reflectors strongly depends on the history of their operation. You can also notice a sharp increase in the concentration of ^{3}He nuclei, which are associated with a long shutdown of the reactor.
The exact number of effective days of operation of the WWR-K reactor at nominal power, shown in Figure 1, namely the time from the first power start of the reactor with LEU fuel until April 2021, was used in the analysis to predict reliable beryllium poisoning values.

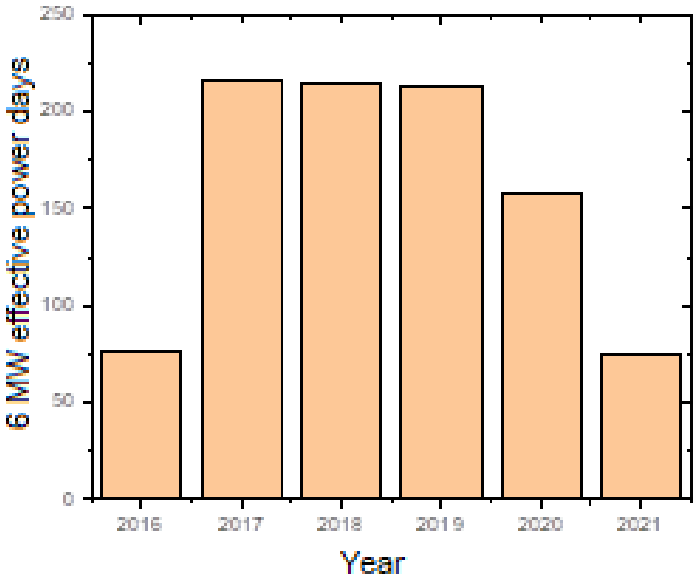

Fig 1. WWR-K reactor operation time from 2016 to the 2021

Figure 2 shows that the accumulation of He-3 and Li-6 in beryllium reflectors strongly depends on the history of their operation. You can also notice a sharp increase in the concentration of 3He nuclei, which are associated with a long shutdown of the reactor.
To study the effect of poisoned elements on reactivity, the reactivity difference between a clean and poisoned core was calculated using the MCNP [6,7] code based on the final concentration of poisoned elements. The effect of poisoning on the reactivity margin was calculated by formula (2):

$$\Delta\rho = \rho_{clean} - \rho_{poisoned}, \tag{2}$$

where it was calculated taking into account fresh beryllium. It can be concluded that the loss of reactivity caused by parasitic absorption in ^{6}Li and ^{3}He in the WWR-K reactor during the actual operating history was 0.4% Δk/k. This is about 7% of the average operating reactivity margin [8].

Figure 3 shows a characteristic section of the process of accumulation of tritium and ^{3}He isotopes. To describe the process of accumulation of these isotopes, three characteristic regions are distinguished in the figure, designated as I, II, and III.

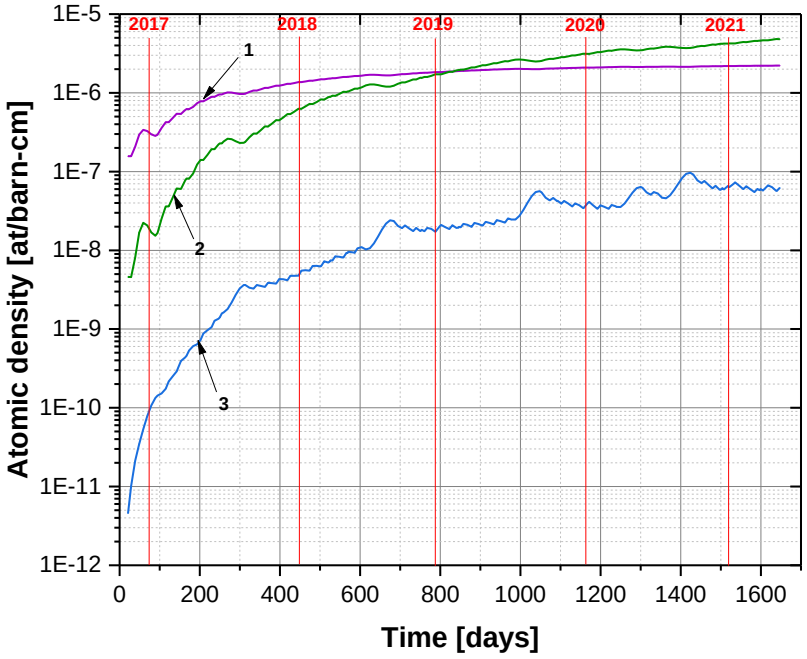

Fig 2. Formation of ^{6}Li (1), ^{3}H (2) and ^{3}He (3) isotopes in a beryllium block

Region I - the period of scheduled preventive maintenance of the reactor equipment, the reactor was in shutdown mode for two months. The figure clearly shows the increase in the nuclear concentration of helium-3, which is associated with the decay of tritium accumulated in beryllium, according to the nuclear reaction $^{3}H \rightarrow {}^{3}He$ ($T_{1/2}$ = 12.4 years, $\sigma_a = 5300 \times 10^{-28} m^2$); the concentration of helium-3 increased by 130% over this period. The nuclear concentration of tritium is decreasing, albeit slightly, this is due to the relatively long half-life of tritium. In absolute terms, the nuclear concentration of tritium decreased by 1%.

Region II is one of the regular irradiation cycles of the reactor at a power of 6 MW. The nuclear concentration of helium-3 is reduced by 22% as a result of the nuclear reaction ($^{3}He + {}^{1}n \rightarrow {}^{3}H + {}^{1}H$). Helium-3 turns into tritium and hydrogen. The nuclear concentration of tritium increases by 10%. Tritium is replenished by two nuclear reactions ($^{6}Li + {}^{1}n \rightarrow {}^{4}He + {}^{3}H$) and ($^{3}He + {}^{1}n \rightarrow {}^{3}H + {}^{1}H$).

Region III is the reactor settling/cooling time after the irradiation cycle. The process of accumulation of tritium and helium-3 is similar to that which occurs in region I, only the absolute values are lower due to the different time durations of these processes.

The beryllium reflector has been used in the WWR-K reactor core for more than 5 years. As is known, nuclear reactions occur on beryllium to produce neutron absorbing nuclei [8], so it is necessary to monitor their production. During the considered period of time, the following nuclear concentrations were accumulated in beryllium: lithium - 2.15 x 10^{18} poison/cm3 and helium - 9.14 x 10^{16} poison/cm3. The production of these poison nuclei led to a loss of reactivity margin by 0.4% Δk/k.

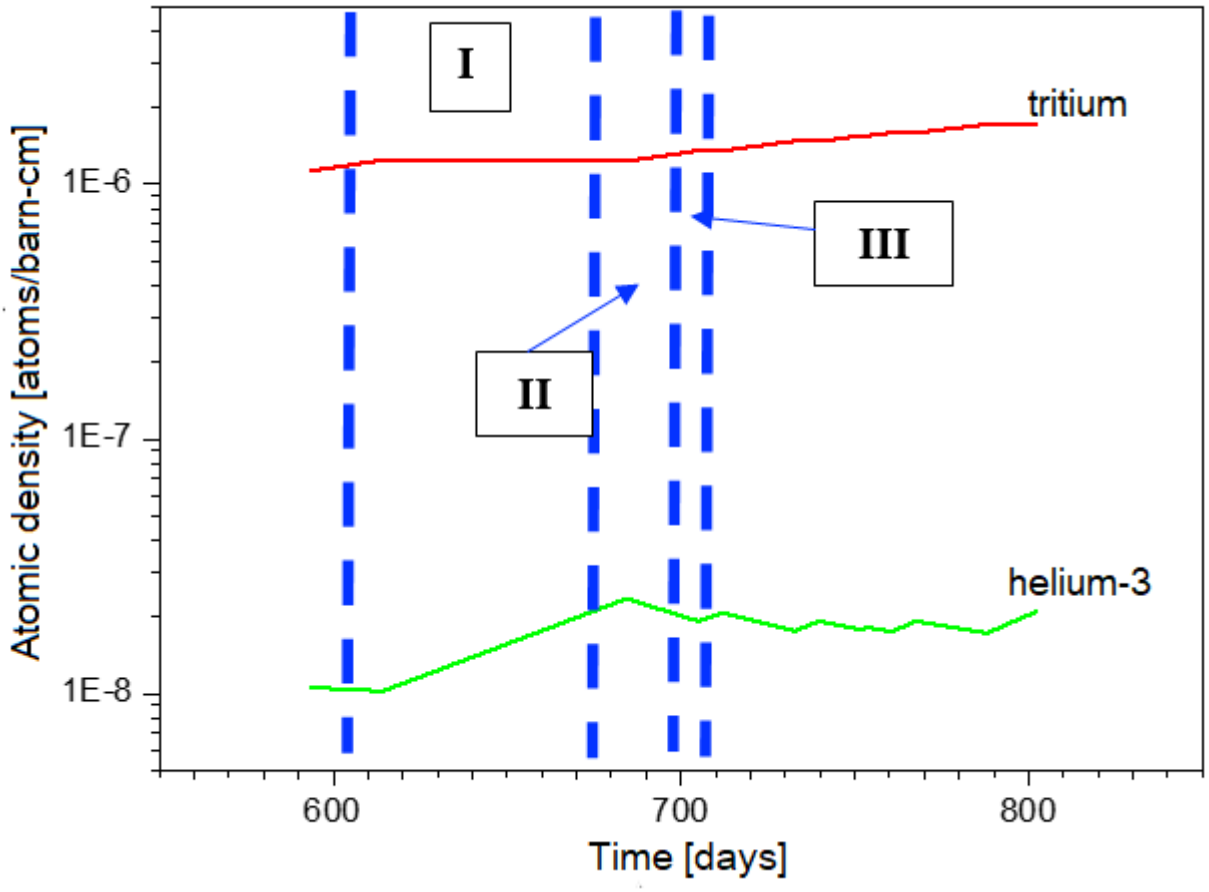

Fig 3. Dynamics of accumulation of ^{3}H and ^{3}He isotopes

Conclusion

At the WWR-K reactor with LEU fuel and an annular beryllium reflector for 952 effective days in beryllium, nuclear concentrations of lithium were accumulated - 2.15 x 10^{18} nuclei /cm^3 and helium - 9.14 x 10^{16} nuclei/cm^3. It was found that the accumulation of ^{3}He and ^{6}Li in the beryllium reflector strongly depended on the history of operation and the loss of reactivity over the period under consideration was approximately 7% of the operating reactivity margin.

References

[1]. Glasstone, S., Sesonske, A., 1967. Nuclear Reactor Engineering, D. Van Nostrand Company, Inc.

[2]. Knoll, G.F., 1989. Radiation Detection and Measurement, 2nd ed. John Wiley & Sons, New York.

[3]. Lamarsh, J.R., 1983. Introduction to Nuclear Engineering, New York, USA.

[4]. Renterghem, W., Van Leenaers, A., Van denBerghe, S., 2008. TEM investigation of long-term annealed highly irradiated beryllium. J. Nucl. Mater. 374, 54–60.

[5]. Andrzejewski, K.J., Kulikowska, T.A., Marcinkowska, Z.E. Computations of fuel management in MARIA reactor with highly poisoned beryllium matrix // Nukleonika. – 2008. – Vol. 53 (4). – P.173–179.

[6]. Briesmeister, J.F.(Ed.), 2000. MCNP- A general Monte Carlo N-Particle Transport code, Version4C.LA-13709-M. Los Alamos National Laboratory.

[7]. Pelowitz, D.B., (Ed.) MCNP6 User's Manual, Version 1.0. LA-CP-13-00634, Rev. 0 // Los Alamos National Laboratory. – 2013.

[8]. Sairanbayev, D.S., Koltochnik, S.N., Shaimerdenov, A.A. et al. Time History of Performance Parameters of WWR-K Reactor during Gradual Replacement of the Water Reflector by a Beryllium One // Russian Physics Journal. – 2020. – Vol. 63, No. 12. – P.2165-2177.

Simulation results of a new WWR-K reactor core aimed to improving the experimental characteristics

A. SHAIMERDENOV, D. SAIRANBAYEV, Sh. GIZATULIN,
N. ROMANOVA, A. MARTYUSHOV
The Institute of Nuclear Physics
1 Ibragimov st., 050032 Almaty, Kazakhstan

ABSTRACT

The increase in demand for irradiation activities in the WWR-K reactor dictates the need to increase the number of irradiation positions in the core. In this case, it is required not only to increase the number of irradiation positions, but also the number of positions with a higher neutron flux intensity. In this regard, in 2021, work began on the search for a new WWR-K reactor core, which will provide an increase in experimental characteristics. Several options of core were considered by simulation, after which a core consisting of 22 FAs of the 1st type and 4 FAs of the 2nd type was selected. In the selected core, the number of irradiation positions in the fuel area increases from 3 to 5. This paper presents the results of neutron analysis of the selected WWR-K reactor core in comparison with the existing core.

This research is funded by the Science Committee of the Ministry of Education and Science of the Republic of Kazakhstan (Grant No. BR10965174)

Introduction

Nuclear and radiation technologies are actively developing all over the world, in particular, on the basis of research reactors. To implement such technologies, additional irradiation positions are required. The effectiveness of some technologies directly depends on the intensity of the irradiation position. According to the IAEA database on research reactors [1], almost 70% of operating research reactors were built and put into operation more than 40 years ago. Consequently, these reactors do not fully meet current trends, which makes it necessary to upgrade the reactors to improve their experimental performance. The first stage is to carry out a neutron-physical justification for the modernization of the reactor with the improvement of its experimental characteristics. The modern development of computational methods and programs makes it possible to carry out sufficiently detailed and accurate calculations, which makes them one of the main scientific research methods. Particularly noteworthy are numerical simulation methods based on the Monte Carlo method, which make it possible to carry out precision calculations [2–4].

The WWR-K reactor was put into operation in 1967 with highly enriched fuel [5]. Since 2016, the operation of a reactor with low-enriched fuel has started [6]. After its conversion, the neutron flux in the center of the core doubled. Currently, there are three irradiation positions in the center of the reactor core. However, recently, the demand for irradiation work has increased significantly, including high-flux irradiation positions located in the fuel part of the core [7-15]. To cover the existing demand, it is necessary to increase the number of irradiation positions. An increase in the number of such positions

at the WWR-K reactor will require a modernization of the core. The layout of the core of the WWR-K reactor was selected by calculation to improve its experimental characteristics. In the MCNP6 transport code, a new core of the WWR-K reactor core was simulated and its main neutronic characteristics were determined.

Materials and methods

The object of study is a new core of the WWR-K reactor, consisting of 22 fuel assemblies of the 1st type and 4 fuel assemblies of the 2nd type (Fig. 1(a)). The new layout of the core has five irradiation positions in the fuel part and at least six in the neutron reflector area, on the periphery of the core. More detailed information on the composition of the new core layout, in comparison with the current core (Fig. 1(b)), is given in Table 1.

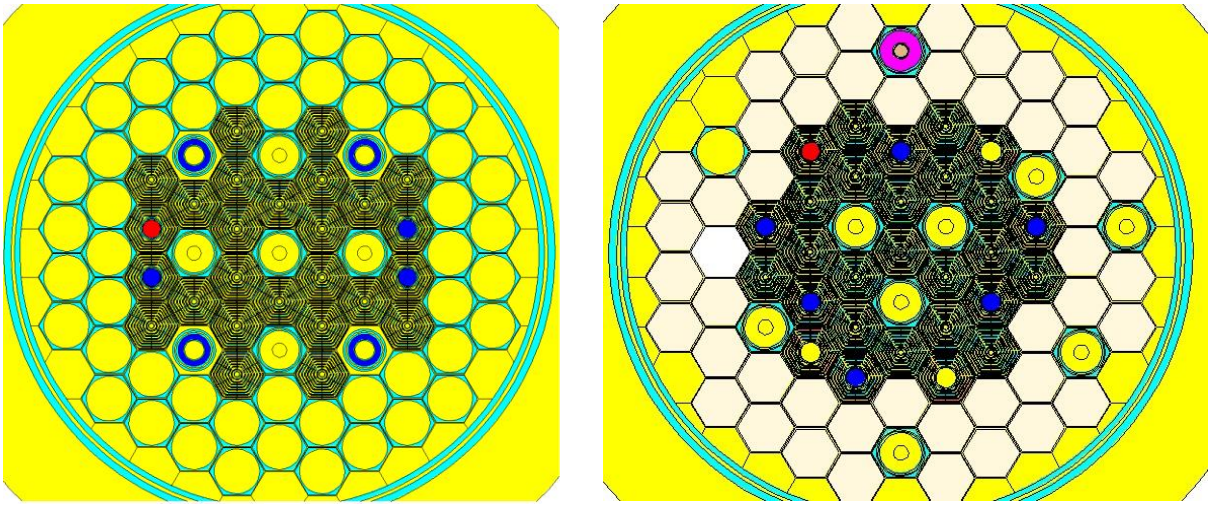

(a) (b)

Figure 1 – The layout of the core of the WWR-K reactor: (a) - new; (b) - existing;

Table 1. The composition of the core of the WWR-K reactor

Parameter	Existing core	New core
Number of FA of the 1st type	18	22
Number of FA of the 2nd type	10	4
FA type	VVR-KN	VVR-KN
Number of irradiation positions in the center of the core (fuel part)	3	5
Number of irradiation positions at the fuel-reflector boundary	2	-
Number of irradiation positions on the periphery of the core (neutron reflector area)	5	6
Type of annular neutron reflector	beryllium	Water (gradual replacement with a beryllium reflector)
Number of reactivity compensation rods	6	4

Number of emergency protection rods	3	3
Neutron absorber in rods	boron carbide	boron carbide

Simulation of the considered layouts of the core of the WWR-K reactor was carried out using the transport code MCNP6 and the library of nuclear data ENDF/B-VII.1 [16, 17]. The MCNP6 transport code is intended for solving problems in the field of nuclear reactor physics, radiation protection, dosimetry, radiography, radiation medicine and nuclear safety. Simulation of the process of neutron transfer in material media is carried out by the Monte Carlo method. The user has the ability to model geometric three-dimensional configurations by setting the mathematical equations of the surfaces limiting them of the first, second and fourth degree, and filling them with an arbitrary material, setting the concentration of the nuclei of the elements that make up the substance. The statistical error of calculations did not exceed 5%.

Results and Discussion

The selected core option has an annular water neutron reflector compared to the existing core, where the neutron reflector is beryllium. In addition, when modeling the new core, it was assumed that the fuel was fresh, i.e. not burned out. In the future, it is assumed that the water side neutron reflector will be gradually replaced by a beryllium one, according to the concept given in [6]. The simulation results are shown in Table 2.

Table 2. The calculation results

Parameter	Existing core	New core
Reactivity margin, % Δk/k	6,6	6,6
Subcriticality, % Δk/k	2,6	1,3
Total efficiency of reactivity compensation rods, % Δk/k	9,2	7,5
Total efficiency of emergency protection rods, % Δk/k	3,1	3,1
Maximum thermal neutron flux (E_n<0,625 eV), $cm^{-2}s^{-1}$	$1,5x10^{14}$	$1,9x10^{14}$
Maximum fast neutron flux (E_n>0,1 MeV), $cm^{-2}s^{-1}$	$8,8x10^{13}$	$9,0x10^{13}$
Minimum thermal neutron flux (E_n<0,625 eV), $cm^{-2}s^{-1}$	$1,4x10^{14}$	$1,3x10^{14}$
Minimum fast neutron flux (E_n>0,1 MeV), $cm^{-2}s^{-1}$	$8,7x10^{13}$	$5,7x10^{13}$
Hardness coefficient of the neutron energy spectrum, arb.unit	0,58	0,47
Maximum generated energy in FA, kW	412*	311

* *the value of generated energy for fresh fuel with a water annular neutron reflector is given*

The values of the neutron flux given in Table 2 correspond to the irradiation positions located in the fuel area.

Based on the data presented in Table 2, the following conclusions can be drawn:

The advantages of the new core are: increase in the number of high-flux irradiation positions in the fuel area from three to five; increasing the maximum flux of thermal

neutrons; reduction of energy release in the most stressed fuel assemblies, which is important for the period when the reactor starts operating with fresh fuel; reduction in the number of reactivity compensation rods, which means a decrease in the probability of their failure.

The disadvantages of the new core is the increase in the range of neutron flux in the irradiation positions located in the fuel area.

Conclusions

The results of computational simulation showed that the new WWR-K reactor core, consisting of 22 FAs of the 1st type and 4 FAs of the 2nd type, makes it possible to improve the experimental characteristics of the reactor. In the fuel part of the core, the number of high-flow irradiation positions is increasing. The maximum value of the thermal neutron flux in high-flux irradiation position is $1.9 \cdot 10^{14}$ $cm^{-2}s^{-1}$. The maximum energy stress of the core is reduced, and the thermophysical reliability of the reactor is increased. The cycle time is saved.

Funding

This research is funded by the Science Committee of the Ministry of Education and Science of the Republic of Kazakhstan (Grant No. BR10965174)

Reference

1 https://nucleus.iaea.org/rrdb/#/home (accessed May 22th, 2022)
2 Bart L. Sjenitzer, J. Eduard Hoogenboom A Monte Carlo Method for Calculation of the Dynamic Behaviour of Nuclear Reactors. Progress in Nuclear Science and Technology, Vol. 2, pp.716-721 (2011)
3 Meysam Ghaderi Mazaher Ali Akbar Salehi Naser Vosoughi A time dependent Monte Carlo approach for nuclear reactor analysis in a 3-D arbitrary geometry. Progress in Nuclear Energy. Volume 115, August 2019, Pages 80-90. https://doi.org/10.1016/j.pnucene.2019.03.024
4 Gomin, E.A., Davidenko, V.D., Zinchenko, A.S. et al. Simulation of Nuclear Reactor Kinetics by the Monte Carlo Method. Phys. Atom. Nuclei 80, 1399–1407 (2017). https://doi.org/10.1134/S1063778817080063
5 A. A. Shaimerdenov, D. A. Nakipov, F. M. Arinkin, Sh. Kh. Gizatulin, P. V. Chakrov, and Ye. A. Kenzhin The 50th Anniversary of the WWR-K Research Reactor // Physics of Atomic Nuclei, 2018, Vol. 81, No. 10, pp. 1408–1411. DOI: 10.1134/S1063778818100162
6 Arinkin F.M., Shaimerdenov A.A., Gizatulin Sh.Kh., Dyussambayev D.S., Koltochnik S.N., Chakrov P.V., Chekushina L.V. WWR-K research reactor core conversion. – Atomic Energy, 2017, Vol.123 – p.15-20. DOI: 10.1007/s10512-017-0294-0
7 Shaimerdenov A., Gizatulin S., Dyussambayev D., Askerbekov S., Kenzhina I. The WWR-K reactor experimental base for studies of the tritium release from materials under irradiation // Fusion Science and Technology. – 2020. - Vol.76(3). p.304-313 https://doi.org/10.1080/15361055.2020.1711852.
8 Y. Chikhray, V. Shestakov, O. Maksimkin, L. Turubarova, I. Osipov, T. Kulsartov, K. Tsuchiya. Study of Li2TiO3+ 5 mol% TiO2 lithium ceramics after long-term neutron irradiation. Journal of nuclear materials 386, 286-289 (2009).

9 L. Chekushina, D. Dyussambaev, A. Shaimerdenov, K. Tsuchiya, T. Takeuchi, H. Kawamura, T. Kulsartov. Properties of tritium/helium release from hot isostatic pressed beryllium of various trademarks. Journal of Nuclear Materials 452.1-3, 41-45 (2014).
10 D. Sairanbayev, S. Koltochnik, A. Shaimerdenov, Y. Chakrova, A. Gurin, Y. Kenzhin Analysis of lutetium-177 production at the WWR-K research reactor // Applied radiation and isotopes. – Vol.169. – 2021. – p. 109561. https://doi.org/10.1016/j.apradiso.2020.109561
11 T. Kulsartov, M.Gabdullin, Ye. Chikhray, Zh. Zaurbekova, G.Kizane, Ye. Kenzhin, A. Tolenova, E. Nesterov, A.Shaimerdenov Experiments on tritium generation and yield from lithium ceramics during neutron irradiation // International Journal of Hydrogen Energy. – 2021, Volume 46, Issue 13, Pages 9186-9192. https://doi.org/10.1016/j.ijhydene.2020.12.224
12 K.M. Nazarov, B. Mukhametuly, S.E. Kichanov, T.K. Zholdybayev, A.A. Shaimerdenov, K.B. Karakozov, D.S. Dyussambayev, M.T. Aitkulov, M. Yerdauletov, P. Napolskiy, M. Kenessarin, E.K. Kalymkhan, N.A. Imamverdiyev, S.H. Jabarov Non-destructive analysis of materials by neutron imaging at the TITAN facility // Eurasian Journal of Physics and Functional Materials, 2021, 5(1), 6-14 DOI: 10.32523/ejpfm.2021050101
13 P.F. Kashaykin, A.L. Tomashuk, S.A. Vasiliev, A.D. Ignatyev, A.A. Shaimerdenov, Yu.V. Ponkratov, T.V. Kulsartov, Y.A. Kenzhin, Sh. Kh. Gizatulin, T.K. Zholdybayev, Y.V. Chikhray, S.L. Semjonov, Radiation resistance of single-mode optical fibres with view to in-reactor applications, Nuclear Materials and Energy (2021), doi: https://doi.org/10.1016/j.nme.2021.100981
14 Merezhko M.S., Merezhko D.A., Rofman O.V., Maksimkin O.P., Short M.P., 2022. Macro-Scale strain localization in highly irradiated stainless steel investigated using digital image correlation. Acta Materialia. 231, 117858.
15 Yarovchuk A.V., Dikov A.S., Tsay K.V., 2022. Peculiarities of stress corrosion fracture of sensitized and neutron irradiated chromium-nickel austenitic steel. Journal of Physics: Conference Series. 2155, 012011.
16 J.T. Goorley, et al., 2013. Initial MCNP6 Release Overview - MCNP6 version 1.0, LA-UR-13-22934.
17 M.B. Chadwick, M. Herman, P. Obložinský, M.E. Dunn, Y. Danon, A.C. Kahler, D.L. Smith, B. Pritychenko, G. Arbanas, R. Arcilla, R. Brewer, D.A. Brown, R. Capote, A.D. Carlson, Y.S. Cho, H. Derrien, K. Guber, G.M. Hale, S. Hoblit, S. Holloway, T.D. Johnson, T. Kawano, B.C. Kiedrowski, H. Kim, S. Kunieda, N.M. Larson, L. Leal, J.P. Lestone, R.C. Little, E.A. McCutchan, R.E. MacFarlane, M. MacInnes, C.M. Mattoon, R.D. McKnight, S.F. Mughabghab, G.P.A. Nobre, G. Palmiotti, A. Palumbo, M.T. Pigni, V.G. Pronyaev, R.O. Sayer, A.A. Sonzogni, N.C. Summers, P. Talou, I.J. Thompson, A. Trkov, R.L. Vogt, S.C. van der Marck, A. Wallner, M.C. White, D. Wiarda, P.G. Young, "ENDF/B-VII.1: Nuclear Data for Science and Technology: Cross Sections, Covariances, Fission Product Yields and Decay Data", Nucl. Data Sheets **112**(2011)2887.

A CRITICAL FLOW MODEL IMPLEMENTATION FOR LEAK BEFORE BREAK ASSESSMENTS

F. BRIGANTE
C&S, Nuclear Research and Consultancy Group (NRG)
Westerduinweg 3, 1755 LE Petten – The Netherlands

ABSTRACT

The Leak Before Break (LBB) criterion in nuclear power plants and research reactors consists in the possibility to detect a small leakage from a cracked pipe before a double ended guillotine break would occur. The demonstration of the LBB failure mode requires the calculation of the coolant leaking over time from the cracked pipe. In this work the Henry modified model for the calculation of the two-phase critical flow is presented and the solutions are compared to experimental data. The thermal-hydraulic code is written in Python and is part of the LBB evaluation software LETO (leak before break probabilistic modular tool). The software is compared to other implementation of the Henry model and the discrepancies of results are discussed.

1. Introduction

The Leak Before Break is a failure more of pressurized pipes that occurs when the through-wall fracture that leads to rupture leaks a measurable volume of coolant before resulting in the double ended guillotine break (DEGB) event [1]. LETO is the latest software for LBB evaluation developed at NRG. Its two-phase critical flow model is presented in this article.

In 2017, the development of a LBB assessment software starts at NRG with the tool DeMoT (Deterministic Modular Tool) [2]. It is written in MATLAB [3], based on the R6 Detectable Leak Before Break procedure [4] and the leak rate module is single phase. In 2018, probabilistic analyses are performed by coupling DeMoT to the probabilistic software RAP++ [5]. The leakage rate calculation module is extended in 2019 with the Henry model to include two-phase leakage rate. The probabilistic results are once again obtained using RAP++. DeMoT has been extensively verified with the results from [6] and [7]. DeMoT is based on the LEAPOR (Leak Analysis of Piping - Oak Ridge) development [8] but the results on experimental test cases [9], [10] differ from LEAPOR with an average relative error of 40%.

The software LETO is developed in 2021 in the Python 3 [11] environment. The model at the basis of the code is the same of the previous NRG tool DeMoT. It relies on the FAD Option 1 assessment procedure in R6 and the Henry two-phase critical flow model [12].

LETO has been carefully validated and verified, comparing results with DeMoT and the previously used benchmarks. The Henry two-phase critical flow model implementation is improved

compared to the previous in-house implementation. Results from LETO for experimental cases in Collier (1984) [9] and Sozzi and Sutherlands (1975) [10] do not differ considerably from LEAPOR [13] as shown in chapter 4.

In chapter 2 the critical two-phase flow phenomenon is illustrated, in chapter 3 the chosen model to represent such phenomenon is reported, chapter 4 shows the validation results and in chapter 5 the conclusions are drawn.

2. Chocked flow

The critical flow rate is the maximum rate of flow of a compressible fluid through a pipe or an aperture for a given set of boundary conditions. Except under highly subcooled upstream circumstances, flow through a fracture linking a high pressure environment to a low pressure one is expected to be a chocked flow [14]. The critical flow problem for a single-phase fluid has been thoroughly investigated, and flow rate may be anticipated using single-phase compressible flow laws. If liquid flashes inside the flow route, flow will be chocked and a two-phase critical flow model is needed for modelling the flow.

The effect of two properties, namely slip and thermal non-equilibrium between the phases, distinguishes two-phase critical flow from single-phase critical flow models. The degree of slip and non-equilibrium is determined by the thermodynamic stagnation conditions and fluid flow channel geometry. These phenomena are often integrated into critical flow models via empirical relations created for specific geometries and fluid conditions [14]. As a result, there are several models, each of which is relevant to a certain geometry [15]. Their applicability to varied settings is determined by the governing equations used in the models creation and the degree of empiricism employed for the interfacial transfer factors.

The Henry modified model is considered for this study. It is used to model the leak rate from a through-wall crack in a pressurized pipe.

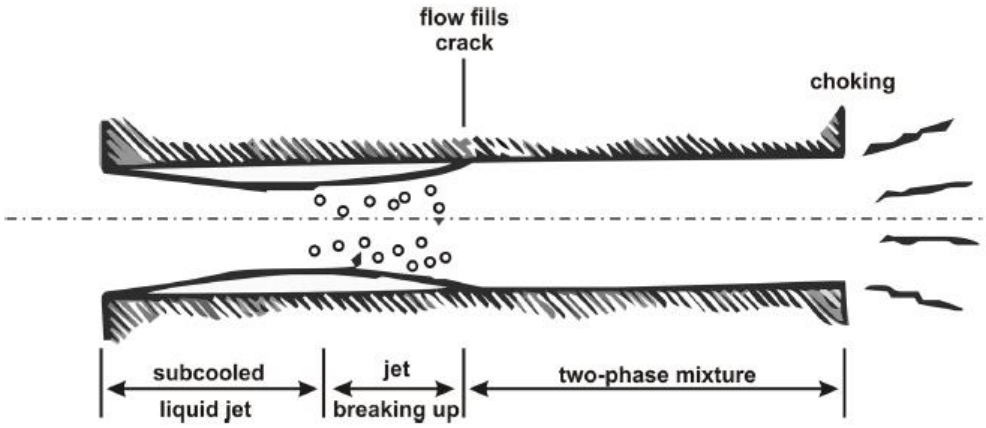

Fig. 1: Representation of the two-phase chocked flow [14].

Henry homogeneous non-equilibrium critical flow model [12] is applicable to subcooled and saturated liquid discharge. The flow is considered homogenous. The non-equilibrium effects are introduced via the parameter N, which is a function of equilibrium quality and the ratio between

the flow route length and the diameter [14]. The modified model takes into account friction and other pressure decreases inside the flow channel. This model is described in the next chapter.

3. Henry modified model [12], [14], [16]

The mass flux equation of the model is derived from the conservation of momentum and conservation of mass.

$$G_C^2 = \left[\frac{X_C v_{g(c)}}{\gamma_0 p_c} - \left(v_{g(c)-} v_{f(c)}\right) N \frac{dX_E}{dp_c}\right]_C^{-1}$$

G_C Mass flux at crack exit $\left[\frac{Kg}{m^2 s}\right]$
X_E Equilibrium vapor quality at crack exit [-]
X_c Non-Equilibrium vapor quality at the crack exit
$v_{g(c)}$ Specific volume of the saturated vapor at the crack exit $\left[\frac{m^3}{Kg}\right]$
$v_{f(c)}$ Specific volume of the liquid at the crack exit $\left[\frac{m^3}{Kg}\right]$
γ_0 Isentropic expansion coefficient for wet or superheated vapor [-]
p_c Pressure at Crack Exit $[Pa]$
N Empirical parameter [-]

The pressure drop constrain equation:

$$p_0 - p_c - p_e - p_a - p_f - p_k - p_{aa} = 0$$

p_0 Initial Pressure $[Pa]$
p_e Crack Inlet Pressure Drop $[Pa]$
p_a Phasic Acceleration Pressure Loss $[Pa]$
p_f Frictional Pressure Loss $[Pa]$
p_k Flow Path Tortuosity Pressure Loss $[Pa]$
p_{aa} Pressure Loss due to Acceleration from Changing Flow Area $[Pa]$

The model is implemented in the software LETO developed at NRG. The inputs for this module of the software are the internal fluid pressure and temperature, the geometry of the pipe and the crack geometry, internal, median and external Crack Opening Area (COA) and Crack Opening Displacement (COD), Critical Crack Length (CCL), crack shape, the global and local roughness values. The outputs are the leak rate from the crack and the pressure drops contributions. The parameters of crack morphology are taken from [17].

The crack morphology parameters are then defined.

$$D_h = \frac{4\,A_0}{pw}$$

D_h : Hydraulic diameter of the entrance flow area $[m]$
A_0: Entrance flow area $[m^2]$

pw: Wetted perimeter [m]

It is assumed a linear variation of the area along the flow path:

$$A_i = A\,(12D_h) \;=\; A_0 + \left(\frac{12D_h}{t}\right)(A_c - A_0)$$

t: Channel length [m].
A_i: Area of the section where two-phase flow starts (at $12D_h$) [m^2].
A_c: Area of the section where the flow is chocked (exit) [m^2].

The number of turns, the surface roughness and the loss term for path tortuosity are then determined based on the ratio between the crack opening displacement and the global surface roughness. The equations for the surface roughness are here reported:

$$\mu = \mu_L \qquad 0 \le \frac{\delta}{\mu_g} < 0.1$$

$$\mu = \mu_L + \frac{\mu_g - \mu_L}{9.9}\left(\frac{\delta}{\mu_g} - 0.1\right) \qquad 0.1 \le \frac{\delta}{\mu_g} \le\ 10$$

$$\mu = \mu_g \qquad \frac{\delta}{\mu_g} > 10$$

μ: Surface roughness of the crack [m].
μ_g: Global surface roughness [m].
μ_L: Local surface roughness [m].
δ: Crack opening displacement [m].

The Darcy friction factor:

$$\mathrm{f} \;=\; \left(\mathrm{C}_1 \log_{10}\frac{D_h}{\mu} + \mathrm{C}_2\right)^{-2}$$

C_1, C_2: Parameters.

The equilibrium vapor quality at the exit:

$$X_E = \frac{s_{l,0}(p_0, T_0) - s_{l,c}(p_c)}{s_{g,c}(p_c) - s_{l,c}(p_c)}$$

$s_{l,0}$ Entropy of the liquid at initial condition $\left[\frac{J}{Kg\ K}\right]$

$s_{l,c}$ Entropy of the liquid phase at crack exit $\left[\frac{J}{Kg\ K}\right]$

$s_{g,c}$ Entropy of the vapour phase at crack exit $\left[\frac{J}{Kg\ K}\right]$

The empirical parameter N is then:

$$N = 0 \quad if\ X_E = 0$$
$$N = 20X_E \quad if\ 0 < X_E \le 0.05$$
$$N = 1 \quad if\ X_E > 0.05$$

This parameter is needed for the non-equilibrium vapor quality. As previously mentioned it is how the non-equilibrium effects are introduced in the model.

$$X_c = NX_E\left(1 - \exp\left(-B\left(\frac{t}{D_H} - 12\right)\right)\right)$$

B: Empirical constant [-]

The isenthalpic vapor quality at crack exit plane:

$$X_h = \frac{h_{l,0} - h_{l,ave}}{h_{g,ave} - h_{l,ave}}$$

$h_{l,0}$ Enthalpy of the liquid at initial condition $\left[\frac{J}{Kg}\right]$

$h_{l,ave}$ Enthalpy of saturated liquid at exit plane $\left[\frac{J}{Kg}\right]$

$h_{g,ave}$ Enthalpy of saturated vapor at exit plane $\left[\frac{J}{Kg}\right]$

The entrance pressure losses:

$$p_e = \frac{v_0\, A_c^2\, G_C^2}{2\, C_D^2 A_0^2}$$

v_0 Specific volume of the liquid at initial condition $\left[\frac{m^3}{Kg}\right]$

C_D Discharge coefficient [-]

The phasic acceleration pressure loss:

$$p_a = \left(\frac{A_c^2}{A_i A_0}\right)\left[(1 - X_h)v_{l,c} + X_h v_{g,c} - v_0\right) G_C^2$$

$v_{l,c}$ Specific volume of the saturated liquid at exit plane $\left[\frac{m^3}{Kg}\right]$

$v_{g,c}$ Specific volume of the saturated gas at exit plane $\left[\frac{m^3}{Kg}\right]$

The frictional pressure loss (for one interval of $\frac{t}{D_h}$):

$$p_f = \left(12\mathrm{f}\, v_0 \frac{A_c^2}{A_i\, A_0} + \mathrm{f}\frac{A_c}{A_i}\left(\frac{t}{D_h} - 12\right)\left(v_{l,ave} + X_{h,ave}\left(v_{g,ave} - v_{l,ave}\right)\right)\right)\frac{G_C^2}{2}$$

$v_{l,ave}$ Specific volume of the saturated liquid at average pressure $\left[\frac{m^3}{Kg}\right]$

$v_{g,c}$ Specific volume of the saturated gas at average pressure $\left[\frac{m^3}{Kg}\right]$

$X_{h,ave}$ Isenthalpic vapour quality at average pressure [-]

The frictional pressure loss elsewhere is:

$$p_f = 12\mathrm{f}\, v_0 \frac{A_c^2}{A_i\, A_0} \frac{G_C^2}{2}$$

The flow path tortuosity pressure loss:

$$p_k = \frac{e_{vloss}}{2} \frac{A_c}{A_i} \left(v_{l,ave} + X_{h,ave}\left(v_{g,ave} - v_{l,ave}\right)\right) G_C^2$$

The pressure loss due to acceleration from changing flow area:

$$p_{aa} = \frac{G_C^2}{2} \left\{ v_0 \left[\left(\frac{A_c}{A_i}\right)^2 - \left(\frac{A_c}{A_0}\right)^2 \right] + \left[v_{l,ave} + X_{h,ave}\left(v_{g,ave} - v_{l,ave}\right)\right] \left[1 - \left(\frac{A_c}{A_i}\right)^2\right] \right\}$$

4. Validation

The code is validated with experimental data from [9] and [10] that has been already collected and compared to two other codes, LEAPOR and SQUIRT in [13]. The same Henry modified model is valid for the cited codes.

The first validation is performed with the data from Sozzi and Sutherland (1975) [10]. It is reported in Fig. 2 and Fig. 3, the average relative error is in Table 1. The temperature ranges from 277 °C to 284 °C and the pressure from 6.2 MPa to 6.9 MPa.

Table 1: Average error respect to Sozzi and Sutherland data.

Code	Relative average error (absolute values)
LETO	4.2 %
SQUIRT	4.9 %
LEAPOR	3.9 %

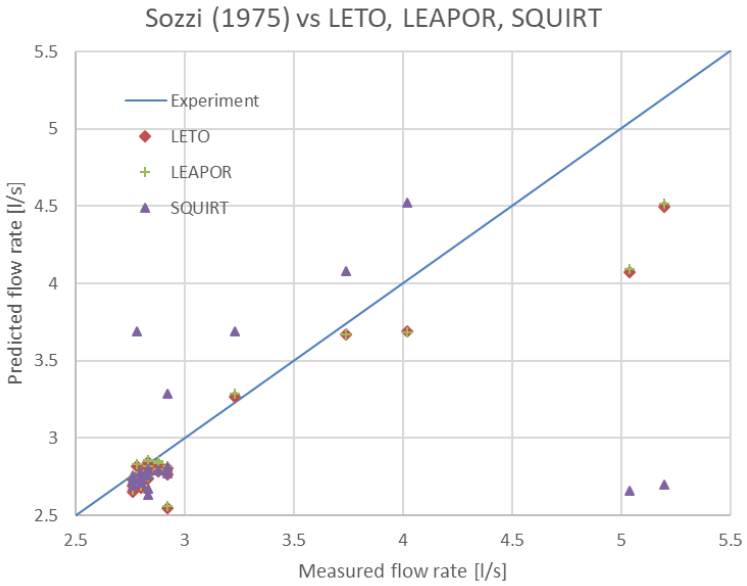

Fig. 2: Experimental data comparison 1.

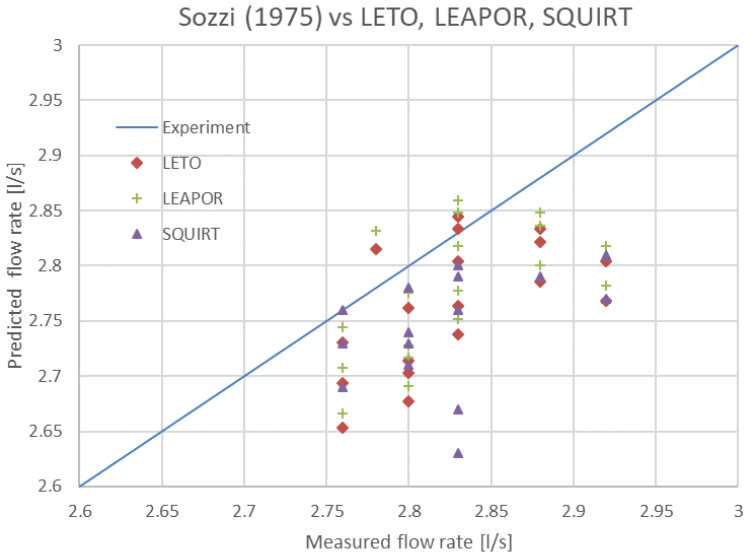

Fig. 3: Experimental data comparison 1, magnification.

The second validation is performed against cases in Collier (1984) [9]. The comparison is shown in Fig. 4 and magnified in Fig. 5. The average relative error is in Table 2. The temperature ranges from 178 °C to 298 °C and the pressure from 3.2 MPa to 11.5 MPa.

Table 2: Average error respect to Collier data.

Code	Relative average error (absolute values)
LETO	32.5 %
SQUIRT	27.7 %
LEAPOR	30.1 %

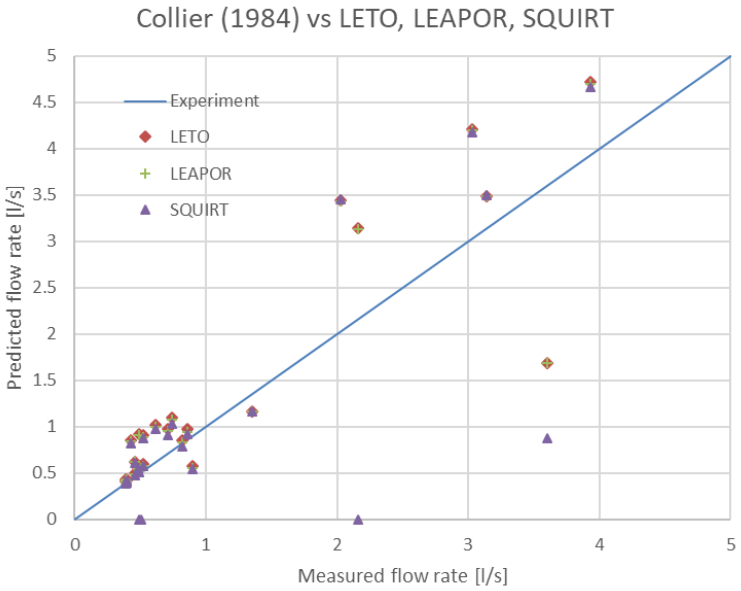

Fig. 4: Experimental data comparison 2.

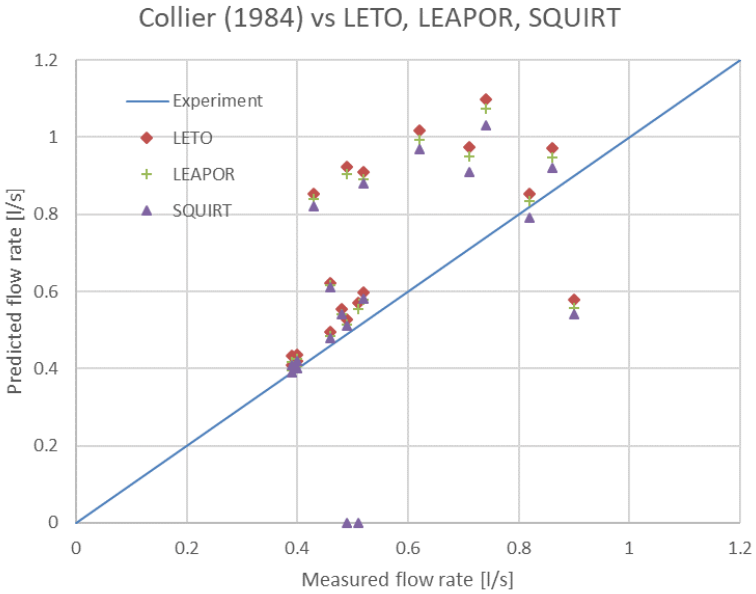

Fig. 5: Experimental data comparison 2, magnification.

It is possible to notice consistency for all the codes; the relative errors differences are negligible. This statement is valid for the region of pressure and temperature of the cases in the cited experiments. As previously demonstrated in [15] not all the two-phase critical flow models have the same results and accuracy for different domains of the problem parameters (pressure, temperature, geometry, etc.); this effect is evident from the accuracy differences of the model (implemented in the three codes) respect to the two cases reported in this study. The relative error respect to Collier cases is still in the range of accuracy of all thermal-hydraulics two-phase critical flow models, ~30% [18].

5. Conclusion

The thermal-hydraulic two-phase critical flow model has been implemented and proven a reliable representation of the experimental cases. This is true for the pressure and temperature intervals of the experiments cited in this study.

The thermal-hydraulic module of the LETO software has been tested and validated. This is one of the most fundamental milestones of the development of the Leak Before Break code LETO.

References

[1] R. Bourga, P. Moore, Y. J. Janin, B. Wang and J. Sharples, *Leak-before-break: Global perspectives and procedures,* vol. 129, Elsevier Ltd, 2015, pp. 43-49.

[2] F. Brigante, "Probabilistic Leak Before Break," NRG, n24644, 2020.

[3] "MATLAB 2007b - The MathWorks, Inc.," Natick, Massachusetts, United States.

[4] D. J. Tipping, "The R6 Theory and Methodology of R-Code: version 5.2," EDF Energy Nuclear Generation Limited, 2016.

[5] F.P. Grooteman, "Reliability Analysis Program RAP++ User Manual v3.3," 2016.

[6] G. Peter, "ATLAS+ Leakage Rate Round Robin".

[7] EDF Energy Nuclear Generation Ltd, "R6 Code - Revision 4," 2015.

[8] R Hardies et al., "xLPR Version 2.0 Technical Basis Document - Acceptance Criteria," 2016.

[9] R. Collier, F. Stulen, M. Mayfield, D. Pape and P. Scott, "Two-Phase Flow Through Intergranular Stress Corrosion Cracks and resulting Acoustic Emissions - EPRI Report No. NP-3540-LD," 1984.

[10] G. Sozzi and W. Sutherland, "Critical Flow of Saturated and Subcooled Water at High Pressure," General Electric Co. NEDO-13418, San Jose, CA, 1975.

[11] G. Van Rossum and F. L. Drake, "Python 3 Reference Manual," *CreateSpace,* 2009.

[12] R. E. Henry and H. K. Fauske, "Two phase critical discharge of initially saturated or subcooled liquid," *Nucl Sic Engng,* 1970.

[13] P. Williams and Y. S., "Prediction of the leakage rate for cracked pipes in nuclear power plants," in *SMiRT-22*, San Francisco, CA, 2013.

[14] D. Abdollahian and B. Chexal, "Calculation of Leak Rates Through Cracks in Pipes and Tubes - EPRI NP-3395," EPRI, Palo Alto, CA, 1983.

[15] F. D'Auria and P. Vigni, "Two-phase critical flow models - CSNI report No. 49," CSNI, Pisa, 1980.

[16] E. Kurth and P. Williams, "xLPR Version 2.0 Technical Basis Document - Leak rate Module Developement (LEAPOR)," U.S. Nuclear Regulatory Commission - Electric power research institute, 2016.

[17] G. Wilkowski, S. Rahman, N. Ghadiali and D. Paul, "Determination of crack morphology parameters from service failures for leak-rate analyses (NUREG/CP--0155))," 1997.

[18] F. D'Auria, Thermal-Hydraulics in water cooled nuclear reactors, Pisa: Elsevier science and technology, 2017.

HIGH FLUX REACTOR – AGEING MANAGEMENT PROGRAM

L. HASA, L. STEFANINI, O. WOUTERS

NRG - Nuclear Research and Consultancy Group
Westerduinweg 3, 1755LE, Petten, Netherlands

ABSTRACT

The High Flux Reactor (HFR) is a research reactor situated in Petten, the Netherlands. The HFR is operating since 1961. The HFR is a one of the key supplier of medical radioisotopes produced worldwide. An Ageing Management Program (AMP) is implemented to ensure the HFR safe operation and its reliability for continued production of the medical isotopes. The Plant Level Ageing Management Program is an outcome of the Continued Safe Operation (CSO) Project. . The Ageing Management Program comes along with good practices, a list of actions for improvement, AMPs for more than five thousands components, improvement of existing Plant Programs (PPs) and implementation of new PPs. The Ageing Management Program is based on the IAEA guidelines (e.g. SRS-3, SSG-48, SSG-10). Many IAEA guidelines used for the realization of the Ageing Management Program focus on the nuclear power plants. These guidelines are graded for a research reactor. The strategy for the Equipment Qualification Program (EQP) is an example of the adaption of these guidelines to the HFR case. In this paper more attention is given to the HFR approach for EQP, the methodology that is followed and the identification of the relevant scope for the EQP.

1. Introduction

The HFR is a multipurpose nuclear reactor and it is a key supplier of medical radioisotopes; HFR supplies 70% of the European demand, and 35% of the worldwide demand. Therefore, safety of operations and production continuity need to be guaranteed in order to guarantee the patient treatment.

The HFR has been in service since the 1961, reaching an operation time of 61 years. The age of the reactor makes ageing related failures more and more important. In order to preserve a safe and reliable production, the HFR developed a centralized Ageing Management Program (AMP-HFR) focussed on the safety relevant Systems, Structures and Components (SSCs).

The AMP-HFR development initiated with the Continued Safe Operation (CSO) project in 2018. The project included three main phases: assessment of current situation and creation of a development strategy (2018-2019), development of the specific AMPs following and policy document (2019-2020), implementation of the Ageing Management Program (2021-ongoing). The Ageing Management Program is an ongoing program needing continue updates from different disciplines. The AMP-HFR is managed and coordinated by the Ageing Management Coordinator of the HFR.

One of the main results of the CSO project is the development of new Plant Programs, such as the Technological Obsolescence Management and the Equipment Qualification Program (EQP). This paper focusses on the EQP In order to develop the EQP, the approach described in IAEA SRS-3 was adapted to the needs of a 45 MW Research Reactor with a graded approach in terms of relevant scope, methodology and qualification assessments.

2. Continued Safe Operation – CSO Strategy

The CSO project initiated in 2018 in order to create a strategy for the development and implementation of a centralized Ageing Management Program in the HFR. The strategy used for the development and implementation of the AMP-HFR is schematized in Figure 1. The three key points in the strategy were the Scope identification, the conception of the policy

document Plant Level Ageing Management [2] (PLAMP) and for the development of specific AMPs (including Ageing Management Review).

A brief description for each of the strategies applied in the CSO project is given below.

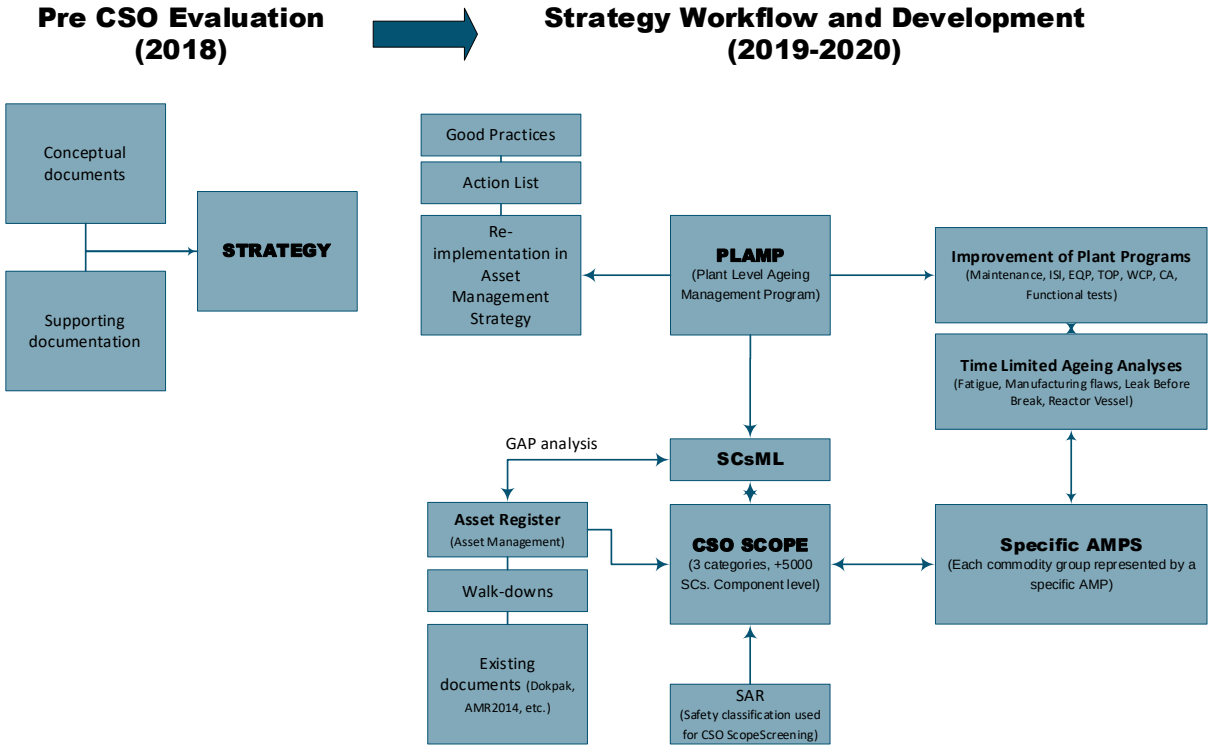

Figure 1. CSO strategy evaluation and development from 2018 to 2020.

2.1. CSO Scope

The determination of the scope is necessary to limit the amount of Structures and Components (SCs) that need to be part of the ageing management. The scoping procedure is busing the utilization of all the available sources and the cyclic gap analysis. The main source is the Asset Register (AR, developed in the framework of the Asset Management strategy [3]). Next to the Asset Register, the units involved in the CSO project and the reactor experts performed different walk-downs at the HFR to identify possible incongruences or missing SCs. Moreover, a cross check with the existing documentation is performed. The dataset retrieved from the AR combined with the other sources is used to create the Structure and Components Master List (SCsML). The SCsML undergoes periodically gap analysis to consider possible changes that might occur to the AR. The screening is based on the safety classification developed in the framework of the Safety Analysis Report (SAR) for the license renewal.

The complete list of the SCs included in the scope of the ageing management program is available in the SCsML, where all the relevant information over the type of each SCs, location, material, safety classification, possible ageing effects and ageing management strategy is given.

2.2. Policy and Ageing Management strategies

The policy of Ageing Management at HFR is described in the license basis document ‘Plant Level Ageing Management Program’ [2] (PLAMP). This is based on the IAEA Requirements and Safety Guidelines SSR-3 [4] , SSG-10 [7] and SSG-48 [8] . The contents of the PLAMP give detailed instruction and extensive information on how to run the ageing management for the HFR.

During the development of the CSO strategy and the creation of the policy, the existing Plant Programs (PPs) and Time Limited Ageing Analysis (TLAAs) were reviewed and analysed.

The TLAAs are used for the quantitative demonstration of the ageing management of the most relevant components that should remain fit for purpose up to the End of Life (EOL). The TLAAs were retrieved when possible and revalidation method were proposed.

The analysis of the PPs highlighted improvements area. For instance, the Technological Obsolescence Management Program, was absent at the HFR. Therefore, a proactive Technological Obsolescence Management Program was developed in order to help minimize the downtime arising by obsolescence issues. The EQP was also absent at the HFR. The most notable issue with the EQP is the fact that the guidelines are referring to Nuclear Power Plants (NPPs). As a consequence the international guidelines are referring to qualified conditions that are not achievable in the RRs (e.g. cooling temperature in accidental conditions). A graded approach that still fulfil the nine attributes presented in the IAEA guidelines was implemented. As a result an EQP was created for the qualification of a limited scope of components. The chapter 4 shows a detailed description of the methodology.

3. Ageing Management Program – HFR

The Ageing Management Program at HFR was developed in a framework (Figure 2) involving:

- IAEA requirements: The AMP-HFR fulfils the Safety Requirements 86 (Ageing Management) and 37 (Design for Ageing Management) of the IAEA Specific Safety Requirements for the Research Reactor (SSR-3).
- ANVS requirements in the operating license: the Dutch National Regulatory Body (ANVS) requires an Ageing Management Program for the issue of the operating license. The ANVS requirements refers to the IAEA Safety Requirements and agrees that the HFR uses the IAEA Specific Safety Guidelines SSG-10 as a guideline.
- Return of external experience: the results from external experiences were analysed to identify common challenges and shortcomings in order improve the AMP-HFR. HFR and other RRs organization meets periodically to exchange information on relevant Ageing Management matters.
- HFR internal experience: the internal experience of the HFR was taken into account by analysing the relevant documentation (e.g. Ageing Management Review 2014) and by reviewing the ageing management strategies applied before the implementation of the actual AMP-HFR.

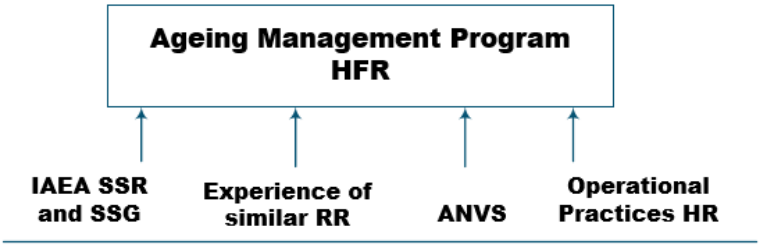

Figure 2 The four pillars approach for the Ageing Management Program.

3.1. (K)PDCA approach

The Ageing Management Program as described in detail in the PLAMP policy, is an ongoing program which and is kept up-to-date in order to ensure the process effectivity. The AMP-HFR follows the (Know)Plan-Do-Check-Act loop for continuous improvement.The whole loop of the Ageing Management Program involves continues activities and interaction between different disciplines and units present in NRG.

The *KNOW* part is referring to the necessity to proper understanding ageing and the framework in which the AMP-HFR is operating. The creation of a SCsML represent the final product of the knowledge gathered about the Scope of the AMP. It includes information about each SC, for instance, location, type, material, possible ageing mechanisms, ageing management strategies (if any).

The *PLAN* part is where the information *(KNOW)* are used to determine the best course of action in the determination of an effective and efficient set of activities for asset and ageing management. The activities are carried out in the framework of the Plant Programs (e.g. maintenance, in-service inspection, functional tests). The specific AMPs documents organize the ageing management related activities and thanks to periodic reviews guarantee the return of operating experience and the possibility of continues improvement as the need arise.

The *DO* part is the practical performing of the planned activities (Detection, Prevention, Mitigation, Corrective Actions and Monitoring).

The *CHECK* is the part that ensure the continuity of improvement and the completeness of the AMP-HFR. To guarantee the continuity, the results from the activities during the *DO* phase are analysed and assessed. The whole ageing management strategy is also re-evaluated periodically in the framework of the Corrective Actions Program. This process represent a strong key-point in the approach.

The *ACT* part is the implementation of the improvement actions defined during the *CHECK* phase. The actions and the analysed results from the *CHECK* phase are added as new information in the *KNOW* part. The (K)PDCA loops is thus closed.

This process guarantees the effectiveness of the Ageing Management Program.

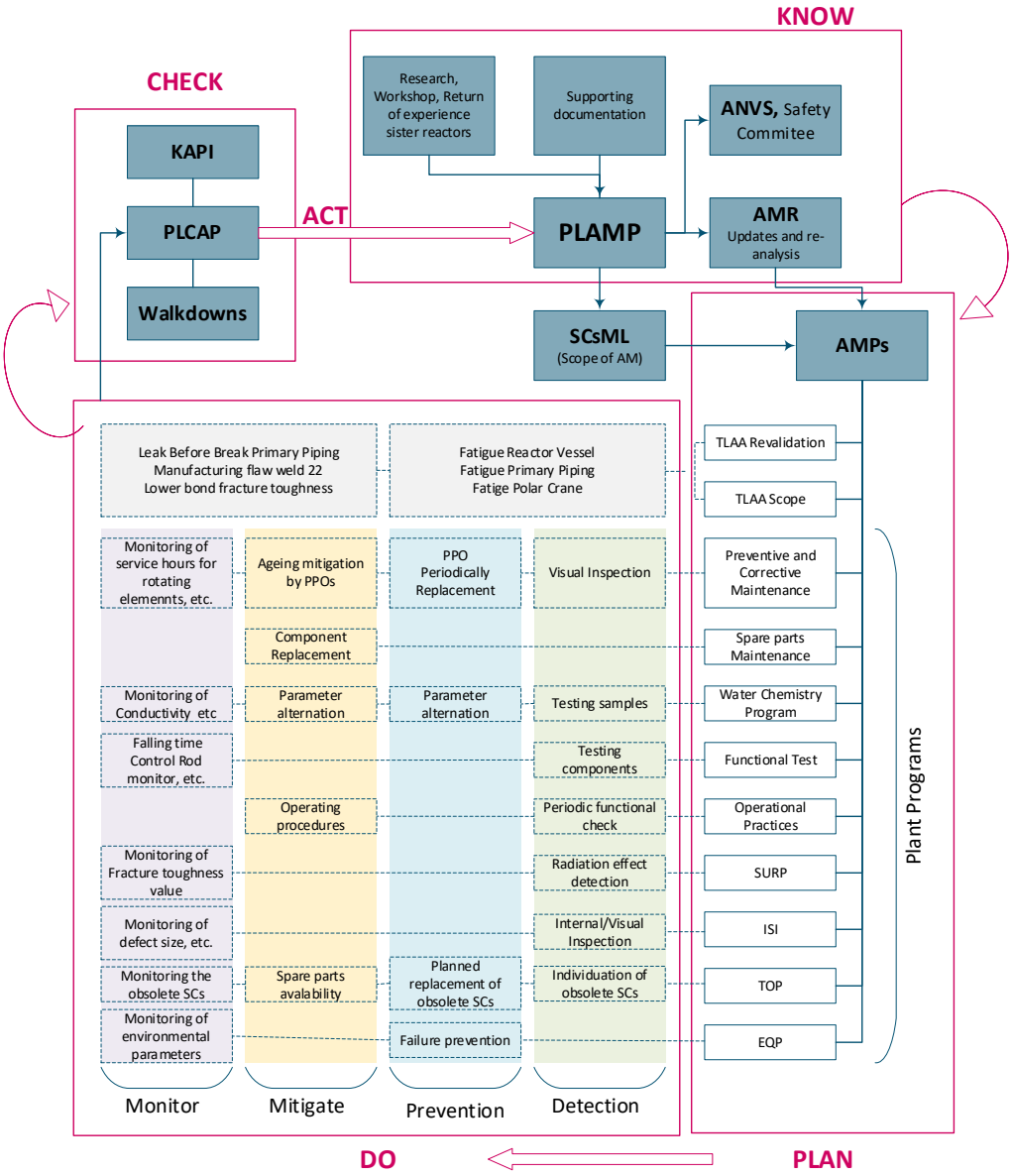

Figure 3 (K)PDCA approach of the Ageing Management process at the HFR.

3.2. Practical case of the (K)PDCA cycle

A practical example of the Plan-Do-Check-Act cycle procedure and effectiveness of the Ageing Management is shown in Figure 4. The (K)PCDA loop shows the performance of the improvement of the ageing management strategies for the piping systems found in the shielding concrete structure in the HFR.

In January 2022, a leakage of primary coolant water was identified through the concrete in the basement ceiling of the pool containment. In-Service inspections (ISI program) were performed to detect the origin of the leakage. Thereafter a Root Cause Analysis (RCA) of the leakage identified the potential causes of the degradation. The ISI inspections (*ACT*) and RCA results, together with historical records (*KNOW*) are used in the framework of AMP-HFR to create an inspection plans of all the piping in similar conditions. The specific AMPs concerning the piping in the concrete are reviewed and modified accordingly (*PLAN*). The implementation, within the framework of the relevant plant programs, of the actions and inspections activities (*DO*) aim to prevent other leakages and monitor possible degradation. The loop is closed with the check of the key performance indicators and monitoring results using acceptance criteria (*CHECK*).

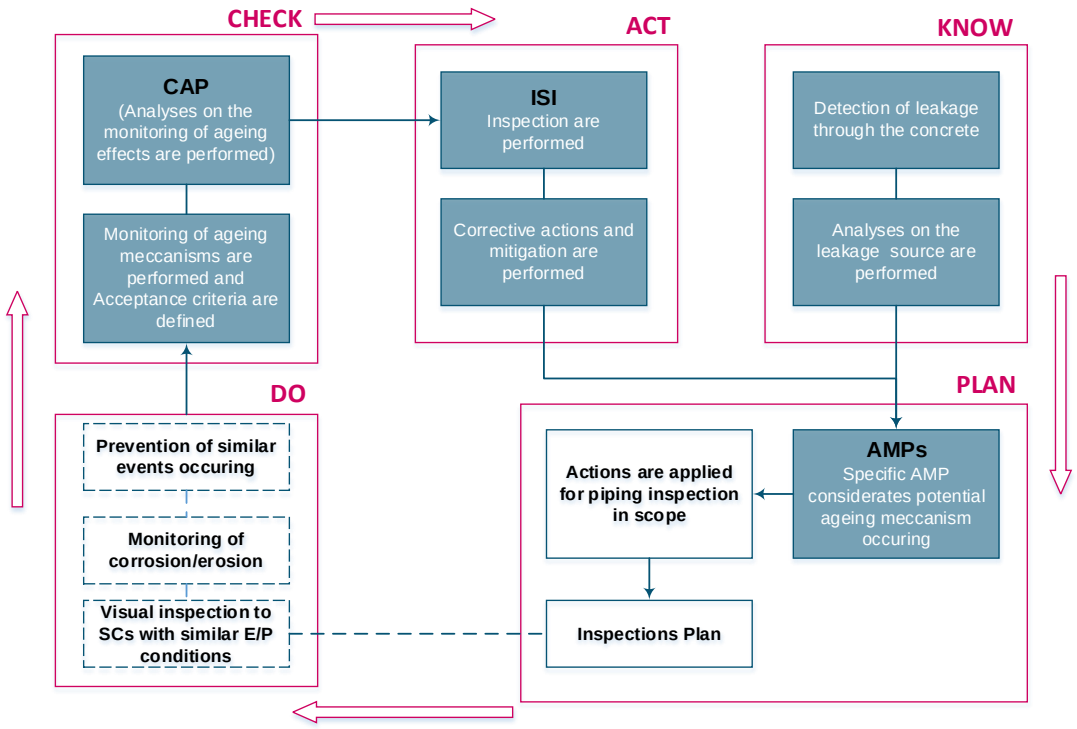

Figure 4: PDCA loop procedure of the Ageing Management of the piping present inside the concrete structure in the HFR.

4. Equipment Qualification

The next paragraphs focus on the HFR Equipment Qualification Program (EQP). An EQP should be in place to ensure that the qualified status of in-scope SSCs is achieved and maintained in order to meet the Requirement 30 of SSR-2/1 [5] and Requirement 13 of SSR-2/2 [6] .

Few literature can be found in international guidelines and external experience for Research Reactors is scarce. The relevant guidelines [8] and [9] for the NPP have been evaluated in order to obtain an effective Equipment Qualification Program that meets the HFR needs. During the implementation phase of the EQP, a new IAEA Safety guide (SSG-69) for the general Equipment Qualification for Nuclear Installation was developed and applied to the EQP-HFR. The SSG-69 is in line with the approach used for developing the EQP-HFR. The new SSG-69 will be considered as the new reference guideline for the review of the approached methodology of the EQP in the HFR.

4.1. HFR approach to EQ

The HFR-EQP is established according to the outlined guidelines SRS-3 [9] . Each phase (see Figure 5) indicated in the IAEA guidelines was analysed and scaled to the HFR.

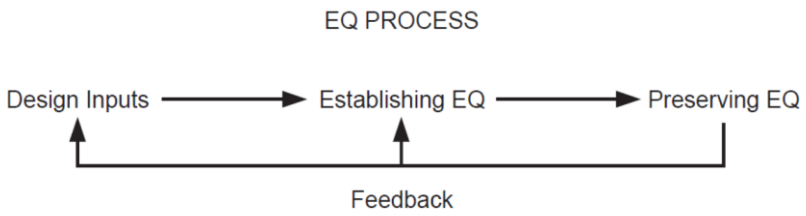

Figure 5 EQ process according to SRS-3.

During the initial phase I, the 'Design Inputs' are retrieved. Equipment Qualification is then established. Whenever it is not possible to establish a qualification for any components, the *'Upgrading EQ'* techniques are used (e.g. relocation, protection). For each SCs, the EQ

process is documented in an EQ File. SCs with same technical specification, location and similar parameters arising from the PIEs are grouped in a single EQ File. Once the SCs are qualified, the qualified status is maintained and preserved.

Environmental conditions

The relevant parameters typically considered during the EQ are analysed and selected for the HFR case. Seismic vibration is considered in the seismic safety analyses [11] of the HFR, therefore will not be considered for the EQP. Water and chemical sprays are not relevant for the HFR configuration. Jet impingement is not relevant due to the absence of high energy lines.

The environmental conditions that may arise from PIEs at the HFR are the following:

- Temperature
- Pressure
- Humidity/ steam and fluid submergence
- Radiation

Relevant Postulated Initiating Events at HFR

Postulated Initiating Events (PIEs) that may occur in the HFR are identified and the service conditions for each Structure and Component are specified. A graded approach is followed due to the fact that conditions arising from PIEs at HFR are not nearly as severe as in a NPP. The HFR identifies the Large Break (LB) Loss-of-Coolant Accident (LOCA) as the most severe PIE, creating the worst conditions in terms of pressure, temperature and humidity/submergence. In terms of radiation dose to components, the failure of experimental facilities is considered a more severe PIE than the LB LOCA.

Therefore the Equipment Qualification at HFR is made against the following relevant PIEs:

- LB LOCA
- Failure of experimental facilities

Scope of EQP

The conditions arising from the PIEs at the HFR might only impact electrical SCs in particularly affected areas of the HFR. Mechanical components are excluded form EQ because the 'harsh conditions' arising from the PIEs are not so severe to impact their functioning. The ageing of these components is managed in the framework of Plant Program in order to assure that they can arrive to the end of life fit for purpose.

Following the graded approach due to milder 'harsh conditions' arising from the PIEs at HFR compared to a NPP, not *'all electrical safety component'* is qualified. The most relevant safety function to guarantee during a PIE is the safe shutdown of the reactor. Therefore the scope of the EQP is limited to the electrical SCs necessary to bring the reactor in a stable shutdown status. The cooling of the reactor core is ensured by mechanically open the convection valves enabling passive cooling. The confinement is ensured by mechanical and civil components, such as the reactor containment.

Therefore, Equipment Qualification Programs is established for the following SCs:

- Electrical components that are part of the reactor shutdown chain sensors.

Methodology of Establishing EQ

The techniques to address the significant ageing mechanisms in the SCs subject to EQ are dealt according to the ways advised in SRS-3 [9] . The SCs are qualified for their mission time. This means that the SCs is qualified against the harshest conditions that it may undergo during the PIEs as long as their function is required.

Each SC has a technical specification and maximum operating time life guaranteed by the producer. The equipment qualification is guaranteed when the operating limits of the technical specification of the SC exceed the value parameter of the maximum harsh conditions by a

safety factor of 1 during its qualified time life. The performance of the intended function of the component is guaranteed by the means of preventive ageing management performed in the SCs and the assurance of the time operating life by the producer.

If qualification is not feasible, the qualified status of the SCs is upgraded (e.g. by means of protection, replacement or relocation of the SCs).

4.2. Ageing and Equipment Qualification

Ageing is a potential common cause of failure mechanism and may affect functioning performances and operational limits, therefore it is evaluated as part of the qualification process.

Three cases are identifies:

- *No relevant ageing and/or minimized/managed ageing*: the SC is considered to arrive at the end of life without significant degradation that renders the equipment vulnerable to failure during PIE.
- *Quantifiable ageing effects:* the effects of the ageing degradation to the operating ranges of the SCs are accounted for.
- *Not quantifiable ageing effects:* An ageing degradation occurs on the SC that cannot be quantified. The operating ranges are affected. The SCs needs to be assessed for qualification by 'Upgrading' the component (e.g. using replacement, relocation or protection approach).

The ageing effects can be considered in during the equipment qualification by simulating them during test (accelerated ageing). The techniques of accelerated ageing are avoided where possible due to the relatively high cost of sacrificial SCs. Relative scarcity on the market of older SCs, non-availability of SCs for testing purpose and the few accelerated ageing methods and models make it difficult to simulate ageing degradation. In case testing is not an option (e.g. due to high costs) the significance of the ageing effects is evaluated by analysis or using operating experience. The HFR policy is to minimize and control ageing in order to remove or limit the impact of possible degradations on the component's operational limit. To do so the HFR identifies the appropriate maintenance and periodic inspection/testing strategies.

4.3. Equipment Qualification Documentation

Each qualified component is provided with the relevant documentation (EQ File) describing the qualification process. Components that have the same type characteristic, location and service condition are grouped in the same EQ File. The EQ File contains all the relevant information on the qualified SC and the process qualification. The layout of the document is as following:

- *Introduction:* Description of the Scope of the EQ file.
- *Location* of the SCs forming the scope of the EQ File
- *Type of SCs:* the type, producer and material properties of SCS forming the scope is stated.
- *Technical specification* of the SCs are presented according to the producer technical datasheet.
- *Service condition and ageing* effects are individuated for the SCs. The ageing strategy is given where applied for each of the ageing mechanisms.
- *Harsh condition* arising from the PIEs affecting the SCs is given. The relevant values of parameters are given.
- *Qualification:* the qualification of the SCs is performed and the equipment qualification of the SCS of the scope is established.
- *Conclusion:* Relevant actions, if any, arising from the final analyse of the equipment qualification are given.
- *References*

Special activities for preserving the qualified status are also included in the EQ File.

In the framework of PLAMP integration matrix, changes to the situation of the SCs in scope for the EQ are evaluated within the framework of the EQP and with the help of specialists. The results of the changes evaluation will indicate if a re-qualification is needed for the components. In the latter case, the Equipment Qualification File is updated.

4.4. Equipment Qualification Assessment effectiveness.

The HFR EQ Program is reviewed in the HFR framework of the Periodic Safety Review. The results of the comprehensive review suggest improvements to the EQ program. Comprehensive review may also be performed by external stakeholders, for instance by IAEA during the Continued Safe Operation (SALTO) mission that results in recommendations of improvements to the EQ program. In case of failure of the SC at less severe conditions than those against which it was qualified, the Failure Reporting, Analysis and Corrective Action System (FRACAS) procedure is started in the framework of the Corrective Action Program.

The FRACAS is a process used to avoid repetitive failures. During the FRACAS procedure, the results of the failure notification (storings meldingen) are analyzed. A team of relevant disciplines is gathered analyze the failure. At the end of the procedure, follow-up actions are defined. The actions may consist of modification of the plant programs, modification to the installation and/or modification in the education and training program of HFR operators and maintenance personnel.

The FRACAS procedure may results in changes to EQ Program. The status of the EQ Program is reviewed yearly in the framework of the self-assessment of the PLAMP. The scheme in Figure **6** presents the approach to EQ effectiveness review at HFR.

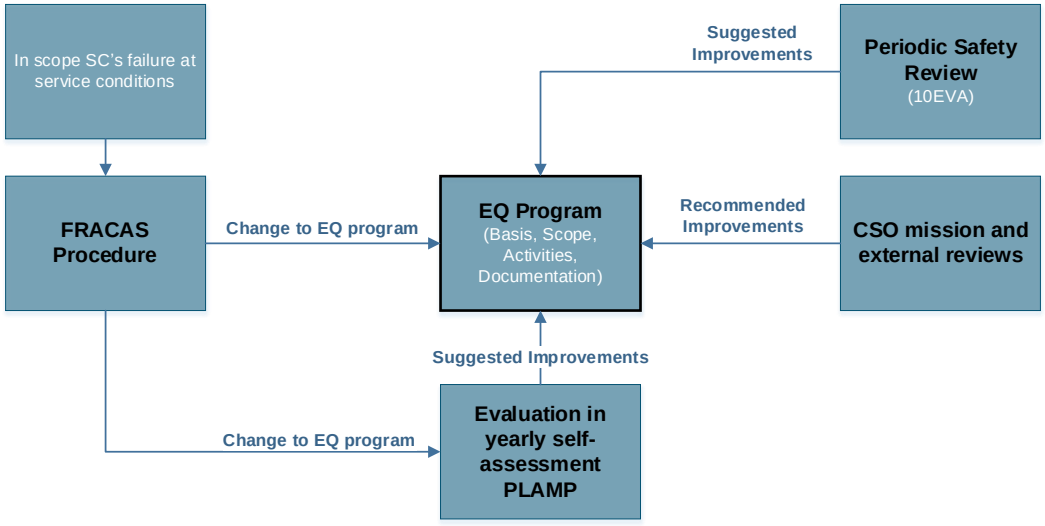

Figure 6**.** Scheme for Equipment Qualification Program Review

5. Conclusion

In this paper the implementation of the Ageing Management Program of the HFR is presented. The implementation of the AMP is overlapped with the last phase of the CSO Project. More attention is given in particular to the Equipment Qualification Program. The EQP Plant Program is still in the implementation phase in the HFR. The used methodology for the EQP development follows the IAEA NPPs guidelines, which were analysed and scaled to for the HFR case. In the next future, the new updated international standards will be considered for the review and effectiveness assessment of the existing EQP methodology. The EQ File will be finalized taking into account all the consideration and recommendation of the SSG-69 [10]
.

6. References

[1] L. Stefanini, 'Continued Safe Operation of the High Flux Reactor – Conceptual document', NRG 25239/18.151802, 21 February 2019.

[2] NRG 'Plant Level Ageing Management Program', 4 August 2020, NO-IB-VE-BD-020392.

[3] NRG 'HFR Asset Management Strategie', 6 February 2020, NO-M-HFR-BD-0002.

[4] IAEA Specific Safety Requirements SSR-3 "Safety of Research Reactors", Vienna 2016.

[5] IAEA Specific Safety Requirements SSR-2/1 "Safety of Nuclear Power Plants: Design", Vienna 2016.

[6] IAEA Specific Safety Requirements SSR-2/2 "Safety of Nuclear Power Plants: Commissioning and Operation", Vienna 2016.

[7] IAEA Safety Guide No. SSG-10, "Ageing Management for Research Reactors", 2010.

[8] IAEA Draft Specific Safety Guide SSG-48, "Ageing Management for Long Term Operation for Nuclear Power Plants", 2018.

[9] IAEA, 'Safety Report Series Nº3 – Equipment Qualification in Operational Nuclear Power Plants: upgrading, preserving and reviewing', Vienna 1998.

[10] IAEA Safety Guide No. SSG-69, "Equipment Qualification for Nuclear Installations", 2021.

[11] F.H.E. de Haan – de Wilde, 'Seismic evaluation of OLP', 23444/17.143704, 12 October 2018.

[12] NRG, 'Failure Report Analysis and Corrective Action System (FRACAS)', NO-IB-HFR-PD-0012.

[13] L. Stefanini, 'HFR Corrective Action Program', NRG-25245/20.175154, 17 June 2020

sck cen

Registered Office
Herrmann-Debrouxlaan 40
1160 Brussel – Belgium

Foundation of Public Utility
VAT BE 406.568.867

Research Centres
Boeretang 200
2400 Mol – Belgium

Chemin du Cyclotron 6
1348 Ottignies-Louvain-la-Neuve – Belgium

Reference N°	Creation Date	
SCK CEN/49224467	2022-05-31	
Alternative Reference N°	Revision	Version
N/A	1.0	1.0
ISC	Revision Status	
Restricted	Approved	

BR2_Research_Fuel_Test_Facilities_RRFM_2022.docx

Authors*
Bert Rossaert Jared Wight

Review information since previous revision*		
Name	**Outcome**	**Date**
Jared Michael Wight	Reviewed	2022-05-24

Approval information for current revision*		
Name	**Outcome**	**Date**
Bert Rossaert	Approved	2022-05-31
Jared Michael Wight	Approved	2022-05-31

Change log*				
Revision	**Version**	**Status**	**Date**	**Description of change**
1.0	1.0	Approved	2022-05-31	

**This automatically generated cover page shows references and document information as were available in the Alexandria document management system on 2022-05-31. Please refer to Alexandria for current and complete metadata, or to the document contents and/or author for additional information.*

BR2 Reactor Irradiation Test Facilities for Research Reactor Fuel Development and Qualification

B. Rossaert and J. Wight
Nuclear Materials Science Institute, SCK CEN,
Boeretang 200, 2400 Mol, Belgium

ABSTRACT

The Belgium Reactor 2 (BR2) has several devices in operation and in preparation that are dedicated to the performance and safety demonstration testing of (research) reactor fuel. Recently, several full size fuel plate irradiations have been performed in the framework of the HiPROSIT, COBRA, FUTURE-HFIR and KIMQI projects in slotted baskets denoted by FUTURE-5. This device is an upgrade of its predecessors, the E-FUTURE baskets, and additional irradiation projects are planned in FUTURE-5 baskets. Furthermore, in support of the US High Performance Research Reactor (USHPRR) LEU conversion project, a new flexible irradiation facility, MUSTANG-R, is being developed in cooperation with INL and ANL to allow for the irradiation testing of a full-size fuel assembly. This device has a flow restriction valve in its inlet structure inside the BR2 upper plenum, which allows the flow to be regulated to typical reactor conditions, to support fuel qualification. The design allows for various materials of the in-core structure of MUSTANG-R, such that appropriate customer-defined neutronic conditions can be achieved. Two irradiations are planned for the Massachusetts Institute of Technology Reactor (MITR) and the National Bureau of Standards Reactor (NBSR) with full size representative fuel elements, denoted by the name Design Demonstration Elements (DDEs). Finally, the conceptual design has started for a generic test assembly (GTA) which will enable the irradiation testing of a box-type fuel assembly/element with up to nine FUTURE size curved plates, to support LEU fuel qualifications.

1. INTRODUCTION

The BR2 **M**aterial **T**est **R**eactor (MTR) is located in Mol, Belgium. The reactor is mainly used for radioisotope production and material testing. The latter includes MTR fuel performance and qualification testing. The fuel tests can be done directly in the BR2 primary circuit which is pressurized (12 barg) and serves as containment. There are 5 irradiation channels of diameter 200 mm, 64 irradiation channels of diameter 84 mm and 10 channels of diameter 50 mm in a hyperboloid configuration within the reactor vessel as shown in Figs. 1 and 2.

At current, the FUTURE-5 devices are being used for irradiation of aluminum clad UMo dispersed and U_3Si_2 dispersed fuel, where irradiation of UMo monolithic is planned.

Furthermore, in support of the **US H**igh **P**erformance **R**esearch **R**eactor (USHPRR) **L**ow **E**nriched **U**ranium (LEU) conversion project, a new flexible irradiation facility, MUSTANG-R, is being developed, in cooperation with **I**daho **N**ational **L**ab (INL) and **A**rgonne **N**ational **L**ab (ANL), to allow for the irradiation testing of a full-size fuel assembly.

Finally, the conceptual design has started for a **G**eneric **T**est **A**ssembly (GTA) which will enable the irradiation testing of a box-type fuel assembly/element with up to nine FUTURE-sized curved MTR fuel plates.

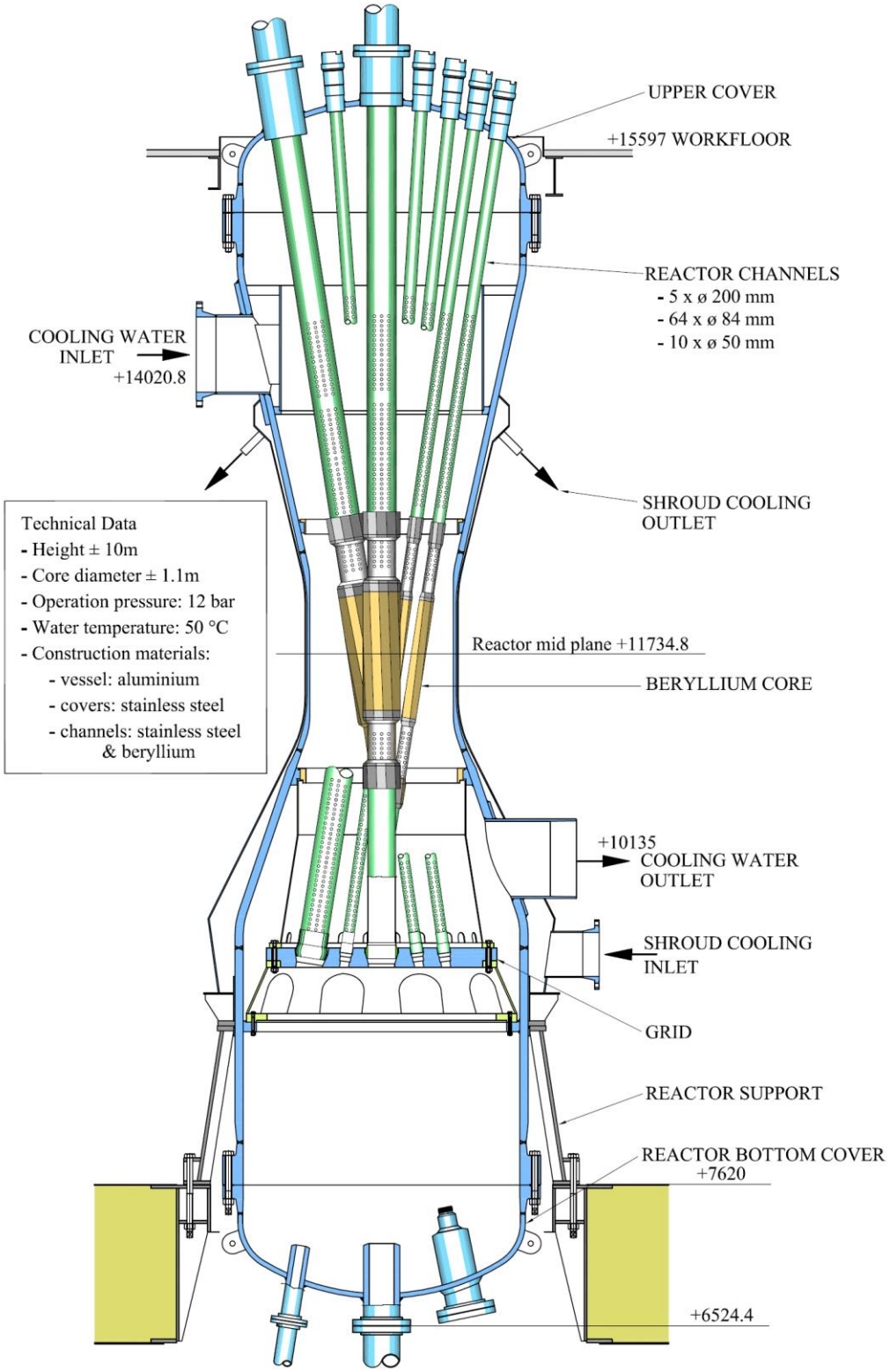

Figure 1 BR2 reactor vessel cross section with annotations

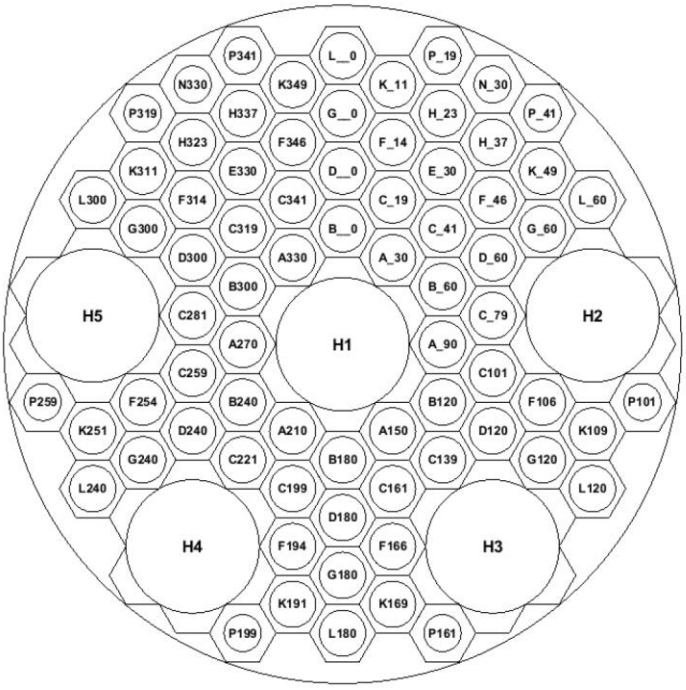

Figure 2 Cross sectional view of the BR2 reactor channel configuration at mid-plane level. Channels are denoted according to their position with respect to the central channel

1. FUTURE-5

The FUTURE-5 basket is an upgraded design qualified in 2019 and is based on its predecessor E-FUTURE from 2010. FUTURE is the abbreviation of **FU**el **T**est **U**tility for **RE**search reactors. It is used for irradiation of up to five full size flat fuel plates (Fig. 3) with dimensions 970 mm x 61 mm with thicknesses in the range 1.27 mm-1.35 mm. These plates are loose in slots in the baskets as shown in Fig. 4 on the right.

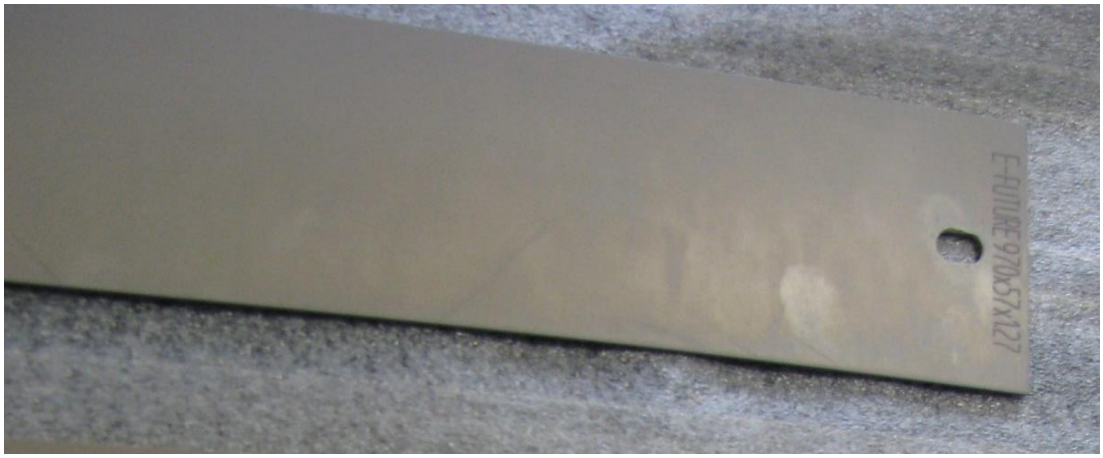

Figure 3 FUTURE type of flat fuel plate

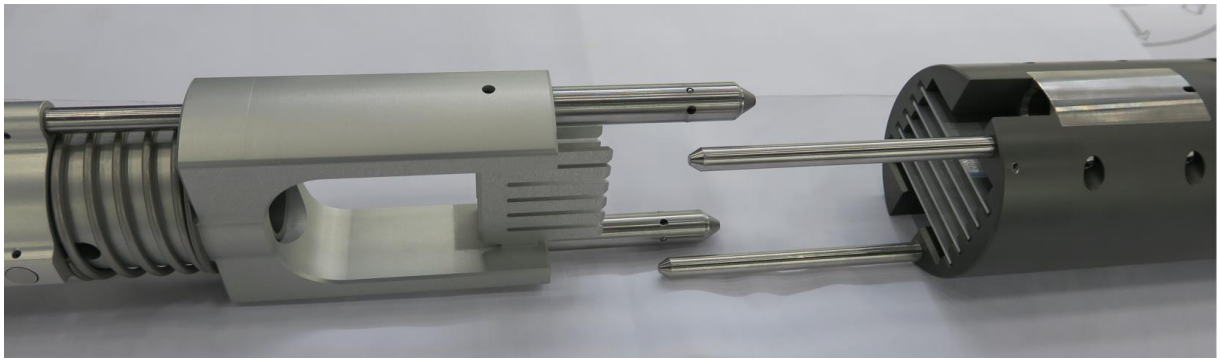

Figure 4 FUTURE-5 suspension fork (left) and basket with five loose plates (right)

The baskets are cooled by the primary coolant and the coolant velocity across the plates is determined by the conditions of the BR2 plena. The BR2 reactor cooling system ensures a well determined pressure drop across the BR2 fuel elements and, thus, across the FUTURE-5 baskets. By having an inter-plate distance of 6 mm, which is a factor 2 larger than for BR2 fuel elements, sufficient cooling margin is ensured in nominal and transient conditions. Therefore, peak heat fluxes up to 600 W/cm^2 are possible.

It should be noted that the design foresees the possibility to put flow orifices in the bottom of the baskets. However, these have never been qualified for in-pile irradiation tests.

Thanks to the large flexibility of the BR2 reactor and the fact that these baskets can be irradiated in any of the 64 diameter 84 mm channels, a large variety of irradiation conditions can be reached.

2. MUSTANG-R

In support of the **US H**igh **P**erformance **R**esearch **R**eactor (USHPRR) reactor program a new capability is being developed at SCK CEN with support of INL. It is denoted by MUSTANG-R (**M**assflow t**U**ning **S**etup for **T**esting of fuel **A**ssemblies of the **N**ext **G**eneration with **R**estrictor). The latter would allow full size (mock-ups of) fuel assemblies to be irradiated in BR2. The devices are designed to be irradiated in one of the large BR2 diameter 200 mm irradiation channels. As illustrated in Figs. 5 and 6 the devices consist of:

- Instrumented **plugs** in beryllium or in aluminum (possibly with absorber rods)
- **Baskets** that contain the **fuel assemblies** that are put in the plugs
- A plug (valve) design denoted by **restrictor** that can regulate the flow (adjustable orifice)

The BR2 coolant in the upper reactor vessel plenum enters the 200 mm channel through perforations in the channel wall as shown in Fig. 7. It then enters the plug suspension tube, flows downward and passes via the restrictor which blocks a part of the flow passage. This coolant cools the baskets with the fuel elements and then discharges into the lower reactor vessel plenum. The minimal cooling, and thus minimal valve opening, required mainly is dependent on:

- Peak heat flux
- Inter-plate distance
- Fuel plate length and width
- Amount of plates

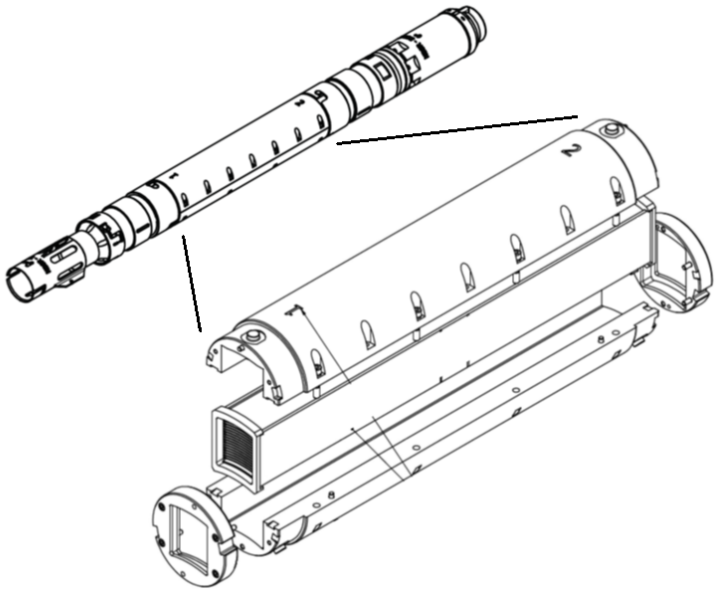

Figure 5 MUSTANG-R basket with connection pieces (top) and example fuel assembly in exploded basket illustration (bottom)

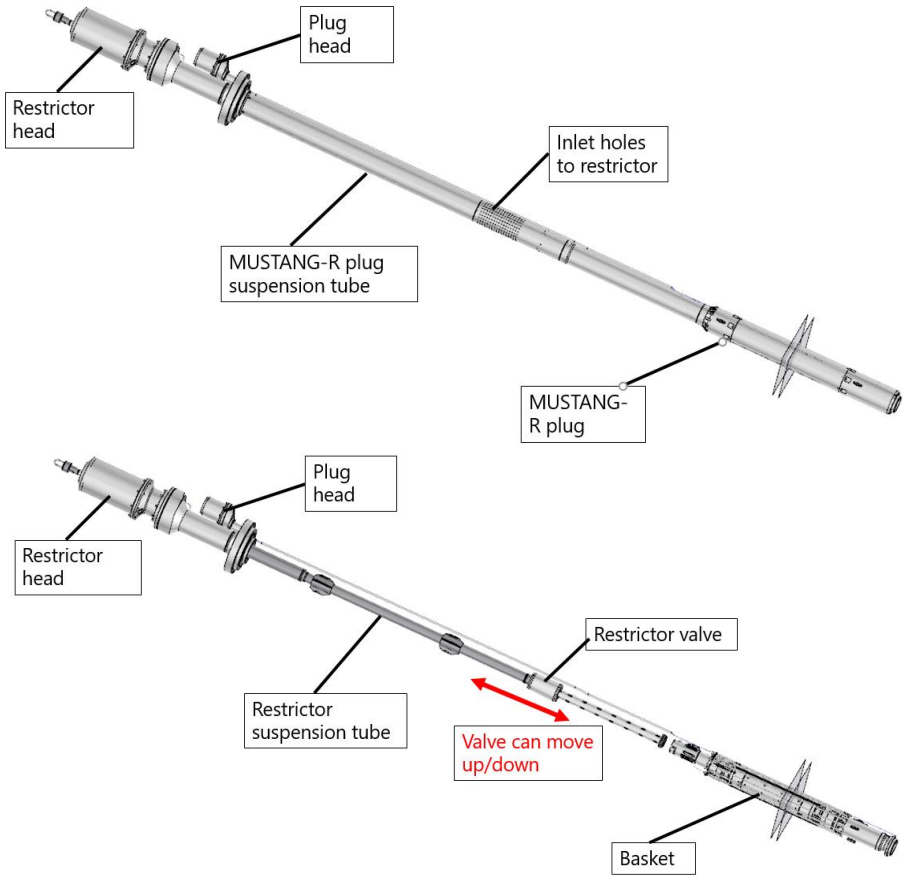

Figure 6 MUSTANG-R plug with inlet holes for the coolant (top) and basket below the restrictor suspension tube (bottom)

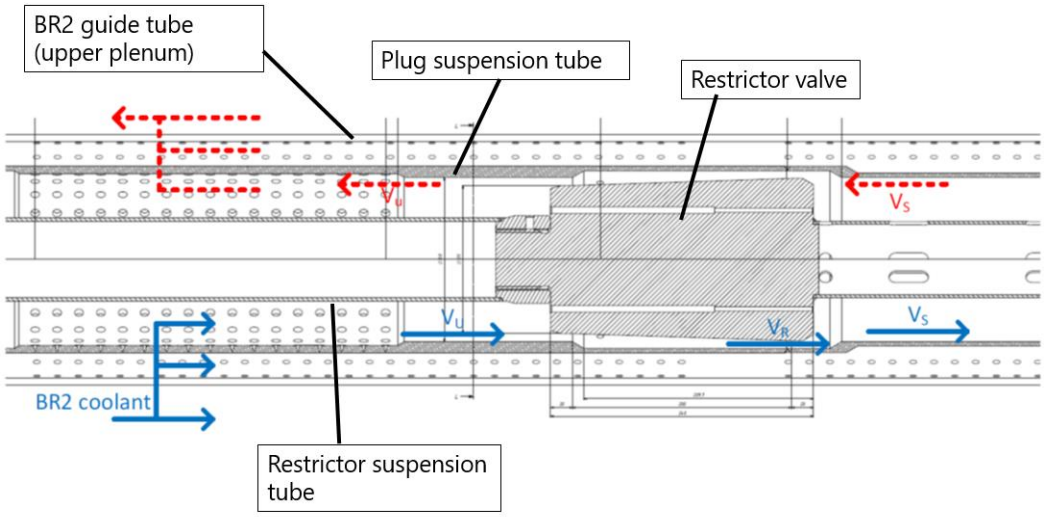

Figure 7 MUSTANG-R restrictor valve (adjustable orifice) in the lowest position (open) possible in the plug suspension tube inside a BR2 200 mm channel guide tube. Arrows in blue denote nominal downwards forced flow whereas dotted arrows in red denote upwards low flow in flow reversal.

The design foresees temperature and pressure sensors in order to have information on differential pressure and temperature across the basket. Furthermore, the intention is to install gamma thermometers and **S**elf **P**owered **N**eutron **D**etectors (SPND) in the plugs.

Safety studies for flow transients are being performed at the moment of writing in cooperation with INL and ANL. MUSTANG-R is being designed and qualified as thermal hydraulically passively safe, thanks to the mechanical design. Ref. [2] for instance focuses on safety during a BR2 flow reversal transient with the help of RELAP.

Design, fabrication, functionality and safety demonstration is supported by full scale mock-ups that are being made and tested by and at SCK CEN. For instance, Fig. 8 shows a mock-up of the restrictor with the restrictor plug (valve) that has been hydraulically tested in 2021. This mock-up provided key feedback for finalizing the design of MUSTANG-R and qualifying special operations and operators.

In collaboration with INL it is foreseen to irradiate two **D**esign **D**emonstration **E**lements (DDEs) in BR2. These are DDEs of the **M**assachusetts **I**nstitute of **T**echnology **R**eactor (MITR) and the **N**ational **B**ureau of **S**tandards **R**eactor (NBSR) [1]. The goal is to mimic the corresponding reactor operating conditions for neutronics and thermal hydraulics. Furthermore, the current design also foresees the possibility to test a **G**eneric **T**est **A**ssembly (GTA) in the MUSTANG-R device. The latter is a FUTURE type of basket in which multiple fuel plates can be swaged/assembled and irradiated.

Figure 8 MUSTANG-R mock-up of restrictor suspension tube with plug (valve)

3. GTA

SCK CEN is working on the conceptual design of a **G**eneric **T**est **A**ssembly (GTA) in collaboration with the **K**orean **A**tomic **E**nergy **R**esearch **I**nstitute (KAERI). For this device, the intention is to swage up to nine full-size fuel plates (970 mm x 55 mm) with thicknesses in the range 1.27 mm-1.35 mm into a generic MTR box type assembly. The fuel assembly will be loaded into a basket inside one of the 84 mm channels of BR2, similar to the FUTURE-5 irradiation device as shown in Fig. 9. This means that neutronic conditions can be similar to that of FUTURE-5.

Equivalent to FUTURE-5, the GTA assembly/basket will be directly cooled by the BR2 coolant and the pressure drop over the basket is similar to that over the BR2 fuel elements. The inter-plate distance minimally is 3 mm similar to the BR2 fuel elements. The thermal hydraulic safety evaluation will determine the maximum heat flux possible which is expected to be in the range 470-600 W/cm^2. It should be noted that configurations with dummy plates or even empty slots are also envisaged in order to tailor the assemblies to the experiment needs. Therefore, it is expected that irradiation studies at elevated heat fluxes can be performed.

The planned projects for the GTA at the moment of writing are KIMQI-GTA and COBRA-GTA.

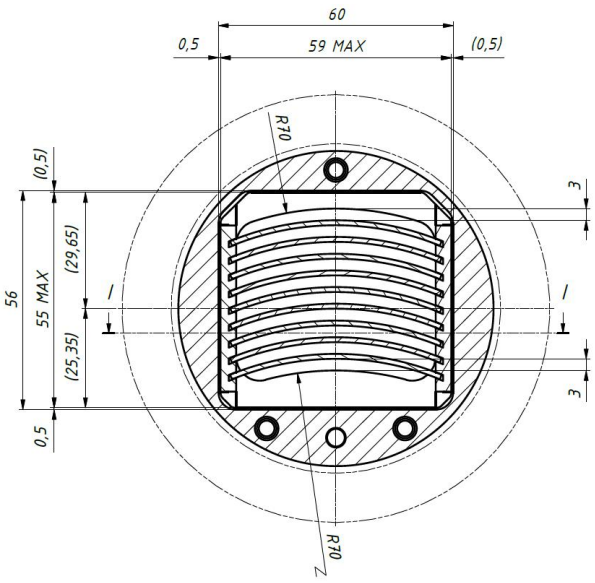

Figure 9 Cross sectional view of the conceptual design of the GTA in a diameter 84 mm BR2 channel

4. Conclusions

The Belgium Reactor 2 (BR2) is designed and qualified for irradiation of MTR fuel plates and assemblies. Several devices dedicated to research reactor fuel plate (assembly) irradiation are in operation and in preparation. A large variety of full size fuel plate irradiations have been performed and are planned in slotted baskets denoted by FUTURE-5. Furthermore, in support of the US High Performance Research Reactor (USHPRR) LEU conversion project, a new flexible irradiation facility, MUSTANG-R, is being developed by SCK CEN in cooperation with INL and ANL to allow for the irradiation testing of full-size fuel assemblies. This device has the possibility to regulate the flow. Furthermore, the design allows for various materials of the in-core structure of MUSTANG-R, such that appropriate customer-defined neutronic conditions can be achieved. Two irradiations are planned for the Massachusetts Institute of Technology Reactor (MITR) and the National Bureau of Standards Reactor (NBSR) with full size representative fuel elements, denoted by the name Design Demonstration Elements (DDEs). Finally, the conceptual design has started for a generic test assembly (GTA) which will enable the irradiation testing of a box-type fuel assembly/element with up to nine FUTURE size curved plates, to support LEU fuel qualifications.

REFERENCES

[1] S. Van den Berghe, S. Kalcheva, V. Kuzminov, B. Rossaert, P. Gouat, J. Valenberghs, H. Ooms, J. Smets, G. Cornelis, Y. Parthoens, F. Joppen, A. Leenaers, P. Jacquet, G. Van den Branden, S. Van Dyck, “Feasibility Study for Performing Design Demonstration Element (DDE) Irradiations in the BR2 Reactor,” SCK CEN/26573864, SCK CEN, 2017.
[2] H. Lin, P. Garner, J. Licht, B. Rossaert, “Transient Safety Analyses for the MUSTANG-R Device in BR2 using RELAP5, Conference Paper RRFM 2022.

AGEING MANAGEMENT AND MODERNIZATIONS AT THE WWR-SM REACTOR IN UZBEKISTAN

S.A. BAYTELESOV, F.R. KUNGUROV, N.R. MAKSUMOV
Institute of Nuclear Physics of Uzbekistan Academy of Sciences, republic of Uzbekistan
Khuroson str. 1, Ulugbek settlement, Tashkent, 100214, Uzbekistan

ABSTRACT

WWR-SM research reactor at the Institute of Nuclear Physics of Uzbekistan Academy of Sciences operates since 1959. Great attention is paid to the nuclear safety of this installation. To avoid any accidents and malfunctions of the reactor systems structures and components (SSC) ageing management is on place. Regular tests and checks of SSC's are carried out and modernization are ongoing periodically. Some of them are listed in this article.

Ageing management and modernizations

In September 1959, the first research reactor was launched in Central Asia, and the construction of the reactor made it possible to carry out research work. As a result of these scientific studies, it was possible to develop radioisotope products for worldwide use as well as republican medical centers, use the reactor for the needs of geology, mining, metallurgical and jewelry industries.
The WWR-SM research reactor of the Institute of Nuclear Physics of the Academy of Sciences of the Republic of Uzbekistan is currently the only nuclear reactor in Central Asia with a capacity of 10 MW. Many foreign experts admit that our reactor is one of the most efficiently used reactors in this category of reactors.
The reactor conducts research in cooperation with international organizations, including the International Atomic Energy Agency (IAEA), the US Department of Energy, the Rosatom Corporation, and other countries as part of various international programs.
In order to increase the lifetime of the reactor and its nuclear safety, with the support of the Government of the Republic of Uzbekistan and the IAEA Technical Cooperation, projects are being implemented on ageing management to improve the safety of the reactor and its more efficient use, including the gradual replacement and modernization of a number of equipment and reactor components.
There is a schedule on testing and checks of WWR-SM reactor components and structures and this work is carried out strictly according to the schedule.
At present, as part of the implementation of ageing management program, work has been carried out to upgrade and replace a number of reactor systems, including by services.

1. Radiation Safety Service of the Reactor

In 2016, an additional section of the automatic radiation monitoring system "Pelikan" was modernized and put into operation to control the release of gases and aerosols in the reactor ventilation system. In November 2020, the components of the "Pelican" system were refurbished.

Fig. 1 automatic radiation monitoring system "Pelikan"

In 2016, one section of the exhaust ventilation and filtration system in case of an accident was modernized and put into operation.

Fig. 2. Exhaust ventilation and filtration system

In 2017, a compactor for the processing of solid radioactive waste was purchased and installed before being removed for disposal in the RWDF.

2. Mechanics Service.

Within the IAEA project framework, the following work will be carried out in the current year 2022:
work is planned to replace the primary cooling system of the reactor (installation of pumps, valves, new pumps and valve control panels).

Fig. 3. primary cooling system pumps

It is planned to carry out modernization by completely replacing obsolete components and assemblies of a 10-ton crane in the main hall of the reactor with new ones.
In addition, the specialized organization "Contexnazoratukuv" carried out a comprehensive check of the nodes and elements of the 10-ton overhead crane by the method of non-destructive testing. According to the results of the examination, a conclusion was made on its satisfactory condition.

Fig. 4. 10-ton overhead crane

In accordance with the approved plan for the technical inspection of the components and equipment of the reactor every 50,000 hours at the WWR-SM facility with the help of the AVJ Technical Center, ultrasonic testing of the central tank, protective tank, and primary circuit pipelines is carried out by the method of non-destructive testing.
In 2021, a "visual" inspection of the components of the reactor core was carried out at the reactor using a special radiation-resistant underwater camera. Having studied the data obtained during the inspection, the experts of the IAEA and the Nur Company concluded that the central tank, the protective tank and the reactor core vessel can be used until 2030.

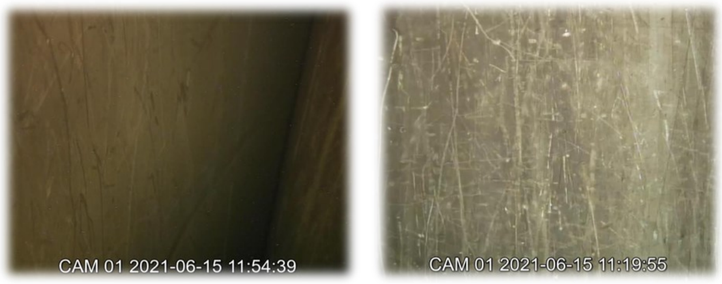

Fig. 5. Components of the reactor core

3. Radiochemistry Service

In 2018, a new steam generator was installed and put into operation to generate distillate water in order to provide the system of the primary cooling circuit and the reactor showering system.
As part of the implementation of the IAEA project, in 2022-2023 it is planned to replace ion-exchange filters (IEF) in the system of the primary cooling circuit of the reactor.

Fig. 6. ion-exchange filters

The technical condition of "IEF No. 1,2" in the system of the primary cooling circuit was checked with a water flow rate of 1320 m^3/h (using pumps in the system of the primary cooling circuit). During testing it became clear that water was flowing from the IEF.

4. I&C service

The control system and instrumentation play a significant role in maintaining the reactor at a stable power and controlling the deviation of technological processes from the established norms. All parts of "Data Acquisition and Processing Device" system (UNO-322R1), which works, with the exception of 1 of 3, were subjected to technical inspection. The technical condition of the equipment located in the reactor control unit (UUP-20R) and on the operator's shield "0"was checked.
In December 2021, within the framework of funding under the IAEA project, an automatic reactor power control device (EMU-electric machine amplifier) was received and put into operation;
As part of the IAEA project, it is planned to install an angular displacement encoder (encoder) for the control rod movement system in 2022.

5. Electricians' service

In 2021, as a result of fluctuations in the electrical network, the reactor was shut down 8 times. In order to reduce the influence of network fluctuations on the operation of the reactor, work is planned to install two large powerful voltage stabilizers with a capacity of 400 kVA to increase the uninterrupted power supply of the facility in 2022;
Also, for this purpose, in the second half of 2022, as part of the implementation of the IAEA project, it is planned to purchase and install an additional powerful diesel generator (200 kVA).

Conclusion

Big attention is paid at the Institute of Nuclear Physics of Uzbekistan Academy of Sciences to ageing management of the WWR-SM research reactor taking into account that it is old enough. All structures of reactor are under permanent control and are replaced and modernized as they become old to keep functioning of reactor safe and reliable as the WWR-SM reactor is the irreplaceable tool for scientific research and radioisotope production in Republic of Uzbekistan.

DEVELOPMENT OF AN APPROACH FOR DOWNBLENDING AND DISPOSITION OF IRRADIATED GRAPHITE FUEL

J. DEWES, P. CHAKROV, R. ROBBINS
International Atomic Energy Agency, Vienna, Austria

I. BOLSHINSKY, K. BATEMAN, S. TOZSER, W. HINTZE
Nuclear Nonproliferation, Idaho National Laboratory
Idaho Falls, ID, USA

V. GNYRYA, Y. KOYANBAYEV
National Nuclear Center of the Kazakhstan Ministry of Energy
Kurchatov, Kazakhstan

K. GAINES
Oak Ridge National Laboratory, Oak Ridge TN, USA

1. ABSTRACT

The IGR reactor, a pulse-type test experimental reactor, reached full power in 1961. The reactor contains a center axial experimental ampoule that is subjected to a large pulse of neutrons (neutron flux maximum density of 7×10^{16} n/cm^2·s, peak power 10GW) when the reactor is operated. The fuel form for the IGR reactor is graphite cubes and rods impregnated with highly enriched (90%) uranyl-dinitrate ($UO_2(NO_3)2\cdot6H_2O$). This fuel is eligible for return to Russia for reprocessing under the Russian Research Reactor Fuel Return program. However due to some technical and licensing issues it was decided to immobilize this fuel in Kazakhstan. The disposition approach thus selected for the spent HEU fuel involves down-blending of the fuel followed by cementation. Development of the process for down-blending and subsequent cementation requires a process that satisfies many criteria, including fissile content, compressive strength, permeability, and containment of radioactivity, among others. One key goal of the final product is to meet the criteria for termination of safeguards. This paper will describe the overall challenge associated with disposition of irradiated HEU graphite spent fuel, the identification of the objectives of the disposition process, and the constraints associated with development of the process and the waste form.

2. THE IMPULSE GRAPHITE REACTOR

The Impulse Graphite Reactor (IGR) was developed as part of the Soviet Union nuclear rocket development program. Although the reactor was not a part of the Soviet nuclear weapons program, the Semipalatinsk site was selected due to its large unpopulated area and proximity to other nuclear activities. Construction of the reactor commenced at the initiative of I.V. Kurchatov, the father of the Soviet nuclear weapons program in 1958 by specialists of the former USSR Kurchatov Institute. Startup commenced in 1960, with first criticality on June 7. Full power was achieved in 1961, and by 1962 experiments were underway. In 1967 a modernization of the core was completed that increased the fissile mass of the fuel from 7.46 to 9.0 kg. The burnup of the initial core was less than 1% when it was removed. The irradiated fuel from this first loading is currently in storage at the IGR

Figure 1. The IGR Reactor Complex

site and represents the initial cache of fuel to be dispositioned. The reactor name, translated as Impulse Graphite Reactor, reflects the fact that it is a graphite moderated reactor generating neutrons in a pulse mode. It is similar in function to the TREAT facility at the Idaho National Laboratory in the USA. The pulse, in this case, is 5.2 GJ in about 0.12 seconds. That's roughly enough energy to liquify 60kg of steel instantaneously.

The reactor has a center ampoule, or test chamber, that is used to hold materials under investigation. This ampoule was initially 180 mm in diameter but was increased to 290 mm during the 1967 modernization.

3. FUEL FABRICATION AND PERFORMANCE

The fuel is comprised of graphite blocks and rods[1] that have been impregnated with a uranium solution enriched to 90% ^{235}U. The graphite is stacked into columns which are encased in a steel vessel filled with helium gas. The use of graphite eliminates issues with variable moderation that would introduce competing phenomena during power-excursion experiments. The core is 1.4 m in diameter and consists of a fixed portion and a moveable portion. Figure 2 shows the movable part of the core in the lowered position with the center ampoule visible. Moving the two portions of the core ensures substantial subcriticality between pulses. The neutron pulses in the reactor are used to simulate accident conditions and accelerate exposure tests. The pulse is self-limiting, as increases in temperature also increase parasitic losses of neutrons which automatically shut down the chain reaction.

Operation of the reactor involves moving the two core portions together, after which control rods are removed to the nearly critical state. Quick removal of additional control rods result in a rapid spike in neutron flux, which is then rapidly quenched by the negative thermal coefficient of reactivity. All 16 gadolinium oxide control rods are in the fixed portion of the core. The fluence of thermal neutrons in the core of the IGR in a pulse is 3.7×10^{16} n/cm^2.

Temperature in the core following a pulse can reach 2000K. The IGR core has no active cooling mechanism, so following a pulse operation, the core must be allowed to cool for a period of time. A cooling water cavity surrounds the sealed vessel containing the core and serves as a heat sink.

4. PROPERTIES OF SPENT FUEL

The fuel removed following the initial operation of the reactor consists of 1220 pieces of uranium impregnated graphite in the form of blocks and rods with a total fuel load mass of 2.6 tons. The fuel is stored in boxes within a vault onsite. As mentioned earlier, the burnup of this fuel was less than 1%. Recent (2017) inspection[2] of the fuel showed a near-contact radiological dose rate of approximately 1.5 mSv/h, a level that requires use of additional protective barriers to ensure safe working conditions. The uranium in graphite matrix after high temperature operation was presumably in the form of carbides, which in finely dispersed state is pyrophoric. Therefore, an inert environment may be necessary for handling of the material.

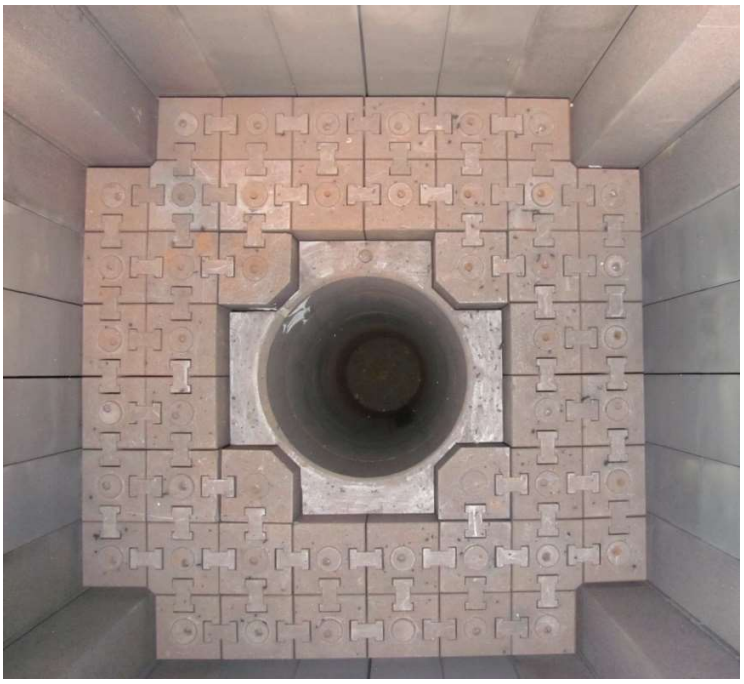

Figure 2. The Movable Portion of the IGR Core

Much has been learned about the fuel while conducting a feasibility study on down-blending 2.5 kg of fresh IGR fuel remaining from the modernization effort that was also located at the IGR site[3]. The distribution of Uranium in the graphite was of interest, as inconsistencies could impact the down-blending process. In addition, the physical properties were desired in support of development of the down-blending process. Each of the three typical shapes of graphite were sectioned, and the uranium content, grain structure, enrichment variation, density, porosity, and other properties were determined using several methods. The results indicated minimal variation in uranium content, even less variation in enrichment, evenly distributed porosity, and otherwise general homogeneity. The Ulba Metallurgical Plant was tasked with development of a method for down-blending this fresh IGR graphite fuel. The process developed included crushing, oxidation of the graphite, dissolution of the residual uranium forming uranyl nitrate, and then mixing with natural uranyl nitrate to a final enrichment of under 19.8 %. The now down blended uranium was precipitated from solution, calcinated, and oxidized to U_3O_8 powder. This approach, however, was not suitable to use for the irradiated graphite fuel, as separation of the uranium was not a desired approach, and due to potentially high rates of release of radioactive gasses.

5. PROCESSING TECHNOLOGIES

The objective of the effort we describe is to disposition the irradiated IGR HEU fuel. Reprocessing is the dominant approach to disposition of irradiated HEU fuel, as it allows

the recovery of the ^{235}U and results typically in a vitrified waste form suitable for disposal. Dissolution of graphite fuels has been studied in support of processing of TRISO fuels, and the process has been deemed feasible. It has yet, however, to be undertaken on a full scale. Preliminary examination of the potential for reprocessing this particular fuel revealed that the high carbon ratio of >7200 C/U was a cause for concern. The risk associated with introducing carbon into a working reprocessing facility was deemed too high, as the carbon had the potential to be carried through the process with unknown effect. In this case, however, extraction of the uranium from the waste is not necessary nor desired. Given the decision to avoid reprocessing, the following key objectives for a Kazakhstan based approach were identified:

a) To downblend the uranium to less than 20% enrichment
b) To exclude stages in the technology that enable ^{235}U separation

Graphite has been used in more than 100 power reactors as a moderator and reflector, and it is estimated that 250,000 tons have been used for this purpose to date. Many technologies have been explored and utilized to deal with disposition of irradiated graphite. Many of these technologies and the precautions of their use are discussed in the IAEA publication TECDOC 1521[4]. Such graphite is contaminated typically with tritium (^{3}H) as well as long lived radioactive contaminants such as ^{14}C and ^{36}Cl. It does not, however, contain uranium and therefore could not be directly applied to this problem.

To identify the best approach for dealing with the graphite fuel, a comprehensive study was undertaken by NNC[5] to investigate potential approaches and select the most suitable. Many chemical processes were identified, however most had the potential for separation of ^{235}U and were therefore eliminated from consideration. Several approaches to destruction of the graphite, either by combustion, oxidation, or other methods were investigated, but the potential rates of release of radioactive gasses would require substantial study.

The potential for dry process remained, with a further question of the means to formulate a radioactive waste form which meets the criteria for storage and disposal. Various approaches were considered, including combustion, cementation, bituminization, compaction, plasma processing, and vitrification. The approach deemed the most durable and most suitable to an ultimate disposal form was cementation. This conclusion was also based on a resulting medium-active waste form where the dilution material serves to both minimize exposure and fixate the radioisotopes.

6. REGULATORY REQUIREMENTS

Regulatory requirements for final disposal of the irradiated graphite fuel will be largely driven by the waste acceptance criteria derived from the safety case for the disposal facility selected for this material. Since the ultimate disposal facility has not been identified, Russian standards for final disposal waste form performance will be used as a reasonable substitute. For the process of producing the waste form, Kazakhstan regulations for management of wastes are well understood and will be applied. These regulations were comprehensively reviewed in a previous report[6].

7. PROCESS DEVELOPMENT

Given the selection of cementation, the issue of the approach to down blending remained. In the case of the unirradiated fuel, recovery of the uranium was desired, and therefore the fuel was crushed and then dissolved in nitric acid to form uranyl nitrate. This was then mixed with sufficient quantities of uranyl nitrate from natural uranium to bring the enrichment down below 20 % From there the uranyl nitrate was precipitated and converted to U_3O_8 powder for subsequent storage and eventual use in fabrication of fuel. In the case of the irradiated fuel, however, liquefaction was to be avoided.

In order to down-blend the uranium, it would need to be mixed in a dry form with sufficient natural uranium (approximately 32 kg) to obtain <20 % enrichment. For this process the mixing of dry components would require some means of ensuring subsequent inseparability. The atomic-scale mixing of enrichments associated with liquid forms was not feasible, so a determination of adequate form for each component to be mixed was needed. Both equivalent particle size and similarity of chemical form was deemed critical to a determination that re-separation of HEU from LEU was not realistically feasible. The chemical form in the irradiated fuel was assumed to be mostly uranium carbide but given the long period of time associated with storage of the fuel it was anticipated that large portions would have oxidized to U_3O_8. This was the form selected for the natural uranium as well. After some consideration it was determined that the form was not critical, as any attempt to chemically separate the HEU from the natural U would require liquification, which would instantly result in a down-blended product.

Once the cementation process was selected, development of the cement matrix composition as well as the mechanism to produce the cement was initiated. Experts from Sellafield Ltd. in the United Kingdom as well as IAEA staff were consulted and have participated in the development process.

Making concrete is a straightforward process, but in this case several aspects have been identified as warranting additional requirements:

a) The final waste form must be easily managed, and therefore steel drums were selected as the container in which the cement matrix will be contained for ease of handling, storage, and ultimate disposal. The drum also qualifies as a “type A” waste container. In order to ensure all of the waste material is contained, the mixing of each portion of waste material must be done within the drum.
b) The product must be homogeneous, without lumps, air bubbles, and stratification. The mixing of the cement is therefore a critical aspect; product drums cannot be comprehensively tested once filled, so uniformity of the mixture will need to be demonstrated with surrogates following a specific protocol that will be implemented for the final product formation. This will require pre-batching of the ingredients.
c) The ability to tolerate operational disruptions such as loss of power is necessary; this places restrictions on the operational temperature, the mixing speed, and the open time of the cement mixture.
d) The operation must minimize the need for proximity to the radioactive uranium material

The process of mixing, curing, and closure of the drums will be developed with these considerations in mind.

8. DETERMINATION OF FINAL WASTE FORM COMPOSITION

What remained to be determined for the final waste form was the cement matrix composition. Lacking a waste acceptance criterion for the final repository, the Russian standards for final disposal waste form performance were taken as a reasonable goal. These include standards for curing time, volume change during curing, water separation, compressive strength, leachability, frost resistance, and moisture resistance.

Preparation of a formula for the cement matrix composition is a multivariate problem. The matrix is a mixture composed of water, cement, and supplementary materials (in lieu of aggregate). The variables include the particle size distribution for the dry waste, cement, and supplemental materials; the choice of supplemental materials (in this case fly ash or blast furnace slag); the ratio of supplemental materials to cement; and the water/cement ratio.

In order to determine the matrix composition, a comprehensive program was established to optimize the performance of the waste form given the many variables. Comparisons of sample compositions involving simultaneous variation of several parameters will be required to determine the optimum mixture as well as the sequence of addition and is expected to require hundreds of samples to be produced. Results of the effort will be discussed in a future paper.

The concentration of uranium in the final product was set reasonably close to the level of concentration that may qualify the final waste form for termination of IAEA safeguards. Termination of safeguards is not a “by the numbers” goal, but also includes the issue of “irrecoverability” as well as other factors. Representatives of the IAEA safeguards department participated in discussions on matrix composition and process development as well and will determine the appropriate course of action once the final process and waste form have been established.

9. CONCLUSION

Disposition of a complex fuel form has been investigated and a path forward has been identified to develop both a waste form that meets performance objectives and a method to package the waste form in an appropriate container. The project is expected to result in production of a waste form that is suitable for final disposition and may qualify for termination of safeguards.

The authors wish to express their sincere gratitude to the experts from Sellafield Ltd. who supported this work by providing valuable expertise for development of the optimized waste form and process.

1. REFERENCES

1. N.V. Gorin, et.al. “Review of Research Results for IGR Impulse Graphite Reactor,” // News of Chelyabinsk scientific center: electron. science-tech. period. – issue 1(22). – 2004 – URL:http://csc.ac.ru/news/2004_1/2004_1_3_1.zip, 2018.
2. V. Baklanov, et al, “Measurement of radiation power of IGR reactor irradiated nuclear fuel and analysis of SNF radionuclide composition” Report on task 3.1.4, “Preparatory work at NNC RK for IGR reactor HEU fuel dilution,” under contract #00173040, Kurchatov Kazakhstan, 2017.
3. V. Baklanov, et al, “NNC Preparations for IGR Fuel Down-blending,” Report on task 3.1.3, “Feasibility Study on the Preparation of the NNC for Down-Blending the IGR Reactor Fuel,” under Contract #00173040, Kurchatov Kazakhstan, 2017.
4. International Atomic Energy Agency, “Characterization, Treatment and Conditioning of Radioactive Graphite from Decommissioning of Nuclear Reactors,” IAEA-TECDOC-1051, IAEA, Vienna, 2006.
5. V. Baklanov, et al, “Preparations of NNC RK for IGR Reactor HEU Fuel Down-blending Process,” SOW-14709, “Analysis of Technical Feasibility for IGR Reactor Irradiated Fuel Down-Blending,” Report 05-00187855, Kurchatov Kazakhstan, 2018.
6. K. Bateman, I. Bolshinsky, E. Batyrbekov, et al., “Immobilization of HEU Graphite Fuel in Kazakhstan,” Proceedings of the Institute of Nuclear Materials Management, 2020.

IMAGE ANALYSIS OF FUEL MEAT MICROSTRUCTURES IN PLATES FROM EMPIRE EXPERIMENT

Z.G. MEI, B. YE, G.L. HOFMAN, Y.S. KIM, L.M. JAMISON, A.M. YACOUT
Argonne National Laboratory, 9700 South Cass Avenue, Lemont, IL 60439, USA

W.A. HANSON, A.B. ROBINSON, D.D. KEISER JR.
Idaho National Laboratory, 1955 North Fremont Avenue, Idaho Falls, ID 83415, USA

ABSTRACT

As a part of destructive examination of the European Mini-Plate Irradiation Experiment (EMPIrE), machine-learning (ML) based image analysis approaches were developed to obtain quantitative information from both fresh and irradiated EMPIrE fuel plates. In this study, ML-based image analysis was applied to measure the volume fraction of fuel meat constituent and fuel particle size distributions from high-resolution optical microscopy of EMPIrE plates. As a verification, the volume fraction of interaction layer (IL) and fuel particle size measured with the automated image analysis compare well with those measured manually. The volume fractions of the fuel meat constituents, including fuel particles, IL, Al matrix and pores, were carefully measured for a set of EMPIrE plates. Additionally, the effect of image location selection on the measurement was studied. The quantitative information will be used to understand the complex fuel irradiation behavior and to support fuel performance evaluations in the future.

1. Introduction

U-Mo dispersion fuels, with U-Mo alloy particles dispersed in an Al matrix, are under investigation as a potential fuel type for the conversion of highly enriched uranium (HEU) fuels currently used for high performance research reactors to low-enriched uranium (LEU). Experiments show that an amorphous interaction layer (IL) forms between U-Mo fuel particles and Al matrix during the fuel fabrication processes and subsequent irradiation [1]. ILs have detrimental effects on the U-Mo fuel performance, such as reducing the thermal conductivity and mechanical stability of fuel meat [1]. Diffusion barrier materials, such as ZrN [2], have been applied to fuel particle surface in order to suppress the formation of IL. Post-irradiation examination (PIE) confirm that such diffusion barriers can effectively reduce the formation of ILs and, therefore, delay the onset of accelerated fuel plate swelling [3]. The European Mini-Plate Irradiation Experiment (EMPIrE) was designed to support the development of ZrN-coated U-Mo dispersion fuels. The focus of the EMPIrE test was to investigate the impacts of various fabrication parameters and irradiation conditions on the performance of coated U-Mo/Al dispersion fuels at relatively high-power conditions. Recently, the non-destructive (ND) PIE of the EMPIrE plates has been completed, and the fuel swelling behavior and overall performance was evaluated using a local fuel swelling analysis as determined through post-irradiation mini-plate profilometry [4]. As was discussed in Ref. [4], destructive examination (DE) results are required to fully assess the effects of the fabrication variables on fuel swelling behavior.

Currently, the optical microscopy (OM) characterization of 15 EMPIrE plates has been completed. To allow the comparison of fuel performance across different plates based on OM results, it is important to collect quantitative microstructure information to evaluate the effects of various variables. Compared to scanning electron microscopy (SEM) images, OM images are usually more challenging for image analysis, because of uneven illumination and color shifting during image acquisition. Thresholding-based image segmentation methods, such as Otsu's algorithm [5], works well for SEM images [6-8] but are not effective for OM images. The manual point counting method (ASTM E562 [9]) therefore remains the most favorable approach for quantitative analysis of OM images of irradiated fuels. However, the manual point counting method is time-consuming, labor-intensive, and subject to the analyst's bias. Therefore, it is difficult to apply the point counting method to process a large quantity of images.

Considering the specific challenges for processing OM images and the large volume of data, it is necessary to develop an effective and reliable tool to automate the extraction of quantitative information efficiently, such as fuel meat constituent volume fractions, particle size distributions, etc. Recent development of machine learning (ML) and computer vision (CV) made it possible to automatically detect various irregular features, such as animals, humans, and vehicles from complex images. In comparison to the traditional image analysis techniques, ML-based image analysis utilizes more complex image features, e.g., Gaussian blur, Sobel filter and difference of Gaussian, and can produce pixel-based segmentations of complex images. In this study, we will apply different image processing techniques, including those based on ML, to analyze high-resolution EMPIrE OM images.

2. Methods

Both manual and automated measurements of fuel particle size distribution and fuel meat constituent volume fractions were performed and compared. A typical workflow for automated image processing usually includes the following steps:

1) Pre-processing of raw images: the purpose of pre-processing is to remove any image noise or artifacts and improve the overall contrast. Several filters have been developed to remove different kinds of noise and defects. For examples, non-local means denoising filter can effectively reduce random noise while preserving textures and edges [10]. For images with uneven illumination, shading correction, such as ball rolling, is crucial for thresholding-based image segmentation.
2) Segmentation: the purpose of image segmentation is to partition a digital image into multiple segments and simplify the representation of the image for easy analysis. Various segmentation methods have been developed for different applications. The commonly used methods include histogram-based thresholding method (e.g., Otsu's method) and Machine Learning based method (e.g., Random Forest classifier [11]).
3) Post-processing: the purpose of post-processing is to remove any artifacts or noise generated from image segmentation using morphological operations, and then measure the regional properties from segmented images. Quantitative information of fuel microstructure, such as volume fraction of fuel constituents, can be obtained.
4) Verification and validation: this is a very important step to verify and validate the results from digital image processing. The manual counting results can be used to adjust the image processing parameters for automated image processing.

Among the four steps, the most challenging and important step for digital image analysis is image segmentation, which determines the quality of image analysis results. There are numerous software available for digital image processing, e.g., MATLAB®, ImageJ, scikit-image, OpenCV, etc. In this work, we selected ImageJ [12] and ilastik [13] for the analysis.

3. Results and discussion

3.1. Fuel particle size distribution in fresh EMPIrE plates

In this study, the OM images with 200 times (200×) magnification taken from archive fresh fuel EMPIrE plates were used to measure fuel particle size distribution using both manual point counting and automated image analysis approaches. For manual measurement, fuel particle size was estimated by measuring the lengths of the major (d_{major}) and minor (d_{minor}) axes of each fuel particle (see examples in Fig. 1(a)) and calculated as (1) the arithmetic mean of the major and minor axes, $d = (d_{major} + d_{minor})/2$; or (2) the geometric mean, $d = \sqrt{d_{major} d_{minor}}$. Due to the imperfect circular shape, the average size of the fuel particles shown in Figure 1 is estimated to be 50.2 μm and 49.8 μm using the arithmetic and geometric means, respectively.

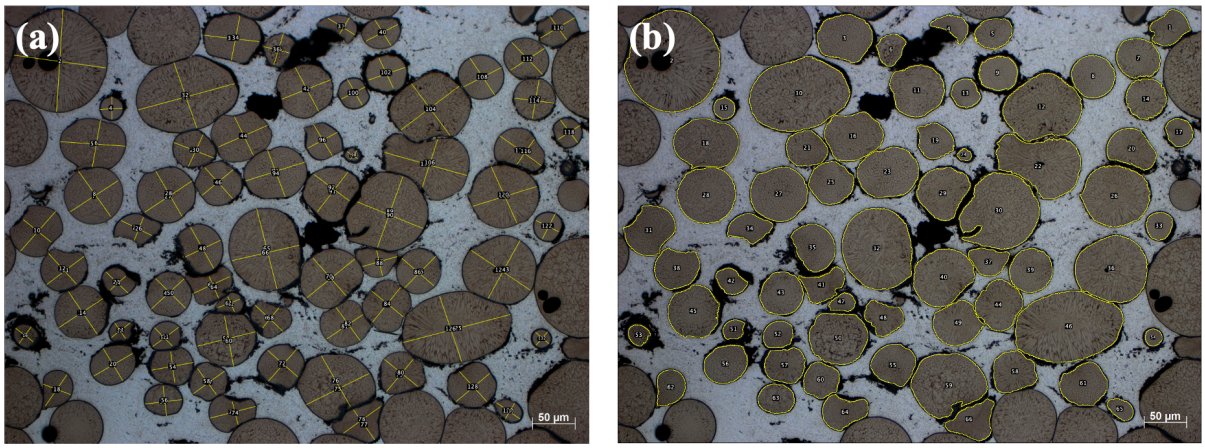

Figure 1. 200× magnification OM image of backup EMPIrE fresh fuel plate EMPI0613. (a) Particle size measured manually from the major and minor axes of fuel particles; (b) Particle size measured from the area of each particle using automated image analysis.

Fuel particle size was also analyzed using an automated image analysis approach. The general procedure for ML-based semantic segmentation of fuel particle in fresh fuel plates is as follows.

1. Select training features for Random Forest-based ML classifiers.
2. Add annotations for fuel particle and background which were used as ground truth for ML training.
3. Train ML classifiers based on annotations.
4. Create segmented binary image by making predictions for each pixel.
5. Perform watershed to separate the contacted fuel particles.
6. Verify the segmentation results by virtual examination.
7. Measure the area and morphology of the fuel particles.

As an example, Fig. 1(b) shows the identified fuel particles with the predicted edges overlayed on the original image. The size of each fuel particle was calculated from the measured particle area, i.e., $= 2\sqrt{S/\pi}$, where S is the area of a fuel particle. The average particle size in Fig. 1 is estimated to be 51.6 μm, which is close to the results estimated from the manual measurement. Additionally, we evaluated the particle morphology by calculating the particle aspect ratio (AR) as d_{major}/d_{minor}. The average aspect ratio of the fuel particles shown in Fig. 1 is estimated to be 1.23, indicating that the shapes of fuel particles deviate from the perfect circular shape. For archive fresh fuel plates, ten 200× OM images for plates EMPI0613, EMPI0715 and EMPI0811,

seven 200× OM images for plates EMPI0516, EMPI0703, EMPI0817 and EMPI2203, four 200× OM images for plate EMPI0104 and five 200× OM images for plate EMPI0115 were used for the fuel particle size measurement. Table 1 summarizes the average fuel particle size (d_{2D}) and aspect ratio (AR) for nine fresh EMPIrE fuel plate measured using the available 200× OM images. As shown in Table 1, the average aspect ratio deviated from 1 due to the deformation of the fuel particles during the fuel plate fabrication processes. The different average particle sizes between different plates might be ascribed to (1) differences in the content of fine fuel particles (< 44 μm in diameter), where zero, 10%, and 25% fines containing plates were fabricated; and (2) the particle size measurement was made at one cross-section of the plate, so the result has uncertainty due to the heterogeneous fuel loading, which explains the differences between the plates with the same nominal particle size distribution.

Table 1. Average measured 2D particle size (d_{2D}), converted 3D particle size (d_{3D}), and aspect ratio (AR)

Plate ID	Percentage of fines	$d_{2D}\ (um)$	$d_{3D}(um)$	AR_{avg}
EMPI0613	0%	57.36	66.96	1.13
EMPI0715	10%	48.10	55.03	1.16
EMPI0811	10%	45.92	52.26	1.20
EMPI0516	0%	48.04	54.13	1.16
EMPI0703	0%	52.68	63.60	1.16
EMPI2203	0%	49.75	60.52	1.17
EMPI0817	0%	47.80	57.26	1.22
EMPI0104	25%	38.29	45.21	1.15
EMPI0115	25%	44.40	52.29	1.16

To gain more insight into the fuel particle morphology, we plotted the particle size distribution and particle aspect ratio distribution in Figs. 2 and 3, respectively. As shown in Fig. 2, although the average fuel particle sizes for plates EMPI0715 and EMPI0516 are very similar, the particle size distributions for these two plates are different. Similarly, plates EMPI0715, EMPI0516, EMPI0703 and EMPI0115 exhibit different particle aspect ratio distributions although their average aspect ratios are the same, as shown in Table 1.

It should be noted that the fuel particle size directly measured from 2D cross-section OM image is not the true particle size. Since the cross-section rarely cut through the equatorial plane of fuel particles, the particle size measured from 2D cross-section is always lower than the true value. To obtain a more realistic particle size distribution, the Schwartz-Saltykov method [14] has been widely used to estimate the 3D particle size distribution from the 2D measurement. In this work, the Schwartz-Saltykov method implemented in MATLAB® by Salvato [15] was utilized to convert the measured 2D particle size distributions to 3D values. After the conversion, the average 3D particle sizes of the fresh EMPIrE plates were estimated. As expected, the 3D particle sizes are notably larger than the 2D measurements. However, the currently estimated 3D particle sizes are still smaller than the targeted average particle size of 80 μm [4]. The causes of the discrepancy could be the uncertainties in the conversion of 3D size distribution from 2D data. Further investigation on the uncertainties is needed. The average 3D particle size distributions were used in the EMPIrE swelling analysis in Ref. [4].

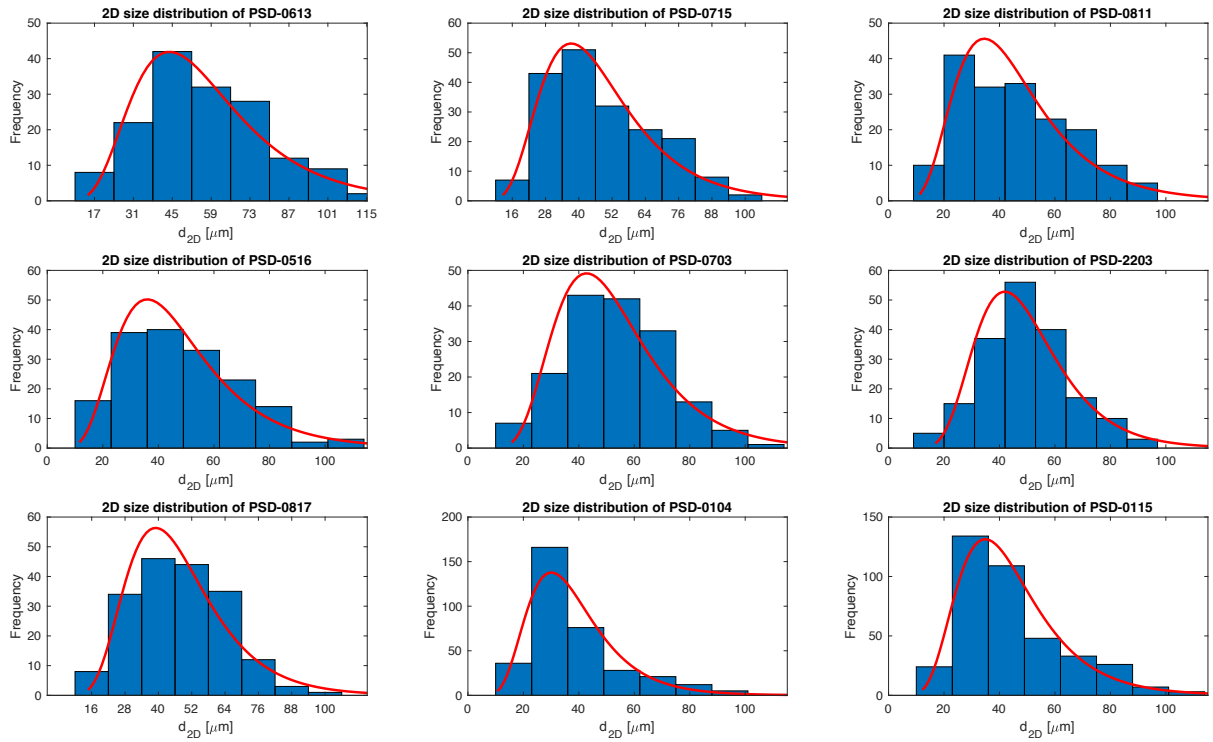

Figure 2. Fuel particle size distributions in nine backup EMPIrE fresh fuel plates with log-normal fit.

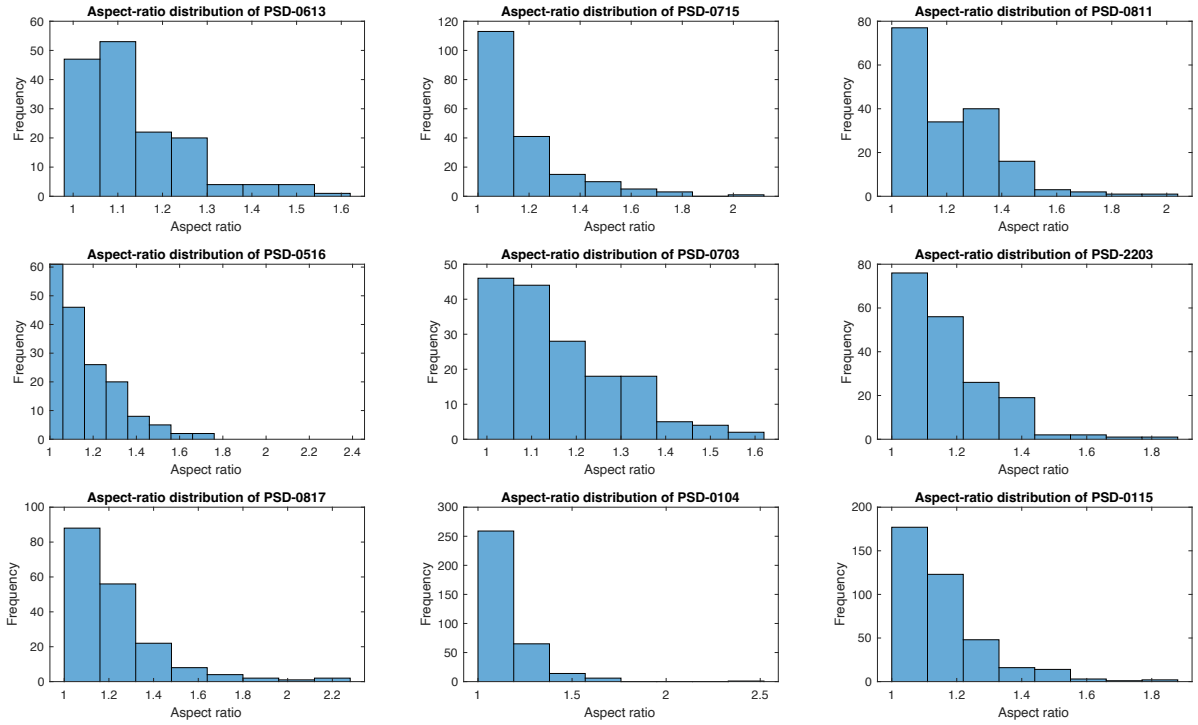

Figure 3. Particle size aspect ratio distributions of the nine backup EMPIrE fresh fuel plates.

3.2. Volume fractions of fuel meat constituents in irradiated EMPIrE plates

Fuel meat constituent volume fraction measurement has been completed for 8 EMPIrE plates, and the measurement for the remaining, already OM characterized, 7 plates is ongoing. For measuring fuel meat constituent volume fractions in irradiated EMPIrE plates, three OM images in the center region of the characterized cross-section were measured. Among the three measured OM images, one was a 500 times (500×) magnification montage of the fuel zone center, and the other two are cropped from the 100 times (100×) magnification whole cross-section montage, because only one 500× magnification OM was provided for the center region. As an example, Figure 4 show the locations of the selected images for measurement on the 100× magnification montage of the cross-section for plate EMPI0109.

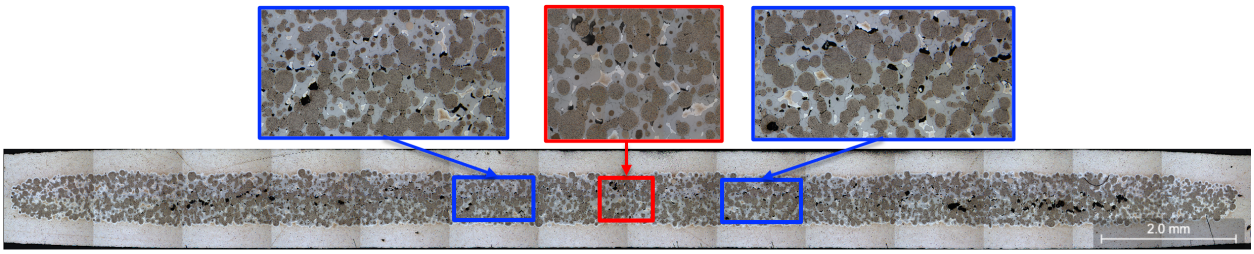

Figure 4. Optical microscopy of the center cross-section of plate EMPI0109. The areas highlighted in red are the location where the 500× magnification OM montage was taken, and the areas highlighted in blues are for the cropped 100× magnification OMs.

The procedure of the volume fraction measurement using ML based image segmentation is similar to the measurement of fuel particle size discussed in section 3.1, except that the IL, matrix and pore of fuel meat were treated as different phases here while treated as a background in section 3.1. Schematic examples of the steps used in the procedure can be found in Figure 5.

1. Select training features, e.g., Gaussian blur, Difference of gaussians filters.
2. Add annotations for each constituent of the fuel meat.
3. Training the classifiers to get semantic segmentation results.
4. Convert the segmented image to an 8-bit grey image.
5. Create selections for each phase using auto threshold method.
6. Modify the selections by virtual examination.
7. Measure the area and calculate the volume fraction of each phase

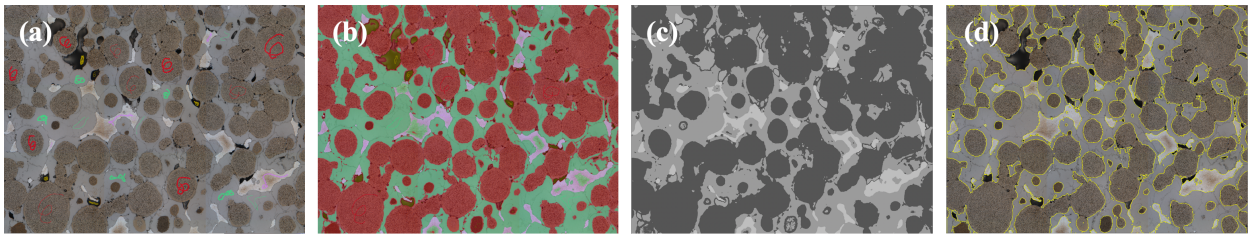

Figure 5. Examples (a-d) showing the results of the sequence steps of (2), (3), (4) and (6), respectively, used for the measurement of the volume fractions of fuel meat constituents in the center region of plate EMPI0109.

IL is the most challenging feature to be determined in automated image analysis because of its irregularity. The volume fractions of the IL measured using manual point count or ML-based image analysis approaches were first compared to test the accuracy of the ML-based image analysis tool. As shown in Table 2, the overall agreement of the IL volume fraction measured by these two approaches is good. The differences should be close to the uncertainty of the manual point count

measurement by different operators. The only exception is for plate EMPI0712. The large differences might be due to the different magnifications of OM images used for analysis. Additional measurement using the same images is ongoing for verification purposes.

Table 2. Comparison of the volume fractions of IL measured with image analysis and manual point count.

Plate ID	ML-based image analysis	Manual point count
EMPI0702	22.7%	22.5%
EMPI0712	10.4%	3.5%
EMPI0818	4.6%	3.5%
EMPI0820	2.6%	2.5%
EMPI0821	6.8%	6.0%

The measured volume fractions of the fuel meat constituents are summarized in Table 3. Generally, the plates with a higher IL volume fraction correspond to lower volume fractions of fuel particle and matrix, because IL formation resulted from the consumption of fuel particles and Al matrix. IL volume fraction is not only a function of fission density but also greatly impact by coating conditions (coating thickness and coverage). For instance, plate EMPI0820 has the lowest IL volume fraction although its fission density is relatively high. On the contrary, plates EMPI0117 and EMPI0109 have similar fission densities as that of EMPI0820 but have much higher IL volume fractions. This is probably because EMPI0820 has thicker coating than the other two plates, i.e., 2.02 μm vs 0.5 μm.

For plate EMPI0905, some areas show different textures from the four regular constituents (i.e., fuel particles, IL, matrix and pore) of the fuel meat. These undetermined areas were labeled as "new phase" and will be further characterized with SEM.

To examine whether there is a location dependence of fuel meat microstructure evolution, the volume fractions of each constituent as a function of distance from the left meat end were measured across the plate width for plate EMPI0109. The results are summarized in Figure 6 and Table 4. As shown in Figure 6, the volume fractions of fuel, IL, and matrix are almost flat in the center region of the cross-section, i.e., between 4 mm and 12 mm from left meat end. At the both ends of the fuel meat zone, the volume fractions of Al matrix are higher because of lower fuel loading in these areas. Meanwhile, the average volume fractions of fuel meat constituents for plate EMPI0109 were measured from the whole cross-section montage. In Table 4, the volume fractions measured from the whole cross-section montage are compared with the data measured from the center region. Only slight differences were observed, indicating that microstructure evolution across the plate width direction is quite consistent.

Table 3. Volume fractions of fuel meat constituents measured from three locations in the center region of cross-section.

Plate ID	Fission Density (fission/cm^3)	Fuel	IL	Matrix	Pore	New phase
EMPI0109	5.90×10^{21}	55.3%	37.8%	4.8%	2.1%	
EMPI0117	4.21×10^{21}	42.9%	48.6%	7.6%	0.9%	
EMPI0512	5.83×10^{21}	54.7%	29.8%	12.7%	2.8%	
EMPI0820	5.16×10^{21}	62.4%	2.6%	34.7%	0.3%	
EMPI0905	6.10×10^{21}	56.3%	18.5%	19.4%	1.2%	3.8%
EMPI2003	2.79×10^{21}	50.9%	21.2%	26.5%	1.0%	

EMPI2007	5.11×10^{21}	54.3%	34.8%	10.9%	0.0%
EMPJ2207	5.19×10^{21}	59.0%	28.2%	17.3%	0.0%

Table 4. Comparison of the volume fractions of fuel meat constituents in plate EMPI0109 measured from the center region or the entire cross-section.

Measured regions	Fuel	IL	Matrix	Pore
Center region	55.3%	37.8%	4.8%	2.1%
Entire cross-section	50.6%	40.0%	6.5%	2.9%

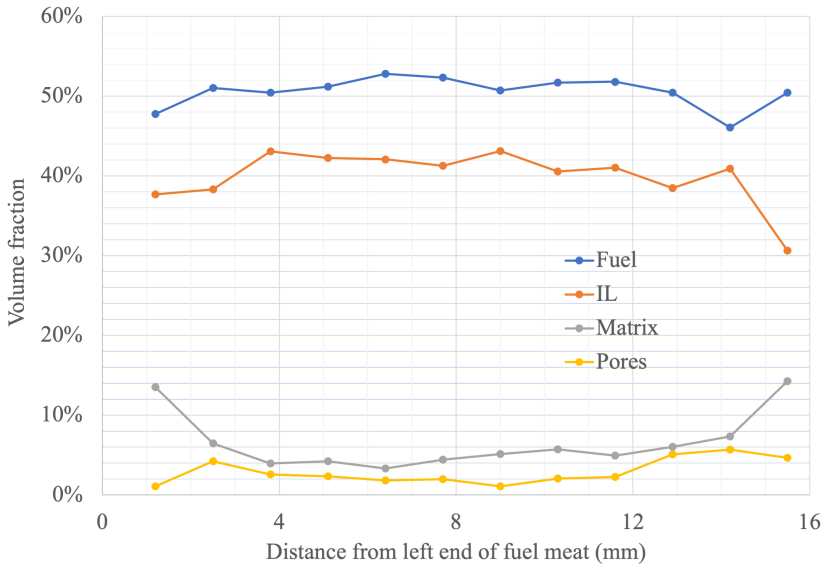

Figure 6. Measured volume fractions of fuel meat constituents across the entire width direction of plate EMPI0109.

3.3. Porosity in irradiated EMPIrE plates

The results in Figure 6 show that in plate EMPI0109, fuel meat porosity is not evenly distributed along the transverse direction of the cross-section. To evaluate the peak porosity in the irradiated EMPIrE plates, two locations showing the highest porosity in the whole cross-section montage were selected for porosity measurement for each plate. An example of the area selection is shown in Fig. 7. The images cropped for peak porosity measurement cover the entire thickness of the fuel meat zone. Meanwhile, the average porosity was evaluated using the entire fuel meat zone in the cross-section.

Figure 7. Cross-section montage of plate EMPI0109 showing the locations for the peak porosity measurement highlighted in blue.

The global and local threshold methods were used to the segmentation of pores from the OM images of fuel meat. The procedure for the porosity measurement is as follows.

1. Crop images from the cross-section montage with the highest porosity or the whole fuel meat zone.
2. Convert images to 8-bit grey images.
3. Segment pores using global threshold method, e.g. Intermodes algorithm.
4. Create selections from threshold result.
5. Modify the selections by virtual examination.
6. Measure the total pore area and calculate the peak or average porosity.

Table 5 summarizes the measured peak and average porosity in PIE of eight EMPIrE plates. Among the eight plates, EMPI0109 shows both the highest peak porosity and the highest average porosity. For the rest of the plates, high peak porosity do not necessarily correspond to high average porosity, e.g., EMPI0512. Because pore formation is highly dependent on local microstructure, which can vary substantially within the fuel meat, for example due to local IL formation. Note that no tears were observed in EMPIrE plates, which were shown in the SELENIUM plate containing ZrN-coated U-Mo powder [16].

Table 5. Measured peak and average porosity in irradiated EMPIrE plates together with the volume fraction of IL.

Plate ID	Fission Density (fission/cm^3)	Peak porosity	Average porosity	Vol. frac. of IL
EMPI0109	5.90×10^{21}	8.5%	2.9%	37.8%
EMPI0117	4.21×10^{21}	4.0%	1.2%	48.6%
EMPI0512	5.83×10^{21}	5.8%	0.9%	29.8%
EMPI0820	5.16×10^{21}	0.3%	0.1%	2.6%
EMPI0905	6.10×10^{21}	2.5%	0.8%	18.5%
EMPI2003	2.79×10^{21}	5.4%	1.5%	21.2%
EMPI2007	5.11×10^{21}	2.4%	0.2%	34.8%
EMPI2207	5.19×10^{21}	0.7%	0.1%	28.2%

4. Summary

ML-based image analysis was applied to quantify microstructure information in EMPIrE OM images. Fuel particle morphology was measured in nine fresh archive EMPIrE plates, including size distributions and aspect ratio. The aspect ratio of fuel particles shows that most fuel particles deformed during fuel plate fabrication processes. The particle size distributions measured from 2D images were converted to 3D size distributions using the Schwartz-Saltykov method.

Fuel meat constituent volume fractions of irradiated EMPIrE plates, including fuel, IL, Al matrix and pore, were measured on high-resolution OM images using the ML-based image analysis tool. The results show that IL volume fraction is not a simple function of fission density but greatly impacted by coating conditions (coating thickness and coverage). The plates with thicker coating developed noticeably less ILs. Additionally, the fuel meat constituent volume fractions measured as a function of location in plate EMPI0109 show that microstructure evolution across the plate width direction is quite consistent except for the end regions, where the initial fuel loading was lower. The measured peak vs. average porosities in the irradiated EMPIrE plates indicate that pore formation is highly dependent on local microstructure, e.g. IL formation, and high peak

porosity do not necessarily correlate with high average porosity. No tears were observed in EMPIrE plates.

As a verification, the average particle sizes in fresh fuel plates and IL volume fractions in irradiated plates were measured manually. The comparison of manual and automated image analysis results shows a good agreement between the two approaches, demonstrating the accuracy of the ML-based image analysis tool and the validity of its application to OM images with greatly improved efficiency.

7. Acknowledgments

This work is sponsored by the U.S. Department of Energy, National Nuclear Security Administration (NNSA), Office of Material Management and Minimization (NA-23) Reactor Conversion Program. The material is also based upon work supported by the U.S. Department of Energy, Office of Science, under Contract DE-AC02-06CH11357. Authors also gratefully acknowledge Dr. Daniele Salvato from Idaho National Laboratory for sharing his MATLAB codes for the analysis of fuel particle size distribution.

8. References

[1] Y.S. Kim, Yeon Soo Kim, Uranium Intermetallic Fuels (U–Al, U–Si, U–Mo). In: Konings R.J.M., (ed.) Comprehensive Nuclear Materials, volume 3, pp. 391-422 Amsterdam: Elsevier, 2012, 2012.
[2] A. Leenaers, S. Van den Berghe, C. Detavernier, Surface engineering of low enriched uranium–molybdenum, Journal of Nuclear Materials 440(1–3) (2013) 220-228.
[3] A. Leenaers, Surface-engineered low-enriched Uranium-Molybdenum fuel for research reactors, University of Ghent-SCK•CEN, 2014.
[4] W.A. Hanson, A.B. Robinson, N.J. Lybeck, J.W. Nielsen, B. Ye, Z.-G. Mei, D.D. Keiser, L.M. Jamison, G.L. Hofman, A.M. Yacout, A. Leenaers, B. Stepnik, I.Y. Glagolenko, Non-destructive analysis of swelling in the EMPIrE fuel test, Journal of Nuclear Materials 564 (2022) 153683.
[5] N. Otsu, A Threshold Selection Method from Gray-Level Histograms, IEEE Transactions on Systems, Man, and Cybernetics 9(1) (1979) 62-66.
[6] R. Collette, J. King, C. Buesch, D.D. Keiser, W. Williams, B.D. Miller, J. Schulthess, Analysis of irradiated U-7wt%Mo dispersion fuel microstructures using automated image processing, Journal of Nuclear Materials 475 (2016) 94-104.
[7] D. Salvato, A. Leenaers, S. Van den Berghe, C. Detavernier, Pore pressure estimation in irradiated UMo, Journal of Nuclear Materials 510 (2018) 472-483.
[8] C.A. Smith, D.D. Keiser, B.D. Miller, A. Aitkaliyeva, Comparison of manual and automated image analysis techniques for characterization of fission gas pores in irradiated U-Mo fuels, Micron 119 (2019) 98-108.
[9] ASTM, Standard test method for determining volume fraction by systematic manual point count, 2019.
[10] A. Buades, B. Coll, J. Morel, A non-local algorithm for image denoising, 2005 IEEE Computer Society Conference on Computer Vision and Pattern Recognition (CVPR'05), 2005, pp. 60-65 vol. 2.
[11] I. Arganda-Carreras, V. Kaynig, C. Rueden, K.W. Eliceiri, J. Schindelin, A. Cardona, H. Sebastian Seung, Trainable Weka Segmentation: a machine learning tool for microscopy pixel classification, Bioinformatics 33(15) (2017) 2424-2426.
[12] C.A. Schneider, W.S. Rasband, K.W. Eliceiri, NIH Image to ImageJ: 25 years of image analysis, Nature Methods 9(7) (2012) 671-5.

[13] S. Berg, D. Kutra, T. Kroeger, C.N. Straehle, B.X. Kausler, C. Haubold, M. Schiegg, J. Ales, T. Beier, M. Rudy, K. Eren, J.I. Cervantes, B. Xu, F. Beuttenmueller, A. Wolny, C. Zhang, U. Koethe, F.A. Hamprecht, A. Kreshuk, ilastik: interactive machine learning for (bio)image analysis, Nature Methods 16(12) (2019) 1226-1232.
[14] J. Takahashi, H. Suito, Evaluation of the accuracy of the three-dimensional size distribution estimated from the schwartz-saltykov method, Metallurgical and Materials Transactions A 34(1) (2003) 171-181.
[15] D. Salvato, Idaho National Laboratory, 2022, personal communications.
[16] A. Leenaers, Y. Parthoens, G. Cornelis, V. Kuzminov, E. Koonen, S. Van den Berghe, B. Ye, G.L. Hofman, J. Schulthess, Effect of fission rate on the microstructure of coated UMo dispersion fuel, Journal of Nuclear Materials 494 (2017) 10-19.

CENTER FOR NUCLEAR TECHNOLOGY RESEARCH AND DEVELOPMENT IN BOLIVIA: PROJECT STATUS

Y.O. DAYRONAS, R.P. KUATBEKOV
RR and CNST technical expertise department, Rusatom Overseas JSC
Leninskaya Sloboda str. 26 b. 2, 115280, Moscow – Russian Federation

ABSTRACT

Center for Nuclear Technology Research and Development (CNTRD) in El Alto (Bolivia) is an innovative project based on the advanced nuclear technologies for the needs of healthcare, agriculture, industry and science.
The CNTRD meets the needs of the Bolivia and is in harmony with the State's scientific program. The CNTRD with a 200 kW research reactor is constructed for ABEN (the Bolivian Nuclear Energy Agency) by the State Atomic Energy Corporation ROSATOM. The facilities of Construction stages 1 and 2 are currently being built at a high pace while the CNTRD's site landscaping works are underway.
The Center´s project is unique for the whole nuclear industry: it is located at 4000 meters above sea level and is currently the highest nuclear facility in the world. All engineering challenges associated with the mountain location of the CNTRD have been resolved in the design, such as seismicity and high altitude (low atmospheric pressure). Project implementation will greatly contribute to the development of science, education, medicine and agriculture in Bolivia.
This paper will give an overview of a current construction status and perspectives of project development.

1. Introduction

The project for the construction of the Center for Nuclear Technology Research and Development in the Plurinational State of Bolivia is being implemented as part of the Intergovernmental Agreement dated March 6, 2016, and in accordance with the general contract signed in September 2017 on the sidelines of the 61st IAEA General Conference in Vienna.

The CNTRD (Layout of the CNTRD is shown in Figure 1) is subdivided into three zones:

- Administrative zone which includes the following main facilities:
  - Cyclotron-Radiopharmacy-Preclinics Complex (CRPC);
  - Training center (which includes research reactor control console model and multipurpose computing center);
  - Administrative common facilities.
- Production zone which includes the following main facilities:
  - Multipurpose Irradiation Center (MIC);
  - Radiobiology and radioecology laboratory;
  - Plasma laboratory.
- Technological zone which includes the following main facilities:
  - Reactor complex which includes:
    Nuclear Research Facility (NRF) with Research Reactor (RR); RR-related services and laboratories (neutron calculations laboratory, thermal-hydraulic calculations laboratory etc.); Neutron activation analysis laboratory; Radioisotope laboratory.
  - Engineering and technological complex (which includes, inter alia, a radioactive waste storage facility and radioactive waste management facility).

CNTRD is being constructed in four stages. The stages and objects to be constructed in the respective stages are described in the Table 1 below.

Stage	Constructed objects
1st stage:	CRPC;
2nd stage:	MIC, part of the administrative zone and part of the production zone;
3rd stage:	Remaining objects of the production zone: plasma laboratory, radiobiology and radioecology laboratory;
4th stage:	Technological zone (RR zone), rest of the objects of the administrative zone.

Tab 1: The CNTRD construction stages

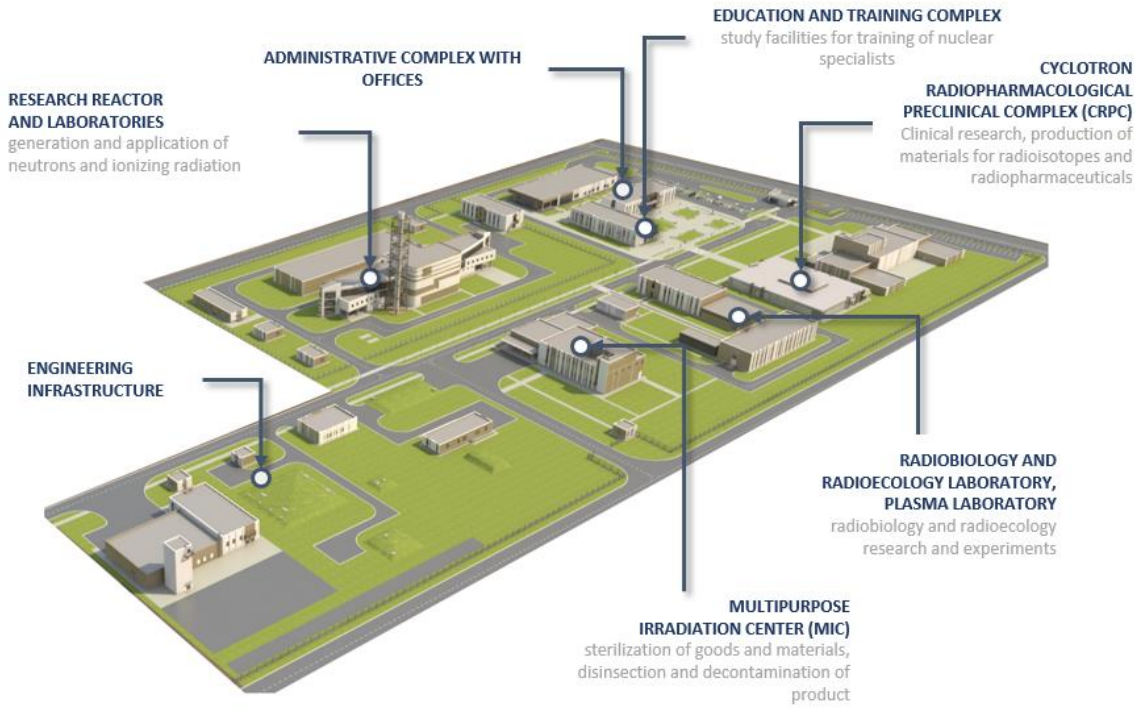

Fig.1 – The CNTRD layout

Currently, all construction works of the 1st and 2nd phases have been completed and the construction works of the 3rd and 4th phases are well underway.
All construction and commissioning of the CNTRD is scheduled for completion in 2024.
As part of the implementation of the EPC-contract for CNTRD construction, an extensive program of training for Bolivian students in leading universities specializing in nuclear science and technology in Russian Federation (Tomsk Polytechnic University, National Research Nuclear University MEPHI) is underway.
University training has now been completed for the personnel who will operate the MIC and the CRPC.

2. Cyclotron-Radiopharmacy-Preclinics Complex

CRPC is an integrated facility for the production of radioisotopes for medical purposes at an on-site cyclotron as well as for the synthesis of radiopharmaceuticals (RPh).
The key facility of the CRPC is a 24 MeV cyclotron equipped with five targeting complexes. Moreover, the complex includes 18 hot cells equipped with all required tools for production of radioisotope products and RPh. The complex has incorporated the best components from those presented in the world market today.

CRPC, constructed in Bolivia, allows production of a wide range of RPh. The facility is designed to produce more than 10 medical isotopes in three aggregate states, including ^{18}F, ^{99m}Tc, $^{123/124}I$, ^{68}Ga, ^{64}Cu, ^{89}Zr, ^{11}C.

Cyclotron complex makes it possible to provide medical centres that are available in Bolivia with their own RPh for conduction of high-quality clinical examinations of up to 5,000 patients annually.
In December 2021, the first batch of FDG-^{18}F was synthesised and tested as part of the CPRC commissioning [1].

3. Multipurpose Irradiation Center (MIC)

MIC includes Laboratory Gamma-Ray Plant (LGRP) and Industrial Gamma-Ray Plant (IGRP). MIC equipment (manufactured by ROSATOM) is aimed for research and industrial applications of ionizing radiation.
The heart of the Industrial Gamma-Ray Plant is a ^{60}Co-based gamma radiation source with a start loadable activity of 100,000 Ci. MIC design and IGPR design provides for the possibility of increasing of source maximum activity of up to 1 million Ci.

LGRP incorporates a lower activity source (12 kCi). LGRP is fully automated and enables studying the effects of radiation on biological objects, quality control and monitoring of production processes to improve their efficiency as well as the development of new production protocols for IGPR. LGRP operates, among other things, as part of the scientific program of the radiobiology and radioecology laboratory.
IGRP is designed to address the following areas:

- Food processing, which consists in the gamma sterilisation of products, by effectively reducing the number of micro-organisms and insects (in their various stages of metamorphosis) contained in the processed products, reducing their volume;
- Sterilisation of medical devices - an area that has come to the forefront due to the epidemiological situation in the country and around the world;
- Preservation of cultural heritage items;
- IGRP can be used to produce polymeric materials by 'cross-linking' them under the influence of gamma rays.

According to the time of irradiation at the IGRP and the depth of gamma radiation penetration, goods treated at the MIC can be divided into three main groups:

- Fruits, vegetables and root vegetables.

In Bolivia, the production of fruits and vegetables is highly developed, the export of which is hampered by spoilage due to the lack of preservation technologies and which could be preserved with the use of IGRP. First of all, these are bananas, including sweet bananas for frying, as well as peaches, tangerines, oranges, pineapples. If we talk about root crops that are produced in Bolivia and that need to be processed to increase the shelf life and suppress germination, then this is, first of all, potatoes.

- Dry foods, spices and meat.

Dry products that are produced in large quantities, which can be irradiated and exported, include primarily oregano, sunflower seeds, cocoa beans, and quinoa. Also, this group includes fresh, chilled or frozen meat.

- Medical devices and materials, cultural values.

These group includes syringes, catheters, droppers, surgical and laboratory materials and equipment, implants and pharmaceutical products. Cultural heritage items that can be preserved by decontamination performed in the IGRP, such as historical documents, antiques and other cultural artefacts.

For the above groups of products, the initial loading of radiation sources into the IGRP (100 kCi) provides the following IGRP production capacity:

- For fruits, vegetables and root crops: 1,700 tpa.
- For dry products, spices and meat: 340 tpa.
- For medical materials and tools: 170 tpa.

Therefore, the IGRP is designed in such a way that its production capacity can be increased by ten times without re-designing, just by additional loading of ^{60}Co sources (up to 1 million Ci). The higher the irradiation power, the less time is required for processing, which leads to a multiple increase in MIC production capacity.

Construction of the MIC has now been completed. In May 2022, permission was obtained to ionising radiation sources (^{60}Co) import into the Plurinational State of Bolivia for charging into the IGRP and the LGRP, with subsequent commissioning of the facility.

4. Research Reactor

The key facility that defines CNTRD's objectives for developing the research and technological capabilities of the Plurinational State of Bolivia in the field of nuclear science is the Nuclear Research Facility with a water-water pool-type research reactor, 200 kW thermal power, designed by ROSATOM.

The core design of the RR under the CNTRD project is shown in Figure 2 and the main performance characteristics of the RR are shown in Table 2.

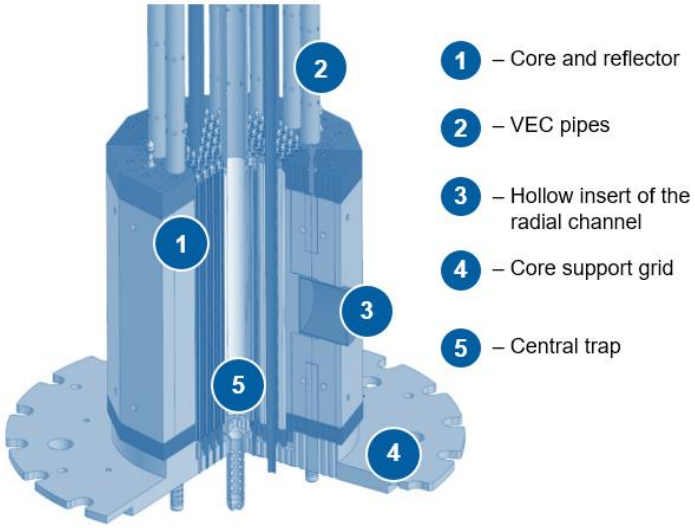

Fig.2 – CNTRD RR core design solutions [2]

Parameter	Value
Maximum design thermal power	200 kW
Core height	600 mm
Fuel used (fuel assembly type): one-section fuel assembly	VVR-M2
Coolant circulation through the core	natural
Coolant	H_2O
Reflector	Be
Uranium-235 content	19.7%
Core	reconfigurable
Number of FAs in the core	72
Number of control rods in the core: - Safety rods, pcs - Shim rods, pcs - Automatic rods, pcs	 2 6 1
Safety and shim rod material	B_4C
Automatic rod material	Steel

Maximum undisturbed neutron flux in the core (thermal, E<0.625 eV), at least	8.0×10^{12} $cm^{-2}s^{-1}$
Number of horizontal experimental channels (HEC): - radial; - tangential (number of outlets).	 1 1(2*)
Number of vertical experimental channels in the reflector:	8 pcs
Central trap	1
Number of vertical experimental channels for the NAA system installation (capsule diameter: 12 mm and 28 mm)	2 pcs
Thermal (E<0.625 eV) neutron flux density at the horizontal radial channel outlet (200 kW): at least	2.0×10^{8} $cm^{-2}s^{-1}$
Thermal (E<0.625 eV) neutron flux density at the horizontal tangential channel outlet for the confirmation of performance guarantees (200 kW): at least	0.6×10^{8} $cm^{-2}s^{-1}$
Average annual operation of RR at maximum design thermal capacity	2,000 hours
Fuel campaign duration (at 200 kW) at average annual operation time of 2000 hours, at least	30 years
* - one outlet is used to confirm guaranteed performance indicators; at the other, the PGNAA system in installed (prompt gamma quanta NAA).	

Tab 2: CNTRD RR main characteristics [2]

The NRF is designed for:

- wide range of research and experimental works, including neutron activation analysis for the needs of various industries;
- production of radioisotope products for scientific purposes;
- performance of applied research using neutron beams;
- training purposes.

The research reactor is equipped with main and backup control panels, experimental devices and experimental channels (vertical (VEC) and horizontal (HEC)).
The facility also provides for Engineering and Technical Complex, which includes fresh fuel storage facility, radioactive waste management facility (waste reduction and immobilization), radioactive waste and spent nuclear fuel storage facility.
It is the first research reactor to be built in Bolivia and is also the highest nuclear facility in the world (the construction site is located at an altitude of 4,000 meters above sea level). At this altitude, the boiling point of water is approximately 85 °C, and this requires careful attention and adaptation of technologies to ensure safe operation in these conditions.

In July 2021, the licence to build a nuclear power plant on the territory of the Plurinational State of Bolivia was obtained. On July 26, 2021, the first concrete of the reactor complex was poured in the presence of the President of Bolivia, Luis Alberto Arce Catacora, and this date marks the commencement of the construction of the facilities of the 4th stage of construction [3].

5. Laboratory complex

CNTRD laboratory complex includes a number of research laboratories designed to carry out a wide range of scientific investigations in various fields of nuclear science. The research laboratories are located in the production area and reactor complex of CNTRD.
The reactor complex includes a neutron activation analysis laboratory and a radioisotope laboratory. The production area includes a radiobiology and radioecology laboratory and a plasma laboratory.

The scientific and production programme, CNTRD configuration and units parameters have been harmonised in line with stakeholder requests, ensuring a high level of RR and laboratory utilisation.

Neutron Activation Analysis Laboratory is designed for mass multi-element analysis of geological, mineralogical and archaeological samples to obtain experimental data on the chemical composition of various materials, as well as investigations of forensic, biological and environmental samples that require a low detection threshold.

The CNTRD project implements two main neutron activation analysis (NAA) methods: instrumental (non-destructive) NAA and prompt-gamma NAA.
Non-destructive instrumental neutron activation analysis is the most common method of NAA. In non-destructive instrumental NAA testing, the radioactive sample is preserved and the radionuclides are identified by determining the difference in decay rates of the elements in the sample being tested, using high energy resolution equipment for gamma irradiation [4]. Irradiation of samples for instrumental NAA is performed in vertical experimental channels placed in the RR reflector and connected to the research station by pneumatic transport system.
PGNAA is a method similar to instrumental NAA. The difference is that instrumental NAA measures the radioactivity of the sample after neutron irradiation in the RR core, while PGNAA detects the prompt gamma rays emitted during neutron capture by element nuclei in the sample under study [4]. The PGNAA facility is placed on one of the tangential horizontal channels of the RR.

Radioisotope Laboratory is designed to handle radioisotopes used to support scientific research in radiobiology and radioecology in accordance with the CNTRD scientific programme.
The list and annual capacity of the radioisotope laboratory is given in Table 3.

Isotope	Produced activity per year, Ci/year
Br-77	5
Cr-51	5
Na-24	5
P-32	5
S-35	5
Sc-46	5
C-14	The laboratory equipment allows for work with these externally supplied isotopes (up to 5 Ci per year for each)
N-15	
Ca-45	

Tab 3: Radioisotopes produced by CNTRD radioisotopes laboratory

Radiobiology and Radioecology Laboratory is designed for scientific research on the development and implementation of irradiation technologies for agricultural raw materials and food products for phytosanitary and microbiological safety, for radiation stimulation and breeding of agricultural crops and for research in the field of radioecology.

Radiobiology and Radioecology Laboratory consists of the following groups:

- plant radiobiology group:
  - analyse the mechanisms of radiation stimulation in order to increase the size and quality of agricultural crops;
  - study radiation mutagenesis and selection of promising crop genotypes;
  - carry out cytogenetic studies.
- microbiology group:
  - conduct research on the effect of ionizing radiation on microorganisms;

- assess the radio sensitivity of microorganisms;
- study changes in the quantitative and qualitative composition of various groups of microorganisms after irradiation.

- group of radiation phytopathology and entomology:
  - application of radiation technologies for the disinfestation of grain, grain products and dried fruits;
  - application of ionizing radiation to treat plant diseases;
  - experimental studies of the use of radiation technologies against insect pests.
- vegetation research group:
  - study of the effect of ionizing radiation on the growth, development and yield of agricultural crops in vitro;
  - mutant screening to select crops;
  - study of the influence of modifying factors (such as lighting, temperature, humidity) on the growth and development of mutant forms.
- chemical research group:
  - determine total N, P, K, Ca, Mg, heavy metals, mobile forms of nutrients, water indicators, physical and chemical properties, pH, granulometric texture;
  - study the content of organic matter in the soil.
- field research group:
  - the study of the effect of ionizing radiation on the growth, development and yield of agricultural crops;
  - the study of the influence of modifying factors (such as lighting, temperature, humidity) on the growth and development of mutant forms.

Also, in line with the development of the scientific programme of the Radiobiology and Radioecology Laboratory and in synergy with the research tools (LGRP) deployed at the MIC on the CNTRD territory, Sterile Insect Technique (SIT) can be implemented. SIT is an environmentally friendly technique to control populations of insect pests and insect vectors of diseases dangerous to humans and animals. The technique consists of gamma-sterilising batches of male target insects and then returning them to their habitat. Sterile male target insects, while maintaining reproductive competition in the habitat, cannot leave offspring, which significantly reduces the population of target insects in subsequent generations [5].

Plasma Laboratory is designed to conduct relevant scientific research and solve applied problems; this laboratory includes a number of benches and necessary equipment, including:

- Glow discharge bench;
- Magnetron discharge bench;
- Atmospheric pressure discharge bench;
- X-pinch bench;
- Plasma focus bench with pulsed gas puffing;
- Bench for electrotechnical and pulse measurements.

6. Conclusions

CNTRD project, which is being implemented in the Plurinational State of Bolivia, is one of the most important sites for the development of the country's research, industrial and medical capacities. The Center will be a key element in ensuring country’s technological sovereignty and its scientific and production programmes will ensure the training of the country's highly qualified human resources.

Due to the joint efforts and effective cooperation between ABEN and the companies of Rosatom State Atomic Energy Corporation, all construction and commissioning works of the CNTRD facilities are planned to be completed in 2025.

References

[1] Bolivia successfully tests radiopharmaceuticals production equipment, https://rusatom-overseas.com/media/news/bolivia-successfully-tests-radiopharmaceuticals-production-equipment.html;

[2] Danil Fomin, RIAR, Russia Federation, report on 24th Topical Meeting on Research Reactor Fuel Management (RRFM) European Research Reactor Conference Helsinki, Finland, 11 – 16 October 2020;

[3] Rosatom launched the construction works for the research reactor complex in Bolivia, https://rusatom-overseas.com/media/news/rosatom-launched-the-construction-works-for-the-research-reactor-complex-in-bolivia.html;

[4] IAEA Nuclear Energy Series No. NP-T-5.3 (Applications of Research Reactors), page 29, page 39, https://www.iaea.org/publications/10491/applications-of-research-reactors;

[5] Sterile insect technique, https://www.iaea.org/topics/sterile-insect-technique.

Prediction of blister-threshold temperature limit for KJRR-LTA fuel plates

Gwan Yoon Jeong, Young-Wook Tahk, Jeong-Sik Yim

Korea Atomic Energy Research Institute, 111, Daedeok-daero 989beon-gil, Yuseong-gu, Daejeon, Republic of Korea

gyjeong@kaeri.re.kr

Abstract

A prediction model of the blister-threshold temperature limit, which is the acceptable operating temperature limit to avoid the blister formation under anticipated transients, has been made based on analytic approaches. It is found that blister-threshold temperature for KJRR-LTA plates can be predicted as a function of burnup with analytic manners and the predicted result was agreeable to experimental data.

1. Introduction

The qualification of U-7Mo/Al-5Si dispersion fuel as a standard fuel designed to be used in Kijang research reactor (KJRR) has been in progress in Korea. For the successful qualification, a full-sized lead test assembly (KJRR-LTA) containing 21 fuel plates had been fabricated by Korea Atomic Energy Research Institute (KAERI) and was irradiated in Advanced Test Reactor (ATR) in Idaho National Laboratory (INL). The irradiation test was successfully completed achieving local maximum burnup of about 84% U235 depletion for 216.6 effective full power days (EFPD).

Post-irradiation examination (PIE) was performed to examine irradiated plates, and eleven fuel plates were selected to conduct the traditional blister threshold test. From the test, it is possible to identify the fuel operating temperature limit under anticipated transient conditions. As a test protocol, each irradiated plate is exposed at the elevated temperature for a period of time and the visual inspection is followed to check whether blisters formed or not. This process is repeated with increasing temperature until blisters are observed. The blister-threshold temperature limit is then determined as the temperature when blisters were observed after the repeated anneal cycles. Fig. 1 shows the observed blisters of an irradiated plate after the anneal cycle with temperature at 425 ℃ with 20 minutes holding time.

It is known that blisters in metals form typically due to the gas coalescence at some preferential sites of excess defects including pores, grain boundaries, or microcrack [1]. For the case of an irradiated dispersion fuel, the gaseous fission products are accumulated inside fuel particles, and they are released toward the fuel meat region by recoil and athermal diffusion during irradiation. It is believed that the released gaseous fission products are entrapped and agglomerate together to form into pores and those pores can be pressurized to cause the formation of blisters on the surface at the elevated temperature condition. Particularly the pore pressurization is possibly facilitated at the laterally-transverse region of the plate where burnup is the highest due to the power peaking.

The formation of blisters on the metal surface entails the plastic deformation when pore pressure increases by the entrapped gases [2]. It implies that the blister formation follows the plastic deformation of the cladding. When the pore pressure is higher than the yield strength of a cladding of aluminum alloy (AA) 6061, the pore pressure becomes high enough to cause plastic deformation of the cladding surface, eventually causing the formation of large-sized blisters.

In this paper, we estimated the pore pressure inside blistered region using fission gas release models and also evaluated the irradiation- and temperature-dependent yield strength of the cladding. Then, the pore pressure was compared to the yield strength of cladding at the elevated temperature of blister threshold tests. It was found that the pore pressure and yield strength at each elevated temperature are comparable and blister-threshold-temperature limit can be estimated as a function of burnup on the irradiated fuel plates of KJRR-LTA.

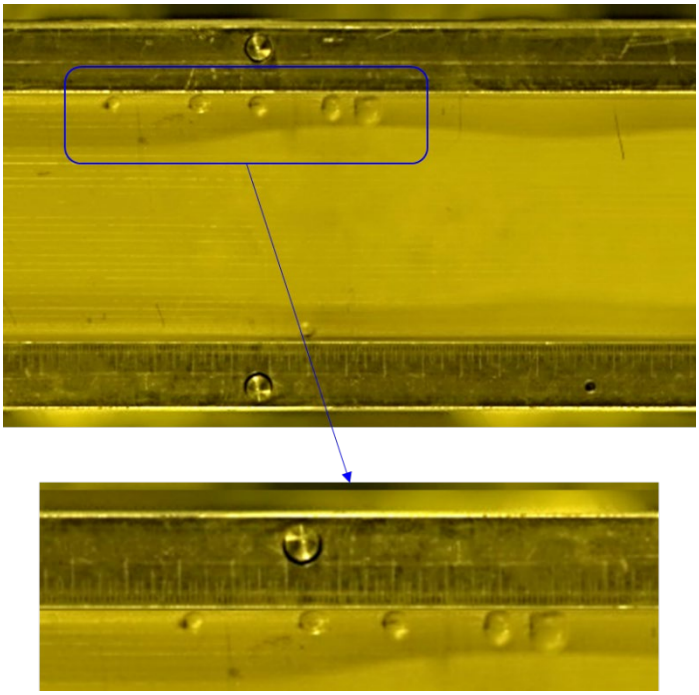

Fig. 1 Image of a surface of irradiated plate from KJRR-LTA after blister threshold test at 425 ℃ for 20 minutes.

2. Methods

2.1. Pore pressure calculation

Fission gases are generated inside fuel particles and they can migrate toward pores in the fuel meat. To estimate pore pressure in the fuel meat region, it is hypothesized that they are released to a porous site in the fuel meat to form pores to be pressurized.

The amount of fission gases generated in the fuel particles are calculated as follows:

$$N_{fg} = 0.26\mathrm{BU} \quad (1)$$

where N_{fg} is the number of fission gases generated in the unit volume of the fuel (#/cm^3-fuel), the value of 0.26 is the sum of fission yield for Xe and Kr which are stable gaseous fission products, and BU is the burnup (fission/cm^3-fuel).

The number of fission gases (n_{fg}) in the pore can be obtained by multiplying the total amount of fission gases generated in the fuel to the total release fraction as follows:

$$n_{fg} = N_{fg} * F_t \quad (2)$$

where F_t is the total release fraction. Two different mechanisms are considered for fission gases to migrate from the fuel particle to the region where blisters form; athermal diffusion and fission-induced recoil. The athermal diffusion of fission gases occurs during irradiation period in the operating temperature regime below 200 ℃. Fission-induced recoil is also the primary migration mechanism

because the fuel particle size is comparable to the fission-recoil range (~6.8 μm) [3].

The total release fraction by athermal diffusion and fission-induced recoil is calculated using Eq. (3) as follows:

$$F_t = F_c + F_d \tag{3}$$

where F_c and F_d is the release fraction by recoil and diffusion, respectively. Each release fraction is calculated using Eqs. (4) and (5):

$$F_d = \frac{4}{r}\sqrt{\frac{Dt}{\pi}} - \frac{3Dt}{2r^2} \tag{4}$$

$$F_c = \frac{3}{4}\frac{\mu}{r} - \frac{1}{16}\left(\frac{\mu}{r}\right)^3 \tag{5}$$

where D is the diffusion coefficient, r is the radius of fuel particle, t is the irradiation time, and μ is the recoil range.

The pore pressure inside blister (P) is calculated using the ideal gas law as follows:

$$\mathrm{P} = n_{fg}\mathrm{RT/V} \tag{6}$$

where R is the gas constant, T is the temperature, and V is the volume of pore. The pore pressure from Eq. (6) represents the pressure of pores having the total volume of V inside a unit cell of the fuel meat. The volume of pore is calculated using the measured porosity in the fuel meat as shown in Fig. 2. The measured porosity is given to be ~5%. This porosity is the nominal value that is determined using optical images obtained during PIE. The volume of pores used in Eq. (6) is believed to represent the volume of pores after irradiation because it could include 1) as-fabricated pores which did not disappear by being filed up with fission gases and fuel particle swelling to consume void space and 2) new pores that are pressurized by fission gases inside/outside of fuel particles.

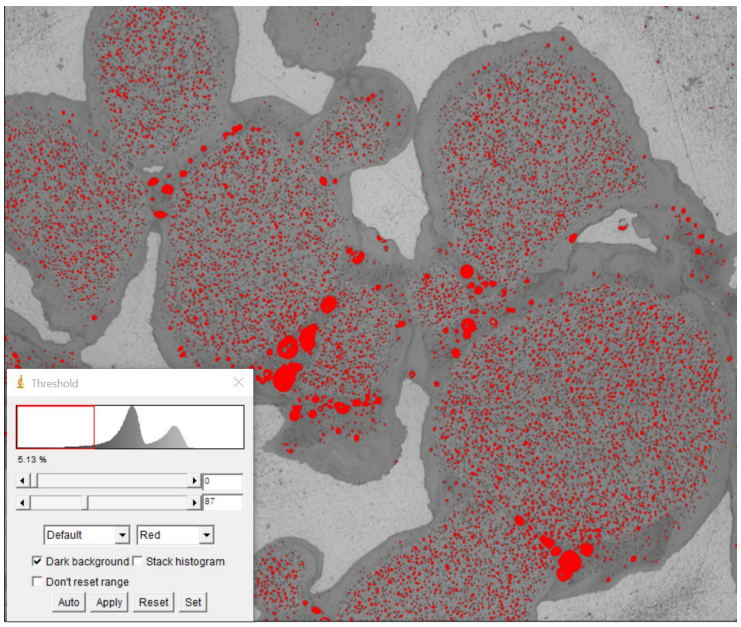

Fig. 2 An optical image showing pores form in the fuel meat of an irradiated plate from LTA.

2.2. Yield strength of the cladding

The yield strength of the cladding at temperature up to 450 ℃ was evaluated based on the available literature data [4-6]. Fig. 3 shows the yield strength for AA 6061 including heat-treated alloys. The widely-accepted data of yield strength for AAs in temperature higher than 94 ℃ are available in ASM Metals handbook [4], Aluminum Design Manual (ADM) [5] or European Code 9 (EN 1999-1-2) [6]. The temperature-dependent yield strength from handbook, manual, or code becomes significantly lower when temperature is higher than 250 ℃ since those properties do not involve effects of not only strain hardening by plastic deformation, but also heat treatments or cold-working from fabrication process. Since they are derived only for the elastic design of structures at high temperature conditions, using these data would lead predicting the blister-threshold temperature limit to be extremely conservative.

The yield strength for the cladding was measured by Kim et al. [7] up to 250 ℃ using specimen from as-fabricated plates, but the data up to 450 ℃ is not available. The additional dataset of yield strength for tempered AA 6061-T6 measured up to 550 ℃ by Mei-Ni Su et al.[8], which is analogous to Kim's data, was combined to predict the yield strength at the temperature higher than 250 ℃.

The yield strength of the cladding generally increases due to the defect generation by the neutron irradiation. Farrell et al. [9] reported the yield strength of irradiated AA6061 exposed up to a neutron fluence of 8.9×10^{22} n/cm^2 (E>0.1 MeV). Based on Farrell's data, the yield strength of the cladding is expected to increase up to 20%, considering the neutron fluence of irradiated plates in KJRR-LTA is estimated as 8.88×10^{21} n/cm^2 (E>0.1 MeV). The yield strength of the irradiated cladding as a function of temperature (i.e., red-solid line in Fig. 3) is used to determine the temperature where the pore pressure with a given burnup equals the yield strength.

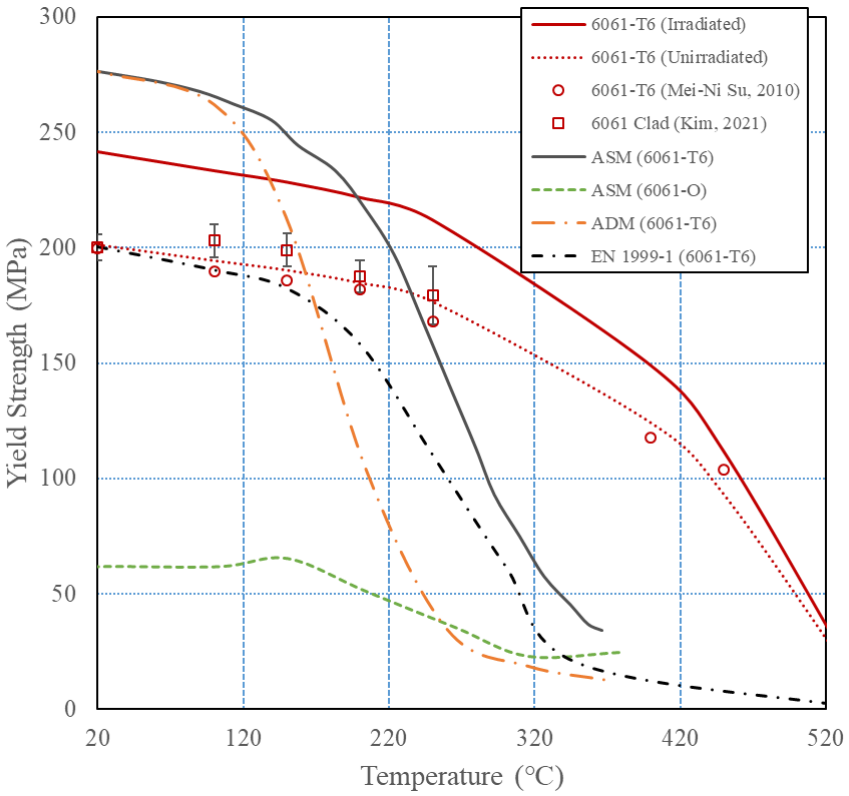

Fig. 3 Temperature-dependent yield strength of the cladding of AA6061-T6.

2.3. Procedure of setting the blister-threshold temperature limit

The blister-threshold temperature limit is the temperature limit, indicating blisters could occur whenever the temperature exceeds the limit for a given fuel burnup. This envelope is typically obtained by an empirical fitting as a function of fuel burnup.

To determine the blister-threshold temperature limit, it is assumed that the formation of a blister is initiated whenever the pore pressure in the fuel meat exceeds the yield strength of the cladding. The calculation procedure is given as follows:

a) Calculate the number of the generated fission gas atoms and the amount of released during irradiation using Eqs. (1) - (3) with time increment.
b) Once the amount of fission gas atoms that is presumed inside the pore in the fuel meat is calculated, obtain the pressure curve for a given burnup as a function of the elevated temperature during blister-threshold test.
c) Find the intersection between the temperature-dependent curve for pressure of a given burnup and the curve for yield strength of the irradiated cladding.
d) Collect all intersection points which contains data of the given burnup and the temperature where the pore pressure equals the yield strength of the cladding

As shown in Fig. 3, it was possible to obtain the temperature limit where the calculated pore pressure (P) at a given burnup starts to exceed the yield strength of the cladding as a function of temperature. The blister-threshold temperature limit was obtained collecting all intersection points of curves for pore pressure and yield strength as a function of temperature.

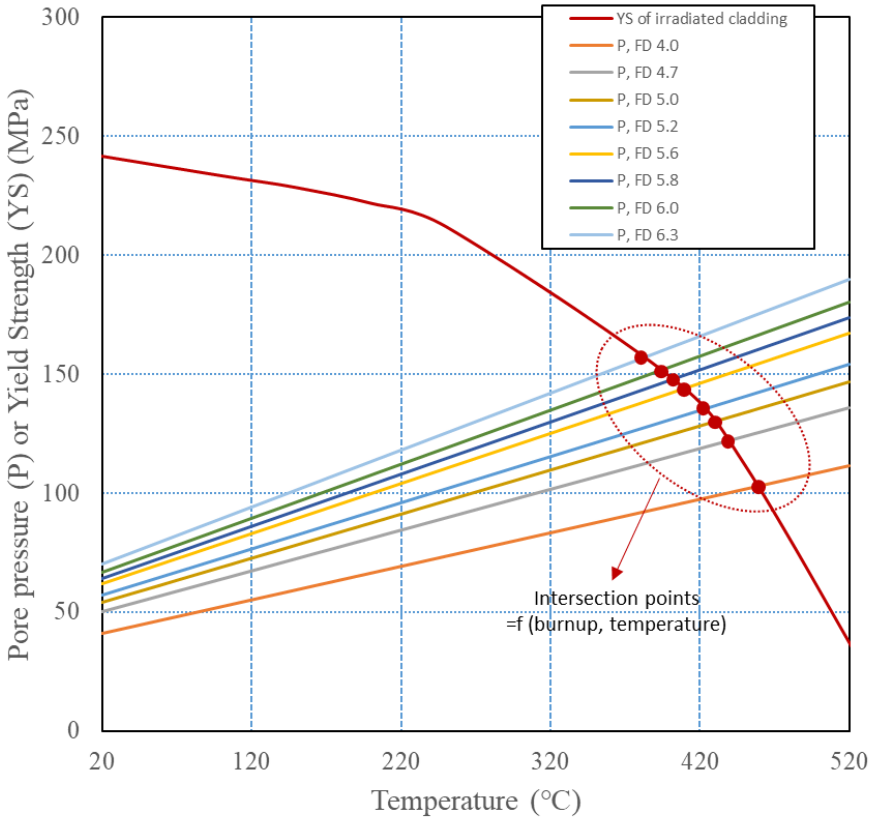

Fig. 4 Comparison among curves for pore pressures with different burnup and yield strength of irradiated cladding. (FD = Fission density in 10^{21} fission/cm^3)

3. Results and discussion

Fig. 5 shows the blister-threshold temperature limit obtained by collecting all intersection points among multiple curves for pore pressures with given fission density and the curve for yield strength of the irradiated cladding in Fig. 4. In Fig. 5, the comparison between test data and the limit curve shows that the model combined with the yield strength of irradiated cladding predicted the agreeable blister-threshold temperature limit as a function of burnup. Using the yield strength of irradiated cladding gives a best-estimated blister-threshold temperature limit. Agreement between the predicted limit and experimental data implies that the blister-threshold temperature is affected by not only the amount of fission gases in the pore, but also the plastic deformation of the cladding determined by temperature- and irradiation-dependent yield strength of the cladding, as was assumed.

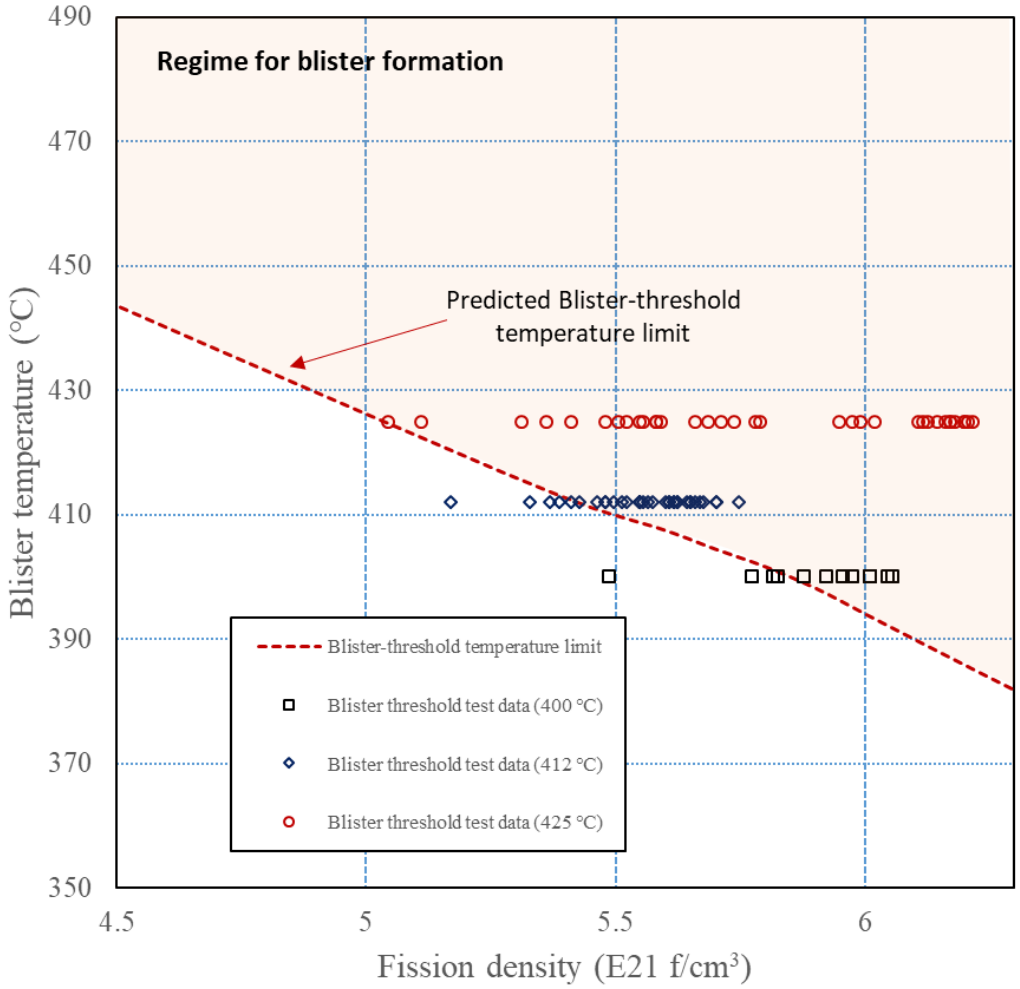

Fig. 5 Comparison between the test data and predicted temperature limit.

Uncertainties from irradiation hardening of the cladding affects the blister-threshold temperature limit as shown in Fig. 6. Parametric studies assuming that the yield strength of the cladding increased ranging from 0 ~ 40% due to the irradiation hardening indicated that the effect of irradiation hardening should be considered in order to obtain a best-estimated limit curve. It appears that using the yield strength of un-irradiated cladding is too conservative to predict the blister-threshold temperature limit.

Thermally-activated diffusion also is likely to occur during annealing of blister-threshold tests at temperature higher than 400 °C. However, a coefficient for thermal diffusion of Xe in metallic U alloys is four orders of magnitude lower than that for athermal diffusion. As reported by Castleman et al. that

Xe was not found to diffuse through aluminum in the temperature range of 295 to 473 ℃ [10], the effect of thermal diffusion of fission gases is minimal taking into account of the time period of each anneal cycle that is much shorter than irradiation period. In this regard, thermal diffusion of fission gases is not considered to calculate the pore pressure.

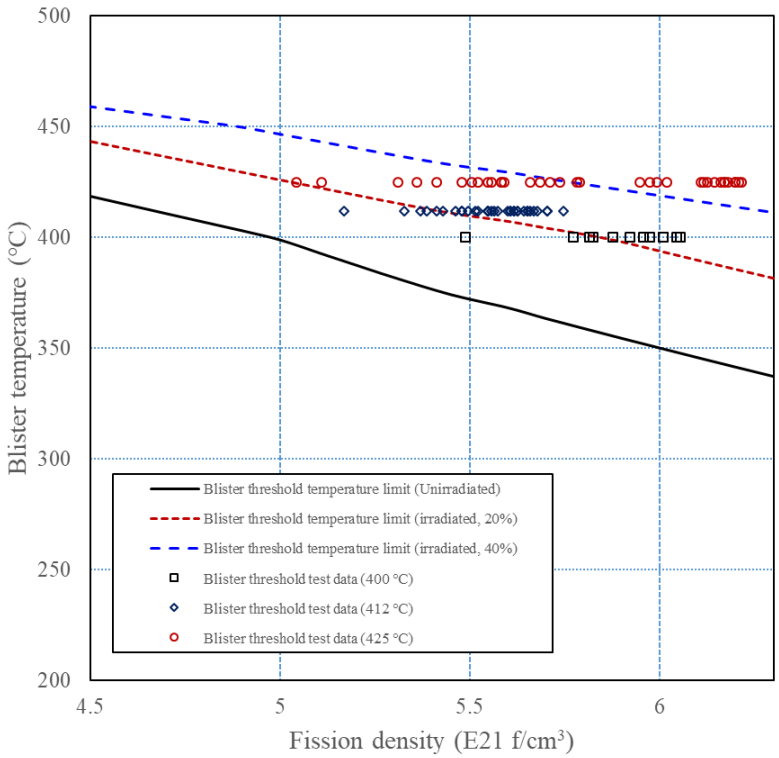

Fig. 6 Comparison of blister-threshold temperature limit obtained using different yield strength of the irradiated cladding.

4. Conclusion

The blister-threshold temperature limit for the fuel plates of KJRR-LTA is obtained by comparing the calculated pore pressure and irradiated yield strength of the cladding. It was found that the blister-threshold temperature limit can be obtained as a function of fuel burnup based on the proposed approaches, which is agreeable to experimental data. It implies that the temperature limits are indeed related to the pore pressure and the yield strength of the cladding. Those approaches could be verified and validated with blister threshold test data from other irradiation campaign in the future.

Acknowledgement

This work was supported by the National Research Foundation of Korea (NRF) grant funded by the Korean government (MSIT: Ministry of Science and ICT) (NRF- 2020M2C1A1061031).

References

[1] F.J. Rice, A. Robinson, M. Meyer, N. Lybeck, Preliminary Blister Anneal Testing Results for U-Mo Monolithic Fuel Plates, INL/LTD-14-33608, Idaho National Laboratory, 2015.

[2] X.G. Hu, Q. Zhu, S.P. Midson, H.V. Atkinson, H.B. Dong, F. Zhang, Y.L. Kang, Blistering in semi-solid die casting of aluminum alloys and its avoidance, *Acta Materialia* 124 (2017) 446-455.
[3] Yeon Soo Kim, G.Y. Jeong, D.-S. Sohn, L.M. Jamison, Pore growth in U-Mo/Al dispersion fuel, *J. Nucl. Mater.* 478 (2016) 275-286.
[4] J.W. Bray, Properties and selection: Nonferrous alloys and special purpose materials, *ASM Metals handbook*, 1990.
[5] Aluminum Association, Aluminum design manual (ADM), Washington, DC, 2000.
[6] European Committee for Standardization, Eurocode 9: Design of aluminum structure – Part 1-2: Structural fire design, BS EN 1999-1-2:2007, Brussels, 2007.
[7] H.-J. Kim, Y.W. Tahk, E.H. Kong, J.Y. Oh, J.S. Yim, Establishment of the design stress intensity value for the plate-type fuel assembly using a tensile test, Nucl. Eng. Technol. 53(3) (2021) 911-919.
[8] Mei-Ni Su, Ben Young, Material properties of normal and high strength aluminum alloys at elevated temperatures, Thin-Walled Structure 137 (2019) 463-471.
[9] K. Farrell, R.T. King, A. Jostsons, Examination of the irradiated 6061 aluminum HFIR target holder, ORNL-TM-4139, Oak Ridge National Laboratory, 1973.
[10] A.W. Castleman, F.E. Hoffmann, A.M. Eshaya, Diffusion of Xenon through aluminum and stainless steel, BNL-624, Brookhaven National Laboratory, 1960.

INSTITUT LAUE-LANGEVIN – HIGH-FLUX REACTOR – ILL2023: AMBITIOUS PROGRAMME FOR FUTURE LONG-TERM OPERATION

J. ESTRADE
Institut Laue-Langevin - 38000 Grenoble - France

Contact author: estrade@ill.fr

ABSTRACT

The Institut Laue-Langevin (the ILL) is an international research centre providing world-leading facilities in neutron science and technology. The Institute operates one of the most intense neutron sources in the world, a 58.3 MW nuclear reactor designed for high brightness.

The ILL recently upgraded the safety of its facilities through its Post-Fukushima reinforcement programme. As part of its regular safety review schedule, it is now working with the regulatory authorities on planning the implementation of new measures to ensure the safe operation of its reactor for the decades to come. In parallel, the ILL is also running an ambitious programme to refurbish its scientific instrument suite. This involves the installation of new types of instrument and higher performance neutron guides, providing gains for fundamental research and nuclear physics, as well as for science addressing societal challenges.

This paper provides an overview of the current long shutdown and the ambitious ILL20-23 programme to ensure that the ILL's scientific instruments and infrastructure maintain the Institute in its world-leading position.

1. Introduction - The Institut Laue-Langevin (ILL)

The Institut Laue Langevin (ILL) is Europe's most advanced neutron research facility. It operates a high-flux reactor (the RHF), one of the world's most intense neutron sources, and delivers beams of neutrons to almost 40 high-technology scientific instruments.
The ILL is managed by France, Germany and the United Kingdom. It has also established scientific partnerships with 11 other countries: Austria, Belgium, Czech Republic, Denmark, Italy, Poland, Slovenia, Slovakia, Spain, Sweden and Switzerland.
In conjunction with the neighbouring synchrotron facility, the ESRF, the ILL is part of a unique complex for the exploration of matter, the European Photon and Neutron science campus. It provides services and expertise to scientists from around the world. Every year, the Institute attracts around 1,200 researchers from more than 40 countries. The research carried out at the ILL focuses on fundamental science in numerous fields, including biology, chemistry, soft matter, nuclear physics and materials science.

Fig 1. The EPN campus

Of the 1,500 experiment proposals received each year, around 800 are selected by the ILL's peer review committees based on their scientific excellence. The number of experiments that can be conducted is determined by the operational constraints of the reactor and the number of instruments available.
The experiments performed in recent years at the ILL have generated an average of over 600 scientific papers per year, including some 150 publications in high-impact journals.

2. Reactor design and continuous refurbishment

The ILL's reactor was designed to provide maximum brightness for the experimental programme. Its fuel assembly is located in a tank of heavy water, from which a series of neutron beam tubes made of aluminium or zircaloy deliver the high flux of neutrons to the instruments. The instruments are located in the reactor building or in the two adjacent guide halls.
Due to its unique, highly compact fuel element and the excellent thermo-hydraulic conditions, the reactor can deliver a thermal neutron flux of 1.5×10^{15} $n.cm^{-2}.s^{-1}$ with a thermal power of 58.3 MW.

The ILL is located in Grenoble, close to the Alps and the river Drac.

Fig 2. Panoramic view from the dome of the RHF reactor

The main characteristics of the ILL reactor are as follows:

- Pool-type reactor
- Coolant: heavy water

- Reflector: heavy water
- Maximum thermal power: 58.3 MW
- Max. thermal flux in the reflector: 1.5×10^{15} $n.cm^{-2}.s^{-1}$
- Cycle length: around 50 days
- 2 cold neutron sources and 1 hot neutron source
- 19 neutron beams
- 40 experimental areas

Fig 3. Reactor core

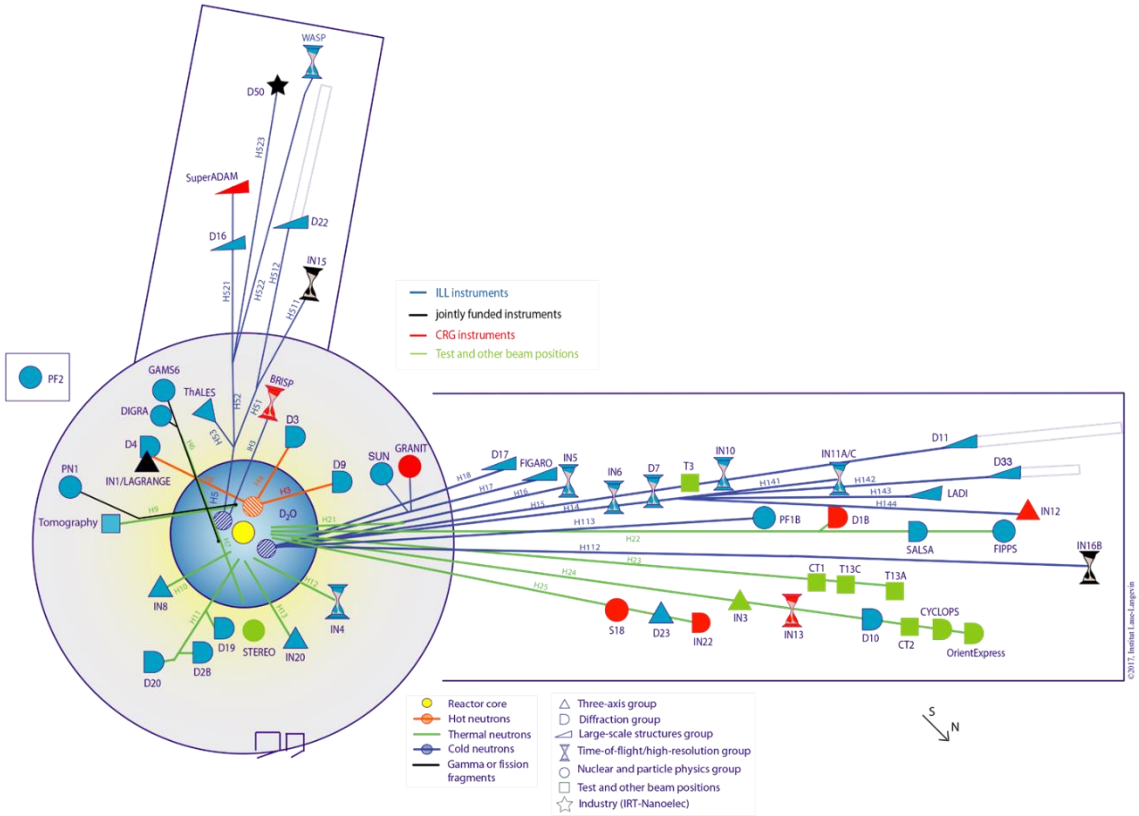

Fig 4. Location of the different ILL instruments

3. ILL2023 programme: ambitious programme for future long-term operation

One of the main ingredients of the ILL's success in maintaining its position as international leader in neutron science is the continuous upgrade of its facilities (both the reactor and the instruments). This is the secret behind its excellent, modern and highly efficient instruments and infrastructure.

Since 2000, two major instrument upgrade programmes have been launched: the Millennium Programme and Endurance.

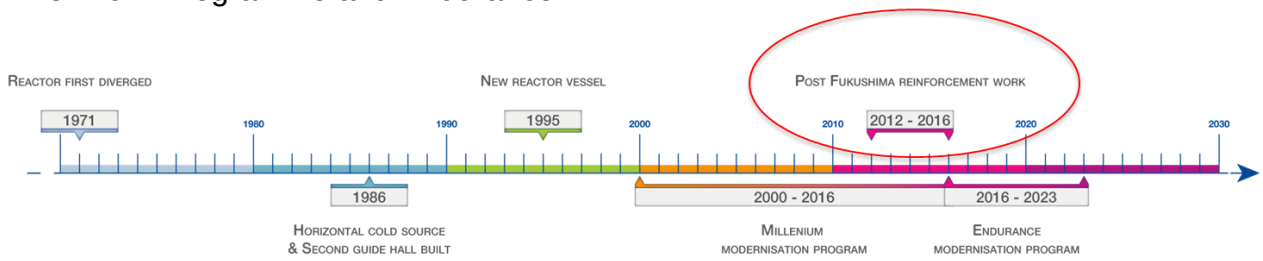

Fig 5. Continuous upgrading of scientific instrument suite

The ILL's "*raison d'être*" is science and innovation with neutrons. Science – both pure and applied - underpins a knowledge-based society and economy, while innovation is the foundation of the advanced, disruptive technology of tomorrow. Addressing societal challenges can only succeed with knowledge and technology of this kind.
Neutron-based research provides unique input for addressing fundamental questions and a wide range of societal challenges, including health, climate change, clean energy and smart materials. In broad terms, these map onto the three main areas of experimental activity at the ILL: biology and soft matter, chemistry and materials, magnetism and correlated electron systems. This mapping and its dependence on scientific and technical support services is illustrated in the figure below, showing specific examples of research topics that are actively pursued through continuous interaction with the user community now and in the coming years – in most cases there is an obvious connection to corresponding challenges. The figure also highlights how scientific progress, technical developments and services go hand-in-hand and how they necessarily combine in an optimal way at the ILL.

Fig 6. Grand challenges, neutron expertise and science at ILL

To consolidate its position at the crossroads of science and innovation and maintain its leadership, the ILL has set up the new ILL20-23 programme. Within this overarching programme, the reactor operating schedule over the period 2021-2025 is interspersed with specific reactor shutdown periods dedicated not only to the implementation of reactor safety improvements but above all to the installation of new instruments within the framework of the modernisation programme Endurance. Endurance phases I & II encompass more than 30 new or upgraded instrument and infrastructure projects. Funded in phases, and with a financial envelope of nearly 60 M€, Endurance is being rolled out over eight years between 2016 and 2023.

4. The H1H2 long shutdown

The first of the three specific shutdowns began after the third reactor operating cycle of 2021. A vast programme involving the refurbishment of existing instruments and the installation of new instruments is planned during this long (14-month) shutdown of 2021-2022. The main objectives are to upgrade two of the ILL's major cold and thermal neutron guides in the ILL7 hall guide (more than 500 m of guide) and install future new flagship instruments.

The work schedule for the 2021-2022 shutdown includes:
- the replacement of the H1H2 beam tube and the replacement of the reactor block chimney (these are periodic replacements associated with the lifetime of these components – aluminium materials under neutron flux)

Fig 7. H1H2 beam tube with its cold source

Fig 8. Top of the reactor core before replacement of the chimney

- the installation of new instruments on the H15 (Vercors side) and H24 guides (Chartreuse side). For information, the H1H2 beam tube has 11 guides, 2 of which - H15, which is connected to the cold source, and the thermal guide H24, will be completely renewed. Between October 2021 and November 2022 we will replace the H1H2 beam tube and in-pile neutron guides that allow the extraction and transport of thermal and cold neutrons to instrumentation in the ILL7 guide hall: 10 of our user instruments have already been disassembled and removed, making way for new and upgraded instrumentation on the renewed H24 thermal- and H15 cold-neutron guides,

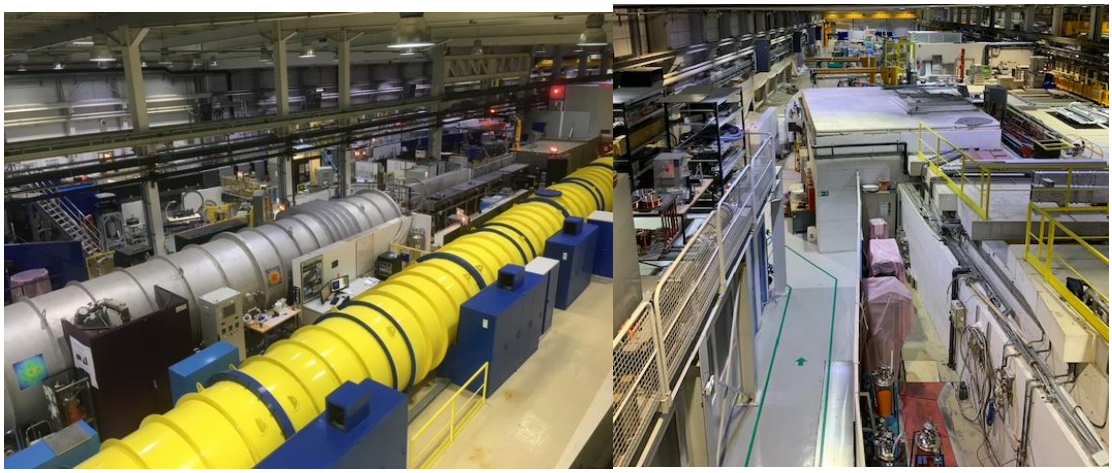

Fig 9. ILL7 guide hall Chartreuse side and Vercors side before the start of work

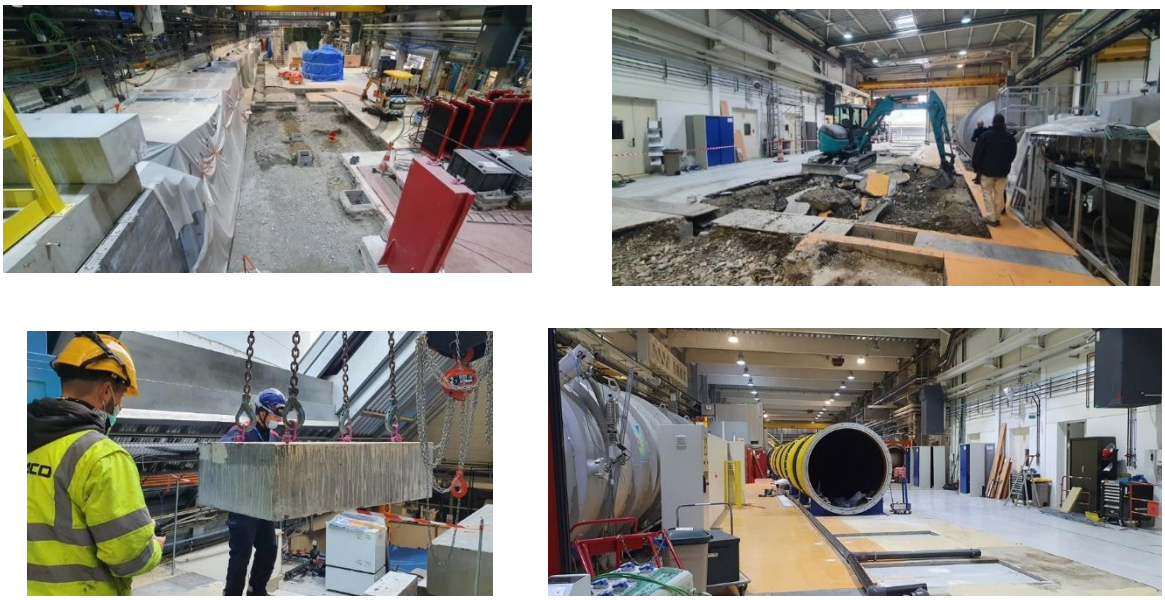

Fig 10. ILL7 guide hall Chartreuse side and Vercors side during the work

The ILL has meticulously prepared the implementation of ILL20-23. All the major components to be installed have been manufactured based on the most stringent quality assurance standards. This does not, however, eliminate risk: particular care will be taken not to damage vital components during installation whilst respecting a very tight schedule and regulatory constraints, since we are committed to providing the scientific community with neutrons again no later than the beginning of 2023.

5. The next ILL 2023 operations and ILL statement

The H1H2 long shutdown will be completed by two other ones in 2023/2024 and in 2025 To finalize the Endurance programme by commissioning of H15 instruments but also improving other independent projects.

Ever since it was founded, the ILL has always invested in innovation programmes as part of a constant effort to enhance the performance of every single instrument by incorporating the latest technological advances, whether it be state-of-the-art detectors and neutron guides, improvements to sample environment equipment, or innovative tools for data analysis and acquisition.

Some of the new instruments included in the Endurance programme are already in operation, such as the new fission fragment spectrometer FIPPS, which saw its first experiment at the end of 2016, and the new thermal time-of-flight (TOF) spectrometer PANTHER.

The instrument performance gains expected from Endurance will also call for research and innovation in other technical fields, including simulation techniques such as virtualisation, to improve the design of the instruments and their environment. The ILL is also currently exploring state-of-the-art computing technology: to illustrate, the ILL has developed an alternative virtual access mode for neutron experiments which allow users to connect to any instrument of the ILL suite via a web portal.

Other projects, including the creation of new detectors and guides as well as innovative data acquisition and storage techniques, will ensure that the ILL's instruments continue to set new standards in their respective fields. One of the ILL's objectives is to develop new detectors that can be tailored to meet an instrument's individual requirements. Another innovative research programme in the field of polarising neutron optics is also currently under way with the aim of developing advanced tools for neutron instrumentation.

One major challenge facing the ILL is how to cope with the ever-increasing volume of experimental data generated by our instruments. In 2011, a full cycle of 50 days and 40 instruments generated approximately 1TB of data. Today, we are generating 3-4TB of data per day and expect this figure to rise to a phenomenal 10TB in the next few years!

Finally, the level of expertise and experience available within the ILL has naturally led to our involvement in a number of European projects and conferences with a view not only to sharing our knowledge but also to helping us further enrich our knowhow, whether it be for the development of new instruments (detectors, guides, instrumentation, electronics, and so on), new data-sharing systems or a new reactor fuel design. And all this, with the aim of constantly improving the capacity for collaboration of our staff and, ultimately, of continuing to provide our users with the excellent instrumentation and quality of service they have come to expect.

6. Conclusion

Once successfully completed, ILL20-23 will provide the ILL with a fully modernised instrument suite and a neutron source compliant with the latest safety requirements.

Thanks to the successful completion of its scientific instrument refurbishment programmes, the ILL has been able to maintain its position as international leader in neutron science for so many years.

By 2025, a two-decade campaign of improvements to the reactor and instruments will be complete, positioning researchers to carry out wholly new types of experiments. Research at the ILL addresses critical challenges across areas ranging from the study of the origin of the universe to the understanding of viral diseases in living organisms.

The resounding success of its successive upgrade and refurbishment programmes can leave us in no doubt as to the ILL’s capacity to continue to operate safely beyond 2030.

INSTITUT LAUE-LANGEVIN – HIGH-FLUX REACTOR – RESULTS OF THE RECENT 10-YEAR SAFETY REVIEW

J. ESTRADE
Institut Laue-Langevin - 38000 Grenoble - France

Contact author: estrade@ill.fr

ABSTRACT

The Institut Laue-Langevin (the ILL) is an international research centre providing world-leading facilities in neutron science and technology. The Institute operates one of the most intense neutron sources in the world, a 58.3 MW nuclear reactor designed for high brightness.

The ILL recently upgraded the safety of its facilities through its Post-Fukushima reinforcement programme. As part of its regular safety review schedule, it is now working with the regulatory authorities on planning the implementation of new measures to ensure the safe operation of its reactor for the decades to come.

This paper provides an overview of the results of the recent 10-year safety review and the ILL's safety commitments aimed at maintaining the Institute in its world-leading position.

1. Introduction - The Institut Laue-Langevin (ILL)

The Institut Laue Langevin (ILL) is Europe's most advanced neutron research facility. It operates a high-flux reactor (the RHF), one of the world's most intense neutron sources, and delivers beams of neutrons to almost 40 high-technology scientific instruments.
The ILL is managed by France, Germany and the United Kingdom. It has also established scientific partnerships with 11 other countries: Austria, Belgium, Czech Republic, Denmark, Italy, Poland, Slovenia, Slovakia, Spain, Sweden and Switzerland.
In conjunction with the neighbouring synchrotron facility, the ESRF, the ILL is part of a unique complex for the exploration of matter, the European Photon and Neutron science campus. It provides services and expertise to scientists from around the world. Every year, the Institute attracts around 1,200 researchers from more than 40 countries. The research carried out at the ILL focuses on fundamental science in numerous fields, including biology, chemistry, soft matter, nuclear physics and materials science.

Fig 1. The EPN campus

Of the 1,500 experiment proposals received each year, around 800 are selected by the ILL's peer review committees based on their scientific excellence. The number of experiments that can be conducted is determined by the operational constraints of the reactor and the number of instruments available.
The experiments performed in recent years at the ILL have generated an average of over 600 scientific papers per year, including some 150 publications in high-impact journals.

2. Reactor design and continuous refurbishment

The ILL's reactor was designed to provide maximum brightness for the experimental programme. Its fuel assembly is located in a tank of heavy water, from which a series of neutron beam tubes made of aluminium or zircaloy deliver the high flux of neutrons to the instruments. The instruments are located in the reactor building or in the two adjacent guide halls.
Due to its unique, highly compact fuel element and the excellent thermo-hydraulic conditions, the reactor can deliver a thermal neutron flux of 1.5×10^{15} $n.cm^{-2}.s^{-1}$ with a thermal power of 58.3 MW.
The reactor first went critical in 1971. Since then it has been maintained through major refurbishment programmes. The reactor core was replaced in 1995, and major work was carried out ten years ago under the Refit Programme to reinforce the facilities to withstand a severe earthquake (5.7 on the Richter scale).

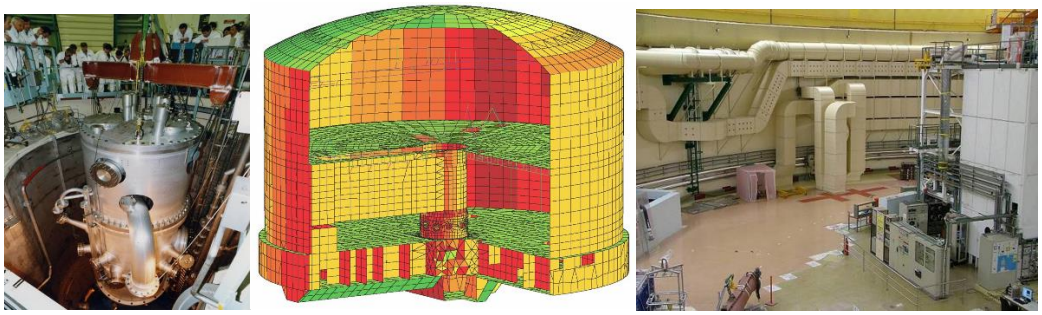

Fig 2. Replacement of the reactor core in 1995 and the 2002-2007 Reactor Refit Programme

The reactor containment was generously dimensioned to house a large number of instruments. It consists of an inner concrete wall some 40 cm thick and an outer steel shell 11 mm thick.

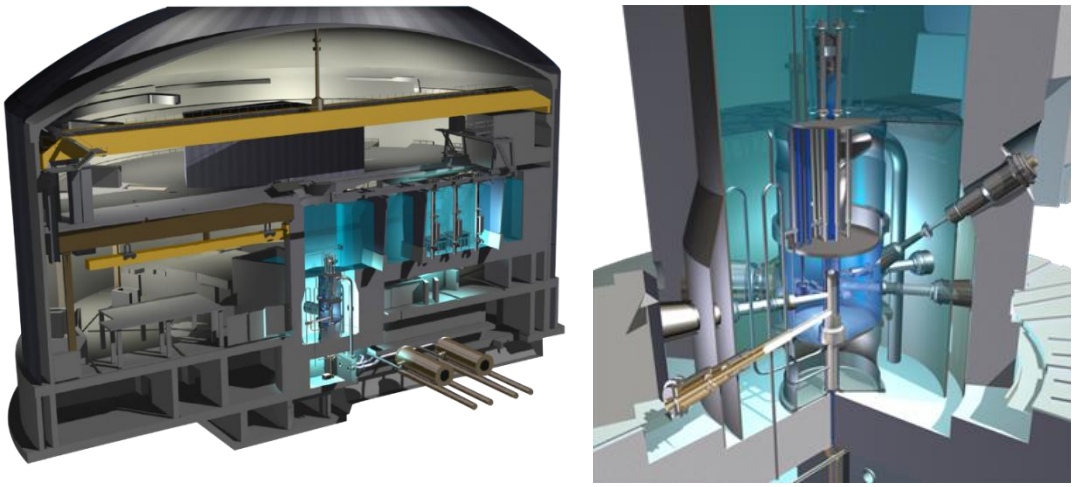

Fig 3. Reactor building and reactor core

The original design basis events underlying the reactor design were the Borax-type accident (rapid reactivity insertion) and a core meltdown in air. It is important to note that, given the type of fuel used by the reactor (highly enriched uranium), its power and its operating mode, the ILL's inventory of radioactive material contains 100 fewer short-lived fission products and 1,000 fewer long-lived fission products than that of a nuclear power plant.
The ILL is located in Grenoble, close to the Alps and the river Drac.

Fig 4. Panoramic view from the dome of the RHF reactor

The main characteristics of the ILL reactor are as follows:

- Pool-type reactor
- Coolant: heavy water
- Reflector: heavy water
- Maximum thermal power: 58.3 MW
- Max. thermal flux in the reflector: 1.5×10^{15} $n.cm^{-2}.s^{-1}$
- Fuel: UAlx with enriched uranium
- Cycle length: around 50 days
- 2 cold neutron sources and 1 hot neutron source
- 19 neutron beams
- 40 experimental areas

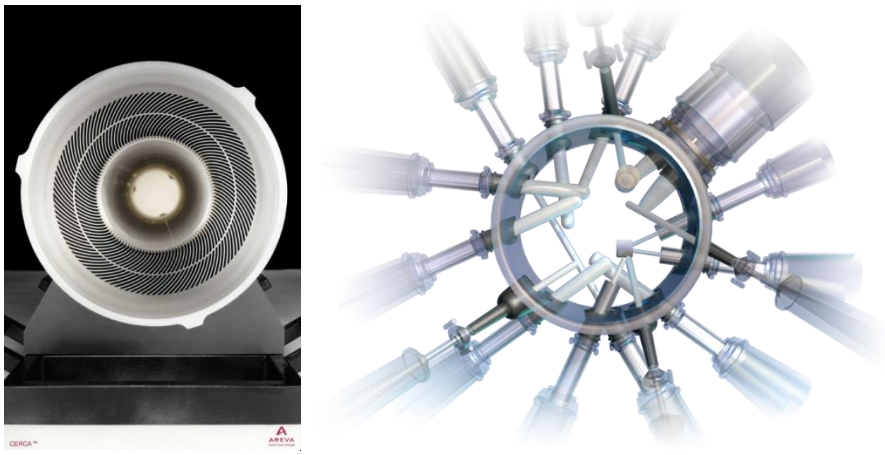

Fig 5. Fuel assembly and reactor core

4. Continuous upgrading of the ILL's scientific instrument suite and safety improvements programme

One of the main ingredients of the ILL's success in maintaining its position as international leader in neutron science is the continuous upgrade of its facilities (both the reactor and the instruments). This is the secret behind its excellent, modern and highly efficient instruments and infrastructure.

Since 2000, two major instrument upgrade programmes have been launched: the Millennium Programme and Endurance. Considering the safety improvements programme, every 10 years, the ILL had a periodic safety review and a dedicated safety review from the feedback of Fukushima accident.

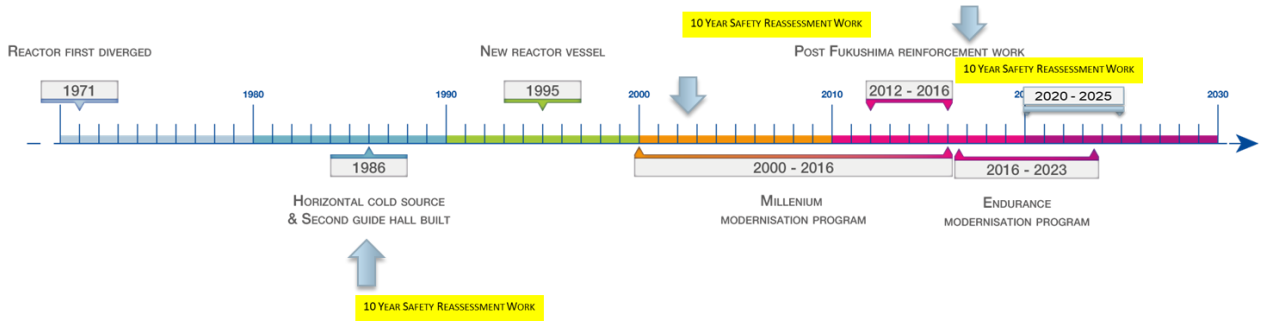

Fig 6. Continuous upgrading of scientific instrument suite and safety improvements

3. Safety reassessment and review of extreme conditions: results of the post-Fukushima stress test

In 2011, following the Fukushima nuclear accident, the French authorities asked the ILL to reassess the risk scenario used in its preparations for a natural disaster (a "stress test"). This request was made to all French nuclear operators. The ILL had to produce a report on the results of its reassessment.
The safety reassessment focused on a verification of the ILL's defence-in-depth procedures for the reactor installations, under specific internal and external conditions, taking into account the hazards associated with the ILL's location (earthquake, flood, and industrial environment). In particular, it examined the safety requirements addressed in the design of the facility, including its resistance to seismic events, flooding, or physical damage (from flooding and/or earthquake), the risk of the loss of its electric power or heat sink, the safety of its spent fuel storage pool, as well as hydrogen control, emergency response arrangements, accident management, and communications.
In the light of Fukushima, and to address the risk of "extreme external events", the severity of the earthquake to be taken into account was raised to 7.3 on the Richter scale (compared to the level of 5.7 used for the relatively recent Reactor Refit Programme). In addition, the authorities added the requirement that the ILL facilities be protected against the simultaneous occurrence of an earthquake and extreme flooding.

The earthquake scenario the ILL had to prepare for was that of a quake such as would occur only every 20 000 years. The hypothesis was that the quake would result in the

breach of the four dams upstream on the river Drac. In less than an hour, the flood waters would reach the ILL and rise in a matter of minutes to the 216-metre level, with a wave 8 metres high sweeping across the city. This was the combination of catastrophes the ILL had to face. The ILL is required, of course, to be able to maintain its reactor under control in these extreme conditions.

Fig 7. Post Fukushima: stress test response for an extreme event

Although earthquake and flooding were the main risks in terms of potential extreme external events, the ILL's industrial environment was also reviewed, particularly regarding the chemical risk for the reactor operator in a post-accident scenario.
The safety reassessment was based on the existing safety analysis report. Its main objective was to confirm the operability of the ILL's basic safety functions. These involve:

- ensuring that the reactor shuts down and remains in a safe shutdown state for all design basis accidents and for all operational states
- providing for the adequate removal of heat after shutdown, in particular from the core, including in the event of design basis accidents
- confining radioactive material in order to prevent or mitigate its unplanned release to the environment.

Following submission of the initial results of the safety reassessment and their validation by the regulatory body, in 2012 the ILL proceeded to install new safety circuits and automated systems, the so-called "hardened safety core", in and around the reactor. There was also a focus on reducing the need for human intervention, particularly during and following an accident situation (the first 30 minutes). The ILL also launched an extensive programme of work to reinforce the existing Structures, Systems and Components (SSC).
This included new buildings capable of resisting "extreme external events" (earthquake conditions and flooding) and modifications to existing buildings.
All the new safety systems were installed in duplicate to ensure that they continue to function in the event of a failure. It is important to note that this is a unique approach, making the ILL reactor one of the safest research reactors in the world, particularly in

the event of an extreme external event. Moreover, all these systems have dedicated power supplies and instrumentation and control systems. To guarantee their timely deployment, instrumentation was developed to monitor and report on the state of the reactor (the level of water in the pool, for example, or the pressure in the reactor building). These improvements and modifications were implemented over the period 2013 to 2018.

5. Ten-year safety review

Following on from these new safety improvements, in 2017 the ILL embarked upon a 10-year safety review. By law (INB decree (arrêté) of 2007 governing nuclear facilities in France), every 10 years, all nuclear facilities must undertake a safety review taking into account the planned future status of the facility (in operation or to be shut down during the coming decade).
For this exercise, the ILL completely reassessed its safety demonstration, which is now based on the most recent standards (IAEA, safety guide...), and undertook a broad review of the current state of its Structures, Systems and Components (SSC), conducting a programme of non-destructive tests to compare the current state with the initial safety requirements associated with each SSC.
Thanks to the additional safety systems put in place in the framework of the post-Fukushima stress test response programme, the ILL now has certain additional safety margins which made it easier to prepare the safety demonstration.

The full examination of the Groupe Permanent 2017 safety review officially started on 11 February 2019; it ended with the meeting of the Groupe Permanent in November 2020. During this period, the IRSN faxed to ILL over 500 questions, 20 technical meetings took place, and more than 200 ILL-internal documents were sent to the IRSN to satisfy requirements. The scope of the safety review was truly exhaustive; all subjects relating to safety issues were examined.

The main issues anticipated were the reinforcement of fire protection and the reinforcement of the polar crane on Level D of the reactor building. The final conclusions were on the whole positive and the ILL has been authorised to operate for a further ten years, provided it fulfils a list of commitments to upgrade certain levels of safety. The ASN is expected to officially finalise its concluding statement by mid-2022.

The ILL has made a number of commitments and elaborated the timeline for the period 2020-2025, also taking into account essential maintenance operations and the ILL scientific programme. Completion of this work schedule in 2025 will mark the end of the major reinforcement measures associated with the safety review. The ILL has defined three major long shutdowns for this work whilst ensuring that time is also optimised for the scientific programme (delivering a maximum number of beam days for science).

The next safety review is scheduled for 2027.

6. Outcome of the ten-year safety review

In the light of the safety review, which was carried out in compliance with both IAEA and French guidelines, the ILL has identified a number of improvements to be made. These concern various areas, such as instrumentation and control to enhance the incident/accident management system, as well as the reinforcement of equipment and the implementation of additional equipment.

Regarding the instrumentation and control system, the safety review identified certain incident/accident scenarios for which shutdown action requests must be added in order to reinforce the safety of the installation. These include:

- Emergency shutdown on reaching the upper threshold for coolant flow rate at core exit (on loss of electricity or on loss of secondary flow)
- Shutdown of primary and shutdown cooling pumps on reaching minimum pressure threshold and upper coolant flow rate threshold at core exit.

The ILL has also proposed to implement redundancy of the primary/secondary exchanger isolation controller.

Fig 8. Redundancy of primary/secondary exchanger isolation controller

Regarding the fuel handling system, a complete review of the existing equipment has been carried out, including the risk of loads falling on to the equipment and the structure of the reactor building. This review was supplemented by a reliability analysis of the polar crane trolley and an analysis of the earthquake resistance of the two main cranes: the polar crane on Level D and the overhead crane on Level C. The trolley of the polar crane will be replaced. Some seismic reinforcement work on the two main cranes is planned.

Fig 9. Overhead crane on Level C and polar crane on Level D

One of the other major modifications to be made involves in the reinforcement of fire protection:

- Installation of a sprinkler system on Level C to avoid a general fire on this level of the reactor building, which houses a large amount of scientific equipment with a high fire load, mainly due to the presence of HDPE (high density polyethylene) used to limit neutron background noise
- The accesses to the casemates on Levels C, B and A containing primary circuit components are classified as red zones from a radiological point of view. Here the installation of sprinklers will make it possible to extinguish a fire by remote control.

Finally, the ILL is rebuilding the fresh-air intake, located close to the reactor building, to reinforce its structure to ensure compliance with seismic resistance requirements.

Fig 10. Rebuilding of the fresh-air intake

7. Conclusion

It is thanks to the quality of the initial design of the ILL reactor and the successful completion of subsequent refurbishment programmes that the ILL has been able to adapt, renew and reinforce its installations in response to new regulatory requirements. This can be seen not only in the ILL's response to the accident in 2011 at the Fukushima Daiichi nuclear power plant in Japan, but also during the recent 10-year safety review.

The ILL has been able to maintain its position as international leader in neutron science for so many years thanks largely to the continuous upgrade of its facilities. This is the secret behind its modern and highly efficient instruments and infrastructure.

By 2025, a two-decade campaign of improvements to the reactor and instruments will be complete, positioning researchers to carry out wholly new types of experiments. Research at the ILL addresses critical challenges across areas ranging from the study of the origin of the universe to the understanding of viral diseases in living organisms.

The resounding success of its successive upgrade and refurbishment programmes can leave us in no doubt as to the ILL's capacity to continue to operate safely beyond 2030.

INVESTIGATION OF THE DEPOSITION CONSTANTS OF NON-GASEOUS FISSION PRODUCTS ON THE INNER SURFACES OF THE I-CIRCUIT OF THE WWR-SM REACTOR.

ALIKULOV SH. A., BAITELESOV S. A., KUNGUROV F. R., KUDIRATOV S. N., TADJIBAEV D. P., TOJIBOYEV D.D, TURDIEVA G.

Institute of Nuclear Physics of the Academy of Sciences of the Republic of Uzbekistan
str. Khuroson, 1, Ulugbek settlement, Tashkent, 100214, Uzbekistan

ABSTRACT

To analyze the state of the core, it is necessary to know the value of the constant removal of radionuclides from the reactor coolant due to their deposition on the inner surfaces of the reactor primary circuit. These values were determined when the cleaning filters were disabled and running.

The experiment was carried out under steady-state reactor conditions (when operating at constant power, with steady-state activity of radionuclides in the primary circuit, with no changes in the release from under the flooring space and unchanged radiation conditions in the reactor process rooms) and with fresh loading of ion exchange filters.

1. Introduction

The activity of the I-st circuit coolant of the WWR-SM research reactor is due to the activation of the coolant and its impurities under the action of the neutron flux density, the ingress of fission products into the coolant from surface contamination of the fuel elements and the violation of the fuel cladding tightness.

During the manufacture of a fuel element, some contamination with the fuel composition remains on its surface, which amounts to a value of the order of 10^{-8}-10^{-9} g/cm^2. When surface contamination is irradiated with neutrons, the fuel will fission and fission products will enter the coolant, increasing its specific activity.

Under the action of uranium fission products, which have high kinetic energies (approximately 60-100 MeV) and temperature, pressure, and corrosion, microcracks (violation of the fuel element tightness) may appear in the fuel element cladding. With small cracks, gaseous and volatile fission products will begin to enter the coolant; with large degrees of leakage, other types of fission products also appear in the coolant.

To analyze the state of the core, it is necessary to know the values of the constants for the removal of radionuclides from the reactor coolant due to their deposition on the internal surfaces of the reactor I-st circuit. These values were defined with purge filters disabled.

2. Theoretical part

The experiment was carried out in the steady state mode of the reactor (when it was operating at a constant power, with a steady activity of radionuclides in the I-st circuit, with no changes

in the release from the space under the floor and a constant radiation situation in the process rooms of the reactor) and with a fresh load of ion-exchange filters.
The condition of the fuel elements in the reactor core can be assessed on the basis of information on the specific activity of uranium-235 fission products in the coolant.
The release of fission products from the fuel composition into the coolant can occur in several ways:
- due to recoil atoms during fission from the surface of the fuel in contact with the coolant (R_{ot});
- due to the diffusion of fission products through the system of cavities and pores that appear in the fuel composition during oxidation and corrosion processes (R_{df});
- due to the blurring of the fuel composition as a result of the abrasive action of the coolant, oxidation and corrosion of uranium dioxide (R_{rz}).
Thus, the entry of fission products into the coolant due to the main three processes listed above will have the following form [1]:

$$R_s = R_{ot} + R_{rz} + R_{df} = A \cdot \lambda + B\sqrt{\lambda} + C \qquad (1)$$

where: R_s - is the entry of fission products into the coolant;
R_{ot} - the release of fission products from the fuel composition into the coolant due to recoil atoms during fission from the fuel surface;
R_{df} - the release of fission products from the fuel composition into the coolant due to the diffusion of fission products through the system of cavities and pores;
R_{rz} - the release of fission products from the fuel composition into the coolant due to the smearing of the fuel composition;
A, B, C - constant values determined experimentally;
λ - the decay constant of a particular radionuclide.
During operation of the reactor, the activity of reference radionuclides in the coolant is measured. The assessment of the reactor core state, using the values of the activity of the reference nuclides, is carried out after converting the value of the volumetric activities of the reference nuclides in the form of normalized rates of nuclides entering the coolant [2]:

$$R_i = \frac{a_i(\lambda^i + \nu_f^i + \nu_o^i + \nu_u^i) \cdot V}{\alpha_i} \qquad (2)$$

where A_i - is the volumetric activity of the i-th nuclide in the coolant, Ci/l;
V - the volume of water in the circulation circuit, l;
λ - decay constant of the i-th nuclide, 1/s;
ν_f - cleaning constant of the i-th nuclide on the filter, 1/s;
ν_o - deposition constant of the i-th nuclide on the surfaces of the circulation loop, 1/s;
ν_u - leakage constant of the i-th nuclide from the water into the space under the floor, 1/s.
α_i - yield of the i-th nuclide per fission, rel. units [3].

$$\nu_f^i = \frac{Q_f\,(\varepsilon_i - 1) \cdot 10^3}{V \cdot \varepsilon_i \cdot 3600} \qquad (3)$$

where Q_f - coolant consumption for cleaning, m/h;
ε_i – activity ratio of the i-th nuclide before and after the filter, rel. units

For non-gaseous radionuclides, the excretion constant due to their release into the space under the floor can be neglected.
When the filters are turned off, the change in the activity of radionuclides in the coolant is described by the expression [2]:

$$a_i = a_i^0 + a_i^n \times \left\{1 - e^{\left(-\left(\lambda^i + v_0^i\right) \times t\right)}\right\}, \text{Ки/л} \qquad (4)$$

where a_i^o - the initial specific activity of the nuclide before the filters are switched off, Ci/l;
a_{in} - the equilibrium level of the specific activity of the nuclide after the filters are switched off, Ci/l.

At equilibrium, i.e. at t≈3 days:

$$a_i^n = \frac{R_i \cdot \alpha_i}{(\lambda_i + v_o^i + v_u^i) \cdot V} \qquad (5)$$

Assume that there is no leakage of the i-th nuclide from the water into the space under the floor, then from expressions 2, 3, 5 it is easy to obtain:

$$v_o^i = \frac{a_i^o \cdot \left(\lambda_i + v_f^i\right) - a_i^n \cdot \lambda_i}{a_i^n - a_i^o}, 1/\text{c} \qquad (6)$$

It should be noted that the deposition constant of radionuclides can also be determined from the activity change curves after the filters are switched off.

3. Experiment results

Water samples are measured in full in accordance with the operating instructions for the WWR-SM reactor [4].

Nuclide	the decay constant of a particular radionuclide [5]	ε_i – activity ratio of the i-th nuclide before and after the filter, rel. units	v_f - cleaning constant of the i-th nuclide on the filter, 1/s	v_o - deposition constant of the i-th nuclide on the surfaces of the circulation loop, 1/s	a_0 - specific activity of the nuclide before the filters are switched off, Ci/l	a_n - specific activity of the nuclide after the filters are switched off, Ci/l
Nb-95	8,24E-04	5,97E-01	-4,01E-05	-8,83E-04	3,56E-07	5,96E-07
Zr-95	4,51E-04	6,88E-01	-2,69E-05	-5,11E-04	2,96E-07	4,30E-07
Mo-99	1,05E-02	3,40E-01	-1,16E-04	-1,06E-02	4,52E-08	1,33E-07
Ru-103	7,34E-04	1,99E-01	-2,40E-04	-7,93E-04	5,68E-08	2,86E-07
Cd-109	6,22E-05	1,78E-01	-2,74E-04	-1,22E-04	8,29E-08	4,65E-07
I-131	3,59E-03	1,66E-02	-3,53E-03	-3,65E-03	1,81E-08	1,09E-06
I-133	3,33E-02	1,33E-02	-4,41E-03	-3,34E-02	5,67E-08	4,26E-06

Cs-134	3,83E-05	3,42E-01	-1,14E-04	-9,79E-05	3,20E-09	9,35E-09
Xe-135	7,61E-02	4,88E-01	-6,25E-05	-7,61E-02	5,17E-06	1,06E-05
Cs-137	2,62E-06	6,27E-01	-3,54E-05	-6,21E-05	3,48E-08	5,55E-08
La-140	2,26E-03	1,76E-01	-2,80E-04	-2,32E-03	1,25E-07	7,12E-07
Ba-140	2,26E-03	1,26E-01	-4,14E-04	-2,32E-03	5,30E-08	4,22E-07
Ce-141	8,89E-04	1,26E-01	-4,12E-04	-9,48E-04	1,35E-07	1,07E-06
Ce-144	1,02E-04	4,25E-01	-8,06E-05	-1,61E-04	1,30E-07	3,06E-07

Table. 1 The results of measuring the activities of nuclides in the water of the 1st circuit and the values of certain deposition constants of nuclides

4. Conclusion

The values of the constants for the removal of radionuclides from the reactor coolant due to their deposition on the internal surfaces of the I-st circuit of the reactor, with the purification filters switched off, were studied.

When fission products are deposited on the internal surfaces of the I-st circuit of the reactor, the content of fission products in water decreases. The higher the rate of deposition during its transportation by the flow in the I-th circuit, the less its release into the atmosphere.

Deposition is due to several physical mechanisms, among which an important place is occupied by recoil atoms during fission from the surface of the fuel in contact with the coolant, as well as the diffusion of fission products through the system of cavities and pores that appear in the fuel composition during irradiation, oxidation, and corrosion.

The results make it possible to estimate the specific activities of fission products in the coolant and show the level of purification of the ion-exchange filters of the I-st circuit in the WWR-SM reactor.

5. References

1. Ashrapov T.B. and others. Express determination of radionuclides in the water of the 1st circuit of the WWR-SM reactor. 2000
2. Pavlenko V.I., Markushev V.M., Timashev V.V. Method for calculating the yield of fission products from leaky fuel rods with fuel based on UO2 // Preprint IAE - Moscow, 1990. - No. 5137/11. – 51 p.
3. Dosimbaev A.A., Baytelesov S.A., Koblik Yu.N. and Salikhbaev U.S., “Water and air activities during operation of the WWR-SM reactor with fuel enriched in 235U up to 36%”, Bulletin of the Russian Academy of Sciences: Physics, 2009, volume 73, no. 2, pp. 270-273.
4. Operating Instructions for the WWR-SM Nuclear Reactor, Inv. №1/28-10, 2020
5. Tables of physical quantities, Reference book, M., Atomizdat, 1976.

INTERNATIONAL SCIENTIFIC RESEARCH PROGRAM ON THE BASIS OF MBIR REACTOR

A.V. GONCHARUK, A.O. KHARCHENKO
International Cooperation Department, IRC MBIR Consortium Leader LLC
Bolshaya Ordynka, 115035 Moscow – Russia

ABSTRACT

MBIR is a multipurpose fast-neutron research reactor with thermal power of 150 MWt and maximal density of neutron flux equal to $5.3 \cdot 10^{15}$ N/cm^{2}s. MBIR Research Reactor which is being constructed on area of JSC “SSC RIAR” in the Dimitrovgrad, Ulyanovsk Region, is the largest research reactor under construction in the world and will allow to expand directions of studies regarding grounds of concepts in two-component nuclear energetics, closure of fuel cycle, creation of safe nuclear Generation IV power plants. Russian Program for Advanced Experimental Research at the MBIR Reactor Facility for 2028 – 2040 was approved in 2021 and will be the basis for creation of the International scientific research program to be implemented on the MBIR reactor. The International Research Center based on the MBIR reactor will become the competence center for fast reactor technologies and research aimed at improving the safety and efficiency of nuclear energy.

1. Introduction

Nuclear power is a stable leader in providing efficient methods of low-carbon electricity generation, responding to the formation of a request for "green" energy. An increasing number of countries inextricably link the future of their energy with nuclear technologies, the development and improvement of which is taking place at an increasing pace.

Currently, State Atomic Energy Corporation Rosatom is acting as a world’s trendsetter in the development of two-component nuclear power, which will allow to combine thermal and fast neutron reactors into a system in order to close the nuclear fuel cycle. In the future, such systems will be the key to the transition to clean, waste-free energy, which makes it particularly important to study the potential of such technologies and conduct the necessary scientific research on the basis of research nuclear reactors. Despite this necessity, the number of research reactors in the world over the past 20 years has decreased by 15% and reached 220, among which only BOR-60 provides relevant technical parameters for testing in-reactor materials and core element designs for fast neutron reactors.

2. MBIR

2.1. General information

The MBIR multi-purpose fast neutron research reactor, which is being constructed at the site of JSC "SSC NIIAR" in the city of Dimitrovgrad, Ulyanovsk region, is a unique installation that allows expanding experimental capabilities to substantiate projects of new fast reactors, closed nuclear fuel cycle technologies and small and medium-power reactor technologies. MBIR is a research reactor with a sodium coolant with a thermal capacity of 150 MW and a maximum neutron flux density of $5.3 \cdot 10^{15}$ N/cm^{2}s, which is almost twice the neutron flux density at BOR-60.

MBIR, which is scheduled for commissioning in 2028, will become the world's largest operating research reactors, which will provide the nuclear industry with a modern and technologically advanced research infrastructure for the next 50 years. Its unique characteristics and technological capabilities will significantly accelerate the creation of safe Generation IV nuclear power plants and open the way to the closure of the fuel cycle.

2.2. Technical features

The modern research infrastructure of the MBIR reactor will allow:

- testing of advanced structural and absorbing materials in support of the development of Generation IV technologies;
- research into advanced fuel, fuel elements and CNFC technologies;
- production of isotopes and raw materials for radiopharmaceuticals, as well as the development of modified materials;
- research with the use of neutron beams in the field of medicine, fundamental and applied physics.

The reactor core will be equipped with:

- 14 non-instrumental channels for material test assemblies and irradiation devices placement;
- 3 instrumented experimental channels with various coolants isolated form the main sodium circuit;
- 3 independent loop facilities for conduction of fuel experiments under conditions of emergency, transient and dynamic modes of reactor operation.

Parameter	**Value**
Thermal power, MWe	150
Electric power, MWe	55
Max / average neutron flux density in the core, $cm^{-2}s^{-1}$	$5.3 \cdot 10^{15}$ / $3.1 \cdot 10^{15}$
Fuel	MOX
Reactor fuel campaign, no less than, days	100
Reactor configuration	Loop-type
Number of loops for heat transfer	2
Number of heat removal circuits	3
Coolant Flow	Bottom – up
Coolant: I and II circuits / III circuit	Sodium / Water
Pressure in the I circuit, MPa	Up to 0,6
Coolant temperature of the I circuit, °C	330-512
Capacity utilization coefficient	0,65
Designed lifetime, years	50
End of construction, year	2028

Tab 1: MBIR reactor design features

2.3. Construction progress

Despite the general recession in the global economy and all the restrictions caused by the Coronavirus pandemic, the implementation of the project in 2021 was carried out ahead of the schedule and the construction program was exceeded by an average of 8%. At the moment about 1400 specialists are working at the construction site and 100 units of equipment are involved. The reactor unit has been already concreted to the +13 meters mark. On April,4 2022 the reactor vessel was delivered to the site.

At the moment MBIR is one of the most technologically advanced projects in Russia. During the construction of this large-scale state scientific facility ROSATOM for the first time implemented advanced technologies and BIM model that allows monitoring the construction progress in real-

time. In September 2021 the full-scale application of integrated remote monitoring tools using digital and unmanned technology (high-resolution satellite survey, UAV survey, and laser scanning) started.

3. Scientific cooperation

3.1. International research centre MBIR

By the time the reactor is put into commercial operation, the International Research Center (IRC), the international fast reactors competence center, will start working on its basis. The IRC MBIR will work under the aegis of the Nuclear Energy Agency of the Organization for Economic Cooperation and Development and the International Atomic Energy Agency and scientists from all over the world will take part in its activities.

The access of foreign partners to the MBIR reactor will be provided through the Consortium "International Research Center based on the MBIR Reactor" (hereinafter – IRC MBIR Consortium). The corresponding agreement was signed in 2021 in Dimitrovgrad. This document made it possible to create a legal platform for foreign partners to join the IRC MBIR Consortium. The main goals of the Consortium are the formation of a competence center for fast reactor technologies and research aimed at improving the safety and efficiency of nuclear energy, as well as the formation of the reactor research market. The IRC will help to create a global platform for conducting experimental nuclear physics research.

3.2. Advanced Scientific Research Programme

In 2021 the Advanced Scientific Research Program for the 2028-2040 period to be implemented at the MBIR reactor facility (hereinafter referred to as the Program) has been issued and approved. This document reflects the key areas of scientific research proposed by the Russian specialists. Among other things, it covers the following areas:

- Fuel studies of different compositions, type and burn up rates;
- Structural materials studies for Generation IV technologies and life-time extension;
- R&D activities in independent loop channels;
- Modelling of the fuel elements behavior in the core with different coolants;
- Testing of new equipment and engineering design configurations;
- Tests of vessel and in-vessel steels for advanced thermal reactors;
- In-core studies into creep rupture strength, creep, strain capacity and irradiation embrittlement of advanced ferritic-martensitic and austenitic steels, including those under high-dose irradiation and at various temperatures;
- High-dose irradiation of materials characterized by radiation-, heat- and corrosion resistance to study their mechanical properties.

In the nearest future, with assistance of our foreign partners, the international scientific research program will be shaped.

3.3. Advisory Board

The Advisory Board of the Consortium "IRC MBIR" (hereinafter referred to as the AB) will conduct the work on expending the Program. The AB is a collegial consultative body of the Consortium, which is responsible for the elaboration of a joint scientific research program, coordination of multilateral research programs, analysis and prioritization of research areas at MBIR.

The AB will consist of representatives of Consortium members and representatives of institutional organizations that have announced their intention to join the Consortium. The Chairman of the Advisory Board is Mr. Stepan Kalmykov. Mr. Kalmykov is the Dean of the Faculty of Chemistry of Lomonosov Moscow State University and a Doctor of Chemical Sciences, Corresponding Member of the Russian Academy of Sciences as well as the Chairman of the Scientific Council of the Russian Academy of Sciences on Global Environmental Problems.

The Advisory Board shall consist of six Committees established in accordance with the main areas of research that will be carried out at the MBIR reactor:

- Materials and fuel research;
- Safety of use of nuclear technologies;
- Code verification;
- Theoretical physics;
- Non-energetic application of nuclear technologies;
- Closing of nuclear fuel cycle.

The first meeting of the Advisory Board is scheduled for the beginning of July this year. It will take place in the city of Dimitrovgrad at the research institute JSC “SSC RIAR” where the MBIR construction site is located. Within the framework of this meeting, participants will have the opportunity to exchange best practices in conducting research in the field of innovative nuclear technologies, discuss the most promising areas of nuclear research, exchange experience with specialists from a wide range of organizations and also learn more about the opportunities for scientific cooperation on the basis of the IRC MBIR.

4. Conclusion

Participation in the IRC MBIR Consortium at the current stage opens up for the members a mechanism to access to the reactor resource for the entire period of reactor operation, creates preferential prices for irradiation of materials in the reactor’s core, provides an opportunity to participate in the work of all its governing bodies and also presents options to introduce changes into the configuration of the research equipment and participate in the international research program development. Thus, joining the Consortium at the investment stage gives the participants a chance to obtain the maximum of economic and scientific benefits from working at the MBIR reactor.

UPDATES FROM THE INVOLUTE WORKING GROUP

AURÉLIEN BERGERON, JEREMY R. LICHT, MARTA SITEK, CEZARY BOJANOWSKI, YIQI YU
Argonne National Laboratory
9700 S Cass Avenue, Lemont, 60439, IL, USA

CHRISTIAN REITER, KALTRINA SHEHU, RONJA SCHÖENECKER
Forschungs-Neutronenquelle Heinz Maier-Leibnitz, Technische Universität München
Lichtenbergstr. 1, Garching, 85748, Germany

KATARZYNA BOROWIEC, EMILIAN L. POPOV, PRASHANT K. JAIN
Oak Ridge National Laboratory
1 Bethel Valley Road, Oak Ridge, 37830, TN, USA

YOANN CALZAVARA, FRÉDÉRIC THOMAS
Institut Laue-Langevin
71 Avenue des Martyrs, Grenoble, 38000, France

ABSTRACT

The HFIR, RHF, and FRM II reactors represent a particular class of Research and Test Reactors that provide some of the most intense and continuous neutron fluxes for science, industry, and medical applications. These high-performance reactors have achieved compact cores by operating with Highly Enriched Uranium fuel (HEU, ^{235}U/U ≥ 20 wt. %) and utilizing fuel plates curved as an involute. Due to the proliferation risks, the international community aims to reduce or eliminate, when possible, the use of HEU fuel in civilian facilities by converting them to a Low-Enriched Uranium fuel (LEU, ^{235}U/U < 20 wt. %). Conversion of these reactors without significantly compromising their performance or safety is a challenging endeavour that can tremendously benefit from advanced computational tools and thus, eliminate unnecessary conservatism to ensure large thermal margins. Therefore, models are being developed using modern Computational Fluid Dynamics (CFD) and Computational Structural Mechanics (CSM) software to evaluate the steady-state safety margins of various LEU designs instead of the more traditional, conservative methods. To gain the confidence and acceptance of high-fidelity modelling by the nuclear regulators, Argonne National Laboratory (ANL) and the involute reactors have formed an informal scientific group, the Involute Working Group (IWG). The IWG is facilitating inter-organizational collaboration on experimental benchmarking, code-to-code comparisons, and Verification and Validation (V&V). This paper describes some of the recent IWG efforts in validating software against the existing experimental data, as well as code-to-code comparisons of different software used by the IWG members.

1. Introduction

There are three research reactors in the world having fuel plates curved as circle-involute (a spiral generated around a circle):

- The Oak Ridge National Laboratory (ORNL) High Flux Isotope Reactor (HFIR) located in Tennessee, USA [1]
- The Laue-Langevin Institute (ILL) High Flux Reactor (RHF) located in Grenoble, France [2]

- The Technical University of Munich (TUM) Research Neutron Source Heinz Maier-Leibnitz (FRM II) located in Garching, Germany [3]

These reactors can produce a particularly intense and continuous flux of thermal neutrons (i.e., ~ 1.0 x 10^{15} n/cm^2/s) to fulfill critical scientific (e.g., neutron scattering experiment) and industrial missions (e.g., isotope production).

All three reactors are currently using Highly Enriched Uranium (HEU, ^{235}U/U ≥ 20 wt. %) as fuel, and all three are actively engaged in activities to convert to Low-Enriched Uranium (LEU, ^{235}U/U < 20 wt. %) fuel.

These reactors have expressed interest in using advanced computational methods and tools to perform some of their safety conversion calculations. These tools represent a significant departure from traditional methods and require thorough qualification before the conversion analyses can be submitted to a regulator. In the context of this paper, qualification means the recognition that the software is able to provide results that are usable for a nuclear safety case.

Thermal-hydraulic experts from Argonne National Laboratory (ANL) and the involute reactors formed an informal group to help each other in this endeavour. This so-called Involute Working Group (IWG) aims, among other things, at supporting the qualification of advanced computational methods to support the conversion to LEU fuel. Activities include benchmarking, code-to-code comparison, Verification and Validation (V&V), as well as technical support and issuance of lessons learned and other relevant publications.

The goal of this paper is to provide an overview of ongoing IWG activities. The paper provides technical information on the involute-plate reactors (Section 2). Then provides more information on the Involute Working Group and its scope (Section 3). Finally, presents an overview of ongoing activities (Section 4).

2. Involute-Plate Reactors

The fuel elements of involute-plate reactors have an annular shape as depicted in Figure 1, which shows a top view, from left to right, of the HFIR, RHF, and FRM II fuel elements. HFIR has two elements, while RHF and FRM II have only one. Fuel elements have to be replaced at every new cycle (i.e., once-through core). Figure 2 provides a more detailed view of the HFIR plates and channels. As one can see in this figure, the fuel plates curved as circle-involute are attached (welded) to two concentric tubes (commonly referred to as side-plates).

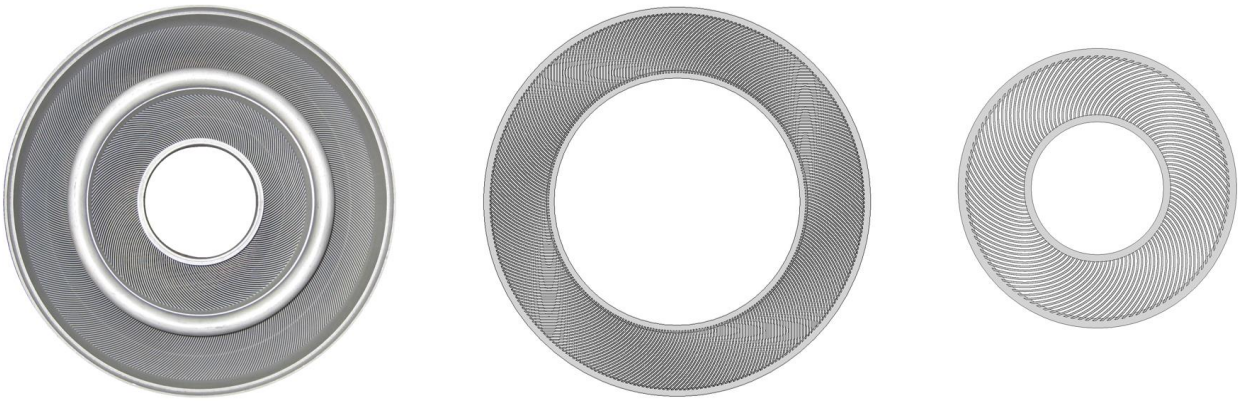

Fig 1. From left to right: top view of the HFIR, RHF and FRM II fuel elements. Source: [4]

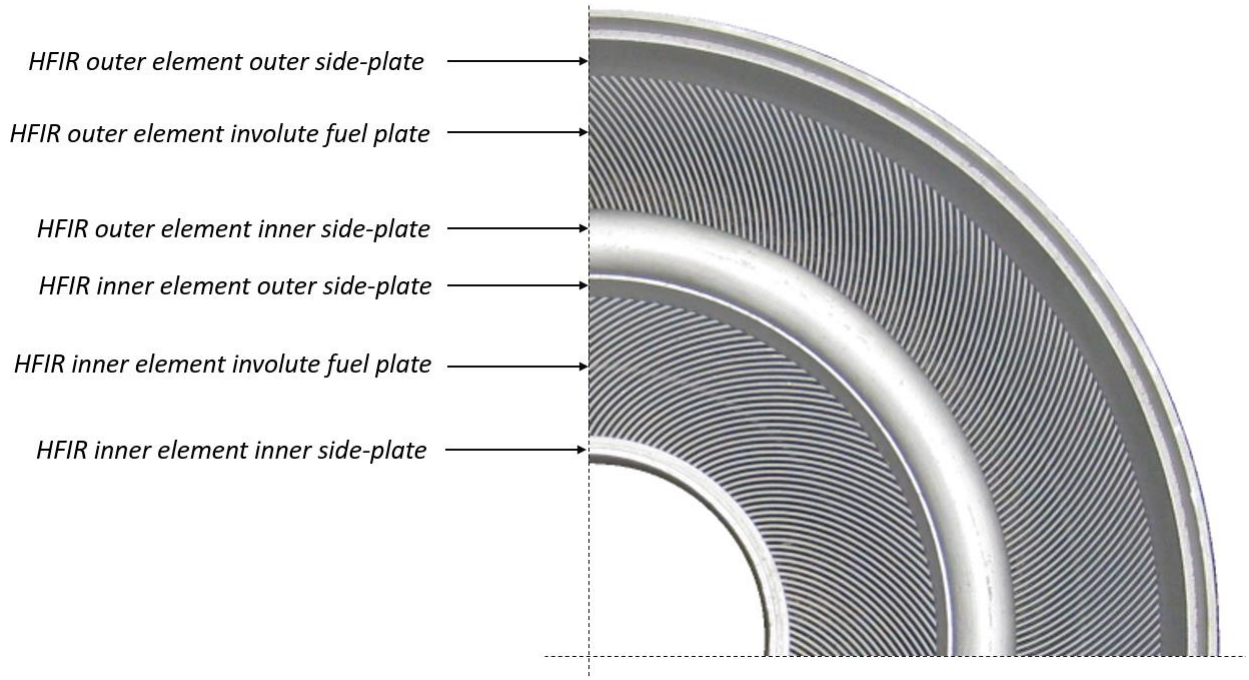

Fig 2. Detailed (top) ¼ view of the HFIR fuel elements. Source: [4]

The space between two adjacent fuel plates forms a coolant channel in which the coolant passes at a very high speed (~15m/s) to remove the heat generated in the fuel plate by nuclear reactions. The fuel plates are very thin (1.27 – 1.36 mm, depending on the reactor) and have a sandwich-like structure. The fuel is made of HEU mixed with aluminium. This so-called “meat” is cladded on each side by aluminium alloy foils. RHF uses heavy water as coolant while FRM II and HFIR use light water. The coolant flows from top to bottom for all three reactors. More information on these reactors and elements can be found in Table I. The involute shape allows for:

- The thickness of a coolant channel to be constant from the inner to the outer edge of the element
- All these channels to be identical (granted some local deviations introduced during the manufacturing process)
- All these fuel plates to experience very similar irradiations conditions (granted some possible local azimuthal variations induced by the presence of safety or experimental components located in the vicinity of the fuel elements)

These features are particularly interesting for Steady-State Thermal-Hydraulic (SSTH) analysis since it only requires modelling one or a few channels (and not all of them) to characterize the entire element. In addition, one could argue that the constant channel thickness allows for modelling the involute-shaped channel as a simple rectangular channel heated on both sides, as depicted in Figure 3. Historically, SSTH analyses have often been carried out following a modelling approach in which the coolant channel is divided into several independent sub-channels (no energy exchange between sub-channels). In this simplified representation, heat comes from the direction normal to the plates, as illustrated in Figure 3 below. Lateral and axial heat conduction, heat-induced mass flow redistribution, or effect of the unfuelled regions are often ignored, translating into a relatively conservative physical representation of the heat transfer in the coolant channel. This, in turn, results in a relatively conservative estimation of the safety margins.

Parameters	HFIR	RHF	FRM II
HEU Fuel type	U_3O_8 / Al	UAlx / Al	U_3Si_2 / Al
Number of elements	2	1	1
Cooling fluid	Light water	Heavy water	Light water
Total nuclear power (MW)	85	57.8	20
Number of plates	540 (171+369)	280	113
Plate thickness (mm)	1.27	1.27	1.36
Plate length (cm)	60.96	90.30	72.00
Channel width along involute arc length between side plates (cm)	8.548 / 7.679	7.594	6.940
Channel thickness (mm)	1.27	1.80	2.20
Cladding thickness (mm)	0.254	0.380	0.380
Meat thickness (mm)	Varies along width, Max: 0.693	0.51	0.60
Meat width along involute arc length (cm)	7.798 / 7.087	6.734	6.240
Width inner unfueled region (from outer radius of inner side-plate to inner fuel radius, cm)	0.234 / 0.218	0.314	0.259
Width outer unfueled region (from outer fuel radius to inner radius of outer side-plate, cm)	0.516 / 0.374	0.547	0.441
Average coolant velocity (m/s)	15.5	17	15.9
Nominal inlet / outlet bulk temperature (Celsius)	49 / 69	30 / 50	38 / 53
Nominal inlet / outlet pressure (Bar)	33.3 / 25.72	14 / 4	8.8 / 2.3
Reynolds number	~100,000	~100,000	~100,000
Peak heat flux (W/cm^2)	< 400	< 400	382.3[1]

Tab 1: Current (HEU) Involute-plate Reactor characteristics. Source: [4]

[1] For FRM II, evaluated using a 3-D heat conduction model. A 1-D model was used for RHF and HFIR

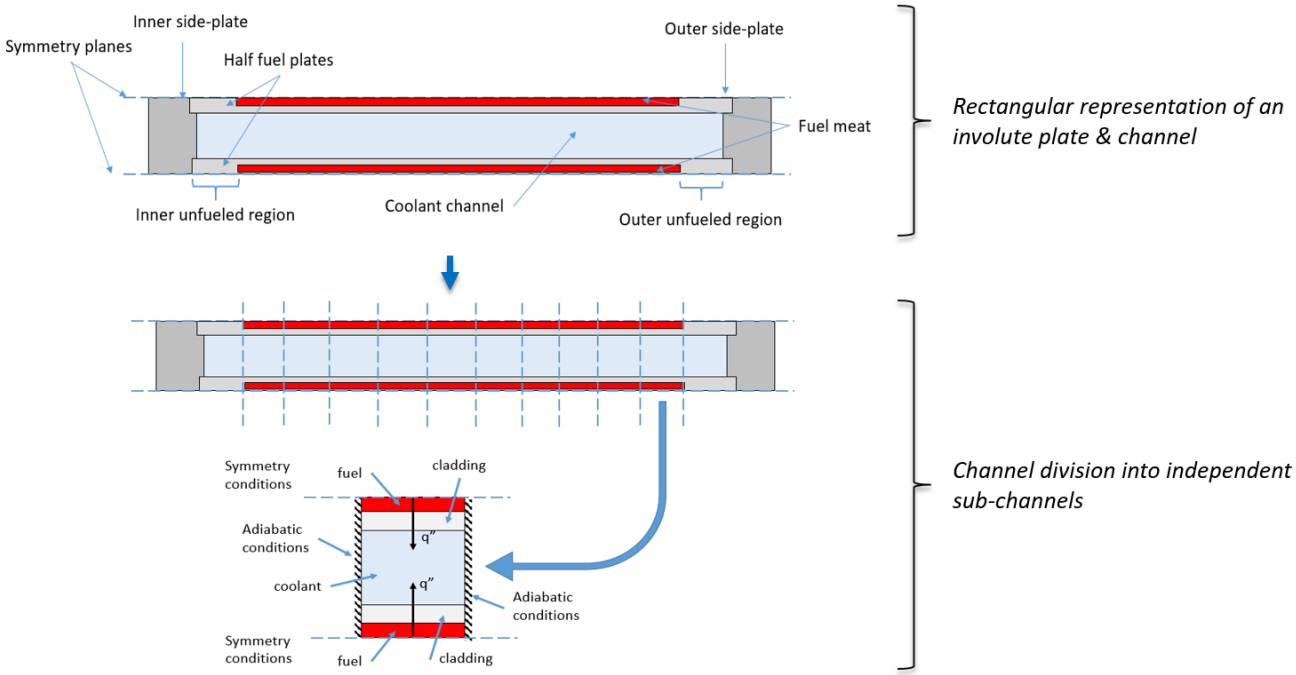

Fig 3. Simplified geometric representation and modelling of an involute plate and channel. Source: [4]

The fuel element of these reactors is located at the centre of a larger vessel that contains the reflector (heavy water for RHF and FRM II, beryllium for HFIR) and experimental and safety devices. The cylindrical volume located at the centre of the annular fuel elements is often referred to as the central cavity. FRM II and RHF use this space for the control elements, which move vertically to control the reactivity during the cycle. HFIR uses this central cavity for isotope production. HFIR reactivity control is assured by an inner and outer shroud located between the outer edge of the outer element and the beryllium reflector.

Due to these geometric characteristics, fast neutrons born from fission thermalize in the reflector and the central cavity. Because the fuel plates are oriented “edge-on,” thermalized neutrons coming back to the fuel elements tend to be captured more frequently on the edges of the fuel, where more fissions and, therefore, more heat is generated.

This leads to a non-uniform distribution of power within the plates where the power tends to spike at the edges. Due to this non-uniformity in power, the involute-plate reactors require additional design features to reduce power peaking locally and satisfy their safety margin requirements. For instance, RHF has borated regions above and below the fuel, FRM II fuel has a lower density near the outer edge, and HFIR fuel thickness is reduced near the inner and outer edges.

While these complex design features are necessary to satisfy the reactor’s safety requirements, it is important to note that they induce substantial fabrication costs and for features involving mass reduction (e.g. reduced thickness or density), may lead to a performance penalty.

3. Involute Working Group

In the framework of its non-proliferation policies, the international community aims to eliminate HEU fuel use in civilian facilities (such as research reactors). Many organizations

worldwide are developing high-density LEU fuel to replace their HEU fuel. All three involute reactors are actively engaged in conversion to LEU activities.

Since the inception of the conversion program, Argonne played a crucial role in helping reactors with their conversion effort by sharing expertise, performing independent analyses, and developing software dedicated to the analyses of research & test reactors. Argonne is actively collaborating with all three involute-plate reactors.

Conversion to LEU implies changing the fuel and, therefore, changing the material properties, which influence the thermal-hydraulic and thermal-mechanical behaviour of the fuel elements. It often also implies making geometric modifications (plate length, channel thickness, and others) that affect the elements' thermal-hydraulic and thermal-mechanical performance.

While performing conversion-related analysis, involute-plate reactors encountered several issues with existing tools and methods:

- Lack of flexibility of legacy codes to model the changes described above and;
- LEU fuels being denser than HEU, power peaking is typically aggravated, increasing the cladding/coolant interface heat flux, increasing local bulk, wall, and fuel temperature, in effect, reducing the calculated safety margins.

To overcome the limitations described above, the organizations operating the involute reactors have expressed interest in using advanced computational codes (e.g., CFD) to perform their conversion safety calculations.

These simulation tools can model virtually any kind of geometry and can model more complex physical phenomena than the legacy codes currently used for involute-plate reactor analysis. The ability to model complex physical phenomena can eliminate some unnecessary conservatism inherently present with legacy methods and provide a better estimate of the margins. Due to the importance of modelling the relevant geometric details and the need for the efficient coupling of multiple physics, modern finite element and/or volume commercial packages such as COMSOL [7], STAR-CCM+ [8] or ANSYS CFX [9] are particularly attractive for involute-plate reactors.

While involute-plate reactors have expressed interest in using these tools to perform their conversion analyses, they generally represent a significant departure from traditional methods. A thorough qualification is required before submitting output results to a regulator.

This is why Argonne National Laboratory (ANL) and the involute reactors formed an informal group to help each other in this endeavour. One of the key objectives of this Involute Working Group (IWG) is to support the qualification of advanced computational methods like CFD that facilitate the conversion to LEU fuel. The IWG has the format of an open forum that is entirely voluntary-based, where thermal-hydraulic experts can exchange, share ideas, design, and execute activities performed in the spirit of collaboration, and that can benefit all.

However, it is essential to note that the IWG is simply a forum and has not been designed to prepare and submit on a reactor's behalf the necessary documentation that could be expected by a given regulator.

4. Overview of Ongoing Activities

This section describes some examples of past and ongoing activities carried out within the IWG that feed into the various qualification steps described in the previous section.

4.1 Turbulence models & Heat Transfer – The Gambill & Bundy experiment

The so-called Gambill & Bundy experiment [10], carried out in the 1960s, aimed to verify the suitability of various heat transfer and flow-instability correlations for the thermal-hydraulic analysis of the HFIR reactor. This experiment is crucial as the conclusions drawn from these studies are still applied today in the HFIR safety basis.

The experiment consisted of a simple rectangular test-section representative of the HFIR geometry (see Figure 4) in which the passing fluid was heated on both sides. Wall temperature was measured and used to deduce the heat transfer coefficient. Enough information is available in the literature to create a CFD model of this experiment.

IWG members performed code-to-code benchmark analysis of this experiment [11] to assess the appropriateness of the standard turbulence models provided with the ANSYS-CFX, STAR-CCM+, and COMSOL software. For illustration, some results obtained with STAR-CCM+ are presented in Figure 5. As one can see, these analyses show that, for this experiment, the use of CFD and standard RANS turbulence models are appropriate as they produce results that are in good agreement with the experimental ones. This is important as it helps justify using these tools and models, a critical step in the qualification process.

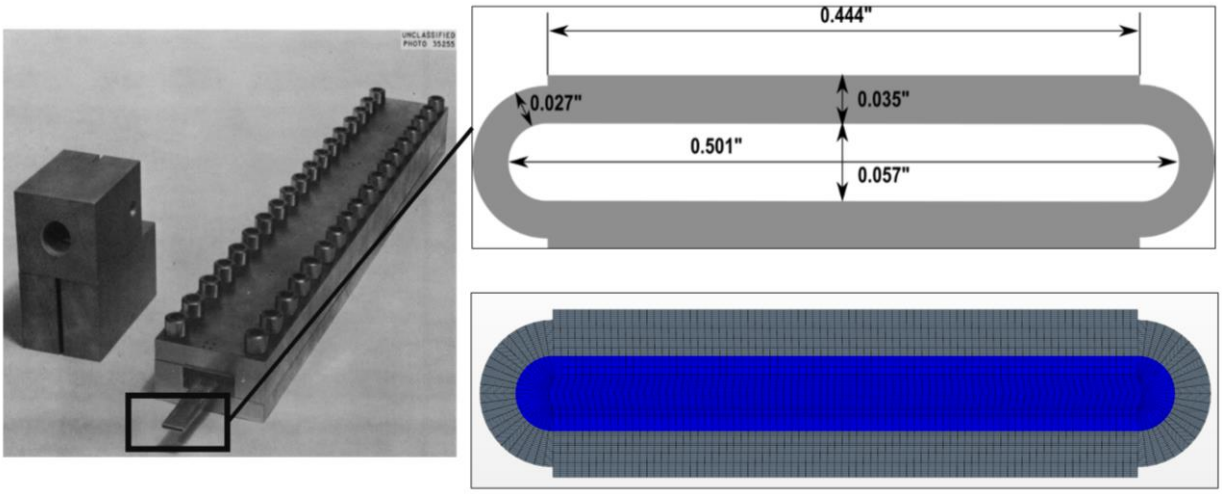

Fig 4. (Left) View of a test section used in the Gambill & Bundy experiment [12]; (right, top) schematic representation of the channel [4]; (right, bottom) view of a CFD model [4], with mesh, of the test section used in the benchmark analysis

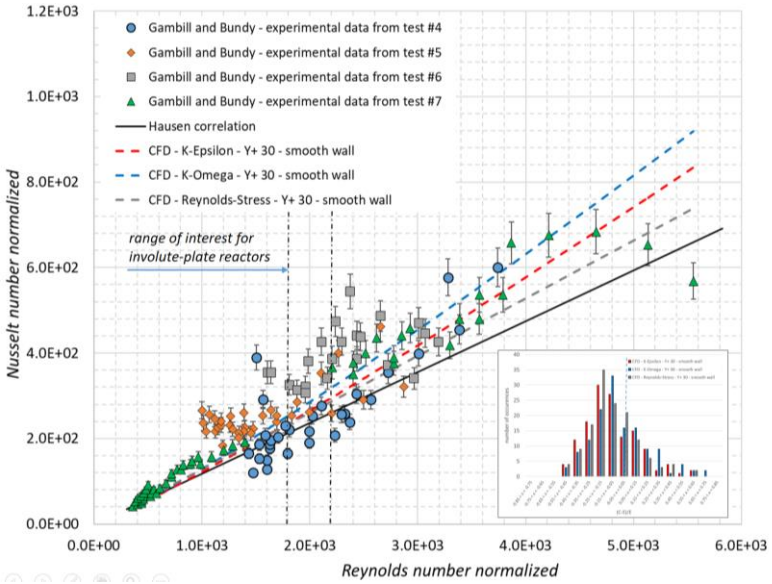

Fig 5. Comparison of experimental and CFD-calculated Nusselt number using the Gambill & Bundy benchmark. Both Reynolds and Nusselt have been normalized following Gambill & Bundy procedure (consult [12] for more details). Source: [4]

4.1. Deflection-induced channel contraction – The Cheverton & Kelley experiment

During normal operation, plate deformation such as deflection induced by pressure and/or temperature load is unavoidable and essential to characterize as they create slight, local perturbations in the flow conditions and ultimately impact heat transfer and, therefore, the margins to boiling. The so-called Cheverton & Kelley experiment, carried out in the 1960s, aimed at understanding these phenomena by applying uniform temperature and/or differential pressure load on plates representative of the HFIR geometry [13] (see Figure 6).

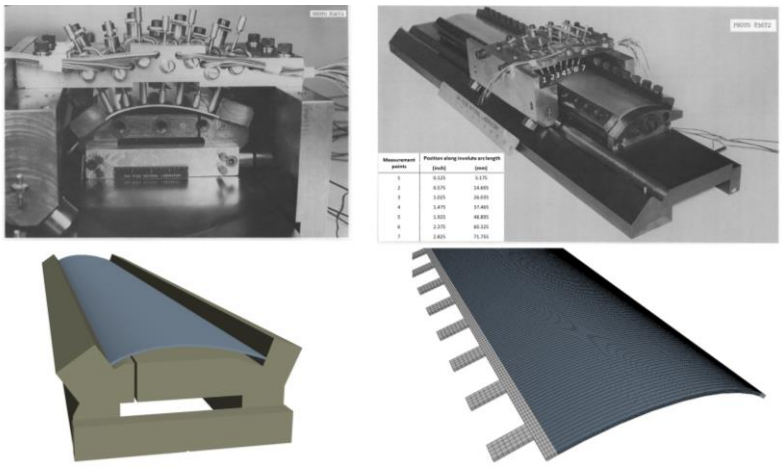

Fig 6. (Top) view of Cheverton & Kelley experimental setup; (Bottom left) View of the CAD model of the experimental setup; (Bottom right) Detailed view of the involute plate mesh model. Source: [14]

Like for the Gambill & Bundy experiment, IWG members performed code-to-code benchmark analysis of the Cheverton & Kelley experiment [13, 14] to assess the appropriateness of the ANSYS-CFX, STAR-CCM+ and COMSOL software. For illustration, some results obtained with COMSOL and STAR-CCM+ are presented in Figure 7. As one can see, these tools can reproduce experimental results relatively well, increasing confidence in their use.

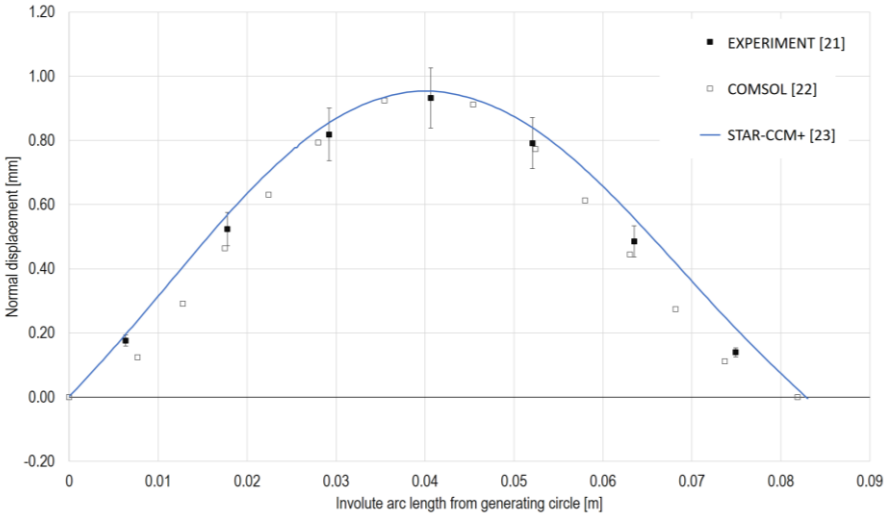

Fig 7. A comparison of experimental and COMSOL, STAR-CCM+ calculated deflection of an involute plate induced by a temperature load. Source: [14]

5. Conclusions

The Involute Working Group (IWG) is leading activities to support the qualification of advanced numerical methods and software and their utilization for safety applications to convert involute-plate reactors to LEU fuel.

The IWG has an open forum format that gathers thermal-hydraulic experts from ANL, ORNL, ILL, and TUM. Following existing best practice guidelines, the IWG carries out benchmarking, code-to-code comparisons, sensitivity analysis, and PIRT analysis. The IWG mandate is not to qualify tools on behalf of a given reactor operator but instead to prepare reference analysis and documentation that reactors could use to support their individual needs.

Examples of some activities aiming at demonstrating the appropriateness of CFD and CSM software were provided. Future work will identify new validation cases, design “CFD grade” experiments, uncertainty quantification and issuance of lessons learned, and recommendations for safety applications.

6. Acknowledgments

Argonne and Oak Ridge National laboratory work was sponsored by the U.S. Department of Energy, Office of Material Management and Minimization in the U.S. National Nuclear Security Administration Office of Defense Nuclear Nonproliferation under Contract DE-AC02-06CH11357.

Technische Universität München work was supported by a combined grant (FRM2023) from the Bundesministerium fur Bildung und Forschung (BMBF) and the Bayerisches Staatsministerium fur Wissenschaft und Kunst (StMWK).

7. References

1. “High Flux Isotope Reactor – User Guide, Revision 2.0,” Oak Ridge National Laboratory, (2015).
2. B. Jacrot, *Neutrons for Science, The Story of the First Forty Years of the Institut Laue – Langevin*, Institut Laue – Langevin (2006).

3. H. Gerstenberg and I. Neuhaus, “A Brief History of the FRM II reactor,” *International Symposium on the Peaceful Applications of Nuclear Technology in the GCC Countries*, Jeddah, 2008.
4. C. Bojanowski et al., “Involute Working Group - Validation of CFD Turbulence Models for Steady-State Safety Analysis,” Argonne National Laboratory, ANL/RTR/TM-19/5 (2020).
5. A. Bergeron, “Review of the Oak Ridge National Laboratory (ORNL) Neutronic Calculations Regarding the Conversion of the High Flux Isotope Reactor (HFIR) to the Use of Low Enriched Uranium (LEU) Fuel,” Argonne National Laboratory, ANL/RERTR/TM-12/49 (2012).
6. C. Bojanowski and Aurelien Bergeron, “Influence of Multi-Dimension Heat Conduction on Heat Flux Calculation for HFIR LEU Analysis,” Argonne National Laboratory, ANL/RTR/TM-17/18 (2017).
7. COMSOL Multiphysics® v. 5.6. www.comsol.com. COMSOL AB, Stockholm, Sweden.
8. Simcenter STAR-CCM+®, Version 2019.2, Siemens PLM Software.
9. Ansys® CFX, Release 18.1, help system, *ANSYS-CFX Solver Theory Guide*, ANSYS, Inc.
10. W. R. Gambill and R.D. Bundy, “HFIR Heat-Transfer Studies of Turbulent Water Flow in Thin Rectangular Channels,” Oak Ridge National Laboratory, ORNL-3079 *(*1961).
11. K. Shehu et al., “First Steps to Coupled Hydraulic and Mechanical Calculations within a Parameter Study to Define Possible Core Designs for the Conversion of FRM II,” Proceedings of PHYSOR-2020 Topical Meeting Cambridge, United Kingdom, March 28 – April 2, 2020.
12. R. D. Cheverton, W. H. Kelley, “Experimental Investigation of HFIR Fuel Plate Deflections Induced by Temperature and Pressure Differentials,” Oak Ridge National Laboratory, ORNL-TM-2325, (1968).
13. P. K. Jain et al., “3D COMSOL Simulations for Thermal Deflection of HFIR Fuel Plate in the “Cheverton-Kelley” Experiments,” Oak Ridge National Laboratory, ORNL/TM-2012/138 (2012).
14. M. Sitek et al., “Involute Working Group – Development and Validation of the Finite Element Models of the Cheverton-Kelley Experiments,” Argonne National Laboratory, ANL/RTR/TM-20/15 (2020).

VALIDATION OF SERPENT 2 USING EXPERIMENTAL DATA FROM THE SPERT-IV D-12/25 RESEARCH REACTOR TESTS

J.C. ALMACHI, V.H. SANCHEZ-ESPINOZA
Institute for Neutron Physics and Reactor Technology, Karlsruhe Institute of Technology
Hermann-von-Helmholtz-Platz 1, 76344 Eggenstein-Leopoldshafen – Germany

M. MARGULIS
Nuclear Futures Institute, School of Computer Science and Electronic Engineering, Bangor University, Bangor, LL57 2DG, United Kingdom

ABSTRACT

In this work, the analysis of two test scenarios of the SPERT IV D-12/25 reactor using the Monte Carlo Serpent 2 code is presented and the results are discussed. A first full 3D model of SPERT was developed to predict the critical condition characterised by four control rods position at 36.70 cm (measured from the lowest part of the fuel plate) and the transient rod completely withdrawn out of the core. The Serpent 2 code is validated against the experimental data described in the nuclear start-up report of SPERT IV. In addition, another full 3D model was elaborated for the simulation of the critical conditions with different positions of the control rods and of the transient rod. The maximal reactivity worth of the new transient rod position was estimated to be 2.64 $. In this case, the control rods position is 44.955 cm and the position of the transient rod is 21.915 cm. These investigations pave the way for the analysis of the transient rod ejection test with the high-fidelity coupled code Serpent2/Subchanflow.

1. Introduction

In recent years, several neutrons and thermal-hydraulic codes have been validated using experimental data in order to improve the prediction capability of simulation tools for both research and power reactors. Large volume of experimental data for research reactors was made available to the research community in the frame of the Coordinated Research Project (CRP) of the International Atomic Energy Agency (IAEA) from 2008 to 2013 this project, *Benchmarking against Experimental Data of Neutronics and Thermohydraulic Computational Methods and Tools for Operation and Safety Analysis of Research Reactors IAEA-TECDOC-1879*, generated a large amount of results of computer simulations for various conditions and geometrical configurations of eight research reactors [1]. For several years, simulation tools have been evolving and computational technological progress has allowed the implementation of innovative analysis methods such as high-fidelity simulations e.g., neutrons and thermal-hydraulics both coupled. High-fidelity simulations are in continuous development and are widely applied in power reactors. Several research groups tried to adapt numerical codes developed for power reactors to research reactors. This approach uses heuristic methods of calculations using equivalent plates, geometrical simplifications, and among other things, specific correlations for power reactors, [2–6]. In recent years several researchers have applied stochastic and deterministic neutronics codes for the analysis of the core of research reactors [7–12].

At the Karlsruhe Institute of Technology (KIT), high-fidelity multi-physics simulation tools for power reactors are under development in the framework of the participation to different European projects, e.g. H2020 McSAFE [13, 14]. The Monte Carlo Serpent 2 and Subchanflow thermal-hydraulic codes have been coupled under the Master-Slave approach at KIT for the analysis of transients. In 2019, the thermal-hydraulic code Subchanflow was

extended and validated for the analysis of research reactor cores [15, 16]. The extended Serpent2/Subchanflow platform of codes has been used to analyse hypothetical transients of an MTR-core defined in the IAEA 10MW benchmark [17] and detailed steady state and transient analysis of an MTR-core at plate-by-plate and subchannel-by-subchannel level were performed and the results discussed in [18]. To validate Serpent2/Subchanflow, the experimental data (neutrons and thermal-hydraulic) of the SPERT-IV 12/25 reactor have been selected. First, in this work, the experimental neutronic data are used for the validation of the full 3D model of Serpent 2. Subsequently, a new criticality position is established based on the recommendations of [19] page 13 in which the transient rod is the one providing the reactivity. These investigations are an important precondition for the subsequent analysis of the transient test with the high-fidelity Serpent2/Subchanflow code. This paper consists of five sections. Section 2 describes the dimensions and initial conditions of the SPERT-IV D12/25 reactor configuration. Section 3 presents the assumptions necessary for the construction of the Serpent 2 model. Section 4 discusses the comparison of experimental data with the predicted results, and it characterises the new critical state of the reactor. Section 5 presents the conclusions and outlook.

2. Description of SPERT-IV reactor

This section presents a brief description of the geometrical parameters of the SPERT-IV reactor. In order to reduce the metrological differences involved in the transformation from imperial to metric units, a 3D model was built using the Autodesk-Inventor program [20]. Figure 1 (a) shows the dimensions in mm of the lower grid assembly made of 6061-T6 aluminium. It contains 81 internal holes to house the fuel assemblies. The active part of the reactor core is located in the centre of the lower grid. The core, Figure 1 (b), consists of 20 standard fuel assemblies, four control fuel assemblies and one transient fuel assembly for a total of 25. The fuel assemblies are housed in an assembly also made of aluminium, Figure 1 (c).

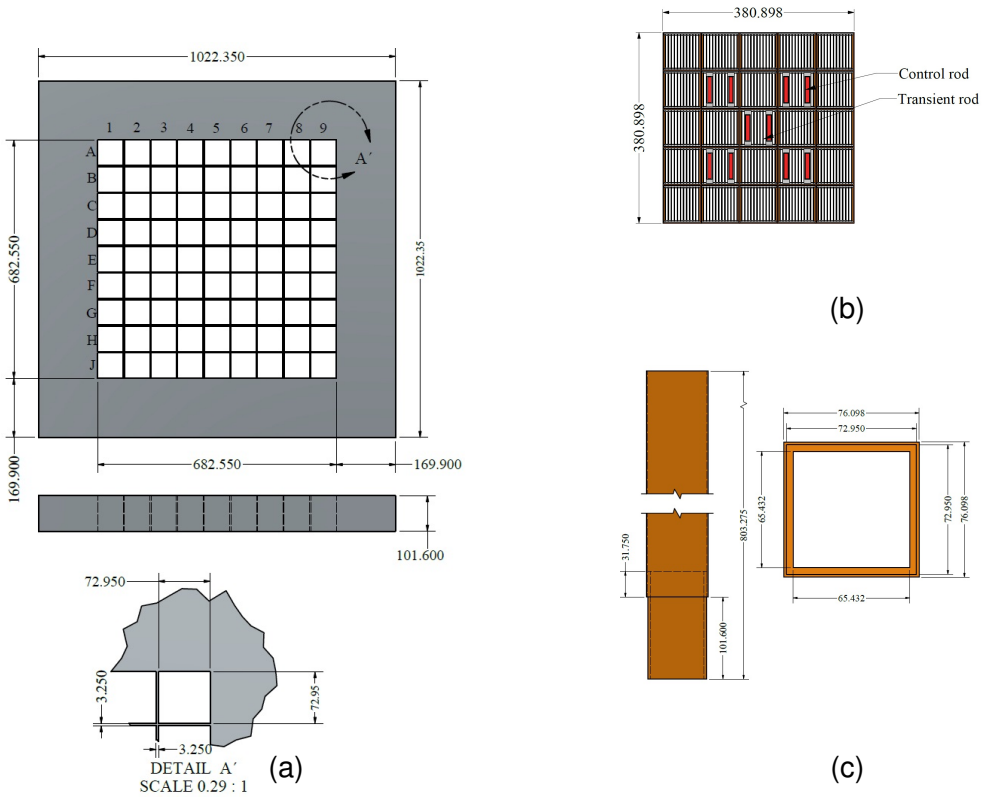

Fig. 1. SPERT-IV dimensions in mm of: (a) lower grid assembly; (b) core; (c) assembly can

Figure 2 (a) shows the dimensions of a standard fuel assembly (SFA) composed of 12 fuel plates (HEU 93 % enriched). Figure 2 (b) shows the dimensions of the control fuel assembly (CFA), which has a total of six fuel plates and at each end a space to accommodate the absorbent material (B-Al). The side plates supporting the cladding of the fuel plates are made of aluminium. The axial dimensions of the meat inside of the aluminium plate can be seen in Figure 2 (c). Finally, the axial dimensions of the control and transient rods are shown in Figure 2 (d).

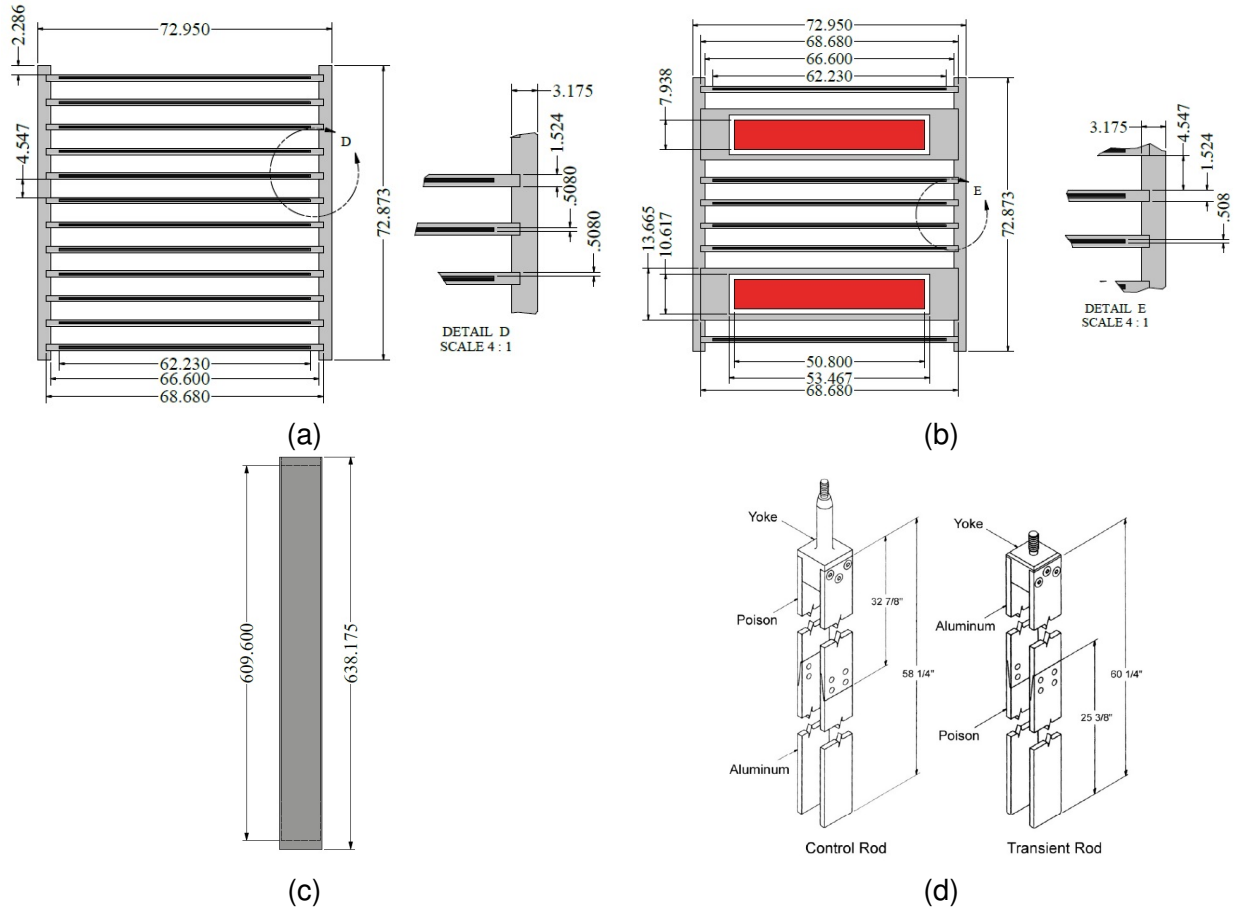

Fig. 2. SPERT-IV dimensions [20]: (a) standard fuel assembly in mm; (b) control fuel assembly in mm; (c) plate-fuel in mm; (d) control and transient rod in inch

Table 1 shows the main operating specifications for the neutronic tests. Material specifications in atomic density required for Monte Carlo calculations can be found in [20] on page 14.

Type of reactor	**Open pool MTR type**
Fuel type	UAl alloy Al cald flat plate fuel
Enrichment	HEU 93 %, 14.0 g ^{235}U
Reference pressure	Pool is open to the atmosphere
Nominal reference temperature	20 °C
Coolant	Light water
Moderator	Light water
Reflector	Light water
Poison material	Binal (B-Al)

Tab 1: Main operation conditions of SPERT-IV

3. Calculation tools

The Monte Carlo code Serpent 2 is used for the core analysis. It is a state-of-the-art code that uses the standard ACE Nuclear Data format for 3D continuous space-energy calculations [21]. This code is widely used for both static and dynamic calculations [22].

3.1 Serpent model and assumptions

A detailed Serpent model, i.e. at plate and subchannel level, was developed following the geometrical description presented in section 2. For the static neutronic calculations, the following aspects were used.

- Nuclear data library: ENDFB-VIII.0 [21]
- The control and transient rod will be moved by Universe Transformation (trans) [23]
- Axially, each plate is subdivided into 60 zones.
- A square detector of 0.1016 cm was used for thermal flux
- The absorber material is Binal (Bi-Al)
- The control rods are extracted in Z+ axis direction
- The transient rod is inserted in the Z+ axis direction
- The criticality calculations are performed with 200 inactive cycles followed by 1000 active cycles, each consisting of 10^6 histories.

In order to validate the results, the measured and calculated thermal fluxes were compared in two positions, E5 and D4, [24]. The data experimental were measured by means of cobalt wires located at different positions, see Figure 3. The energy cutoff for thermal flux was set to 0.5 eV.

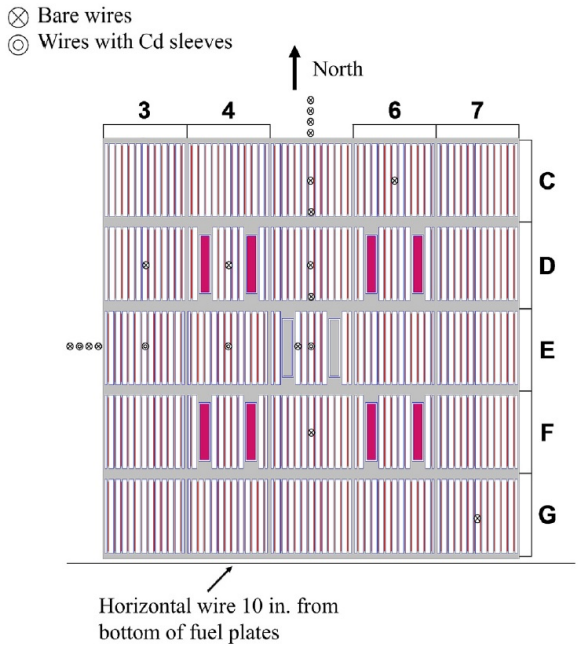

Fig. 3. Radial position of cobalt wires for thermal flux measures, [10]

To obtain the new critical state of the reactor, first, the control rods are extracted until a reactivity of $\sim$ 2.64 $ is reached. Then the transient rod is inserted until the reactivity is reduced to $\sim$ 0 $, see [19] page 13.

4. Comparison of the experimental data with the Serpent predictions

Figure 4 and 5 show the normalised axial thermal flux at positions D4 and E5 with a statistical error of $\pm$ 2 sigma compared with the measurement data. The highest statistical error is found around the peaks of the flux profile. The thermal flux has also been normalised, and a higher statistical error can be observed in the lower major peaks. In general, the results of Serpent are very close to the measured data at the two positions, and they are comparable to those presented in [10].

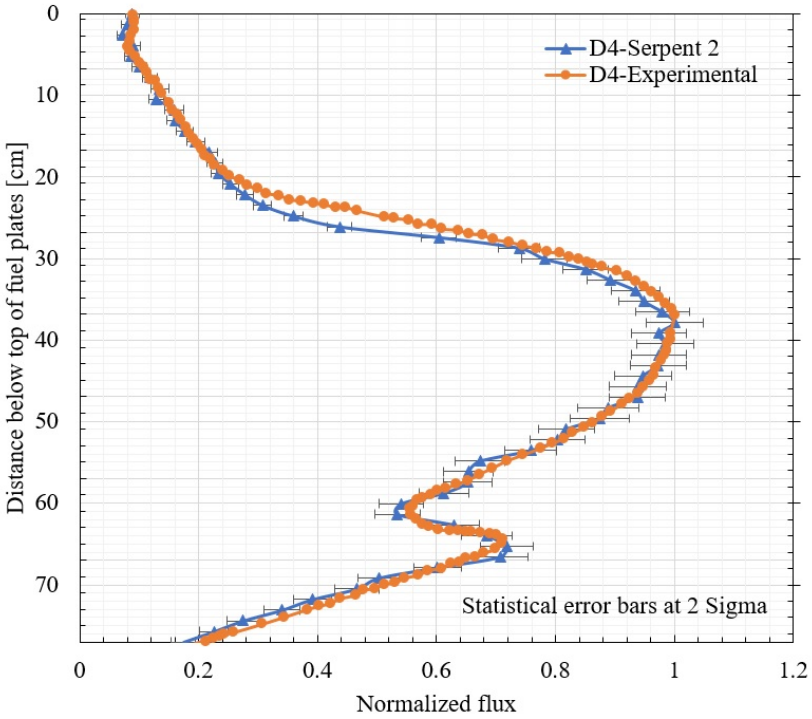

Fig. 4. Comparison of thermal flux detectors at location D4

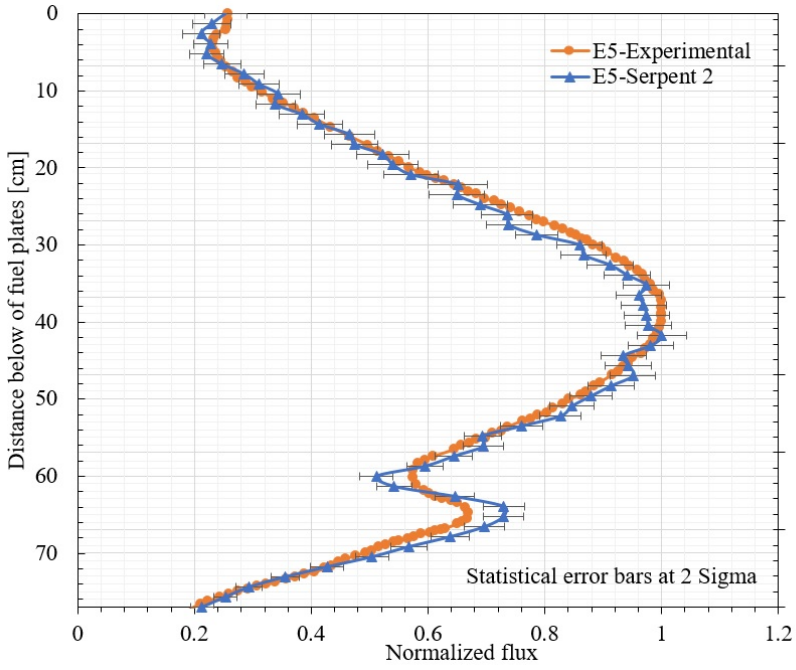

Fig. 5. Comparison of thermal flux detectors at location E5

Figure 6 shows the reactivity added to the reactor when the control rods are extracted step-by-step. The simulations were performed at different rod positions (6 positions measured from the lowest part of the active region of the plate, see Figure 2 (c). The βeff value calculated by Serpent, for reactivity estimation, was 749 $\pm$ 2 pcm using the Meulekamp Method [25]. A good agreement of the predictions with the experimental data is observed.

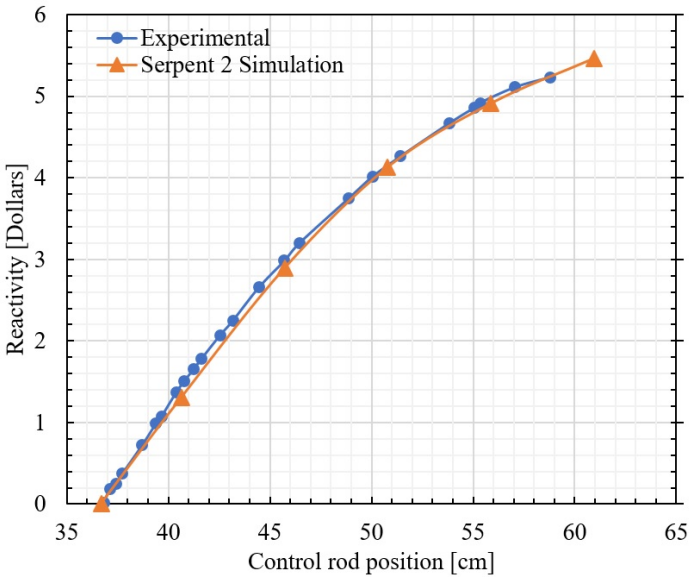

Fig. 6. Integral control rod worth comparison

The Serpent simulation time was about $\sim$ 5 hours for each position using an OpenMP compiler with 48 cores Linux 4.9.0-18-amd64. Figure 7 shows the positions of the control and transient rods for a new critical state with a factor keff of 1.00001 $\pm$ 0.00002. The dark part of the rods corresponds to the Binal absorber material. The control rods are extracted to add reactivity in the z+ direction, whereas the transient rod is introduced in the z- direction to decrease the reactivity.

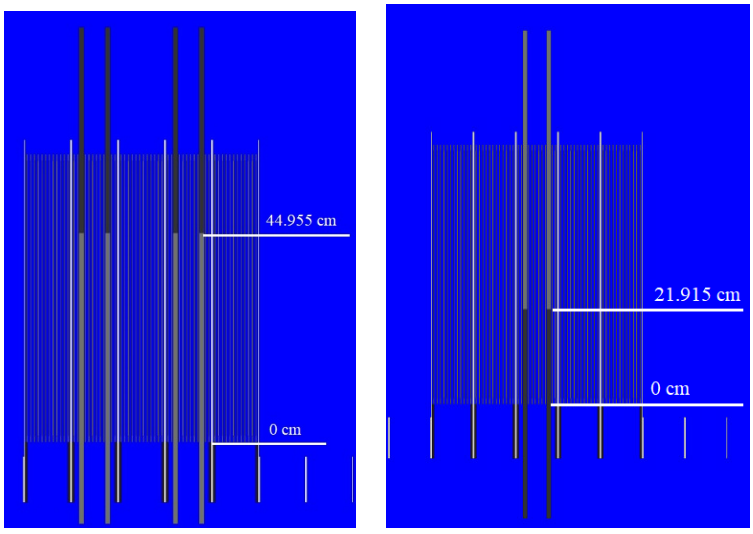

(a) (b)

Fig. 7. Critically positions of: (a) control rods; (b) transient rod

Figure 8 shows the normalised thermal flux at positions D4 and E5 predicted by Serpent 2 with a statistical error of $\pm$ 2 sigma. Higher uncertainty is observed at the peaks. The curves were obtained with the control and transient rods inserted at the positions described in Figure 7.

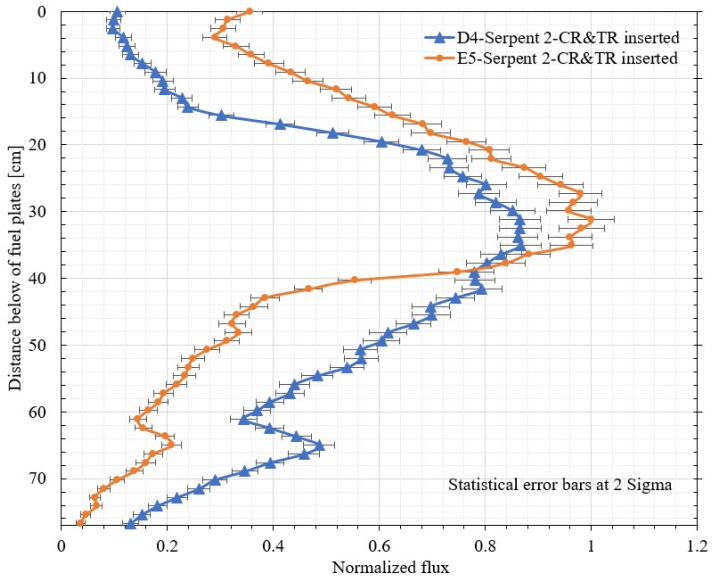

Fig. 8. Thermal flux normalised simulation, control and transient rods (CT & TR) inserted

Finally, Figure 9 shows the reactivity added by the transient rod at seven different positions. In case the transient rod is fully extracted from the core, a maximum reactivity of \$ 2.64 will be inserted into the core. The simulation time for each simulation was about $\sim$ 5 hours for each position using an OpenMP compiler with 48 cores Linux 4.9.0-18-amd64.

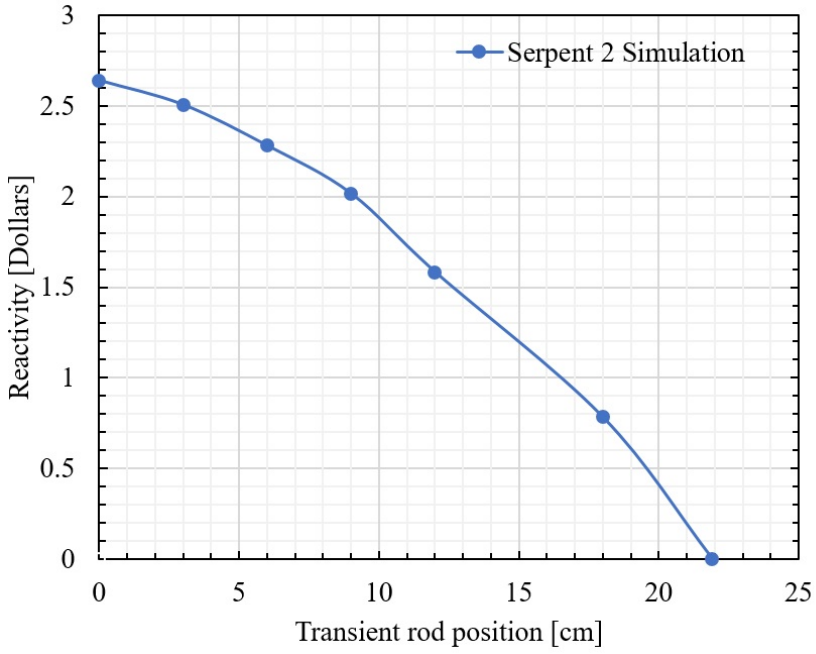

Fig. 9. Transient rod worth

5. Conclusions and outlook

The Serpent 2 code has been successfully validated against the experimental data of the SPERT-IV D12/25 reactor measured for static core conditions at two different radial positions (normalised thermal neutron flux obtained from the E5 and D4). The reactivity at different positions of the control rods was calculated, and the obtained reactivity curve was compared with the experimental data showing a good agreement. The new critical state of the core is characterised by a keff of 1.00001 $\pm$ 0.00002 with a position at 44.955 cm for the control rods and 21.915 cm for the transient rod. This new configuration will be used to determine the extraction rate of the transient rod for the high-fidelity calculations.

Acknowledgements

The authors acknowledge the financial support of the NUSAFE program at the Karlsruhe Institute of Technology (KIT) and of the Welsh European Funding Office (WEFO), project Sêr Cymru II 80761-BU-103.

References

[1] INTERNATIONAL ATOMIC ENERGY AGENCY, *Benchmarking against Experimental Data of Neutronics and Thermohydraulic Computational Methods and Tools for Operation and Safety Analysis of Research Reactors*, IAEA: Vienna, Austria, 2019; Volume TECDOC Series. [CrossRef]

[2] V. Koppers and M. K. Koch, "Heuristic methods in modelling research reactors for deterministic safety analysis," ATW-INT J NUCL POWER, vol. 63, no. 8-9, pp. 464-468, 2018. [CrossRef]

[3] K. Ahmed, "Thermal-hydraulic fortran program for steady-state calculations of plate-type fuel research reactors," Nucl. Technol. Radiat., vol. 23, no. 1, pp. 19-30, 2008. [CrossRef]

[4] J. Chao, Y. K. Cheung and A. P. Olson, "COBRA-3C/RERTR, a subchannel code for research and test reactors," Trans. Am. Nucl. Soc., vol. 34, 1980. [CrossRef]

[5] A. Hainoun, N. Ghazi and B. M. Abdul-Moaiz, "Safety analysis of the reference research reactor MTR during reactivity insertion accident using the code MERSAT," Annals of Nuclear Energy, vol. 37, no. 6, pp. 853-860, 2010. [CrossRef]

[6] A. Salama and S. E.-D. El-Morshedy, "CFD simulation of the IAEA 10MW generic MTR reactor under loss of flow transient," Annals of Nuclear Energy, vol. 38, no. 2, pp. 564-577, 2011. [CrossRef]

[7] M. A. Motalab, M. S. Mahmood, M. J. H. Khan, N. H. Badrun, Z. I. Lyric and M. H. Altaf, "Benchmark analysis of SPERT-IV reactor with Monte Carlo code MVP," Annals of Nuclear Energy, vol. 65, pp. 365-369, 2014. [CrossRef]

[8] A. Zoia, C. Jouanne, P. Siréta, P. Leconte, G. Braoudakis and L. Wong, "Analysis of dynamic reactivity by Monte Carlo methods: The impact of nuclear data," Annals of Nuclear Energy, vol. 110, pp. 11-24, 2017. [CrossRef]

[9] T. Mahmood, M. Iqbal and I. H. Bokhari, "Benchmark analysis of SPERT IV reactor," Progress in Nuclear Energy, vol. 58, pp. 6-10, 2012. [CrossRef]

[10] M. Margulis and E. Gilad, "Simulations of SPERT-IV D12/15 transient experiments using the system code THERMO-T," Progress in Nuclear Energy, vol. 109, pp. 1-11, 2018. [CrossRef]

[11] N. H. Badrun, M. H. Altaf, M. A. Motalab, M. S. Mahmood and M. J. H. Khan, "Modeling of SPERT IV Reactivity Initiated Transient Tests in EUREKA-2/RR Code," International Journal of Nuclear Energy, vol. 2014, pp. 1-8, 2014. [CrossRef]

[12] J.-M. Labit, N. Seiler, O. Clamens and E. Merle, "Thermal-hydraulic two-phase modeling of reactivity-initiated transients with CATHARE2 – Application to SPERT-IV simulation," Nuclear Engineering and Design, vol. 381, 2021. [CrossRef]

[13] D. Ferraro, V. Valtavirta, M. García, U. Imke, R. Tuominen, J. Leppänen and V. Sanchez-Espinoza, "OECD/NRC PWR MOX/UO2 core transient benchmark pin-by-pin solutions using Serpent/SUBCHANFLOW," Ann. Nucl. Energy, vol. 147, p. 107745, 2020. [CrossRef]
[14] D. Ferraro, M. García, V. Valtavirta, U. Imke, R. Tuominen, J. Leppänen and V. Sanchez-Espinoza, "Serpent/SUBCHANFLOW pin-by-pin coupled transient calculations for the SPERT-IIIE hot full power tests," Ann. Nucl. Energy, vol. 142, p. 107387, 2020. [CrossRef]
[15] J. C. Almachi, U. Imke and V. H. Espinoza-Sanchez, "Extensions of Subchanflow for Thermal Hydraulic Analysis of MTR-Cores," In Proceedings of the European Research Reactor Conference, Online, 12–15 October, pp. 1-10, 2020. [CrossRef]
[16] J. C. Almachi, V. Sánchez-Espinoza and U. Imke, "Extension and validation of the SubChanFlow code for the thermo-hydraulic analysis of MTR cores with plate-type fuel assemblies," Nuclear Engineering and Design, vol. 379, 2021. [CrossRef]
[17] J. C. Almachi, V. H. Espinoza-Sanchez, U. Imke and L. Mercatali, "High-Fidelity Analysis of MTR Cores Using Serpent2/Subchanflow," In Proceedings of the European Research Reactor Conference, Helsinki, Finland, 24–29 September, pp. 1-10, 2021. [CrossRef]
[18] J. C. Almachi , V. H. Sánchez-Espinoza and U. Imke, "High-Fidelity Steady-State and Transient Simulations of an MTR Research Reactor Using Serpent2/Subchanflow," Energies, vol. 15, no. 4, p. 1554, 2022. [CrossRef]
[19] J. G. Crocker and L. A. Stephan, "REACTOR POWER EXCURSION TESTS IN THE SPERT IV FACILITY," United States, 1964. [CrossRef]
[20] S. Day, "SPERT IV D-12/25: Facility specification," International Atomic Energy Agency (IAEA), Hamilton, Canada, 2015. [CrossRef]
[21] M.B. Chadwick and P. Obložinský and M. Herman and N.M. Greene and R.D. McKnight and D.L. Smith and P.G. Young and R.E. MacFarlane and G.M. Hale and S.C. Frankle and A.C. Kahler and T. Kawano and R.C. Little and D.G. Madland and P. Moller and R.D. Mosteller and P.R. Page and P. Talou and H. Trellue and M.C. White and W.B. Wilson and R. Arcilla and C.L. Dunford and S.F. Mughabghab and B. Pritychenko and D. Rochman and A.A. Sonzogni and C.R. Lubitz and T.H. Trumbull and J.P. Weinman and D.A. Brown and D.E. Cullen and D.P. Heinrichs and D.P. McNabb and H. Derrien and M.E. Dunn and N.M. Larson and L.C. Leal and A.D. Carlson and R.C. Block and J.B. Briggs and E.T. Cheng and H.C. Huria and M.L. Zerkle and K.S. Kozier and A. Courcelle and V. Pronyaev and S.C. van der Marck "ENDF/B-VII.0: Next Generation Evaluated Nuclear Data Library for Nuclear Science and Technology," Nuclear Data Sheets, vol. 107, pp. 2931-3060, 2006. [CrossRef]
[22] J. Leppänen, M. Pusa, T. Viitanen, V. Valtavirta and T. Kaltiaisenaho, "The Serpent Monte Carlo code: Status, development and applications in 2013," Annals of Nuclear Energy, vol. 82, pp. 142-150, 2015. [CrossRef]
[23] J. Leppänen, Serpent – a Continuous-energy Monte Carlo, VTT Technical Research Center of Finland, 2015, pp. 28-30. [CrossRef]
[24] J. G. Crocker, J. E. Koch, Z. R. Martinson, A. M. Mcglinsky and L. A. Stephen, "NUCLEAR START-UP OF THE SPERT IV REACTOR," 1963. [CrossRef]
[25] Robin Klein Meulekamp and Steven C. van der Marck "Calculating the Effective Delayed Neutron Fraction with Monte Carlo," Nuclear Science and Engineering, vol. 152, pp. 142-148, 2006. [CrossRef]
[26] D. Ferraro, "Monte Carlo-based multi-physics analysis for transients in Light Water Reactors". Ph.D. dissertation, Karlsruher Institut für Technologie (KIT), Germany, 2021. [CrossRef]

New Concept of Hybrid Low-power Research Reactor Developed by KAERI

KYUNG-O KIM, GYUHONG ROH, and BYUNGCHUL LEE

Research Reactor Design Division, Korea Atomic Energy Research Institute
111, Daedeok-daero 989 Beon-gil, Yuseong-gu, Daejeon, Republic of Korea

ABSTRACT

Korea Atomic Energy Research Institute (KAERI) has designed a second-generation Hybrid Low-Power Research Reactor (H-LPRR), which can be used as a critical assembly and conventional research reactor. Of note, the fuel assemblies and the reflectors of the H-LPRR are designed to standalone without any supporting equipment and to allow replacement with each other. Its eight irradiation holes are located on the edge of the core, and are applicable to neutron activation analysis and radioisotope production. In this study, some of important nuclear characteristics are provided, such as kinetic parameters, Control Absorber Rods' (CARs) worth, and so on, which were calculated by using the MCNP6.1 code with the ENDF/B-VII.0 library. Following a Reactivity Insertion Accident (RIA), the power trend as a function of the time was also analysed using the RELAP5 code. As a result, excess reactivity and β_{eff} at the beginning of life were evaluated to be 3.84 mk and 7.29 mk, respectively, and the integral CARs' worth and maximum value in the differential CARs' worth were 9.17 mk and 0.035 mk/mm, respectively. The results of a RIA analysis showed that the reactor power instantly reaches a plateau after increasing up to about 650 kW. From these results, it can be confirmed that the H-LPRR possesses high performance in terms of nuclear design and safety analysis, and it can be a suitable option for countries considering replacement of existing, aged low-power research reactors.

1. Introduction

The IAEA Research Reactor Database (RRDB) provides information on all of the world's 206 research reactors, classifying them by operational status, age, flux, power, and so on. Based on the information, 44.3% of the operational and temporary shutdown reactors are included in the range from zero to 100 kW_{th}, and major types of these are the Argonaut (30 kW_{th}), TRIGA (18 kW_{th}), and Miniature Neutron Source Reactor (MNSR, 30 kW_{th}). The MNSR is a compact Low-Power Research Reactor (LPRR) designed mainly for training and research, and commercial versions of this reactor have been installed in China, Ghana, Iran, Nigeria, Pakistan, and Syria [1]. The functions of LPRRs are similar to those of higher-power (> 1 MW_{th}) research reactors, although there is a difference in terms of performance and quality; (a) Radioisotope (RI) production, (b) studies of reactor characteristics, (c) uses of extracted neutrons, and (d) Neutron Activation Analysis (NAA). Hence, many countries introducing nuclear power programs have constructed or are planning to build LPRRs to establish a fundamental infrastructure prior to the introduction of nuclear power plants.

For the past 10 years, Korea Atomic Energy Research Institute (KAERI) has been working on a new concept LPRR, called the Hybrid Low-Power Research Reactor (H-LPRR), to meet the needs of not only conventional research reactor utilization but also as a critical assembly that

can be used as part of the training of nuclear engineering students at higher education institutions (see Fig. 1) [2]. A core of 70 kW_{th} power is submerged in a pool and cooled by natural convection. The use of LEU UO_2 fuels makes the core have a strong negative fuel temperature coefficient and a negative power coefficient. One very specific feature of the H-LPRR is that the core is horizontally separable into two sub-cores. The central space between the sub-cores provides an area that can be used for experiments under critical or subcritical conditions such as kinetic parameter measurements, neutron spectrum measurements for a fuel array, and measurements of the neutron detector characteristics.

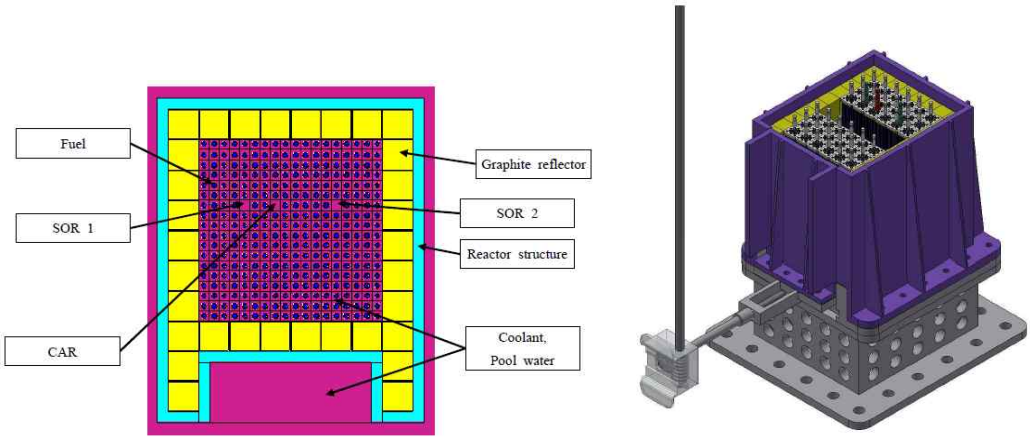

Fig. 1. The first-generation H-LPRR

Recently, KAERI has modified the existing model to increase the flexibility and cost-effectiveness, and an inherent safety function has also been reinforced to prevent a power excursion caused by a Reactivity Insertion Accident (RIA). In this study, it is demonstrated with some neutronics results in order to introduce the second-generation H-LPRR, and all of the design calculations, including fuel burnup behaviour, are performed using the MCNP6.1 code with the ENDF/B-VII.0 library [3].

2. Core characteristics of the second-generation H-LPRR

The newly designed H-LPRR is an open tank-in-pool type, of 50 kW thermal power (see Fig. 2), which is designed for training purposes, producing medical radioisotopes (e.g., ^{32}P, ^{198}Au, ^{99m}Tc, ^{192}Ir, and ^{131}I), and applying Neutron Activation Analysis (NAA). The reactor core comprises 20 fuel assemblies and reflector blocks with irradiation holes. Whenever an additional excess reactivity is required, the vacant region at the center of the core is partially changed to the reactivity compensator made with beryllium.

The fuel assembly includes a 3×3 UO_2 fuel rod array distributed on a square lattice, and the basic specifications (e.g., enrichment, radius, material, etc.) are similar to the ones used in the OPR-1000, except for the axial length (see Table 1). The reactor core has two kinds of reflectors of beryllium and graphite, which are designed to enable replacement with the fuel assemblies. Beryllium is used as an inner reflector, and this is surrounded by an outer reflector of graphite canned with aluminium. The beryllium and graphite reflectors are located on the grid plate, and standalone without any support equipment. The reactivity control is performed by four Control Absorber Rods (CARs) filled with natural B_4C, and the reactor core is cooled by natural convection. There are eight irradiation holes on the edge of the core, classified into two types: IR (for RI production) and NA (for NAA) holes.

The second-generation H-LPRR aims to operate for at least 20 years without refueling and to simultaneously provide the functions of a research reactor and critical assembly. Furthermore, it can be instantly started up and shut down without considering the xenon dead time, and it can be sequentially operated without a limitation such as the maximum continuous operation time (e.g., MNSR: < 7 hours). The concept of an in-core reactivity compensator is introduced to provide sufficient excess reactivity and to easily approach the core, and the inherent safety function is increased to prevent the damage of nuclear fuel and the power excursion caused by a RIA. The nuclear requirements considered in the design process of the H-LPRR are as follows:

(a) The temperature coefficients of fuel and coolant should be negative.

(b) The power coefficient should be clearly negative for any operating conditions.

(c) The power peaking factor should be no>3.0.

(e) The flux shape and level should be maintained even if nuclear fuels burn.

(f) Reactivity compensator should provide a sufficient reactivity to operate the reactor for a reasonable period.

(g) The maximum unperturbed thermal neutron flux level at BOL should be 4.0×10^{12} n/cm^2-s or higher. The thermal neutron flux in irradiation holes for RI production and NAA application should be ~9.0×10^{11} n/cm^2-s and ~4.5×10^{11} n/cm^2-s, respectively.

In this study, the MCNP6 code was used to evaluate the kinetic parameters (delayed neutron fraction and decay constant in each group), excess reactivity, differential and integral CARs' worth, and neutron flux distribution in each irradiation hole at the Beginning of Life (BOL). When the reactivity was suddenly inserted as much as excess reactivity in the core, the power trend as a function of time was also analysed using the RELAP5 code [4].

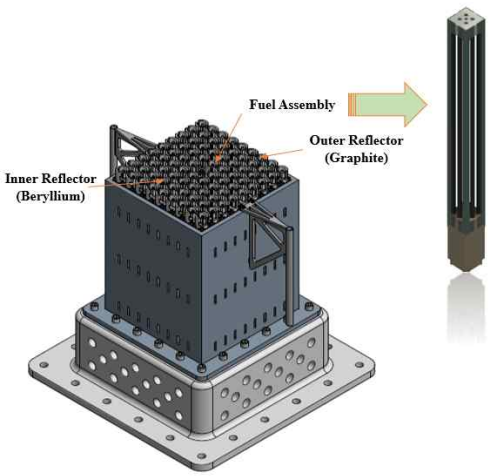

Fig. 2. Conceptual design of the second-generation H-LPRR

	Parameter	Values
Reactor	Type	Open Pool
Core	Thermal Power	50 kW_{th}
	Core Size [W×L×H]	53.7cm×53.7cm×58.32cm
Fuel Assembly	Geometry	3×3 Square Lattice
	Assembly Pitch	5.5 cm

Fuel	Type	Rod
	Material	UO_2
	Enrichment	4.65 wt%
	Clad Material	Zirlo
	Active Fuel Length	39.32
Coolant	Material	Light Water
	Core Cooling	Natural Convection
Reflector	Material	Beryllium and Graphite
Absorber	Material	B_4C (Natural)
	Use	CAR

Table 1. Design Specifications of H-LPRR

3. Results of neutronic calculations

At the BOL, excess reactivity of the newly designed H-LPRR was evaluated to be 3.84 mk, and the kinetic parameters including delayed neutron fraction in each group are presented in Table 2. As shown in the table, the effective delayed neutron fraction (β_{eff}) is 729 pcm, which is similar to that of UO_2 fuel used in a commercial Pressurized Water Reactor (PWR). Based on these results, it was expected that there is no rapid increase in reactor power (i.e., no prompt jump) because excess reactivity is considerably less than β_{eff}.

Precursor Group	Delayed Neutron Fraction [β_i]	Decay Constant [s^{-1}]
1	2.40E-04	1.249E-02
2	1.15E-03	3.176E-02
3	1.19E-03	1.097E-01
4	3.37E-03	3.184E-01
5	1.05E-03	1.351E+00
6	2.90E-04	8.741E+00
Total or β_{eff}	7.29E-03	

Table 2. Delayed neutron fraction and decay constant

In order to investigate the reactivity worth of four CARs, their moving distance was axially segmented into 10 regions, and the calculated results are shown in Fig. 3. As shown in the figure, the curves of reactivity worth are shown as typical shapes, and the integral CARs' worth and maximum value in differential CARs' worth are 9.17 mk and 1.29 mk, respectively. That is, it can be confirmed that this reactor has a sufficient shutdown margin of about 5 mk.

Figure 4 shows the thermal neutron flux distribution in the irradiation holes for RI production and NAA. As shown in the figure, the thermal neutron flux in IR holes was about two times higher than that of NA holes, and the maximum neutron flux in IR and NA holes were 9.09×10^{11} n/cm^2-sec and 4.78×10^{11} n/cm^2-sec, respectively. In terms of the thermal neutron flux, it was almost the same level as the performance of the MNSR irradiation holes (Hole for RI Production: 9.23×10^{11} n/cm^2-sec and Hole for NAA: 4.90×10^{11} n/cm^2-sec).

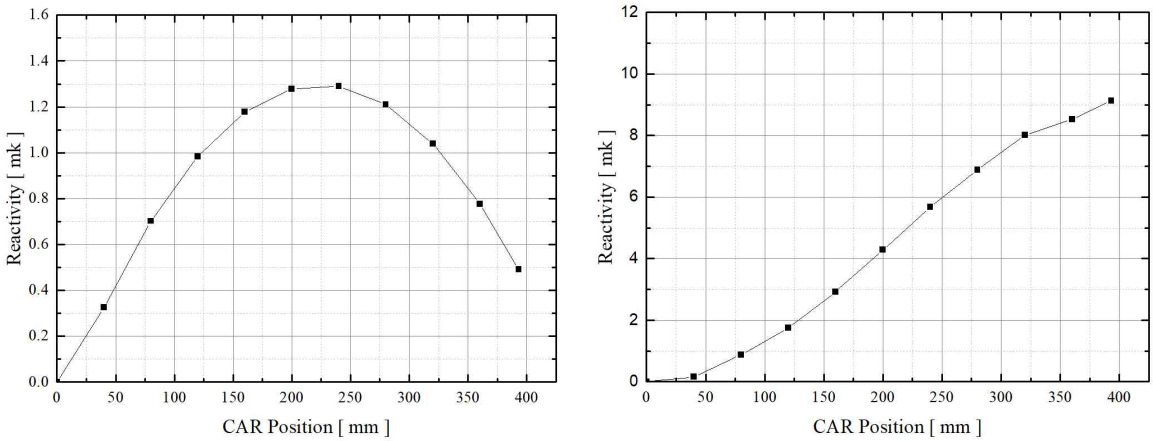

(a) Differential CAR worth (b) Integral CAR worth

Fig. 3. Reactivity worth of four CARs

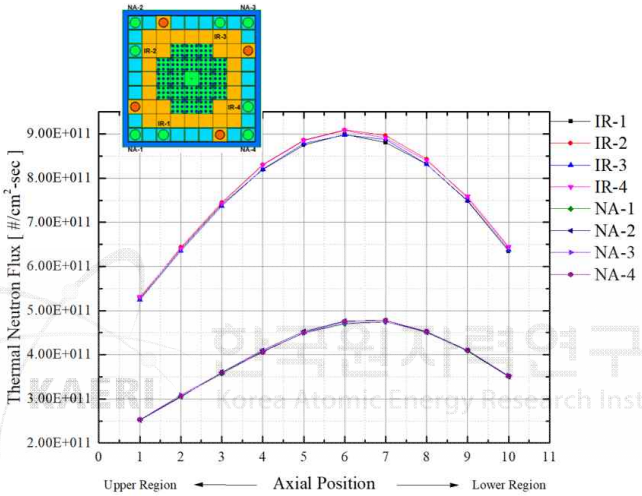

Fig. 4. Neutron flux distribution in each irradiation hole

When the reactivity was suddenly inserted as much as excess reactivity, the time-dependent power change is represented in Fig. 5. As shown in the figure, the reactor power exponentially increased up to about 650 kW at an accident moment, and after that time, the power excursion was self-limited by the reactivity feedbacks from the fuel and coolant temperatures. During the transient period, fuel integrity was assured in terms of critical heat flux and fuel temperature.

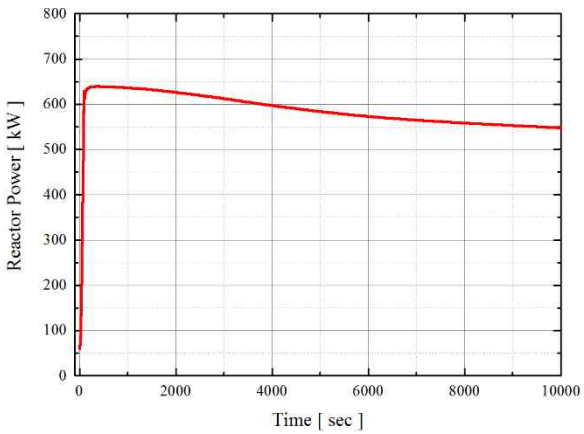

Fig. 5. Results of safety analysis for RIA

4. Conclusions

KAERI designed a new concept of H-LPRR that could be used as a research reactor and a critical assembly. The excess reactivity of the core was restricted to prevent a rapid increase in reactor power by RIA, and the fuel assembly and the reflectors are designed to be interchangeable. Two types of reflectors are employed in the core; the beryllium reflector is surrounded by an outer reflector of graphite canned with aluminum. The neutronics calculation and the safety analysis are progressed using the MCNP6.1 code with the ENDF/B-VII.0 library and the RELAP5 code. As a result, excess reactivity and β_{eff} at the BOL were evaluated to be 3.84 mk and 7.29 mk, respectively, and the integral CARs' worth and maximum value in differential CARs' worth were 9.17 mk and 0.035 mk/mm, respectively. Furthermore, the reactor power does not increase above 650 kW in spite of a RIA being as large as the core excess reactivity. Consequently, it can be evaluated that the newly designed H-LPRR possesses sufficient inherent safety against a RIA and good performance in terms of nuclear design.

ACKNOWLEDGEMENTS

This work was funded by the Ministry of Science and ICT of Korea (522110-22).

References

1. T.S. Azande, G.I. Balogun, A.S. Ajuji, Y.A. Ahmed, and S.A. Jonah, Determination of LEU Core Safety Related Parameters of NIRR-1 Using WIMS and CITATION Codes, Continental J. Applied Sciences, 6, 71-76, 2011.
2. S. T. Hong, I. C. Lim, S. Y. Oh, S. B. Yum, and D. H. Kim, Hybrid Low-Power Research Reactor with Separable Core Concept, TRTR 2016 Meeting, Aug. 21-25, 2016, USA.
3. D.B. Pelowitz (Ed.), MCNP6 User's Manual Version 1.0, LA-CP-13-00634, LANL, 2013.
4. C. D. Fletcher and R. R. Schultz, RELAP5/MOD3.3 Code Manual, NUREG/CR-5535, 2001.

Recent Results of Scanning Electron Microscopy Characterization of Fuel Plates Irradiated in the EMPIrE Irradiation Experiment

Dennis Keiser Jr., Daniele Salvato, Charlyne Smith, Tammy Trowbridge, William Hanson, Adam Robinson, and Irina Y. Glagolenko
Idaho National Laboratory, P. O. Box 1625, Idaho Falls, ID 83415 USA

Bei Ye, Laura M. Jamison, and Gerard L. Hofman
Argonne National Laboratory, 9700 S. Cass Ave., Lemont, IL 60439, USA

Corresponding Author Contact Information:
Dennis D. Keiser, Jr.
Idaho National Laboratory
P.O. Box 1625
Idaho Falls, ID, 83415 U.S.A.
Phone: 1 (208) 526-7298
E-mail: dennis.keiser@inl.gov

For Publication in the Proceedings of the Research Reactor Fuel Managment Conference

(June 6-10, 2022 in Budapest, Hungary)

Recent Results of Scanning Electron Microscopy Characterization of Fuel Plates Irradiated in the EMPIrE Irradiation Experiment

Dennis Keiser Jr., Daniele Salvato, Charlyne Smith, Tammy Trowbridge, William Hanson, Adam Robinson, and Irina Y. Glagolenko
Idaho National Laboratory, P. O. Box 1625, Idaho Falls, ID 83415-6188 U.S.A.

Bei Ye, Laura M. Jamison, and Gerard L. Hofman
Argonne National Laboratory, 9700 S. Cass Ave., Lemont, IL 60439, USA

ABSTRACT

Irradiation of fuel plates in the European Mini-Plate Irradiation Experiment (EMPIrE) has been completed. The mini-plates (2.54 cm in width by 10.16 cm in length) were irradiated in the Advanced Test Reactor (ATR) located at the Idaho National Laboratory (INL). The dispersion fuel plates were comprised of zirconium nitride (ZrN)-coated U-Mo fuel particles in an aluminum (Al) matrix, clad in Al-alloy. Several fabrication parameters were varied as a part of the experiment design to evaluate their influence on the fuel performance, including fuel powder heat treatment, coating methodology, coating thickness, fuel particle size distribution, Mo-alloying content, and fuel powder source. Of interest is the swelling behavior of the fuel particle, the effectiveness of the ZrN coating in mitigating fuel/matrix interaction during irradiation, and the possible development of relatively large pores in the fuel meat. This paper discusss the most recent results of the microstructural characterization of transverse cross-sections taken at the midplane for the top priority fuel plates using scanning electron microscopy (SEM). The SEM was used to produce secondary electron (SE) and backscattered electron (BSE) images, and composition analysis was conducted using energy dispersive spectroscopy (EDS) and wavelength dispersive spectroscopy (WDS). Results of this analysis showed how fission gas bubbles developed in the fuel particles, how the coating performed during irradiation, and how fission products partitioned amongst the different phases.

1. Introduction

The Material Management and Minimization (M3) Fuel Development program (earlier known as the Reduced Enrichment for Research and Test Reactors program) has been working with international collaborators over the years to develop low-enriched uranium (LEU) fuel to reduce the demand of highly-enriched uranium (HEU) fuels currently used in research and test reactors throughout the world [1]. One fuel type being evaluated for use is a U-7Mo disperison fuel with a barrier coating deposited on the U-7Mo particles that are encased in Al matrix to comprise the fuel meat which is then contained in Al alloy cladding [2]. Recently, the European Mini-Plate Irradiation Experiment (EMPIrE) experiment was completed in the Advanced Test Reactor (ATR) to test the performance of this fuel where the barrier coating is ZrN [3]. Initial, microstructural characterization of the different fuel plates has begun using scanning electron microscopy (SEM). The SEM was used to produce secondary electron (SE) and backscattered electron (BSE) images, and composition analysis was conducted using energy dispersive spectroscopy (EDS) and wavelength dispersive spectroscopy (WDS). To date, three fuel plates (EMPI 0818, 0820, and 0821) have been characterized, and the results of this analysis provide an initial assessment of the evolution of fission gas bubble morphology with increasing fission density in the fuel particles, of the

coating performance during irradiation, and of the partitioning behavior of fission products amongst the different fuel meat phases.

2. Experimental

During irradiation in the Advanced Test Reactor the EMPIrE fuel plates were oriented face-on to the core resulting in fairly uniform flux profiles across the width of the fuel plates. Transverse cross-section were produced near the midplane of the fuel plates at the Hot Fuels Examination Facility (HFEF) at the Idaho National Laboratory, and some of these cross-sections have been shipped to the Irradiated Materials Characteriation Laboratory (IMCL) for SEM characterization. The cross-sections were mounted and polished for SEM analysis. To date, samples from three fuel plates have been characterized (EMPI 0818, 0820, and 0821). Some details of the irradiation conditions for these fuel plates are presented in Table 1. These three fuel plates have ZrN coating on heat-treated U-7Mo fuel particles that was applied using physical vapor deposition (PVD), and there were no particles less than 40 μm in size. Both secondary electron (SE) and backscattered electron (BSE) images were produced from the polished samples. Since the radiation levels of the cross-sections are too high for the SEMs that have compositional analysis capability, FIB samples were produced from the polished samples and used for composition analysis using energy dispersive spectroscopy (EDS) and wavelength dispersion spectroscopy (WDS). The first step when generating a FIB sample is to deposit a Pt protective layer on the sample surface to reduce curtaining and minimize damage to the specimen surface during milling operations. This is followed by the generation of "lift-outs", which are ultimately obtained at specific locations by coarse trenching an approximately 50 μm x 50 μm x 1 μm sample. Figure 1 shows four FIB samples that were produced for characterization from fuel plate EMPI 0820.

Table 1: Calculated irradiation parameters for EMPI 0818, 0820, and 0821.

Sample	Average Burnup (% ^{235}U)	Peak Heat Flux (W/cm^2)
EMPI 0818	45	444
EMPI 0820	68	241
EMPI 0821	79	285

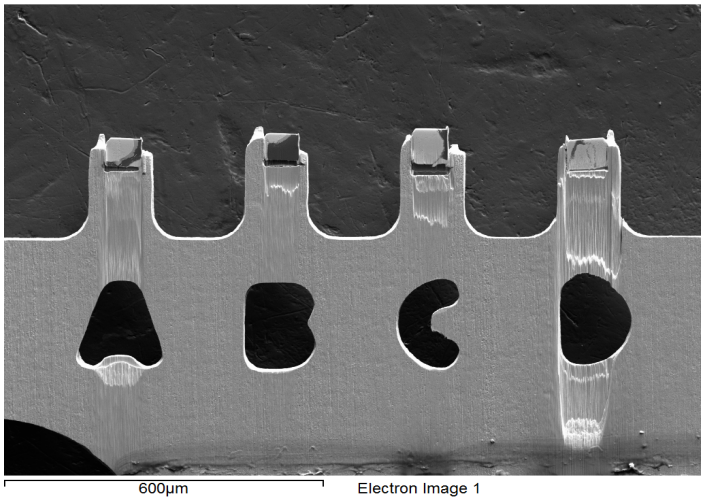

Figure 1. BSE image of four FIB samples produced from fuel plate EMPI 0820.

3. Results

3. 1 SEM Images

3.1.1 EMPI 0818

Figure 2 shows the microstructure observed for EMPI 0818. Negligible fuel/matrix interaction was identified, and intact ZrN coating could be found. Fission gas bubbles could be resolved on grain boundaries.

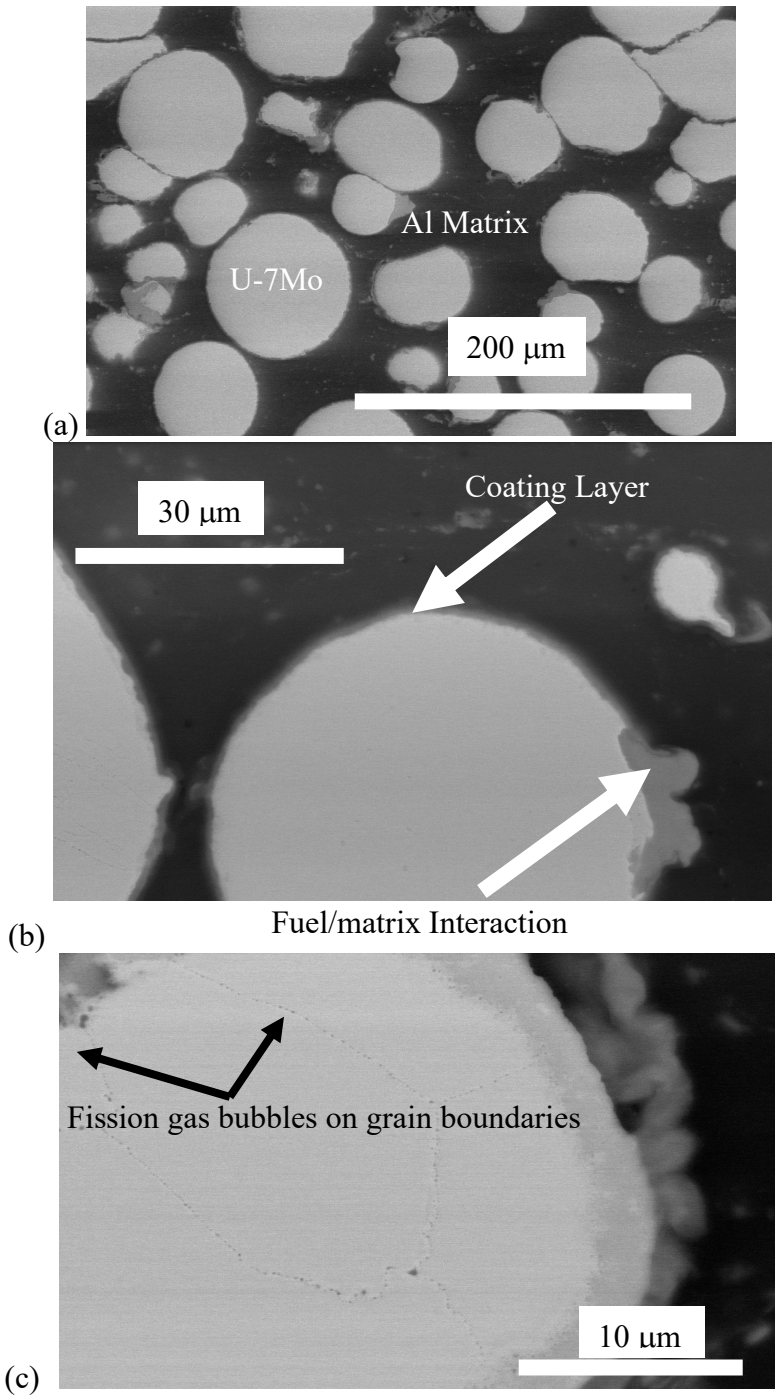

Figure 2. BSE images (a-c) of the polished surface of a EMPI 0818. In (a), the microstructure exhibits very small amounts of interaction layer. In (b), is a higher magnification image showing the coating and interaction layer. In (c), fission gas bubbles on grain boundaries are shown.

3.1.2 EMPI 0820

Figure 3 shows BSE of the EMPI 0820 microstructure, where some interaction layer could be found along with intact ZrN coating, and more fission gas bubbles could be found in the U-7Mo fuel paritcles viz-a-viz EMPI 0818 fuel particles.

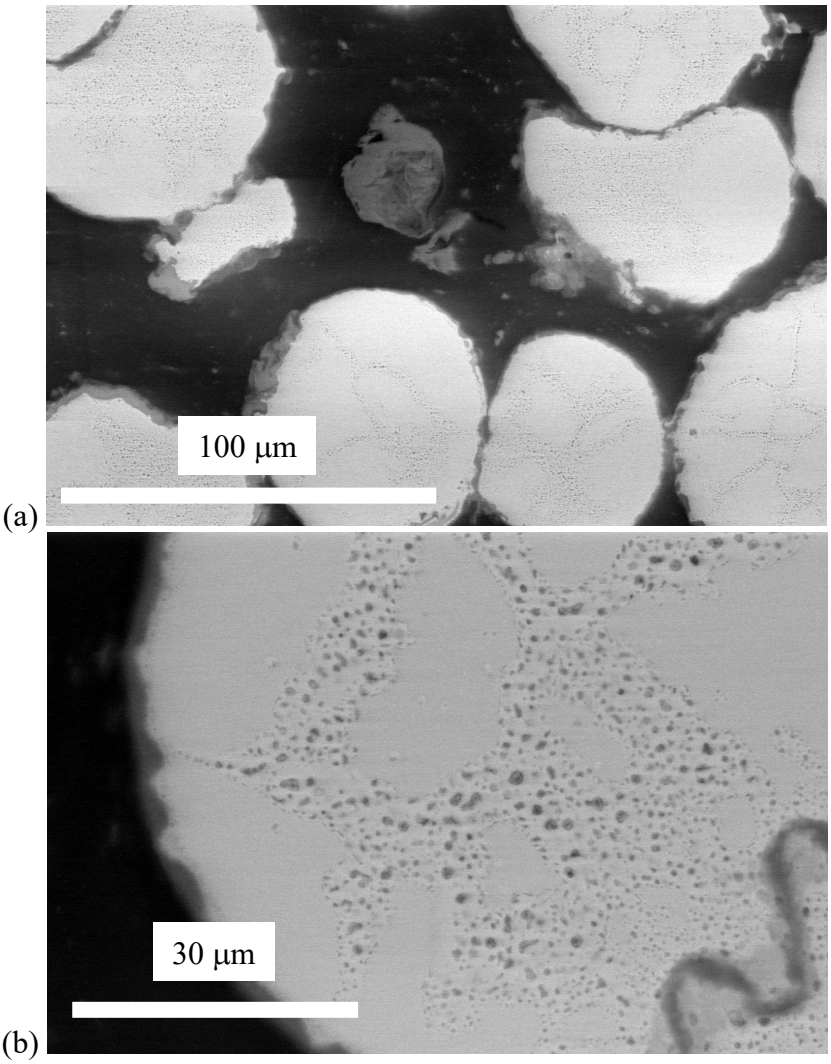

(a)

(b)

Figure 3. BSE images (a and b) of the microstructure observed for EMPI 0820, where (a) shows limited fuel/matrix interaction layer formation and intact ZrN coating, and (b) shows fission gas bubbles in a U-7Mo fuel particle.

3.1.3 EMPI 0821

Figure 4 shows the microstructure for EMPI 0821, which achieved the highest burnup during the irradiation experiment. Like was the case for the other two fuel plates, only limited fuel/matrix inteaction was observed, along with intact ZrN coating. The U-7Mo fuel particles exhibited more fission gas bubbles than the type 8 plates discussed previously.

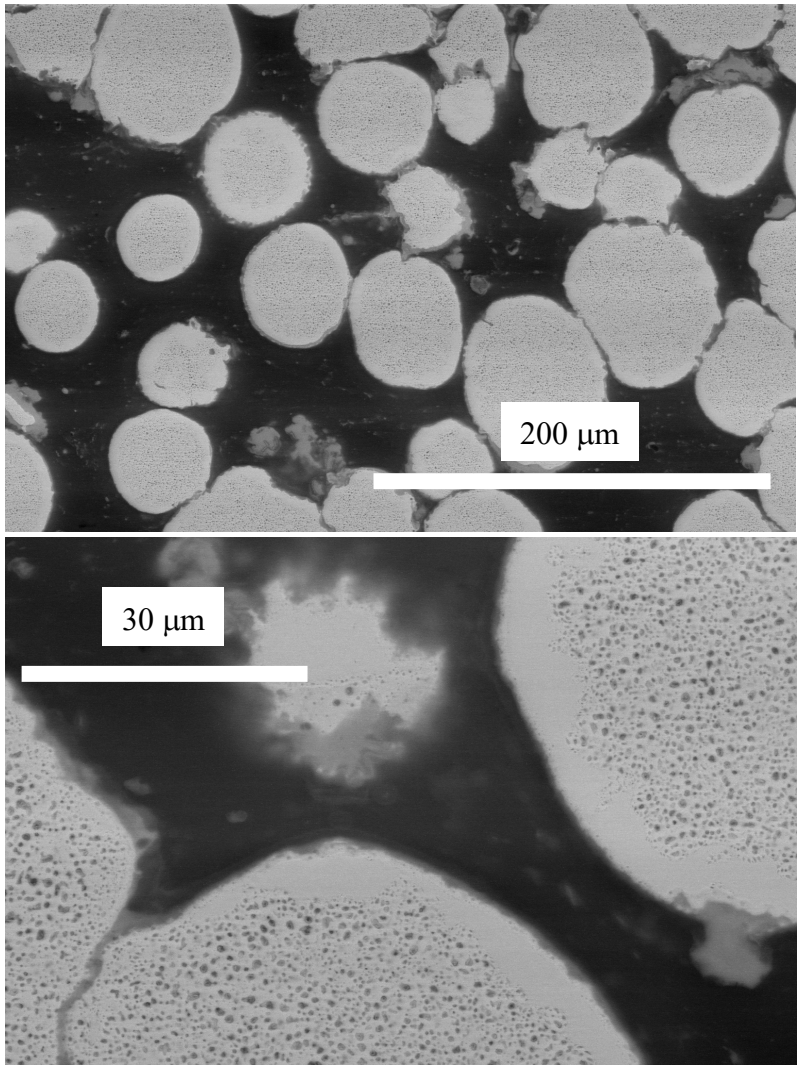

Figure 4. BSE images (a and b) of the microstructure observed for the EMPI 0821 fuel plate sample. (a) shows the limited fuel/matrix interaction and intact ZrN coating, and (b) shows the presesence of more fission gas bubbles in the U-7Mo fuel particles compared to the other fuel plates. Some regions around the periphery of the U-7Mo fuel particles were devoid of observable fission gas bubbles.

3. 2 Compositional Analysis

The first compositional analysis has been generated for the EMPI 0820 fuel plate. Analysis is currently ongoing for the EMPI 0818 and 0821 fuel plates. Figures 5 and 6 shows WDS x-ray maps for a region of this fuel plate with a relatively thick interaction layer and relatively thin interaction layer, respectively. In areas with relatively thick fuel/matrix interaction layers, negligible Zr was observed near the U-7Mo/matrix interface, and in regions of the sample where fuel/matrix interaction layers were realatively thin more appreciable amounts of Zr could be found. A relatively large amount of oxygen is present in regions with high levels of Zr.

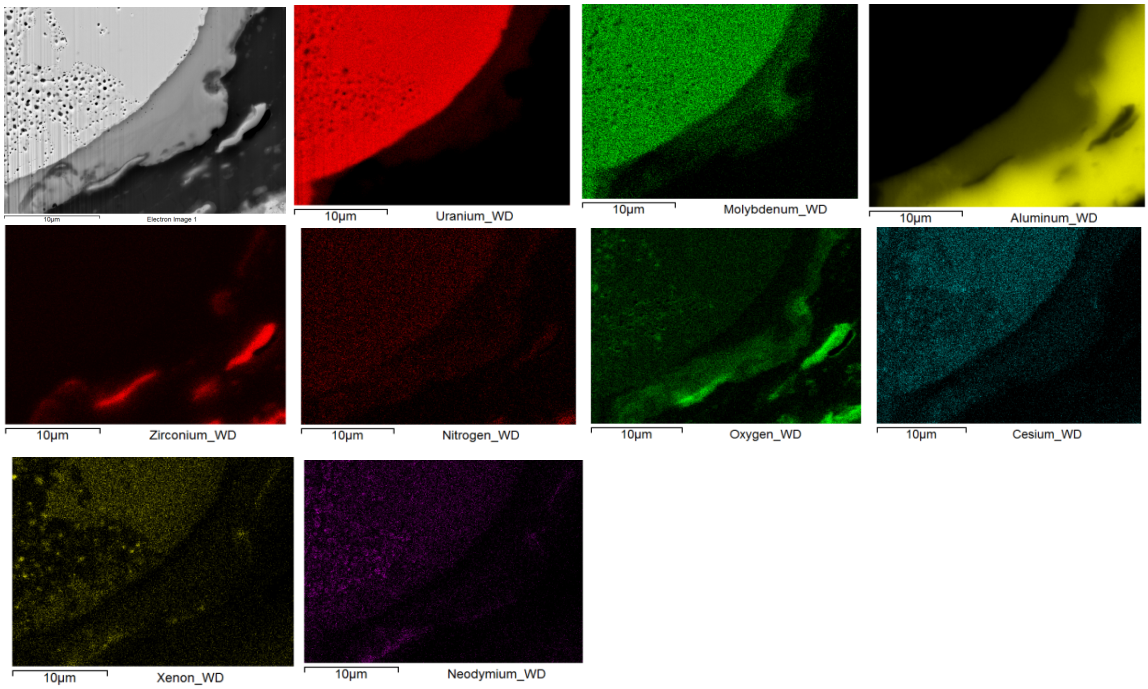

Figure 5. BSE image (upper left) and WDS x-ray maps for U, Mo, Al, Zr, N, O, Cs, Xe and Nd taken in a region of the EMPI 0820 fuel plate sample.

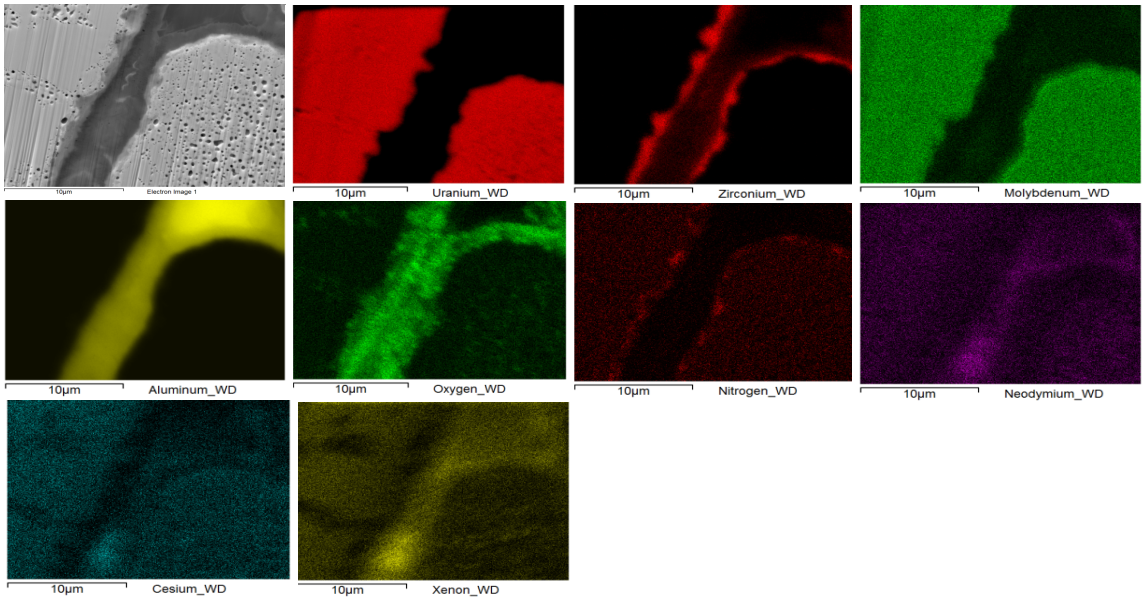

Figure 6. BSE image (upper left) and WDS x-ray maps for U, Zr, Mo, Al, O, N, Nd, Cs, and Xe taken in a region of the EMPI 0820 fuel plate sample.

4. Summary

Based on the microstructural characterization of EMPIrE fuel plates with PVD-deposited ZrN coating on the U-7Mo fuel particles that were irradiated up to 79% burnup, only limited fuel/matrix interaction occurs during irradiation, and in many regions the original coating exhibits limited degradation. The result of this behavior is a lack of development of relatively large pores in the fuel meat, which is favorable in terms of limiting the swelling of the fuel plate and in terms of maintaining the mechanical integrity of the fuel plate.

Acknowledgments
This work is supported by the U.S. Department of Energy, under DOE Idaho Operations Office Contract DE-AC07-05ID14517. Accordingly, the U.S. Government retains a nonexclusive, royalty-free license to publish or reproduce the published form of this contribution, or allow others to do so, for U.S. Government purposes.

References
[1]. J. Snelgrove et al., Nucl. Engr. Design 178 (1997) 119-126.
[2]. M. K. Meyer, J. Gan, J. F. Jue, D. D. Keiser, E. Perez, A. Robinson, D. M. Wachs, N. Woolstenhulme, G. L. Hofman, and Y. S. Kim, "Irradiation Performance of U-Mo Monolithic Fuel," Nucl. Energy and Tech. 46 (2) (2014) 169-182.
[3]. William A. Hanson, Adam B. Robinson, Nancy J. Lybeck, Joseph W. Nielsen, Bei Ye, Zhi-Gang Mei, Dennis D. Keiser Jr, Laura M. Jamison, Gerard L. Hofman, Abdellatif M. Yacout, Ann Leenaers, Bertrand Stepnik, Irina Y. Glagolenko," Non-destructive analysis of swelling in the EMPiRE fuel test, " J. Nucl. Mater. 564 (2022), published on-line. https://doi.org/10.1016/j.jnucmat.2022.153683

HIGH RESOLUTION NEUTRON DIFFRACTION STUDIES OF ADDITIVELY MANUFACTURED INCONEL 718 SAMPLES

P. Mikula, V. Ryukhtin,

Nuclear Physics Institute CAS, 250 68 Řež, Czech Republic

ABSTRACT

In our contribution we present the results of the experimental feasibility studies of neutron powder diffraction profiles of several samples of Inconel 718 material which was used as the 3D printing material. Though the measurement at the medium power research reactor is rather time consuming, together with the γ phase matrix, it was possible to distinguish small portions of some other phases corresponding to created precipitates which could have influence on the material properties.

1. Introduction

When looking for good mechanical properties and corrosion resistance at elevated temperatures a Ni-based superalloy 718 (also known as Inconel 718) is widely used for components e.g. in gas turbines in jet engines. The excellent properties of the Inconel 718, namely, strength and ductility, results from a good combination of the phases [1-3]: γ phase matrix with the fcc crystal structure, the coherent γ'' phase precipitates with Ni3Nb composition and a tetragonal bct ($D0_{22}$) crystal superstructure. Less often a fcc crystal structure of γ' precipitates is present. The precipitation of either γ' or γ'' is dependent on the concentration of Ti and Nb. Typically, Inconel 718 is used in applications carried out at medium temperature, because above 650 °C the thermodynamically stable δ phase forms, with Ni3Nb composition and an orthorhombic crystal structure (at the expense of the γ''phase) which degrades the mechanical properties of the material. The δ phase precipitates either at the grain boundaries or intragranular.

Thanks to their excellent properties, fabricating components of the Alloy 718 using additive manufacturing (AM) methods are very attractive for different applications because they provide large possibilities of design flexibility. The most usually used AM processes are the so-called powder bed fusion ones, which include the following methods: direct metal laser sintering (DMLS), electron beam melting (EBM), selective heat sintering (SHS), laser powder bed fusion (LPBF usually referred as selective laser melting, SLM), and selective laser sintering (SLS). In the LPBF method a laser source is utilized for melting and selectively fusing together metallic powders, which are spread on a moving plate when the designed component is built. In the LPBF method, processing parameters as the laser power, scanning speed, hatch spacing, and layer thickness, are the most influential ones when producing microstructure for particular metals/alloys. For the studies of the microstructure and determination of the individual phases in the material X-ray diffraction and neutron diffraction are usually used. Namely, synchrotron XRD, providing the high flux, is very important for indexing and quantifying different phases in low fractions in the material. However, it is well known that due to a low penetration of X-rays into the material (for low energies X-rays), XRD provides required information related to the surface of the studied samples. On the other hand, neutron diffraction can use much larger probed volumes when

fighting with a relatively much lower flux and thus also with much longer measurement time. As a feasibility study, in this paper we introduce neutron powder diffraction results of several samples of Inconel 718 as obtained by unconventional high-resolution neutron diffraction method in order to determine some phases having very close lattice spacings to the matrix one.

2. Experimental procedure

The neutron diffraction experiment was carried out by a high-resolution three-axis setting as schematically shown in Fig. 1. Following the sketch shown in Fig. 1 (for small widths of the samples), a maximum resolution from this arrangement can be achieved for minimal dispersion of the whole system [4,5]. When treated it in momentum space, meaning that the orientation of the Δk momentum domains related to the monochromator and analyzer should be matched to that of the sample, and this can be achieved by proper radii of curvature of the bent perfect crystal monochromator and analyzer. Contrary to the conventional two axis diffractometer, the diffraction profiles with the three-axis set-up are obtained by rocking (step-by step) the bent perfect crystal (BPC) analyzer situated on the third axis of the diffractometer and the neutron signal is registered by a point detector (see Fig. 1). When

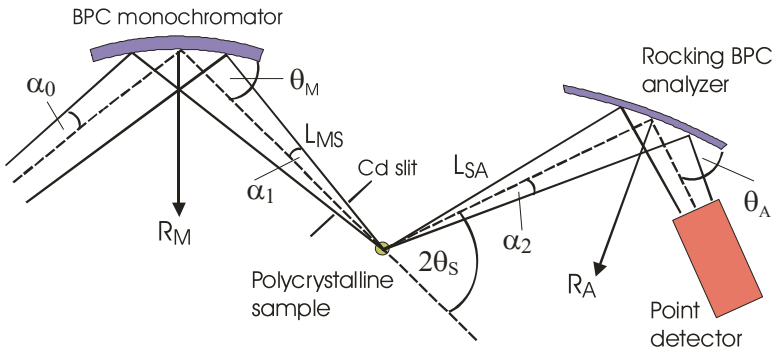

Fig. 1. Three-axis diffractometer setting employing BPC monochromator and analyzer as used in the experiment (R_M, R_A - radii of curvature, θ_M, θ_A - Bragg angles).

treating the resolution of the setting in momentum space, this means that the orientation of the Δk domains of the wave vectors related to the monochromator and analyzer are matched to that of the sample. For $L_{MS}/(R_M \cdot \sin\theta_M) \neq 1$ and $L_{SA}/(R_A \cdot \sin\theta_A) \neq 1$, a general form for focusing in momentum space (not dependent on α_1 and α_2) which minimizes the dispersion between all elements can be derived as [6]

$$2 \tan\theta_S = \tan\theta_M /(1 - L_{MS}/(R_M \cdot \sin\theta_M)) + \tan\theta_A /(1 - L_{SA}/(R_A \cdot \sin\theta_A)). \quad (1)$$

When fulfilling the condition (1) a maximum peak intensity and a minimum *FWHM* of the analyzer rocking curve can be expected. Due to its high resolution, the three-axis setting can be used for plastic strain studies on the basis of diffraction profile analysis as e.g. in deformation studies on samples under the external thermomechanical load [8,9]. Recently, it has been found out that the setting providing a sufficiently high resolution, can be used to distinguish diffraction profiles corresponding to very close lattice constants e.g. of different phases, as it is in the case of Inconel 718. The experimental tests were carried out on the 3-axis neutron diffractometer installed at the Řež research reactor LVR-15. The diffractometer employs the Si(111)-monochromator and Si(311)-analyzer single crystals which have the

dimensions of 200x40x4 mm^3 and 20x40x1.3 mm^3 (length x width x thickness), respectively. The monochromator Si(111) provides the neutron wavelength of 0.162 nm and has a fixed curvature with a radius R_M of about 12 m. The radius of curvature of the analyzer was changeable in the range from 3.6 m to 36 m. It permitted us to determine an optimum analyzer curvature minimizing the dispersion and thus optimizing the resolution of the setting. The dimensions of the Inconel 718 samples were of 2x7x18 mm^3 and put on the second axis in the vertical or horizontal position. The impinging beam on the sample was limited by a 5 mm Cd slit in order to be smaller than the width (7 mm) of the sample.

3. Experimental results

Examples of an excellent resolution of the 3-axis setting as documented by *FWHMs* of the rocking curves obtained on well annealed α-Fe(110) standard samples are shown in Fig. 2. High resolution of the setting points out a feasibility to use it for studying special material research tasks e.g. determination and volume content of different material phases having very close values of lattice spacing, or microstructure analysis of plastically deformed samples on the basis of diffraction profile analysis [7-10]. Both samples were put on the second axis in the vertical position. Recently, it has been found out that the setting provides a sufficiently high resolution, though slightly relaxed, when wider slits (e.g. up to 20 mm) or wider samples are used [11]. This phenomenon can be used e.g. for measurements of peak shifts $\Delta\theta_S$ on samples of large dimensions when the resolution is comparable to the one of

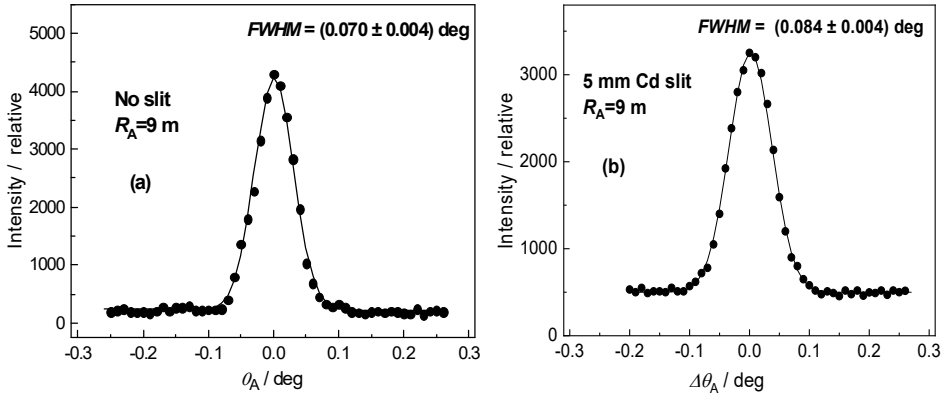

Fig. 2. α-Fe(110) diffraction profiles when using a well annealed 2 mm pin and a small steel plate of the dimensions of 2x7x15 mm^3 – (b).

conventional strain/stress scanners. For the high-resolution measurement test we used several samples of Inconel 718 of the dimensions of 2x7x18 mm^3. Figs. 3-5 show several results obtained on the wrought, SLM and wrought–aged samples which document the feasibility of the three-axis diffraction setting for such demanding experimental investigations. When using the values of the lattice spacings from ref. 2 and a simple formula $\Delta\theta_A \approx -\Delta(2\theta_S)$ valid for large values of R_A, our results well correspond to the ones obtained in ref. 1. The inspection of Fig. 3 reveals that the main maximum (the red line) corresponds to the γ phase of the matrix while the small maxima at the shoulders correspond to the separated γ' (green line) and γ'' (blue line) phases, respectively. Then, Fig. 4 reveals that the main maximum (the red line) corresponds to the γ phase while the

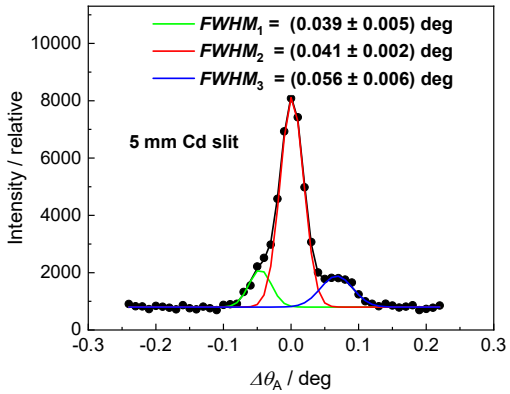

Fig. 3. Analyzer rocking curve related to the wrought Inconel 718 sample.

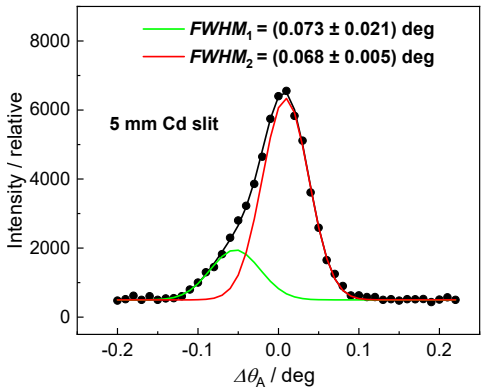

Fig. 4. Analyzer rocking curve related to the SLM Inconel 718 sample.

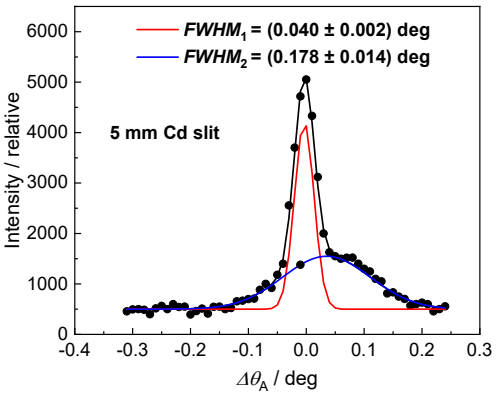

Fig. 5. Analyzer rocking curve related to the wrought-aged Inconel 718 sample.

small maximum at the shoulder (green line) corresponds to the γ' phase. On the other hand, Fig. 5 shows that together with the main γ phase, there is a considerable contribution of a mixture of γ' and γ'' *phases* (blue line). Then, the difference of the lattice spacings of the individual phase in the particular sample can be determined from the relation $\Delta\theta_S = -(\Delta d_S/d_{0,S})\cdot\tan\theta_S$.

4. Conclusion

The feasibility of using the high-resolution three axis diffractometer setting in some special studies exploiting diffraction profile analysis (e.g. strain/stress analysis of plastically deformed samples, determination of phases having very close values of the lattice spacings etc.) is presented, thus namely, in the case of samples subjected to thermo-mechanical load. In our case, the resolution of the diffractometer setting was tested on samples of Inconel 718 material which due to its excellent mechanical properties is often used in demanding applications. The mechanical properties considerably depend on the volume content of additional phases accompanied the main γ one and their determination is highly important. Therefore, we hope that the presented neutron diffraction setting can offer an additional support to complement the information achieved by using the other conventional characterization methodologies. Of course, this high-resolution diffraction setting can also be used for conventional macro-strain scanning from the angular shifts $\Delta\theta_A$ of the obtained diffraction profiles, but due to the step-by-step analysis with the analyzer, rather time-consuming measurement would be impractical as a result of a rather low detector signal.

5. Acknowledgements

Measurements were carried out at the CANAM infrastructure of the NPI CAS Řež supported through MŠMT project No. LM2015056. The presented results were also supported in the frame of the following MŠMT projects: LM2015048 and the infrastructural one - "Experimental nuclear reactors LVR-15 and LR-0." We thank Ms. B. Michalcová for a significant help in the measurements and basic elaboration of the data.

6. References

[1] J. Čapek, E. Polatidis, M. Knapek, C. Lyphout, N. Casati, R. Pederson and M. Strobl, The effect of γ'' and δ phase precipitation on the mechanical properties of Inconel 718 manufactured by selective laser melting: An in-situ neutron diffraction and acoustic emission study, JOM **75**, (2021) 223-232. https://doi.org/10.1007/s11837-020-04463-3.

[2] C. Solís, J. Muske, M. Bergner, A. Kriele, M.J. Mülbauer, D.V. Cheptiakov, B. Gehrmann, J. Rosler and R. Gilles, In-situ characterization at elevated temperatures of a new Ni-based superalloy VDM-780 Premium, Metallurgical and Materials Transaction A, **49** (2018) 4373-4381. https://doi.org/10.1007/s11661-0184761-6.

[2] J. Repper, PhD Thesis, Einfluss mikroskopischer Eigenspannungen auf die makroskopische Eigenspannungsanalyse mittels Neutronenbeugung, Technische Universität München, 2010.

[4] P. Mikula, J. Šaroun, V. Ryukhtin and J. Stammers, An alternative neutron diffractometer performance for strain/stress measurements, Powder Diffraction, **35** (2020)185–189. https://doi.org/10.1017/S0885715620000329.

[5] P. Mikula, J. Šaroun and V. Ryukhtin, High-resolution residual strain/stress measurements on three-axis neutron diffractometer, Advanced Materials Research, **1166** (2021) 33-40. https://doi.org/10.4028/www.scientific.net/AMR.1166.33.

[6] M. Vrána, P. Lukáš, P. Mikula and J. Kulda, Bragg diffraction optics in high resolution strain measurements, Nucl. Instrum. Methods in Phys. Research, A **338** (1994) 125-131. https://doi.org/10.1016/0168-9002(94)90172-4.

[7] R. Delhez, T.H. de Keijser, E.J. Mittemeijer, 1982, Determination of crystallite size and lattice distortions through X-ray diffraction line profile analysis, Fresenius' Zeitschrift für analytische Chemie, **312**(1) (1982) 1-16. DOI:10.1007/BF00482725.

[8] V. Davydov, P. Lukáš, P. Strunz and R. Kužel, Single-line diffraction profile analysis method used for evaluation of microstructural parameters in the plain ferritic steel upon tensile straining, Materials Science Forum, **571-572** (2008) 181-188. https://doi.org/10.4028/www.scientific.net/MSF.571-572.181

[9] K. Macek, P. Lukáš, J. Janovec, P. Mikula, P. Strunz, M. Vrána and M. Zaffagnini, Austenite content and dislocation density in electron beam welds of a stainless maraging steel, Mat. Sci. Eng. A **208** (1996) 131-138. DOI:10.1016/0921-5093(95)10047-4.

[10] K. Hirschi, M. Ceretti, P. Lukáš, N. Ji, C. Braham and A. Lodini, Microstrain measurement in plastically deformed austenitic steel, Textures and Microstructures, **33** (1999) 219-230. DOI: 10.1155/TSM.33.219.

[11] P. Mikula, V. Ryukhtin, J. Šaroun and P. Strunz, On possible high-resolution residual strain/stress measurements by three-axis neutron diffractometer, Materials – MDPI, **13** (2020) 5449-5455. DOI:10.3390/ma13235449

MULTIPURPOSE OR DEDICATED RESEARCH REACTORS?

A. DOVAL, E. VILLARINO
Nuclear Technology Department, INVAP S.E.
Comandante Luis Piedrabuena 4950, 8400, San Carlos de Bariloche, Río Negro, Argentina
D. FERRARO
Nuclear Engineering Department, INVAP S.E.
Esmeralda 356, 1035ABH, Buenos Aires, Argentina

ABSTRACT

Research reactors proved to be a useful tool, not only for academic and research purposes but also as a versatile and reliable radioisotope "factory". Although the well-known applications of these facilities, the increasing demand of medical radioisotopes observed in the global market - mostly related to the 99Tc - is shifting the operation goals towards the production of diverse radioisotopes. This goal became the driving force for the design of several new research reactors, likewise grounded the modernization, upgrade and optimisation of existing ones.
This production-driven activity demands specific requirements when compared with a traditional facility purely dedicated to basic scientific research, which will be reflected in specific aspects that drive the neutronic and thermal-hydraulic design. This paper describes the most relevant aspects to take into account within the process of defining these tailored design requirements that reflect main application of a Research Reactor, showing the INVAP's perspective as a nuclear vendor.

1. Introduction

More than 220 research reactors (RR) are nowadays in operation in more than fifty countries, whereas about 20 are planned or under construction [1]. These complex facilities are known to represent a cornerstone in the countries' scientific and technological infrastructure, enhancing not only research purposes, but also academic and human resources training goals. On top of that, the high demand of diverse Radioisotopes, suited to be massively produced at low cost within these facilities, has converted several RR in radioisotope "factories". As a consequence, this latter application has become the driving force for the design of several new research reactors, likewise grounded the modernization, upgrade, reconversion and optimisation of existing ones.

INVAP has more than four decades of experience in the design, analysis, optimisation, upgrade, construction and commissioning of research reactors [2], with on-going projects in Argentina, Brazil, The Netherlands, Saudi Arabia and Algeria. As a vendor, INVAP focuses on the expected customer´s performance goals, tailoring the facility design to match the client's and stakeholders' expectations. For such purpose, a high degree of versatility in the design and analysis process is commonly required, likewise a custom-oriented approach.

In this line, the design of a Dedicated (for example, a radioisotope-production reactor) can present some distinctive characteristics with respect to a Multipurpose Research reactor, both regarding the neutronic design, the associated core and out-of-core thermal-hydraulics and several additional aspects. To consider such specific attributes in early engineering stages represents a key aspect to develop a successful project, regarding not only performance, but also timing and costs. The following sections thus describe some of the most relevant aspects to consider in this process when dealing with dedicated or multipurpose reactors, aimed to be interpreted as a rough description based on INVAP´s experience rather than a mandatory path to follow.

2. Description of the main aspects of a Dedicated and a Multipurpose RR

Before starting this description of the main aspects to take into account within this process, it is important to stress that dedicated RRs do not only refer to the production of radioisotopes. Conversely, this classification could be also used to identity an education and training RR, a fully research or material testing facility, just to mention a few, which could have either low, medium or high power ranges. Nevertheless, this work will refer to a dedicated RR as a facility that massively produces radioisotopes in a market-oriented schedule, whereas a the Multipurpose reactor will refer to high-performance facilities, where for both cases the power operational ranges is in the order of the tens of MWth.

As a general rule, the versatility in the design and analysis tools for the core and out-of-core facilities of a research reactor is key to reach the stated goals regardless of the reactor type. In particular, INVAP develops its designs with a tailored (and own-developed) calculation line [3], proved to be suited to handle both Dedicated and Multipurpose Research Reactor designs.

In this process, some specific aspects are to be considered, here divided in neutronics, thermal-hydraulic and additional features for simplicity, described in the following sections.

2.1 Neutronic design

To begin with the description of the most relevant aspects to take into account within the process of defining tailored design requirements for a Research Reactor, the neutronic design, analysis and performance optimisation shall be considered.

As a general rule, the global trend is oriented to consider high-performance compact core designs, where the following features are commonly considered regardless of the foreseen application:

a. Safety-oriented designs: High safety-margins, with a mandatory fast First Shutdown System (usually composed by absorber plates) plus a Secondary Shutdown System (diverse and redundant, usually non-fast and mandatory for high-power reactors).
b. Non-proliferant designs: considering both the core design and the out-of-core irradiation facilities.
c. Utilization of Low Enriched Uranium (LEU) Fuels: Mostly plate-type U_3Si_2 (dispersed) designs, but also rodded-type (UO_2), with enrichment lower than 20%wgt for all cases. Alternative compounds such as UMo_x (dispersed or monolithic) are sometimes considered.
d. Optimization of core performance and safety margins using Fuel assemblies with burnable poisons: To improve global performance of the shutdown systems and to improve power distributions it is a common approach to include burnable poisons, where the incorporation of cadmium wires within the fuel frames is the preferred solution by INVAP.
e. Consideration of LEU targets: Regarding ^{99}Mo production (if fission within mini-plates is chosen), the consideration of LEU targets (usually U-Al_x) is nowadays a standard approach.
f. High availability designs: State-of-the-art design are oriented to provide an availability of more than 300 FPD per year.
g. Provide versatile design solutions: Core and out-of-core devices are to be customized to current customer's and stakeholders goals, but considering by design room to optimisation/upgrade/reformulation of applications.

In particular, within INVAP's RR designs, such features are tailored depending on the main application both for the core and out-of-core devices [4]. At the end, this customization process is reflected into the global layout, as is schematically shown in Fig 1 for the alternative approaches for reactor utilization discussed above.

For both alternatives presented in Fig 1, the design considers a core composed of fuel assemblies (i.e. the refuelling is optimised to enhance performance), where main irradiation

applications are placed out-of-core. Nevertheless, it shall be considered that is a common approach to complement those with some in-core positions. It is clear thus that a Multipurpose reactor design (Fig 1 a)) leads to a crowded out-of-core layout. Standard applications such as neutron science (i.e. Cold/Thermal neutron sources, beams, etc.) lead to a small amount of space to place irradiation devices (such as bulk positions, fuel performance facilities or Silicon Doping devices). Conversely, a dedicated design (Fig 1 b)) allows to count with a bigger amount of bulk facilities with a wide range of neutronic flux levels.

Fig 1. Scheme of the core and out-of-core design for Multipurpose or Radioisotope production Dedicated reactors.

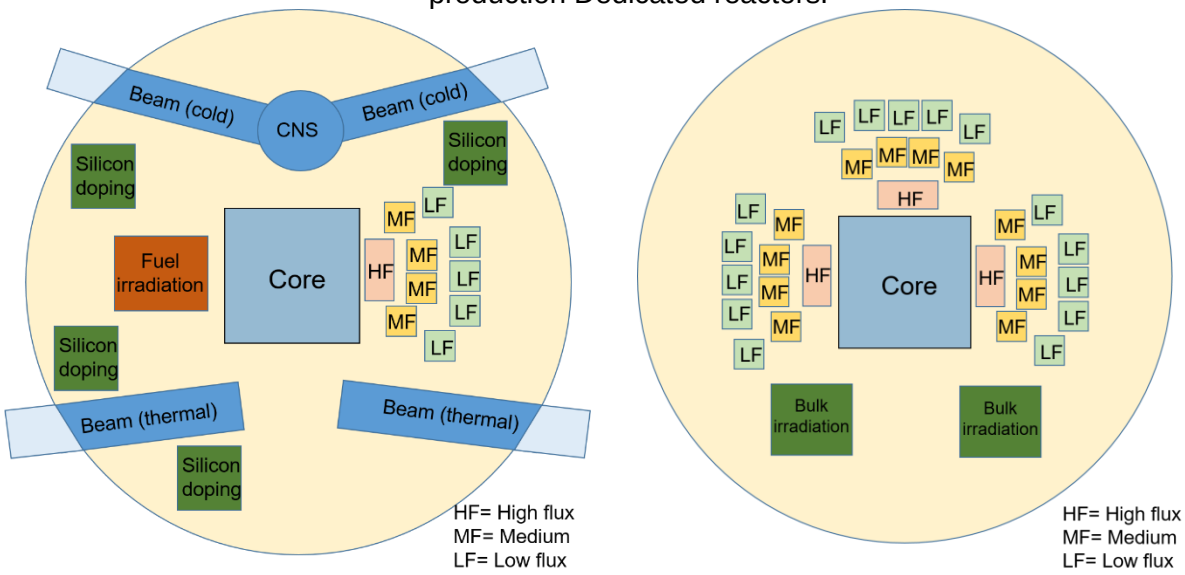

a) Schematic neutronic layout of a Multipurpose Research Reactor

b) Schematic neutronic layout of a RI Dedicated Research Reactor

Examples of INVAP designs for the former case (i.e. Multipurpose reactor) are the well-known OPAL reactor (Australia, in operation since 2006 [5]), the ETRR-2 (Egypt, in operation since 1998 [2]) the RA-10 (Argentina, under construction [6]) and RMB (Brazil, end of detailed design [7]). Regarding Radioisotope dedicated reactors, INVAP has developed tailored design for customers such as Coqui (USA, end of conceptual design [8]) or PALLAS (The Netherlands, in detail engineering stage [9]).

From the neutronic point of view, both options have their peculiarities, where the main aspects to consider are the following:

a. Minimize operational costs: The total core power is to be minimized through the optimisation of the layout. This leads to a minimization of fuel consumption and lowers the overall facility costs, where core powers lower than 30MWth are reachable.
b. Minimize perturbation within facilities: The layout is to be in-depth optimised to minimize the neutron flux perturbation due to the load/unload of irradiation rigs (e.g. bulk devices) or shutdown of facilities (i.e. CNS) during operation. This optimisation process is made to reach perturbations levels that are usually below 10%.
c. Enhance safety: The reactivity worth of the removable devices has to be carefully analysed in order to limit the maximum reactivity introduced. This is the case of the ^{99}Mo production rigs, since the load/unload during reactor's operation is foreseen and thus potential reactivity insertion accidents shall be bounded. A well-performed optimization process shall lead to maximum values lower than 0.5 β_{eff}.

d. Enhance safety margins: The shutdown margins and power peaking factors are optimised through a combination of refueling strategies and control rod movement strategies. As a result, power peaking factors below 3 are commonly reached, with shutdown margins for the first shutdown system (i.e. control rods) with single failure higher than 1000 pcm.
e. Enhance safety features: The consideration of a Second Shutdown System (SSS) is a standard-approach for high-performance INVAP core designs. When the reflector is D_2O within a reflector vessel, this SSS consists of the sudden drainage of D_2O. This is the most common approach, where other alternatives exist (e.g. through the poisoning of ad-hoc zones).

As a general rule, when dealing with Multipurpose reactors the more restrictive aspects are the items a), b) and e) above. This is mainly due to the fact that the crowded layout leads to a high level of interaction within the facilities, likewise tends to jeopardize the reactivity worth of the SSS.

Conversely, the dedicated Radioisotope reactors are easier from the layout point of view, but the high amount of irradiation rigs tend to make the aspects c) and d) above more difficult to optimize.

2.2 Thermal-hydraulic design

In the same line as the neutronic design, the thermal-hydraulic design is developed to fulfill high-safety standards as well as customer's goals. Some of the thermal-hydraulic aspects to be considered are:

a. Coolant flow direction: for reactor powers higher than 10 MWatts the upward forced cooling is the preferred choice for the core with flowrates higher than 1000 m^3/h, depending not only on the power but on the maximum heat flux, as well. Conversely, the out-of-core bulk facilities are commonly downwards cooled to facilitate the handling during reactor operation, which allows a "cleaner" layout for loading/unloading tasks. Regarding in-core irradiation positions (meaning upward cooling), the loading/unloading tasks will require special strategies, such as perform these tasks during refuelling state or dedicated cooling circuits.
b. Core configuration: a fixed core configuration is always desirable from the thermal-hydraulic point of view but it depends on the purpose of the facility. Moreover, a close core cooling system totally independent of the cooling system of the out-of-core devices would be viable for the case of no in-core irradiation positions.
c. Versatile coolant flow: a smart design of calibrated restrictors and plugs, both for the core grid and for the out-of-core irradiation position allows the adequate cooling in case of a non-fixed core configuration and for changing radioisotopes demand, either type or quantity.
d. Core coolant inlet temperature: some standard applications such as neutron science (i.e. Cold/Thermal neutron sources, beams, etc.) could require additional control systems for operational parameters such as temperature whereas this would not be a requirement for the targets' irradiation.

As for the neutronics description in the former Section, the details for the INVAP's approach for the thermal-hydraulic designs both for MPR and dedicated research reactors can be gathered in [5], [2], [9], [10] and [11].

Needless to say that the thermal-hydraulic design of Dedicated radioisotopes production reactors is simpler although the challenge is to:

i. Ensure the adequate flowrate for the variety of irradiation positions, all along its irradiation time, i.e., loading/unloading tasks performed, and during normal reactor operation avoiding undesired by-pass flow. Removable calibrated orifices (restrictors) is a way to fulfil this requirement.
ii. Optimise the design to provide the maximum coolant velocity with the minimum pressure drop in a downward flow condition to avoid cavitation at the exit. In open

pool type RR the inlet pressure for the out-of-core devices is fixed by the water column above these devices (namely, around 10 – 12 m of water column).

2.3 Additional aspects

When dealing with Multipurpose reactors it is important to define from the beginning whether the reactor will be a “research-slave” reactor, i.e. neutron science is the priority, or a “production-slave” reactor, meaning that radioisotope production is the main goal.

Although the focus was on the neutronic and thermal-hydraulic aspects, there are others not less relevant such as (not exhaustive):

a. Reflectors: the design and materials will differ according to the purpose of the facility. For example, beryllium blocks allow discrete neutron flux changes likewise provide some flexibility if a grid is considered. Although this could not be the best choice when large volume facilities for radioisotopes production are required, it is a good option when reconfiguration and/or relocation of irradiation loops for research applications is foreseen. Conversely, when the choice is to count with a reflector vessel filled with D_2O, precise locations for optimised irradiation purposes are defined, but reconfiguration is not possible. In this sense, some mixed approaches are usually considered (i.e. reflector vessel with localized Be grids).
b. Staff: although the difference is obvious it is an important issue to consider particularly regarding the training requirements when several (and complex) devices are to be operated at the same time.
c. Operational modes: for the case of a dedicated Radioisotopes production factory, the reactor should operate almost uninterruptedly, minimising the shutdown times with strict irradiation schedules. On top of that, the market-oriented operation of the facility will demand a fast recovery of full-power after a spurious reactor trip in order to preserve such production schedules. On the contrary, Multipurpose reactors could require longer shutdown times for the assembling and disassembling of research devices, for example, regardless the shutdown times due to failures.

3. Conclusions and main remarks

The most relevant aspects to take into account within the process of defining tailored design requirements for both Multipurpose of Radioisotope production Research Reactors were roughly presented and discussed. The INVAP’s perspective as a nuclear vendor and reactor designer were also presented, focusing mainly in the neutronic and thermal-hydraulic aspects. Furthermore, some practical examples were provided in order to show how this process is tailored according to the customer´s objectives.

It is key to note that each research reactor is, in a way, one of a kind when its purpose and design are evaluated. As it was described along this paper, there is not a unique set of rules for a Dedicated or for a Multipurpose research reactor.

As a final remark, from INVAP’s perspective, it is key to encourage the customers to prioritize each of the performance and production requirements from the beginning of the design process, since the success of the project is heavily attached to a well-balanced design path.

4. References

[1]. IAEA Research Reactor Database. https://nucleus.iaea.org/rrdb/#/home . Accessed on 12/May/2022.
[2]. Eduardo Villarino, Alicia Doval, "INVAP's Research Reactor Designs", Science and Technology of Nuclear Installations, vol. 2011, Article ID 490391, 6 pages, 2011. https://doi.org/10.1155/2011/490391 .
[3]. Eduardo Villarino et at. “INVAP Nuclear Engineering Department Calculation Suite” RERTR 2018 – 39TH international meeting on reduced enrichment for research and test reactors

[4]. Ferraro, Diego and Eduardo Villarino, Eduardo. (2018). “Neutronic Design of customized Research Reactors”. AYNG conference 2017.
[5]. The OPAL research reactor. https://www.ansto.gov.au/research/facilities/opal-multi-purpose-reactor
[6]. J.M.Tuñón et al. “Neutronic Design of the RA10 Research Reactor´s Core” IGORR Conference 2014.
[7]. J.M.Tuñón et al. “Neutronic Design of the RMB Research Reactor” IGORR Conference 2014.
[8]. Ferraro, Diego, Boschetti, Facundo, Villarino, Eduardo and Sardella, Federico. “Neutronic Design of the Coqui Reactor”. European Research Reactor Conference 2015
[9]. PALLAS reactor. https://www.pallasreactor.com/en/en-pallas-van-levensbelang-voor-miljoenen/
[10]. Lupiano Contreas, J. et al. “Thermal-hydraulic aspects of RMB design” IGORR Conference 2014
[11]. Francioni, F. et al. “Thermal-hydraulic aspects of RA-10 design” IGORR Conference 2014

TRANSIENT SAFETY ANALYSES FOR THE MUSTANG-R DEVICE IN BR2 USING RELAP5

H. LIN, P. GARNER, J. LICHT
Nuclear Science & Engineering Division, Argonne National Laboratory
9700 S. Cass Ave, 60439 Lemont, U.S.A.

B. ROSSAERT
Nuclear Engineering Office, SCK CEN
Boeretang 200, 2400 Mol, Belgium

ABSTRACT

To support US High Performance Research Reactor low-enriched uranium reactor conversion project, two Design Demonstration Elements (DDEs) for Massachusetts Institute of Technology Reactor (MITR) and the National Bureau of Standards Reactor (NBSR), are planned to be irradiated in the Belgium Reactor 2 (BR2). Irradiations of a Generic Test Assembly (GTA) are also being considered. The irradiations target to mimic their reactor operating conditions. MUSTANG-R, an experimental device with a flow restrictor, is designed to regulate flow rates. This study provides thermal-hydraulic analyses during loss-of-flow and loss-of-pressure scenarios for the DDEs and GTA in the MUSTANG-R device using RELAP5-3D. The MUSTANG-R device has been implemented as a parallel branch to the BR2 RELAP5-3D model. The results demonstrate that DDEs and GTA in the MUSTANG-R device are sufficiently cooled and experience less severe conditions than the limiting BR2 fuel element when comparing cladding and coolant temperatures, voids, and critical heat flux ratios.

1. Introduction

In support of the US High Performance Research Reactor (USHPRR) reactor program, two Design Demonstration Elements (DDEs), including the Massachusetts Institute of Technology Reactor (MITR) and the National Bureau of Standards Reactor (NBSR) are planned to be irradiated in the Belgium Reactor 2 (BR2) [1]. The DDE irradiations are targeted to mimic their reactor operating conditions for neutronics and thermal hydraulics. Mass flow tuning Setup for Testing of fuel Assemblies of the Next Generation (MUSTANG) device is designed to be placed in one of the BR2 200 mm irradiation channels. MUSTANG-R, an experiment irradiation device with a flow restrictor, is designed to achieve the relatively lower flow rates of the MITR and NBSR DDEs. In addition to the DDE irradiations in BR2, the intention is to also test a generic test assembly (GTA) in the MUSTANG-R device.

BR2 is a research and test reactor located in Mol, Belgium and is mainly used for radioisotope production and material testing as shown in Fig 1. The BR2 reactor core contains 79 irradiation channels in a hyperboloid configuration within the reactor vessel and uses pressurized water as a coolant. During normal operation, coolant in the upper reactor vessel plenum enters the channels through perforations in the channel walls, flows downward to cool the core region, and then discharges into the lower reactor vessel plenum.

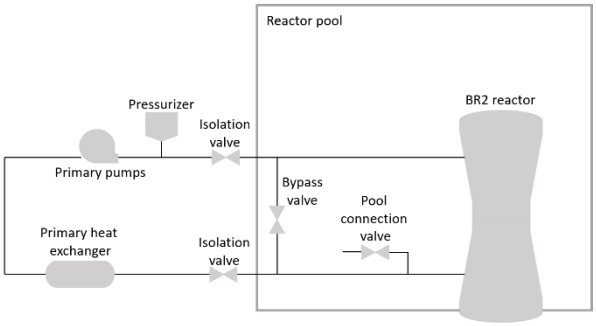

Fig 1. Schematic of BR2

To meet the flow requirements of the irradiation experiments, MUSTANG-R uses a plug design, denoted by restrictor, to regulate the flow by blocking a part of the flow passage area above the fuel testing section. During DDE and GTA irradiation experiments, it is needed to ensure that experiments are properly cooled in the event of reactor accidents, such as loss of flow (LOF) and loss of pressure (LOP) scenarios.

The safety analysis was performed for the MUSTANG-R device in BR2 during transients using RELAP5. RELAP5-3D version 4.3.4 [2] is used for transient analyses of the BR2 reactor. Briefly, a RELAP5/MOD 3.3 model for BR2 has been validated against historical experimental data which shows agreement with measured cladding temperatures during various reactor transients [3]. Following validation, the BR2 model was converted to the representative core and extensively used for various transient analyses including loss of coolant accidents (LOCA) and beyond design basis accidents (BDBA) [4,5,6]. During this work, the BR2 RELAP5/MOD 3.3 model has been converted to RELAP5-3D version 4.3.4 with several model updates and modifications implemented [4]. Regression testing [7] has been performed, confirming that the RELAP5 model used as a starting point for this work is consistent with the analyses supporting the BR2 safety analyses. This study shows the transient analyses of the MUSTANG-R device model during LOF and LOP scenarios. The results are compared with the hot stripe located in the 6th channel of the limiting BR2 fuel element (high heat flux fuel element).

2. MUSTANG-R RELAP5 Model

Fig 2 shows the BR-2 RELAP5 model with MUSTANG_R added that contains MITR DDE, NBSR DDE and GTA. The MITR and NBSR DDE are divided into three subchannels based on their heat flux distributions, whereas the GTA only uses one flow channel for this preliminary analysis. The RELAP5 point kinetics model is utilized for the steady state and transient fission power. The ANSI/ANS-5.1-1979 is chosen for the decay heat model [4].

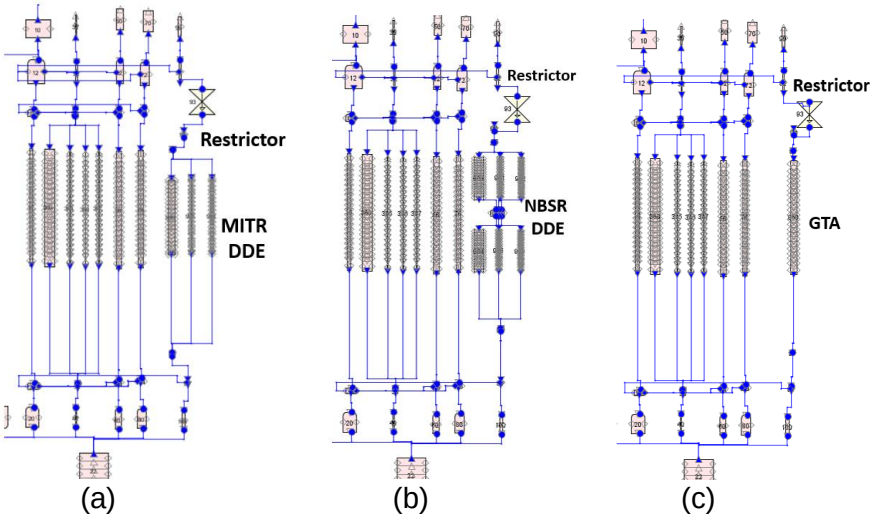

Fig 2. MUSTANG-R RELAP5 models with (a) MITR DDE, (b) NBSR DDE and (c) GTA

For the MITR DDE fuel, component 961 represents the coolant channel between plates 18 and 19. Component 962 represents the coolant channel between plate 19 and the fuel basket. Component 960 represents the remainder of the coolant channels, as shown in Fig 3 [8]. For this work, the peak heat flux of MITR DDE is 74.9 W/cm^2 at plate 19. The average flow velocity in the fuel flow channel is 3.36 m/s [9].

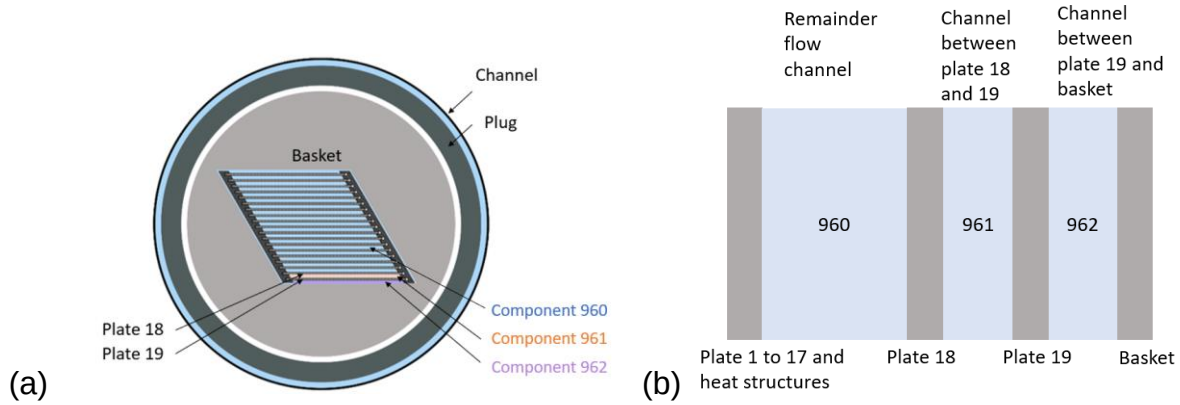

Fig 3. MITR DDE coolant channels in the MUSTANG-R RELAP5 model

For the NBSR DDE fuel, components 961 and 965 are the coolant channels between plates 16 and 17 for the upper fuel and lower fuel, respectively. Components 962 and 966 are the coolant channel between plate 17 and a dummy plate. The remainder of the flow channels are lumped into components 960 and 964. Component 963 represents the gap between the upper and lower fuel, as shown in Fig 4 [10]. For this work, the peak heat flux of NBSR DDE is 179 W/cm^2 at lower fuel plate 17. The average flow velocity in the fuel channel is 6.6 m/s [11].

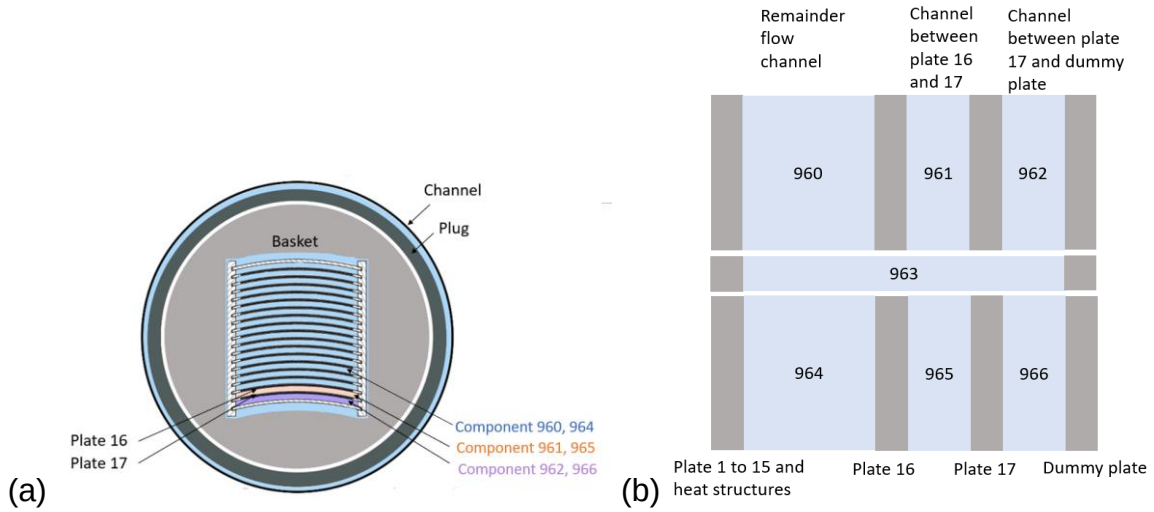

Fig 4. NBSR DDE coolant channels in the MUSTANG-R RELAP5 model

The GTA consists of 10 fuel plates and 11 coolant channels as shown in Fig 5. The power distribution in the BR2 high heat flux channel is utilized in GTA fuel plates for this preliminary analysis. It is assumed that the 10 fuel plates in GTA all have the same power distribution which is a conservative modeling approach. Due to the same power distribution in every plate, only one coolant channel (component 960) is sufficient to simulate the whole coolant area for GTA. The peak heat flux and target average flow velocity of GTA used in this work are 350 W/cm^2 and 8 m/s, respectively.

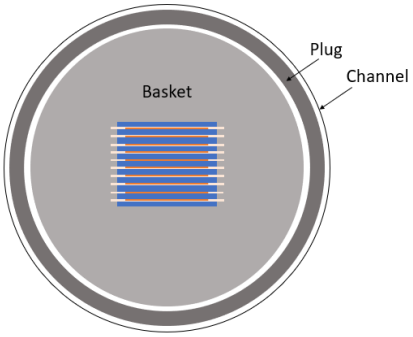

Fig 5. GTA in the MUSTANG-R RELAP5 model

The flow restrictor as shown in Fig 6 is used for regulating and reducing the flow rate in the MUSTANG-R device. The flow restrictor is designed to be moveable in the axial direction to vary the flow area, and hence the flow rate, and will be set at a position specific to the assembly/element being tested. The restrictor is moved in a downward direction to reduce pressure drop and increase the flow rate. The restrictor upper position is limited by a mechanical blockage. This mechanical blockage is adjustable depending on irradiation requirements and can ensure the minimum flow area through the restrictor during flow transients. For the purposes of transient safety analysis, it is conservatively assumed that the restrictor moves from its nominal position to the fully closed position, neglecting the mechanical blockage. Note that in a closed position there is still some small flow area around the restrictor for coolant to pass. Therefore, the restrictor model in RELAP5 needs to account for both the nominal and closed positions, as well as for upward and downward flow. Nevertheless, to make the model more realistic, the model is implemented in a way that is consistent with pressure drop values predicted by CFD analysis [12,13]. The servo valve model with the CSUBV function is used, it is a user-defined function that allows the form loss coefficients to change with time.

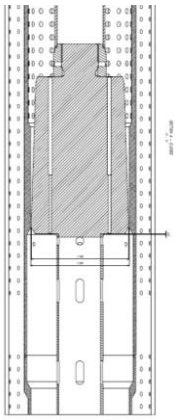

Fig 6. Restrictor in the MUSTANG-R device [13]

3. Steady State Results

Tab 1 summarizes the parameters of the MUSTANG-R device at steady state. The inlet temperatures in the three models are 40 °C. The form loss coefficients (K_forward) represent that the restrictor is manually adjusted to reach the nominal target velocities in the DDEs and GTA fuel channels. K_reverse = 0 is set at steady state. The K_reverse in the open position is not used in the simulation since the restrictor is fully closed at 5 s. However, the flow starts to reverse at 20 s.

Tab 1. Steady state values of the MUSTANG-R device

	MITR DDE	NBSR DDE	GTA
Average velocity in the fuel section (m/s)	3.36	6.60	8.0
Form loss coefficient in restrictor, K_forward	56.2	2.5	5.7
Outlet temperature (ºC)	53.6	48.2	75.3
Mass flow rate (kg/s)	7.6	23.2	13.7
Pressure drop across restrictor (bar)	2.23	0.98	0.76
Pressure drop across DDE/GTA (bar)	0.33	1.43	1.76
Power (MW)	0.44	0.80	2.07

4. Transient Results

The transient results of the MUSTANG-R device with DDEs and GTA are evaluated. The peak cladding and peak coolant temperatures in the MUSTANG-R device are compared to the limiting BR2 fuel element. The short-term transient results are focused since the peak temperatures occur during flow reversal within 100 s into LOF and LOP transients. It is assumed that the restrictor reaches a closed position (with minimal flow area available) at 5 s. Hence, the form loss coefficients representing the restrictor are linearly changed from nominal values in Tab 1 to coefficients corresponding to a closed restrictor K_forward = 126.75 and K_reverse = 93.37 for Test A, F and G.

4.1 Test A

Test A transient is a total loss of flow followed by opening of the bypass valve between the BR2 coolant inlet and outlet pipes. To initiate Test A, the primary pumps are tripped at 0 s. At this time, it is assumed the restrictor accidentally changes to a closed position from 0 s to 5 s. In Fig 7 (a), after the pump trip at 0 s, the cladding temperatures in all the fuel elements start to increase due to a sudden decrease in coolant flow rate. The reactor scrams at 1.88 s since the pressure difference across the core is low and then causes a decrease in fission power and cladding temperatures. As the coolant flow rate keeps decreasing, the cladding temperatures start to rise and then reach peak values during the flow reversal process. In the MUSTANG-R device, the peak cladding temperature occurs at plate 19 for MITR DDE; and lower plate 17 for NBSR DDE. The peak cladding temperatures in the BR2 fuel element are higher than DDEs and GTA. As shown in Fig 7 (b), the peak coolant temperatures occur when the coolant flow rates reach 0 kg/s. The peak cladding and coolant temperatures in the MUSTANG-R device are significantly lower than the temperatures in the limiting BR2 fuel element. In Test A, the coolant temperatures are below saturation temperatures.

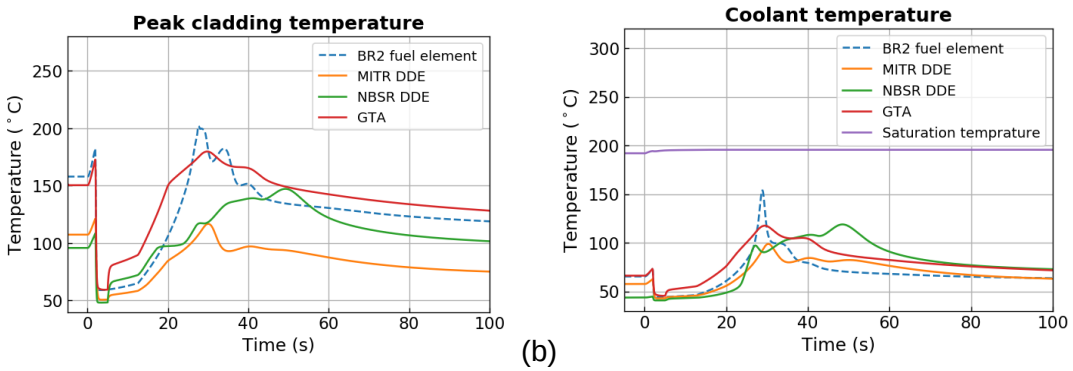

(a) (b)

Fig 7. Test A (a) peak cladding and (b) peak coolant temperatures

In Fig 8, the sudden drop of mass flow rate at 5 s is due to the restrictor reaching a closed position. The downward flow in the reactor vessel is defined as positive flow and vice versa. The flow reversal starts after ~25 s in the MUSTANG-R device followed by a steady natural circulation flow.

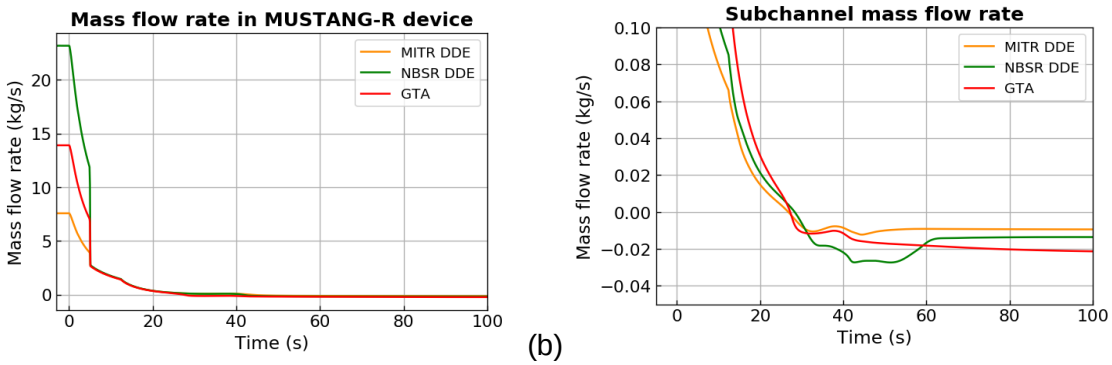

(a) (b)

Fig 8. Test A mass flow rates in (a) the MUSTANG-R device and (b) high heat flux channels

4.2 Test F

Test F is defined as an untimely opening of the pool connection valve (total loss of pressure) followed by the opening of the bypass valve. At 0 s, the transient is initiated by the pool connection valve opening. The restrictor is also assumed to accidentally start to close at 0 s. Peak cladding temperatures are shown in Fig 9 (a). The reactor scram at 0.39 s due to low pressure in the primary loop causes the initial decrease in cladding temperatures. After the primary pump trip at 2.25 s, the cladding temperatures increase as the flow rate decreases. The cladding temperatures in Test F are lower than temperatures in normal operations. GTA is slightly higher than BR2 due to higher heat flux. Fig 9 (b) shows peak coolant temperatures in each fuel element. Depressurization in Test F causes saturation temperature to decrease. During flow fluctuations in flow reversal in Fig 10, all fuel elements undergo nucleate boiling near the location of the peak heat flux and voids are generated. For the fuels in the MUSTANG-R device, the boiling periods are shorter than the BR2 limiting fuel element.

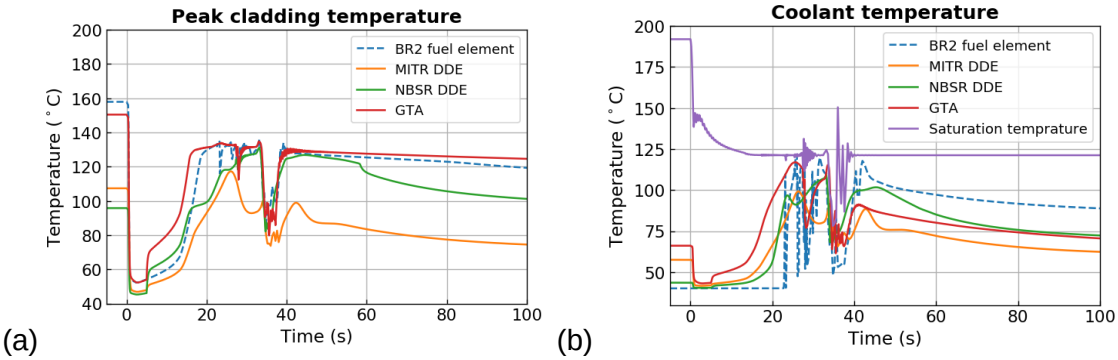

(a) (b)

Fig 9. Test F (a) peak cladding temperatures (b) peak coolant temperatures

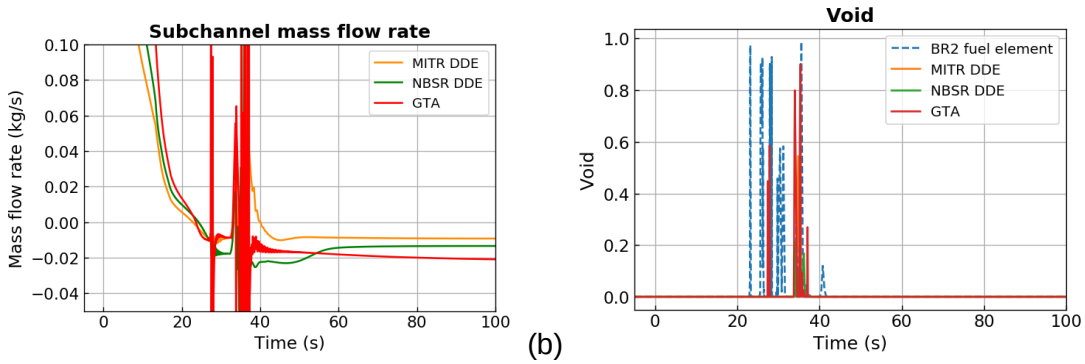

(a) (b)

Fig 10. Test F (a) channel mass flow rates and (b) voids

4.3 Test G

Test G is defined as an untimely opening of the pool connection valve (total loss of pressure) without opening the bypass valve. The initiation condition of Test G is identical to Test F, except the bypass valve is failed to open in Test G. Therefore, the natural circulation flow mainly occurs within the reactor core after flow reversal. In Fig 11, the trends of peak cladding temperatures in the limiting BR2 fuel element are close to NBSR DDE and GTA. After flow reversal, nucleate boiling starts to occur in the MUSTANG-R device, as shown in Fig 12. CHFR is also investigated using the extended version of 2006 Groeneveld look-up tables [14,15]. Though the boiling periods in NBSR DDE and GTA are longer due to higher heat flux, Fig 13 shows the CHFR of NBSR DDE and GTA are higher (less limiting) than the limiting BR2 fuel element. Except for the flow reversal period, the remaining CHFR is higher than 1. Though the CHFR decreases below 1 at 25 s and 31 s in the BR2 channel during the flow reversal in which the temperature and flow rates are fluctuating, the CHF is at the local condition and the heat flux is not sufficient to sustain dryout.

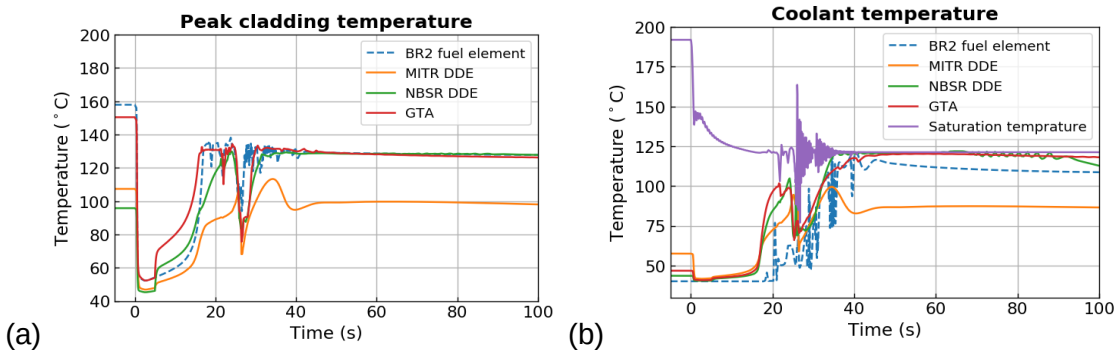

Fig 11. Test G (a) peak cladding temperatures and (b) peak coolant temperatures

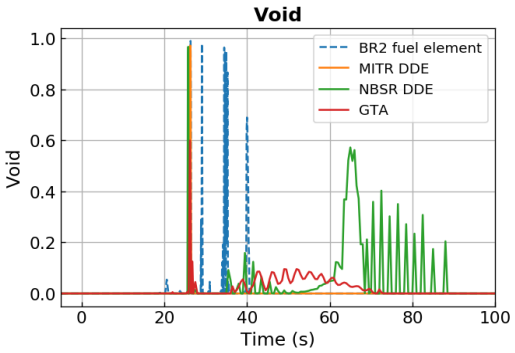

Fig 12. Test G voids

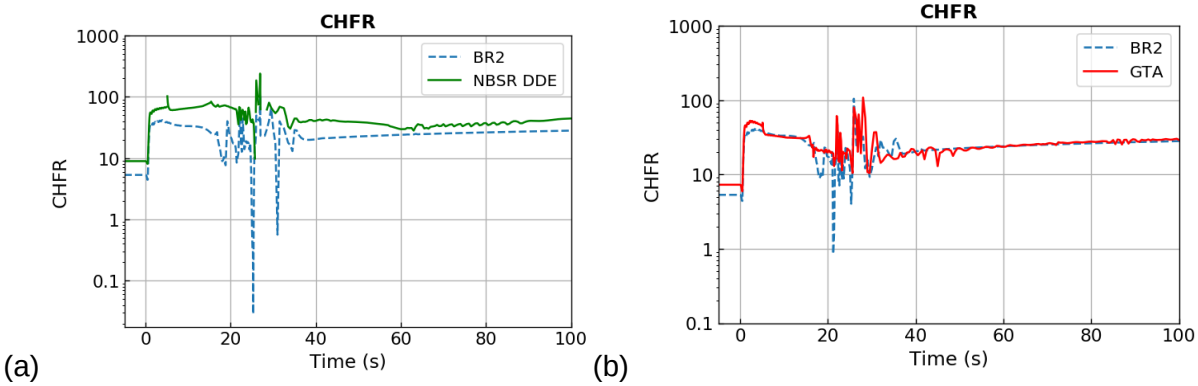

Fig 13. Comparisons of CHFR in Test G

4.4 Test A and test F (long-term transient)

The coolant temperatures keep increasing after 100 s, so it is necessary to also evaluate the temperatures in transients for a longer time. Fig 14 shows the coolant temperature results for Test A and Test F remain in single-phase heat transfer following flow reversal.

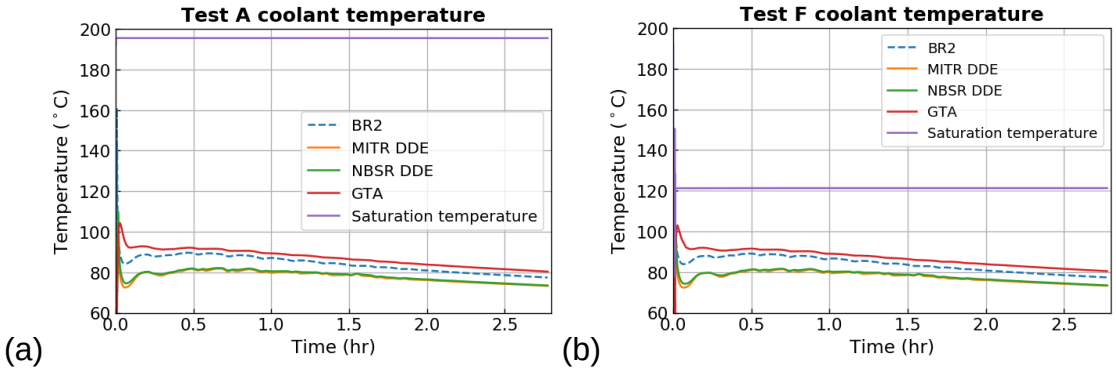

Fig 14. Comparison of coolant temperatures Test A and F within 2.7 hours

4.5 Test G (long-term transient)

Fig 15 shows the long-term transient results of Test G. Without opening the bypass valve, the coolant temperature is heated up to saturation temperatures in fuel elements. Nucleate boiling lasts 1.4 hrs for BR2 fuels, 0.75 hrs for MITR DDE, 0.8 hrs for NBSR DDE and 1.1 hrs for GTA. After that, the coolant temperatures decrease with time and nucleate boiling terminate.

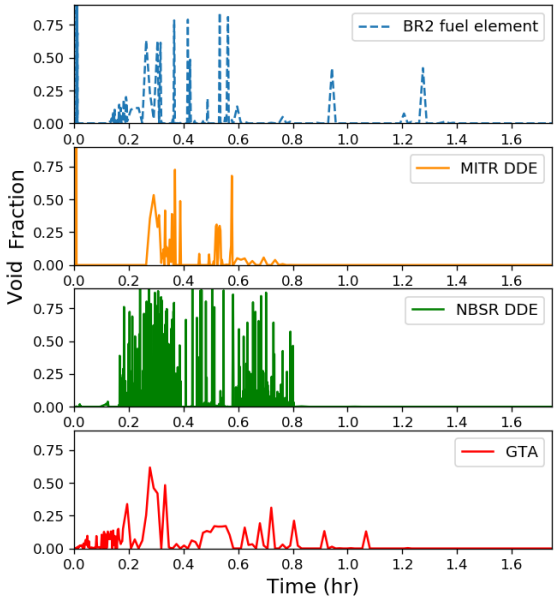

Fig 15. Test G voids within 1.7 hours

5. Summary and Conclusion

This study provides the transient simulation results of the DDEs and GTA in the MUSTANG-R device during LOF and LOP scenarios. A MUSTANG-R device with MITR DDE, NBSR DDE and GTA have been implemented into separate BR2 RELAP5-3D models as a parallel branch to the representative core configuration. CFD simulation results were used to determine the form loss coefficients for the restrictor at various positions in the RELAP5 model. A valve model with the CSUBV function was used to represent the restrictor and regulate the flow in the MUSTANG-R device.

At the initiation of the scenarios, it was conservatively assumed that the restrictor moved to a closed position with a decreased flow area compared to nominal flow conditions. For MITR DDE, NBSR DDEs and GTA, the peak cladding temperature and peak coolant temperature results during flow reversal are lower than the values of the limiting BR2 fuel element during Test A. During flow reversal in Test F and G, coolant in the MUSTANG-R device undergoes nucleate boiling as the flow stagnates during the flow reversal process. Due to higher heat flux in NBSR DDE and GTA, nucleate boiling last longer within the first 100 s in Test G. However, the CHFR in NBSR DDE and GTA are still higher than the value in the limiting BR2 fuel element. The short-term transient results also demonstrate that MUSTANG-R with different testing fuels are in less severe thermal hydraulic (boiling) conditions during transients than the limiting BR2 fuel element.

In the long-term transients of Test A and F, the coolant temperatures are all below coolant saturation temperatures with the assistance of the bypass valve opening and enabling better natural circulation. In Test G, where the bypass valve remains closed, nucleate boiling lasts 0.75 hours for MITR DDE, 0.8 hours for NBSR DDE and 1.1 hours for GTA. Following this, the coolant temperatures decrease to the subcooled region. The boiling time in the MUSTANG-R device is shorter than the limiting BR2 fuel element. It is noted that the simulation is assumed to be conservative since the restrictor moves to a closed position and in absence of a mechanical blockage that is foreseen in the design and will limit the closing of the restrictor.

To summarize, the simulation results of the MUSTANG-R RELAP5 model demonstrate that the MUSTANG-R device in BR2 is sufficiently cooled during LOF and LOP transient accidents. The DDEs and GTA in the MUSTANG-R device experience less severe conditions than the limiting BR2 fuel element when comparing the cladding temperatures, coolant temperatures, voids and CHFR. In addition, there is no over-heating observed in the DDEs or GTA fuel plates during LOF and LOP scenarios.

6. Reference

[1] S. Van den Berghe, S. Kalcheva, V. Kuzminov, B. Rossaert, P. Gouat, J. Valenberghs, H. Ooms, J. Smets, G. Cornelis, Y. Parthoens, F. Joppen, A. Leenaers, P. Jacquet, G. Van den Branden, S. Van Dyck, “Feasibility Study for Performing Design Demonstration Element (DDE) Irradiations in the BR2 Reactor,” SCK CEN/26573864, SCK CEN, 2017.

[2] RELAP5-3D© Code Manual, INL/MIS-15-36723, Idaho National Laboratory, 2015.

[3] J. Licht, B. Dionne, G. Van den Branden, E. Sikik and E. Koonen, “RELAP5 Model Description and Validation for the BR2 Loss-of-Flow Experiments,” ANL/GTRI/TM-14/10, Argonne National Laboratory, July 2015.

[4] J. Licht, A. Bergeron, B. Dionne, E. Sikik, G. Van den Branden and E. Koonen, “Loss-of-Flow and Loss-of-Pressure Simulations of the BR2 Research Reactor with HEU and LEU fuel,” ANL/RTR/TM-15/8, Argonne National Laboratory, March 2016.

[5] J. Licht, B. Dionne, E. Sikik, G. Van den Branden and E. Koonen, “Supplemental Thermal-Hydraulic Transient Analyses of BR2 in Support of Conversion to LEU Fuel,” ANL/RTR/TM-16/3, Argonne National Laboratory, September 2016.

[6] J. Licht, F. Wols and G. Van den Branden, “Beyond Design Basis Accident Analyses of BR2 in Support of Conversion to LEU,” ANL-RTR-TM-19/1 Rev. 1, Argonne National Laboratory, June 2019.

[7] H. Lin, P.L. Garner and J.R. Licht, “Regression Testing for BR2 RELAP5 Models,” ANL/RTR/TM-21/2, Argonne National Laboratory, May 2021.

[8] G. Housley et al., “MITR DDE Element Conceptual Design Assembly and Details,” DWG-606748, Rev 1, Idaho National Laboratory, November 2019.

[9] K. Sun, A. Dave, L. Hu, D. Jaluvka, S. Pham, J. Stillman, and E. Wilson, “Irradiation Demonstration Element Design Parameters for MITR LEU U-Mo Fuel Conversion,” MIT-NRL-18-03 Revision 2, Massachusetts Institute of Technology, 2020.

[10] G. Housley et al., “NBSR DDE Element Conceptual Design Assembly and Details,” DWG-606745, Rev 1, Idaho National Laboratory, October 2019.

[11] D. J. Diamond, P. Kohut, and A. Varuttamaseni, “Irradiation Experiment Design Parameters for NBSR Fuel Conversion,” BNL-211807-2019-IR-R1, Brookhaven National Laboratory, 2020.

[12] M. Sharabi, “CFD Simulations of the MUSTANG-R Restrictor,” SCK CEN/39693934, SCK CEN, 2021. “105081-A001/1,” SCK CEN, 2019

[13] B. Rossaert, S. Stevens, “MUSTANG-R: results and feedback from the construction and testing of the restrictor mock-up”, Restricted contract report R-8688, NT 4986/N0BRIDDES/30/BR/SS, SCK CEN/ 43527939, September 2021.

[14] D.C. Groeneveld, J.Q. Shan, A.Z. Vasić, L.K.H. Leung, A. Durmayaz, J. Yang, S.C. Cheng, and A. Tanase, “The 2006 CHF look-up table,” Nuclear Engineering and Design, 237, pp. 1909-1922, 2007.

[15] M. Kalimullah, et al., “An evaluation of subcooled CHF correlations and databases for research reactors operating at 1 to 50 bar pressure,” RERTR 2012 – 34th International Meeting on Reduced Enrichment for Research and Test Reactors, October 14-17, Warsaw, Poland, 2012.

Acknowledgement

This work was sponsored by the U.S. Department of Energy, Office of Material Management and Minimization in the U.S. National Nuclear Security Administration Office of Defense Nuclear Non-proliferation under Contract DE-AC02-06CH11357. The authors would like to thank Silva Kalcheva, from SCK CEN, for providing MITR DDE and NBSR DDE MCNP simulation results.

MANUFACTURING OF DISPERSION TYPE TARGETS FOR FISSION ^{99}Mo PRODUCTION

LUIS OLIVARES, MARIO BARRERA, JAIME LISBOA,
Research and Nuclear Applications Division, Chilean Nuclear Energy Commission
Nueva Bilbao 12501, Postal code 7600713, Santiago, Chile

ALLISON CASTRO, GISEL CARTER, JORGE MARIN,
Metallurgy Engineering Department, University of Santiago of Chile
Av. Lib. B. O'Higgins 3363, Postal code 9170022, Santiago, Chile

ABSTRACT

One of the methodologies to produce the ^{99}Mo radioisotope for medical use is the nuclear fission of low-enriched uranium (LEU). This technique uses targets based on particles made of uranium alloys, usually UAlx aluminide type, dispersed in an aluminium matrix.
CCHEN is currently developing an R&D project aiming to develop the methodology to obtain dispersion-type targets, based on our experience and available facilities. This was an outcome of our developed capacity to produce fuel assemblies for research reactors.
Although this technology allows advances in terms of supply and availability, there are still improvement opportunities, in terms of productivity and process efficiency. An improvement proposal is to increase the uranium load inside the targets. This parameter, in order to maintain homogeneity in the dispersion of UAlx-type compounds, is limited to less than 3 gU/cm^3. This limited uranium load could be significantly increased by using uranium-molybdenum alloy particles, an alloy which would allow to reach homogeneous dispersions of up to 8 gU/cm^3.
This study summarises the results of targets manufactured with U-Mo alloy particles, dispersed in an aluminium matrix, and then subjected to heat treatments. In the U-Mo particles, it was possible to observe phase transformations, initially forming UAl_2 compounds and then UAl_3 and UAl_4 for more than 8 hours of annealing.
Finally, it was possible to induce in situ phase transformations in the U-Mo alloy particles, as a first step to obtain uranium targets with loads higher than the technological limit specified for the use of UAlx-type compounds.

1. Introduction

^{99}Mo is the father of ^{99m}Tc, which is the most widely used radioisotope in nuclear medicine in the world, applied annually in approximately 20 to 25 million diagnostic medical procedures, comprising about 80% of all diagnostic procedures worldwide. ^{99m}Tc is a gamma emitter with an energy of 141 keV and a half-life of 6.0 hours, which is produced by the decay of its parent, ^{99}Mo, with a half-life of 66 hours [1]. The most efficient way to have the radioisotope ^{99m}Tc at any time and in any place, even far from the production centres, is by elusion from Mo-Tc generators. These generators have a useful life of up to 2 weeks to obtain ^{99m}Tc. For these generators, high specific activity ^{99}Mo is used as raw material, only possible to obtain from the fission of uranium in a nuclear research or intermediate-high power reactor [2].

In Chile, between 50,000 and 100,000 nuclear medicine procedures using ^{99m}Tc are performed annually.

A limited amount, which can only be applied in capital city (Santiago) due to its low specific activity, is produced in the RECH-1 nuclear reactor by neutron activation (which is another less effective technique), and most of it is obtained from imported Mo-Tc generators. CCHEN

developed the technology and infrastructure for assembling Mo-Tc generators from imported fission ^{99}Mo, which it produced and sold with excellent results until 2007.

The development of the production of ^{99}Mo in the CCHEN had as its first objective to satisfy the national demand, which reaches 55 Ci per week.

Between 2005 and 2011, CCHEN participated in an IAEA CRP “Developing Techniques for Small Scale Indigenous ^{99}Mo Production using LEU Fission or Neutron Activation” (T1.20.18), for which a relevant objective was to develop capacities for fission ^{99}Mo production based on Low Enriched Uranium (LEU) targets [3].

As a result of CCHEN's participation in the IAEA CRP, it was possible to achieve objectives related to the production of thin uranium foils, assembly and disassembly of annular targets, cold dissolution tests, separation and purification of solutions, calculations, design and manufacture of irradiation devices. Pending activities, not completed in the CRP were:

- Safety Analyses
- Irradiated waste Management
- Target irradiation in research reactor
- Cintichem process with irradiated LEU
- Dissolution of irradiated foils in nitric acid
- Recovery of 99Mo by precipitation
- Purification of the solution through ion exchange columns
- Quality controls of purified 99Mo solution. Validation for radiopharmaceutical use.

In 2009 the fission ^{99}Mo development activities were stopped at CCHEN. Nevertheless, the capabilities for manufacture and inspection of annular and plate type targets are still valid [4]

Currently CCHEN produces ^{99m}Tc by Neutron Activation of purified molybdenum trioxide (Merck ® MoO_3) in RECH-1 research reactor.

Production schedule: 11 capsules with 40 g of MoO_3 each one, irradiated by 22 hours. After 24 hours of cooling, radiochemical process start on Saturday midnight and ends on Sunday about 04:00 AM. ^{99}Mo is produced at CCHEN weekly, starting on Friday

^{99m}Tc Activity (Daily production level):

Day 1 (Monday): 31 Ci
Day 2 (Tuesday): 25 Ci
Day 3 (Wednesday): 19 Ci
Day 4 (Thursday): 15 Ci
Day 5 (Friday): 11 Ci

Coverage Area: Limited to capital city (Santiago) and surroundings. There is a private company that supplies ^{99m}Tc to some far cities, extracted from imported generators [5]

In 2021, CCHEN's Nuclear Research and Applications Division - DIAN, launched an internal R&D project aimed at the development of manufacturing technology of dispersion type targets [6] The main objectives planned for this R&D project are the following

1. Study phase transformations observed in dispersions of uranium compounds in aluminium matrix, considering manufacturing parameters and heat treatment conditions for phase transformations of the U-Al system.

2. Develop the technology for manufacturing plate-type targets based on UAlx compounds dispersed in aluminium matrix.

3. Develop the radiochemical-metallurgy processes of dissolution, separation, extraction and purification of the ^{99}Mo.

4. Study the irradiation conditions and the radioactive activity that would be generated in the target once irradiated, in positions of known fluxes, inside the core of the RECH-1 reactor.

5. Develop treatment and management technologies for radioactive waste generated from fission ^{99}Mo production processes

1.1 Problem Description

The radioisotope ^{99}Mo currently produced at the CCHEN by neutron activation has limited radioactive activity, which is the cause for it is not available to patients living in remote areas far of the capital city.

The specific radioactive activity of ^{99}Mo produced by neutron activation is several times lower than the activity obtained by nuclear fission methodology of U-235. It is necessary to produce radioisotopes with greater radioactive activity, so that they can be transported to and made available in the farthest regions of the country.

1.2 Proposed solution

The dispersion of uranium compound particles in disperse-type targets must be homogeneous. When using aluminide-type compounds, the volumetric fraction is limited and they can only contain charges of up to 3 gU/cm^3.

Then, in this study it is proposed to evaluate the use of uranium alloy particles with 7% weight of molybdenum (U-7%Mo), dispersed in an aluminium matrix, to then induce phase transformations, by means of thermal treatment, to UAlx compounds.

The nominal uranium loading or uranium density of disperse-type targets is 2.6 gU/cm^3, while using U-Mo particles, the core of the plate could reach densities of up to 8 gU/cm^3.

For the objective 1, the main goal will be to study phase transformations in the U-Al system, considering U-Mo alloy particles dispersed in an aluminium matrix.

1.3 Specific goals

- Obtain a dispersion of U-Mo alloy particles in an aluminium matrix using standard methodology for the manufacture of plate type fuel.
- Induce phase transformations of the U-Al system by means of thermal treatments.
- Analyse the effects of heat treatments using available analysis techniques.

2. Materials and methods

2.1 Preparation of U-Mo alloy powders

The U-Mo alloy was prepared with natural uranium and 7% by weight of metallic molybdenum in a high alumina crucible and subsequently cast in a graphite mould. The melting was carried out in an induction furnace, located inside a chamber with an inert argon atmosphere, obtaining U-Mo ingots, which were then vacuum annealed (10^{-4} Torr) at 950 °C for 24 hours, in order to homogenize the microstructure, inducing the transformation of the residual alpha phase, located at grain boundaries, into metastable gamma phase.

To obtain disperse-type plates necessary for studies of phase transformations, it is necessary produce fine powders. The methodology used was obtaining metal shavings extracted by a rotating file immersed in water. These shavings were subjected to milling in a rotating blade mill to obtain fine particles.

2.2 Target manufacture (miniplates).

U-Mo alloy and Al powders were blended and compacted to required density. The picture-frame technique was used to clad the dispersions of U-Mo particles with aluminium. Figure 1 summarises the targets fabrication process, manufactured by thermo-mechanical processing (hot rolling & annealing) of the U-Mo/Al matrix contained in an assembly of 6061 alloy (frame and covers). The fabricated plates were characterised by non-destructive testing techniques and small samples extracted by punching were annealed to achieve the required phase of uranium aluminide for proper dissolution in basic media.

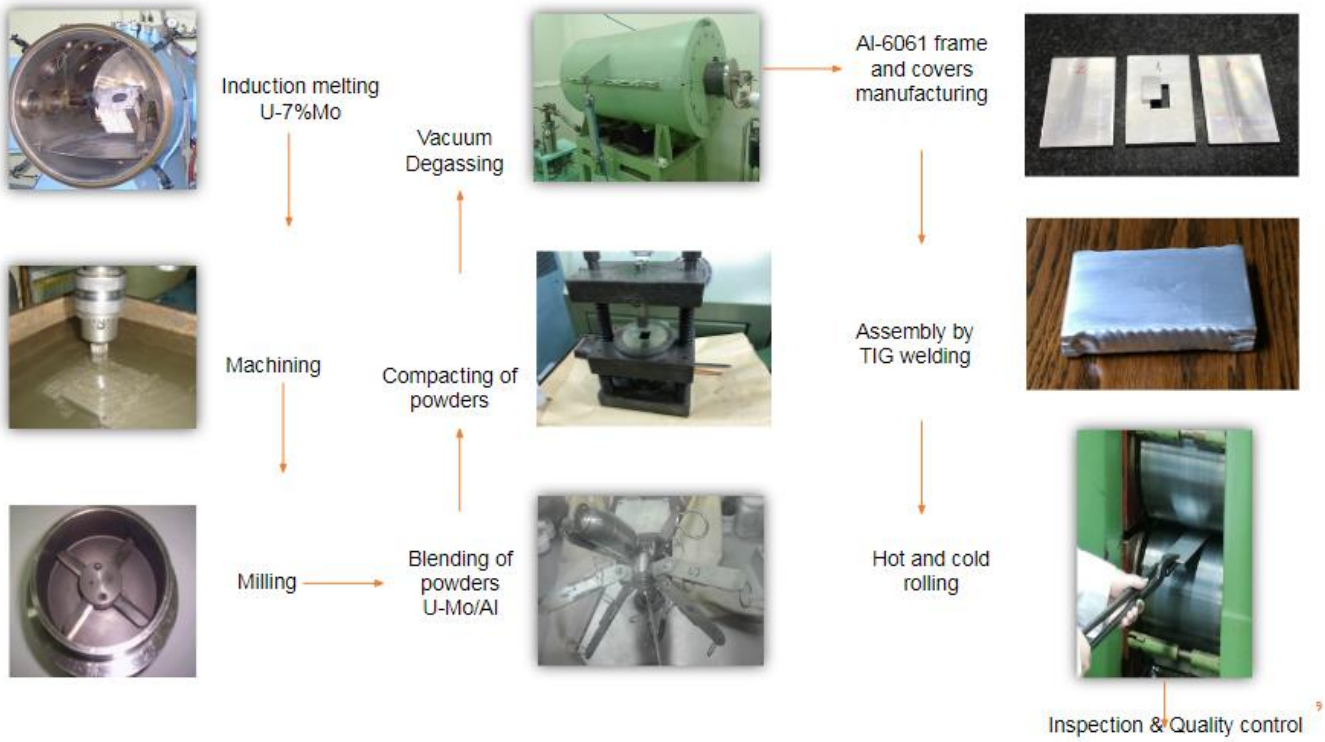

Figure 1. Manufacturing of plate type targets

2.3 Extraction and preparation of samples from plates

1 cm. diameter discs, extracted from meat zone of target plates by punching, were sealed in quartz capsules for thermal treatment. Figure 2 shows radiography of punches plate, vacuum sealed capsules (< $2*10^{-4}$ Torr) and a sample mounted and polished for SEM analysis

Figure 2. Photo and radiography of UMo/Al plate type target, punched for samples extraction. At centre, samples sealed in vacuum into quartz capsules and at right, sample mounted for SEM analysis

2.4. Thermal treatments for phase transformations

Phase transformations annealing were performed on the vacuum encapsulated samples at 550 °C for times between 2 and 48 hours. Table 1 shows the thermal treatments applied to each sample.

Sample Id.	Temperature (°C)	Time (hr)
14	as fabricated, not annealed	
10/6	550	2
5	550	4
11	550	14
9	550	24
8	550	48

Table 1. Samples subjected to phase transformation annealing

2.5 Samples characterisation

The annealed samples were characterised by means SEM with microanalysis. The idea was to verify the interaction of particles with the aluminium matrix and the evolution of U-Al compounds with the annealing time. For their part, the plate targets are being characterized by industrial radiography, ultrasonic scanning and metrology, whose results will be verified by destructive metallographic analysis. All inspections of plate type targets are being performed in accordance with the technical specifications of targets for fission Mo production.

3. Results

Figure 3 shows the U-Mo particles obtained by milling of machined shavings. For plate type target manufacturing, all U-Mo particles were sieved under 150 µm.

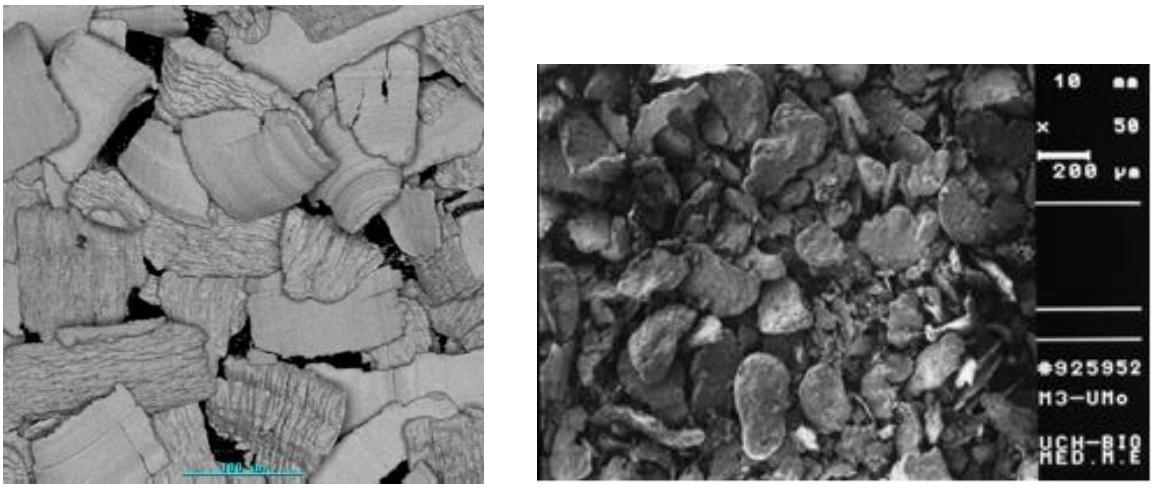

Figure 3. U-Mo shavings produced by machining and at right, particles obtained by milling

Micrographs in figures 4 and 5 shows U-Mo particles total or partially transformed to UAlx phase and below of each image, a table with the microanalyses results. The formed compounds have at the beginning, chemical composition close to UAl_2 and then, the interaction progress with the annealing time to convert U-Mo particles to UAl_3 or UAl_4 compositions.

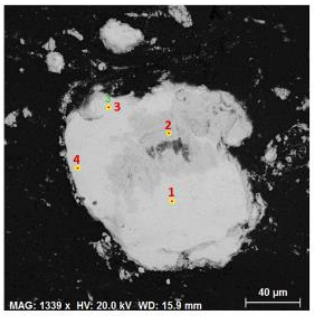

U-Mo/Al sample as fabricated (without annealing)

Point	1	2	3	4
U (%p)	90.45	88.67	90.46	89.78
Mo (%p)	6.80	6.96	6.53	6.74
Al (%p)	0.80	1.15	0.85	0.95

Microanalysis results for as fabricated sample.

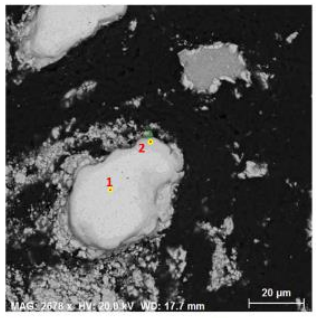

U-Mo/Al sample annealed at 550°C - 2 hours.

Point	1	2
U (%p)	90.23	88.66
Mo (%p)	6.52	3.08
Al (%p)	0.82	4.46

Microanalysis results for sample annealed at 550 °C - 2 hours.

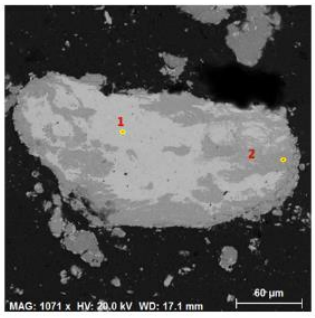

U-Mo/Al sample annealed at 550°C - 4 hours.

Point	1	2
U (%p)	90.46	70.06
Mo (%p)	6.17	3.05
Al (%p)	0.62	25.5

Microanalysis results for sample annealed at 550 °C - 4 hours.

Figure 4. Dispersive energy microanalyses results for U-Mo/Al particles dispersed in aluminium matrix. Left, as fabricated sample, centre after 2 hours and at right, after 4 hours of annealing at 550 °C

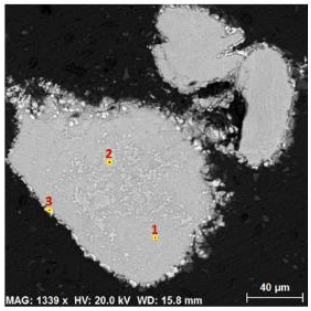

U-Mo/Al sample annealed at 550°C - 14 hours.

#	1	2	3
U (%p)	62.30	65.39	71.58
Mo (%p)	2.54	1.80	3.30
Al (%p)	32.99	31.78	22.05

Microanalysis results for sample annealed at 550 °C - 14 hours.

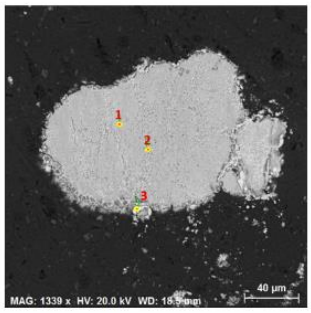

U-Mo/Al sample annealed at 550°C - 24 hours.

#	1	2	3
U (%p)	58.79	58.22	61.58
Mo (%p)	2.97	2.70	1.90
Al (%p)	34.93	35.60	33.46

Microanalysis results for sample annealed at 550 °C - 24 hours.

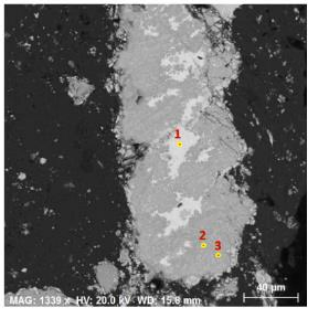

U-Mo/Al sample annealed at 550°C - 48 hours.

#	1	2	3
U (%p)	88.79	63.49	68.27
Mo (%p)	7.23	5.31	2.05
Al (%p)	1.06	30.10	28.56

Microanalysis results for sample annealed at 550 °C - 48 hours.

Figure 5. Dispersive energy microanalyses results for U-Mo/Al particles dispersed in aluminium matrix. Left, after 14 hours, centre after 24 hours and at right, after 48 hours of annealing at 550 °C

Table 2 summarize the nominal composition of aluminides and according to the results of microanalyses, an estimation of possible uranium aluminides formed is shown in table 3.

	Concentration (weight %)	
Formula	**U**	**Al**
UAl_2	81.52	18.48
UAl_3	74.62	25.38
UAl_4	68.80	31.20

Table 2. Uranium contents for aluminides UAl_2, UAl_3 and UAl_4.

Time (hours)	Centre			Interfase		
	U (weight %)	**Al (weight %)**	**Possible UAlx**	**U (weight %)**	**Al (weight %)**	**Possible UAlx**
0	93.95	6.05	**UAl_2**	94.49	5.51	**UAl_2**
2	94.40	5.60	**UAl_2**	88.25	11.75	**UAl_2**
4	93.97	6.03	**UAl_2**	72.09	27.91	**UAl_3**
14	64.96	35.04	**UAl_4**	72.58	27.42	**UAl_3**
24	59.26	40.74	**UAl_4**	61.54	38.46	**UAl_4**
48	93.22	6.78	**UAl_2**	68.79	31.21	**UAl_4**

Table 3. Concentration values of U and Al in the centre and the interface of particles, considering them as the total of an aluminide UAlx.

As explained above, the study of phase transformations [7], corresponding to the objective 1, was carried out with U-Mo/Al plates. For its part, for the objective 2, a set of plate-type targets was manufactured, based on UAlx/Al. The format of the targets and an image of the set are shown in Figure 4, while the manufacturing parameters are detailed in Table 2.

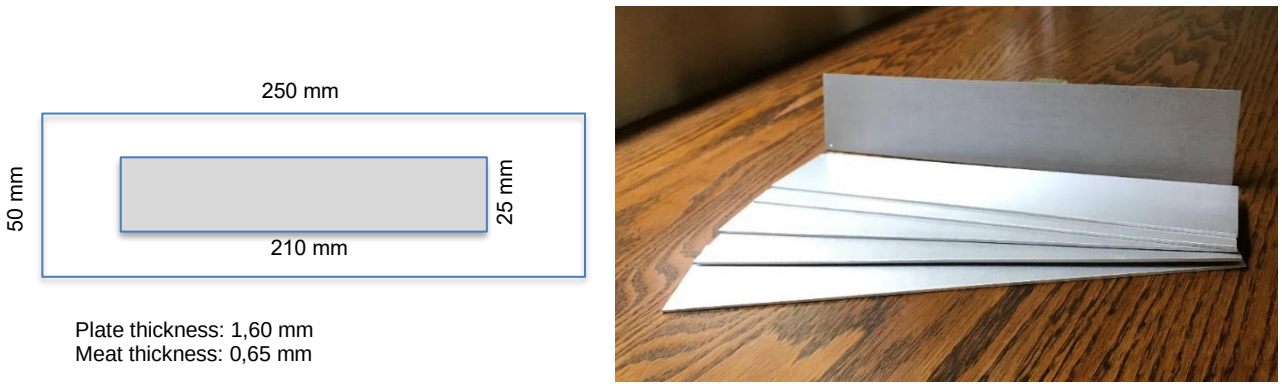

Figure 6. Plate type targets manufactured with UAlx particles dispersed in an aluminium matrix

Target identification		UAlx-1	UAlx-2	UAlx-3	UAlx-4	UAlx-5	UAlx-6
Uranium type		NU	NU	NU	NU	NU	NU
UAlx density g/ cm^3		8,14	8,14	8,14	8,14	8,14	8,14
Nom Loading gU/cm^3		2,6	2,6	2,8	2,8	3,0	3,0
UAlx weight (g)		8,53	8,53	9,19	9,19	9,84	9,84
Matrix weight (Al) (g)		4,01	4,01	3,79	3,79	3,58	3,58
Compact measures	Wide (mm)	20,53	20,52	20,50	20,53	20,54	20,51
	Length (mm)	30,52	30,48	30,48	30,49	30,49	30,49
	Thickness (mm)	4,38	4,47	4,49	4,51	4,50	4,51
Meat measures	Length (mm)	172,8	174,3	175,1	174,3	172,8	173,8
	Wide (mm)	21,9	22,3	22,0	21,9	21,7	22,2
	Thickness (mm)						
Targets measures	Length (mm)	250	250	250	250	250	250
	Wide (mm)	50	50	50	50	50	50
	Thickness (mm)	1,64	1,65	1,66	1,66	1,66	1,66
Initial thickness (mm)		11,38	11,42	11,42	11,44	11,44	11,43
Total Reduction (%)		85,6	85,6	85,5	85,5	85,5	85,5
Reduction rate		1: 6,941	1: 6,92	1: 6,88	1: 6,89	1: 6,89	1: 6,89

UAlx alloy: 81.5 wt% U + 18,5 wt% Al

Table 4. Manufacturing parameters for plate type targets

4. Conclusions

It was possible to obtain a dispersion of particles of the U-7%Mo alloy in an aluminium matrix with proper characteristics for disperse-type targets for fission ^{99}Mo production.

Both in the centre of the particles and in the interface, it was possible to verify the formation of uranium aluminides such as UAl_2, UAl_3, and UAl_4 in thermal treatments carried out at 550°C, from 2 to 48 hours. However, the confirmation of phase transformations by X-ray diffraction analysis is not completed yet.

Observing the evidence of the formation of aluminides, it is concluded that, by means of a thermal treatment carried out at 550°C for around 14 hours, an equilibrium is achieved between the formation of aluminides at the centre of the particles and the presence of UAl_2, UAl_3, and UAl_4 in all its volume.

At times greater than 24 hours, the UAl_4 compound is the predominant constituent, and then the reactions in the particles have already reached a stable state.

5. References

[1]. IAEA. Feasibility of Producing Molybdenum-99 on a Small Scale Using Fission of Low Enriched Uranium or Neutron Activation of Natural Molybdenum. Technical reports series n°478. Vienna, 2015

[2]. R. Schrader, J. Klein, J. Medel, J. Marín, J. Lisboa, L. Birstein, L. Ahumada, M. Chandía, R. Becerra, X. Errazu, C. Albornoz, G. Sylvester and J.C. Jiménez Status of the Chilean Implementation of the modified Cintichem Process for Fission 99Mo production using LEU, RERTR 2008 30th International Meeting on Reducer Enrichment for Research and Test Reactors, October 5-9, 2008, Washington, D.C. USA

[3]. Medical Isotope Production without Highly Enriched Uranium, Nuclear and Radiation Studies Board Division of Earth and Life Studies, National Academy of Sciences, 2009.

[4]. Olivares, Luis, PPT “Status Report of ^{99}Mo Production at CCHEN” Technical Meeting on Global Capabilities for the Production and Manufacture of Non-High Enriched Uranium ^{99}Mo Targets, IAEA Headquarters, Vienna – Austria, October 2018

[5]. Andres Núñez, Radioisotope Production Laboratory, CCHEN internal communication

[6]. R&D CCHEN Project P01_P2905 “Desarrollo de blancos tipo disperso para producción de Mo de fisión”

[7]. Carter Garín, Gisel Vannesa “Estudio de Transformaciones de fase en el sistema U-Al para producción de ^{99}Mo de fisión” Graduate thesis of metallurgy engineering, Universidad de Santiago de Chile, 2020.

6. Acknowledgments

The authors wish to acknowledge the support of the Nuclear Research and Applications Division (DIAN) of CCHEN and to the IAEA for their support for attending to this international conference.

POINT KINETIC PARAMETERS CALCULATION FOR MTR-TYPE FUEL ASSEMBLIES USING CONDOR CODE

I. FERRARI, D. FERRARO
Nuclear Engineering Department, INVAP SE
Esmeralda 356, C1035, Buenos Aires,
Argentina

E. VILLARINO
Nuclear Technology Department, INVAP SE
Av. Cmte. Luis Piedrabuena 4950, R8403, S.C.
Bariloche, Argentina

ABSTRACT

The accurate calculation of the reactor kinetic parameters is mandatory regarding both the safety analysis and the design of operational support facilities, such as full-scope simulators. These parameters are dependent in the reactor states (i.e. burnup, operation condition, etc.) and are usually obtained using deterministic particle transport calculation methodologies, namely the standard cell-core level approach.
CONDOR is a cell-level code which solves the multigroup transport equation using the Collision Probabilities and the Heterogeneous Response methods in 2D geometries. In this work we present the methodology implemented in CONDOR v2.8.07 for computing the burnup-dependent point kinetic parameters (delayed neutron fractions and prompt-neutron generation time) at cell level. A verification case is proposed for a realistic MTR-type fuel assembly, where the results are compared with those from the Monte Carlo transport code Serpent 2, and thus addressing CONDOR's capabilities to handle such calculations.

1. Introduction

The calculation of the effective kinetic parameters represents a key aspect for the design and operation of a research reactor. This is due to their impact in numerous aspects of safety, such as the modelling of neutronic transients derived from accident situations; likewise their impact in operational support, such as the follow-up of the core through short-term transients or full scope-simulator applications, which are essential for the training of human resources.

As part of the continuous improvement of INVAP's calculation line, an update of its current methodology for computing the kinetic parameters is being developed. The main objective of this effort is to develop a fast and accurate methodology based on a standard cell-core calculation scheme using Condor-Citvap codes [1].

In this work, the implementation of the calculation of the kinetic parameters developed in Condor is presented, which is the first mandatory step within this proposed cell-core scheme. The ultimate goal of this first step is to generate homogenized multigroup constants condensed in a few-group energy structure (3 groups in INVAP's calculation methodology) to be later used to perform full core diffusion calculations. These constants should take into account not only the contribution of each fissile isotope (in terms of delayed neutron fraction, delayed neutron spectrum and decay constants), but also other aspects such as the involved operational conditions.

In this line, an initial verification of the implementation is provided for the obtained results at cell level. For such purpose, a burnup-dependent modelling of a MTR-type fuel assembly with Condor code is proposed, where the obtained results are compared with those from the state-of-the-art Montecarlo code Serpent 2 [2].

2. Calculation of kinetic parameters within Condor cell-code

INVAP calculation line [1] is composed of a set of in-house developed computational codes, utilities and third-party codes, together with nuclear data libraries and calculation procedures which encompasses the different aspects of the design of the reactor.

The deterministic line, composed of the cell-core codes Condor and Citvap provides a fast methodology for the design of the main features core, together with the definition of the operation cycle. Condor-Citvap is also integrated with general multipurpose 3D Montecarlo transport codes, which allows the design of ex-core irradiation facilities. Additional computational codes are also frequently used for specific calculations, including dynamic coupling, inventory and activation calculations or independent core-level verifications.

Condor is a cell-level neutronic calculation code that applies multi-group collision probabilities with heterogeneous response coupling method, aimed to provide results within generic geometry configurations. As it was previously mentioned, the main goal of this step is to generate homogenized multigroup constants condensed in a few-group energy structure to be later used with Citvap code in order to perform a full core calculation.

Taking these objectives in consideration, the flow of the execution within Condor cell-level calculations is the following (to be applied for each burnup step and reactor state):

a. A transport calculation is performed in order to compute the neutron flux in the energy structure of the library (typically, 69 energy groups), using collision probabilities plus heterogeneous response method.
b. The critical spectrum is computed for the homogenized geometry.
c. Homogenization and condensation of the standard macroscopic cross-sections in a few-group energy structure (typically, 3 energy groups) is done according to zones and energy structures defined by the user.
d. A calculation of the adjoint flux for the homogeneous system in the few-group energy structure is done.
e. A calculation of the kinetic parameters using the few-group energy constants is done.

It should be noted that using this methodology it is not required to compute the adjoint flux in the heterogeneous system with the energy structure of the library, thus reducing the required computational effort.

3. Implementation of calculation approach within Condor cell-code

The calculation of the kinetic parameters is based on the perturbation theory. First, the total ν-fission reaction rate ($RR_{R,i}^{\nu f}$) is computed for each fissile isotope present in the homogenization region R as:

$$RR_{R,i}^{\nu f} = \sum_{r \in R} V_r \sum_{g} ND_{r,i}\, \nu\sigma_{i,r,g}\, \emptyset_{r,g} \qquad (1)$$

where V_r is the volume of the mesh r, $ND_{r,i}$ is the number density of fissile isotope i in mesh r, $\nu\sigma_{i,r,g}$ is the ν-fission microscopic cross-section for the fissile isotope i in the mesh r for the library group g and $\emptyset_{r,g}$ is the critical neutron flux in mesh r and library group g.

Then, the total ν-fission reaction rate ($RR_R^{\nu f}$) can be computed from the partial reaction rates as follows:

$$RR_R^{\nu f} = \sum_i RR_{R,i}^{\nu f} \tag{2}$$

Using these quantities, the nuclear parameters are computed, which take into account the contribution of each fissile isotope, which in turn, depends on the burnup of the fuel. The delay neutron fraction in the homogenization region R for the precursor family p ($\beta_{R,p}$) and the decay constant in the homogenization region R for the precursor family p ($\lambda_{R,p}$) are computed as:

$$\beta_{R,p} = \sum_i \frac{RR_{R,i}^{\nu f}\,\beta_{p,i}}{RR_R^{\nu f}} \tag{3}$$

$$\lambda_{R,p} = \sum_i RR_{R,i}^{\nu f}\,\beta_{p,i} \Big/ \sum_i \frac{RR_{R,i}^{\nu f}\,\beta_{p,i}}{\lambda_{p,i}} \tag{4}$$

where $\beta_{p,i}$ represent the delayed neutron fractions for precursor family p and fissile isotope i, $\lambda_{p,i}$ is the decay constant of precursor family p and fissile isotope i and $RR_R^{\nu f}$ and $RR_{R,i}^{\nu f}$ are given by equations (1) and (2) respectively.

Being the calculation of the kinetic parameters based on perturbation theory, the adjoint flux ($\emptyset_{R,G}^*$) for each condensation group G of the NG groups of the few-group structure (defined by the user) is then computed using a diffusion model:

$$\nu\Sigma_{R,G}^f = \left(\Sigma_{R,G}^{tr} - \Sigma_{R,G\to G}^{s_0} + D_{R,G}\,B^2\right)\emptyset_{R,G}^* - \sum_{G'\neq G}^{NG} \Sigma_{R,G\to G'}^{s_0}\,\emptyset_{R,G'}^* \qquad \forall\, G \in NG \tag{5}$$

where $\nu\Sigma_{R,G}^f$, $\Sigma_{R,G}^{tr}$, $\Sigma_{R,G\to G'}^{s_0}$, $D_{R,G}$ are the homogenized macroscopic ν-fission, transport and scattering cross-sections and the diffusion coefficient in the region R respectively, and B^2 is the buckling of the system.

The following quantities are also required for the condensation within the user-defined energy group structure, i.e., the reciprocal of the neutron velocity ($1/V_{R,G}$) and the delayed neutron spectrum for region R, defined for each condensation group G and for each precursor family p ($\chi_{R,G,p}$):

$$1/V_{R,G} = \sum_{r\in R} V_r \sum_{g\in G} \emptyset_{r,g}/v_{r,g} \Big/ \sum_{r\in R} V_r \sum_{g\in G} \emptyset_{r,g} \tag{6}$$

$$\chi_{R,G,p} = \sum_i RR_{R,i}^{\nu f}\,\beta_{p,i} \sum_{g\in G} \chi_{g,p,i} \Big/ \sum_i RR_{R,i}^{\nu f}\,\beta_{p,i} \tag{7}$$

where $v_{r,g}$ is the neutron velocity in group g and $\chi_{g,p,i}$ is the delayed neutron spectrum for group g, precursor family p and fissile isotope i.

The effective delayed neutron fractions for each precursor family p ($\beta_{eff}{}_{R,p}$) and the effective prompt-neutron lifetime ($\Lambda_{eff}{}_{R}$) are computed as:

$$\beta_{eff}{}_{R,p} = \beta_{R,p} \sum_{G} \chi_{R,G,p}\, \emptyset^{*}_{R,G} \Big/ \sum_{G} \chi_{R,G}\, \emptyset^{*}_{R,G} \tag{8}$$

$$\Lambda_{eff}{}_{R} = \sum_{G} \emptyset^{*}_{R,G}\, \frac{\emptyset_{R,G}}{V_{R,G}} \Big/ \sum_{\forall G} \emptyset^{*}_{R,G}\, \chi_{R,G}\, RR^{\nu f}_{R} \tag{9}$$

Finally, the total delayed neutron fraction can be obtained by summing the contribution of each precursor family.

$$\beta_{eff}{}_{R} = \sum_{p} \beta_{eff}{}_{R,p} \tag{10}$$

4. Verification of results

The implemented methodology for computing the kinetic parameters within Condor code was verified by comparing the burnup-dependent results obtained for a generic MTR-type fuel assembly with the results obtained with Serpent 2 code.

The fuel assembly consists of 21 parallel fuel plates with an U_3Si_2 slab (^{235}U enrichment of 19.75%) cladded in Aluminium. The plates are housed between two parallel Aluminium plates which also allow the positing of Cadmium wires which are used as burnable poisons.

The fuel assembly was modelled using Condor and Serpent codes, preserving all geometric details (1/4 of the fuel assembly was modelled in both cases), the discretization of the burnable materials and fuel zones as well as the compositions (Fig. 1).

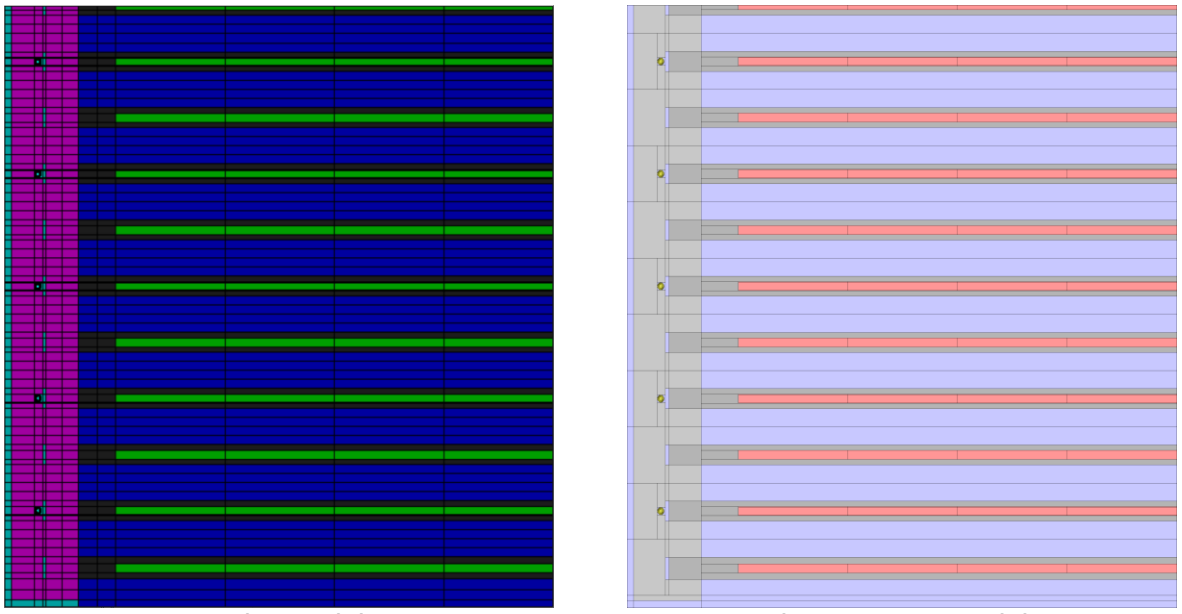

a. Condor model b. Serpent 2 model

Fig. 1: Models for the MTR-type FA assembly

In both cases the nuclear data is based in ENDF/B-VII.1 [3] evaluation. For the case of Condor, the multigroup library is based on IAEA's WLUP 69-group library 'endfb7.lib' [4]. Additional Cadmium isotopes were added to the library by means of NJOY21 [5] and ESINLM [1], as well as the required nuclear data for the kinetic parameter calculations (i.e., nuclear delayed neutron fractions, delayed neutron spectra and decay constants for the precursor families).

For verification purposes, several parameters are proposed to be compared, aimed to show that the global behaviour is properly modelled (i.e. infinite multiplication factors) likewise the kinetic-parameters dependence with burnup are captured with the proposed implementation.

To begin with, a verification of the models was performed by comparing the evolution of the infinite multiplication factor as a function of the average burnup (Fig. 2) showing a reasonable agreement between the results, with differences ranging from -500 to 700 pcm in the whole burnup scope considered.

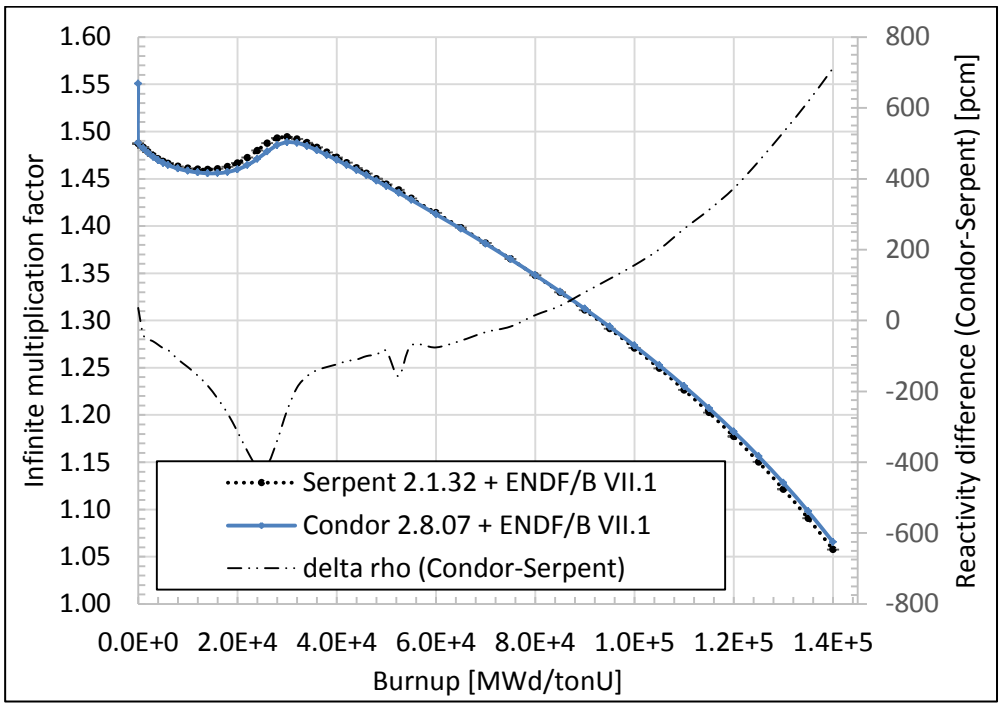

Fig. 2: Comparison of the Infinite multiplication factor for Condor and Serpent models

Being the global consistency addressed, the comparison of kinetic-parameters is proposed. Thus, the effective delayed neutron fraction and the effective prompt-neutron lifetime were obtained with both models. In the case of Serpent 2, the results computed with the Iteration Fission Probability methodology were used [6]. The comparison between the results is shown in Fig. 3 and Fig. 4.

For both β_{eff} and Λ_{eff} parameters, there is a reasonable level of agreement between the results obtained with the different codes (lower than 3% for the former and 1% for the latter).

It should be noted that both parameters have a noticeable dependence with burnup, which is captured by the proposed implementation within Condor code. In this line, is key to remark that it is necessary to take into the burnup profile in order to obtain accurate estimations of the dynamic behavior of the core during operational or accident transients.

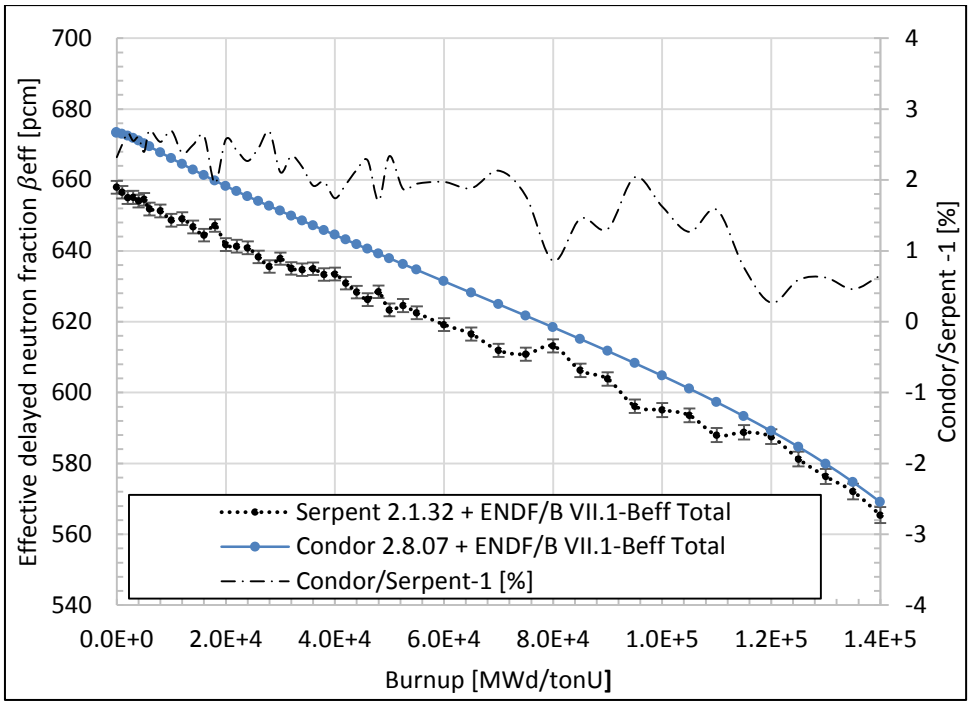

Fig. 3: Comparison of the effective delayed neutron fraction for Condor and Serpent models

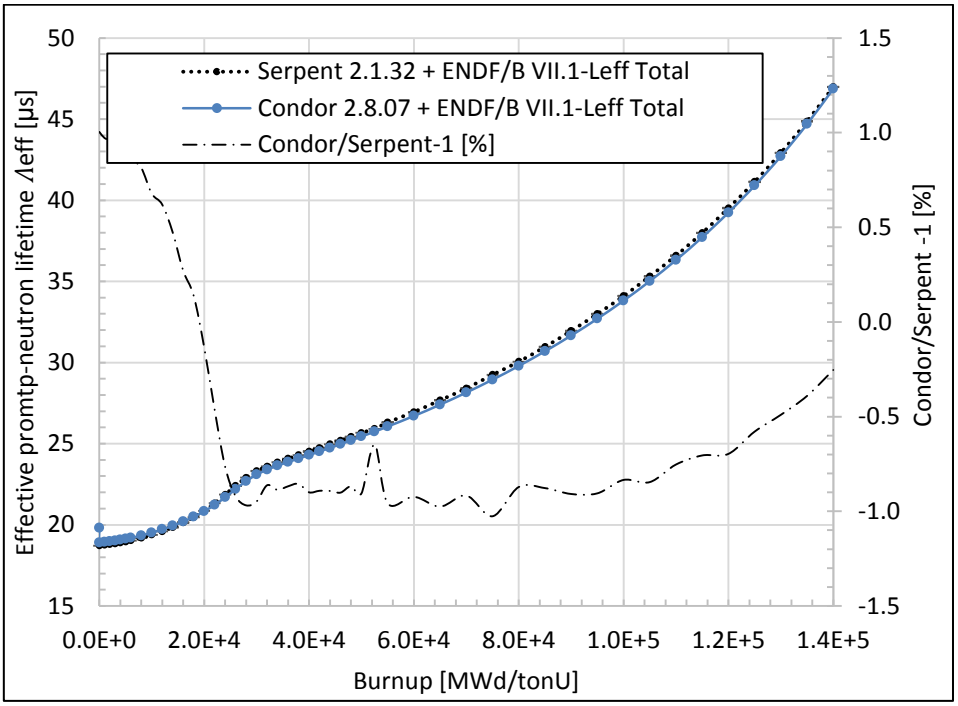

Fig. 4: Comparison of the effective prompt-neutron lifetime for Condor and Serpent models

As a final remark, is key to note that the developed methodology is intended to be applied in design stages; therefore the minimization of the computational effort required for the computation of the parameters is of great interest.

For the Condor run a total CPU time of 4.5 minutes was required in order to complete the full calculation up to 1.4×10^5 MWd/TonU.

Conversely, for the Serpent run, 3000 cycles of 90000 particles (a total of 2.7×10^8 particles) were computed (64 cores, AMD Opteron(tm) Processor 6282 SE) requiring 7.4×10^3 minutes of running time (4.7×10^5 minutes of CPU time), achieving a statistical uncertainty of approximately 1% for each $\beta_{eff\ p}$.

5. Conclusions and further work

The methodology for computing the effective kinetic parameters at cell-level was implemented in Condor; this constituted the first step in the development of the methodology for computing the effective kinetic parameters for the full core using a standard two-step cell-core calculation scheme.

The capability of Condor to address the burnup-dependency was shown, allowing to obtain few-group constants that take into account the main characteristics of the operational conditions of the reactor likewise the contribution of each fissile isotope (including isotope-dependent delayed neutron fractions, delayed neutron spectra and precursor family decay constant).

The comparison of results with Serpent 2 calculations showed that the implemented methodology is a fast and accurate alternative for computing the kinetic parameters at cell level.

The next step in the development of the methodology implies the integration of these new capabilities with the rest of INVAP calculation line in order to compute the kinetic parameters in full-core diffusion calculations.

6. References

[1] E. Villarino, I Mochi and P. Sartorio. “INVAP neutronic calculation line”. XXI Congreso sobre Métodos Numéricos y sus Aplicaciones 23-26 September 2014, Bariloche, Rio Negro, Argentina.

[2] Leppänen J., Pusa M., Viitanen T., Valtavirta V. and Kaltiaisenaho T. – “The Serpent Monte Carlo code: status, development and applications in 2013”. Ann. Nucl. Energy 82, 142–150.

[3] M.B. Chadwick et al. “ENDF/B-VII.1: Nuclear Data for Science and Technology: Cross Sections, Covariances, Fission Product Yields and Decay Data", Nucl. Data Sheets 112(2011)2887.

[4] https://www-nds.iaea.org/wimsd/

[5] Conlin, J.L, et al. “NJOY21: Next generation nuclear data processing capabilities”, EPJ Web Conf. 146 09040 (2017).

[6] Leppänen J., Aufiero M., Fridman E., Rachamin R. and van der Marck S. - "Calculation of effective point kinetics parameters in the Serpent 2 Monte Carlo code", Ann. Nuc. Energy 65 (2014) 272–279.

PRODUCTION OF FULL-SIZE MONOLITHIC U-MO FUEL PLATES

C. SCHWARZ[1], B. BAUMEISTER[1], E. FUCHS[1], L. FISHER-SKIPPER[1], W. PETRY[1], S. LORAND[2], K. BUDUCAN[1,2], B. STEPNIK[2]

[1]Forschungs-Neutronenquelle Heinz Maier-Leibnitz (FRM II), Technische Universität München
Lichtenbergstr. 1, 85748 Garching b. München – Germany
[2]Framatome
2 Rue Professeur Jean Bernard, 69007 Lyon - France

ABSTRACT

In the EMPIrE irradiation test, two mini-size fuel plates with monolithic U-Mo and a PVD Zr coating have been successfully irradiated and showed promising results in non-destructive as well as destructive examinations. Since then, TUM's PVD coating and Framatome-CERCA™'s C2TWP cladding process have been steadily improved and up-scaled to full-size geometry in preparation for the upcoming full-size irradiation test FUTURE-MONO-1.

For the PVD device, the handling of the substrates has been enhanced step by step with different generations of substrate holders that now prevent the foils from bending, while still being able to apply a voltage to the substrate, which was shown to be a valuable tool for the controlled manipulation of coating properties. Finally, several batches of depleted U-10wt%Mo foils have been coated in order to investigate the influence of biasing voltage, Zr purity, coating thickness and quality of the bare U-Mo foils.

At Framatome-CERCA™ the coated foils were cut to the right size by precision laser cutting and cladded with the C2TWP process. The produced plates were then investigated by ultrasound transmission scans and destructive examination, where a continuous improvement of the coating layer was observed.

1. Introduction

U-Mo foils of mini-size geometry (82.5 mm x 19 mm) have been successfully coated with Zr diffusion barriers [1] and cladded with Framatome-CERCA™'s C2TWP process in order to fabricate fuel plates for the EMPIrE irradiation test, which showed stable and predictable swelling behavior [2,3]. As a step towards industrialization of the fuel plate production the process was scaled up for the use of full-size foils (762 mm x 45 mm) [4]. This includes the Zr coating process by sputtering – a physical vapor deposition (PVD) method – at TUM and the proprietary C2TWP cladding application process by CERCA™.
Sputter parameter tests of the full-size coating device have been performed to ensure comparability with the mini-size samples produced for EMPIrE. For this, extensive studies have been carried out on stainless steel substrates to achieve Zr coatings with desirable properties, i.e. a low hardness and high ductility in order to withstand the mechanical stresses caused by the cladding application [5]. Substrate holders were developed and continuously improved to solve the issue of foil bending due to internal tensile stresses in the coating [6]. Furthermore, the substrate holders were designed for application of voltage to the substrate during coating. This technique called *biasing* has shown to be a crucial parameter to achieve suitable coating properties. In this context, the robustness of the substrate holder had to be adjusted to avoid short circuits.

These successful preparations completed, the process was ready for the coating and cladding of monolithic U-10wt%Mo foils. In the following, the production and characterization of the resulting fuel plates is described, which will be the preliminary tests for the subsequent production of low-enriched uranium (LEU) fuel plates for the FURURE-MONO-1 irradiation test [7].

2. PVD coating device & substrate holder development

The complete sputtering device as seen in Figure 1 consists of a vacuum chamber with the sputtering source and the substrate holder, which is placed inside a glove box with argon atmosphere. The gas purification system of the glovebox ensures a low oxygen and water vapor content (usually below 5 ppm). In contrast to the previously used mini-size device it uses a rotary magnetron target, where the rotating target has the geometry of a hollow cylinder through which the cooling water flows. This design is common in industrial applications due to its robustness and high target material utilization [8]. Also inside the target is an interchangeable magnet bar for different magnetic field configurations. Furthermore, the magnet bar is swivel-mounted which allows an operation in a distinct *cleaning position* where the target is sputtered free from possible impurities without depositing those onto the substrate. This way, no additional shutter mechanism is needed between target and substrate.

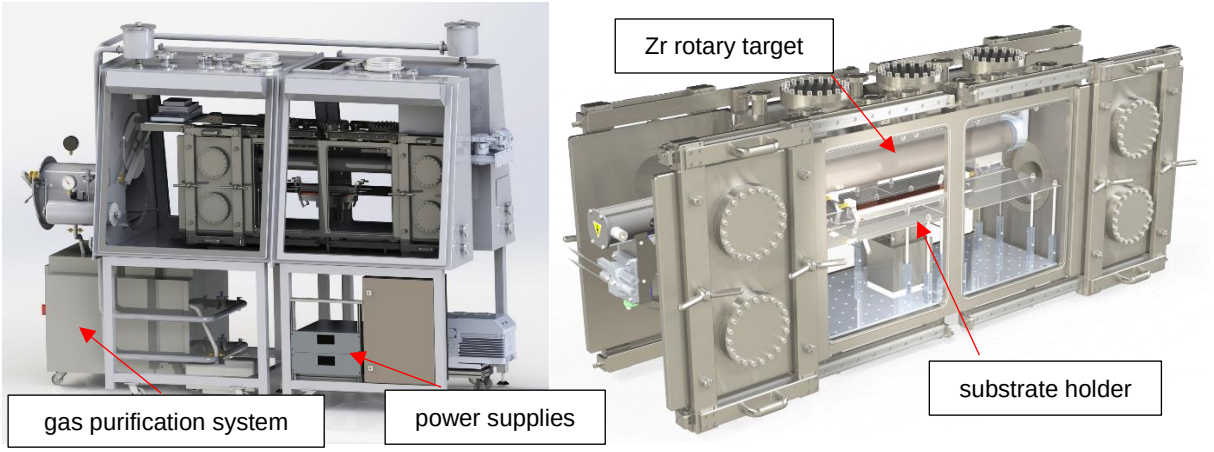

Fig. 1. The complete sputtering device inside the glovebox system (left) and a closer look at the vacuum chamber with the rotary target and the substrate holder (right).

The substrate holder plays an important role in a coating process as it not only fixes the substrate to a certain position, but is also a means to apply additional process parameters. For example, the device used prior for the EMPIrE samples was equipped with external heating, bias voltage application and variable substrate-to-target distance. Except for the substrate heating, these features were retained, while an additional mechanism was implemented to keep the foil flat during coating. This latter feature was necessary as the substrates bend under the tensile stresses in the coatings. For substrates that are just loosely placed onto a holder, this poses the risk of bent foils short-circuiting the target, which can cause severe damages to power supplies. Furthermore, bent foils will have a more inhomogeneous layer thickness distribution as the local substrate-to-target distance changes across the foils' surface.

Voltage application was shown to be crucial for the control of coating properties [4, 9]. With this technique, the growing thin-film can be bombarded with an adjustable amount of ions from the plasma, which introduce energy to the substrate's surface, allowing the condensing Zr adatoms to find more suitable lattice sites by diffusion. Furthermore, the voltage application can be used for *plasma cleaning*. It has been shown repeatedly [10] that it is of critical importance for the layer adhesion that the substrate surface is cleaned off from impurities like

thin water films. This can otherwise be achieved either by evaporation via heating, but due to the absence of an external heating system it is done by bombardment with Ar ions from the plasma that sputter off impurities.

Figure 2 shows a model of the first substrate holder at which all the described features were implemented. Two holes had to be drilled at the short ends of the substrate foils each to fix them inside the clamping blocks of the substrate holder. These clamping blocks were placed horizontally movable on two guiding rods and a central threaded rod was used to tension the foil with springs. This not only resolved the bending issue, but also created the opportunity to work with different foil lengths, while the springs ensured a dynamical adaption to thermal expansion and contraction of the foil during the coating.

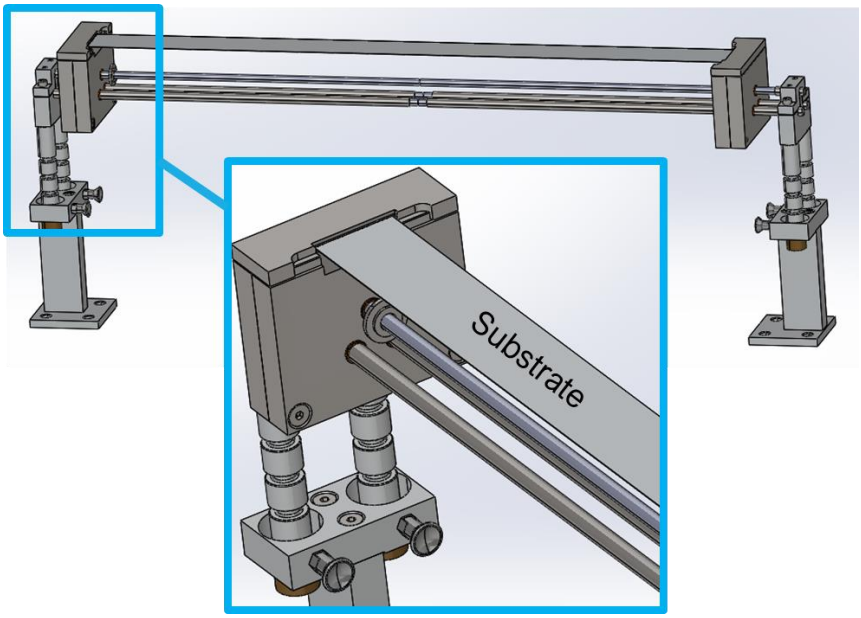

Fig. 2. Model of the substrate holder used for the half-size foils.

This substrate was used for the coating of two half-size batches (see section ‘Plate production’). However, the reliability had to be improved. One problem were occasional short circuits inside the clamping blocks. This resulted from the fact that the inner parts were the foil was fixed had to be energized for the application of the biasing voltage, while the outer parts are grounded. The distance between these parts needs to be well-adjusted: if too large, parasitic plasmas may ignite inside, if too small, the risk of short circuits increases. Another issue was that the contractive force of the substrate acted almost tangential to the top of the blocks, which caused the blocks to get stuck on the guiding rods due to the slight tilting. Additionally, abrasive wear and sputter coating, which could not be avoided completely even with the use of screening plates, increased the friction of the guiding rods.
The problems were resolved with an improved version of the substrate holder shown in Figure 3. It features better separation of energized and grounded parts using ceramic insulators and the tensioning mechanism was improved in a way that the force on the clamping block is more evenly distributed and no guiding rods are used. Additionally, the substrate holder was equipped with appropriate connections for resistive substrate heating for potential future experiments. The main innovation, however, was the rotatable mounting of the substrate. This way the substrate no longer needs to be removed and inserted again for the coating of the second side of the foil. A mechanism is provided that makes the installation of a motor possible in the future to remote-control the turning of the foil. This would significantly reduce the fabrication time of a coated foil as the vacuum chamber would no longer need to be vented and re-evacuated for turning of a foil.

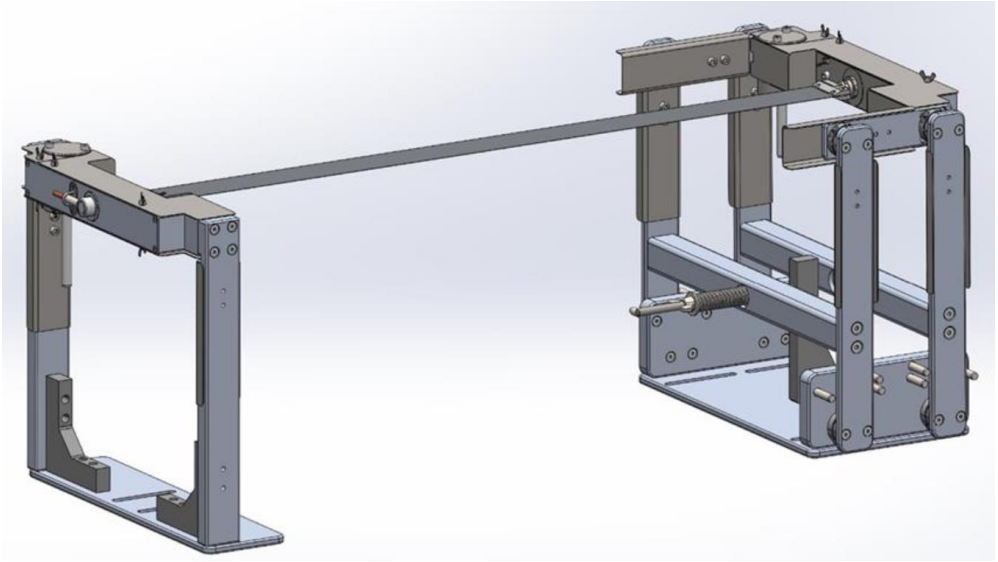

Fig. 3. Model of the improved substrate holder used for the full-size foils.

3. Plate production

Three batches (two half-size, one full-size) of 4 plates each were produced so far. The production steps for each foil include preparation and coating, cutting of the end pieces and subsequent cladding application by Framatome-CERCA™. A finished batch of plates has been characterized first before the next batch was produced in order to incorporate the gained knowledge and adjust the coating parameters if necessary.

Preparation of the U-Mo foils for coating involves drilling the holes for mounting on the substrate holder and chemical cleaning. The latter is necessary to remove the oxide from the foils' surface which would otherwise strongly reduce the coating adhesion. As uranium oxidizes rather quickly while exposed to air, this cleaning step is performed shortly before the coating. The cleaning solution is based on hydrogen peroxide in combination with an alkaline builder [11]. Two transparent basins, depicted in Figure 4, were designed for the cleaning of full-size foils; one containing the cleaning solution and the other deionized water for a rinsing step. Both containers were equipped with pumps to circulate the liquids for a more efficient cleaning. The foils are then transferred into the argon atmosphere of the glovebox.

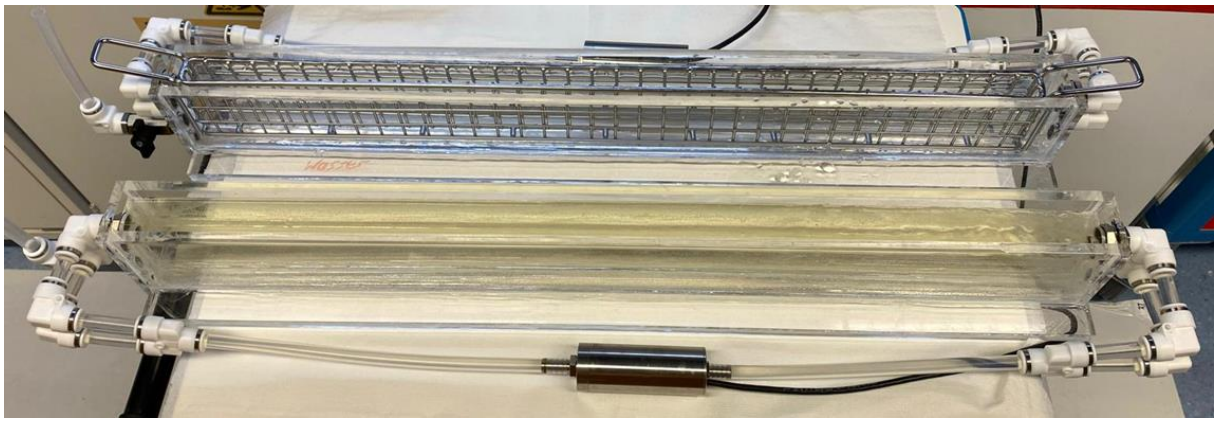

Fig. 4. Cleaning basins for full-size foils with circulation pumps. One filled with cleaning solution (front) and the other one with deionized water (back).

For the coating, the foils were fixed on the substrate holder and the vacuum chamber was evacuated to a base pressure of $< 2 \cdot 10^{-6}$ mbar. After a plasma-cleaning step the foils were coated at an argon pressure of about $5 \cdot 10^{-3}$ mbar and a sputtering power of 5 kW. The substrate-to-target distance was 30 mm for the half-size and 40 mm for the full-size foils because of geometrical reasons due to the substrate holder.
Table 1 shows the parameters varied for the different batches. Every parameter set was used on two foils to increase the reliability of the results. For the first batch the parameters from the previous test on stainless steel substrates were adopted. Afterwards the Zr target of the sputtering device was exchanged for a reactor-grade (rg) one, which is significantly purer than the one made of industrial-grade zirconium (Zr 702) and as a consequence the coatings are expected to be significantly more ductile. Thus, the second batch was produced with the new target and otherwise same parameters as before. Finally, the third batch was produced with full-size foils and different coating thicknesses; two samples with the 8 µm of the previous batches and two foils with 20 µm, which is more similar to the plates produced for EMPIrE. Additionally, the influence of foil quality is to be investigated by using foils obtained from different sources (BWXT and Los Alamos National Laboratory) for the two trials on each coating thickness. The initial appearance of these foils with different oxidation conditions can be seen in Figure 5. After the chemical cleaning, the differences are not so prominent anymore, however, the surface texture is still different.

Tab. 1. Overview of coating parameters for the produced batches.

Batch	Amount / foil size	Biasing voltage	Zr quality	Coating thickness
#1	2x half-size	100 V	Zr 702	8 µm
	2x half-size	-	Zr 702	8 µm
#2	2x half-size	100 V	rg	8 µm
	2x half-size	-	rg	8 µm
#3	2x full-size	100 V	rg	8 µm
	2x full-size	100 V	rg	20 µm

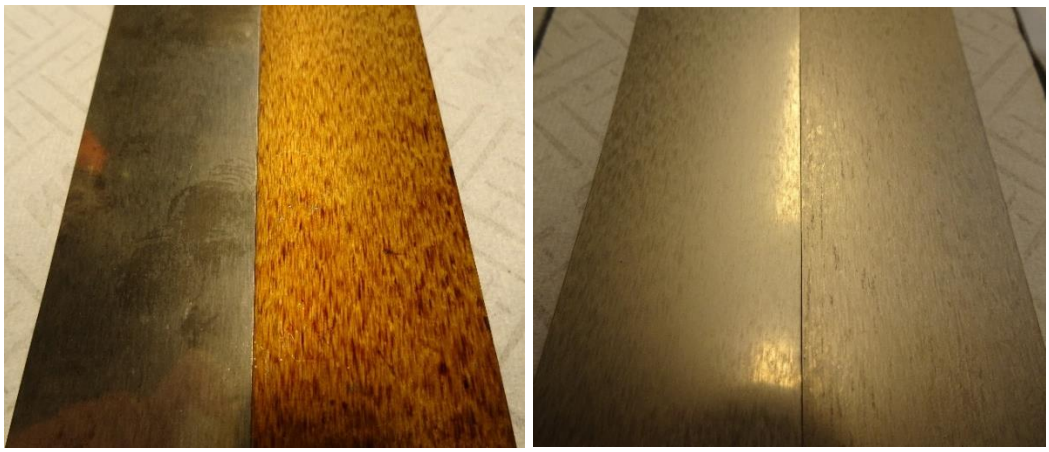

Fig. 5. Two full-size foils of different surface condition before (left) and after chemical cleaning (right).

Figure 6 shows a half-size foil with a finished coating. The uncoated ends with the drill holes had to be cut after that. This was done with a workshop guillotine at TUM for the half-size foils. For the full-size foils, Framatome-CERCA™ performed this step by precision laser cutting. Subsequently, the foils undergo the C2TWP cladding application process resulting in the finished U-Mo fuel plates.

Fig. 6. Half-size foil after coating with the drilled und uncoated ends still to be cut.

4. Sample characterization

As a means of non-destructive examination ultrasound transmission (UT) scans have been performed for each plate. Common defects like debonding of interfaces and other voids like end gaps at the short edges of the foils are visualized by blue areas in the UT scans corresponding to lower transmission.
Figures 7 and 8 show UT scans of two plates from batch #1 and #2 respectively. One small defect is visible in each batch, which could be traced back to a delamination of the Zr coating at the corresponding position. These defects have been there already prior to the cladding application and resulted in one case from a less effective plasma cleaning process close to the edge of the U-Mo foil, while the other one was due to an electric arc from a short circuit. Apart from this, a good overall quality of all the plates could be confirmed. The same goes for the first two full-size foils of batch #3 shown in Figure 9. The big spots at the right side of each foil are an artefact of the cladding process that does not affect the result.

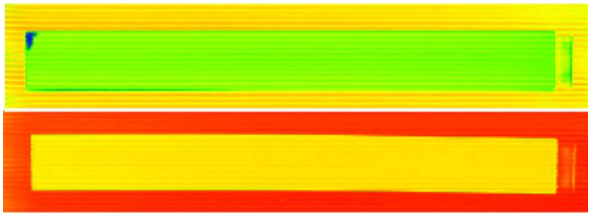

Fig. 7. UT scans of two plates of batch #1.

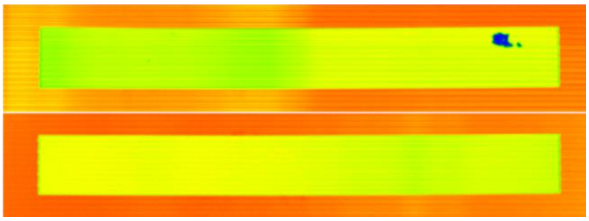

Fig. 8. UT scans of two plates of batch #2.

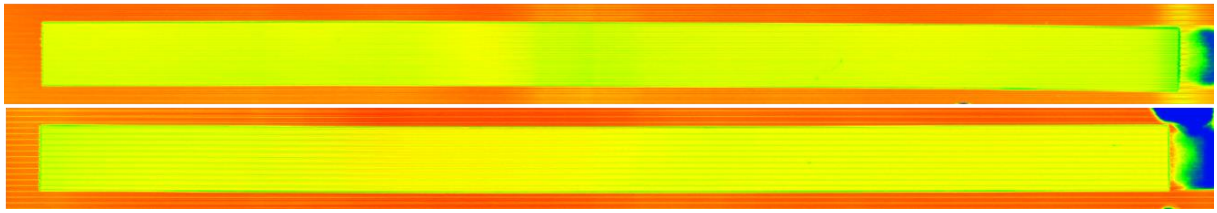

Fig. 9. UT scans of two plates of batch #3.

For destructive examinations, the plates were sectioned according to the scheme shown in Figure 10. Apart from the general interest of adhesion between U-Mo foil and Zr coating as well as between Zr coating and AlFeNi cladding, a special focus is on the edges of the foils to see how the cladding behaved there. Because of this, most sample pieces are from the edges. Furthermore, it is important to know how the coating behaves in longitudinal and transversal direction as the cladding process creates different mechanical stress in those directions. To account for this, 5 of the cross sections are orientated in a way that it shows the longitudinal direction and 4 show the transversal direction. Cutting of the plates from the first batch was performed at TUM with a precision saw (Isomet 1000 by Bühler) and from the second batch

with precision laser cutting at Framatome-CERCA™. The obtained sample pieces were subsequently mounted in epoxy resin using a vacuum impregnation unit (CitoVac by Struers) and then polished for optical inspection.

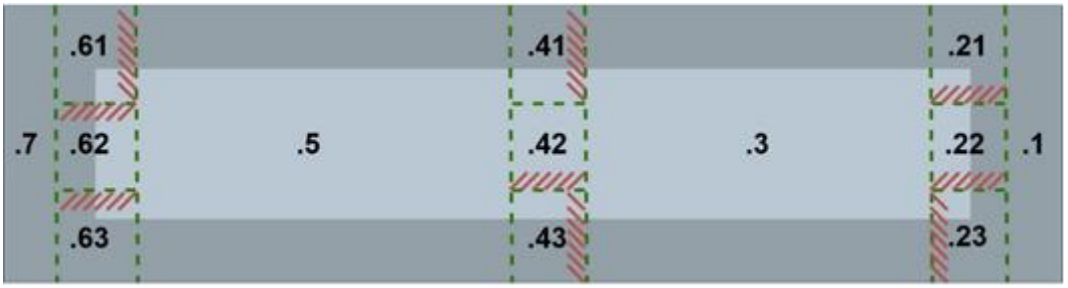

Fig. 10. Sectioning scheme for the half-size U-Mo plates with the U-Mo foil inside in light grey. The dashed green line indicates the sections that are to be investigated with the corresponding cross-section in dashed red.

When looking at the cross sections, the most noticeable feature of the plates are the end gaps at the foil edges. These voids remain when the cladding material does not completely enclose the foils. The gaps are most pronounced at the short edges of the foils, while the long edges show little to no voids. Figure 11 shows exemplary cross sections of foil edges from the first batch. The voids are too small to be visible in the UT scans. With maximum dimensions of about 300 µm x 200 µm they are within the success criterion of defects with a maximum diameter of 1.5 mm defined in [12].

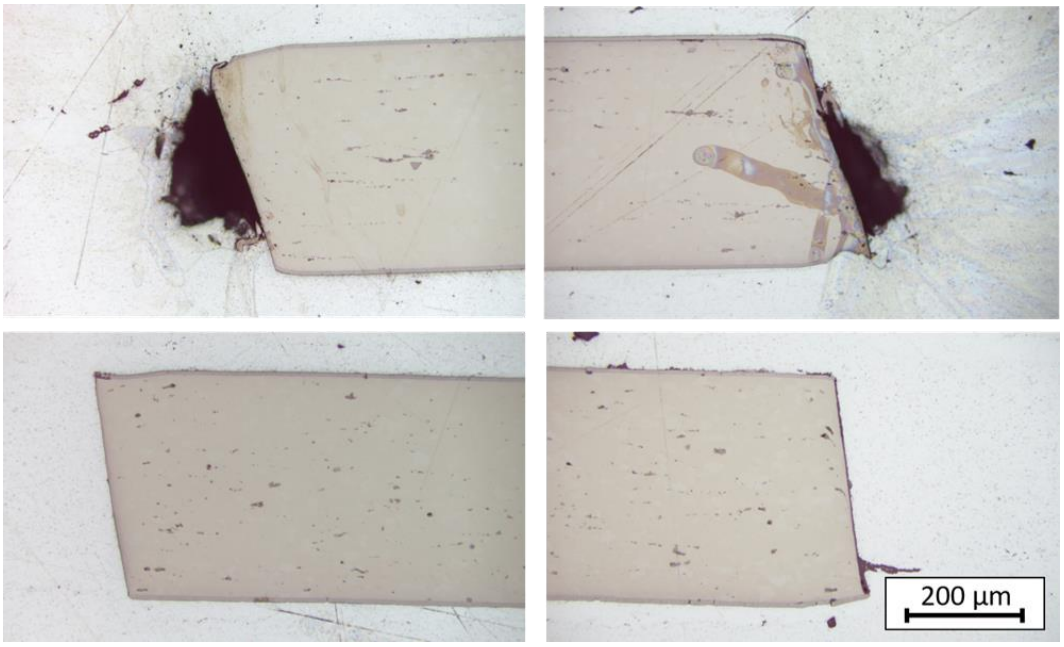

Fig. 11. Cross section of a plate showing the foil edges of short sides (top) corresponding to sample pieces 22 and 61, and the long sides (bottom) corresponding to sample pieces 41 and 43.

A special focus is on the integrity of the coating as the EMPIrE samples displayed a fair amount of cracks [13, 14] that are caused by the cladding process when the coating is too brittle. It has been shown that this was also the case for the first sample batch. Figure 12 shows a section of unbiased coating with a severe amount of cracks. This also led to oxidation of the U-Mo fuel that is no longer protected by the coating. However, it was observed that the samples with biasing showed fewer cracks, which makes sense as the coating is supposed to be less brittle. The shift to the reactor-grade Zr target in batch #2 again brought a significant improvement as coatings were even more ductile. As a result, cracks were rarely observed. Still, some defects

could be observed as depicted in Figure 13. These defects are mainly due to grooves and steps in the surface topology of the bare U-Mo foils. Sometimes surface-near carbide inclusions in the U-Mo also cause defects. This was the reason why for the third batch different foil qualities were chosen to be investigated. However, the results of destructive examination are still pending.

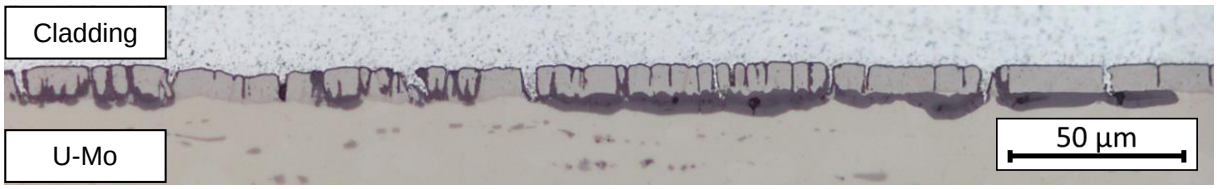

Fig. 12. Cross section of unbiased coating from batch #1 with cracks and oxidation.

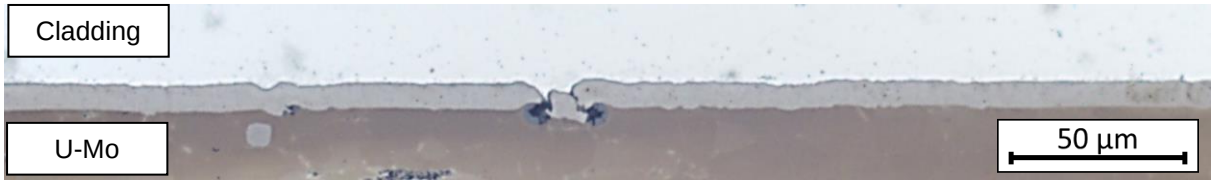

Fig. 13. Cross section of biased coating from batch #2 with single defect.

5. Summary

U-Mo foils of mini-size geometry (82.5 mm x 19 mm) have been successfully coated with Zr diffusion barriers and cladded with Framatome-CERCA™'s C2TWP process in order to fabricate fuel plates for the EMPIrE irradiation test, which showed stable and predictable swelling behavior. This fabrication process has been upscaled to full-size geometry (762 mm x 45 mm) as a step towards industrialization and tested on stainless steel foils.
Now the process was done with depleted U-Mo foils, including a chemical cleaning step before coating. Two batches of four half-size plates each were produced as well as a full-size batch with 4 plates. Different parameters were tested like biasing voltage, Zr purity, coating thickness and foil quality. During these tests the coating procedure was improved by implementation of a new substrate holder that eliminated weak spots of the previous model.
The produced plates were investigated by ultrasound transmission scans as well as with destructive examinations. Overall it was shown that fuel plates can be manufactured within the success criterion of defects smaller than 1.5 mm. End gaps on the foil's edges from the cladding process were within this criterion. Occasional defects seen in the UT scan could be traced back to small coating delaminations that were known before the cladding process. Cracks in the coating, as already seen at the EMPIrE test, and oxidation of the U-Mo resulting from this has been observed, but was gradually minimized by suitable coating parameters.

6. References

[1] Steyer, C., "Production of Monolithic UMo Plates for the EMPIrE Irradiation Experiment", RERTR 2016, Antwerp, Belgium.

[2] Breitkreutz, H., "European developments for monolithic UMo fuel: A status report", RERTR 2017, Chicago, United States.

[3] Robinson, A.B., "EMPIRE Monolithic Plates NDE Results", Technical report, Idaho National Laboratory, Report number: INL/LTD-19-56501, United States, 2019.

[4] Baumeister, B., “Advancements in Monolithic U-Mo Fabrication: Demonstration of Gradient Foil Fabrication and Development of a Pilot Physical Vapor Deposition Process for Full-Size U-Mo Foils”, PhD thesis, Technische Universität München, Germany, 2022.

[5] Schwarz, C. et al., “Scale-Up of the TUM PVD Zr Coating Process for Monolithic U-Mo Fuel Foils”, RRFM 2020.

[6] Fisher-Skipper, L., “Development, Construction and Commissioning of an Improved Substrate Holder for the Sputter Coating of Uranium-Molybdenum Nuclear Fuels”, Bachelor’s Thesis, Technische Universität München, Germany, 2021.

[7] Proposal “EU-QUALIFY”, Proposal No. 945009, EURATOM Call NFRP-2019-2020-15.

[8] robeko GmbH & Co. KG**,** Homepage: https://www.sputteringcomponents.com/.

[9] Ploessner, N., “Commissioning and Parametrization of an Upscaled Sputtering Device for Nuclear Fuel Development“, Bachelor‘s thesis, Technische Universität München, Germany, 2019.

[10] Steyer, C.; “Plasma- und festkörperphysikalische Optimierung eines Beschichtungs-verfahrens für monolithische UMo-Kernbrennstoffe“, PhD thesis, Technische Universität München, Germany, 2019.

[11] Schwarz, C. et al., “All-in-one chemical cleaning and deoxidation process for monolithic Uranium-Molybdenum foils”, RRFM 2016, Berlin, Germany.

[12] Proposal “Horizon 2020 - FOREvER”, Proposal No. 754378, EURATOM Call NFRP-2016-2017.

[13] Felbinger, P.J., “Präparation und Charakterisierung von monolithischen Uran-Molybdän-Brennstoffen mit Zr-Diffusionsbarriere und AlFeNi-Cladding“, Bachelor‘s thesis, Hochschule für angewandte Wissenschaften München, Germany, 2018.

[14] Iltis, X. et al., “Microstructural characteristics of a fresh U(Mo) monolithic mini-plate: Focus on the Zr coating deposited by PVD”, Nuclear Engineering and Technology 53 (8), 2021, DOI:10.1016/j.net.2021.02.026.

This work is part of the LEU-FOREvER Project that received funding from the European Union’s HORIZON 2020 Euratom programme through Grant Agreement 54378.

European Commission

PREPARING AN OPTIMIZATION STRATEGY FOR EUROPEAN RESEARCH REACTORS - ADVANCEMENTS IN THE TOURR PROJECT

R. CIRILLO, G.L. PAVEL
European Nuclear Education Network
Rue d'Egmont 11, 1000 Brussels – Belgium

ABSTRACT

"Towards Optimized Use of Research Reactors in Europe" or, in short, TOURR it is a coordination action among 9 partners across the European Union (EU), out of which 6 are EU Research Reactors Operators. Main targets of the project are to assess the impact of the decreasing number of research reactors (RRs), identify future needs (including new neutron sources), draw a roadmap for upgrade of the existing RR fleet, and develop a model for harmonized resource utilization. Another aim of the project it is to evaluate the current and future need for neutron sources and for medical radioisotopes in Europe. Currently the TOURR project has reached its half-life and important progress has been made with respect to the assessment of RRs capabilities. A dedicated questionnaire has been developed and distributed across Europe to gather input from Research Reactors on both their specific experimental work but also for opportunities offered to researchers. The received data have been analyzed and three GAP analysis compiled. Project activities are currently running in parallel: to create tools for optimized of use of European research reactors and optimize education and training actions and to assess needs and opportunities to support the supply of medical radioisotopes. At this stage, we are ready to start drafting the optimization strategy which will be a report publicly available at the end of the project (September 2023). At the same time, a platform will be developed also and made publicly available, for all RRs in Europe. This paper aims to illustrate the progress of the TOURR project achieved so far and to cast some light on the next step for the project. The TOURR project has received funding from the Euratom research and training programme 2019-2020 under grant agreement No 945 269.

1. Introduction

TOURR is the acronym of "Towards Optimized Use of Research Reactors in Europe" project. It is a EURATOM funded project whose consortium is composed by 9 partners across the European Union (EU) out of which 6 are EU research reactors operators.
The institutions participating in TOURR represent a significant part of RRs in EU whose production lines are able to supply medical radioisotopes while simultaneously offering significant portion of their irradiation time for Science and Technology (S&T) activities.
The coordinator of the project is the 'European Nuclear Education Network' (ENEN).
The TOURR Project aims first and foremost at proposing a strategy for the optimization of the European Research Reactors (RRs) fleet and at the same time realize the tools to facilitate the achievement of the same optimization.

This project is a coordinated action that answers to the challenge of:

- assessing the impact of the decreasing number of RRs,
- identify future needs (including new neutron sources),
- draw a roadmap for the upgrade of the existing RR fleet,
- and a model for harmonized resource management.

2. Background

Nuclear research reactors (RRs) have been widely used across Europe in both experiments necessary to develop commercial reactors and training programmes.
At the same time, neutron irradiations techniques have found new applications in the adaption and production of existing and new materials, as well as medical radioisotopes.
These latter, radioisotopes, some of them very rare, enabled the development of new diagnosis and treatment techniques, for the benefit of millions of citizens.
Europe has a broad and very diverse landscape of RRs, many of them operating since long time, well maintained and regularly upgraded.
Yet the current scenario has seen a combination of the public lowered interest in nuclear facilities (perceived as some sort of relic of the past nuclear era) and the absence of a sound financial model. This resulted in the closure of many RRs already and a few more will close soon. Only a few are currently under construction.
The TOURR project kicked off on October 2020 with the ambition to be the first very well coordinated action to offer the European RRs fleet an optimization strategy. This way it will contribute the European Research Area (ERA) and also help in achieving a stable production of radioisotopes. TOURR is also listed in SAMIRA[1] action plan as one of the outputs.
The project specific objectives can be summarized as follows:

1. Assessment of the current status of the EU RR fleet
2. Estimation of future needs
3. Plan for the upgrade of the reactor fleet
4. Plan to maintain the fleet
5. Developing tools for optimal use of the RR fleet
6. Rising awareness of decision makers and the public on the role of RR

3. Project current status (half-life)

The TOURR project has currently reached a bit more than half of its implementation period.
The work performed so far allowed to achieve **objective 1 – 'Assessment of the current status of the EU RR fleet'.**
In order to meet this objective, the TOURR consortium prepared a detailed questionnaire that has been distributed to RRs across Europe. The questionnaire collected answers from 84% of the facilities it has been sent to.
A more detailed description on the process that led to the creation of the questionnaire, and its structure, can be found in [1].
The first output of this questionnaire is a public report, containing only bulk considerations, describing the EU RRs fleet through the answers provided. The choice of providing only general conclusions has been made to grant the confidentiality to the respondents.

[1] SAMIRA: Strategic Agenda for Medical Ionising Radioisotopes Applications [1]

The report is titled “Data Base of European RR fleet” and can be found at [2] (a blank questionnaire is provided as appendix of the same report).
Questions were articulated into 7 main sections:

1. Location of the RR
    a. Name of the facility and country
2. Technology of the RR
    a. What is the focus of the RR
3. Exploitation
    a. Users distribution
    b. Scientific and technological utilization of the RR
    c. Education and Training Applications of the RR
    d. Medical and industrial radioisotope production of the RR
    e. Radioisotopes production related questions
    f. Users distribution by field
    g. Users distribution by origin (academia, industry…)
    h. Information about the RR ability to satisfy all the demands
    i. Information about cooperation with other research reactors to ensure continuity of supply
4. Sustainability
    a. Information about any problems/issues the RR may have encountered
5. Future
    a. Future developing plans
    b. Current needs
    c. Future needs
6. Conclusions
    a. A definition of the “SCIENTIFIC STRENGTH” of the RR
    b. Information about updates with respect to the characteristics described in the RR IAEA database
7. Contact details

When closing the data collection, answers have been received from Austria, Belgium, Czech Republic, France, Germany, Hungary, Italy, The Netherlands, Poland, Romania and Slovenia. For reference, see figure 1.

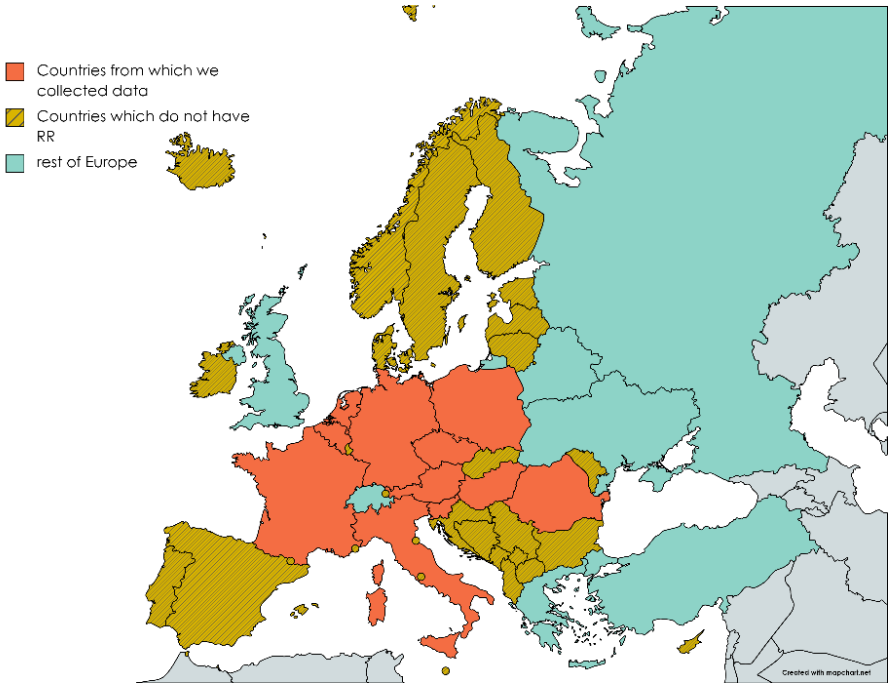

Figure 1 Countries whose RR answered the TOURR questionnaire

The ambition of TOURR is to evaluate the current and future needs of RR and neutron sources in Europe along 5 science and technology axes:

- Education and training
- Basic and fundamental research and its instruments
- Medical applications, including isotope R&D as well as beam applications
- Material testing, including fuel, structural material and its instrumentation
- Core physics testing for reactors in "zero power" installations

The questions allowed for multiple answers (as well as for blank answers in case the respondent preferred not to disclose some details).
Since the ultimate scope of the project is to provide an optimisation strategy, several questions were aimed at assessing if the actual RR fleet can satisfy all the demands it receives and if they collaborate with other institutions in order to ensure continuity of supply.
This type of questions allowed to understand if the availability of RR is too low for example and if some cooperations are already in place.
The work on the questionnaire outputs proceeded with the production of 3 gap analysis (confidential) that contributed to achieve **objective 2 – estimation of future needs** in highlighting gaps versus opportunities per each main area:

- Technological applications
- Medical applications
- Education & training

Furthermore, another confidential deliverable presents the evaluation of current and forecasted needs and production capabilities for medical isotopes produced using research reactors in Europe. It is dedicated to analysis of medical isotopes in EU market and focuses on the following chapters:

- Market driving factors, types of markets trading/contracts with isotopes and nuclear materials
- Market functioning, rules and relationships

- Isotopes and nuclear materials trading in the EU including legal framework and regulations
- Supply/Demands chains, supply side analysis, demand side analysis
- Source material production capacities
- Opportunities of Global Radiopharmaceuticals Market

To complete the overview of what has been achieved already, TOURR has been presented and promoted at several international conferences in the nuclear field and the general public is being made more and more aware of the TOURR initiative thanks to the publications on the project website [3], on the webpage under ENEN website [4] and on social media channels.

4. Plans until the end of the project

TOURR primary objective is to develop a strategy for RR in Europe and prepare the ground for its implementation. The ambition of TOURR project is to secure access and availability of RRs as a vital part of the European Research Area and to support stable supply of medical radioisotopes.
The data gathered via the questionnaire definitely allowed the TOURR consortium to have insights about the current scenario of EU RR. The three gap analysis have highlighted were the opportunities and the gaps can be identified in the various sectors of science & technology, medical applications and education & training.
TOURR project will not only draft the “optimization strategy” but will also produce an online platform based on an innovative model for coordinating the European RRs in the areas of their respective exploitation area (material testing, education and training, basic research, energy research, isotope production, cancer therapy, etc.)
The model will assume complementary utilization patterns and synergies among the participating research reactor facilities with the aim to allow for a more efficient use of research reactors in Europe.
Both the “optimization strategy” and the “platform” will be made publicly available.
Once they will be ready, **objective 5 – Developing tools for optimal use of the RR fleet**, will be achieved
It is foreseen that the TOURR project will also have a major impact on the planning and eventual refurbishment or construction of new RRs in Europe. Specific deliverables are foreseen in this domain also and will allow to achieve **objective 3 - plan for the upgrade of the reactor fleet** and **objective 4 – plan to maintain the fleet.**
It will contribute to a more effective utilization planning of the EU RR fleet.
The achievement of **objective 6 – Rising awareness of decision makers and the public on the role of RR** happens on a continuous basis, thanks to the dissemination actions carried on by all partners.

5. Ackowledgements

The TOURR project has received funding from the Euratom research and training programme 2019-2020 under grant agreement No 945 269.

The authors of this paper wish to thank all the TOURR consortium partners for their efforts in achieving outstanding results in this project.

6. References

[1] SAMIRA website:
https://ec.europa.eu/commission/presscorner/detail/en/IP_21_265
[2] Bor Kos, Roberta Cirillo, Anže Pungerčič, Gabriel L. Pavel, Luka Snoj, Gathering of Data on the European Research Reactor Fleet as Part of the TOURR Project, https://www.djs.si/nene2021/proceedings/pdf/NENE2021_318.pdf
[3] Database of European RR fleet (public report)
https://www.tourr.eu/fileadmin/user_upload/TOURR_D1.1_Data_Base_of_European_RR_fleet.pdf
[4] TOURR project website : https://www.tourr.eu/
[5] Webpage under the ENEN website: https://enen.eu/index.php/portfolio/tourr-project/

EFFICIENT BALANCE BETWEEN RESEARCH AND PRODUCTION TASKS AT IVV-2M RESEARCH REACTOR

Joint-Stock Company “Institute of Nuclear Materials” (INM JSC),
Rosatom State Corporation
P.O. Box 29, Zarechny, Sverdlovsk region, 624250 — The Russian Federation

ABSTRACT

The research nuclear reactor IVV-2M was built and put into operation in 1966 and is located on a site in the city of Zarechny, Sverdlovsk Region, Russian Federation. The IVV-2M is a pool type reactor with pressurized water. The nominal power of the reactor is 15 MW. The IVV-2M reactor is designed to solve various scientific and industrial problems, such as pre-reactor research, radiation testing, post-irradiation examinations, non-destructive testing of irradiated elements, production of radiochemical equipment and isotopic raw materials for the production of radiopharmaceuticals, as well as the implementation of advanced isotope projects. Continued modernization of IVV-2M allows us to solve all these problems, maintaining an effective balance between research and production tasks.

1. Introduction

Research reactors are the most versatile and convenient powerful sources of neutrons for producing radioisotopes. They are flexible and use a wide spectrum of neutrons which makes them easy to be reconfigured to solve new research problems. The installations at the beginning of the operation cycle seemed to be one of many scientific tasks and now it has become the most important application program implemented on most RRs. Maintaining a balance between research and application programs has become a key for rational use of such a powerful research reactor.

2. The Experimental and production base of INM JSC

IVV-2M reactor is next to a Hot Cell laboratory, which allows for post-reactor studies. This complex lets you do scientific work and produce industrial isotopes. Also the Experimental and production base of INM JSC consists of Experimental equipment manufacturing workshop and Radiochemical laboratory.

3. Research nuclear reactor IVV-2M

IVV-2M is a pool-type water-cooled research nuclear reactor with a nominal power of 15 MW. In 1991 and 2018, the reactor was upgraded for operational safety, and future planned improvements will open up new opportunities for R&D and the production of radioisotope products as well as extend its service life.

4. R&D Services

R&D services are including such areas as:

• Reactor, pre- and post-reactor testing of materials for advanced power plants;
• Testing the materials (mechanical, corrosion testing, and release of radionuclides from heavy liquid metal coolant);
• Testing the promising fuel combinations, and determining gaseous fission products;
• Post-reactor studies of structural materials and fuel of Fast Reactors during current operation, as well as finding ways to increase their service life;
• Post-reactor studies of fuel channels, Control and Protection System channels and elements of the core of graphite moderated RBMK reactors. (high power channel reactors)

All in all, R&D volumes have tripled since 2018.

5. Production Tasks

INM JSC has been building a manufacturing complex based on nuclear technologies for the production of highly competitive raw materials using the capabilities of IVV-2M reactors, including radiopharmaceutical precursors, radionuclide sources for medical and industrial purposes, to provide high quality products. With customers INM JSC follows the principles of quality, stability, efficiency and a flexible product delivery schedule. INM is implementing a number of projects aimed at the company's competitiveness in the foreign market with products of higher level processing. At the moment, the Institute produces such isotopic raw materials as:

Isotopes for medical and industrial use
- Lutetium-177 (177Lu)
- Carbon-14 (14C)
- Iridium-192 (192Ir)
- Cesium-131 (131Cs)
- Selenium-75 (75Se)

Production of 177Lu:

The specific activity of 177Lu is quite high, >(more than) 30 Ci/mg on ship date. Also, it's available about 300 days a year. INM JCS has created a technology for the production of research grade radiopharmaceutical precursor 177LuCl3.

Production of 14C:

Carbon-14 is a rare isotope, but INM JSC produces more than 10 varieties of 14C precursors with a purity of more than 97%.

Production of 192Ir:

Typica requirements for specific activities of at least 500 Ci/g for natural iridium and 900 Ci/g for 191Ir, enriched to 80% in 191Ir on the day of delivery to the customer.

Production of 131Cs:

The advantages of production at INM JSC are high radiochemical purity (99.99%), and also weekly deliveries during the year.

Production of 75Se:

Selenium-75 is widely used in industrial flaw detection. Preservation of the source geometry during irradiation makes it possible to obtain an image with minimal blurring of the edges.

166Ho Microspheres:

During the tests the INM successfully solved the problem of destruction of organic microspheres during irradiation in a nuclear reactor. And also confirmed the quality of the products by validation tests.

As in case of R&D, production volumes for the radioisotope product line have doubled since 2018.

6. Flexibility in the operation of the IVV-2M research reactor:

Depending on the current priority goals, the layout of the fuel in the reactor can be flexibly changed for various R&D tasks or industrial production of isotopes:

Fuel layout examples:

R&D predominance

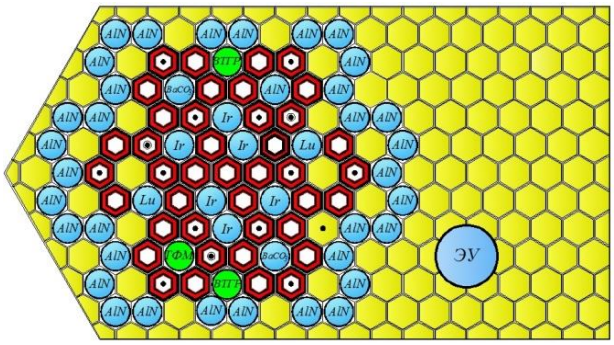

Predominance of industrial isotope production

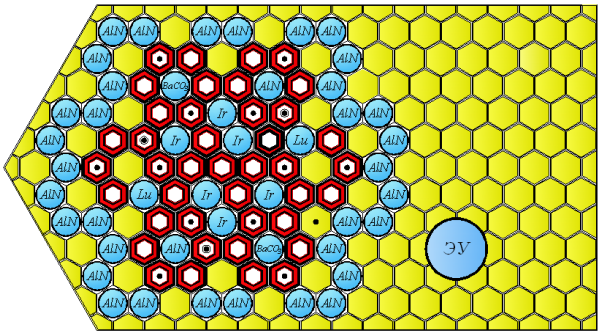

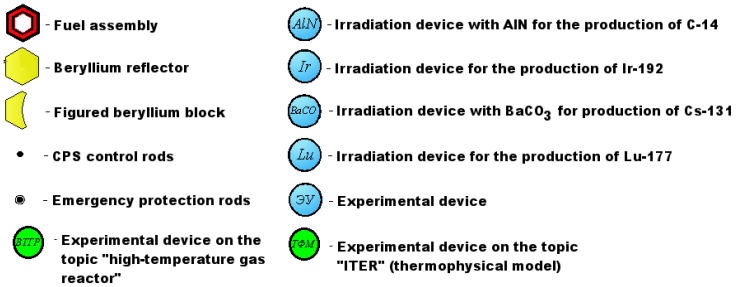

7. Conclusions

The reactor upgrades in 1991 and 2018 ensured operational safety, and future planned improvements to the reactor will open up new opportunities for R&D and radioisotope production, as well as will extend service life.

With development of alternative ways of using the IVV-2M reactor INM has started designing technologies in radioisotope production for applied tasks and scientific research. Also the company launched the production and commercial supply of radioisotope products for flaw detection, nuclear medicine and pharmaceutical research.

Flexibility in the operation of the IVV-2M research reactor for various tasks makes the production and research as efficient as possible. A special feature of this reactor is its effective balance between research and production tasks without downtime. This is also confirmed by statistics: since 2018, thanks to earlier upgrades, the reactor was capable to increase production volumes by 2 times and R&D volumes by 3 times.

It is also worth noting that more than 85% of the time in a year the reactor operates, the rest of the time is devoted to complex technological repairs and refueling.

Contacts
P.O. Box 29, Zarechny, Sverdlovsk region, 624250 — The Russian Federation
Tel.: +7(34377) 3-54-54
E-mail: irm@irmatom.ru

Core and Reactor Block: From the Beginning to the Final Assembly at Jules Horowitz Reactor

M. BOYARD, C. BERNARD
TechnicAtome
CS 50497, 13593 Aix en Provence, France

L. CHABERT, D. ERARD
CEA, JHR project
F-13118 Saint-Paul-lez-Durance, France

ABSTRACT

This paper backs up on the feedback of the Jules Horowitz Reactor to illustrate the process of designing a reactor block and all its main components, including the core. The publication covers the basic design stage and explains that even if the technical requirements and the conceptual design have been clearly defined beforehand, both core and fuel assembly have been significantly modified during this stage. During the detailed design stage, studies have been carried out in order to improve the main performances of the reactor and its experimental load (in-core and ex-core experimental devices, thermal and fast flux, quality of the irradiations, cost of the experiments). These studies have been based on a combined approach (neutronics, thermal hydraulics, mechanics, safety). The easiness of the operation, the flexibility and the adaptability of the reactor also have been upgraded.
Usually, the core and its reflector are schematized as a 2D cross-section but this paper illustrates the prominence of the 3D constraints related, among other reasons, to the design and manufacturing of the reactor block.
To summarize, this paper bridges the gap between core design and reactor block design. It explains the origin of some key choices such as the cylindrical core vessel, irregular hexagonal core lattice, control rod insertion in the centre of fuel assembly but also the main feedback related to the manufacturing of the reactor block components during the procurement.

1 INTRODUCTION

In the beginning of the design phase of a reactor, it is fruitful to gather a small and well-balanced group of specialists and general engineers in different technical fields for a brainstorming meeting. These experts, based on simple considerations and on their knowledge of similar facilities, define and adapt the major options for the reactor [1]. This team manages through discussions with the customer and with other projects in which they are all involved simultaneously and that have reached different maturity stages (conceptual design, basic design, detailed design and procurement).
The importance of exchanges with the customer, the project organisation, the application of System Engineering methods, human resources management, availability of modelling and calculation tools have already been underlined in other publications.
This paper focuses on the sole case of the JHR reactor, from the beginning of its design, to the assembly of its components, in order to highlight the importance to know exactly when to draw a sketch from scratch, to use rules of thumb, to use part of an existing solution to a given problem and when to enrich it all with detailed CAD 3D modelling and exhaustive assessments.
Generaly speaking, if dealing with a reactor including the core, reflector and experimental load, one can point out that:

- A reactor block is a theoretical object during a limited in time design phase which will further be involving real components during operation.
- This reactor block is considered through modelling during studies, based on validated tools and through a monitoring system during operation.
- In order to get a license for full power operation, this reactor block undergoes a safety assessment based on a methodology involving a mix of principles that are shared on national and international levels and of historical aspects deriving from feedback obtained on currently operated facilities. These analyses include performances of the protection system, fed by the monitoring system.
- A reactor block should be feasible, maintainable, easily operated, adaptable and for a reasonable price [2].

Thus, as said, this paper illustrates these points using the example of the JHR reactor block, from the beginning of its design, to the assembly of its components.

2 CONCEPTUAL AND BASIC DESIGN

2.1 GENERAL OUTLINE OF THE CORE – STRUCTURING REQUIREMENTS

Design of the JHR is led by its experimental load and is basically about:

- Having a high fast neutron flux level in material irradiation devices. This requirement places some of them in the core, which has a high power density. Cooling fluid speed is thus high which means that pressure drops are important inside the core. Primary circuit then has to be pressurised and a variable pressure difference exists between the inside and the outside of the primary circuit. Required performances, higher than those of OSIRIS, lead to the JHR being a tank-in-pool (closed primary circuit).
- Benefiting from important OSIRIS feedback concerning the performance of power ramps on fuel samples. This leads to choosing an OSIRIS-type displacement device (radial movement). Due to the number of devices, inserting such a device is facilitated in the case of a light water and/or beryllium reflector (versus a heavy water tank).
- Having the possibility to withdraw these reactor fuel samples at full power, which goes along with positioning the devices (certain of which having in addition a NPP primary circuit –like loop) in a reflector which is open on the pool and thus having the primary circuit vessel between the core and its reflector.
- Having a high neutron in the reflector, in particular thermal, which leads to seek to minimise the distance and optimise materials between the core and the reflector (neutron transparency, low heating, variable internal pressure resistant). This material minimising along with considerations on the manufacturability of the components leads towards cylindrical geometries for the reactor block and to separate the core rack from the reactor block compartment (manufacturing, operation), the whole being made of aluminium in order to minimise thermal neutron capture and to maintain a high fast flux.

In addition, the whole system is constrained by the general requirement on cost constraints leading to an optimisation of the core power – fuel consumption – facility availability at full power system, while reaching a high experimental quality.

In order to finalise structuring options, in core coolant flow being greater than 10 m/s, curved fuel plates were chosen, in accordance with state of the art (see Figure 1 from the IAEA RR database). Given curved fuel plates, many fuel assembly types are possible on the powder technology used by CERCA, which yields important advantages in terms of achievable fuel plate and assembly geometry tolerances and of meat homogeneity. After a review of possible geometries (curved type plates: HFR, R2, KUR, MNR; tubular type: BR2, FRJ2, JRR2; ring-shaped type: RHF, FRM II), the tubular type was chosen [3].

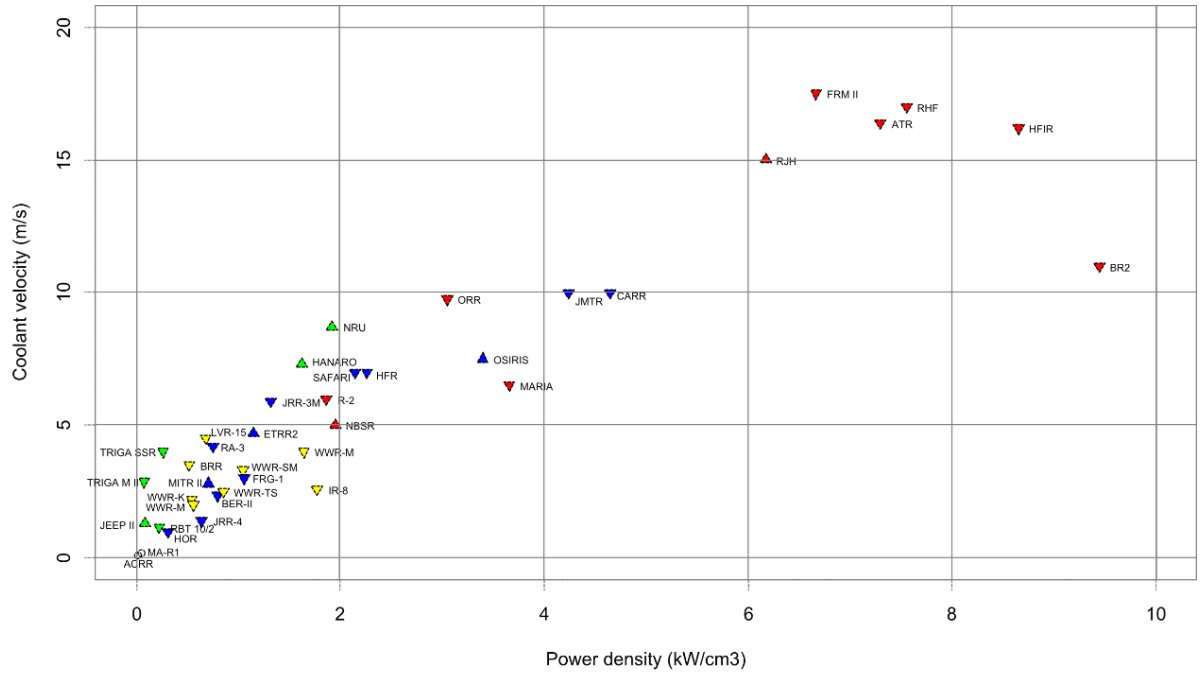

Figure 1: Coolant velocity versus power density - Fuel element shapes (color) and downward-upward streams (shape) - (red: curved plane, blue: flat plane, green: rod, yellow: extruded fuel element; downward triangle: downward flow, upward triangle: upward flow, empty circle: natural convection)

At this stage, here is the reactor concept:

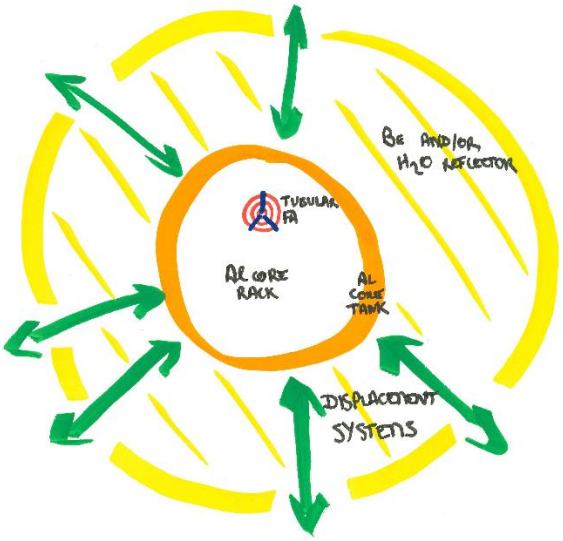

Figure 2: Beginning of the design

2.2 CORE CELL AND COLOURING

Major options having been reminded, we can now move on to what is essential for a core: the cell and the related lattice.
At this stage, it is all about cooperation between architects, mechanical, neutronics and thermal hydraulics engineers, on the basis of a white board and markers to discuss in-core experimental devices [4], fuel and control assemblies.
In the JHR case, a cell must house, for the reference core:

- Small sized devices (around ∅ 32mm): 7 in the bill of specifications,

- Large sized devices (around ∅ 92mm), also called “triple devices”: 3 in the bill of specifications,
- Tubular fuel assemblies, initially 3 sectors with 6 plates,
- Control assemblies, to be defined,

the whole inside a rack that privileges a high fast neutron flux level, thus with a lattice as compact as possible and given manufacturing and handling constraints.
In addition, besides requirements concerning flux homogeneity inside a triple device and a minimum discrepancy between flux levels between two of the three devices (in order to have an irradiation interval), requirements are associated concerning devices geometry above the core:

- 3 positions with a 140 mm diameter at 30 cm above the core,
- The others with a rise up to 120 mm.

From this point, it is mostly a geometry problem:

- 120 and140 mm diameters are greater than the foreseen cell diameter (around 92 mm), even considering the isthmus between two cells, the latter being anyway limited by target core densities (see Figure 3). Moreover, a BR2 type solution was not conceivable:
  - ⇨ The design option for the core was then not to place two experimental devices in two adjacent cells (see Figure 5),
  - ⇨ Choice was made at this stage to move to a 98 mm cell that is capable to receive a triple device or a tubular type fuel assembly with three sectors of 8 plates: a rise in the U-235 mass per assembly while remaining in proven design for the fuel assembly (see Figure 4),

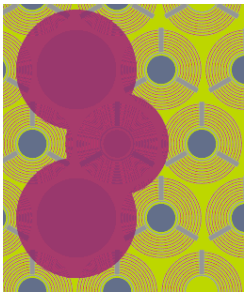

Figure 3: Not compliant

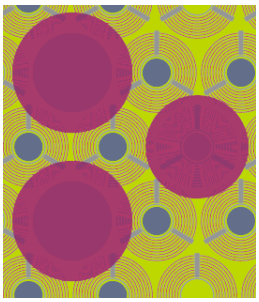

Figure 5:Compliant

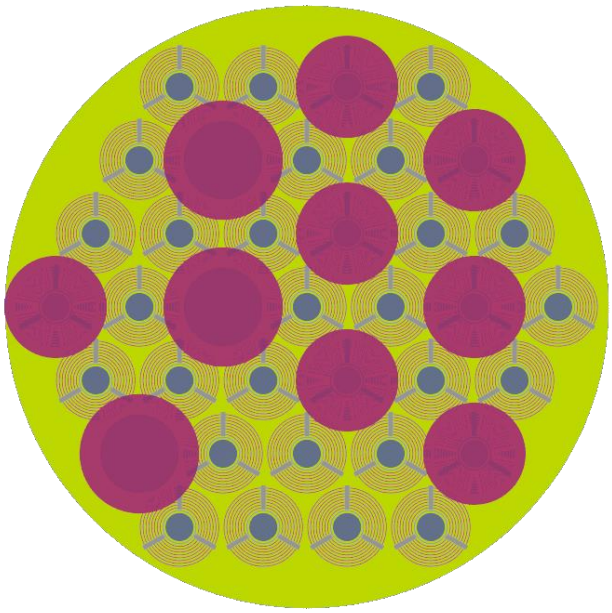

Figure 4: At core level

- Let us return for a while on the size of the core, now that the above design option is made (non connected devices). The most compact lattice based on cylindrical cells is a triangular one, which leads to a hexagonal shape for the core (if one choses a regular shape). A simple geometry scheme shows that a lattice with a central element is preferred to a three-element centred one. The first leads to 37 cells and can receive 10 slots for devices such as required (objective achieved). The second leads to 48 cells (see Figure 6) and can house 14 devices with the same rules (+30% of fuel volume with identical active height and a decrease in fuel rating at a given core power level).

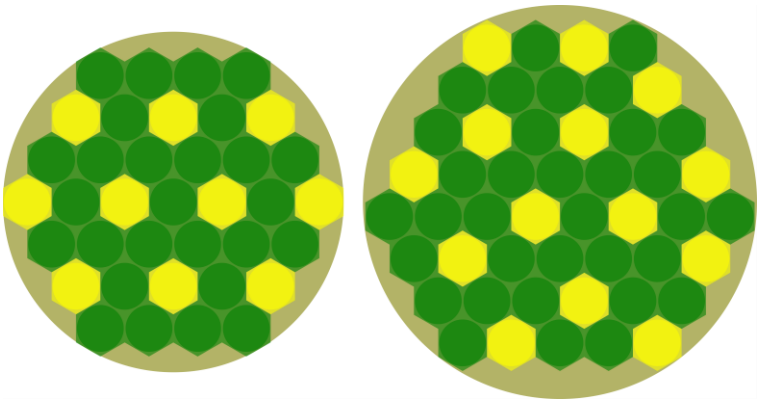

Figure 6: Core - 37 slots and 48 slots

Now with the positioning of control assemblies. Since design input rule out a follower type assembly solution such as in OSIRIS (tedious with high in-core flow rates) and since a significant part of the reflector is dedicated to the second part of the experimental load, the three options are:

- In the central part of the fuel assemblies: 27 slots are available because they do not interfere with devices above the core (see Figure 4),
- In the place of some fuel assemblies: discarded solution because of its high volume cost,
- Between fuel elements, along with an increase of the lattice length: discarded because of either leading to complex geometries, either also high volume costs and locally interacting with the above-core part of the experimental load and thus disrupting some devices.

Even if above reasonings are sometimes simplified and neutronic and thermal hydraulic assessments were performed in parallel, this shows that is mostly geometry considerations that have led to these global choices.

2.3 DESIGN: THE CORE AND THE REFLECTOR IN INTERACTION

Paragraph 1.1 gives major options concerning general shape of the core and the reflector, as well as main components as seen from above the core (rack and cylindrical vessel.
Paragraph 1.2 shows how a 37 cells hexagonal core meets requirements on the experimental load as well as core reactivity control.
At this stage, the core is hexagonal and the vessel cylindrical.

From an experimental load in the reflector perspective, the situation is then:

- Reflector slots in which neutron flux is greatest are slots positioned opposite the hexagon angles,
- Irradiation of fuel pins require a strong neutron flux and to minimise sample heating due to gamma irradiation from the core, which means gammas that do not come from fissions within the sample itself,
- Minimal distance between an experimental device and the vessel is affected by the closing of the tank in pool above the core if one wishes to keep simple geometries and devices handling (axial movements and devices without tilts,
- The outlet of the primary circuit makes part of the reflector unavailable, hopefully in a limited way.

At this design stage, it is no longer geometry assessments and engineer judgement, it is:

- Monte-Carlo neutronic calculations in order to explore solutions concerning performances of the whole experimental load [5] [6],

- Deterministic depletion calculations in order to determine core safety and operation features along the cycle: fuel management, reactivity control, thermal hydraulic assessments input, material balance for Monte-Carlo [7],
- A 3D CAD model and mechanical assessments,
- Typically, most technical fields have taken note of each and other's constraints to give birth to a profusion of solutions prior to a wrap-up between all of them.

Without getting too much into details (see Figure 7), search for the maximisation of experimental quality in the reflector has led to examining several avenues, certain of which only to better frame the solution:

- Impact of fuel assemblies in the reflector, in pressure tubes,
- Transformation of the last ring of the core into a circle,
- Adjustment of in-going channels inside the vessel to bring reflector inside the core,
- …

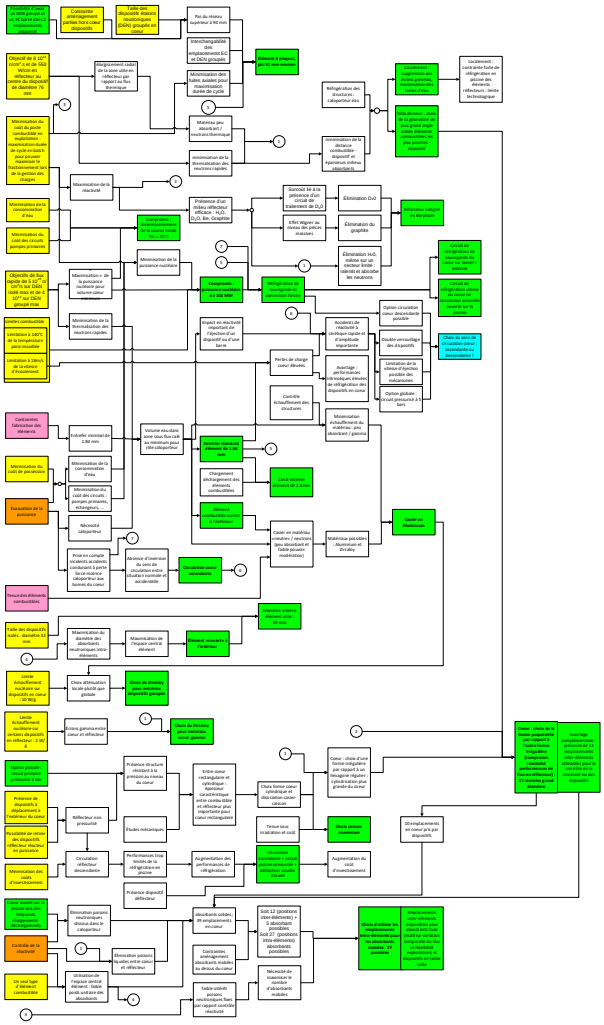

- *Figure 7: To illustrate the complexity of the design process: "simplified" logical links between some main requirements (yellow) and some design options of the reactor block (green)*

This led to a propose a slight twist in the core lattice, less bold than that of BR2 but quite effective.

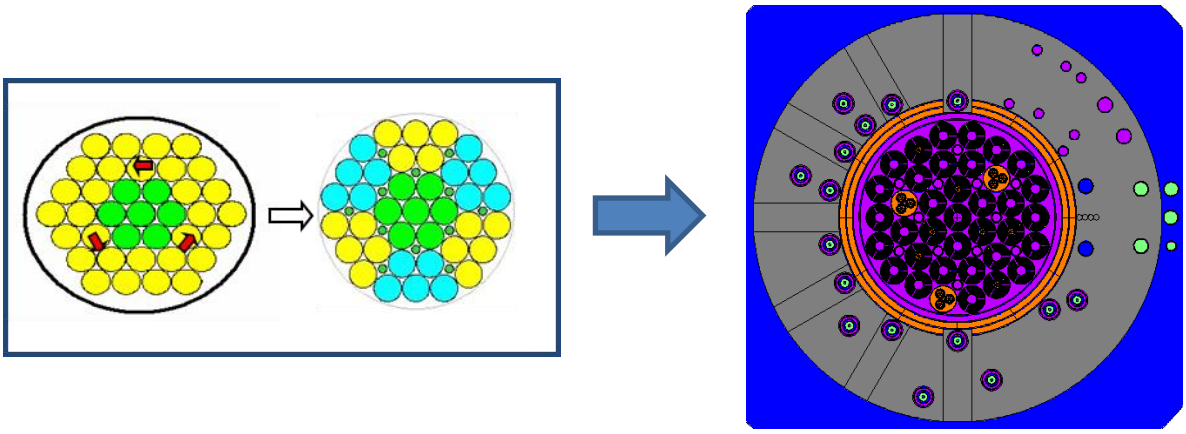

Figure 8: From hexagonal to daisy shape

This twist and the addition of Zircaloy gamma screens between the core and the reflector enabled to meet many demands:

- Increase the experimental load performance in the reflector: 12 fuel assemblies are now very close to the reflector,
- Clear 12 inter-assembly slots that are very useful to introduce reactor instrumentation (this aspect is not addressed in this paper) and to introduce neutron poisons for start-up cores,

without impeding performances of the in-core experimental load as well as other core features and without increasing constraints on mechanical components from the reactor block.

Note: Even though this issue has not been detailed here, choice for the aluminium grade and manufacturing process of the vessel has undergone many R&D actions along with foreseen manufacturers.

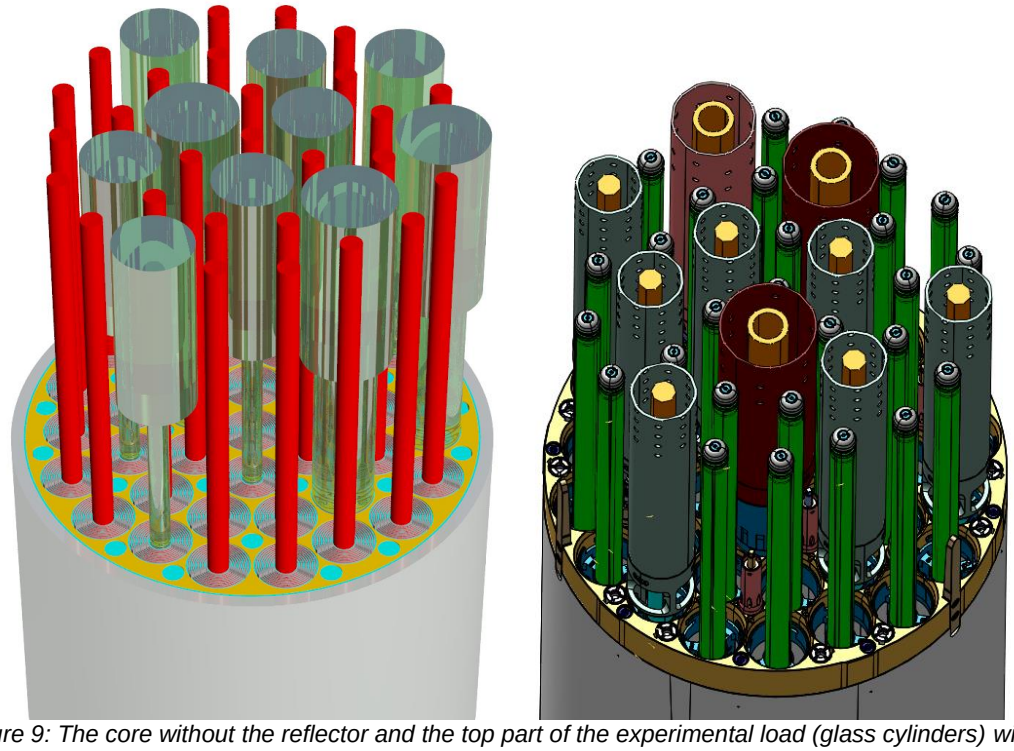

Figure 9: The core without the reflector and the top part of the experimental load (glass cylinders) with the absorbers (in red) – Engineer synthesis view during basic design (left) and CAD view (right)

3 DETAILED DESIGN AND PROCUREMENT

The objective of this paper is not to provide complete lists of all the subjects that were treated on the reactor block on the neutronic, thermal hydraulic, mechanic, safety and manufacturing [6] points of view during detailed design and procurement. Nevertheless, it is interesting to continue illustrating structuring issues and interfaces between mechanics and core physics and of its environment.

Globally, high fast neutron flux performances as well as safety constraints (maximum fuel rating) lead to a minimising of many water gaps and thus to a constraint of manufacturing tolerances for mechanical components and for their relative positioning. In addition, intrinsically due to high target performances for the experimental load, present mechanical structures undergo high irradiation levels and heating (rack, vessel, gamma screens, reflector structures, displacement structures, grids, control absorbers, …) [8].

These two main issues led to many exchanges between previously mentioned technical fields in order to adjust the pattern of mechanical components [9]. To illustrate this point, one can use three examples:

- Assessment and supply to mechanical engineers by neutronics teams of neutron fluences (fast, thermal) and heatings on a great number of components (see Figure 10) in order to verify RCC-MX 2008 requirements [10] (justify exemptions and take place in the processing of certain non-compliances during fabrication. These assessments were performed in 4 cycle points (beginning of cycle, xenon equilibrium, half cycle and end-of cycle) and also providing sensitivities to future flux tilts due to experimental loads:
    - Radially: core rack, core mandrels, pressure taps, irradiation samples, vessel, Zircaloy gamma shields, devices (displacement systems, cooling tubes, dummy devices…)
    - Axially : upper grids, absorber (Aluminium mandrel, Hafnium tubes, followers, guide tubes, absorber caps)
    - In all the core volume and core environment, in the region of binding components: screws, bolts, keys, springs, locking buttons…
- Adjusting certain interface constraints. For instance, it has already been mentioned that the closing the vessel, on the lid and near the top of the vessel, induces a minimum distance between the vessel and experimental devices in the reflector. In the case of two devices, this minimal distance is reduced thanks to a specific design of the top of the vessel (see Figure 11) after iterations between neutronics and mechanical engineers,
- Adjustment of the design of reflector components due to detailed safety assessments on the thermal hydraulic side.

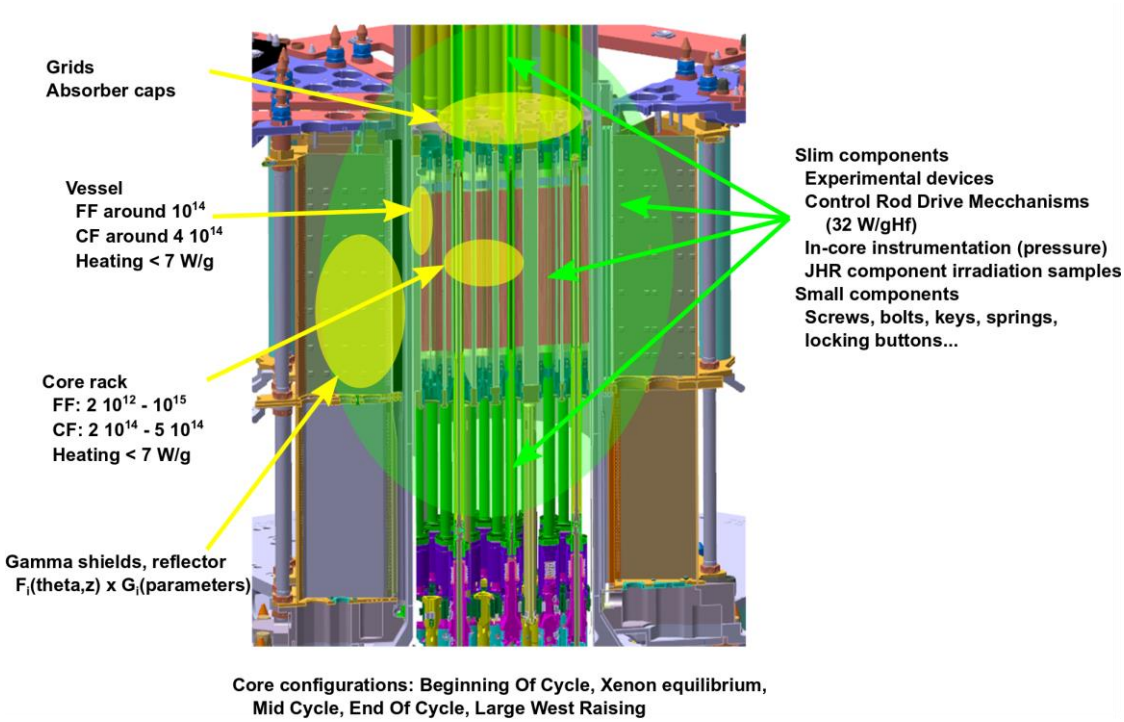

Figure 10: Block-reactor components - Neutron flux, heating

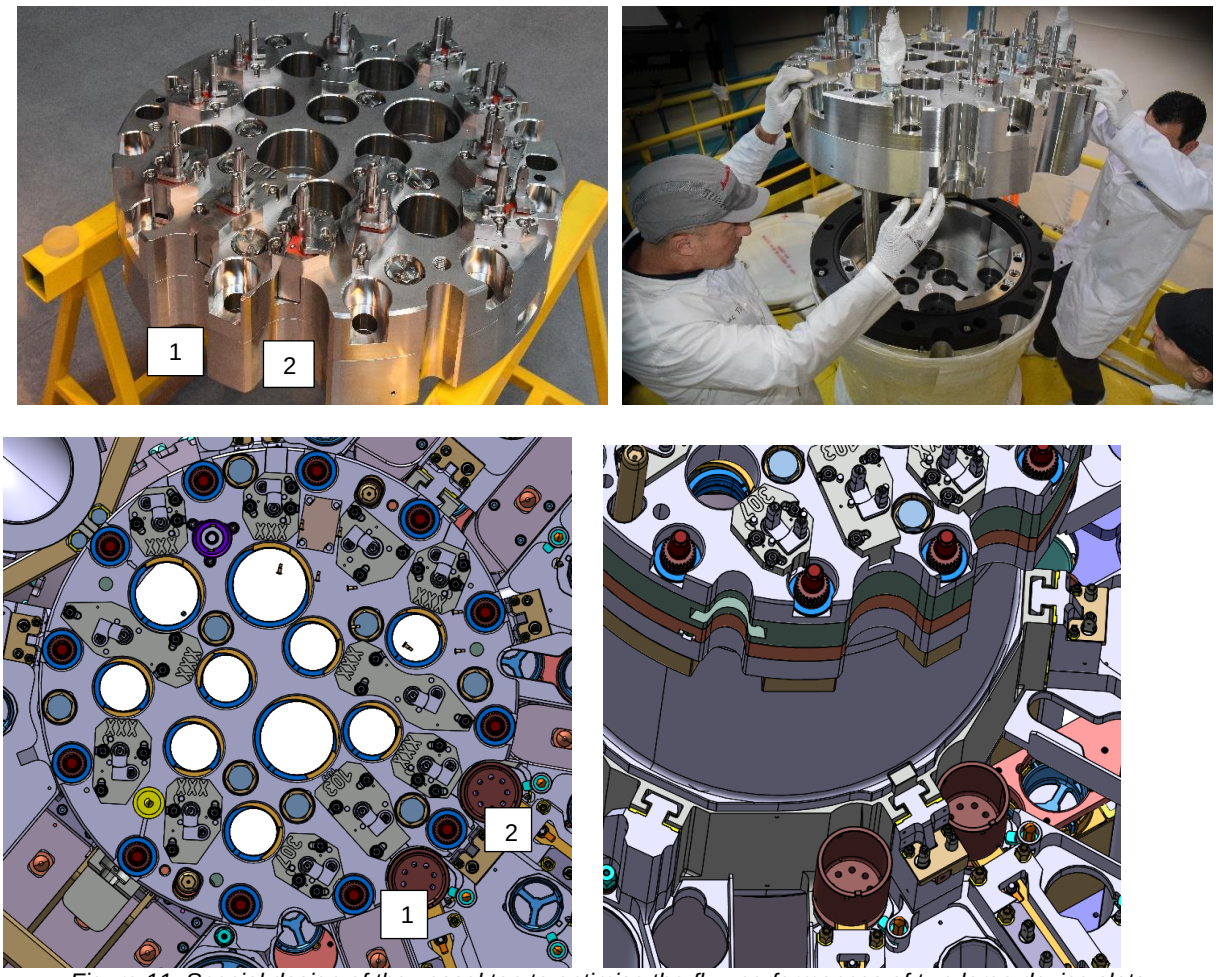

Figure 11: Special design of the vessel top to optimise the flux performances of two large device slots

In addition, the choice of a beryllium reflector made at the beginning of the design helped adapt the reflector to an increased production of Tc99m [11], thanks to readjustment of a reflector sector to receive necessary production devices (see Figure 12). This refurbishing benefited from the technological brick of the displacement system that had been developed for fuel pins power ramps, a brick that was simplified for this purpose. This example illustrates the adaptability of a Be reflector. Figure 13Figure 13 illustrates evolution of the reflector through its modelling during the project.

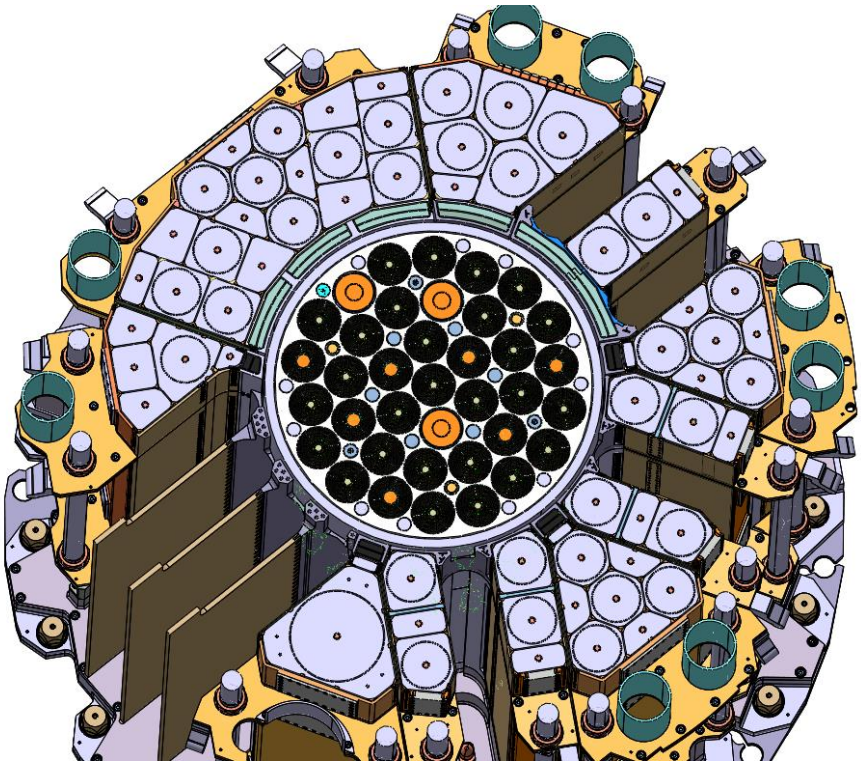

Figure 12: Core and reflector – Adaptation of the Be blocks for the four Tc99m displacement systems (empty slots at bottom left)

Finally, this stage led to an important feedback in each technical field [12]. On the main reactor block components side, one can highlight main subjects assessed:

- Materials (Aubert et Duval, Forgital Maurice Dembiermon, CEZUS, Brush Wellmann…): procurement of small quantities, acceptance tests, introduction of new materials that were not in the RCC-MX 2008 scope (hafnium for neutron absorbers, beryllium for the reflector, Inconel 718 for screws),
- Full scale demonstrators and mock-ups: first reactivity control system (Control Rod Drive Mecchanisms, CRDMs), assembly of the rack and vessel, introduction of the internal grid on the 27 CRDMs, test bench for the vessel internals…
- Industrialisation (taking into account the industrial tools capacity during design phase): water boxes, vessel, rack, internals, covers (see Figure 14 and Figure 15),
- Execution procedures (CNIM, SEIV,…): utilisation of 3D design files (CATIA) to put together component fabrication and control procedures, deep boring (core rack), alignment, installation, cleaning, tightening, welding, surface treatments (Aluminum Anodization),
- Utilisation of numerical dimensional meters (scatter plots metered with 3D laser tracker for instance) in order to adjust components with one another and have a 3D reliable view of the reactor block (numerical twin),
- Monitoring and assessment of fabrication non compliances,
- Assessment of the putting into practice of RCC-MX and exemptions feedback, as well as investigation of the ESPN decree (French regulation on nuclear pressurised

equipment) with the agreed notified body (APAVE). JHR was the first nuclear reactor to put into practice this new regulation.

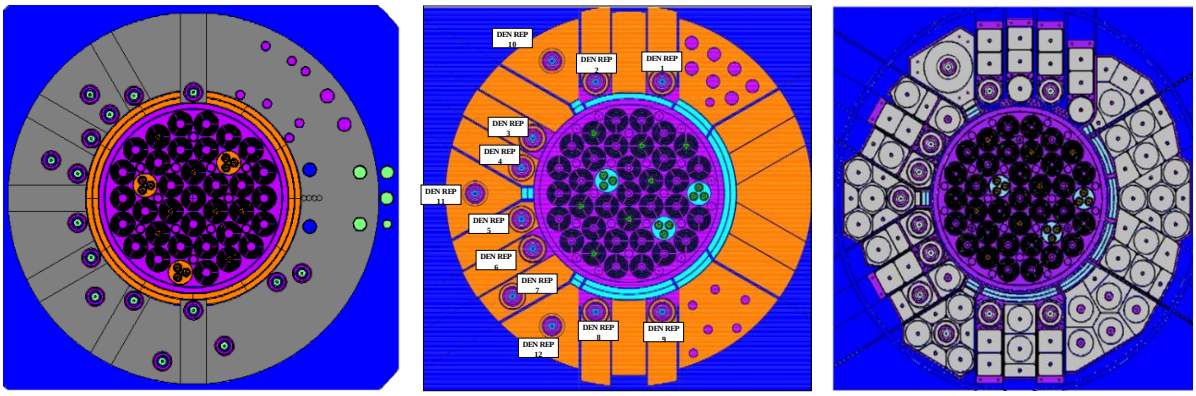

Basic design Detailed design Procurement

Figure 13: Reflector – Modelling for neutron calculation - From Basic Design to Procurement

Figure 14: Manufacturing of reactor block components: core rack (VALLA), vessel and outlet of the primary circuit, top view of the upper grids and core rack, test lifting of the upper internals (CNIM)

4 CONCLUSION

This paper illustrates different levels of processing for the design of a reactor block: from basic geometry considerations to detailed multi disciplinary assessments (neutronics, thermal hydraulics, mechanics, …). In this perspective, besides everything that establishes the riches of such a project on the human and systems engineering sides, JHR consisted in an important milestone for CEA and TechnicAtome concerning the update of completeness of the assessment of the different phenomena intrinsic to neutron and gamma fluxes induced by high

targets for the experimental load. This completeness was driven by the manufacturing of the components and of their assembly

Moreover, the design and manufacturing of the pile-block components enabled a practical application of the RCC-MX that had been put together in the perspective of the JHR, using feedback from CEA nuclear facilities. This use of RCC-MX has concerned of course as well CEA and TechnicAtome as well as other companies acting in different supply chains.

A rich feedback was obtained from this set of experiences and very practically, components of the reactor block have been manufactured, accepted and mounted.

Figure 15: Jules Horowitz Reactor Block - Final setting of some internals

Acknowledgements: Special thanking to Laurent Manifacier for his advice and his contribution to this paper.

Références :

[1] “Contributions Of Previous Projects To The Design Of New Research Reactors”, C. Pascal, P.Mignone , G.Airieau , J.S.Zampa, 18th IGORR Conference and IAEA Workshop on Safety of research reactors in light of Fukushima Daichi accident

[2] “Graded approach Practices for mechanical components of French research reactors projects”, C. Pascal, IAEA 2011 - International Conference on Research Reactors: Safe Management and Effective Utilization, Rabat, Morocco

[3] “Qualification program for the JHR fuel elements: Irradiation of the first JHR test assembly in the BR2-EVITA loop”, S. Brisson, G. Miras, MC. Anselmet, PM. Lemoine, E. Koonen, P. Benoit, P. Gouat, W. Claes, F. Geens, RRFM 2010, Marrakech, Morocco

[4] “Jules Horowitz Reactor (JHR): Start-Up Equipements And Experimental Utilities”, J.-P. Coulon, RRFM 2019, Jordan

[5] “Practices for Neutronic Design of RRs: Safety and Performances”, M. Boyard, P. Péré, L. Chabert, L. Lamoine, T. Bonaccorsi, IAEA 2011 - International Conference on Research Reactors: Safe Management and Effective Utilization, Rabat, Morocco

[6] “JHR core features based on TRIPOLI-4 and code comparison with MCNP-6”, E. Privas, J. Couybes, PHYSOR 2018, Cancun, Mexico

[7] “HORUS3D/N neutron calculation tool, a deterministic scheme dedicated to JHR design and safety studies: development, validation, biases and uncertainties quantification”, F. Jeury, J. Politello, C. d’Aletto, L. Gaubert, C. Vaglio-Gaudard, J.-F. Vidal, J.-M. Vidal

[8] “Irradiation damage and material limit: illustration of a way to codify rules with RCC-MRx”, C. Pascal, C. Pétesch, T. Lebarbé, S. Dubiez, Le Goff, IGORR 2014, Bariloche, Argentina

[9] “Contribution of CAD and PLM for research reactor design and construction”, X. Bonnetain, P. Guillou, E. DridiI, C. Pascal, IGORR 2013, Daejon, Korea

[10] “Code of Design and Construction Rules for Mechanical Component in Nuclear Installations (RCC-MRX)”

[11] “Production Of Radioisotopes At The Jules Horowitz Reactor”, J.-P. Coulon , M. Antony, C. Chapuis, RRFM-IGORR 2019, Jordan

[12] “Jules Horowitz Reactor (JHR): Manufacture Of The Reactor Pile-Block”, F. Duquesnoy, P. Parraud, RRFM-IGORR 2019, Jordan

CHARACTERIZATION OF U_3Si_2/Al FRESH FUEL PLATES WITH DIFFERENT URANIUM LOADINGS

X. Iltis, J. Havette, J. Gousseau, N. Tarisien, V. Klosek, S. Valance, H. Palancher
CEA, DES, IRESNE, DEC, Cadarache, F-13108 Saint-Paul-Lez-Durance - France

J. Allenou, B. Stepnik
FRAMATOME, CERCA, SPL, ZI Les Bérauds, 54 Avenue de la Déportation, BP 114, F-26104 Romans-sur-Isère - France

ABSTRACT

The HiProsit irradiation was completed in 2020, in the frame of the LEU-FOREvER EURATOM project. This experiment aimed at evaluating the performance of high-loaded U_3Si_2 full size plates. Four plates were irradiated. They differed in terms of fuel core thickness, uranium loading and cladding. The detailed characterization of samples from non-irradiated sister plates was performed at CEA Cadarache to support the interpretation of post-irradiation examinations.
The microstructure of the fuel core and the composition of the U_3Si_2 fissile particles are found very close to what could be expected from literature data. Moreover, it is shown that the increase of the uranium loading does not seem to induce a significant modification of the porosity of the fuel core (measured by helium pycnometry) and of the regularity of its thickness (evaluated by image analysis) but it affects the mechanical strength of the plate (according to three points bending tests at room temperature). It also results in an increase of the fragmentation of U_3Si_2 particles.

1. Introduction

The High Performance research Reactors Optimized Silicide Irradiation Test (HiProsit) was completed in 2020, in the frame of the LEU-FOREvER EURATOM project aimed to develop Low Enriched Uranium (LEU) fuels for medium and high power research reactors in Europe [1]. It was performed in the BR2 reactor (in Belgium) on four plates with U_3Si_2+Al dispersed fuel. Its main objective was to evaluate the impact on irradiation behaviour of an increase of the uranium loading in the fuel core from 4.8 gU/cm^3 to 5.6 gU/cm^3 (4.8 gU/cm^3 corresponding to the silicide fuel loading qualified since the 1980s [2]).
Tab.1 summarizes the main fabrication and irradiation characteristics of these four HiProsit plates. It shows that the thickness of the fuel core varied depending on the U loading and that two different claddings were tested (AG3NE and AlFeNi). The mean and maximum burnups reached at the end of the irradiation were similar for the four plates, i.e., respectively about 55 and 80 % ^{235}U.
The first non-destructive post-irradiation examination results pointed out a globally satisfactory behaviour of the four plates, with a limited fuel swelling [3].
In parallel, samples taken from either Depleted uranium (DU) or LEU non-irradiated sister plates were cut at FRAMATOME CERCA and sent to CEA Cadarache for detailed characterization.

Tab.1. Main fabrication and irradiation characteristics of the U_3Si_2/Al fuel plates tested in the HiProsit experiment (from [3] [4]).

Plate designation	U loading (gU/cm^3)	Specified fuel core thickness (µm)	Cladding alloy	Heat flux (W/cm^2) at beginning of irradiation	Mean/maximum burnups (%^{235}U)
HIPL 2001	4.8	690	AG3NE	450	56.2/81.1
HIPL 1002	5.3	630	AG3NE	427	55.1/81.1
HIPL 1003	5.3	630	AlFeNi	396	54.6/80.0
HIPL 1102	5.6	600	AlFeNi	451	56.2/81.2

2. Experimental details

2.1. Characteristics of the samples received

The main fabrication characteristics and the designation of the non-irradiated plates examined in the present work are presented in Tab. 2. Samples were taken by FRAMATOME CERCA in the central area of each plate, using a punch tool. Their size and number were respectively:

- 80×20 mm, three per plate, for DU plates,
- 28×10 mm, one per plate, for LEU ones.

Tab.2. Main fabrication characteristics of the non-irradiated U_3Si_2/Al fuel plates, made with DU and LEU fuels, studied at CEA Cadarache.

U loading - Cladding *(specified fuel core thickness)*	**DU plates (HIPX series)**	**LEU plates (HIPL series)**
4.8 gU/cm^3 – AG3NE *(690 µm)*	HIPX 2005	HIPL 2002
4.8 gU/cm^3 – AlFeNi *(690 µm)*	HIPX 2008	/
5.3 gU/cm^3 – AG3NE *(630 µm)*	/	HIPL 1001
5.3 gU/cm^3 – AlFeNi *(630 µm)*	HIPX 1007	HIPL 1005
5.6 gU/cm^3 – AlFeNi *(600 µm)*	HIPX 1102	HIPL 1101

Note that HIPX and HIPL series correspond respectively to DU and LEU plates. In both cases, the plate designation number refers to its uranium loading: 2xxx for 4.8 gU/cm^3, 1xxx for 5.3 gU/cm^3 and 11xx for 5.6 gU/cm^3.

2.2. Characterization methods and samples preparation

Depending on the measured property and the size of the sample required for its determination, LEU and/or DU samples were used, as indicated in Tab. 3. For structural and microstructural characteristics, LEU samples were selected but one DU sample was also studied to make sure that no significant differences had to be taken into account when comparing DU and LEU samples.

Tab. 3. Characterizations performed on DU and LEU samples.

Measured characteristic	Method(s)	Origin of the samples (plates)
Structural and microstructural characteristics		
Structure of the fuel core (phases)	XRD[(1)]	Samples from the 4 LEU plates + 1 DU sample (HIPX 2005)
Microstructure and phase composition of the fuel core	SEM[(2)] EDS[(3)] EBSD[(4)]	Samples from the 4 LEU plates + 1 DU sample (HIPX 2005)
Physical characteristics		
Fuel core thickness	OM[(5)] + image analysis	▪ HIPL 2002 (LEU) ▪ HIPL 1101 (LEU)
Mechanical strength	Three-points bending (room temperature)	Samples from the 4 DU plates
Fuel core porosity (feasibility)	Helium pycnometry	▪ HIPX 2008 (DU) ▪ HIPX 1102 (DU)

[(1)]X-Ray Diffraction – [(2)]Scanning Electron Microscopy – [(3)]Energy Dispersive Spectroscopy – [(4)] Electron BackScatter Diffraction – [(5)]Optical Microscopy.

XRD analyses were performed on about 7×7 mm samples polished parallel to the fuel-cladding interface down to the middle of the fuel core, using a Bragg-Brentano θ-θ Bruker D8 advance X-ray diffractometer using Cu Kα1 and Kα2 radiations (1.5406 and 1.5444 Å respectively) from a conventional tube source. The angular range analysed was 10-140° with a 0.01° step and a counting time of 3 seconds per point was chosen.
The SEM examinations and the EDS analyses were performed using a Nova NanoSEM 450 from FEI equipped with an Oxford Instruments EDS silicon drift detector with an active surface of 80 mm^2. EDS data were processed with the AZTEC software, using its standard database for quantification of elements.
EBSD analyses were achieved with the Nova NanoSEM 450. This microscope is equipped with a Symmetry camera (maximum resolution: 1244×1024 pixels) from Oxford Instruments. AZTEC and AZTEC Crystal softwares were respectively used for data collection and analysis. No camera binning was applied and the step size was adapted on a case-by-case basis.
To evaluate if the increase of the uranium loading affects the regularity of the thickness of the fuel core, this thickness was measured by image analysis on two LEU samples (with U loadings of 4.8 and 5.6 gU/cm^3 respectively), using the “layer thickness” module of the Olympus STREAM software. These samples corresponded to 28 mm long cross-sections, observed by optical microscopy, on which measurements were taken every 50 µm. Each sample was polished and examined three times (the examination plans being separated by several hundred µm), in order to get data on a total length of about 28×3 = 84 mm.
The mechanical strength of the four DU plates was evaluated at room temperature using a three-points bending device mounted on an INSTRON 3342 single column testing machine. The size of the specimens was 40×4×1.33 mm and the distance between the two support points was 24 mm. The tests were carried out up to different deflection values (from 1.7 to 9 mm, depending on the plates) with a displacement speed of 100 µm/min. Cross-sections were prepared by cutting and polishing the most deformed part of the samples. They were observed by SEM in order to study the appearance and propagation of defects within the fuel core and the cladding.
Finally, as requested by the european Fuel Development Expert Group (FDEG), first characterizations of the local porosity within the U_3Si_2 + Al fuel core were undertaken: helium pycnometry measurements were performed on samples from two DU plates, previously de-cladded by mechanical polishing. Four samples per plate (about 20×10×0.5 mm each) were measured simultaneously using a Micromeritics AccuPycII 1340 system, with a cell volume of 3.5 cm^3. These measurements were repeated three times to check their reproducibility.

3. Results

3.1. Structural and microstructural characteristics

XRD analyses were performed in the fuel core on the four LEU plates and on one DU plate. In all these cases, the same phases were evidenced. As expected, Al and U_3Si_2 were the major constituents of the core but two minor phases were also systematically found: $U_{34}Si_{34.5}$, in accordance with results obtained on arc melted ingots slightly over-stoichiometric in silicon [Havette, 2020] and UAl_3 and/or $U(Al,Si)_3$. The presence of this (these) latter phase(s) can be attributed to an interaction between some free uranium and aluminium, during the plate manufacturing [5]. Few very small diffraction peaks remained unindexed. The quantification of minor phases by Rietveld refinement is considered unreliable, given the quality of these laboratory XRD data.

SEM examinations (in Back-Scattered Electrons (BSE) mode) point out a significant increase of the U_3Si_2 particles fragmentation with the increase of the uranium loading (Fig. 1), that can be attributed to numerous direct contacts between these particles, non-accommodated by the ductile Al matrix during plate rolling.

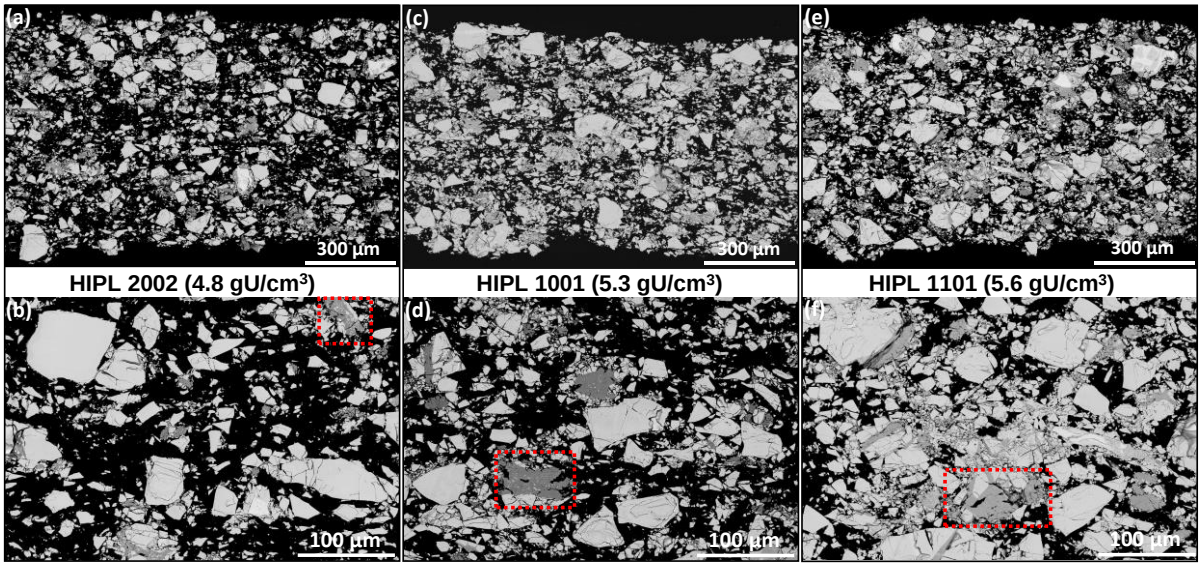

Fig. 1. SEM examination (BSE mode) of (a) (b) HIPL 2002, (c) (d) HIPL 1001, (e) (f) HIPL 1101 plates, at two different magnifications.

EDS and EBSD results presented hereafter were all obtained on a plate with 4.8 gU/cm^3 (HIPL 2002), because it contains larger particles without cracks than the plates with higher loadings, which are thus easier to characterize. Except for this difference, the results presented are representative of all the plates studied.

Red-dotted boxes in Fig. 1b, 1d and 1f highlight uranium-based particles in which several phases are present according to grey levels variations. EDS analyses were performed on such particles to get information about their composition. Fig. 2 presents the results obtained on two representative particles commonly encountered in LEU and DU plates. In the first one (Fig. 2a), a vein of secondary phase corresponding to a binary U-Si compound with about 50 at.% Si is present (Fig. 2b). The second one also exhibits a vein of minor phase (Fig. 2c) with a composition very close to UAl_3 (Fig. 2d). In that case, a few at.% of Si are also detected and that area could thus correspond to an $U(Al,Si)_3$ phase. Note that the Si content in such areas varies depending on particles, perhaps because of a contribution of underlying U_3Si_2 or the presence of a mixture of phases with different Al and Si contents. The detection of some Al in the U_3Si_2 phase surrounding this vein is due to a slight contamination by the Al matrix that occurred during polishing.

These results fully confirm those obtained by XRD, concerning the presence, in small amounts, of the USi (more exactly $U_{34}Si_{34.5}$) and UAl_3 (and/or $U(Al,Si)_3$) phases in the fuel core.

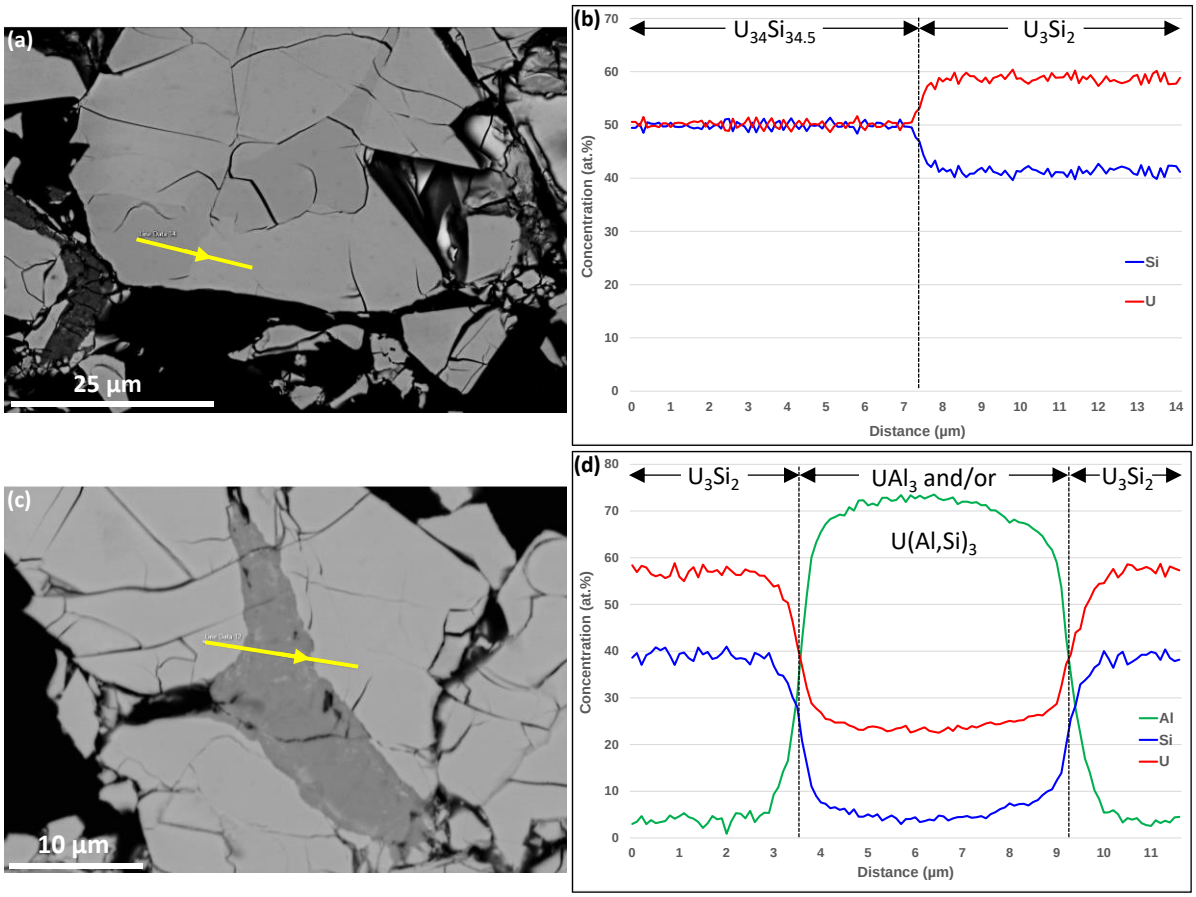

Fig. 2. EDS analyses performed on two particles from HIPL 2002 plate, (a) SEM image of particle 1 (BSE mode), (b) composition profiles acquired along the yellow line drawn in (a), (c) SEM image of particle 2 (BSE mode), (d) composition profiles acquired along the yellow line drawn in (c).

In addition to these common features, some large fuel particles presenting areas made of nearly pure uranium (very probably in the α-U form) are also relatively often encountered in all studied samples. Fig. 3 gives an example of such a particle. Its heterogeneous light grey core with slightly darker areas (Fig. 3a and 3b) is the part where metallic uranium is present. Its mean concentration in Si is about 11 at.%. The composition profiles shown in Fig. 3d can be interpreted as representative of the alternation of U and U_3Si_2 areas. As the U_3Si_2 particles are very small (typically of the order of 1 µm in diameter) and close to the EDS spatial resolution limit, it is difficult to determine undoubtedly if some Si is present or not in solid solution in U and if a small U_3Si rim is formed around U_3Si_2 particles (as expected according to the intermediate contrast visible in Fig. 3c and literature [6]). Sub-micrometric precipitates containing metallic elements (Fe, Ni…) can also be found more scarcely in these metallic areas. Their presence is probably due to segregation phenomena.
Finally, few “exotic” particles are encountered from place to place with often an U_3Si_5 composition. All these phases could not be detected by XRD, due to their small amount and/or to overlaps of their diffraction peaks with those of major phases.

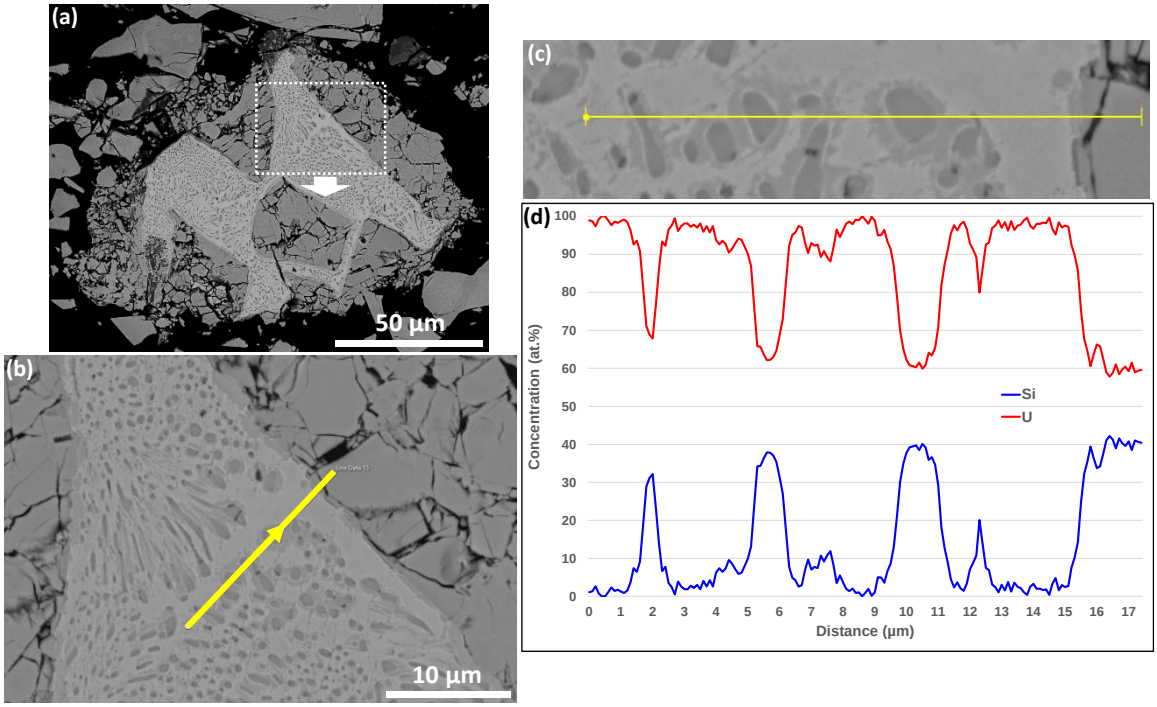

Fig. 3. Example of particle containing nearly pure U (plate HIPL 2002), (a) (b) (c) SEM images (BSE mode) at three magnifications with the position of the line-scan drawn as a yellow line in (b) and (c), (d) corresponding composition profiles.

Fig. 4 corresponds to a typical EBSD map acquired on plate HIPL 2002. Fig. 4a, colorized in IPF-Z, shows that many of the U_3Si_2 particles are single crystalline, as also concluded by Havette *et al.* when examining crushed arc-melted U_3Si_2 ingots and a DU archive plate from the SHARE irradiation experiment (with a 4.8 gU/cm^3 loading) [7]. Fig. 4b shows the same map colorized in phase distribution.

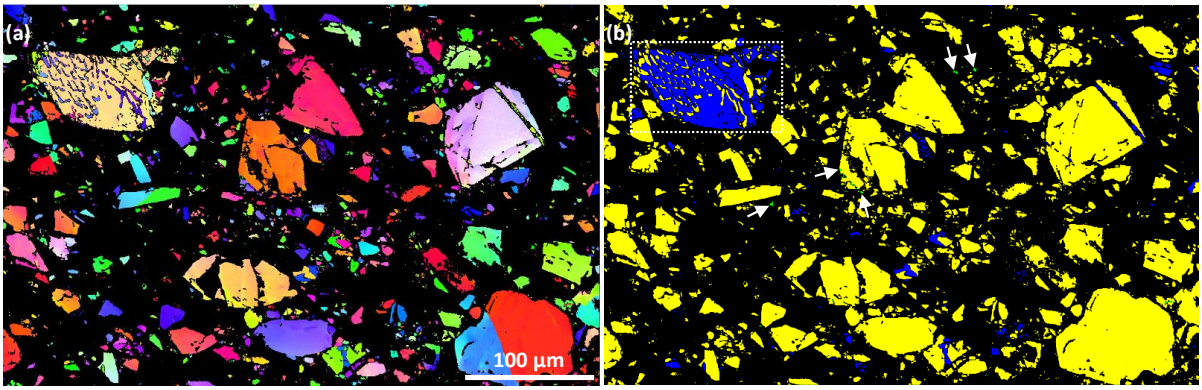

Fig. 4. EBSD map acquired with a 0.25 µm step size on plate HIPL 2002, (a) colorized in IPF-Z, (b) colorized in phase distribution with U_3Si_2 in yellow, $U_{34}Si_{34.5}$ in blue and U_3Si_5 in green. Non indexed pixels are in black.

Three phases were detected by EBSD (excluding the Al matrix which was not taken into account when indexing this map and appears thus in black): U_3Si_2 (in yellow), $U_{34}Si_{34.5}$ (in blue) and U_3Si_5 (in green). Note that the areas within U_3Si_2 particles containing α-U or UAl_3 could not be analyzed here, since they did not diffract well enough. This limitation is due to surface preparation issues which need further work to be overcome. In accordance with Fig. 2a, $U_{34}Si_{34.5}$ generally forms veins in large U_3Si_2 particles or isolated small fragments but it can sometimes also constitute the major phase in some large particles (as it is the case for that white-boxed in Fig. 4b). U_3Si_5 is observed more rarely, in the form of small veins within U_3Si_2 particles or small isolated fragments (some being pointed by white arrows in Fig. 4b).

It is difficult to quantify the fraction of uranium-bearing minor phases present in the fuel core. On the basis of several EBSD maps, this fraction was estimated roughly by measuring the relative surface fraction of diffracting phases (based on IPF-Z maps) and non-diffracting ones (based on pattern quality maps, where areas corresponding to cracks and pull-outs were selected manually and disregarded). This fraction was estimated at 15-20 % of the whole surface of U-bearing phases, at the most.

3.2. Physical characteristics

In this section, results relative to the fuel core thickness (measured by image analysis) and to the mechanical strength of the plates are presented. Data acquired by helium pycnometry in the frame of feasibility tests are also given.

Fig. 5 summarizes the results obtained by OM + image analysis concerning the variability of the fuel core thickness in two plates which differ by their uranium loading (4.8 and 5.6 gU/cm^3). The inset corresponds to a partial view of one of the optical images used for the measurements. The blue lines delimitate the fuel core, the green one corresponds to the medium position between them and the yellow ones mark the positions where the measurements of the fuel core thickness were done. This figure shows that the fuel core thickness varies a little bit more (by reference to its mean value) when the uranium loading increases. This variation is quantified by the values given in Tab. 4 for about 1500 measurements per plate.

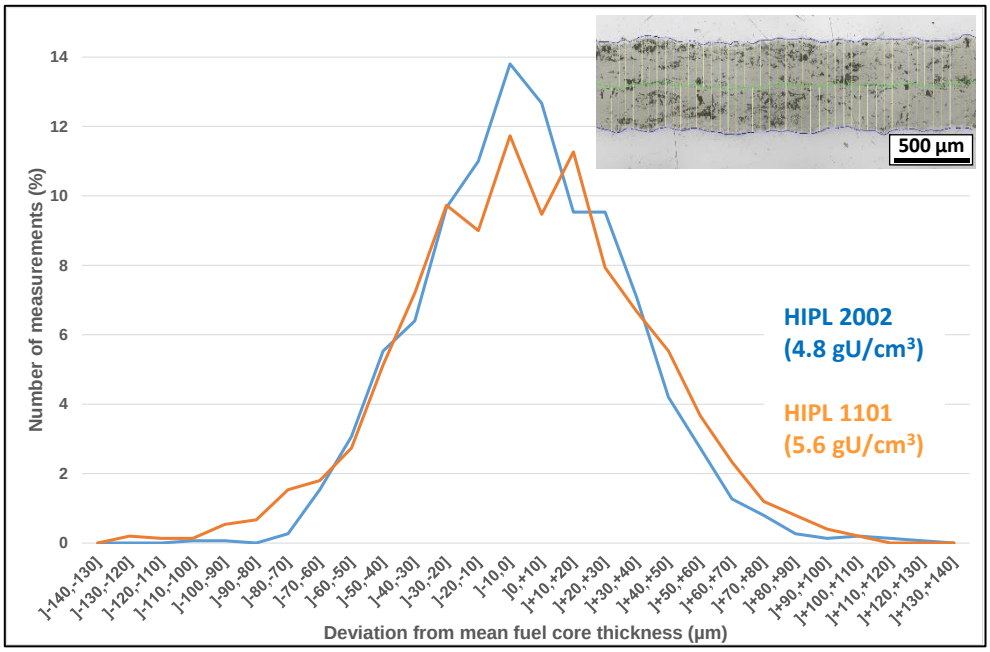

Fig. 5. Results of the fuel core measurements performed by image analysis on two LEU plates differing by their uranium loading. The inset illustrates the measurement method.

Tab. 4. Statistical data associated to the measurements displayed in Fig. 5.

	Fuel core thickness (µm)				
Plate *(U loading)*	Mean value	Standard deviation	Minimum value (Min)	Maximum value (Max)	Total spread (Max – Min)
HIPL 2002 (4.8 gU/cm^3)	694	31	592	817	225
HIPL 1101 (5.6 gU/cm^3)	610	37	486	715	229

As regards the fuel core average thickness, they are in good agreement with the manufacturing specifications. As they are related only to one sample per plate (taken in its central part), it would be interesting to perform complementary measurements on other samples taken at different locations.

Fig. 6 illustrates the results of three-points bending tests performed up to a deflection of 4.5 mm on specimens taken from the three DU plates with AlFeNi cladding. The stress-strain curves clearly point out a decrease of the mechanical strength of the plates when the uranium loading increases. A partial breakage of the specimens occurred as shown by SEM images (taken in BSE mode): this breakage is all the more advanced that the uranium loading is high. According to examinations carried out on samples deformed at different levels, the failure of the specimens takes place in several stages: first, cracks roughly parallel to the direction of solicitation appear in some of the largest U_3Si_2 particles, second a main tear forms in the fuel core, third this tear gets bigger and propagates within the cladding. When the uranium loading increases, the tearing process occurs earlier (i.e., for lower deflections) and can initiate at several locations (as pointed by the white arrow in Fig. 6d).

These results were obtained at room temperature and could be useful to address some safety questions such as the behaviour of the plates in the event of a fall during handling, for example. However, they are not representative of their mechanical properties in reactor, i.e., at a temperature of the order of 200°C or even more [8]. That is why complementary mechanical tests are planned at different temperatures on specimens from HiProsit plates.

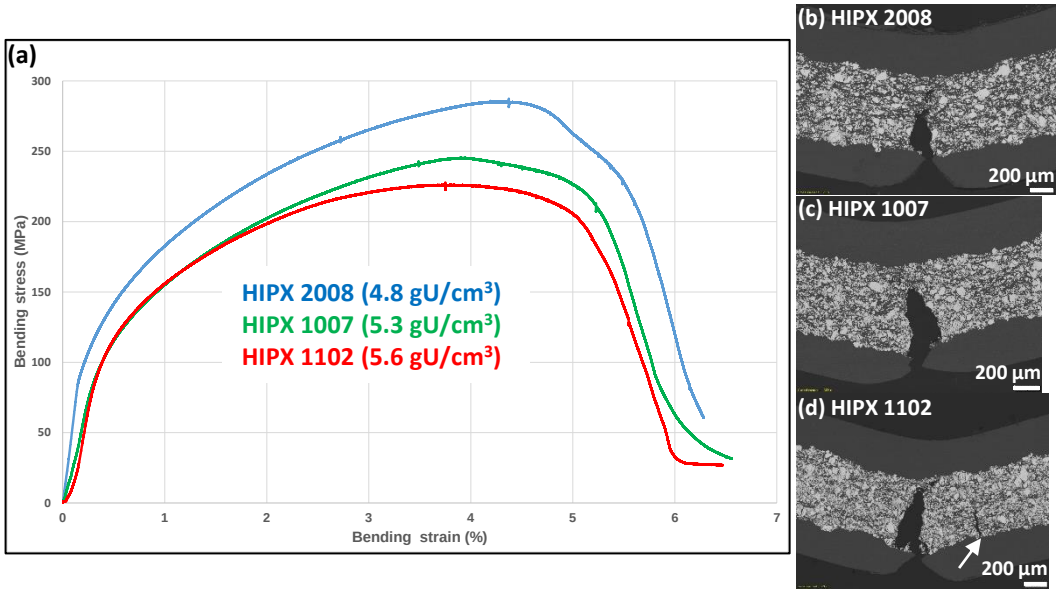

Fig. 6. Results of three-points bending tests performed at room temperature up to a deflection of 4.5 mm on specimens taken from HIPX 2008, 1007 and 1102 plates – (a) stress-strain curves, (b) (c) (d) SEM images (BSE mode) of cross-sections taken from the most deformed part of each specimen.

Tab. 5 gathers the results obtained by helium pycnometry on de-cladded samples from HIPX 2008 and HIPX 1102 DU plates, in the frame of preliminary tests. Density measurements had a very good repeatability, as assessed by the low standard deviation values. The mean closed porosity of the fuel core was deduced from these measurements using the following relation:

$$V_{porosity}\ (vol.\%) = [1 - (measured\ density/theoretical\ density)] \times 100$$

where the theoretical density of the fuel core was calculated from data given by FRAMATOME CERCA [9]. It is worth noting that the measured porosity is almost the same for the two plates, which tends to indicate that it does not increase significantly with the uranium loading. To confirm these first values, it would be interesting to perform complementary measurements on samples taken from different locations in the plates. Inter-comparison tests between several laboratories equipped with a He pycnometry apparatus would also be very interesting.

Tab. 5. Results of helium pycnometry measurements.

Plate *U loading (cladding)*	Measured density (g/cm^3)	Theoretical density (g/cm^3)	Mean closed porosity (vol.%)
HIPX 2008 *4.8 gU/cm^3 (AlFeNi)*	Mean value: 6.6824 Standard deviation: 0.0029	6.905	3.2
HIPX 1102 *5.6 gU/cm^3 (AlFeNi)*	Mean value: 7.5431 Standard deviation: 0.0107	7.763	2.8

4. Main results, conclusion

Samples from eight fresh fuel plates (four made with DU fuel and four with LEU fuel) manufactured for the HiProsit irradiation experiment were subjected to extensive characterizations.

Microstructural examinations evidenced a significant increase of the fragmentation of U_3Si_2 particles (often single crystalline) with the U loading. Several minor uranium-bearing phases were found in all plates, the most common ones being $U_{34}Si_{34.5}$ and UAl_3 (and/or $U(Al,Si)_3$) according to XRD data. The presence of some α-U must also be noticed.

The fuel core thickness was measured by image analysis on optical images, on two LEU plates with different uranium loadings. Results pointed out a very slight increase of this thickness variability, when increasing the uranium loading from 4.8 to 5.6 gU/cm^3. Complementary measurements on samples taken at different locations in the plates should be performed to confirm these results. Three points bending tests at room temperature showed that the increase of the uranium loading leads to a damage of the plate that occurs for lower deflection values.

Prospective studies regarding the local measurement of the fuel core porosity were initiated. Measurements were carried out by helium pycnometry on de-cladded samples from two DU plates (with 4.8 and 5.6 gU/cm^3 respective U loadings). In both cases, a mean closed porosity of the fuel core of the order of 3 vol.% was measured with a high repeatability. Other measurements on samples taken from different locations in the plates and inter-comparison tests between several laboratories would be of great interest.

These results are in general agreement with literature data [2] [5] [7] and will provide a basis for the interpretation of post-irradiation examinations currently in progress on plates from this irradiation experiment.

Acknowledgements:

This work was supported by the European Commission in the framework of HORIZON 2020 through Grant Agreement 754378 in the LEU-FOREvER project. The members of the european Fuel Development Expert Group (FDEG) are warmly thanked for their interest and their insightful comments on this study.

References:

[1]. S. Valance *et al.*, *The H2020 European project fuel for research reactors LEU-FOREvER: LEU fuel for medium and high power research reactors in Europe*, RRFM 2018, March 11-15, Munich, Germany.

[2]. *Safety evaluation report related to the evaluation of low-enriched uranium silicide-aluminum dispersion fuel for use in non-power reactors,* U.S. Nuclear Regulatory Commission NUREG-1313 report, 1988.

[3]. A. Leenaers *et al.*, *Status of the SEMPER FIDELIS and HiPROSIT post-irradiation examinations*, RETR 2021, April 20-22, online.

[4]. B. Stepnik *et al.*, *Manufacturing of the HiProsit irradiation experiment: High density U_3Si_2 fuel plates*, RERTR 2019, October 6-9, Zagreb, Croatia.

[5]. M. Mirandou *et al.*, Study of the interaction between U_3Si_2/Al in dispersion plates at the end of the fabrication process, Nuclear Technology 199 (2017) 96-102.

[6]. J.M. Harp *et al.*, *Uranium silicide pellet fabrication by powder metallurgy for accident tolerant fuel evaluation and irradiation*, Journal of Nuclear Materials 466 (2015) 728-738.

[7]. J. Havette *et al.*, *From arc-melted ingot to MTR fuel plate: A SEM/EBSD microstructural study of U_3Si_2,* Journal of Nuclear Materials 537 (2020) 152224.

[8]. G. Hofman *et al.*, *Projection of irradiation behaviour of U_3Si_2-Al dispersion fuel at high fuel loading and high power,* RERTR 2019, October 6-9, Zagreb, Croatia.

[9]. J. Allenou *et al.*, *Report on improvement process on U_3Si_2*, LEU-FOREvER project EURATOM H2020 WP 2016-2017 / NFRP-11 Deliverable # D2.2.1, Framatome CERCA report SPL/19-242/JA, 2019.

EMPIrE FUEL MEAT SWELLING ANALYSIS

L.M. JAMISON, G.L. HOFMAN, B. YE, Z. MEI, A. YACOUT
Chemical and Fuel Cycle Technologies Division, Argonne National Laboratory
9700 S. Cass Ave, 60439 – United States

A.B. ROBINSON, W.A. HANSON, D.D. KEISER, JR.
Post Irradiation Examinations, Idaho National Laboratory
2525 North Fremont Ave, 83402 – United States

ABSTRACT

Following initial challenges in the processing of the non-destructive (ND) post-irradiation examination (PIE) results of the European Mini-Plate Irradiation Experiment (EMPIrE), analysis of the fuel particle swelling has been completed [1]. It is timely to start interpreting those results in conjunction with currently available partial set of destructive examination (DE) results. Typically, the effects of test variables on fuel behaviour is expressed in terms of fuel swelling, as was done in [1]. It should be stressed, however, that reported fuel particle swelling includes a correction factor for as-fabricated porosity determined with average fabrication parameters. In order to avoid the uncertainty and variability of those parameters, an evaluation of the fuel meat swelling (dependent only on the pre- and post-irradiation thickness and nominal plate and fuel meat thicknesses) was conducted. Preliminary results of this analysis, and connection to preliminary DE results, are reported here.

1. Introduction

As discussed above, due to the sensitivity of fuel swelling calculations on the as-fabricated porosity and fabrication parameters, and the uncertainties and variation involved in those values, analysis of the plate-average fuel meat swelling of EMPIrE plates was pursued. In this report, the analyses related to plate types 1, 5, 7A, and 8A are discussed. The measured thickness change of a fuel plate, $\Delta_{t,plate}$, is related to the actual U-Mo swelling as follows:

- Because these plates are thin, all fuel swelling is expressed in plate thickness change ($\Delta_{t,plate} \sim \Delta_{V,plate}$). Any lateral swelling is converted by creep to thickness change only due to the constraint of the thicker cladding in the lateral direction (compared to the thickness direction). Additionally, swelling within the cladding is negligible at the temperatures and fluences experienced here, so all plate thickness swelling can be attributed to the fuel meat ($\Delta_{V,plate} \sim \Delta_{V,meat}$). The contributing factors to fuel meat swelling are porosity formation in the interaction layer (IL) (and any other changes in fuel meat volume attributable to IL formation), U-Mo fuel particles volume change, and as-fabricated fuel meat porosity (assumed to close completely under irradiation, which is to be confirmed with DE, accommodating fuel swelling). These contributing factors are not treated separately in the equations below, as their influence is incorporated into the overall fuel meat swelling behavior.
    - $Plate\ Fractional\ Swelling = \frac{t_{plate}^{post} - t_{plate}^{pre}}{t_{plate}^{pre}}$ where t_{plate}^{pre} is the pre-irradiation plate thickness and t_{plate}^{post} is the post-irradition plate thickness, as measured by profilometry

- $Meat\ Fractional\ Swelling = (Plate\ Fractional\ Swelling) \times \left(\frac{t_{plate}^{nom}}{t_{meat}^{nom}}\right)$ where t_{plate}^{nom} and t_{meat}^{nom} are the nominal plate (1.28778 mm) and meat thicknesses (0.508mm for U-7Mo, 0.5334mm for U-10Mo), respectively.

The formation of large fission gas pores in the IL has occurred in previous tests at high fission rate [2], and testing the effectiveness of various fabrication parameters in eliminating this undesirable radiation effect was the main purpose of the EMPIrE experiment. The as-fabricated meat porosity in previous and concurrent coated-particle fuel tests, i.e. SELENIUM and SEMPER FIDELIS [3, 4], has been small, on the order of 1-2%, and its influence on fuel swelling calculations is easily masked by uncertainties in the measurements. As shown in Table 1 this appears to hold for the ALD coated fuel particles but not for the PVD coated ones. The CERCA supplied porosity values were obtained with their standard immersion density procedure, which does not include the impact of the coating volume. The as-fabricated porosity was re-calculated to incorporate the influence of the coating volume [1], using the average coating thickness of literature values [5-8], or the minimum thickness range from the fresh fuel report [9], as applicable. As can be seen in Table 1, the recalculated values for as-fabricated porosity, although closer than in the as-reported values, are in disagreement with the ongoing optical microscopy analysis, especially for the plates with PVD coated particles.

Table 1. Plate type descriptions and characterizations.

Plates	Description	Powder Batch	Average Coating Thickness (μm)	As-Fabricated Porosity (Powder Type Average)		
				As-reported	Recalculated values from [1]	Measured from Optical Microscopy Images
Type 1	ALD/HT/25%fines	12	0.5 [9]	2%	0.23%	
Type 5	ALD/HT/0% fines	4R	0.79 [7]	1%	0.90%	0.54%
Type 7A	PVD/nHT/0%fines	LA1/A	1.17 [6-8]	7%	7.31%	1.4%
Type 8A	PVD/HT/0%fines	LA3/A	1.65 [6-8]	9%	3.79%	2.8%
		LA4/A	2.02 [6-8]	10%	2.47%	1.2%
		LA5/A	1.32 [6-8]	6%	2.19%	

HT=particles were heat-treated before coating, nHT=particles were not heat-treated, ALD=atomic layer deposition coating, PVD=physical vapor deposition coating, fines are defined as particles between 20 and 44μm diameter, while coarse (the balance of the particles) are 45-125μm diameter..

2. Plate Types 1 and 5

Plate types 1 and 5 were both heat-treated and ALD-coated plates. The primary differences between these two plate types are the amount of included fines (25% versus 0%) and the average particle coating thickness (0.5 µm versus 0.79 µm). A comparison of the plate-average meat swelling thickness of these two plate types is shown in Figure 1.

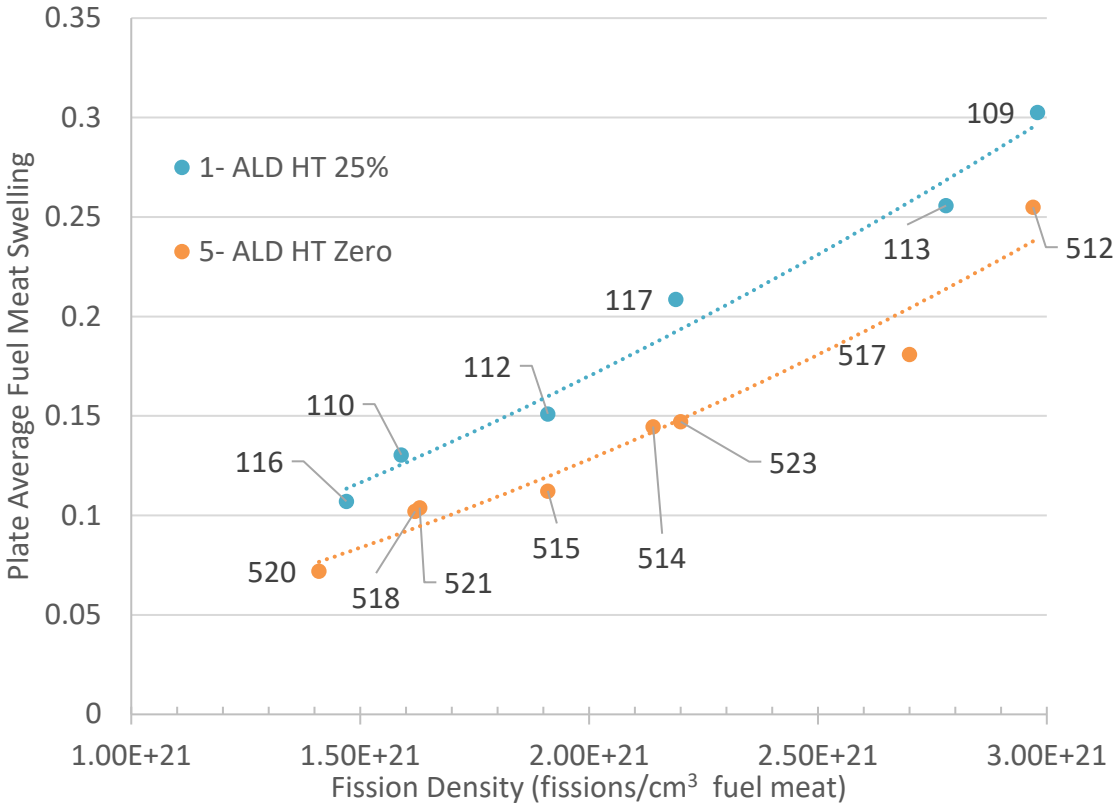

Figure 1. Plate average fuel meat swelling of plate types 1 (ALD coating, heat treated, 25% fines) and 5 (ALD coated, heat treated, zero fines).

Although the fines content between these two plate types is substantially different, it was discussed in [1] that fines content alone cannot explain the observed difference in swelling behaviour, as increased swelling in plates with higher fines content was not consistently observed across the plate type variations. The thickness of the coating, introduced in the EMPIrE test to mitigate the formation of the IL, which leads to the formation of fission gas bubbles, in these two plate types is significantly different. It was proposed that the difference in coating thickness may have contributed to the elevated swelling observed in the type 1 plates [1], and these results corroborate this.

Optical microscopy of plate 117, a mid-range fission density (2.2×10^{21} fissions/cm^3 fuel meat) type 1 plate, is shown in Figure 2.

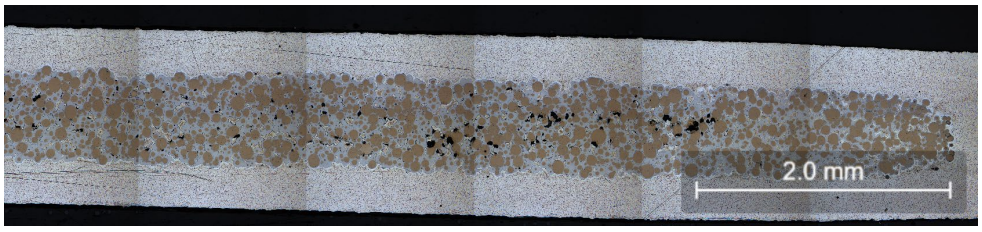

Figure 2. Optical Microscopy of plate 117 (IL volume fraction = 48.6%)

A large volume of interaction layer has formed, in addition to larger fission gas bubbles. The formation of these fission gas bubbles is what causes the increased swelling. Figure 3 compares the optical micrographs of plates 109 and 512, which are higher burnup plates with similar fission densities.

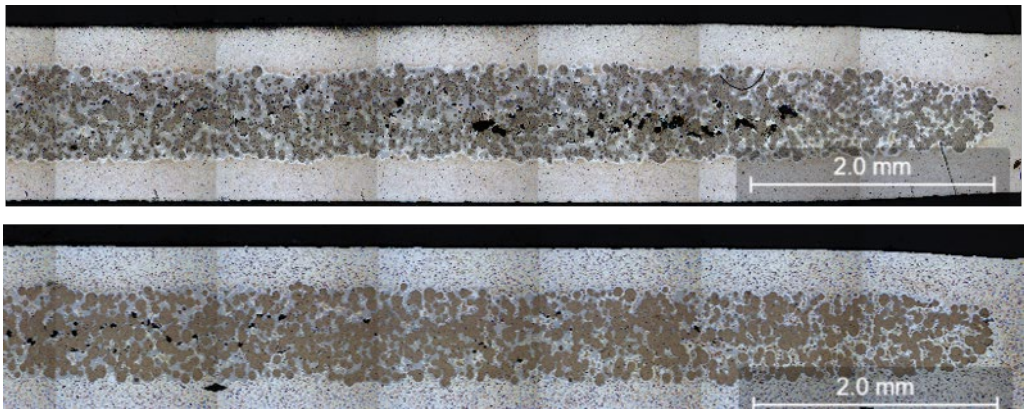

Figure 3. Optical microscopy images of plate 109 (top, IL volume fraction = 37.8%) and plate 512 (bottom, IL volume fraction = 29.8%).

At this fission density (~3.1 × 10^{21} fissions/cm^3 fuel meat), type 5 plates exhibit similar microstructure as the type 1 plates, an indication that the coating has been consumed, allowing for the formation of extensive interaction layer and fission gas bubbles. A further indication of this coating consumption is that the swelling of plate 512 has started "catching up" to the swelling behaviour of plate 109. Higher-resolution electron microscopy will be needed to confirm the consumption of the coating.

3. Plate Types 7A and 8

A comparison of plate types 7A (PVD coated, not heat treated, zero fines) and 8A (PVD coated, heat treated, zero fines) was conducted. A comparison of the plate average fuel meat swelling of these two plate types is shown in Figure 4.

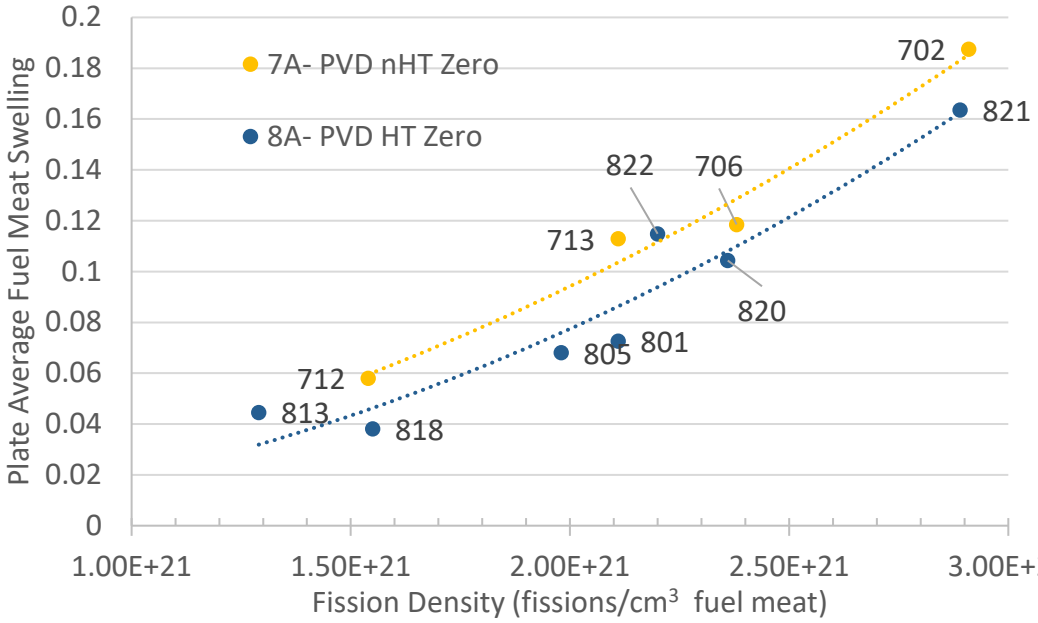

Figure 4. Plate average fuel meat swelling of plate types 7A (PVD coated, not heat treated, zero fines) and 8A (PVD coated, heat treated, zero fines).

Although the heat treatment could be influencing the difference in plate-average fuel meat swelling observed here, the analysis presented in reference [1] did not find that heat treatment had a significant impact on swelling behaviour. The other difference between these two plate types is the coating thickness. Plate type 7A coating thickness was 1.17μm, while plate type 8A coating thicknesses ranged from 1.32μm to 2.02μm (three different coating batches). In fact, the only type 8A with a coating thickness of 1.32μm (plate 822), has plate average fuel meat swelling in line with the type 7A plates. The optical microscopy of the two highest fission density plates are shown in Figure 5.

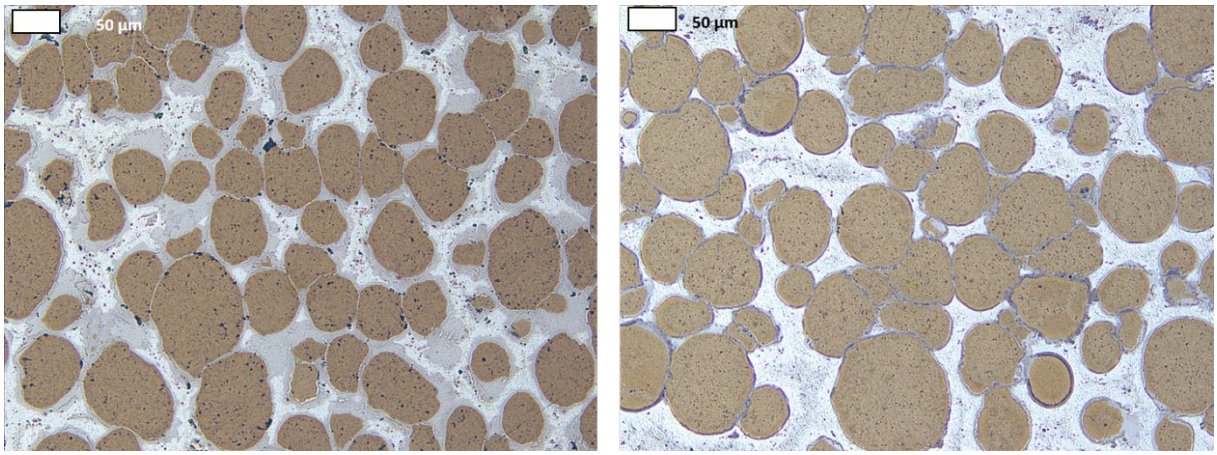

Figure 5. Optical microscopy of plates 702 (left, IL volume fraction = 22.7%) and 821 (right, IL volume fraction = 6.8%).

Figure 5 shows plate 702 has more IL than plate 821, though similar fuel meat swelling. This indicates that the IL likely formed later in the irradiation than in plate 109 (where IL and bubbles can be observed, and the fuel meat swelling is high). The late formation of the IL in plate 702 might be attributed to the larger coating thickness compared to plate 109. Meanwhile, the lack of observable large fission gas formation in the IL of plate 702 can be attributed to the fact that the fission rate at higher burnups is low enough that fission gas mobility decreases, inhibiting the formation of large gas bubbles in the IL.

4. Conclusions and Future Work

The EMPIrE experiment demonstrated that the coated UMo-dispersion fuel system is robust and generally insensitive to most fabrication parameters, with the exception being coating thickness .The following may be deduced from the completed non-destructive examination [1], the current meat swelling analysis, and the partially completed destructive part of the PIE:

- The ZrN coating on the U-Mo particles is effective in reducing fuel-Al interaction layer formation. However, depending on the thickness of the coating layer, it may lose its protective capability under irradiation and enable IL formation.
    - This was evidenced in PVD plates by comparison of the IL growth in type 7 and 8 plates. This increase in IL formation in type 7 plates (thinner coating, see Table 1) likely occurred closer to the end of the irradiation, as the IL volume fraction in type 7 plates was similar to type 8 plates at lower fission densities. At sufficiently high burnups, the fission rate is low enough that fission gas mobility decreases such that large gas bubbles do not form in the IL.
        - Increased IL formation (~22 volume %) was observed in type 7 plates at ~3×10^{21} fissions/cm^3 fuel meat (equivalent to ~ 6×10^{21} fissions/cm^3 fuel particle) while type 8 plates only exhibited ~7 volume % IL at similar fission densities
        - Plate type 7A has higher plate swelling and IL formation than plate type 8A. Bubbles in the IL can be observed in plate 702, while they are absent in plate 821.

        - The bubbles observed in plate 702 are smaller than those observed in the type 1 plates.
    - In the case of the ALD coated particles, which had a relatively thin coating (particularly type 1 plates), an increase in IL volume fraction occurred early in the irradiation, when the fission rate is still high. This may lead to a condition where large fission gas bubbles can form at the IL-matrix interfaces (as seen in Figure 2), resulting in increased plate swelling and probability of plate failure by pillowing.
        - Type 1 plates (amongst the thinnest coatings in the experiment, see Table 1), exhibited high IL formation (up to ~48% in plate 117at a fission density of only 2.2×10^{21} fissions/cm^3), indicating that the increased IL formation started earlier (when fission gas mobility was higher) than type 7 plates, which exhibited increased IL formation at fission densities closer to 3×10^{21}, and had thicker coating than Type 1 plates.
    - This experimental observation indicates that specification of the ZrN layer is important.
- The lower swelling of the type 8 plates indicates that heat treatment of the U-Mo particles seems to have the expected reducing effect on plate swelling, although the ALD plates do not show a clear influence of heat treatment on plate swelling.
    - DE is needed to determine the effect of heat treatment on the irradiated fuel particles, in particular if recrystallization was delayed.
- The non-destructive examination is inconclusive on the impact of the fraction of fines on the plate swelling behavior. Destructive examination is needed to determine this behavior.

While differences are observed between plate-types non-destructively, until high precision destructive examination is available, the full mechanistic effect of EMPIrE variables on fuel swelling cannot be fully determined. Therefore, the information obtained in this analysis cannot to be used for the purpose of fuel design specification. However, it should be emphasized that, with the exception of plate type 1 (which exhibited a high level of interaction layer formation), all plates in the EMPIrE experiment exhibited acceptable irradiation performance.

5. Acknowledgment

This work was supported by the U.S. Department of Energy, National Nuclear Security Administration (NNSA), Office of Material Management and Minimization (NA-23) Reactor Conversion Program. The submitted manuscript has been created by UChicago Argonne, LLC, Operator of Argonne National Laboratory ("Argonne"). Argonne, a U.S. Department of Energy Office of Science laboratory, is operated under Contract No. DE-AC02-06CH11357. The U.S. Government retains for itself, and others acting on its behalf, a paid-up nonexclusive, irrevocable worldwide license in said article to reproduce, prepare derivative works, distribute copies to the public, and perform publicly and display publicly, by or on behalf of the Government.

6. References

1. Hanson, W. A., et al., *Non-Destructive Analysis of Swelling in the EMPIrE Fuel Test.* Journal of Nuclear Materials, 2022. **564**.
2. Van den Berghe, S. and P. Lemoine, *Review of 15 years of high-density low-enriched UMo dispersion fuel development for research reactors in Europe.* Nuclear Engineering and Technology, 2014. **46**(2): p. 125-146.
3. Van den Berghe, S., A. Leenaers and C. Detavernier. *The SELENIUM Fuel Experiment - Progress Report After 2 Cycles*. in *International Meeting on Reduced Enrichment for Research and Test Reactors*. 2012. Warsaw, Poland.
4. Leenaers, A., et al., *ZrN coating as diffusion barrier in U(Mo) dispersion fuel systems.* Journal of Nuclear Materials, 2021. **522**.
5. Iltis, X., et al.; *CEA. 2018.* Private communication to FDEG.

6. Iltis, X., et al. *Characterization of fresh EMPIrE and SEMPER FIDELIS plates made with PVD-coated U(Mo) particles*. in *RRFM*. 2018. Munich, Germany.
7. Housaer, F., et al., *Morphological characterization of the fresh ZrN coated UMo powders used in EMPIrE irradiation experiment: A practical approach.* Journal of Nuclear Materials, 2020. **533**.
8. Leenaers, A.; *Production Report EMPIRE Powder*. SCK-CEN/12662511. SCK-CEN (2016).
9. Trowbridge, T., D. Keiser and C. Brizzee; *EMPIrE Fresh Fuel Characterization Report*. INL/EXT-20-59404. Idaho Falls, ID:Idaho National Laboratory (2020).

CURRENT STATUS OF KIJANG RESEARCH REACTOR

S. H. KIM, J. S. RYU, H. C. KIM, D. W. LEE, M. H. KIM
New Research Reactor Project Group, Korea Atomic Energy Research Institute (KAERI)
111, Daedeok-daero 989 Beon-Gil, Yuseong-gu, Daejeon – Republic of Korea

ABSTRACT

The KiJang Research Reactor (KJRR) is a research reactor with thermal power of 15 MW. KJRR aims to produce and supply important medical radioactive isotopes such as Mo-99 and to produce semiconductors through the Neutron Transmutation Doping (NTD). The KJRR will be constructed in Gijang-gun, located in the southeast of the Korean Peninsula, and the construction site is near the Kori Nuclear Power Plant. KJRR obtained a construction permit from NSSC, a regulatory body, on May 10, 2019. Preparations for construction were completed and construction began in May 2022. The operation permit application is scheduled to be made in the middle of 2023. The first criticality is planned for early 2027 considering the five-year construction period and time required to review the application for operating license.

1. Introduction

The KiJang Research Reactor (KJRR) is an open-tank-in-pool type research reactor with thermal power of 15 MW. The KJRR aims to produce and supply important medical radioactive isotopes such as Mo-99 and to produce semiconductors through the Neutron Transmutation Doping (NTD). Currently, in South Korea, the major medical radio-isotope, Mo-99, has been supplied entirely by importing it from foreign countries. The KJRR is going to supply Mo-99 more than enough to meet the national demand and look for a chance to supply it for the international market. The NTD service will assist in expanding the semi-conductor industry after the KJRR operation.
By constructing and operating the KJRR, we are going to demonstrate new technologies such as U-Mo fuel, Bottom-mounted control rod driving mechanism, and Fission-Molybdenum production process. As one of the outcomes we are willing to achieve through this construction project, technologies for these items relating to the design, construction, installation, and operation would be advanced enough to apply to future research reactor projects. The key technical specification [1] is summarized in table 1.

Parameter	Value
Power	15 MW
Reactor Type	Open-tank-in-pool type
Max. thermal neutron flux	> 3×10^{14} (n/cm^{2}s)
Annual operation	~ 300 days
Fuel	Plate type, U-7Mo (19.75% enriched)
F-Mo Target	UAlx plate type (LEU, 2.6 g/cc)
Reflector	Be and Al
Coolant and Cooling method	H_2O, downward forced convection flow
Decay heat cooling	SRHRS and natural circulation by flap valves
Reactor building	Confinement

Tab 1: KJRR Design Specification

Before the KJRR, there are four research reactors in South Korea. Two of them are TIRGA-type research reactors built in the 1960s and they are decommissioned now. Kyung Hee University has been operating AGN-201K (10 W) since 1982 for the education service of reactor experiments. HANARO (High-flux Advanced Neutron Application ReactOr) is a 30 MW thermal power multi-purpose research reactor. Korea Atomic Energy Research Institute (KAERI) has designed, constructed, and operated the research reactor since 1995. This research reactor works as a national nuclear basic research platform by fulfilling national demands and various needs from outside of the institute. HANARO has equipped various thermal neutron beam instruments such as the High-Resolution Powder Diffractometer, the Residual Stress Instrument, the Neutron Radiography Facility, and so on.
The KJRR will be constructed in Gijang-gun, Busan, located in the southeast of the Korean Peninsula, and the construction site, which is 130,000 square meters in total, is near the Kori Nuclear Power Plant. The KJRR will be one of the most important facilities in the Southeast Area radiological & medical Sciences industrial complex along with Dongnam Institute of Radiological and Medical Sciences (DIRAMS) and Heavy Ion Medical Accelerator (KIMA).
Reactor building, Utility building, Fission Molybdenum Production Facility (FMPF) building, Radio-Isotope Production Facility (RIPF) building, Radio-Waste Treatment Facility (RWTF) building, and other supporting facilities are going to be constructed on the same site. Figure 1 shows the bird's eye view of the KJRR. The RIPF building houses hot cells and ancillary facilities and produces radio-isotopes and radiopharmaceuticals. In the RWTF building, liquid and solid radioactive waste generated during the research reactor operation are processed and the treated waste is stored.

2. Characteristics of KJRR [2]

The core is composed of several nuclear fuel assemblies, control devices, and irradiation holes. The core is located inside the rectangular core box, and the beryllium and aluminum reflectors are located outside. A total of 22 nuclear fuel assemblies are loaded in the core, 16 are standard fuel assemblies and six of them are follower fuel assemblies. The uranium density of a standard fuel plate is 8.0 g-U/cm^3. The follower fuel assembly is loaded in an aluminum alloy control rod guide tube. A neutron absorber made of hafnium (Hf) is connected to the upper part of the six follower fuel assemblies and can move up and down in the control rod guide tube. Four of them are control rods used for reactor control and primary shutdown system. During operation, the fuel assembly moves to the lower part of the core, and the neutron absorber is partially inserted into the core. The remaining two control fuel assemblies are used as secondary stopping rods. During operation, the neutron absorber is completely withdrawn to the top of the core so that the fuel assembly can be positioned at the same height as other standard fuel assemblies. And when the reactor shuts down, the follower fuel assemblies move to the lower part of the core and the neutron absorber is inserted.

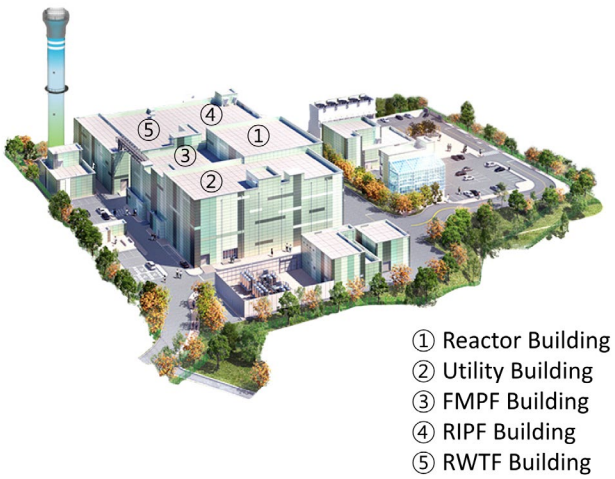

Fig 1: Bird's Eye View of the KJRR

The reactor structure assembly is positioned at the bottom of the reactor pool, which is filled with demineralized water. It consists of reactor cover assembly, neutron detector assembly, grid plates, upper guide structure assembly, fuel assemblies, reflectors, and control rods. It provides flow paths of the cooling water, supports the fuel assemblies and reflectors, and controls movements of the control rods and shutdown rods. The reflectors are beryllium and aluminum. The outer core reflectors have irradiation holes for the NTD.

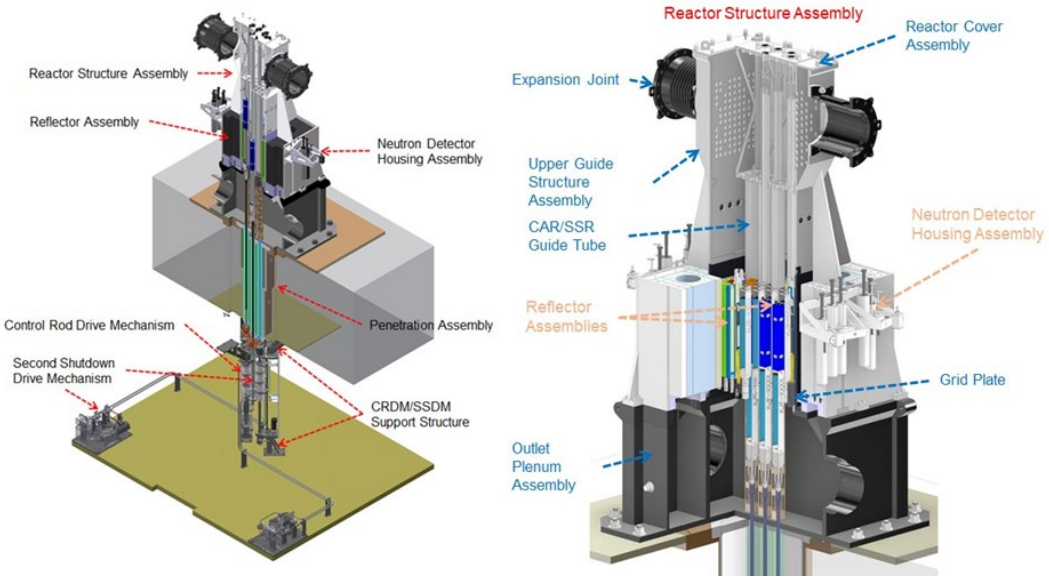

Fig 2: Reactor Structure Assembly

The pool is a concrete structure including a stainless steel plate liner and consists of the reactor pool, the service pool, and the spent fuel storage pool. The reactor assembly, reactivity control device, fuel assemblies, primary cooling system piping, FM cooling device, reactor pool platform, etc. are installed inside the reactor pool. The reactor core is loaded with radio-isotopes and irradiated materials for semiconductor production. The reactor pool plays a role in removing residual heat generated from the core when the primary cooling system loses its function and shields the upper part of the pool.

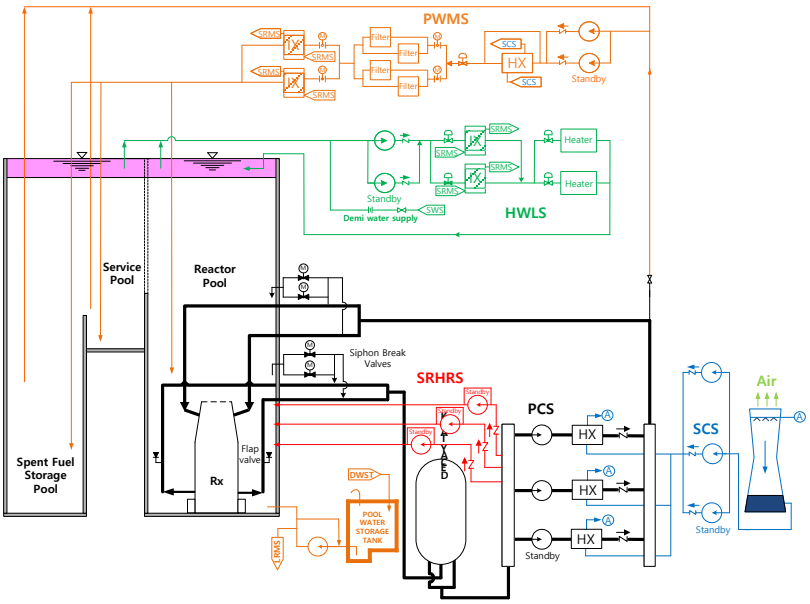

Fig 3: Reactor Cooling and Connected System of the KJRR

The service pool is connected to the reactor pool through the pool door, and the irradiated object handling device and storage rack, the reactor components storage rack, the service pool platform, etc. are installed in the service pool. The spent fuel storage rack and the transfer elevator are installed inside the spent fuel storage pool. The pool water plays a role in cooling the decay heat of spent nuclear fuel and providing a shield from radiation. In addition, the transfer elevator connects the reactor area and the hot cell of the FMPF building and provides a passage for the transport of the irradiated object.

Reactor Cooling and Connected System of the KJRR consists Primary Cooling System, Secondary Cooling System, Pool Water Management System, Hot Water Layer System, and Safety Residual Heat Removal System. The Primary Cooling System provides flow to remove the heat generated in the reactor core and transfer it to the secondary side through the heat exchanger. The Secondary Cooling System dissipates the heat from the Primary Cooling System through cooling towers. The Pool Water Management System purifies and cools down the pool water. The Hot Water Layer System generates the hot water layer on top of pool water. It lowers radiation exposure on the workers at the pool top by preventing highly radioactive water at the pool bottom from rising to the top.

The Safety Residual Heat Removal System maintains downward flows in the core for a certain time after the Primary Cooling Pumps are stopped. Before the upward natural circulation occurs, it prolongs the downward flow time with the flywheel on the Primary Cooling Pumps to provide enough flow to cool down the core. With this engineering safety feature, the reactor can operate within the safety limit even during the core flow reducing accidents such as loss of external power. When the core flow is diminished to a certain value, flap valves installed at the core outlet pipe open passively and provide the natural circulation path to cool the core afterward.

The instrumentation and control system is a system for protecting, controlling, and monitoring nuclear reactor facilities, and it is a system that provides related equipment so that the operator can safely operate the research reactor. The design criteria for the instrumentation and control system of the KJRR are divided into control, protection, and monitoring functions by the defense-in-depth philosophy. Digital technology to improve operation and maintainability and ergonomic design principles to reduce operator's human error and operational burden are applied to the instrumentation and control system of the long-term research reactor. The I&C systems of KJRR consist of Reactor Protection System, Reactor Regulation System, Accident Monitoring System, Alternative Protection System, Automatic Seismic Shutdown System, Radiation Monitoring System, and Main Control Room.

The FM target is produced by dispersing UAlx particles on an aluminum matrix. In order to produce Mo-99, it is irradiated for a short irradiation period of about a week at a target irradiation hole in the core. It is irradiated with a low burnout of about 5% U-235. The FM production facility produces a solution of Mo-99, a radiopharmaceutical raw material, through a series of chemical processes from irradiated low-enriched uranium FM targets. For this purpose, the FMPF is equipped with a transfer elevator, hot cells, waste handling and storage facility, testing and quality inspection facility, transfer facility, and ventilation facility. The irradiated target is transported via a transfer elevator from the reactor pool to the FMPF. The FMPF is equipped with a connecting passage for the transfer of the irradiation target and solution to the RIPF building, and a connecting passage and transfer pipe for transferring liquid and solid waste to the RWTF building. The FM production process equipment is installed inside the FM production hot cell, and after dissolving the FM target with an alkaline solution, Mo-99 is separated from other fission products such as inert gas and radioactive iodine and purified.

3. Works after Construction Permit

Several experiments as preparation for the operating license application have been conducted during this time.

For utilization of U-Mo fuel in KJRR, it is required to verify the design and manufacture of fuel and to qualify for supply it. The irradiation test of the fuel assembly is performed at the Advanced Test Reactor (ATR) of the Idaho National Laboratory (INL) in the US to confirm the

fuel integrity and irradiation stability. The manufacture of the test fuel assembly was completed and delivered to INL in October 2014. The requirements of the irradiation test were set so that the achieved burnup and heat flux conditions included those of the research reactor conservatively. The irradiation test started in November 2015 and was completed in February 2017 [3, 4]. The cooling of the irradiated fuel assembly was finished and the post-irradiated examination (PIE) is completed expect the publication of the PIE report.
Critical Heat Flux experiments for the narrow rectangular channel flow are conducted to verify the appropriateness of the Sudo-Kaminaga correlation to the fuel assembly geometry. This correlation has been widely used in various research reactors. The experimental results obtained for the same geometries and flow conditions as a flow channel of the fuel assembly and a flow channel between the fission molybdenum target plates showed a good match with the correlation.
An experiment is designed as a full scale and performed to obtain the flow rate distribution at each fuel assembly in the core. The result will be used to be compared to the previous results by a simple hydraulic code and computational fluid dynamics.
Another experiment is performed for understanding the flow characteristics inside the decay tank. To get an idea of the flow in the tank during and after the accident, we have designed the experiment with a full-scale decay tank and a water level of the reactor pool to remove questions that may arise after scaling.
Aside from those experiments, several works that are required to support licensing documents are planned and in progress. Those works are cyber security assessment and evaluation, preparation of the operational technical specification and radiological impact on the environment review, etc.

(a) CHF experiment loop (b) Decay Tank test loop

Fig 5: Experimental facilities for KJRR

4. Brief History and Future Plans

The KJRR project has started in 2012. The two-step licensing process for the construction of a research reactor in South Korea is applied. As the first step, the construction permit was applied to the Nuclear Safety and Security Commission (NSSC), the national nuclear regulatory body, in 2014 after a conceptual and basic design for 2 years. During the review by NSSC and the KINS, the entrusted technical reviewer, the strongest earthquake in the national history (M_L 5.8) near the construction site occurred in September 2016. And there was another earthquake of M_L 5.4, the second-strongest, in another city in November 2017. After a detailed review was performed to verify the safety of the KJRR structural design, NSSC finally approved the construction permit in May 2019.

Last three years, KAERI has been preparing for the KJRR construction. The project team was recruited and reorganized to get ready for the construction. We made contracts with vendors for major components, such as Reactor Structure Assembly, Primary Cooling Pumps, Flap Valves, and Heat Exchangers. Recently, a consortium of construction companies, which has much experience in nuclear power plant construction projects, has joined the project. Several construction change permits are applied recently. The first stage of the preoperational inspection was submitted to the regulatory body.
To name a few milestones for the construction, the first concrete will be poured in February 2023. It was planned to be 60 months for the construction of the whole facility. The documents are planned to be prepared for submission of the operating license in mid-2023. The Final Safety Analysis Report (FSAR) and other documents for the operating license are being prepared. As the construction has proceeded, preoperational inspection and test will be performed by the regulatory body following the pre-determined schedule.
We made a plan to obtain an operating license for KJRR in early 2027. And then we will load fuel assemblies in the core and conduct the Reactor Performance Test to verify whether the reactor works as it has been designed.

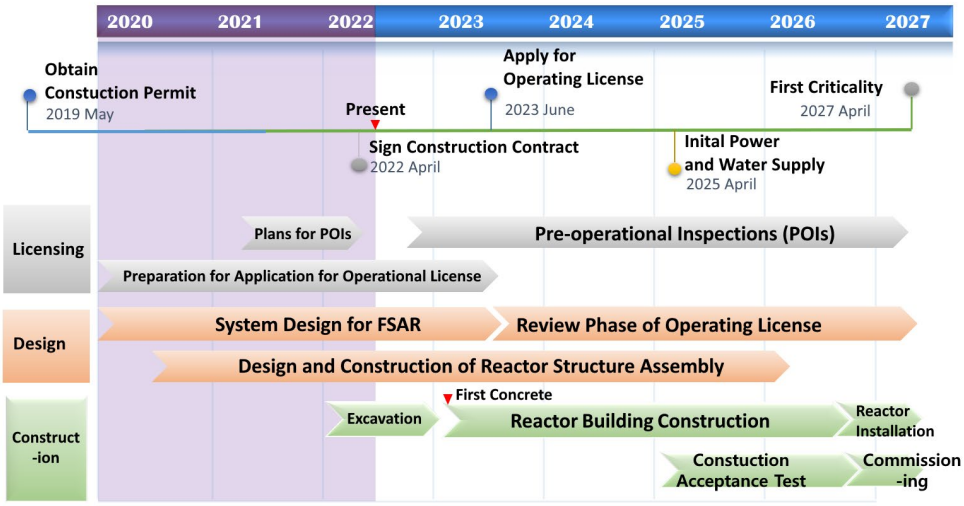

Fig 6: Brief Schedule

5. Conclusions

The KJRR construction project started in April 2012. This project has been planned and proceeded in order to meet the national and regional demand for medical and industrial radioisotopes, to expand the semiconductor industry, and to demonstrate the new research reactor technologies. KAERI has been reorganizing the project team and has made contracts with the construction company and major components suppliers since the construction permit was obtained. To obtain the operating license in April 2027, as in the schedule, construction work along with licensing is going to be conducted.

6. References

[1] Top Tier Requirements of Kijang Research Reactor, KJ-000-KT-405-001.
[2] Preliminary Safety Analysis Report of KJRR, 2015.
[3] K. H. Lee et al., “Current Status of Kijang Research Reactor Project,” KNS Spring Meeting, Jeju, Korea, 2018.
[4] J. S. Yim et al., “On-going Status of KJRR Fuel (U-7Mo) Qualification,” No. INL/CON-17-41243, Idaho National Lab., Idaho Falls, ID (United States), 2017.

DELICENSING THE CONSORT NUCLEAR LICENSED SITE

H.J. PHILLIPS,
Corporate risk Associates, V407 Vox Studios, 1-45 Durham Street, London, SE11 5JH

T. CHAMBERS, R. MANSON
Imperial College London, South Kensington Campus, London SW7 2AZ

S. WILCOX, L. TAYLOR
Orano Ltd, Suite 7, Hitching Court, Abingdon Business Park, Abingdon, Oxfordshire, OX14 1RA

ABSTRACT

The final part of the CONSORT 100kW research reactor decommissioning programme was to revoke the nuclear and environmental regulatory requirements on the site and to return it to a brown field site suitable for any use.
In early 2021, dismantling of site was completed with the demolition of the reactor building and the adjoining laboratory and office building. The ground slab and drainage systems which ran beneath them were removed, leaving only the final land remediation to be completed, which was put on hold awaiting regulatory confirmation that no further sampling of the site was required prior to deregulation.
Imperial College held a nuclear site licence for the CONSORT reactor and environmental permits for both the nuclear site and the adjoining laboratories. The process of revoking the site licence and permits was approached as one project, although separate cases had to be submitted to the nuclear and environmental regulators. Delicensing cases were based on a historical review of site activities and sampling and analysis with the objective of demonstrating that residual radionuclides and other contaminants presented no danger to the public or environment.
The College contracted Orano, who had experience of delicensing other UK nuclear sites using the Data Quality Objectives (DQO) methodology, to support the CONSORT delicensing Project.
Early engagement with the regulators (Office for Nuclear Regulation (ONR) and the Environment Agency (EA)) was essential to agree the approach to deregulation prior to completion of decommissioning. This ensured that required sampling took place at the right points in the decommissioning programme.
The DQO methodology allowed the College to optimise the sampling process, by designing a targeted, statistically robust sampling plan based on site history and pre sampling data.
The sampling programme covered

- pre sampling of the building and base slabs for radiological and chemical contaminants and off-site soil sampling to characterise the local background levels.
- the main sampling programme for radiological contaminants of concern and asbestos in soil from below the buildings and ground slabs.
- Ground water sampling from the area around, and on the licensed site.

Sample analysis was a mix of in-house gamma spectroscopy and beta counting, and independent laboratory measurements for some specific radionuclides, asbestos and chemicals. Some parallel independent monitoring, sampling and analysis was carried out on behalf of the regulator.

1. Introduction

The CONSORT Reactor was a 100kW, light water cooled and moderated research reactor which operated at Imperial College's Silwood Park Campus from first criticality in April 1965 to final shutdown in December 2012.

The reactor was defueled in June 2014 under a modification to the operational safety case. Decommissioning started in November 2015 following regulatory approval of the decommissioning safety case. Decommissioning was divided into a number of phases. The early phases were carried out in-house and included removal of the reactor start-up source, the control rods and the remaining in-core fixed items. A specialist decommissioning contractor was bought in for the later phases, including dismantling of the reactor vessel and surrounding concrete bioshield, asbestos removal, demolition of the buildings and removal of the ground slab and underground structures.

The final part of the CONSORT 100kW research reactor decommissioning programme was to revoke the nuclear and environmental regulatory requirements on the site and to return it to a brown field site suitable for any use. The Nuclear Site Licence was revoked on 31st March 2022. This paper discusses the approach taken to deregulate the site, revoking the Nuclear Licence and Environmental Permits.

2. Approach to deregulation of site

Imperial College London adopted the use of the DQO methodology for the deregulation project to ensure that technically and statistically robust decisions were made relating to the radiological status of the site. The DQO methodology streamlines procedures, minimises time requirements and eliminates unnecessary costs while balancing the need for reliable environmental data that addresses regulatory requirements and other stakeholders' concerns.

The College brought in specialist support from Orano Ltd, who were experienced in applying the DQO methodology to delicensing/deregulation of nuclear licensed sites in the UK.

Throughout the decommissioning programme, the College had sought to maintain open communications with the nuclear and environmental regulators, to ensure that they were informed of proposed plans and kept up to date with progress. The College set up a regulatory interface forum (RIF) for delicensing, which incorporated the key stakeholders in the delicensing process.

- Office for Nuclear regulation (Safety and Security)
- Environment Agency
- UK Health Security Agency (UKHSA) (Providing independent sampling and analysis for ONR)
- Orano Ltd (Contractor Support for delicensing using the DQO methodology)

This had benefits of early agreement on deregulation criteria and ensuring sampling and analysis were scheduled in the decommissioning programme.

3. Details of Site to be Deregulated

The Imperial College Reactor Centre (ICRC) comprised of an area of grounds (~ 3000 square metres) at the College's Silwood Park Campus. Part of the ICRC was a Nuclear Licensed Site (NLS) which also held an environmental permit (blue area in figure 1), while the rest of the ICRC, or Non-NLS, held separate environmental permits (pink area in figure 1).

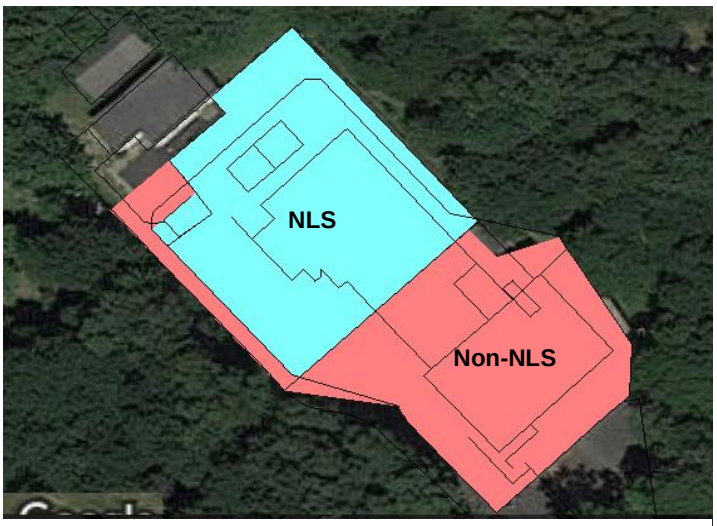

Figure 1: ICRC Footprint for Deregulation

All of the following structures and services were removed from the ICRC as part of the decommissioning programme, and disposed of via the most appropriate waste route:

- Reactor Building (including all internal equipment and structures) and its foundations
- Adjoining Office and Laboratory Building (EAS), (including all internal equipment and structures) and its foundations
- Workshop (including all internal equipment and structures) and its foundations
- Delay Tank and its pit base / bund
- All manholes and drainage structures
- All made ground, including all brick, concrete and tarmac
- All services (electric cabling, pipework, etc.) in the ICRC footprint, including all structures located below ground
- All soil / overburden from excavation activities.

Figure 2: Imperial College Reactor Centre

4. Clearance Criteria for deregulating the site

4.1 Delicensing

The CONSORT NLS operated under a licence issued by the ONR in accordance with the Nuclear Installations Act 1965 (NIA65). For a nuclear site licence to be revoked at the same time as the licensee is released from their period of responsibility for the site, the ONR has to be satisfied that there is "No danger" from ionising radiation from anything on the site to be delicensed [Ref. 1].

The "No danger" criterion requires: *"…a demonstration that any residual radioactivity, above background radioactivity, which remains on the site, which may or may not have arisen from licensable activities, will lead to a risk of death to an individual using the site for any reasonably foreseeable purpose of no greater than 1 in a million per year*" [Ref. 2, 3].

Such a level of risk is considered to be "broadly acceptable" and broadly equates to doses to members of the public of the order or 10 μSv per year or less. The IAEA safety guide on the Application of the Concept of Exclusion, Exemption and Clearance (RS-G-1.7) [Ref. 4] defines activity concentration levels (in Bq/g) that correspond to annual doses of up to 10 μSv per year for the exposure of receptor groups via different pathways. These are nuclide specific and are the most limiting activity concentrations from the different pathways considered.

In addition, the overarching requirements of the Health and Safety at Work Act 1974, which requires that risks are reduced As Low As Reasonably Practicable (ALARP), still apply. ONR expect the operator to demonstrate that it has also considered the overall ALARP requirements. However, if the ONR judges that the operator has demonstrated that the residual risk has been reduced to less than 1 in a million ("No Danger"), this will usually be sufficient to satisfy all of its substantive concerns [Ref. 1].

4.2 Environmental Permit Surrender

In order to surrender the Environmental Permit(s) and hence be released from Radioactive Substances Regulation (RSR), the EA expectation is that the requirements set out in the Guidance on Requirements for Release from Radioactive Substances Regulation (GRR) [Ref. 5] are met. This guidance states that operators of a NLS intending to be released from the obligations of their Environmental Permit are required to fulfil the "Fundamental Protection Objective", which is to ensure that their site is returned to a condition in which it can be safely released from RSR, known as the "Site Reference State". To meet this objective, the guidance requires operators to:

- Produce a waste management plan
- Produce a site-wide environmental safety case and ensure the condition of their site meets EA standards for protection of people and the environment, now and in the future.
- GRR sets out fifteen individual requirements that form the key obligations of the guidance. The EA expects an operator's case for the release from RSR to demonstrate; either that no radiological hazard remains on a site; or that all the requirements set out in the guidance are met.

GRR states that *"…we presume that any site (or part of a site) in which levels of radionuclides do not exceed the RSR out-of-scope values* [Ref. 6]*, meets the standard for release from RSR."*.

The derived activity concentration limits in RS-G-1.7 are equal to, or more restrictive than the Out of Scope criteria in the Environmental Permitting regulations (EPR) [Ref. 6]. Hence, if the ONR "No danger" criterion is met, the site also meets the radiological standard for release from RSR.

4.3 Selected Deregulation Criteria

To maintain a consistent approach to deregulation, the College decided to apply the same decision-making and sampling process to both the NLS and N-NLS regions, using the most restrictive activity concentration limits. This was a conservative approach as there is no legal requirement to meet “No danger” in areas outside the NLS.

In order for the College to satisfy both the requirements of the ONR and EA, a comparison of the “No danger” and Out of Scope target criteria were made. The most restrictive criteria were carried forward which resulted in a set of Deregulation Criteria for all radionuclides.

An individual assessment of each identified Contaminant of Concern (COC) was undertaken to determine whether the activity of individual radionuclides is less than or equal to its respective Deregulation Criterion.

Additionally, an assessment of whether the sum of the identified radionuclide activities divided by their respective Deregulation Criteria is less than or equal to 1 was carried out, i.e.

$$\frac{C_1}{D_1} + \frac{C_2}{D_2} + \cdots + \frac{C_n}{D_n} \leq 1$$

Where:

C is the activity of the COC;

D is the deregulation criterion for that COC

This ensured the “No danger” criterion was still met when all radionuclides were considered collectively.

5. Data Quality Objective / Data Quality Assessment (DQO/DQA) methodology

5.1 The DQO Process

The DQO process, as defined by the United States Environmental Protection Agency (USEPA), is a series of planning steps used to identify more efficient and timely data collection programmes. The process relies heavily on customer-supplier communication to define data requirements and acceptable levels of errors in decisions before major resources are expended, to ensure the customer is satisfied with the results.

There are seven steps in the DQO process. Stakeholders decide and record the logic required to define the type, quality, and quantity of data needed for environmental decision-making by working through these steps.

5.2 History File

A History File for the ICRC was produced, which documented the operational history of the ICRC, with the main aim to identify the Contaminants of Potential Concern (COPCs) for the site and any areas of higher radiological risk. This document formed the basis for the DQO study and therefore supported the generation of the Sampling and Analysis Plans (SAPs).

The information presented in the History File was generated from various sources including, but not limited to:

- periodic safety reviews of the site
- incident reports
- decommissioning safety case and associated modifications
- analysis of samples taken and surveys of buildings
- site visits and discussions with ICRC personnel
- interrogation of Imperial College London archives

5.3 Contaminants of Potential Concern (COPCs)

A set of contaminants of potential concern were identified from the history file. As an example, those initially identified for the reactor building included

Reactor Building	Ac-228, Ag-109m, Ag-110m, Al-28, Am-241, C-14, Cd-109, Cd- 113m, Cf-252, Co-59, Co-60, Cr-50, Cr-51, Cs-134, Cs-137, Eu- 152, Eu-154, Fe-55, H-3, Kr-85, Mg-27, Mn-54, Mn-56, Na-24, Ni- 63, Rb-87, Sb-125, Tl-204, W-186, W-187, Zn-65

These COPCs were reviewed as part of the DQO process to determine whether any could justifiably be removed from the scope of the study. In the first instance a set of high-level exclusion criteria were applied which consisted of the following:

- radionuclides with very short half-lives and short-lived daughters
- radionuclides present as sealed sources with no relevant abnormal events
- noble gases
- naturally occurring radionuclides not present as a result of operations.

Following this, further radionuclides were excluded after a more detailed evaluation of operations and recent characterisation data.

5.4 Pre-sampling programme and contamination monitoring

The College carried out a pre-characterisation sampling and monitoring campaign prior to the DQO process, in order to gain additional evidence to exclude certain radionuclides from further assessment. This work involved taking core samples from the exposed building slabs of the Reactor Hall, EAS, Workshop and Delay Tank, in areas of perceived higher risk. A non-intrusive radiological walkover survey (ScanPlot) across the full site was carried out to identify any contamination hot spots present on the ICRC site.

5.5 DQO Workshop

ICRC held a DQO Workshop (January 2021), which was delivered by Orano, who were facilitating the DQO process for the deregulation project and was attended by a multi-disciplinary team of ICRC personnel who collectively formed the DQO Planning Team. Representatives from UKHSA (see section 6) were in attendance in their role as formal stakeholders. PHE attended to observe the DQO process and did not participate in the decision-making activities. However, they were undertaking an independent verification of the process for the ONR. Members of the ONR were also in attendance as observers.

The workshop began with a presentation of the ICRC History File findings and a full review of the recorded Abnormal Events. Following this, the DQO Planning Team were taken through the steps of the DQO process to agree on the sampling and monitoring strategy for the site.

5.6 DQO Decision - Zoning Strategy and Sampling Requirements

Following a full review of the information collected, including the History File, recorded abnormal events and recent pre-characterisation sampling results, the DQO Planning Team applied a set of exclusion criteria to the list of COPCs identified in the History File. After detailed discussions Am-241, Co-60, Cs-137, Eu-152 and H-3 were identified as the final COCs for assessment as part of the DQO process.

Contaminants of Concern	Selected Deregulation Limits (Bq/g)
Am-241	0.1
Cs-137	0.1
Co-60	0.1
Eu-152	0.1
H-3	100

Table 1 – COCs and deregulation limits

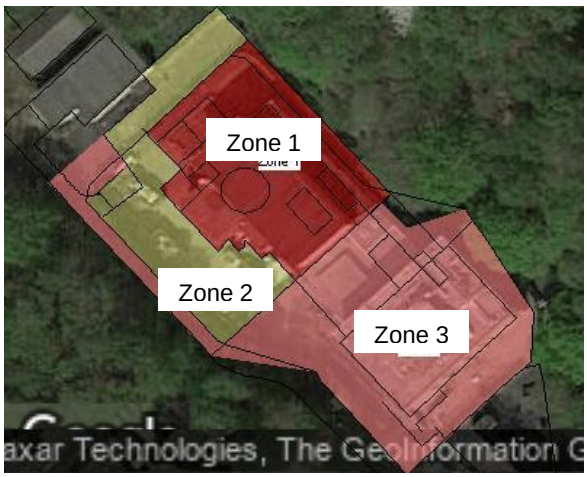

Figure 3: A map of the zoning strategy

For sampling purposes, the DQO Planning Team decided to consider the ICRC site as three discrete zones. The NLS was split into Zones 1 and 2, while the remainder of the site (N-NLS) was named Zone 3.

The DQO Planning Team decided that the 95% Upper Confidence Limit (UCL) on the sample mean (in Bq/g) would be used as the appropriate parameter to compare against the deregulation criteria.

It was also decided that the Minimum Detection Limit (MDL) (in Bq/g) would be substituted as the reported result, for all non-detects. This was a conservative approach.

Zones for the DQO process were assigned a classification which determined the type of sampling regime required. Each zone was given a Type B classification which resulted in 5% α / β error rates (and 95% confidence in the survey design). This aligns with the industry best practice to have a 95% confidence level [Ref. 7].

Classification	Definition	Intrusive Samples	Surface Contamination Surveys
Type B	Areas that have potential for contamination but are unlikely to be above the relevant criteria.	Random grid sampling. Some limited, intrusive judgemental sampling may be required to provide assurance that relevant thresholds have been achieved	Some limited targeted surface contamination surveys on non-absorbent surfaces may be required to further underpin the intrusive regime.

Table 2**:** Definition Type B Area Classification and Associated Sampling Regime

The agreed sampling matrix in each zone was grounds (soil, clay, sand, etc.), as this was the only remaining material following the decommissioning process. Samples were to be taken from the ground surface.

The DQO Planning Team also decided that additional judgemental samples should be added in the footprint locations of some of the former structures, as additional reassurance, including the storage pits, bioshield base, delay tank and water plant room. These supplemented the statistical sampling designs for each Type B zone.

6. Sampling and Analysis Plans

6.1 Background Soil Sampling

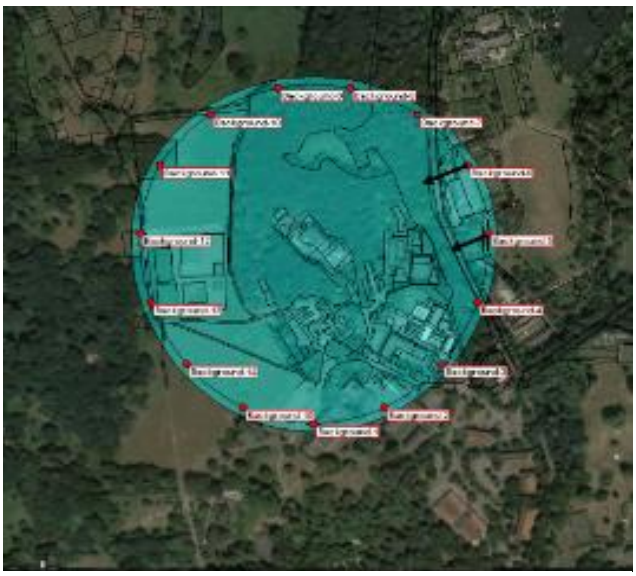

Figure 4: Background sampling points

A Sample and Analysis Plan (SAP) was created for determination of background levels for certain radionuclides in the local environment, which may have been present due to their natural occurrence or due to human activities not associated with the College. Following a review of the Contaminants of Potential Concern (COPCs) for the site, Caesium-137 was considered to be the only radionuclide that required a background radioactivity study. This was because Caesium-137 is the only radionuclide both potentially present as a result of ICRC operations, and also from natural means or other human activities (in this case radioactive fallout from global weapons testing). Soil samples were taken from 15 locations in a ring around the site at a distance of 200m.

6.2 Second ScanPlot

A second ScanPlot survey was undertaken at the time of DQO sampling, across the full site to provide additional reassurance that no significant hotspots (gamma) were present. The survey identified three areas of interest, but these were later attributed to variations in NORM [Ref. 14]. Two additional samples were taken in NLS Zone 2 to confirm this. These samples were included in the population of results assessed as part of the Data Quality Assessment (DQA) (see Section **Error! Reference source not found.**).

6.3 Main Sampling Programme - NLS and N-NLS

Following the DQO Workshop the statistical sampling designs were generated using Visual Sample Plan (VSP), and two SAPs were produced: one for the whole ICRC (NLS and N-NLS) [Ref. 10] and one just containing the design for the NLS [Ref. 9]. These contained the necessary information and instructions to enable the sampling team to collect the samples from the generated locations, and for the correct radiological analysis to be performed at the laboratory.

Samples were collected from the three zones.

Zone	Total collected and analysed
NLS Zone 1	31
NLS Zone 2	22
Non-NLS Zone 3	24

Table 3: Deregulation Samples

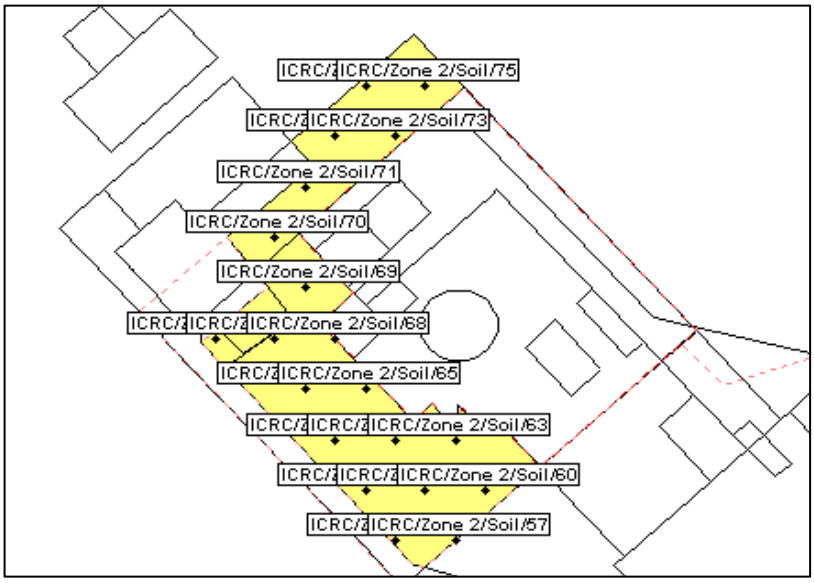

Figure 5: Sample grid for NLS Zone 2

6.4 Sample Analysis

Sample analysis plans (SAPs) were prepared, covering details of the sampling process, including data acquisition and measurement, sample handling, shipping and custody requirements, documentation, quality control and data management.

Samples were analysed using the following techniques listed in Table 4.

Technique	Laboratory	Sample type	Sample Programme
High resolution gamma ray spectrometry	ICRC	Concrete core samples, soils, water	• Pre-sampling • Background • Deregulation • Borehole
Sample oxidation by pyrolysis, extraction of 14C, measurement by liquid scintillation counting	External	Concrete core samples, soils,	• Pre-sampling
Sample oxidation by pyrolysis, extraction of 3H, measurement by liquid scintillation counting	External	Concrete core samples, soils,	• Pre-sampling • Background • Deregulation • Borehole
Chemical separation of 55Fe, measurement by liquid scintillation counting	External		• Pre-sampling
Chemical separation of 63Ni, measurement by liquid scintillation counting	External		• Pre-sampling
Liquid scintillation counting	ICRC	water	• Borehole
Gross alpha and beta counting	ICRC	water	• Borehole

Table 4: Analytical Techniques used for radiological measurements

Where possible, sample analysis was carried out in-house using the ICRC UKAS accredited analytical laboratory. The remaining analyses, where no in-house capability existed, were performed by an external accredited analysis service (GAU Radioanalytical Laboratories).

6.5 Independent Verification of Clearance Process

An independent verification of the clearance process for delicensing was undertaken by Public Health England on behalf of ONR. (PHE has since been replaced by the UK Health Security Agency (UKHSA) an executive agency, sponsored by the Department of Health and social Care, responsible for protecting every member of every community from the impact of infectious diseases, chemical, biological, radiological and nuclear incidents and other health threats.)

Representatives from UKHSA were closely involved throughout the key stages of the process, attending DQO/DQA workshops, witnessing samples being taken in the field and taking some material for their own analysis. UKHSA have also undertaken their own independent surface sampling campaigns across the NLS (NLS Zones 1 & 2), as well as a separate monitoring survey. All DQO sampling results for the NLS were reported at very low levels and this was consistent with UKHSA's analysis of their own samples.

7. DQA Process

The DQA process is a strategic review approach used to evaluate the quality of the data collected during the sampling and analysis activities. The process provides a systematic procedure for documenting the ability of the data to meet the original project objectives or identify data deficiencies that impact data interpretation. The DQA process involves a scientific and statistical evaluation of data to determine if it is of the correct type, quality, and quantity to support the intended use.

7.1 DQA Workshop

The ICRC DQA Workshop was held in August 2021. This was facilitated by Orano with the DQO Planning Team as participants. Representatives from UKHSA and the ONR were also present as observers. The primary objective of the DQA Workshop was to present the outcome of the statistical assessment of radiological DQO sampling results.

7.2 Assessment Against the Selected Deregulation Criteria

All COCs passed the individual contaminant assessment in NLS Zones 1 and 2, as well as the summation calculations. This showed that the dose from the remaining grounds within these zones is not greater than 10 µSv per year and hence meets the "No danger" criterion which ensures that the additional mortality risk is not greater than 1 in a million per year.

In addition to the DQO sampling results that have been assessed as part of the DQA, the sampling team took samples from areas of deeper excavations for further reassurance. These areas include the footprint of the former delay tank as well as former manholes. All but one sampling result was reported as MDL. The single positive sampling result was for Cs-137 and this was an order of magnitude below the deregulation criterion of 0.1 Bq/g. Hence, these results were consistent with the DQO sampling results.

7.3 DQA Conclusions

Following assessment against the Selected Deregulation Criteria, it was concluded that in all zones, all COCs passed the individual contaminant assessment as well as the summation calculations. Hence, in all zones the future dose was not greater than 10 µSv per year and hence the "No Danger" criterion was met, which showed that the additional risk of death from ionising radiations was not greater than one in a million per year. As a result, the remaining grounds is also Out of Scope of the EPR regulations. Therefore, the ICRC was fit to be deregulated.

8. Additional Sampling Programmes

8.1 Ground water sampling from the area around the licensed site.

The College undertook a groundwater sampling campaign, to demonstrate that the groundwater had not been contaminated as a result of ICRC operations.

The College prepared a Site Investigation Plan, which identified suitable bore hole locations to determine the groundwater flow direction and enable representative ground water samples to be taken. The DQO Planning Team converted this into a sampling plan. In addition to groundwater sampling, surface water from static bodies was also collected and soil from the boreholes was sampled at regular intervals, in order to determine whether there was any contamination present in the soils at depth.

Figure 6: Proposed Borehole Drilling Locations

The depths of the boreholes ranged from 5.6 m to 19.5 m below ground level (bgl) to achieve the target depth of 2 m below the water table.

One borehole was located on the NLS and its soil was to be sampled at 1 m depth intervals. All groundwater and soil samples from this borehole were analysed using high resolution gamma spectrometry (with the emphasis on the COCs identified during the DQO process). The groundwater samples were also tested for gross alpha and beta. In addition to radiological analysis, chemical analysis was performed for levels of hydrocarbons, volatile organic compounds and metals. The remaining boreholes were located off the NLS and their soils were sampled at 5 m intervals. The analysis requirements for these boreholes were similar to that for the NLS borehole, except that tritium analysis was only to be performed if the gross beta results were greater than the MDL.

There were no positive detections of radionuclides in any of the borehole samples taken (at all depths). This is true for samples taken from the borehole on the NLS, as well as those located off the ICRC site footprint. Hence, there was no evidence to suggest that there was any leaked contamination in the surrounding Silwood Park Campus as a result of ICRC operations, and no radiological risk to water receptors in the vicinity of the site.

8.2 Chemical Results

Low levels of hydrocarbons and metals were identified in the chemical results in some groundwater samples. However, given the limited / sporadic detections of the hydrocarbons, the low mobility of these compounds and the distance to surface water, these were considered

unlikely to pose a risk to surface water. Metals were reported to be typical of background concentration for the vicinity of the site. None were considered to be related to activities on the ICRC Site.

8.3 Asbestos

Asbestos had been present in the ICRC buildings. This material was all removed from the site by a licensed contractor as part of the asbestos strip of the buildings, prior to demolition. However, there was a known risk of asbestos present in the remaining ground across the site, which was thought to be present as a result of legacy activities prior to ICRC operations.

Two investigations were carried out, where samples were taken from trial test pits. The first was within the site boundary and found seven positive results which indicated asbestos might be present outside the boundary. This was confirmed by the second investigation which found positive results outside the boundary.

The College decided, after taking specialist advice, to do no further asbestos remediation, as the positive asbestos samples had levels below the waste acceptance criteria and thus, the soil from the site was deemed non-hazardous with respect to asbestos for the current projected land use of a grassland amenity. The residual asbestos was not an issue for deregulation, however, the College continues to have a ‘duty of care’ under the asbestos regulations for management of the site going forward.

9. Controls to Maintain ‘Cleared’ Status

Following sampling of the ICRC site, it was necessary for the College to maintain adequate control of site to ensure that the radiological status of the area could not have been compromised by any incidents/events or modifications before formal agreements with the ONR and EA to deregulate was in place. The construction site fencing around the site was kept in place to demarcate the boundary of the site and to help protect the area from unauthorised access. Final landscaping of site was put on hold until the site was deregulated.

9.1 Conclusions

Following the extensive decommissioning programme and a comprehensive sampling and monitoring strategy to support the deregulation case, it was concluded that

- There was “No danger” from exposure to ionising radiation in the future from the remaining ground of the ICRC site
- The conditions of the site also meet the standards for release from RSR.
- The case was approved by the regulator, with the site achieving deregulation on the 31st March 2022.

10. References

1. ONR, ONR Criterion for Delicensing Nuclear Licensed Sites, March 2021.
2. HSE, Reducing Risks, Protecting People, 2001.
3. HSE, The Tolerability of Risk from Nuclear Power Stations, 1992.
4. IAEA, IAEA Safety Standards Series RS-G-1.7, Application of the Concepts of Exclusion, Exemption and Clearance, International Atomic Energy Agency, 2004.
5. Scottish Environment Protection Agency, Environment Agency and Natural Resources Wales, Management of radioactive waste from decommissioning of nuclear sites: Guidance on Requirements for Release of Nuclear Sites from Radioactive Substances Regulation, July 2018.
6. The Environmental Permitting (England and Wales) (Amendment) (No. 2) Regulations 2018, SI 2018 No. 428.
7. Clearance and Radiological Sentencing: Principles, Processes and Practices for Use by the Nuclear Industry. A nuclear Industry Code of Practice, Issue 2, Dec 2012

REQUIREMENTS FOR NUCLEAR INSTRUMENTATION SYSTEMS FOR A NEW KOREAN RESEARCH REACTOR

YONGSUK SUH, SEUNG KI SHIN, DANE BAANG
Kijang Research Reactor Design and Construction Project Dept., Korea Atomic Energy Research Institute (KAERI),
111, Daedeok-daero 989 Beon-gil, Yuseong Gu, Daejeon, 34057, Korea Republic of

ABSTRACT

A new Korean research reactor, called the Kijang Research Reactor (KJRR), is currently under construction to reach its first criticality in early 2027. Nuclear instruments for the KJRR will be installed in early 2026. We developed requirements for the nuclear instruments and will open them for bidding in late 2022. We categorized them into six systems: NMS, PGMS, PNMS, PRMS, FRMS and RMS. Foreign entities will be encouraged to bid for manufacturing these very sophisticated systems. This paper describes detail requirements for the systems to help foreign entities to take part in the 2022 bid.

1. Introduction

The KJRR is a 15 MWth open-tank-in-pool type research reactor to mainly produce fission moly 99 [1]. The construction schedule has been changed since 2012. This paper concerns only nuclear instrumentation systems (NIS) of the KJRR. We categorized the NIS into six systems: Neutron Measurement System (NMS), PCS Gamma Monitoring System (PGMS), PCS Neutron Monitoring System (PNMS), Pool surface Radiation Monitoring System (PRMS), Fission Moly Production Building (FMPB) Radiation Monitoring System (FRMS) and Radiation Monitoring System (RMS). We first published the safety requirements for the NMS, PGMS, PNMS, PRMS and FRMS at the RRFM 2020 conference [2].

No.	System name	I&C Systems that use it	Location of detector installation (Harsh environment)	Location of processor installation (Mild environment)	Safety Class (Nuclear/Electrical)	Seismic Category	Quality Group
1	NMS WRGFC Ch. A/B/C	RPS	Neutron Detector Housing in Rx Pool	Main Control Room	SC 3/Class 1E	I	Q
2		RPS	Neutron Detector Housing in Rx Pool	Safety Instrument Room	SC 3/Class 1E	I	Q
3		RPS	Neutron Detector Housing in Rx Pool	Main Control Room	SC 3/Class 1E	I	Q
4	NMS WRGFC Ch. X/Y	RRS, APS	Neutron Detector Housing in Rx Pool	Non-safety Instrument Room	NNS/Non Class 1E	II	T
5		RRS, APS	Neutron Detector Housing in Rx Pool	Non-safety Instrument Room	NNS/Non Class 1E	II	T
6	NMS CIC Ch. A/B/C	RPS, AMS	Neutron Detector Housing in Rx Pool	Main Control Room	SC 3/Class 1E	I	Q
7		RPS, AMS	Neutron Detector Housing in Rx Pool	Safety Instrument Room	SC 3/Class 1E	I	Q
8		RPS	Neutron Detector Housing in Rx Pool	Main Control Room	SC 3/Class 1E	I	Q
9	PRMS GIC Ch. A/B/C	RPS, AMS	Reactor Pool Top Gallery Wall	Main Control Room	SC 3/Class 1E	I	Q
10		RPS, AMS	Reactor Pool Top Gallery Wall	Safety Instrument Room	SC 3/Class 1E	I	Q
11		RPS	Reactor Pool Top Gallery Wall	Main Control Room	SC 3/Class 1E	I	Q
12	PNMS BF3 (B10) Ch. A/B/C	RPS, AMS	PCS Decay Tank Pipe Access Room	Main Control Room	SC 3/Class 1E	I	Q
13		RPS, AMS	PCS Decay Tank Pipe Access Room	Safety Instrument Room	SC 3/Class 1E	I	Q
14		RPS	PCS Decay Tank Pipe Access Room	Main Control Room	SC 3/Class 1E	I	Q
15	PNMS BF3 (B10) Ch. X/Y	APS	PCS Decay Tank Pipe Access Room	Non-safety Instrument Room	NNS/Non Class 1E	II	T
16		APS	PCS Decay Tank Pipe Access Room	Non-safety Instrument Room	NNS/Non Class 1E	II	T
17	PGMS GIC Ch. A/B/C	RPS	PCS Decay Tank Pipe Access Room	Main Control Room	SC 3/Class 1E	I	Q
18		RPS	PCS Decay Tank Pipe Access Room	Safety Instrument Room	SC 3/Class 1E	I	Q
19		RPS	PCS Decay Tank Pipe Access Room	Main Control Room	SC 3/Class 1E	I	Q
20	FRMS GIC Ch. A/B/C	FIDAS, AMS, PICS	FMPB HVAC Duct Wall	Main Control Room	SC 3/Class 1E	I	Q
21		FIDAS, AMS, PICS	FMPB HVAC Duct Wall	Safety Instrument Room	SC 3/Class 1E	I	Q
22		FIDAS, PICS	FMPB HVAC Duct Wall	Main Control Room	SC 3/Class 1E	I	Q

Tab 1: The list of NMS, PGMS, PNMS, PRMS, FRMS equipment

This paper provides more requirements such as interfaces between the NIS and instrumentation and control (I&C) systems, installation of detectors, dimensions of signal processors, etc. We list the number of NMS, PGMS, PNMS, PRMS, FRMS equipment in Table 1 and RMS equipment in Table 2.

In Table 1, nuclear safety class SC3 means safety critical class 3 defined in ANSI/ANS 51.1[3] and is equivalent to Category A of IEC 61226 and Safety Critical Software of IEC 60880. NNS means Non-Nuclear Safety and is equivalent to Category B of IEC 61226. Seismic category I shall require the system to perform its required function and II shall require the system to maintain its integrity under Safe Shutdown Earthquake. Quality Assurance (QA) group Q shall meet ASME NQA [4] and group T meets QA requirements lower than ASME NQA but higher than Industrial QA.

2. Requirements of the NMS (Neutron Measurement System)

The one channel of output signals of the Wide Range Guarded Fission Chamber (WRGFC) for one channel of the safety Rector Protection System (RPS) shall include:

1) One 4-20mA (0 ~ 150%FP) analog current output signal for linear power
2) One 4-20mA (1.0E-8 ~ 150%FP) analog current output signal for log power
3) One 4-20mA (-15%PP/s ~ 15%PP/s) analog current output signal for log rate
4) One relay dry contact signal for WRGFC NMS channel failure alarm

The one channel of output signals of the WRGFC for one channel of the non-safety Reactor Regulating System (RRS) and the non-safety Alternate Protection System (APS), and one the non-safety Reactivity Calculator shall include:

1) Three 4-20mA (0~150%FP) analog current output signals for linear power
2) Three 4-20mA (1.0E-8 ~ 150%FP) analog current output signals for log power
3) Three 4-20mA (-15%PP/s ~ 15%PP/s) analog current output signals for log rate
4) One 4-20mA (1.0E-1 ~1.0E+5 CPS) low power level neutron count rate
5) One square pulse for low power level neutron count (pulse from the discriminator), TTL level (5V or 3V), 1μs pulse duration
6) One 4-20mA (1.0E-3 ~ 150 %FP) Campbell signal for intermediate/high power level
7) Two relay dry contact signals for WRGFC NMS system failure alarm

The one channel of output signals of the Compensated Ion Chamber (CIC) for one channel of the safety RPS and the safety AMS shall include:

1) Two 4-20mA (0~150%FP) analog current output signals for linear power
2) Two 4-20mA (1.0E-5 ~ 150%FP) analog current output signals for log power
3) Two 4-20mA (-15%PP/s ~ 15%PP/s) analog current output signals for log rate
4) One relay dry contact signal for CIC NMS system failure alarm

The NMS detector shall be installed into the housing located at a 12m-depth inside the reactor pool as shown in Fig. 1. The housings are provided by KAERI.

The flexible watertight conduit is connected from the detector to the signal processor and the distance between the two is about 100m. We recommend to fill Nitrogen gas into the watertight conduit. We recommend to install the signal processors for the FC and CIC in the main control room and instrument room where is mild zone, the total integrated dose (TID) requirement is negligible.

The active length of the WRGFC and CIC detectors shall be minimum 200 mm and maximum 500 mm. In addition, we recommend the active area of the detectors as

1) WRGFC: height 235 mm and radius 41.4 mm
2) CIC: height 355.6 mm and radius 41.4 mm

In this paper, we use abbreviations: FP means Full Power, PP means Present Power, CPS means Count Per Second, and FS means Full Scale.

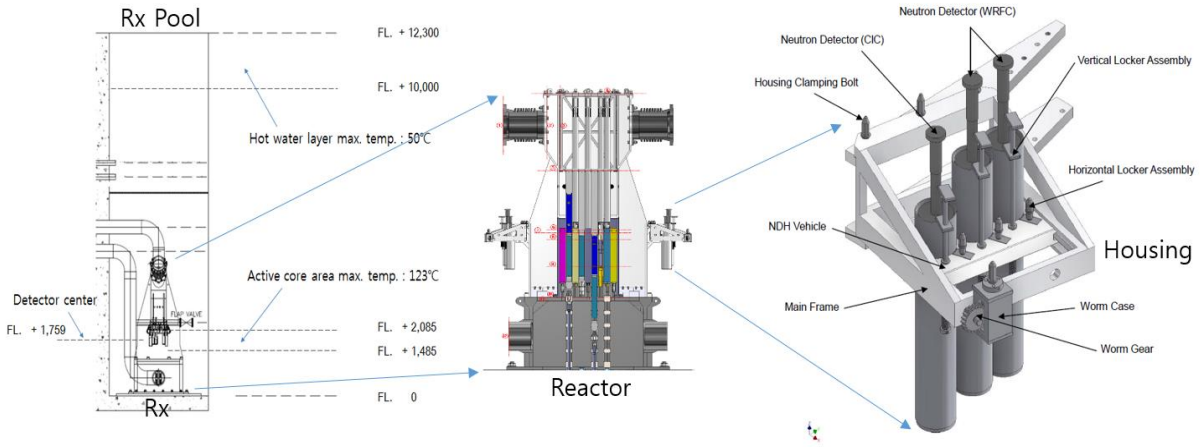

Fig 1. The housing of NMS detectors

3. Requirements of the PGMS (PCS Gamma Monitoring System)

The one channel of output signals of the Gamma Ion Chamber (GIC) for one channel of the safety RPS shall include:

1) One 4-20mA analog current output signals per channel, corresponding to full range of gamma power level from 0%FP to 150%FP from PCS water flow.
2) One relay dry contact signal for high radiation alarm
3) One relay dry contact signal for equipment failure alarm

The PGMS detector shall be installed on the wall of Primary Cooling System (PCS) Decay Tank Pipe Access Room (harsh environment) next to the reactor pool.

4. Requirements of the PNMS (PCS Neutron Monitoring System)

The one channel of output signals of the BF3 (or B10) for one channel of the safety RPS and the safety AMS shall include:

1) Two 4-20mA (1.0 ~ 1.0E+4 CPS) analog current output signals per channel, corresponding to full range of delayed neutron counts from PCS water flow.
2) One relay dry contact signal for high PCS neutron alarm
3) One relay dry contact signal for equipment failure alarm

The one channel of output signals of the BF3 (or B10) for one channel of the non-safety APS shall include:

1) One 4-20mA (1.0 ~ 1.0E+4 CPS) analog current output signal per channel, corresponding to full range of delayed neutron counts from PCS water flow.
2) One relay dry contact signal for high PCS neutron alarm
3) One relay dry contact signal for equipment failure alarm

The PNMS detector shall be installed on the movable supports located in PCS Decay Tank Pipe Access Room (harsh environment) next to the reactor pool as shown in Fig. 2. The movable supports are provided by KAERI.

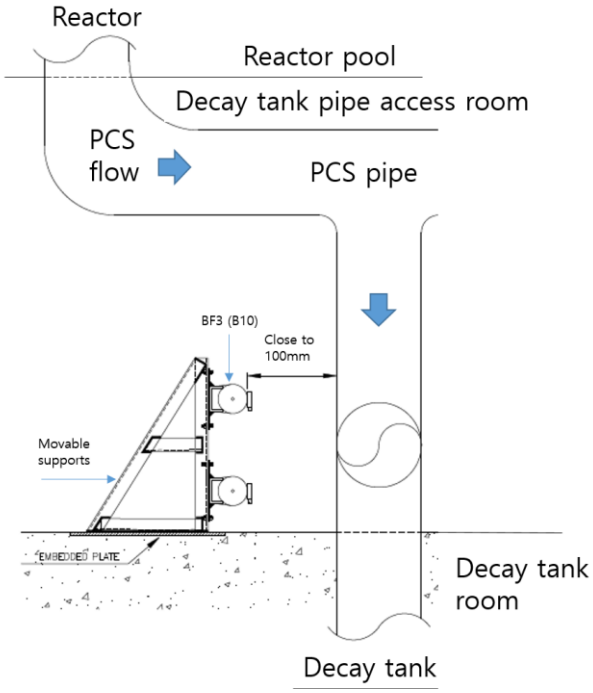

Fig 2. The support of PNMS detectors

5. Requirements of the PRMS (Pool surface Radiation Monitoring System)

The one channel of output signals of the GIC for one channel of the safety RPS and the safety AMS shall include:

1) Two 4-20mA (1.0 ~ 1.0E+6 μSv/h) analog current output signals per channel corresponding to full range of gamma radiation in reactor pool water.
2) One relay dry contact signal for high radiation alarm
3) One relay dry contact signal for equipment failure alarm

The PRMS detector shall be installed on the wall of reactor pool top gallery as shown in Fig. 3.

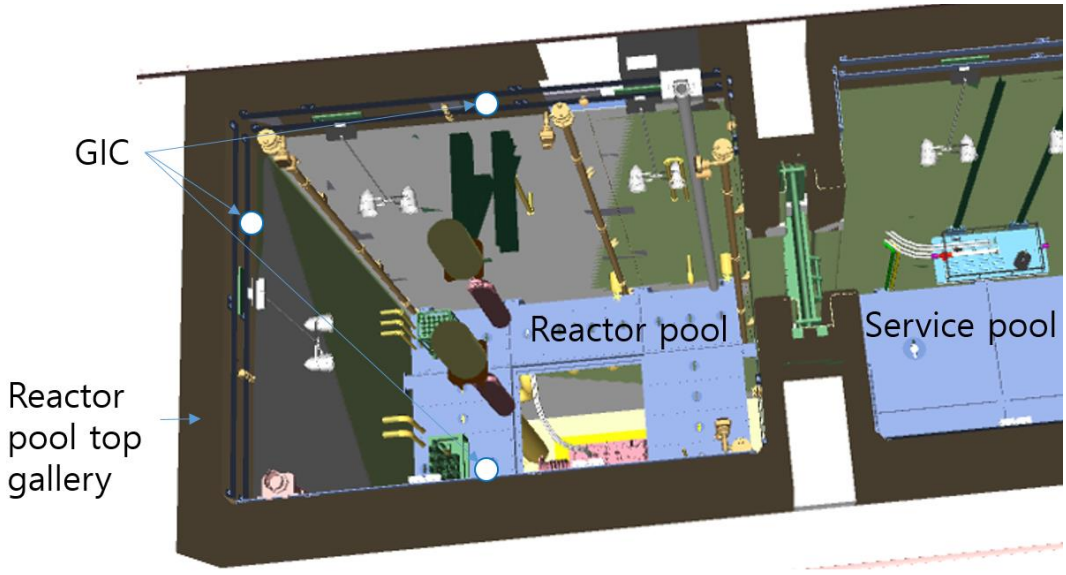

Fig 3. The location of PRMS detectors

6. Requirements of the FRMS (FMPB Radiation Monitoring System)

The one channel of output signals of the GIC for one channel of the safety FMPB Isolation Damper Actuation System (FIDAS) and the safety AMS, and one channel of the non-safety Process I&C System (PICS) shall include:

1) One relay dry contact signal for high radiation alarm to the safety grade FIDAS
2) One 4-20mA (1.0 ~ 1.0E+6 μSv/h) analog current output signals corresponding to full range of gamma radiation in air flow to the safety grade AMS
3) One 4-20mA (1.0 ~ 1.0E+6 μSv/h) isolated analog current output signals corresponding to full range of gamma radiation in air flow to the non-safety grade PICS
4) One isolated relay dry contact signal for high radiation alarm to the non-safety grade PICS
5) One isolated relay dry contact signal for equipment failure alarm to the non-safety grade PICS

The FRMS detector shall be installed on the wall of Heating, Ventilation and Air Conditioning (HVAC) duct line room in the Fission-Molybdenum Production Building (FMPB)

7. Requirements of the RMS (Radiation Monitoring System)

The NMS, PGMS, PNMS, PRMS and FRMS provides nuclear signals in order for I&C systems to actuate protection, control and monitoring functions. On the other hand, the RMS provides nuclear signals for KJRR's physical protection purposes. The RMS is a non-safety grade and Category B system. The NMS, PGMS, PNMS, PRMS and FRMS are order-made production systems whereas the RMS is a commercial off-the-shelf item. The RMS local units are installed in mild area. Some of RMS equipment installed in the main control room, the reactor hall, or near the safety system equipment shall maintain their integrity under Safe Shutdown Earthquake events. The RMS equipment is described in Table 2 and in the design specification for the RMS [7].

Main server cabinet and display computer workstations				
Equipment name				Number of equipment
Main server computer and cabinet in a health physics room				1
Display computer workstations				7
Laser printers				2
Local monitors				
Equipment name	Measurement signal	Measurement range	Detector type	Number of equipment
Area radiation monitor	Gamma	1.0E-5 ~ 1.0E+6 mSv/hr	Silicon	77
Liquid monitor	Gamma	1.0E+2 ~ 1.0E+7 CPM	NaI Scintillation	2
Gaseous effluent for duct	Beta	1.0E+2 ~ 1.0E+7 CPM	Plastic Scintillation	6
Gaseous effluent for stack of reactor building	Particulate	1.0 ~ 3.7E+6 Bq/㎥	Silicon	1
	Iodine	3.7 ~ 3.7E+6 Bq/㎥	NaI Scintillation	
	Noble gas (normal)	3.7E+4 ~ 3.7E+10 Bq/㎥	Silicon	
	Noble gas (high)	1.0E+6 ~ 3.7E+15 Bq/㎥	Ion	
	Tritium	3.2E+3 ~ 3.2E+12 Bq/㎥	Ion	
Gaseous effluent for stacks of other building	Particulate	1.0 ~ 3.7E+6 Bq/㎥	Silicon	3
	Iodine	3.7 ~ 3.7E+6 Bq/㎥	NaI Scintillation	

	Noble gas	3.7E+4~ 3.7E+10 Bq/㎥	Silicon	
Air monitor	Particulate	1.0 ~ 3.7E+6 Bq/㎥	Silicon	5
Air monitor	Particulate	1.0 ~ 3.7E+6 Bq/㎥	Silicon	5
	Iodine	3.7 ~ 3.7E+6 Bq/㎥	NaI Scintillation	
Air monitor	Particulate	1.0 ~ 3.7E+6 Bq/㎥	Silicon	8
	Iodine	3.7 ~ 3.7E+6 Bq/㎥	NaI Scintillation	
	Noble gas	3.7E+4 ~ 3.7E+10 Bq/㎥	Silicon	
Air monitor	Noble gas	3.7E+4 ~ 3.7E+10 Bq/㎥	Silicon	2
Cell door monitor	Gamma	1.0E-2 ~ 1.0E+6 mSv/hr	Ion	29
Portal monitor				3
Portable air sampler				1

Tab 2: The list of RMS equipment

8. Conclusions

The requirements for the nuclear instrumentation systems were first described in a previous paper [1]. The total integrated dose (TID) in the reactor hall is changed from 100 to 200 Gy for three hours in the case of one fuel melting accident. KAERI provides an embedded plate, H-beam and support. The supplier provides accessories such as bracket, bolt and nut, tie-band, etc. to mount the supplier's equipment on the embedded plate, H-beam and support. All these fixtures shall meet the seismic requirements. Thus, the supplier shall clearly propose the installation instructions of the NIS equipment in their proposals at the bidding time. It has been hard to repeat the measurement of response time after installation. Thus, the supplier shall provide equipment for measuring the total response time. For safety grade digital equipment, an independent third-party certificate is required for verification and validation of software according to IEEE Std. 1012 [5] and evaluation of cyber security according to USNRC RG 5.71 [6].

Acknowledgement

This work was supported by Korea Ministry of Science and ICT (MSIT) (Grant Code: 2020M2C1A1061034).

References

[1] C. Park, et. al, "Overall Design Features and Key Technology Development for KJRR", Transactions of the Korean Nuclear Society Autumn Meeting, Gyeongju, Korea, 30 Oct., 2015.
[2] Y. Suh, "LESSONS LEARNED FROM THE PREPARATION OF TECHNICAL SPECIFICATIONS OF SAFETY GRADE NUCLEAR INSTRUMENTATION SYSTEMS FOR A NEW KOREAN RESEARCH REACTOR", European Research Reactor Conference 2020, Online, 12-15 October 2020.
[3] ANSI/ANS 51.1-1983, "Nuclear Safety Criteria For The Design of Stationary Pressurized Water Reactor Plants", American Nuclear Society, 1983.
[4] ASME NQA-1–2008, "Quality Assurance Requirements for Nuclear Facility Applications", THE AMERICAN SOCIETY OF MECHANICAL ENGINEERS, 2008.
[5] IEEE Std. 1012-2004, "IEEE Standard for Software Verification and Validation", IEEE Computer Society, 2004.
[6] USNRC RG 5.71, "CYBER SECURITY PROGRAMS FOR NUCLEAR FACILITIES", U.S. NUCLEAR REGULATORY COMMISSION, 2010.
[7] KJ-678-DJ-416-001, Design Specification for Radiation Monitoring System, 2021.

ENRICHED LANTHANIDES SUPPLY PROJECT TO THE RESEARCH REACTORS COMMUNITY

PHILIPPE BERTRAND, LAURENT BIGOT,
JEAN-NOEL LACROIX, JEAN-LUC VINCENT
Stable Isotopes, Orano Chemistry & Enrichment,
125 avenue de Paris, 92320 Chatillon - France

ABSTRACT

Pursuant to last year presentation, Orano is leveraging on its unique competencies and technologies to produce stable isotopes for the research, medical and industrial communities. 2022 is a key milestone for our project. First, the civil work for the construction of the stable isotope laboratory has been finalized last year, the heart of the process is being installed and erection of the key process equipment is on-going. Production of stable isotopes based on centrifugation technology will start mid-2023, on time and on budget with our initial commitments.

Among the 61 stable elements that can be separated circa 40 cannot be enriched by the centrifugation technology. The latter are predominantly separated by calutron, a technology widely used in the previous century, energy intensive and nowadays almost exclusively in operation in non-Western countries. Therefore, Orano is launching the second phase of its project to define the operational conditions and develop business models for enriching other heavy stable elements, like lanthanides, based on laser separation technology. Such expansion of Western enrichment capabilities, based on a technology historically proven on uranium, is a timely answer to the growing demand of OECD needs

1. Orano presentation and positioning

Orano is one of the world leaders and global players in uranium mining, conversion and enrichment activities with almost 75 years of industrial experience. Based on solid foundations laid by its predecessors, Orano is an integrated industrial actor focusing on the nuclear fuel cycle encompassing the following activities[1] :

- Mining
- Chemistry & Enrichment
- Used fuel recycling
- Nuclear Packages and Services
- Dismantling and services
- Engineering

Orano has approximately 3.7 Bn € per year of revenues, employs 16,500 persons world-wide and has a strong backlog of orders covering 7 years ahead of activities.

The purpose of Orano is to develop know-how in the transformation and control of nuclear materials, for the climate, for a healthy and resource-efficient world, for today and tomorrow.

Based on its best-in-class separation and chemistry technologies and unique knowhows developed for the transformation of uranium, Orano is developing a stable isotopes

[1] website: www.orano.group/en

activity. The project has been validated by the board in 2020 as a key milestone of Orano's growth strategy in the medical field.

The first phase of Orano Stable Isotopes project targets the circa 20 elements that can be separated with the centrifugation process, a process currently used for the enrichment of uranium. These elements include the very large category of stable isotopes precursors for radioisotopes that are mainly used for specific needs, such as medical imaging, oncology treatment and industrial radiation sources.

Fig 1. Stable isotopes currently separated by centrifuges

The second phase of the project targets other stable elements, key in growing markets, and that cannot be enriched with centrifugation technology. For example, lanthanides and among others Ytterbium, key in oncology treatments both in the short and the medium term.

2. Current project status and next steps

The civil work of the Stable Isotopes Laboratory ended last year on the Tricastin site (South of France) in a non-nuclear zone as stables isotopes are non-radioactive. Since the beginning of this year key equipment are being delivered. The mounting of the test benches and of the assembling of the first cascade shall be completed by the end of the year. Testing and first production will take place in 2023.

Fig 2. Stable Isotopes Laboratory building

The facility will be used for producing stable isotopes and for performing research & development customized on client's needs. The first production line is a flexible cascade of centrifuges (multi-isotopes per production line). Our industrial scenario for additional lines permits the construction of dedicated capacities for future client's needs. The production capacity is fully modular and can be replicated to meet increasing market needs.

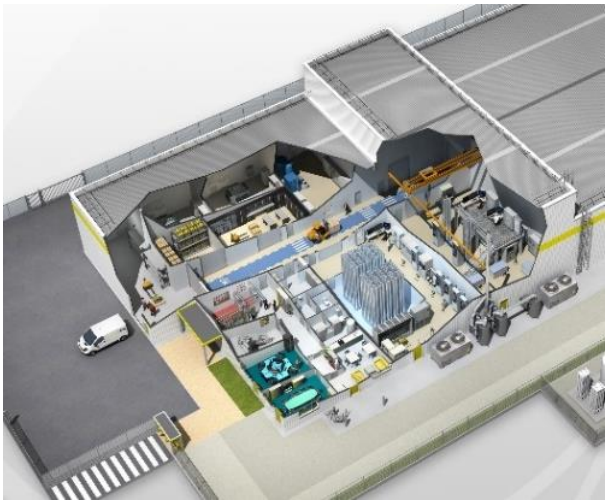

Fig 3. Stable Isotopes Laboratory overview

3. Enrichment of lanthanides

Among the elements that cannot be enriched by centrifugation, circa 10, like O, C, or N, are produced in several industrial plants around the world. The supply of these elements is not a concern for our industrial community.
But the production of the remaining 30 elements is only located in Russia and some, like Yb, are essential in oncology applications to produce nca 177-Lu. In 2021, the share of Yb among these 30 elements was about 80% (around 2kg in 2021 of enriched Yb in oxide form).

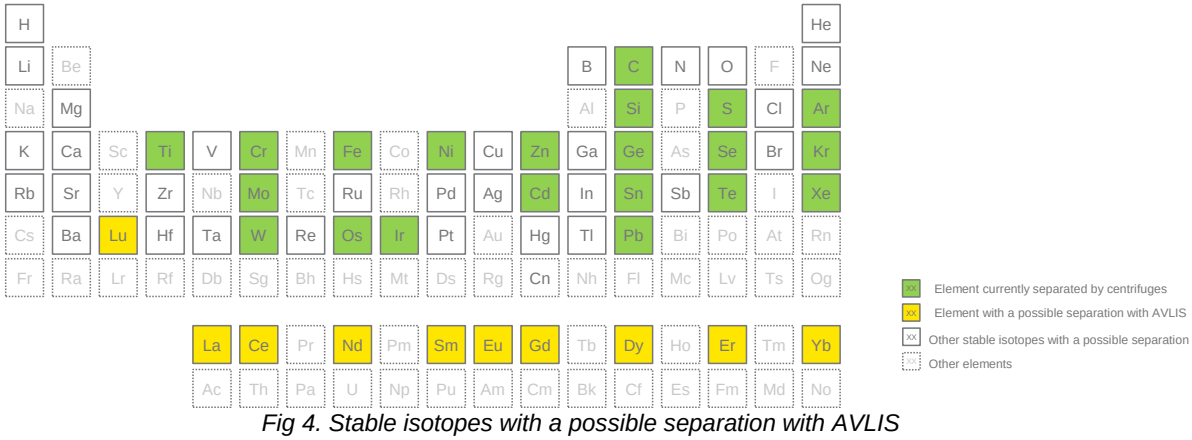

Fig 4. Stable isotopes with a possible separation with AVLIS

CEA has developed a laser enrichment technology, Atomic Vapor Laser Isotope Separation technology (AVLIS), with Orano as a stakeholder. In 2003, the efficiency of AVLIS was proven on a large scale on uranium isotopes by separating more than 200kg of enriched uranium from two tons of natural uranium. The principle of this technology could be successfully applied for the separation of lanthanides including Ytterbium. Given the performance of the AVLIS technology we believe that it will be the cheapest and the most efficient way for industrially enriched Ytterbium in the Future. Such expansion of

Western enrichment capabilities is a timely answer to the growing demand of OECD needs.

An ALVIS equipment can easily be implemented into the Stable Isotopes Laboratory after a first phase of validation. The objectives of this preliminary phase are to adapt the parameters set for uranium on ytterbium, to demonstrate the feasibility to produce an Ytterbium sample at the isotopic composition required for an efficient nca 177-Lu production and to determine the key data for the upscaling to an industrial capacity.

4. Conclusion

While some recent positive developments have been observed on the fight against cancer, the establishment of a sustainable, a competitive and an independent supply chain is crucial for the continuation of research in this field. Among others, the predicted importance of 177Lu in future cancer therapy has deemed the development of an enrichment facility to produce enriched Yb176 one of the top priorities for our community.

CEA has developed in the recent past a laser enrichment technology, AVLIS, with Orano as a stakeholder. The performances of this technology, proved on uranium, are suitable to enrich ytterbium as well as other elements only enriched by calutron so far. AVLIS technology being much more efficient and cost effective compared to calutron, Orano is launching the translation of the production parameters from uranium to ytterbium and the scaling to an industrial production capacity. This second phase of Orano stable isotopes laboratory project shall last for about two years and bring the technology to TRL 7.

ANALYSIS OF THE ROD-DROP EXPERIMENTS IN JRTR COMMISSIONING STAGE

HANJONG YOO, KYUNG-O KIM, BUMWOO PARK
Kijang Research Reactor Design and Construction Project Dept.,
Korea Atomic Energy Research Institure (KAERI)
111, Daedeok-daero 989 Beon-gil, Yuseong-Gu, Daejeon, 34057, Korea

ABSTRACT

Results of rod drop experiment during commissioning stage of Jordan Research and Training Reactor (JRTR) is analysed. Reactivity worth measurement for reactor commissioning was based on the rod-swap method. Rod-drop experiment is also performed however this experiment was intended for measuring control rod drop time. During rod-drop experiment, detector signals and reactivity readings by reactivity meter are recorded but direct reading from reactivity meter was far from designed value. Steady state calculation of MCNP code is used to make correction factors for both of detector signal and designed reactivity worth. After correction two values showed a good agreement.

1. Introduction

During the Jordan Research and Training Reactor (JRTR) commissioning program, experiment for measuring Control Absorber Rod (CAR) worth was performed based on rod-swap method. Calculated and measured shape curves for the CAR worth were similar, but the measured integral CAR worth values were about 11% ~ 15% smaller than the calculation.
Rod-drop test was also performed but main purpose of this experiment was to measure rod-drop time. As a side task, during this experiment, neutron detector signals are collected and directly converted to reactivity values. However, reactivity values were far from the designed values without correction of spatial effects. Spatial effect significantly affect reactivity measurement but application of spatial correction factor can reduce it. Concept of spatial correction factor is well described in the literature [2, 3].
M. Maillot and his colleagues [1] reviewed theoretical background of conventional rod-drop experiment and introduced spatial correction factor, called Modified Source Method (MSM) factor, to take into account the modification of the detector efficiency. MSM factor worked well for conventional rod-drop experiment.
In this paper, rod-drop test result of the JRTR is revisited and spatial correction factor is applied in different manner. Spatial correction factor is produced from series of steady state MCNP calculation with modified nuclear data of variable delayed neutron fraction, then spatial correction factor is applied to detector signal. Reactivity value is obtained from inverse point kinetics equation based on this signal.
Dynamic effect from delayed neutron source to the static reactivity worth is also taken into account. In normal steady state calculation, delayed neutron source is always proportional to prompt fission neutron source with fixed fraction. In real situation, this fraction changes after rod drop due to redistribution of fission source. Through the iterative calculation process described in section 3, spatial correction factor for detector signal is produced and static reactivity is corrected during iterative process.

In section 2, JRTR reactor is introduced and conditions for rod-drop experiment is described. Theoretical background is explained in section 3. After brief comments on conditions of MCNP calculation, test results are given in section 5 and conclusions are followed.

2. JRTR reactor core and CAR worth measurement

2.1 Reactor core configuration

JRTR is 5Mth, open-pool type research reactor located in Jordan, and is in operation since 2016. JRTR is designed and constructed by KAERI-Daewoo E&C consortium for education and training of nuclear engineers and to produce radioisotopes. Space for beam tubes and cold neutron source is available for the future use.

JRTR core consists of 18 plate-type fuel assemblies, four CARs and two Second Shutdown Rods (SSRs) and three vertical irradiation holes are in the core. The reactor core is reflected by both beryllium block and heavy water tank as seen in Fig 1.

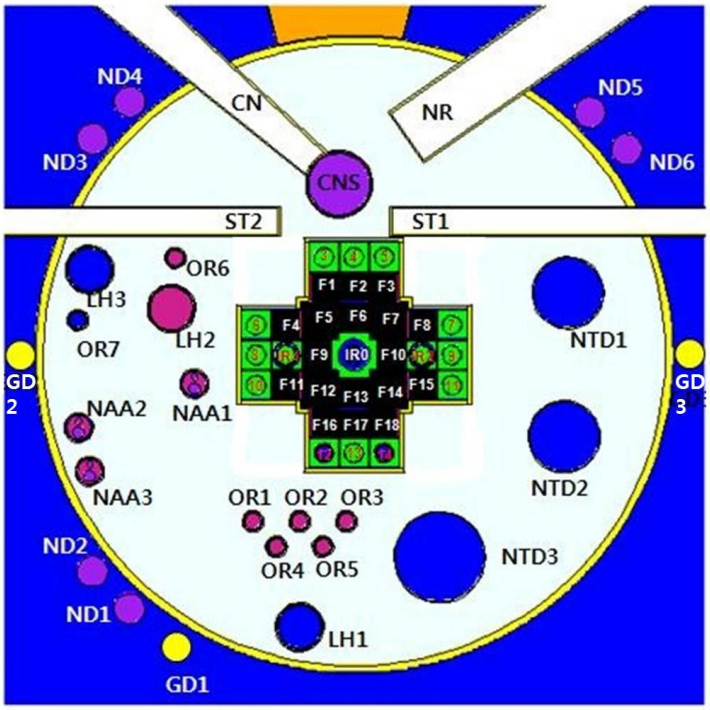

Fig 1. JRTR core and reflector layout

The JRTR fuel is a plate type fuel which is widley used in research reactors. In standard fuel assembly, 4.8gU/cc, 19.75wt% enriched U_3Si_2 fuel in Al matrix is encapsulated in Al cladding. 21 fuel plates consist one box-type fuel assembly. Fuel assembly of different U density (4.0gU/cc, 2.6gU/cc, 1.9gU/cc) but with same geometry consists the initial core.

Four CARs are made of natural hafnium (Hf) and regulates the reactor power. A hollow, square-shaped CARs travel up and down with the guide of tube made of Al. CARs are located at F5(CAR1), F7(CAR2), F12(CAR3), F14(CAR4) position.

2.2 Experiment condition

During normal operation, all CARS are kept at almost same position. For rod-drop experiment, CAR under measurement is fully withdrawn while others are at the critical position. Four CARs are kept at this position for enough time to reach saturated state of delayed neutron precursor density. Then fully withdrawn CAR is dropped at operator's signal.

Drop time of CAR is around 1second and total rod worth (of each CAR) is expected to be around -10$ which is very large negative reactivity insertion in short period of time. Precise power profile is obtained by adjusting the BF3 detector sampling rate. Two BF3 detectors are located at the vertical hole of the thermal column extension (TCE2 and TCE3 @ Fig 2) which is very far from inner core.

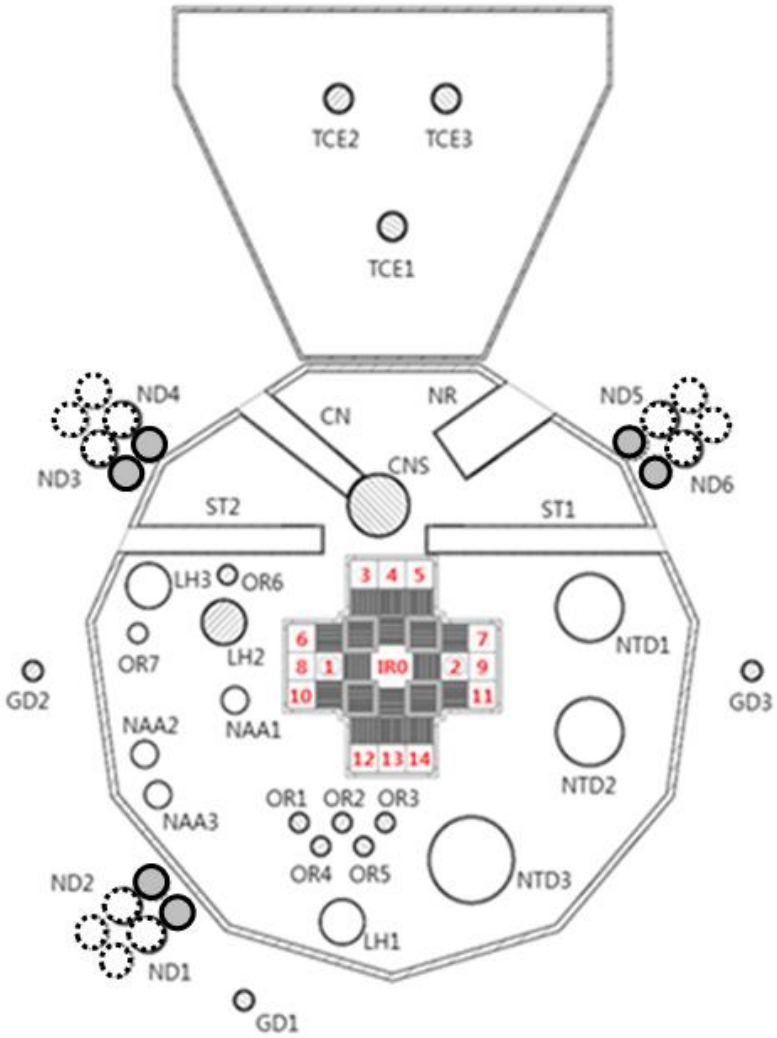

Fig 2. Plan view of core and surrounding area

3. Theoretical Background

3.1 Neutron flux distribution and reactivity

Reactivity of the reactor core is monitored by reactivity meter. It solves inverse point kinetics in real time from the detector signal. In the exact inverse point kinetics equation, *n(t)* should be the core averaged neutron density. However, detector signals represent the neutron density of few peripheral fuel assemblies near the detector. Therefore, reactivity readings from reactivity meter can underestimate or overestimate reactivity of reactor core depending on the flux distribution and detector position. Lee's work [3] described how to relate core average neutron density to detector current (signal) using spatial correction factors and Jeon, et al.[4] quantitatively analysed by comparing the ratio of neutron density at detector and core average neutron density before (*critical* state) and after rod-drop (*subcritical* state). This ratio (written as ***a*** in [4]) is described in Eq. (1)

$$\boldsymbol{a}\ n(t)_{detector,\ critical} / n(t)_{core\_avg,\ critical} = n(t)_{detector,\ subcritical} / n(t)_{core\_avg,\ subcritical} \quad (1)$$

Through the analytic and numerical analysis, it was concluded that when negative reactivity ρ_{true} is inserted, reactivity $\rho_{detector}$(calculated from $n(t)_{detector,subcritical}$) converges to the reactivity value of $\rho_{true}/\mathbf{a}$ around 25~50 seconds past after rod drop in [4]. If **a** can be calculated precisely estimated, ρ_{true} can be estimated. In [2,3], a correction factor similar to **a** was obtained from fast flux(or power) distribution during transient(control rod movement) situation and adjoint flux for detector response for given control rod position.

3.2 Reactivity and delayed neutron source strength relative to the prompt neutron source

Delayed neutron plays an important role in dynamics of reactor core. At critical state, among total source neutrons, specific portion of neutrons born as delayed neutron and the ratio between two is called delayed neutron fraction (β). For non-critical reactor core, with given amount of reactivity (ρ_{given}), the fraction of delayed neutron source can be calculated from point kinetics equation. Neutron production rate is $n(t)/\Lambda$, where Λ is prompt neutron generation time and $(\rho_{given}-\beta_{eff})\cdot n(t)/\Lambda$ is prompt neutron production rate. In point kinetics equation, density of delayed neutron precursors can be calculated and the strength of delayed neutron source, $\sum \lambda_i C_i$, can be easily obtained either, where λ_i is decay constant of delayed and C_i is density of delayed neutron precursor of group i.

3.3 Calculation procedure for reactivity correction

(1) Steady state calculation for critical state (before rod drop)

Perform steady state calculation for critical state and save neutron flux distribution and effective multiplication factor.

(2) Steady state calculation of subcritical state (after rod drop)

Perform steady state calculation for subcritical state and save neutron flux distirubion and effective multiplication factor. From the flux distribution of both states, relative local flux to the core average flux(=n_{local}/n_{core_avg}) and ratio between two states (=***a,*** let's call this Local Flux Ratio(LFR) factor hereafter) can be obtained (see Eq. 1 in section 3.1). Reactivity of the control rod under measurement ($\boldsymbol{\rho}_{steaty}$) can be calculated from the effective multiplication factor.

(3) Point kinetics calculation

Assume reactivity is calculated from the power profile of z'th axial segment of i'th fuel assembly, and LFR factor this section is $\boldsymbol{a}_{i,z}$. Then reactivity will converge to the $\boldsymbol{\rho}_{steaty}/\boldsymbol{a}_{i,z}$ as described in section 3.1. From point kinetics equation of reactivity $\boldsymbol{\rho}_{steaty}/\boldsymbol{a}_{i,z}$ inserted condition, fraction of delayed neutron($\beta_{i,z}$) can be calculated. $\beta_{i,z}$ should be calculated for every local fuel segments.

(4) Nuclear data modification

For local fuel segment (i,z), update nuclear data so that fraction of $\beta_{i,z}$ are generated as a delayed neutron among source neutrons.

Go back to (2) and perform steady state calculation for subcritical state with updated nuclear data. Iterate (2~4) until power distribution and criticality of the core converge.

After convergence of step (2~4), calculate neutron flux at detector position. Calculate LFR factor of neutron flux at detector position and apply it to detector signal (LFR factors for CAR partially inserted state are linearly interpolated between CAR fully withdrawn and full inserted case). Recalculate reactivity from modified detector signal.

Schematic diagram of whole procedure is described in Fig 3.

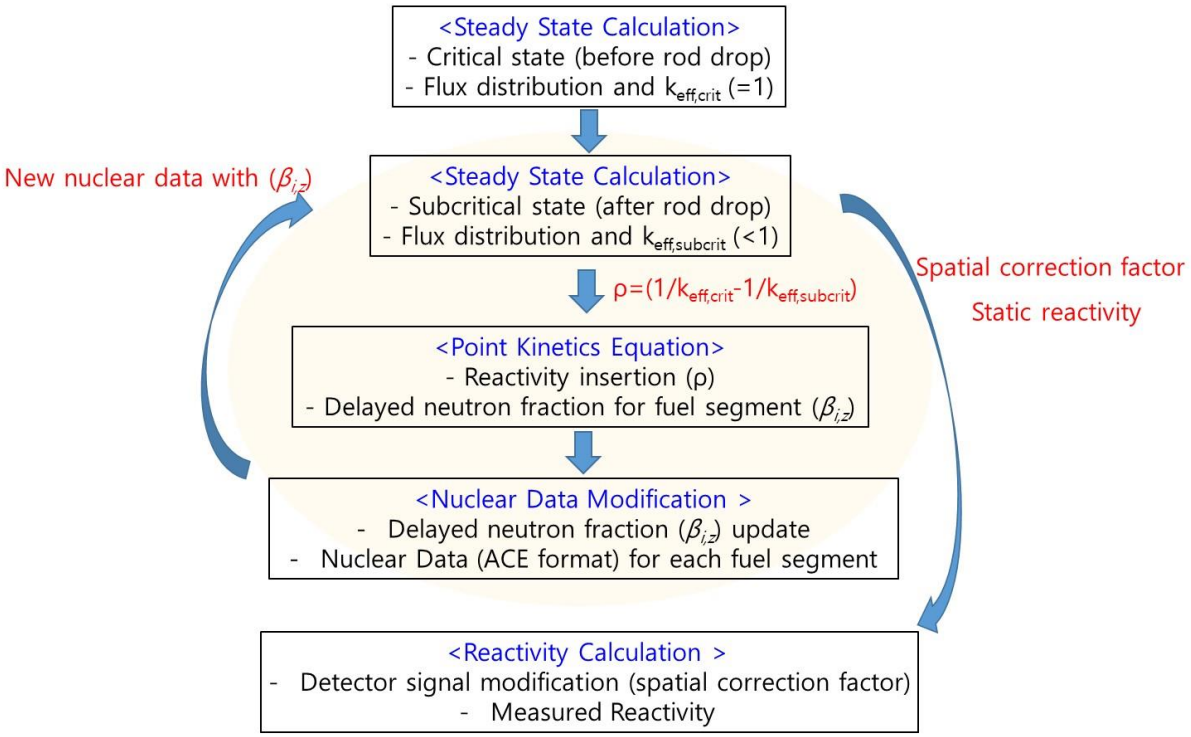

Fig 3. Schematic diagram of calculation process

4. MCNP code calculation

MCNP code is used for numerical simulation to verify the method described in section 3. MCNP is one of the JRTR core design code and core model is prepared in detail. Although ENDF/B-VII.0 was used for JRTR design, ENDF/B-VIII.0 was used for this research. Each MCNP calculation was done with total 64million particles in eigenvalue mode.

4.1 Fuel Segmentation and nuclear data preparation

As described step (4) in section 3, nuclear data should be prepared for every local fuel segments. In this research, each fuel assemblies is divided into ten axial segments and there are total 180 fuel segments. ACE format files for U-235 and U-238 are created and modified for each fuel segment. Data structure and location of delayed neutrons is well explained in [5] and some information is extracted from U-235 ACE file and given in Fig 4.

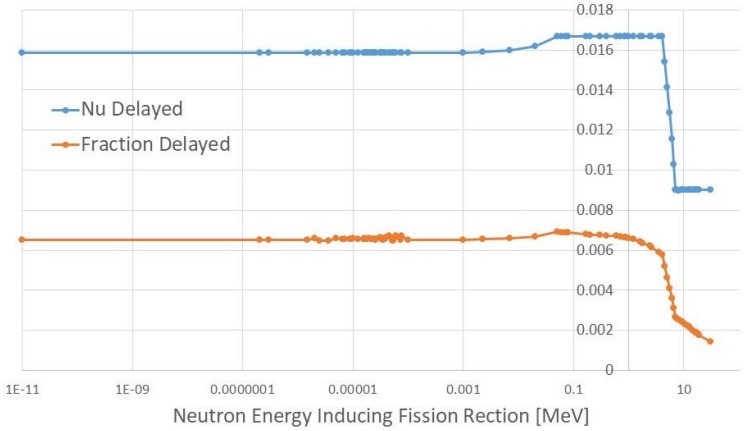

Fig 4. Number of delayed neutrons produced per fission of U-235 atom (ENDF/B-VIII.0)

4.2 Multiplication factor

When MCNP calculation is performed with nuclear data of modified delayed neutron fraction, effective multiplication factor given in output file is not reliable. To calculate correct multiplication factor, total number of fission neutrons produced is tallied with F4 tally card and tally multiplier card '*(1 (mat #) -6 -7)'* where reaction number -6 means total fission cross section and -7 is fission ν. Tally results are post processed by multiplying volume and U number density. As a final result, total number of fission neutron produced per one source neutron was obtained and this is the same with multiplication factor by track length estimator in definition.

5. Results

As shown in Fig 1 and Fig 2, CAR1 and CAR2 are closer to the BF3 detectors (at TCE2 and TCE3) than CAR3 and CAR4. Characteristics of detector signal of CAR1 is similar to that of CAR2 (CAR3 and CAR4 are similar either). Therefore, in this paper, test results of CAR1 and CAR3 are analysed. For production of correction factor of CAR1 calculation results during iterations are shown in Fig 5 and Fig 6. Both power of fuel assemblies and effective multiplication factor are converged in 5 iterations. FA power is converged within 1% relative error between iterations and k_{eff} converged within 10pcm. In Tab 1, reactivity worth of CAR1 and CAR3 are summarized.

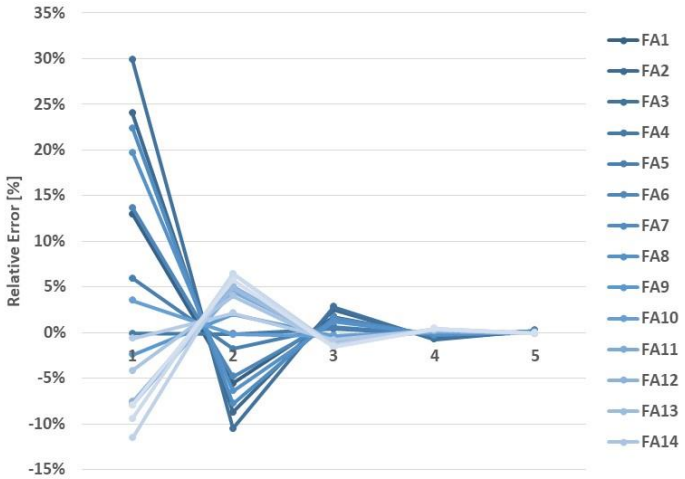

Fig 5. Convergence of power of fuel assembly

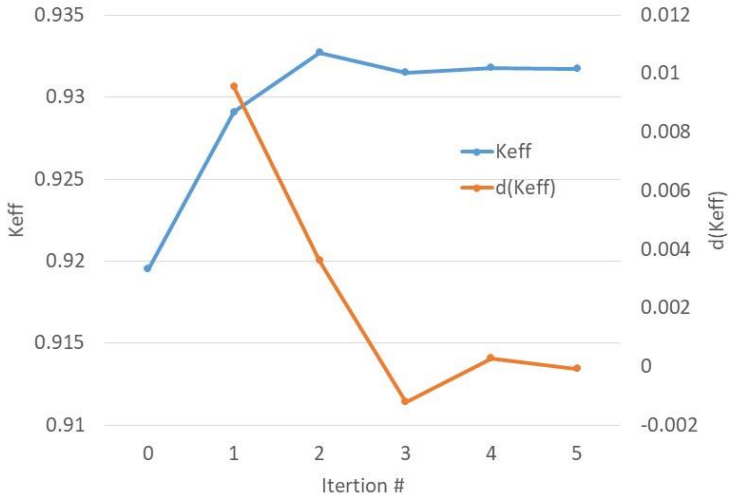

Fig 6. Convergence of multiplication factor

Tab 1: Summary of CAR rod worth [mk]

Case		CAR1	CAR3
No correction	MCNP (C)	-84.96	-81.48
	Measurement (M)	-83.24	-49.66
	Error ((C-M)/M) [%]	2.1	64.1
Correction	MCNP	-70.58	-67.94
	Measurement	-70.23	-68.74
	Error ((C-M)/M) [%]	0.5	1.2

Calculated reactivity of CAR1 and CAR3 are both well agreed with measured one after correction with spatial correction factor. Without correction process, reactivity value of calculation seems accurate but results of CAR3 shows the reason why spatial effect should be corrected properly and CAR1 result looks like coincidence. During the iterative calculation process there is a change between MCNP calculation results. Obviously this is due to redistribution of delayed neutron source and it can be concluded dynamic effect is taken into account from modified static calculation.

6. Conclusions

JRTR rod drop tests are revisited and test results are corrected with spatial correction factor. Spatial correction factor was produced with series of steady state calculation and modification of delayed neutron fraction. Importance of correction of static spatial effect is clear as measured reactivity values converge to similar values. Static reactivity also should reflect the spatial effect but actual value (-70.58 and -67.94) need to be verified with transient calculation.

Acknowledgement

This work was supported as a part of the Technology Development and Enhancement for Supporting the Export of Research Reactor Systems project sponsored by the Ministry of Science and ICT of the Korean government (2020M2D5A1078126).

7. References

1. M. Maillot et al., “Analysis of the Rod-Drop Experiments Performed during the CABRI Commissioning Tests”, RRFM2018, Munich, Germany, March 11-15, 2018.
2. Y. A. Chao et al., “Dynamic Rod Worth Measurement”, *Nuclear Technology*, Vol. 132, p. 403, 2000.
3. E. K. Lee et al., “New Dynamic Method to Measure Rod Worths in Zero Power Physics Test at PWR Startup”, *Annals of Nuclear Energy*, Vol. 32, p.1457-1475, 2005.
4. B. Jeon, et al., “Analysis of Complex Effect of Neutron Source, Gamma-ray and Neutron Flux Distribution in Rod-Drop Experiment for Control Rod Reactivity Worth Measurement”, *Proceedings of the Korean Nuclear Society Autumn Meeting*, Taegu, Korea, October, 1997. (in Korean)
5. J. L. Conlin et al., A Compact ENDF (ACE) Format Specification, Loa Alamos National Laboratory, LA-UR-19-29016.

INITIAL POST-IRRADIATION OPTICAL MICROSCOPY RESULTS FROM PRIORITY PLATES IN THE EMPIRE FUEL TEST

W.A. HANSON, A.B. ROBINSON, D.D. KEISER JR., I.Y. GLAGOLENKO
Idaho National Laboratory
P. O. Box 1625, Idaho Falls, ID 83415 – United States of America

B. YE, Z.-G. MEI, L.M. JAMISON, G.L. HOFMAN
Argonne National Laboratory
9700 Cass Ave, Lemont, IL 60439 – United States of America

ABSTRACT

Initial optical microscopy was completed for the European Mini-Plate Irradiation Experiment (EMPIrE). Several fabrication parameters were varied as a part of the experiment design, but the primary fuel consisted of a dispersion core of zirconium nitride (ZrN) coated low-enriched uranium (LEU) U-Mo fuel particles in an aluminum (Al) matrix, clad in Al-alloy, in a mini-plate geometry. The mini-plates were irradiated within the Idaho National Laboratory (INL) Advanced Test Reactor (ATR) at a high meat power density (~21 kW/cm^3) and to a high fuel particle fission density (~6.4 × 10^{21} fissions/cm^3). Following non-destructive post-irradiation examination (PIE), a priority subset of the EMPIrE mini-plates were sectioned for destructive PIE, based on their combination of fabrication variables and irradiation conditions. Observations on the differences in microstructural evolution between these mini-plates will be discussed as will an initial comparison to the trends noted within the fuel particle swelling analysis.

1. Introduction

1.1 Experimental Details

The European Mini-Plate Irradiation Experiment (EMPIrE) was intended to support the conversion of select high-performance research reactors (HPRRs) to utilize low-enriched uranium (LEU) by evaluating the performance of coated uranium molybdenum (U-Mo) dispersion fuel. The EMPIrE experiment consisted of 44 dispersion LEU U-Mo mini-plates, irradiated in the Idaho National Laboratory (INL) Advanced Test Reactor (ATR) to a high particle fission density (~6.4 × 10^{21} fission/cm^3) at high meat powder density (~21 kW/cm^3). These conditions are similar to the SCK CEN BR2 reactor bounding conditions, where the irradiation was performed for the concurrent full-size plate experiment, SEMPER FIDELIS [1]. The full background of the EMPIrE experiment, including design, fabrication details, and irradiation parameters, have been discussed thoroughly [2, 3], so only a brief summary is provided here. The aluminum (Al)-alloy clad mini-plate fuel meat primarily consisted of zirconium nitride (ZrN) coated LEU U-Mo fuel particles, dispersed in an Al-matrix. During the EMPIrE fabrication, several of the parameters were varied to evaluate their influence on the fuel performance. These included fuel powder heat treatment prior to coating, coating methodology, fuel particle size distribution, Mo alloying content, and fuel powder source. The focus of this work are the optical microscopy results for EMPIrE plates that were previously identified as having the highest analysis priority, due to their combination of fabrication variables

(plate-type) and irradiation conditions. A summary of these priority plates, along with their plate-type and other parameters are detailed below in Tab 1.

1.2 Sample Preparation and Irradiation History

Following non-destructive post-irradiation examination (NDE-PIE) of all 44 EMPIrE dispersion plates, 15 priority mini-plates were sectioned using a low speed diamond saw for destructive (DE)-PIE, according to the diagrams in Fig 1, where the diagram for each plate is detailed in Tab 1. DE-PIE include optical and electron microscopy (7 mm and 3 mm transverse cross-sections, respectively), chemical burn-up analysis (two 2.5 × 3.5 mm samples), and thermophysical property measurements (3.5 mm DSC sample strip and 6 mm Laser Flash sample strip). All samples were sectioned based off an initial, transverse section at the fuel-zone midplane (50 mm from the mini-plate non-ID end), to locate the initial transverse metallography cross-section (Met in Fig 1).

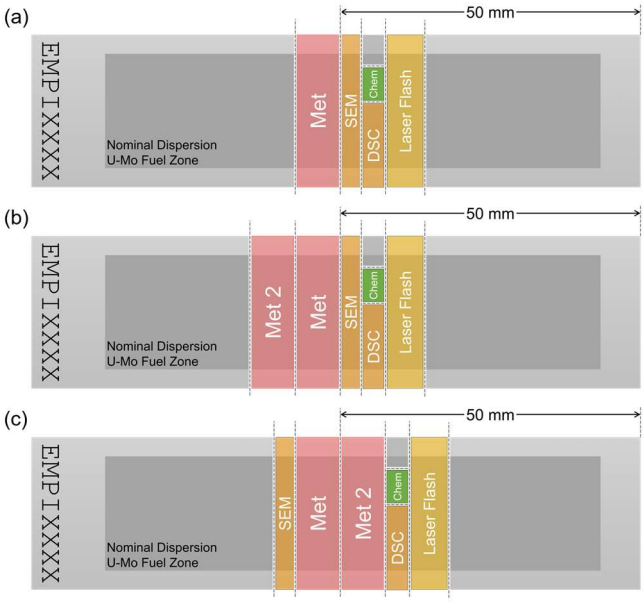

Fig 1: Sectioning diagrams illustrating metallography sample locations.

Due to an epoxy curing sample preparation issue, image analysis was not possible using the first metallography sample for many of the priority mini-plates. Following modification to the sample preparation process, including the inclusion of glass beads to improve edge retention, a second 7 mm metallography cross-section (Met 2) was sectioned for the affected plates. The locations for the second samples are shown in the diagrams in Fig 1 (b) or (c) and were dependent on the status of other DE-PIE sectioning performed. The sectioning diagram and metallography sample used for the analysis presented in this work is detailed for each priority mini-plate in Tab 1.

A neutronics analysis was performed for the EMPIrE irradiation and validated with test-train flux wire analysis [4]. The resulting 4 × 16 grid of analysis nodes over the nominal fuel zone of each mini-plate have a calculated end-of-life (EOL) meat fission density that was corrected to EOL particle fission density using the as-fabricated volume fraction of fuel in the meat [3]. Using the as-fabricated plate dimensions, sectioning diagrams, and a conservative 0.5 µm saw-loss, the metallography cross-sections for each priority-plate were placed into the same reference frame as the neutronics nodes, and a weighted average particle fission density was calculated for each DE-PIE sample, provided for the metallography samples examined in this work in Tab 1.

Plate-Type	Fabrication Variables	Powder Batch Average Coating Thicknesses (μm)	Plate ID	Sectioning Diagram (sample)	Sample Fission Density (fission/cm^3)
Type 1	ZrN/ALD/HT/25% Fines	0.5*	EMPI0117	(c) (met 2)	4.21×10^{21}
			EMPI0109	(a) (met)	5.90×10^{21}
Type 20A	U-10Mo/ZrN/ALD/HT/0% Fines	0.5*	EMPI2003	(a) (met)	2.79×10^{21}
Type 20B	U-10Mo/ZrN/ALD/HT/22% Fines	0.5*	EMPI2007	(a) (met)	5.11×10^{21}
Type 22	ZrN+AlN/ALD/HT/0% Fines	0.5*	EMPJ2207	(a) (met)	5.19×10^{21}
Type 5	ZrN/ALD/HT/0% Fines	0.79	EMPI0518	(c) (met 2)	3.10×10^{21}
			EMPI0512	(a) (met)	5.83×10^{21}
Type 7A	ZrN/PVD/NoHT/0% Fines	1.17	EMPI0712	(b) (met 2)	3.00×10^{21}
			EMPI0706	(a) (met)	4.64×10^{21}
			EMPI0702	(b) (met 2)	5.73×10^{21}
Type 8A	ZrN/PVD/HT/0% Fines	2.02	EMPI0813	(a) (met)	2.79×10^{21}
			EMPI0818	(b) (met 2)	3.32×10^{21}
			EMPI0820	(c) (met 2)	5.16×10^{21}
			EMPI0821	(b) (met 2)	6.24×10^{21}
Type 9	Lab-Scale U-7Mo/ZrN/PVD/HT/0% Fines	1.53	EMPI0905	(c) (met 2)	6.10×10^{21}

*minimum specified coating thickness

Tab 1: Summary of the EMPIrE priority plates sorted by their plate-type, fabrication variables [2, 5, 6, 7], and irradiation conditions. The particle fission density reported is the average for the 7 mm transverse metallography cross-section as identified in Fig 1.

2. Results

Optical microscopy was performed from low to high magnification (50-500x) for each priority-plate transverse cross-section. A selection of the optical micrographs are shown for the mini-plates containing U-Mo powder coated via ALD in Fig 2 and via PVD in Fig 3, for brevity referred to as ALD and PVD plates, respectively. It should be noted, a limited selection of optical microscopy results for EMPIrE PVD priority plates were presented previously [8]; however, these latest results were gathered at a higher resolution. In each case, a high magnification (500x) montage of the center of the fuel zone, encompassing the meat thickness is shown with an accompanying zoomed view from the montage. In both figures, grain refinement appears to increase with fission density, with small micron-size fission gas bubbles observed to accumulate at the grain boundaries. Additionally, a thin fission gas bubble denuded region is readily observed in the heat-treated particle peripheries at fission densities exceeding 5.1×10^{21} fissions/cm^3.

From initial examination of the ALD plates in Fig 2, an Al-U-Mo interaction layer (IL) forms and appears to increase with fission density for both the U-7Mo Type 5 and U-10Mo Type 20A&B plates. Significantly increased IL is observed in both Type 1 plates as compared to the other ALD plates while the IL observed around the Type 22 plate particles appears slightly less than the similar fission density Type 5 plate. Large pores are also observed in the IL of the Type 1 plates and the highest fission density Type 5 plate.

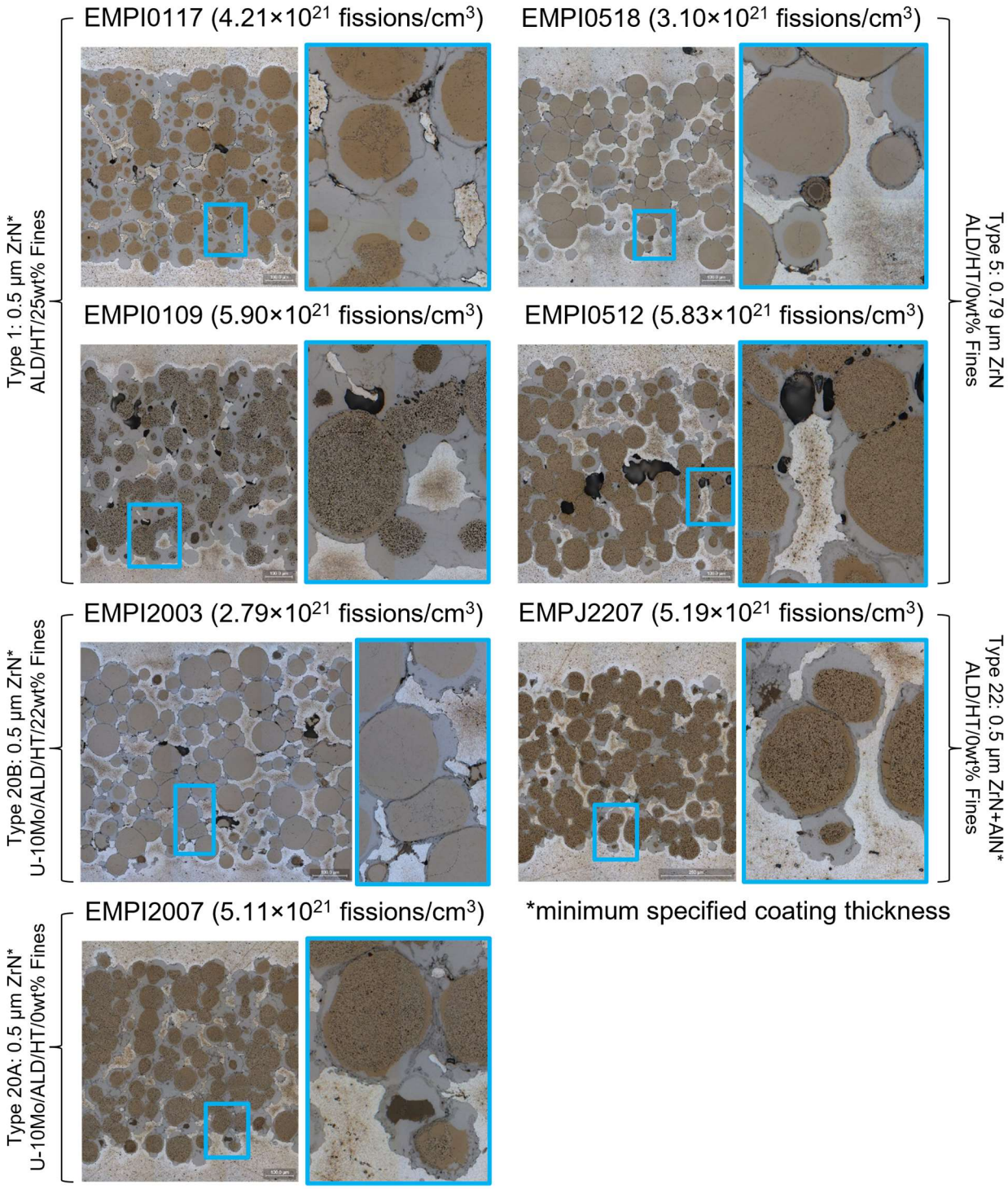

Fig 2: Select 500x optical microscopy montages with zoomed views of Type 1, 20A, 20B, 22, and 5 priority mini-plates, each of which was fabricated with heat-treated fuel powder that was coated with ZrN via ALD. The Type 22 U-7Mo powder received an additional AlN coating via ALD. In all cases the images are located in the center of the fuel-zone, and the 500x montage encompasses the fuel meat thickness.

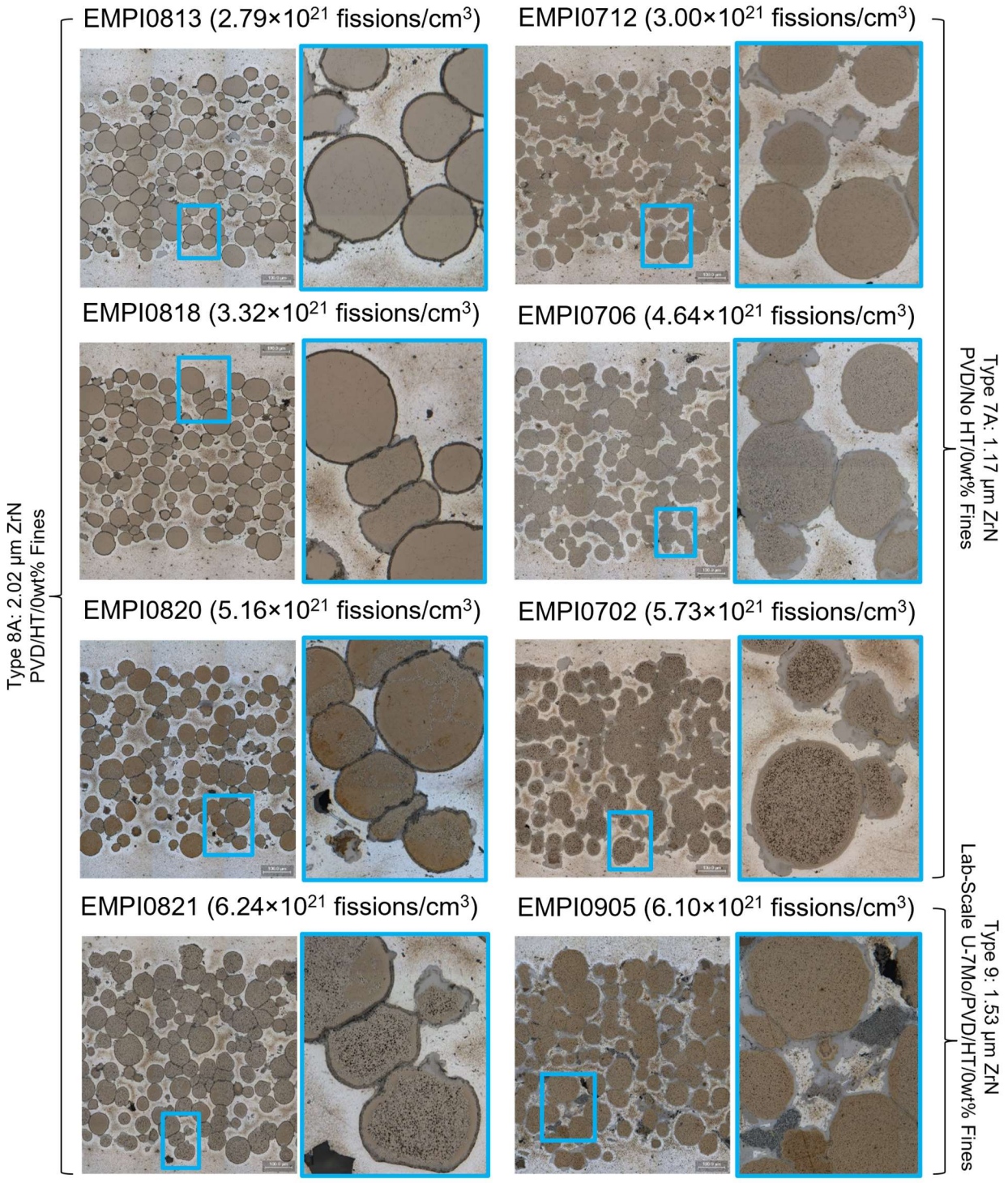

Fig 3: Select 500x optical microscopy montages with zoomed views of Type 7A, 8A, and 9 priority mini-plates, each of which was fabricated with fuel powder that was coated with ZrN via PVD. The Type 8A and 9 U-7Mo powder was heat-treated prior to coating while the Type 7 fuel powder was retained in the as-atomized condition. Additionally, the Type 9 powder was fabricated via an independent lab-scale process. In all cases the images are located in the center of the fuel-zone, and the 500x montage encompasses the fuel meat thickness.

From initial examination of the PVD plates in Fig 3, the initial grain size effect is apparent between the Type 7A and Type 8A plates, with grain subdivision and accumulation of micron-size bubbles at new grain boundaries delayed to higher fission densities in the heat-treated Type 8A plates. While the Type 8A plates appear to have IL limited to regions where the ZrN coating appears damaged, for the Type 7A plates, some IL is also observed in a thin layer, external to the coated fuel particles, at all fission densities. Significantly more IL is observed in the Type 9 plates; though, these appear predominantly in the vicinity of what appears to be a secondary fissile phase scattered throughout the meat.

3. Discussion

3.1 Fuel Microstructural Evolution

The microstructural behaviour of the U-Mo particles observed from examining the 15 EMPIrE priority plates appears consistent with previous studies characterizing U-Mo performance [9, 10, 11]. The microstructure appears generally unchanged at lower fission density (<3 × 10^{21} fissions/cm^3) with small, micron-size fission gas bubbles observed in low density at the grain boundaries. At moderate fission densities (3–4 × 10^{21} fissions/cm^3), grain refinement, often referred to as subdivision, results in additional grain boundary interfaces for the larger intergranular fission gas bubbles to coalesce. Eventually the fuel particle is fully recrystallized with micro-grains fully surrounded by the increasing fission gas bubbles, currently observed in this study >5 × 10^{21} fissions/cm^3 [9].

A primary hypothesis tested within EMPIrE irradiation experiment was that heat treating the U-Mo fuel particles would increase the initial grain size, and thus delay the grain refinement and coalescence of the micron-size intergranular fission gas bubbles [1, 2, 5, 9]. At this stage of the analysis, this hypothesis appears confirmed within the PVD plates. Comparing the Type 7A and 8A plates in Fig 3, the initial grain size afforded by the heat treatment applied to the Type 8A plates clearly delays the full recrystallization of the fuel particles from <4.6 × 10^{21} fissions/cm^3 to between 5.1–6.2 × 10^{21} fissions/cm^3. It should be noted that it is likely the grain refinement was only partially delayed in the heat-treated Type 9 plates as uranium carbide (UC) contamination was detected during fabrication as intergranular UC precipitates in the U-Mo particles, suspected to have reduced the grain growth through pinning grain boundaries [3]. However, as the only sectioned Type 9 plate exceeds a fission density of 6 × 10^{21} fissions/cm^3, analysis of lower fission density plates will be necessary to further evaluate this.

Some additional observations should be made regarding the micron-scale fission gas bubble denuded zone observed in the periphery of the U-Mo particles at higher fission density. This is not the first time these denuded zones have been observed in U-Mo dispersion fuel [12], and substantial microstructural characterization, including SEM, WDS/EDS, and potentially TEM will be needed to characterize them more fully. Initial observations note that the denuded zones are more readily observed in the higher fission density samples (>5.1 × 10^{21} fissions/cm^3); however, the resolution of the optical microscopy makes observing the region at fission densities where grain subdivision is reduced a challenge. It seems likely that higher resolution analysis using SEM will reveal evidence of the denuded periphery at lower fission densities. It can be readily observed that the denuded region is reduced in proximity to other U-Mo particles, so its formation may be related to a reduced local fission environment. This seems corroborated by the reduced denuded zones adjacent to Al-U-Mo IL containing a high density of fission gas bubbles as this IL contained sufficient U for increased fission events. Admittedly, the reduced periphery in these cases may

also be due to particle periphery loss to the IL formation. Ultimately, the precise mechanism remains unclear at this time and substantial microstructural and chemical analysis will be necessary to characterize the regions.

3.2 Al-U-Mo Interaction Layer

One of the more common IL formations observed in the EMPIrE experiment is unsurprisingly at regions where the fuel powder coating appears damaged. These have a striking resemblance to the “erupting volcano” features observed in the ZrN SELENIUM plate [9], with the coating appearing to “curl” as the IL forms at what was likely a separation in the coating. The most clear examples may be observed in the Type 7A and 8A plates where less overall IL is apparent. The highest fission density Type 8A plate (EMPI0821) also shows a few examples of small IL formations on the inside of intact ZrN coating in the particle periphery as were observed in the highest fission density regions of the ZrN SELENIUM plate [9].

While the erupting volcano features were also observed in the Types 20A&B, 22, and 5 priority plates, more commonly, the IL in these mini-plates appears to form in a layer that surrounds the fuel particles. Further, a more extreme example of this IL formation was observed in the Type 1 plates, where little matrix appears to remain. In these cases, a darker phase is often observed near the IL/Al-matrix interface or at interfaces where multiple IL formation fronts intersect. SEM analysis along with WDS/EDS will be needed to identify this phase.

Based on the interaction layer formation observed to this point in the EMPIrE DE-PIE, it appears that the IL formation is heavily influenced by the initial fuel particle coating thickness. The thickest ZrN coating (~2 μm) in the EMPIrE experiment was applied via PVD to the Type 8A plates examined here, which showed very little IL formation beyond where the coating was damaged. A slightly thinner ZrN coating was applied in the case of the priority Type 7A plates and the Type 9 plate (~1.2–1.5 μm), and in these cases, a thin IL layer was observed exterior to the coating at higher fission densities. These results appear consistent with the preliminary results reported previously for the PVD priority EMPIrE plates [8]. Further, examining the ALD plates in Fig 2, this trend appears to continue, culminating in the most IL formation observed in the Type 1 plates, which likely had the thinnest ZrN coating [5]. It should be acknowledged the increased surface area afforded by the inclusion of fines in the Type 1 plates likely contributed to the increased IL formation. It is also interesting to note that the secondary AlN coating applied via ALD in the Type 22 plate appears to have reduced the IL formation slightly as compared to the slightly thicker ALD ZrN coating in the Type 5 plates. Image analysis to quantify the fuel, matrix, and IL phase fractions will aid in identifying mechanisms for the behaviour observed here.

3.3 Initial Comparison to NDE-PIE

At this time, it is appropriate to make some initial comparisons between the NDE-PIE results, specifically the fuel particle swelling analysis, to those observed in this work. In the fuel particle swelling analysis, detailed previously [3], the Type 8A plates had the lowest swelling at all fission densities. Comparing this result to the optical micrographs in this analysis, it seems likely that the general lack of IL formation in this plate-type consequently reduced the area for insoluble micron-size fission gas bubble formation that increased the meat swelling in the other examined plate-types. The thicker ZrN coating clearly contributed to this response as the thinner coated powder batches exhibit both increased IL formation and fission gas bubble accumulation external to the

fuel particles at the interface with the IL. It also seems likely that the slight delay in grain refinement contributed to reduced swelling in the Type 8A plates as compared to the Type 7A plates [3]; though, the difference appears subtle at this stage. Additional characterization comparing the Type 5 and Type 6 ALD plates will reveal more on this mechanism.

The results presented here also provide some insight into the swelling response of the Type 9 plates. The presence of significant IL within the matrix, containing coalesced fission gas bubbles, as well as a currently unidentified secondary phase that appears fissile likely contribute to the increase swelling observed [3]. Microstructural and chemical analysis of this secondary phase are anticipated to improve the understanding of the swelling response.

4. Acknowledgements

This work is supported by the U.S. Department of Energy, under DOE Idaho Operations Office Contract DE-AC07-05ID14517. Accordingly, the U.S. Government retains a nonexclusive, royalty-free license to publish or reproduce the published form of this contribution, or allow others to do so, for U.S. Government purposes. The authors would like to acknowledge the Korea Atomic Energy Research Institute for providing the U-7Mo powder for this experiment, S. Bhattacharya's efforts in applying the ALD coating, and Y. S. Kim's effort in the EMPIrE test design. The authors would like to thank Xavière Iltis for providing ZrN coating thickness measurements for select powder batches. The authors would also like to acknowledge the staff, engineers, and operators of the INL Materials and Fuels Complex (MFC) Hot Fuel Examination Facility (HFEF) for their efforts during the post-irradiation examinations. Argonne National Laboratory's work was supported by the U.S. Department of Energy, Office of Science, under contract DE-AC02-06CH11357.

5. References

[1] B. Stepnik, M. Grasse, C. Rontard, D. Geslin, Y. Guinard, S. Van den Berghe, A. Leenaers, H. Breitkreutz, W. Petry, H. Palancher, E. Hervieu, Y. Calzavara and H. Guyon, "Manufacturing in the SEMPER FIDELIS UMo irradiation experiment," in *RRFM 2018, European Research Reactor Conference 2018*, MUNICH, GERMANY, 2018.

[2] X. Iltis, H. Palancher, J. Allenou, F. Vanni, B. Stepnik, A. Leenaers, S. Van Den Berghe, D. Keiser and I. Glagolenko, "Characterization of fresh EMPIrE and SEMPER FIDELIS U(Mo)/Al fuel plates made with PVD-coated U(Mo) particles," *EPJ Nuclear Science and Technology,* vol. 4, no. 49, 2018, doi:10.1051/epjn/2018048.

[3] W. A. Hanson, A. B. Robinson, N. J. Lybeck, J. W. Nielsen, B. Ye, Z.-G. Mei, D. D. Keiser Jr., L. M. Jamison, G. L. Hofman, A. M. Yacout, A. Leenaers, B. Stepnik and I. Glagolenko, "Non-destructive analysis of swelling in the EMPIrE fuel test," *Journal of Nuclear Materials,* vol. 564, no. 153683, 2022, doi:10.1016/j.jnucmat.2022.153683.

[4] J. Nielsen, B. Curnutt, D. Choe, M. Reicheberger, D. Nigg, I. Glagolenko and J. Henley, "Experiment Validation Protocol for Flux Wire Measurements in the Advanced Test Reactor," *PRS/JOU-21-00957, Idaho National Laboratory,* submitted to Nuclear Technology, manuscript under review.

[5] F. Housaer, F. Vanni, M. Touzin, F. Béclin, J. Allenou, A. Leenaers, A. Yacout, H. Palancher, B. Stepnik and O. Tougait, "Morphological characterization of the fresh ZrN coated UMo powders used in EMPIrE irradiation experiment: A practical approach," *Journal of Nuclear Materials,* vol. 533, no. 152087, 2020, doi:10.1016/j.jnucmat.2020.152087.

[6] T. Trowbridge, D. Keiser and C. Brizzee, “EMPIrE Fresh Fuel Characterization Report,” *INL/EXT-20-59404, Rev 0., Idaho National Laboratory,* September 2020.

[7] X. Iltis, H. Palancher, F. Vanni, J. Allenou, B. Stepnik, A. Leenaers, S. van den Berghe, I. Glagolenko and D. Keiser, “Characterization of fresh EMPIrE and SEMPER FIDELIS plates made with PVD-coated U(Mo) particles,” in *RRFM 2018, European Research Reactor Conference 2018*, Munich, Germany, (2018).

[8] G. Hofman, L. Jamison, B. YE, Z.-G. Mei, A. Yacout, A. Robinson, W. Hanson, J. Nielsen, D. Keiser and A. Leenaers, “Analysis of Preliminary PIE Results for PVD Coated U-7Mo Dispersion Fuel Plates Irradiated in the EMPIrE Experiment,” *RRFM2020 Conference Proceeding, Fuel Cycle from Front End to Back End,* pp. 27-31, 2020.

[9] A. Leenaers, S. Van den Berghe, E. Koonen, V. Kuzminov and C. Detavernier, “Fuel swelling and interaction layer formation in the SELENIUM Si and ZrN coated U(Mo) dispersion fuel plates irradiated at high power in BR2,” *Journal of Nuclear Materials,* vol. 458, pp. 380-393, 2015, doi:10.1016/j.jnucmat.2014.12.073.

[10] J. Gan, B. Miller, D. Keiser Jr., J. Jue, J. Madden, A. Robinson, H. Ozaltun, G. Moore and M. Meyer, “Irradiated microstructure of U-10Mo monolithic fuel plate at very high fission density,” *Journal of Nuclear Materials,* vol. 492, pp. 195-203, 2017, doi:10.1016/j.jnucmat.2017.05.035.

[11] J. Rest, “Evolution of fission-gas-bubble-size distribution in recrystallized U–10Mo nuclear fuel,” *Journal of Nuclear Materials,* vol. 407, no. 1, pp. 55-58, 2010, doi: 10.1016/j.jnucmat.2010.07.009.

[12] J. D. D. KEISER, J.-F. JUE, B. D. MILLER, J. GAN, A. B. ROBINSON, P. G. MEDVEDEV, J. W. MADDEN and G. A. MOORE, “Microstructural Characterization of a Mg Matrix U-Mo Dispersion Fuel Plate Irradiated in the Advanced Test Reactor to High Fission Density: SEM Results,” *Metallurgical and Materials Transactions E,* vol. 3, no. 2, pp. 71-89, 2016, doi: 10.1007/s40553-016-0071-3.

The IVG.1M Reactor Conversion: Current State and Prospects

Irkimbekov R.A.[1], Gnyrya V.S. [1], Prozorova I.V.[1]

Hanan, Nelson A.[2], Garner, Patrick L.[2], Stevens, John G.[2]

[1] National Nuclear Center of the Republic of Kazakhstan

[2] Argonne National Laboratory, USA

The conversion of research reactors to low-enriched fuel is supported by the Office of Material Management and Minimization of the US Department of Energy. The IVG.1M reactor designed and built by Russian specialists has been operating since its inception in 1972 with Russian high-enriched uranium (HEU) fuel (with 90% enrichment in U^{235} isotope). The NNC RK (National Nuclear Center of the Republic of Kazakhstan) and ANL (Argonne National Laboratory, USA) jointly carried out the conversion of the IVG.1M reactor from high enriched uranium (HEU) fuel to low enriched uranium fuel (LEU), with an enrichment of less than 20% in U^{235} isotope using the geometry of a fuel element identical to that one used in the core with HEU fuel. ANL provided analytical support to NNC in the feasibility study of IVG.1M reactor conversion, selection of a suitable type of LEU fuel and fuel assemblies for conversion, development of technical requirements for LEU fuel, fuel testing and safety analysis.

The Legal Framework was developed, which included the following organizations and agreements:

- International Atomic Energy Agency and Republic of Kazakhstan
  - Bilateral Safeguards Agreement between the IAEA and the Republic of Kazakhstan, June 1995.
- United States and Russian Federation
  - Agreement Between the Government of the United States of America and the Government of the Russian Federation Concerning Cooperation for the transfer of Russian-Produced Research Reactor Nuclear Fuel to the Russian Federation, May 2004.
- United States and Republic of Kazakhstan
  - Agreement Between the Department of Defense of the United States of America and the Ministry of Defense of the Republic of Kazakhstan Concerning Control, Accounting, and Physical Protection of Nuclear Material to Promote the Prevention of Nuclear Weapons Proliferation, December 1993;
  - Agreement Between the United States of America and the Republic of Kazakhstan Concerning the Destruction of Silo Launchers of Intercontinental Ballistic Missiles, Emergency Response, and the Prevention of Proliferation on Nuclear Weapons, December 1993.
- Republic of Kazakhstan and Russian Federation.
  - Agreement Between the Government of the Republic of Kazakhstan and the Government of the Russian Federation in the Field of Peaceful Use of Nuclear Energy, September 1993.

Description of the IVG.1M Reactor

IVG.1M reactor (Fig.1) is modified IVG.1 reactor commissioned in 1975. IVG.1 reactor was gas cooled and used for testing of fuel assemblies of high-temperature gas cooled reactors, including reactors of nuclear rocket engines. The IVG.1M is water cooled. The power of the IVG.1M reactor is limited by 10 MW, because of the available flow rate of the water coolant. Preliminary studies have shown that the conversion of the reactor when replacing the fuel with low-enriched fuel makes it possible to keep the reactor design unchanged. [1-3].

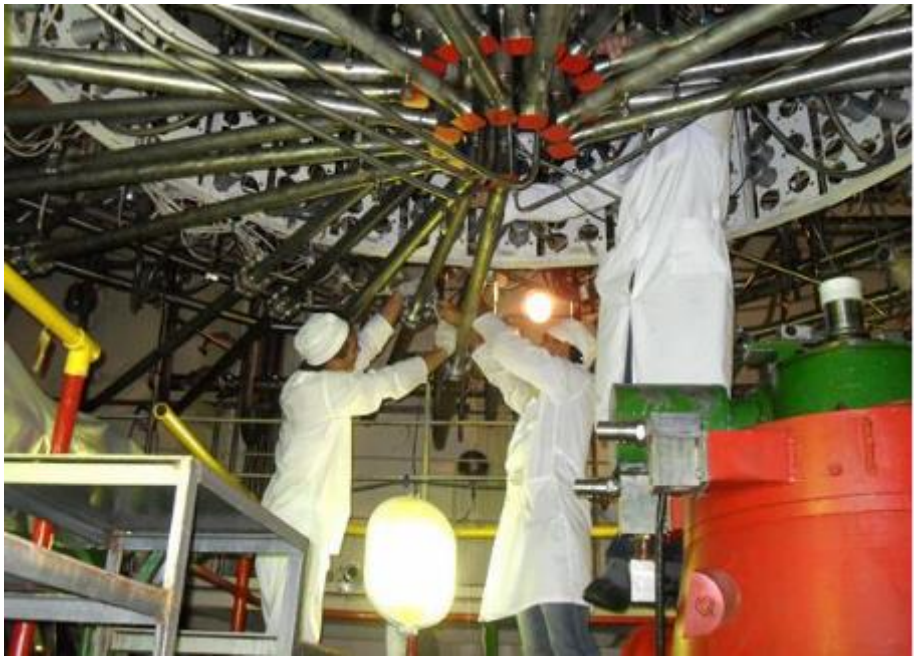

Figure 1. The IVG.1M reactor

The IVG.1M Conversion Roadmap

- Now the project has completed the following:
  - collaboration established in 2010
  - analysis showed that conversion from HEU to LEU was feasible (2012) [4];
  - technical requirements for LEU fuel were developed;
  - neutronic models and code for reactor kinetics calculations were developed [5];
  - calculations were made to produce a Safety Analysis Report (SAR) for LEU fuel [6];
  - irradiation experiments and post-irradiation studies of LEU fuel were carried out [7, 8];
  - physical start-up of the IVG.1M reactor was prepared and is in progress (2022);
  - preparations are under way for the energy start-up of the IVG.1M reactor (2022-2023).

During the process of the IVG.1M reactor conversion to LEU, the design of each fuel assembly and the design of the reactor in whole remained unchanged. The Russian company JSC NPO "LUCH" developed and manufactured water-cooled technological channels with fuel enrichment of 19.75%.

Experimental LEU fuel assemblies and single fuel pins were delivered to Kazakhstan from Russia in July 2014. The fuel was examined in great detail, including destructive studies of single fuel elements. In the course of these studies, some deviations of the characteristics of the fuel elements from the technical requirements were revealed. As a result, the technology of manufacturing low-enriched fuel was improved.

The experimental LEU fuel was then irradiated in the IVG.1M (with the remainder of the core HEU) in order to demonstrate good performance with burnup. To accelerate the test program and according to proposal of Argonne National Laboratory, NNC performed design, construction and commissioning of a coolant cooling system (Fig. 2) that allowed the reactor to be operated once per week, rather than once per month. This will be an enduring benefit of the conversion process, allowing more frequent irradiations in the IVG.1M.

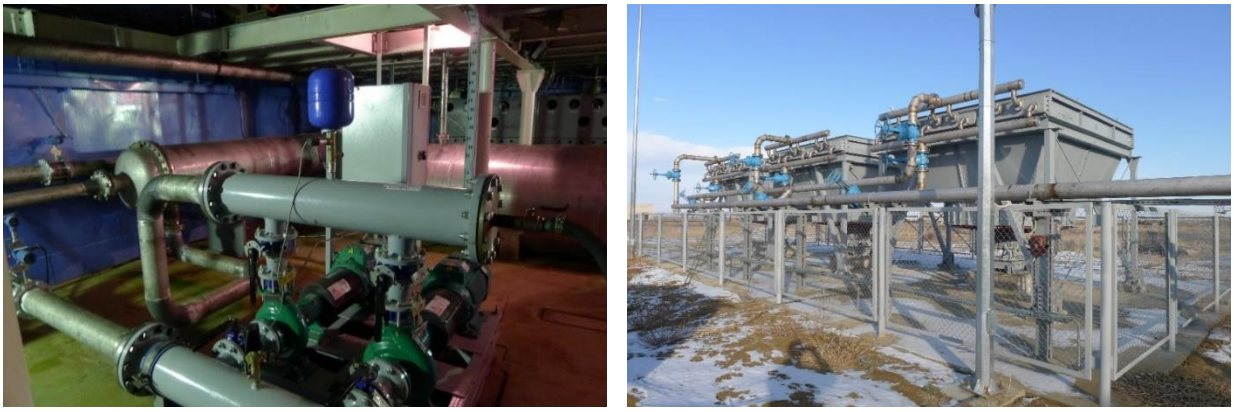

Figure 2. Cooling system for the primary coolant of the IVG.1M reactor
a) Heat exchanger and pumps premise; b) Chillers

After the success of the test irradiation program and Post Irradiation Examinations performed by NNC, the full load of conversion fuel that took into account the changes made at the previous stage was delivered from Russia to Kazakhstan (Fig 3). The conversion fuel was again examined in great detail by NNC, including complete non-destructive examinations and destructive analysis of randomly selected “witness pins”.

Once the full load of fuel was determined to be acceptable the loading of the LEU fuel into the IVG.1M was able to commence in March 2022.

Figure 3. Fuel was delivered from Russia to Kazakhstan
The fuel was transported via an airplane to the Semipalatinsk airport, then by special trucks to the research reactor complex.

Stages of Physical Start-Up

At present, the first stage of commissioning the reactor with LEU fuel is being implemented, namely, the stage of physical start-up of the IVG.1M reactor. On May 05, 2022, the physical start-up of the IVG.1M reactor with low-enriched uranium fuel was successfully carried out at the National Nuclear Center of the Ministry of Energy of the Republic of Kazakhstan [9]. To fix the critical state, the reactor was brought to a power of 2 W. The critical state was reached when the control drum system was rotated by 91.5°.

The overall purpose of the physical start-up program of the IVG.1M will determine the main neutronic characteristics of the reactor with LEU fuel.

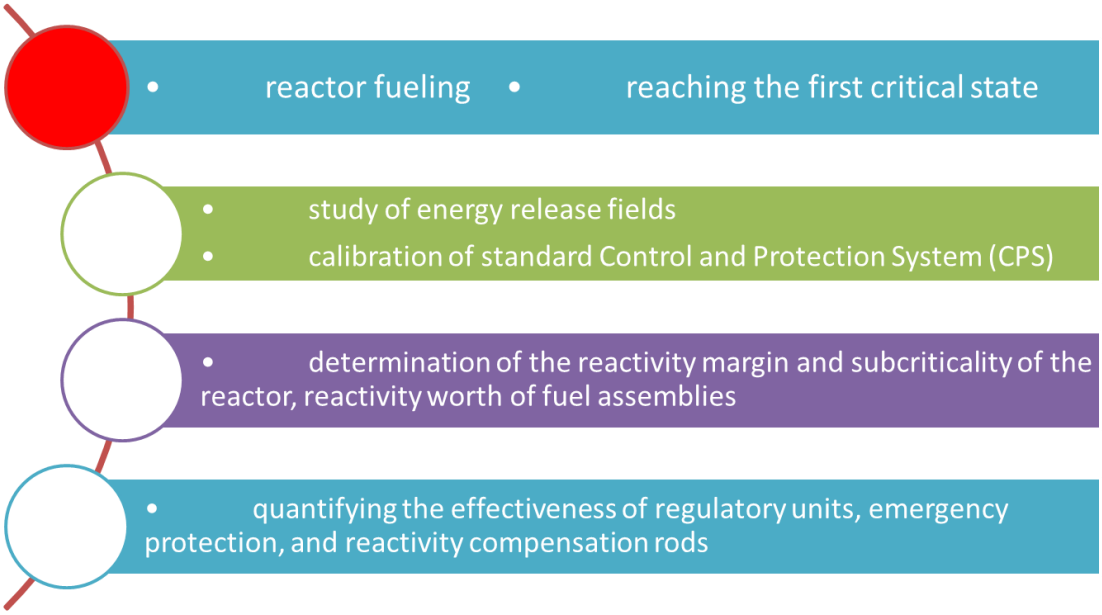

Figure 4. Stages of physical start-up

- The multiple steps will include:
  - reactor fueling;
  - reaching the first critical state;
  - study of energy release fields [10];
  - calibration of standard Control and Protection System (CPS) sensors in units of absolute power;
  - determining the reactivity margin and subcriticality of the reactor;
  - determining the reactivity worth of fuel assemblies of the first, second, and third rows;
  - determining the reactivity worth of voiding fuel assemblies of the first, second, third rows;
  - quantifying the effectiveness of regulatory units, emergency protection, and reactivity compensation rods;
  - examining the radiation fields surrounding the reactor.

After the completion of the next stage - the power start-up of the reactor, and the experimental determination of all the necessary characteristics of the new core at power, the IVG.1M reactor will be put into operation. Thus, as early as 2023, research work in the field of peaceful atomic applications will be resumed at the IVG.1M reactor. At that time, according to the calculations, we will be able not only to maintain, but also significantly improve the output characteristics of the reactor.

Acknowledgement

This work was sponsored by the U.S. Department of Energy, Office of Material Management and Minimization (M3) in the U.S. National Nuclear Security Administration Office of Defense Nuclear Nonproliferation under Contract DE-AC02-06CH11357. This paper describes the collaboration between Argonne and NNC for the M3 Conversion Program aspects of the overall project. The M3 Remove Program team of the Idaho National Laboratory and NNC performed tremendous work to assure the site was ready for HEU fuel removal and LEU fuel delivery.

The work was supported by the Ministry of Education and Science of the Republic of Kazakhstan [grant project № AP08856242].

Argonne, LLC, nor any of their employees or officers, makes any warranty, express or implied, or assumes any legal liability or responsibility for the accuracy, completeness, or usefulness of any information, apparatus, product, or process disclosed, or represents that its use would not infringe privately owned rights. Reference herein to any specific commercial product, process, or service by trade name, trademark, manufacturer, or otherwise, does not necessarily constitute or imply its endorsement, recommendation, or favoring by the United States Government or any agency thereof. The views and opinions of document authors expressed herein do not necessarily state or reflect those of the United States Government or any agency thereof, Argonne National Laboratory, or UChicago Argonne, LLC.

References

1 Kotov V.M., Rajkhanov N.A., Prozorova I.V. (2005). *Modernization of IVG1 reactor fuel*. Vestnik Natsional'nogo Yadernogo Tsentra Respubliki Kazakhstan, **3** (23), 3-9.

2 Pakhnits V.A., Aleinikov Y.V., Popov Y.A., Prozorova I.V., Toktaganov M.O. (2009) *Experiment–calculated researches to substantiate options of IVG.1M reactor fuel replacement* NNC RK Bulletin; **1** (37), 46-54. (In Russ.)

3 Prozorova I.V., Ganovichev D.I., Kirichek E.A. (2013) *Justification of the Thermophysical Characteristics of the IVG.1M Reactor during the Conversion of the Core to Low-Enriched Fuel*. Bulletin of the Tomsk Polytechnic University. Geo Assets Engineering Vol. **01**, 5-10.

4 Y. Aleynikov, A. Azimkhanov, E. Beisembayev, D. Ganovichev, P. Garner, V. Gnyrya, N. Hanan, V. Ignashev, Yr. Vassiliev, A.Vurim, A. Kolbaenkov, A. Kolodeshnikov, Yu. Popov, I. Prozorova, V. Zuev, *Study of Feasibility of HEU to LEU Conversion for IVG-1M Reactor*, paper S4-P3, RERTR 2011: International Meeting on Reduced Enrichment for Research and Test Reactors, Santiago, Chile (October 23-27, 2011).

5 Irkimbekov R.A., Zhagiparova L.K., Kotov V.M., Vurim A.D., Gnyrya V.S. (2019) *Neutronics Model of the IVG.1M Reactor: Development and Critical-State Verification*. Atomic Energy.– Vol.– **127**.– Issue 2.– P. 69–76., https://doi.org/10.1007/s10512-019-00587-1

6 R.A.Irkimbekov, A.S. Akayev, L.K. Zhagiparova, A.S. Khazhidnov, V.S. Gnyrya, A.D. Vurim, P.L. Garner, N.A. Hanan, *Safety analysis of the IVG.1M reactor with LEU fuel*, paper S13-P2, RERTR-2019: International Meeting on Reduced Enrichment for Research and Test Reactors, Zagreb, Croatia (October 6-9, 2019). <https://www.rertr.anl.gov/RERTR40/pdfs/RERTR-2019-program.pdf >.

7 V.S. Gnyrya, A.D. Vurim, I.K. Derbyshev, E.T. Koyanbaev, V.V. Baklanov, A.S. Azimkhanov, D.A. Ganovichev, Yu. A. Popov, A.N. Kolbayenkov, P.L. Garner, N.A. Hanan, *Status of the IVG.1M Fuel Test*, paper S10-P2, RERTR-2019: International Meeting on Reduced Enrichment for Research and Test Reactors, Zagreb, Croatia (October 6-9, 2019). < https://www.rertr.anl.gov/RERTR40/pdfs/RERTR-2019-program.pdf >

8 Skakov M.K., Vurim A.D., Gnyrya V.S., Azimkhanov A.S., Kolbayenkov A.N., Derbyshev I.K., Nurzhanov Y.B. (2018) *In-pile tests of water-cooled technological channels with low-enriched uranium fuel within conversion of IVG.1M research reactor*. NNC RK Bulletin; Vol **3**, 18-21. (In Russ.)

9 NNC [online]. National Nuclear Center of the Republic of Kazakhstan (Kazakhstan) < https://www.nnc.kz/en/news/show/341/ > [Reviewed on May 2022].

10 R.R. Sabitova, I.V. Prozorova, RA. Irkimbekov, Yu. A Popov, S.V. Bedenko, A.A Prozorov, A.K. Mukhamediyev (2022) «Methods to study power density distribution in the IVG.1M research reactor after Conversion». «Applied Radiation and Isotopes», Volume 185, Jury 2022,110259, https://doi.org/10.1016/j.apradiso.2022.110259 .

LEVERAGING ADVANCED SMR I&C TECHNOLOGIES FOR RESEARCH REACTORS

A. DUTHOU
Framatome Grenoble
23, Chemin du Vieux Chene, Meylan 38240, France

ABSTRACT

This paper draws a parallel between Small Modular Reactors (SMR) and research reactors' (NRR) I&C needs, to identify shared challenges and the solutions that can be applied in both cases, still assessing the specific issues of each project.
In particular, we extract the main requirements and constraints imposed on Research Reactors and SMRs' Instrumentation and Control (I&C), more particularly on the safety platforms used for the Reactor Protections System (RPS) and other safety applications (Neutron Instrumentation System, Diverse Reactor Protection System…). As an illustration, we present Framatome technologies and products currently developed to address these markets.

1. Introduction

Starting in the 1960s, Framatome has been a major stakeholder in the deployment of the Nuclear Research Reactors (NRR), supplying, among others, several key safety Instrumentation and Control (I&C) systems such as Reactor Protection, Neutron Instrumentation and Rod Control. More recently, it also modernized some of their I&C systems, transitioning from original analogue technology to modern Digital safety systems. In total, Framatome has supplied key I&C systems to nearly 60 research reactors in the world.
At the same time, Framatome has been providing its Digital or Analog safety and safety-related technologies to Nuclear Power Plants (NPP) all around the world; resulting in installed and operating equipment in more than 200 NPPs worldwide. More recently, it has developed new I&C products optimized for SMRs and Research Reactors.

SMRs are setting a new trend in the market of civil nuclear reactors. Thanks to their novel business model favouring serial production, their different applications: electricity production but also other uses (industrial heat, desalinization, district heating…), their various core technologies (PWR, BWR, MSR, HGTR…) and of course their sizes that can address many types of needs, SMRs are generating a lot of interest in the nuclear world. Because of these various aspects, there is a multitude of SMR designs (IAEA [1] identified at least 70 developments) with different impact on their architecture and systems, including their Instrumentation and Control (I&C).

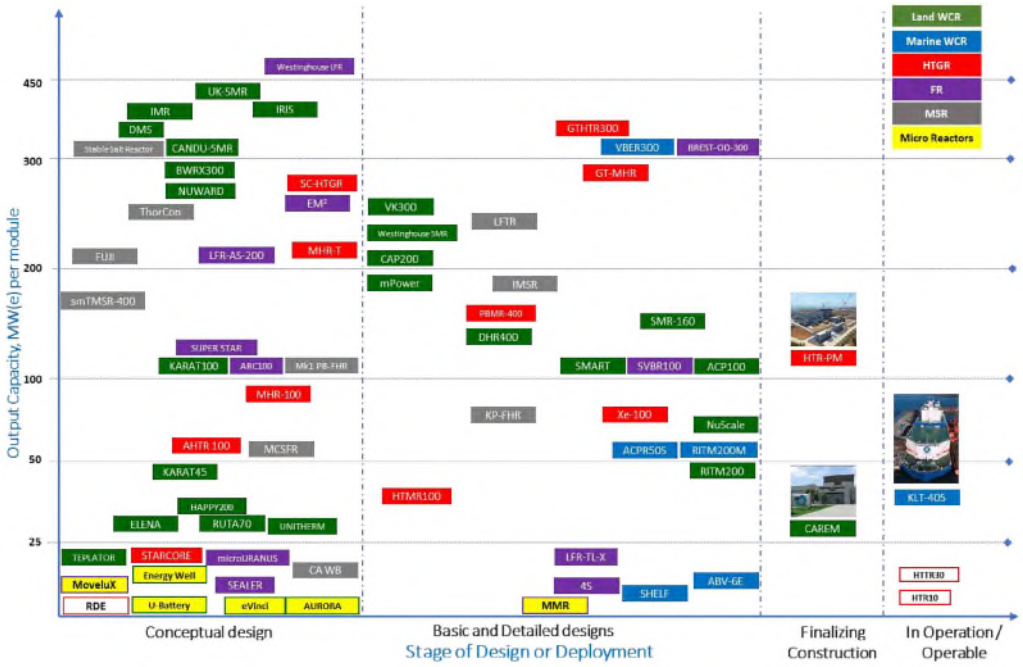

Figure 1: Stage of Design or Deployment of SMRs in term of output Capacity [1]

Research reactors share a lot of similarities with SMRs: their power range is limited (generally less than 100 MW), they are small -with footprint constraints-, they aim to maximize the use of inexpensive equipment and they must fulfill nuclear safety regulations.

This paper draws a parallel between SMR and Research Reactors' needs, more specifically I&C needs, to identify shared challenges and the solutions that can be applied in both cases, still assessing the specific issues of each project.
In particular, we extract the main requirements and constraints imposed on Research reactors and SMRs' (including advanced Reactors -ARs-) I&C. We will notably focus on the safety platforms used for the Reactor Protections System (RPS) and other safety applications (Neutron Instrumentation System, Diverse Reactor Protection System…).
As an illustration, we present Framatome technologies and products currently developed to address these needs.

2. Defining SMRs & Research Reactors I&C specificities

The I&C characteristics of the SMRs I&C result from 2 kinds of specificities: their design and their financial model.

2.1 SMR Design specificities:

As illustrated by " Figure 1: Stage of Design or Deployment of SMRs in term of output Capacity [1]" there is a multitude of SMR designs, that greatly vary in term of: power (from a few kWe for very Small Modular Reactors, upto ~400 MWe), usage (Power production, desalinization, heat generation…) and nuclear type (PWRs, BWRs, Molten Salt Reactors, Travelling Wave Reactor, etc). This leads to great variations of architecture and design, which impacts their I&C. Nevertheless, we can extract similarities between all these SMRs:

- Power output & Size: by definition all these reactors are less powerful and smaller than "traditional" Nuclear Power Plants (NPP) and target a small footprint
- Scalability: several reactors can be added in parallel but usually share a single MCR
- Simpler design: many components integrated to reduce piping, cables etc and favour passive safety

Economics specificities:

- Fleet approach: ideally manufactured in large series, with reduced equipment costs
- Modular: the reactors must be factory built and pre-assembled
- Easy to license internationally: to avoid costly changes in production line

These will lead to specific constraints for I&C.

2.2 Research Reactors characteristics

There are also multiple types of research reactors [2]: among the 220+ NRRs in operation in the world (23 countries), we find that the most frequent are Pool-type (47 units), Tank type (21 units) & tank in pool type. Triga (36 units) and Slowpoke reactors designs are the most frequent, more uncommon types are fast reactors, heavy water reactors (10 units) or Homogenous reactors.

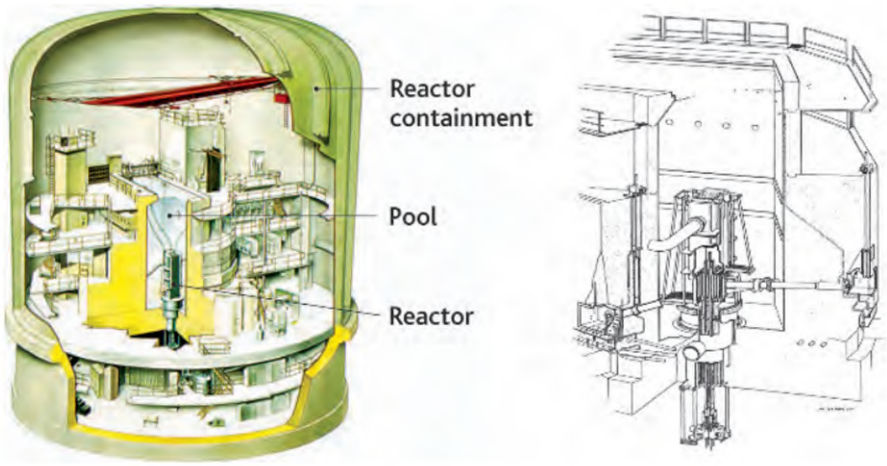

Figure 2: HFR reactor at Petten, closed-tank pool-type reactor: NRG [3]

So, as for SMRs, this multitude of NRR designs leads to great variations and impacts on I&C, nevertheless we can extract similarities that match some of SMRs' key characteristics and requirements:

- Power output & Size: NRRs' power output can range from 0 up to 200 MW(th) which is quite similar to SMRs. They are also smaller than NPPs, with similar footprint to SMRs
- Simpler design: most of the NRRs have a very straightforward architecture that translates into basic safety functions to implement and thus simple I&C systems
- Because Research Reactors operators usually have less resources (financial & expertise) to dedicate to the licensing phase, "easy-to-license" technologies are preferred (same as SMRs)
- Equipment costs: also due to limited funding, there is a need for equipment cost limitation.
- Also, as SMRs can address multiple applications (electricity production, industrial heat, desalinization…). Research reactors have multiple applications: analysis and testing of materials, neutron scattering, non-destructive testing, production of radioisotopes, education. This calls for solutions that can be adapted to these different purposes

We can see that SMRs and research reactors share key characteristics, it is not surprising as many SMR designs are being developed by teams coming from the nuclear research field.

As we focus on I&C in this paper, we will now see how these shared characteristics impose specific constraints on the I&C systems and technologies present in SMRs and NRRs.

3. Main characteristics of SMRs and NRRs I&C safety Platform

3.1 Size, Footprint

The size constraint can directly be applied to I&C. To reduce footprint, several means are available: use of digital technology, modern components and modular architecture. Fortunately, simpler design of the reactor means that fewer functions and cabling are needed thanks to the removal or reduction of some elements (valves, specific equipment…). Moreover, fewer and simpler functions also mean that Hardwired platforms will be able to implement the Reactor Protection System (RPS) safety functions within a limited number of cabinets, and thus fulfilling the requirement for reduced footprint.

3.2 Costs, Standardization

The SMR fleet approach also impacts I&C: the components shall be manufactured / programmed in series to limit costs and shorten production time. Modularity is also key here.
For NRRs, only the cost aspects are relevant, but, if we consider that the more reactors use the same technology, the cheaper it will be, we can see that it also points toward the use of technology with a potentially large installed base. For the safety systems, this can be achieved thanks to a strong standardization strategy but allowing for parameterization until the last minute (for example to conform to local regulation requirements).

3.3 “Easiness of licensing” worldwide

This is a crucial factor, as it is needed to guarantee the economic model for SMRs and the project feasibility for Research reactors. This must first be addressed by safety authorities to edict clear, and ideally shared, guidance, such as edicted by WENRA (see Figure 3: Refined structure of the levels of DiD, WENRA RHWG [4]). Nevertheless, proven architecture, design, manufacturing and verification & validation processes and experience will contribute to worldwide acceptability. So, for simple systems, a Hardwired safety platform could be an advantage, as this technology is widely accepted and does not need the more complex licensing process as its digital counterparts. For more complex functions where it would be too difficult to use hardwired platform, digital platforms are necessary (Software or FPGA based). In this case, depending on the design architecture and local regulations it may be necessary to add a diverse protection system as recommended by WENRA [4]

Levels of defence in depth	Objective	Essential means	Radiological consequences	Associated plant condition categories
Level 1	Prevention of abnormal operation and failures	Conservative design and high quality in construction and operation, control of main plant parameters inside defined limits	No off-site radiological impact (bounded by regulatory operating limits for discharge)	Normal operation
Level 2	Control of abnormal operation and failures	Control and limiting systems and other surveillance features		Anticipated operational occurrences
Level 3 (1) 3.a	Control of accident to limit radiological releases and prevent escalation to core melt conditions (2)	Reactor protection system, safety systems, accident procedures	No off-site radiological impact or only minor radiological impact (4)	Postulated single initiating events
Level 3 (1) 3.b		Additional safety features(3), accident procedures		Postulated multiple failure events
Level 4	Control of accidents with core melt to limit off-site releases	Complementary safety features(3) to mitigate core melt, Management of accidents with core melt (severe accidents)	Off-site radiological impact may imply limited protective measures in area and time	Postulated core melt accidents (short and long term)
Level 5	Mitigation of radiological consequences of significant releases of radioactive material	Off-site emergency response Intervention levels	Off site radiological impact necessitating protective measures(5)	-

Figure 3: Refined structure of the levels of DiD, WENRA RHWG [4]

The same factors can also be applied to other nuclear specific systems. For example, the use of a wide range excore Neutron Instrumentation System (NIS) allows the replacement of multiple detectors, conditioning and processing channels (Source / Intermediate / Power) by a single channel. This simplifies the design and reduces the footprint necessary.
Such enhancements are also possible for other systems or instrumentation but are highly dependent on the design architecture and technology used

4. Framatome new Safety technologies for SMRs & Research reactors

4.1 Teleperm XS Compact (TXS-Compact) Digital Safety platform

Framatome has a long history with digital safety technology. Based on the return of experience of its installed base of digital safety systems and, in particular, using the proven concepts of Teleperm XS platform, Framatome has developed a new digital safety (1E / Cat. A) I&C platform: Teleperm XS Compact (TXS compact) designed to fulfil small reactors needs: especially for SMRs & research reactors' I&C.

It is based on FPGA technology, does not have any software, and features a large range of functions implemented on compacts modules, racks and cabinets. Its standard FPGA module allows for high throughput, including for complex numerical calculation.

It is very well adapted to implement Research reactors and SMRs safety functions and matches perfectly the requirements and characteristics we have extracted previously.

4.1.1 Compactness / footprint reduction

Digital technology allows the implementation of very complex systems (many data and/or complex algorithms & computations) in a reduced footprint compared to analogue technologies. Teleperm XS compact features modern compact modules (3U) and cabinets.
Its IO boards also allow for remote IOs, which can reduce furthermore the footprint necessary in electrical rooms and reduce the cabling necessary.

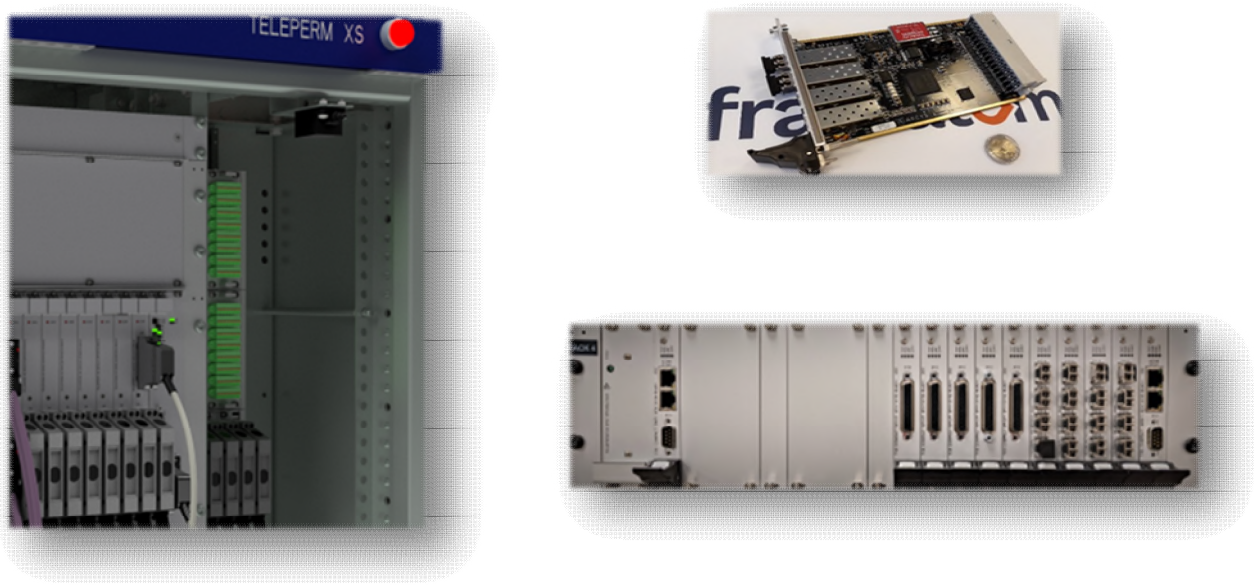

Figure 4: TXS Compact cabinet, rack and module

4.1.2 Costs, High level of standardization

In addition to the cabling reduction, other costs are reduced thanks to high level of modules standardization. Moreover, advanced engineering software allows for a shorter project design phase, leading to noticeable savings.
Finally, as TXS compact follows the Teleperm XS mechanical aspects and is compatible with its modules, it benefits from a mature Serial manufacturing organization already in place.

4.1.3 Worldwide Licensing & use

TXS compact has been designed specifically for nuclear, leveraging Framatome's experience with digital safety platforms licensing and operation, in particular with Teleperm XS. It is designed with advanced application programming using functional blocks diagrams only, which limits the risks of errors and facilitates V&V demonstrations. It can be parameterized without hardware/firmware modification which also limits the risks.
Teleperm XS compact also features advances cybersecurity features (such as cryptographic signatures authentication, data encryption, physical access detection…).

4.2 Hardline Safety Hardwired platform

Even though non-programmed technologies still have limited data processing, which reduce their ability to implement complex system or architectures, they are ideal for main, or

diverse, protection systems implementing simple functions such as NRRs' and SMRs' because they are usually simpler and cheaper to qualify than digital.
Framatome has a long history with safety analogue technology. Based on its previous analogue platforms installed on more than 200 nuclear I&C systems in the world. Framatome has developed a new Hardwired safety I&C platform: Hardline.
This new safety (1E / Cat. A) Platform, where the safety functions are completely hardwired (no software no FPGA), is particularly oriented towards SMRs & NRRs thanks to:

- Compactness / footprint reduction
- High level of standardization and delayed differentiation
- Highly modular approach
- Highly developed Self-Testing, diagnostics with modern IHM

4.2.1 Compactness / footprint reduction

One of the usual shortcomings of hardwired technology is the difficulty to implement complex calculations and the high number of cabinets necessary for numerous or complex functions. Fortunately, as the NRRs and SMRs I&C functions are usually simpler and less numerous, Hardwired technology becomes a possible choice for safety platforms. Nevertheless, the targeted reduced footprint can still be a challenge to existing platforms.

A special focus has been directed towards technology compactness. In particular, an optimized cabinet internal cabling has resulted in a cabinet front-access only (see Figure 5: Hardline Cabinet). This allows placing the cabinets against a wall or two cabinets back to back significantly reducing the footprint necessary for these systems.

4.2.2 High level of standardization and delayed differentiation

The high degree of standardization is completely in line with the SMR modular and series approach, as the modules and cabinets can be manufactured in advance and parameterized later thanks to an innovative configuration board that replaces tedious manual wiring. Therefore, the modules can be manufactured in series, parameterized, and tested in the factory at "the last moment" before being sent on site.

The modules can be combined to implement many different kinds of functions and thus allow for a modular approach, for example to add functionalities to NRRs or to accommodate additional SMR units.

The system design flow is supported through advanced automatic development tools that facilitate the choice of an optimized combination of modules and allow for a last minute differentiation / parameterization on the already built modules.

4.2.3 Worldwide Licensing & use

With Hardline, all the safety functions are implemented exclusively with non-programmed components (no FPGA and no CPU/Software). This guarantees a much simpler licensing process than for digital platforms as it is largely based on environmental qualification (seismic, EMC, temperature etc…) and therefore requires less justifications and documentation related to digital V&V.

Hardline has also been designed specifically for nuclear, based on Framatome's very extensive return of experience on the design, operation and maintenance of Hardwired safety I&C platforms.

4.2.4 Advanced Self-Testing and diagnostics with modern HMI

Another limitation of previous analogue technologies was the lack of self-testing and diagnostic capabilities. Hardline eliminates this weakness thanks to dedicated components that provides capabilities and interfaces similar to the most modern digital technologies (see

Figure 6: Example of Hardline HMI). This reduces the need for frequent physical inspection and facilitates the simultaneous management and operation of several reactors.

Figure 5: Hardline Cabinet

Figure 6: Example of Hardline HMI

4.3 New Wide-Range ex-Core Neutron Instrumentation System (WR NIS):

Although wide range channels have existed for a long time, they are seldom used in commercial Nuclear Power plants (NPP). However, new requirements lead by regulators (need for diversity) and new architectures (SMRs) have led to the development of a new ex-core wide range NIS.

This new safety (1E / Cat. A) technology, is very well adapted to small reactors in term of:

- Footprint reduction
- High level of standardization
- Licensing

4.3.1 Footprint reduction

The new ex-core Wide Range NIS can cover the full neutron flux range from 1nv to $2*10^{10}$ nv. This is usually sufficient to address Research reactors complete neutron flux range from reactor start-up to full power operation (see Figure 7: Traditional and wide range neutron flux measurement). Thus, it can replace several channels of a “traditional” NIS (that features at least 3 separate channels Source/Intermediate/Power for each division), resulting in significant footprint reduction: less detectors, cables, conditioning and processing cabinets. Notice that it may be necessary for regulatory compliance to have diversity on the Neutron flux measurement on all on some of the ranges (Source, Intermediate or Power). It is then possible to use a combination of Wide Range and traditional channels to reach the desired configuration.

Moreover, this NIS does NOT need a pre-amplifier near the reactor building. This eliminates the risk of failure on this additional equipment and the need for its location and cabling.

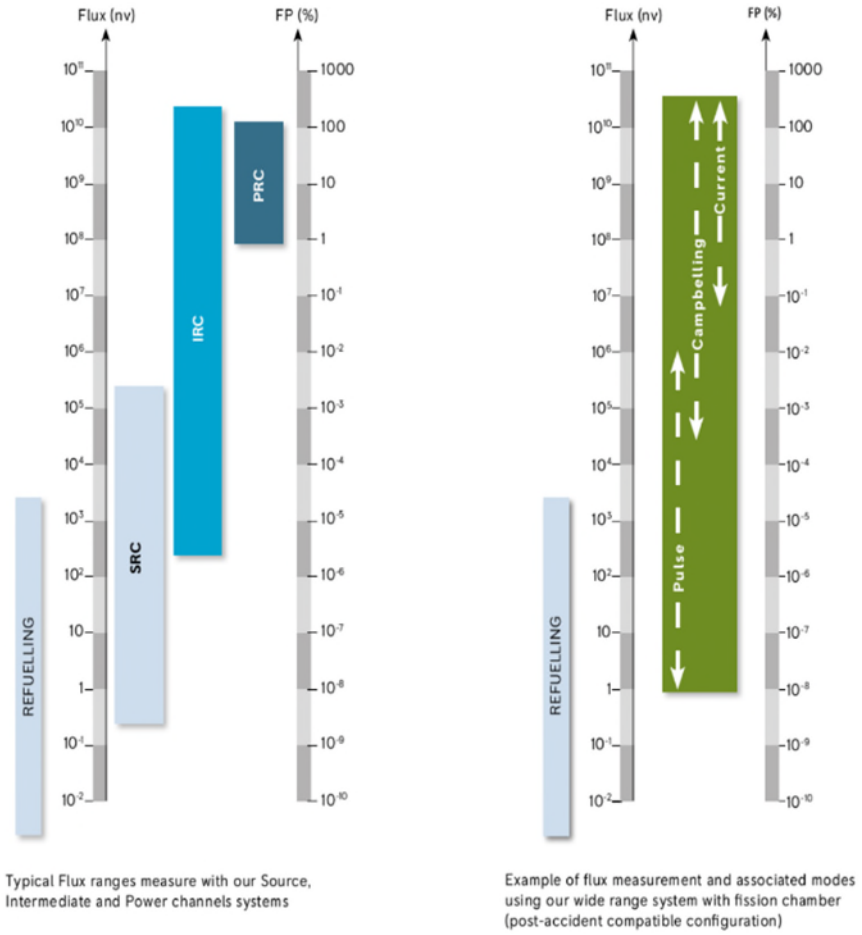

Figure 7: Traditional and wide range neutron flux measurement

4.3.2 Licensing

The processing can be done with our digital safety platform Spinline®, currently used in more than 90 plants in the world, or third party safety platform. Spinline's existing qualification and licensing in many countries complying with their safety regulations will facilitate the licensing of the system.

The complete system is certified to implement 1E / Cat. A safety functions.

In addition, the WR meets post-accident requirements as defined by NRC RG 1.97 when coupled to adequate Fission chamber-based detector.

4.3.3 High Level of standardization

The wide range module (see Figure 8: Wide Range Module) is standardized and can be manufactured in series and implemented in cabinets for testing before being sent to the reactor location.

Figure 8: Wide Range Module

In conclusion, the Wide Range NIS perfectly matches NRRs and SMRs constraints: adaptable to specific configurations, compactness (usually needs only one detector to cover full range, no pre amplifier), can meet post-accident requirements and is based on highly standardized components that can be produced in series.

5. Conclusion

Some of the existing technologies found in traditional NPPs are not optimized for Research reactors and SMRs that have specific requirement dictated by their particular designs and also economic model. Notably for the I&C, several factors will affect the type and architecture of the platforms and technologies chosen: footprint, scalability, licensing easiness, modularity and compatibility with manufacturing in series.

It is possible to address SMRs and Research Reactors I&C needs with optimized I&C technologies that meet these reactors' specific requirements. Moreover, the use of equipment and technologies benefiting from a large installed base will ensure the lasting sustainability and long term support of the solution.

Framatome is the I&C Original Equipment Manufacturer (OEM) of 47 research reactors in the world and has modernized more than 15. Based on this extensive and long standing experience, Framatome has recently developed new safety I&C technologies that were designed to meet the SMRs' and Research reactors' specific challenges but that can also be applied to regular NPP.

6. References

[1] IAEA. (2020). Advances in Small Modular Reactor Technology Developments. Vienna.

[2] World Nuclear association. (2021, June). Research Reactors. Retrieved from World Nuclear Association: https://world-nuclear.org/information-library/non-power-nuclear-applications/radioisotopes-research/research-reactors.aspx

[3] J. Couturier, H. Abou Yéhia, E. Grolleau (IRSN). (2019). Elements of nuclear safety-Research reactors.

[4] WENRA. (2013). Safety of new NPP designs - Study by Reactor Harmonization Working Group RHWG. . WENRA - Reactor Harmonization Working Group (RHWG).

GAMMA IRRADIATIONS USING SPENT FUEL ELEMENTS AT FRM II

X. LI, V. HUTANU, S. BULLA, J. MOLCH, F. JESCHKE
FRM II, TU München
Lichtenbergstraße 1, D-85748 Garching, Germany

ABSTRACT

A gamma-irradiation facility is constructed for irradiations of samples in the spent fuel elements at the FRM II. It consists of a double-walled watertight sample container and a positioning device to adjust the sample position for a homogeneous irradiation. Samples can be heated up to 140°C with a temperature stability <1°C over a long irradiation time (weeks). A control system monitors the sample irradiation and visualizes the process parameters remotely on-line. The typical γ dose rate ranges from 0.05 kGy/h up to 50 kGy/h depending on the cooling time of the fuel elements. Decay of the γ dose rate and its axial profile in a total length of 70 cm in the active zone was detected using Harwell PMMA-dosimeters. Concepts for achieving an irradiation uniformity for research of microstructure in halite with a typical target dose up to 4 MGy will be introduced.

1. Introduction

Spent fuel elements (FE) of nuclear reactors are usually treated as useless waste and stored for cooling on site for a long time, before being moved to a final disposal place. However, the intense gamma rays arising from many radionuclides generated by the fission process of the fuel material ^{235}U or ^{239}Pu and neutron activation in the spent fuel elements during reactor operation can be used for many research purposes and technical applications. Irradiation facilities in spent fuel assemblies have been developed and are being used at research reactors and nuclear power plants worldwide for several years [1, 2].

Just like all other ionizing radiation, gamma rays with high energy up to MeV can change chemical, physical and biological properties in the materials. Industrial irradiation facilities using ^{60}Co or ^{137}Cs normally designed for sterilization of medical products, microbial decontamination of foods or modification of polymer reach a typical desired dose between 0.02 and 250 kGy [3]. Also at some research institutes, gamma ray irradiation facilities of ^{60}Co are available; however, the intensity of most sources is usually not high enough for some special scientific purposes. For example for the study of microstructures in rock salt mineral through the generation of colour centres under gamma radiation or the investigation of radiation resistance of electronic components or isolating materials to be used in nuclear reactors, a high dose up to many MGy is required.

The research reactor FRM II with a thermal power of 20 MW represents a high flux neutron source for various applications in science, industry and medicine. The concept of the reactor design is based on the use of a single compact core, with about 8 kg highly enriched uranium (>90%). Heavy water is used for the neutron moderation. Light water is used as a cooling medium [4]. After the operation, all spent fuel elements are stored in the cooling pool of the FRM II for years. A gamma dose rate of more than 100 kGy/h is accounted in a fresh spent element within the first 50 days.

A dedicated gamma ray irradiation facility with heating function was developed at the FRM II in cooperation with the Institute for Endogenous Dynamics of RWTH Aachen University in order to use this spare radiation. The main scientific motivation for this development is based on the so-called method of “gamma decoration of the grain boundaries” in the study of microstructure in halite [5]. The information drawn from an untreated salt sample is normally

limited. However, gamma irradiation of rock salt can make microstructures in halite visible through creation of colour centres in the material. A high ambient temperature over 100°C can accelerate this process [6]. Thus, many details of the microstructure (e.g. grain and sub-grain boundaries, growth zones) giving information about deformation and recrystallization processes and the transport of liquids in the sample can be studied and were properly understood using irradiated samples only. Earlier for the same purpose, a similar irradiation facility was developed and operated at the Jülich research reactor (FRJ-2) until the rector shutdown in 2006. Useful knowledge was transferred to the FRM II for further development.

2. The fuel element (FE) at FRM II

The compact reactor core of the FRM II consists of one 1.3 m high single FE with a 72 cm long uranium zone in the middle. 113 separate involute-shaped fuel plates are welded between two concentric tubes with diameters of 237 and 118 mm respectively. The core with ca. 8 kg of highly enriched (93%) uranium in form of silicide dispersed in Al matrix provides in combination with heavy water as a moderator a peak thermal neutron flux of 8E14 /cm²s at about 30 cm radial distance from the FE centre in the moderator tank [7, 8]. Figure 1 shows a photograph of the FRM II FE viewed from the bottom. During the reactor operation, the control rod, made of Hafnium, is inserted into the central tube and moves slowly from the bottom to the top of FE to regulate the reactor power during the 60 days of an operating cycle.
After the reactor cycle, the spent FEs are placed for cooling vertically about 6 meters under the water in a storage rack with a total of 50 positions in the reactor cooling pool. The spent FEs remain there for at least 6.5 years before being transported to a national storage site for highly radioactive waste (dry storage). There are currently 47 spent FE's with different cooling times stored at the FRM II since the reactor's commissioning in 2004. They can be easily reached from the top by the crane or from the handling bridge over the cooling pool for gamma irradiation.

The main γ-ray intensity in the FE originates from the fission products of ^{235}U, while the contribution of the transuranium actinides and activation products built during the reactor cycle is relatively limited. According to the MCNP calculations, the total activity of fission products is ca. 1 MCi at 120 days after the reactor cycle and it decays to a level of 180 kCi after one year [9].

3. Design of the irradiation facility

The gamma irradiation facility at the FRM II is constructed for irradiation of samples directly in the central tube of a spent FE or in a free position in the storage rack surrounded by 4 or 8 fuel elements. The choice of the irradiation position depends on the targeted dose and the current dose rate of the chosen fuel element. The hall crane transports the irradiation facility to the selected position according to the stored coordinates automatically. The entire load chain of the irradiation system is designed based on the requirements of the KTA 3902 4.2 stipulated by the German Nuclear Safety Standards Commission.

Fig. 2 shows the facility in the irradiation position with some details of design. The irradiation system consists essentially of two watertight cylindrical concentric vessels (irradiation tube and sample container), a watertight bell-shaped connection box and a positioning ring for height adjustment. All of them are made of $AlMg_3$ alloys. The sample container designed for an overpressure of 2 bar has an inner diameter of 7.6 cm. Regarding the length of the active zone of the FE of ca. 70 cm, the maximum sample volume is about 3 litres.

During irradiation, the facility sits on the cone of a spent FE and its lower part is inserted into the central pipe. The positioning ring adjusts the actual position of samples in the radiation field. The inner sample container is double-walled. An electric heating coil is welded spirally from top to bottom on the inner pipe in the 4 mm gap between the double walls, so that the

irradiated samples can be heated during the irradiation simultaneously. The gap is filled completely with thermal insulating material perlite due to its chemical stability and radiation resistance. The minimal operating temperature is limited by the temperature of the cooling water inside the FE tube (about 30°C) and the maximum operating temperature is currently limited to 140°C according to the operation permit. Higher temperatures are still possible technically. Temperature stability <1°C is provided over a long period of days or weeks.

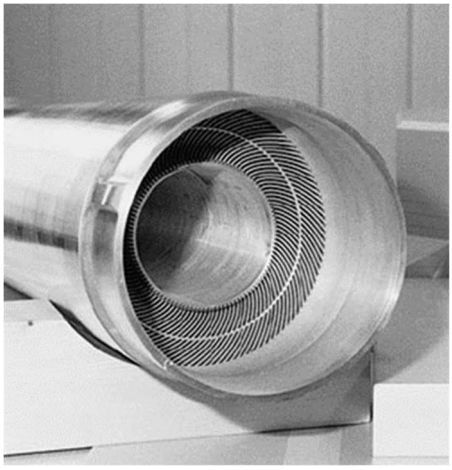

Fig 1: Fuel element of the FRM II.

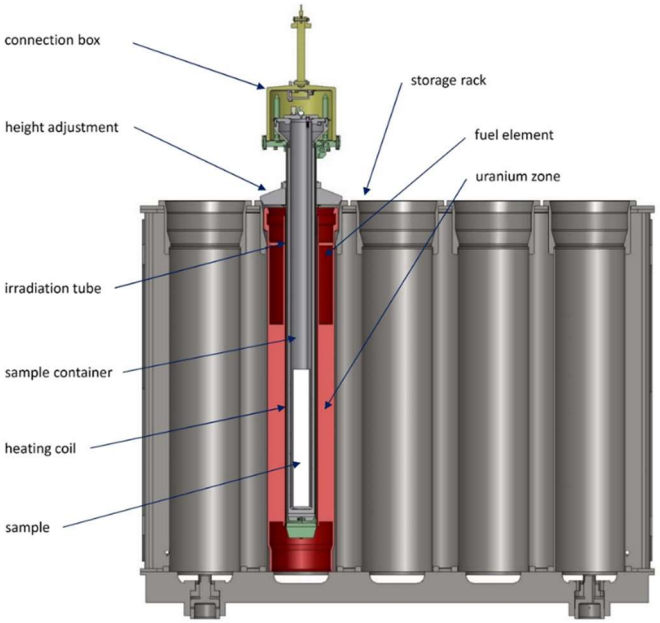

Fig 2: Gamma irradiation facility in a spent FE.

Altogether five resistance temperature detectors (RTDs) of the type Pt100 are mounted on the irradiation facility. The sensitive zone and the connection cable of the thermometers are enveloped in the stainless steel tube to ensure their radiation resistance and a long operating life. One of them is fixed between the wrappings of the heater and regulates its power, according to the target temperature during the irradiation. The heater has a maximum electric power of 500 W. However, due to the efficient thermal insulation, only a tiny part of this is actually used. The output of less than 20 W is fully sufficient to keep a thermal equilibrium at 140°C. This thermal power is very small compared to the residual heat of ca. 11 kW from the “fresh” spent FE element directly after the reactor operation. Additionally, there is still a pool water column/layer of 4 mm between the inner tube of the spent FE and the outer tube of the irradiation device. The natural convection of the pool water is sufficient for an effective cooling. Regarding the safety, three other temperature sensors are fixed at different heights and in 120° geometry to each other on the outer side of the irradiation tube. They work according to the 2 of 3 selection principle, which means the heater will be automatically switched off, if the temperature limit of 90°C on the outer surface is exceeded at any two of the three sensors. However, our real values recorded during the routine irradiation processes show that the local outer temperature of the irradiation facility always remains below 50°C, denoting an efficient thermal isolation.

A fifth thermometer located between the samples monitors the actual local temperature in the sample container and acts as a secondary safeguard in addition. It is connected to the regulator of the heating coil through a logical switch, in order to avoid overheating within the container. The parameters in the heating unit dTRON304 of the company JUMO are so optimized that the pre-selected target-temperature can be approached smoothly without significant overheating.

Considering the radiation damage on the conventional electronics in the high dose field, all electrical plugs and sockets (LEMO-connectors) are mounted in a bell-shaped connection box made of 1.2 cm thick $AlMg_3$ at the top of the irradiation facility away from the direct radiation field. A reliable humidity sensor installed inside the bell triggers the alarm and switches off the heating system, if water is detected in the box. Two O-rings of EPDM (ethylene propylene diene monomer rubber) are used at the opening site of the inner sample container and the connection box. Additionally, the tightness of the whole facility is proven using compressed air shortly before each irradiation. The EPDM O-rings are located at least 70 cm above the active fuel zone to avoid radiation damages. Measurements have confirmed that the gamma dose rate there is generally less than 5 Gy/h. This O-ring material stands out for its excellent radiation resistance and can be used for up to a total gamma dose of at least 100 kGy [10]. For safety, the O-rings are changed preventively on a regular base after an operation period of one year.

A software written using JUMO LOGOSCREEN nt controls the whole system during gamma irradiation. The processing values displayed on a control panel mounted close to the reactor cooling pool can be also read out remotely by using the PC Evaluation software PCA3000 for archiving and analysis after each batch. The target temperature can be only set and confirmed manually at the heater unit on site, in order to avoid an unforeseen access from internet. The control unit is connected to the reactor monitoring system. In case of warning signals, e.g. water leakage or overheating, the heater is switched off immediately and a warning message is sent to the reactor control room and the person responsible for the system via e-mail and SMS, correspondingly.

4. Gamma dosimetry and dose rate profile

Due to the limited length of the cylindrical geometry of the FE's on the one side and the asymmetrical burn-up process of the fuel material in the FE during the reactor operation on the other side, the local distribution of the γ-ray intensity within the central tube is not homogeneous. To investigate the axial profile of γ dose rate in the spent FEs, poly-methylmethacrylate (PMMA) dosimeters (Harwell 4034 Red and 3042 Amber) with sensitive ranges from 5 kGy to 50 kGy and 1 kGy to 30 kGy were used. The uncertainty is 2% over the entire calibrated ranges [11].

The dosimeters were placed discretely at 11 different heights with an equal distance of 7 cm on a sample holder in the irradiation container. The total length covered the entire active zone of 70 cm in the fuel element. According to the expected dose rate, the irradiation duration was adjusted accordingly to fit well into the sensitive range of dosimeter. During the measurement of the dose rate, the heater in the sample container was switched off. The ambient temperature in the spent FE was under 40°C. The temperature influence on the dosimeters was limited at this temperature [12].

Based on the single core concept of the reactor and the same burn-up history of each fuel element, the shape of measured axial profile of dose rate is quite similar in all fuel elements apart from the absolute value decaying with time. Using values normalized to the maximum in each measurement, a representative axial profile of dose rate was obtained for all spent FEs at the FRM II independent of their individual decay time. This made a general investigation of the lateral dose distribution within the irradiated samples possible. Fig. 3 demonstrates the normalized dose rate profile derived from measurements performed in seven spent FEs with different cooling times. Standard deviation of the seven measurements is given as the measurement error bar at each position in the FE. The curve shows that the γ dose rate decreases to both edges of the FE rapidly, where the values fall to ca. 50% (bottom) and 20% (top) of the maximum in the centre. The profile curve is quite symmetric around the burn-up centre about 8 cm below the geometrical centre of FE. This observation is in the good agreement with the MNCP calculations for the position of the maximal reactor neutron flux.

The axial dose profile R(x) over the symmetrical part of about 60 cm can be well fitted with a polynomial function of fourth degree:

$$R(x) = 1.05E\text{-}07\ x^4 - 8.56E\text{-}06\ x^3 - 5.24E\text{-}04\ x^2 + 4.03E\text{-}02\ x + 4.10E\text{-}01,\ (0<x<60) \qquad (1)$$

R(x) is dose rate at x cm from the bottom of the FE in Gy/h.

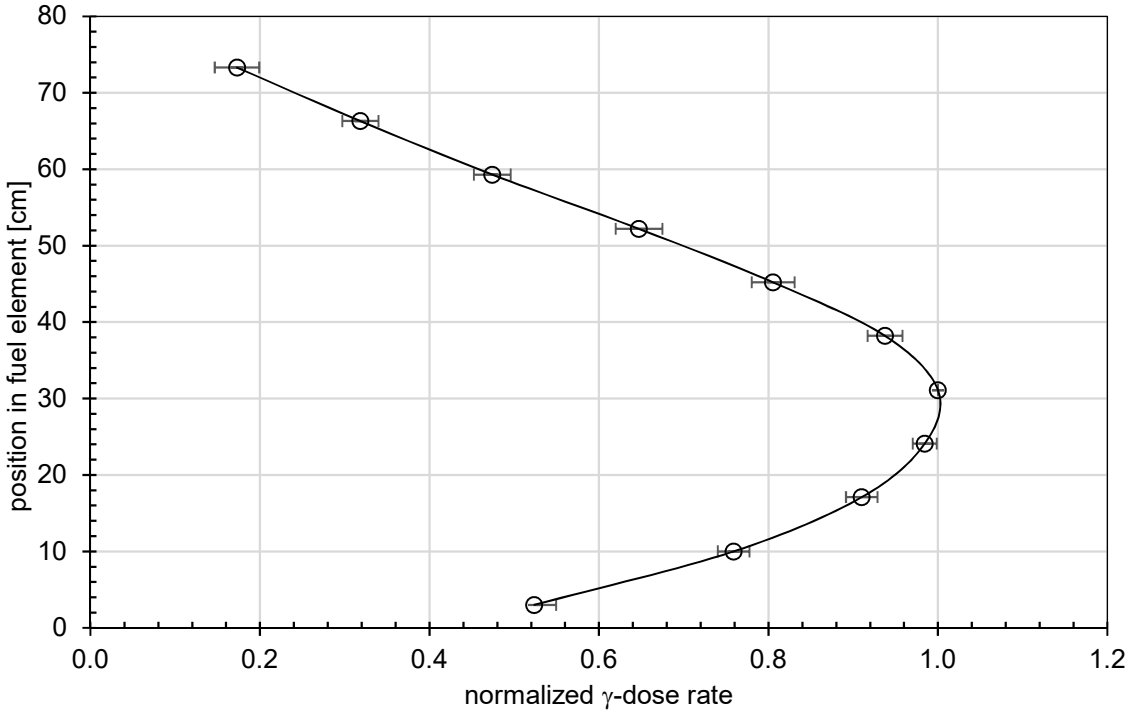

Fig. 3: axial dose rate profile inside FE, normalized to the maximum.

Performing measurements of the dose rate in the spent FEs of different cooling times, the time dependence of the dose rate in the FEs was build. Fig. 4 presents the decay curve of the dose rate at the maximum in the centre of fuel elements. The dose rate decreases very rapidly from 75 kGy/h after a cooling of 80 days down to blow 2 kGy/h after 1½ years. Afterwards it decays slowly. For the first 1.5 years of cooling, in which most irradiation with very high target dose of up to several MGy are normally performed, the decay of γ dose rate R(t) can be fitted with a fourth degree polynomial function (Eq. 2):

$$R(t) = 65.49\ t^4 - 320.7\ t^3 + 586.4\ t^2 - 483.9\ t + 158.7, \qquad \text{for } t < 1.5 \text{ a} \qquad (2)$$

with $R(t)$: dose rate [kGy/h] at time t [a] passed after the reactor cycle completing.

The total dose D [kGy] deposited in the samples over a long irradiation time is the integration of the dose rate R(t) expressed by the fitting function (2):

$$D = \int_{t_b}^{t_e} R(t) * dt \qquad (3)$$

with t_b, t_e : begin and end time of an irradiation in [a]. For a given target dose D, the expected irradiation duration can be calculated by solving the Eq. 3 for t.

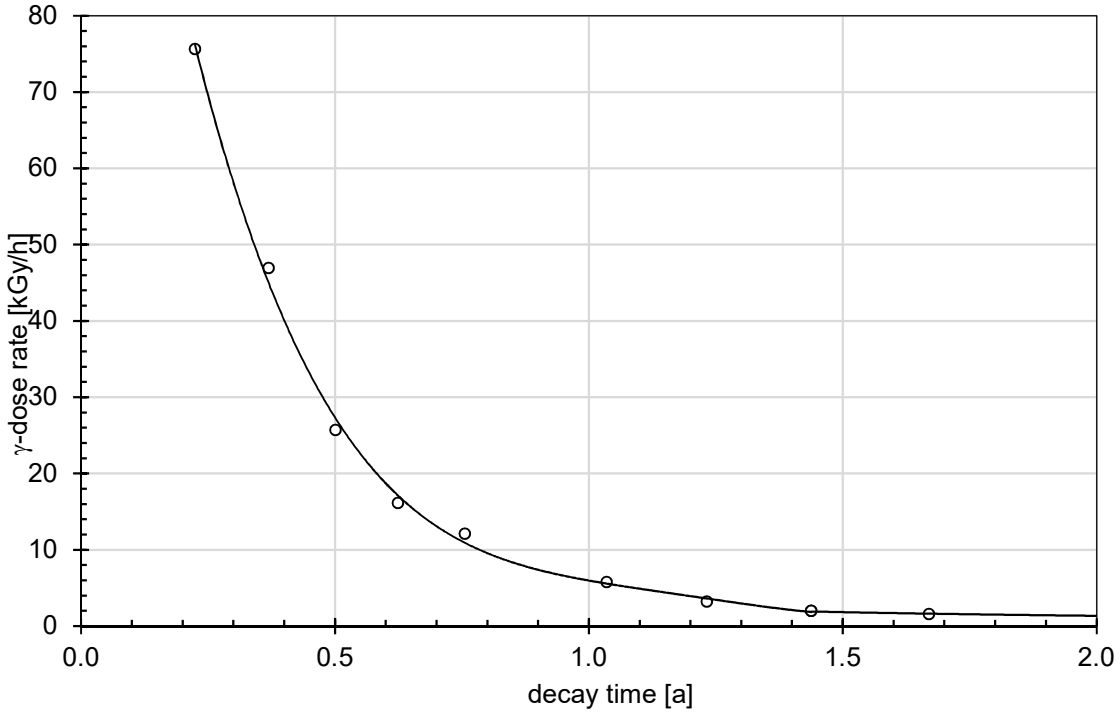

Fig. 4: decay of γ dose rate in spent FE in the first two years after reactor cycle.

5. Example of application: microstructure investigation in halite samples

One of the main applications of our γ-ray irradiation facility up to now is irradiation of rock salt. Salt domes are actively investigated as a potential geological nuclear waste storage places. The flowing and recrystallization dynamic in rock salt mineral is an important criteria for the long-time stability forecast prediction of the certain site. Samples collected at different geological sites over the world are prepared in a suitable size (cube or cylinder) with a diameter smaller than 7.5 cm and a height between 2 and 5 cm. They are wrapped into aluminium foil separately and numbered before irradiation. In order to reach a best homogenous irradiation for all samples, the samples are normally stacked up to 40 or 50 cm in the height (70 cm is the maximum length of the sample carrier). Fig. 5 shows an example of typical halite samples stack before irradiation.

During the irradiation, the samples are usually heated to 100°C. After the high dose gamma irradiation, the white halite crystals become deep blue. Under a microscope, the fine microstructures, domain gran and sub-grain boundaries responsible for plastic behaviour of mineral and initially invisible in the white salt, became clearly visible after irradiation. Plastic behaviour in dependence on grain size could be studied. The typical target dose is about 4 MGy and can be reached in ca. 60 h or in 30 d in a spent FE with a cooling time of three months or one year respectively.

Due to the cylindrical design of the FE, the samples located along the central axial are irradiated from all sides homogeneously. A high radial dose uniformity is provided. However, the axial dose profile should be compensated in order to achieve a high lateral dose uniformity for the whole sample length.

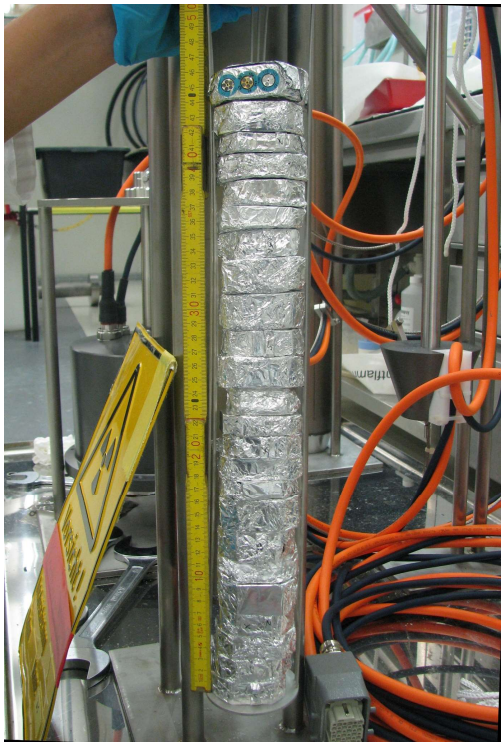

Fig. 5: Example of typical halite sample stack before irradiation

The IAEA recommends a lateral dose uniformity ratio ($DUR=D_{max}/D_{min}$) of 1.05, which is the ratio of the maximum to the minimum dose in the irradiated samples [3]. The mathematical analysis of the axial dose rate profile by means of the fitting function (Eq. 1) shows that this value can be guaranteed without any additional measures for our facility only in a region of 17 cm height. DUR value of 1.1 is reached in an irradiation length of 23 cm. If the whole length of the active zone of 70 cm should be used for the sample irradiation, an additional measures like absorber tubes [13] or sample restacking can be implemented. Due to the limited space in the irradiation tube, an extra absorber tube is a less favourite solution. However, changing the order of samples during the irradiation process is a simple and viable alternative. That means the samples irradiated in the middle area of the FE with a higher dose rate in the first half of irradiation time will be moved to the edge area with a lower dose rate, so that all samples absorb approximately the same total dose at the end of the irradiation process.

	total sample length		
restacking	DUR < 1.05	DUR < 1.1	DUR < 1.15
0	17 cm	23 cm	28 cm
1	34 cm	44 cm	50 cm
2	60 cm	70 cm	-

Tab 1: Sample-restacking concept for different requirements of the lateral dose uniformity ratio DUR and different sample lengths.

This measure is applied in our routine irradiation procedure of halite samples. With one restacking, DUR value of 1.05 can be guaranteed for a total sample length of 34 cm. Further calculations show, that this value can be also reached for a length of 60 cm, if samples (each assumed 5 cm high) are divided into 3 groups and restacked twice after each 1/3 of the total irradiation duration. For thinner samples (<5 cm), the total sample length with homogenous irradiation can be further extended. Table 1 shows the restacking concept for different requirements of the DUR-values. These results indicate the effectively uniform irradiation region around the point with the maximum dose rate in the spent fuel element. According to the requirement for the DUR, the sample package with a suitable length can be located exactly by adjusting the positioning ring on the irradiation facility.

6. Conclusions and outlook

The gamma irradiation facility using spent FE has been successfully designed, built, commissioned and operates at FRM II. It is equipped with a heating element and control system to ensure a safe operation in the centre of the spent FE providing irradiation under required temperatures between 30-140°C. The challenges of the rapid decay of the fission products on the one side and the strongly curved profile of the dose rate in the axial direction on the other side could be corrected mathematically and compensated effectively using an

optimized sample restacking concept. Effective sample lengths were determined for required DUR values.

Glass dosimeters can be used and co-irradiated together with the samples for better dosimetry, especially for high dose measurements in the future, as they detect the total gamma radiation dose deposited in the samples during the whole irradiation process. However, the evaluation of the dosimeters is only possible after the irradiation process. The glass dosimeters can be re-used after a reset.

According to the current operating license, only inorganic substances are allowed to be irradiated using our facility at this time. Applications on other materials will be extended. The gamma irradiation system at the FRM II is assessed by TÜV Süd Industrie Service GmbH within the frame work of the nuclear safety management and is expected to be ISO 9000 certified in the future for more industrial applications.

Acknowledgement

The authors would like to thank the German Research Foundation (DFG) for funding (DFG-Project-No. 126157913) and Prof. Urai and his coworkers at the RWTH for their kind cooperation. We thank also our colleagues of the engineering group, especially Mr. Franz Tralmer for the technical design and Mr. Manfred Thomé at the FRJ-2 for sharing his expertise.

7. References

[1] A. Fernandez, H. Ooms, B. Brichard, M. Coeck, S. Coenen, F. Berghmans, M. Decréton, "SCK/spl middot/CEN gamma irradiation facilities for radiation tolerance assessment," IEEE Radiation Effects Data Workshop, 2002, pp. 171-176, doi: 10.1109/REDW.2002.1045549.

[2] I. Sánchez-García, H. Galán, A. Núñez, J.M. Perlado, J. Cobos, “Development of a gamma irradiation loop to evaluate the performance of a EURO-GANEX process”, Nuclear Engineering and Technology, Vol. 54, Issue 5, 2022, p1623-1634, doi: 10.1016/j.net.2021.11.024.

[3] International Atomic Energy Agency (IAEA), Industrial Applications and Chemistry Section, Vienna (Austria) (2006), “Gamma irradiators for radiation processing” (INIS-XA--862). ISBN 83-909690-6-8.

[4] W. Petry, “Neutron Research and Applications at FRM-II” in TRANSACTIONS of the 8th International Topical Meeting Research Reactor Fuel Management (2004) pp. 3-10.

[5] J.L. Urai, C.L. Spiers, H.J. Zwart and G.S. Lister, „Weakening of rock salt by water during long-term creep”, Nature 324 (1986) 554p.

[6] H. Donker & A. García Celma, “Saturation of radiation damage in natural rock salt irradiated at moderate dose rate2, Radiation Effects and Defects in Solids (1996) 139:4, 241-252, DOI: 10.1080/10420159608212929.

[7] A. Axmann, K. Böning, M. Rottmann, “FRM-II: The new German research reactor”, Nuclear Engineering and Design, 178 (1997) 127 – 133. Doi: 10.1016/S0029-5493(97)00215-X.

[8] C. Ailloud, P. Colomb, J.P. Durand, G. Harbonnier, CERCA: Status of development, main features of plates and dummy element fabrication for FRM-II. Proceedings of the Fourth Meeting of the International Group on Research Reactors (IGORR-4). Gatlinburg, TN, USA, 24 – 25 May 1995.

[9] A. Röhrmoser, internal report FRM II OPA00482 rev. A (2014).

[10] European Organization for Nuclear Research (CERN), Technical inspection and safety commission, “compilation of radiation damage test data”, CERN 89-12, part I, 2nd edition, p8, 31. Dec. 1989.

[11] Harwell Dosimeters Limited, accessed Sept. 07. 2021, http://www.harwell-dosimeters.co.uk/harwell-red-4034/.

[12] B. Whittaker, M.F. Watts, “The influence of dose rate, ambient temperature and time on the radiation response of Harwell PMMA dosimeters”, Rad. Phys. and Chem., vol. 60, Issues 1–2 (2001) 101-110, doi: 10.1016/S0969-806X(00)00316-9.
[13] X. Li, H. Gerstenberg, I. Neuhaus, „Silicon doping system at the research reactor FRM II”, Applied Radiation and Isotopes, Volume 67, Issues 7–8 (2009) 1220-1224, Doi: 10.1016/j.apradiso.2009.02.017.

REBUILD OF THERMOSTATIC IRRADIATION SYSTEMS CAPABILITIES IN MARIA. LESSONS LEARNED FROM THE ISHTAR THERMOSTATIC DEVICE OPERATION.

M. MIGDAL, M. LIPKA, A. TALAROWSKA, G. WOJTANIA
Nuclear Facilities Operations Department, National Centre for Nuclear Research
A. Sołtana 7 Street, 05-400 Otwock – Poland

ABSTRACT

MARIA reactor team has rebuilt its competences related to irradiation of material samples in irradiation devices, especially in conditions of very high temperatures. The hiatus in research was caused by the generation gap and declining community interest in various research conducted in research reactors. Recently, on the wave of increasing worldwide interest we have returned to work on the subject of in-core irradiation in various irradiation systems.
Contemporary development of fission and fusion power technologies requires scientific equipment enabling advanced studies of material behaviour in high-temperature, neutron-intensive environments. In response to mentioned scientific interest a novel irradiation device, ISHTAR, was constructed and irradiated by the MARIA Research Reactor's Nuclear Facilities Operations Department. The irradiation conditions in the device reflect those occurring in the core of the advanced helium-cooled nuclear reactor at very high temperatures reaching 1000°C. Additionally, the highly flexible core of MARIA reactor enables studies in various neutron conditions, including the fusion-related neutron spectrum.
This work shows the experience from the operation of the ISHTAR device in the reactor core, and comparison of pre-design calculations and real data from the period of in-core irradiation. Comparing computational data with the experimental data gathered during ex-core and in-core test campaigns proves that the device is reliable, inherently safe, and provides required irradiation conditions. Additionally lessons learned concerning the design, and some need for further investigation are presented.

1. Introduction

After more than 40 years of hiatus, MARIA reactor team has rebuilt its competences related to irradiation of material samples in irradiation devices, especially in conditions of very high temperatures. The hiatus in research was caused by the generation gap and declining community interest in various research conducted in research reactors. In the late 1970s and up to the mid-1980s, many projects related to the testing of irradiated materials in various types of irradiation devices were carried out in the MARIA reactor. The following irradiation devices operating in the past in MARIA are worth mentioning: SR-1 (after changing the sample holding insert the name was also changed to KAMA-1), which could work with replaceable inserts and tested samples of stainless steel and zirconium alloys, another device – GAPISZON enabled long-term testing of detectors in the reactor core, the KRS-M device was designed in cooperation with Czechoslovakian research institute to study zirconium alloys in a water vapour atmosphere, and finally the BARTEK device that was used to study fuel materials in the field of neutron radiation [1]. Recently, on the wave of increasing worldwide scientific interest MARIA team is returning to work on the subject of in-core irradiation performed in various irradiation systems. One of those systems is ISHTAR

high temperature irradiation device (ISHTAR stands for Irradiation System for High Temperature Reactors).

2. ISHTAR high temperature irradiation system

As the high-temperature reactors (HTR) seem to be considered by the Polish government as a meaningful branch of scientific studies in the field of nuclear energy [2][3], however separate from the Polish Nuclear Power Programme, the need for the development of thermostatic rig that will enable irradiations in the HTR conditions emerged. As a result of this interest, a state-funded research programme GOSPOSTRATEG-HTR was initiated, which in its part was aimed at the development of methods for testing of structural materials in a nuclear research reactor [4]. ISHTAR irradiation rig, was designed and built at the Nuclear Facilities Operation Department in National Centre for Nuclear Research. It enables irradiation of material samples in MARIA reactor under conditions prevailing in high-temperature gas reactors, i.e. temperature up to 1000°C and in helium atmosphere. This level of temperature inside the rig is ensured through simultaneous nuclear and electric heating, and thermal insulation of gas gap. The goal of conducted tests of samples placed in the rig were to determine the effect of radiation field and high temperature on the strength and structure of materials intended for use in the construction of new reactors, in particular core elements.
The initial rig design was carefully optimized to minimize heat flux in axial direction and homogenize the temperature field within the holder filled with materials samples. Results of CFD calculations of the axial temperature distribution inside the ISHTAR irradiation rig are shown in Figure 1. The optimization process, which lead to the final axial insulation arrangement, required tight cooperation between analysts and design engineers. Test of the prototype was performed to measure thermal and hydraulic conditions in the external mock-up of the vertical irradiation channel of the MARIA reactor – coolant flow correlated with the known pressure drop. When the hydraulic conditions were known (and derived from them – heat transfer coefficient), thermal measurements became possible: the temperature at various points inside and outside the rig was measured to map the temperatures and compare them with calculation results of the measurements to prove the adequacy of the design, as shown in Figure 2. Now, after several irradiation cycles in-core, it has been shown that the calculated temperatures correspond very well with those measured in actual irradiation conditions [5].

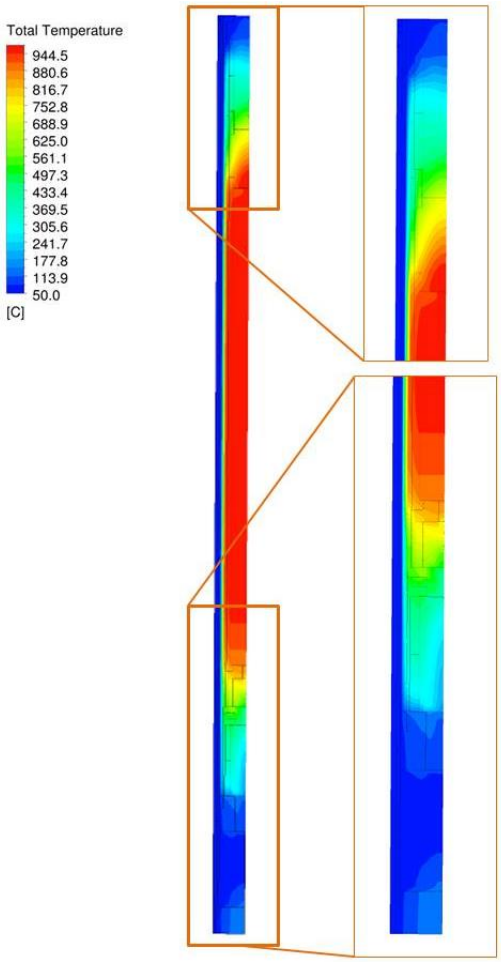

Fig. 1. CFD calculations of axial temperature distribution inside the ISHTAR device.

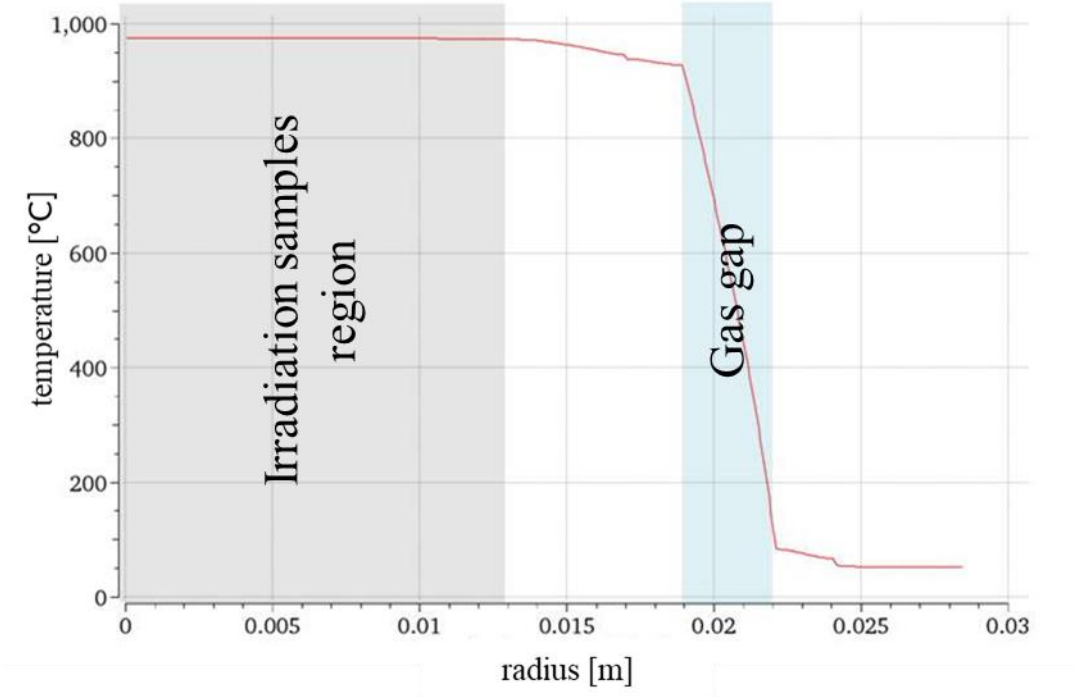

Fig. 2. Radial temperature distribution inside the ISHTAR device.
Coolant temperature outside the capsule – 30°

3. ISHTAR capsule design

The main feature of the rig is the homogeneous irradiation temperature of 40 cm specimen's holder length which is impressive comparing to the 1 m of active reactor core height. The homogenous temperature of 1000°C was achieved by helium gas insulation layer. The outer diameter of the rig d = 48.3 mm can be easily fitted to the vertical channel which internal diameter equals 54 mm. The rig is cooled by the forced convection of water in reactor pool. The main goal of ISHTAR thermostatic device was to demonstrate the possibility of graphite specimen irradiation in high temperatures. The thermostatic device irradiates four graphite specimen, each 100 mm long. Samples from this irradiation campaign are intended for the pull tests. The samples are fitted with six thermocouples as part of the temperature monitoring inside the thermostatic device. The specimen is implemented inside the rig's tray, with cylindrical loading space of diameter 28 mm and 400 mm long. The tray encapsulating the loading space is wrapped in 7 high-temperature heaters. The heaters are placed in spiral grooves and interlaced at the bottom, allowing both cold ends of each heater directly upwards. The heater interfaces stainless steel sleeve tube's outer diameter allows maintaining 3.15 mm isolating gap between thermostatic device tray and thermostatic device outer tube. The gap is filled with helium with a pressure of 1.5 bar, providing isolation necessary to reach a temperature of 1000°C inside the tray. Thermal expansion shrinks the gap to about 2.85 mm, which was taken into account in the calculations. The Upper and lower ends of the tray in the sleeve are additionally isolated by rings manufactured from Zirconium-Yttrium ceramic with low thermal conductivity of 2 $Wm^{-1}K^{-1}$ combined with the helium volumes. The whole assembly is locked within the stainless steel (AISI316) cylinder, providing structural rigidity to the assembly [6]. In the Figures below some details of the ISHTAR irradiation device structure are shown.

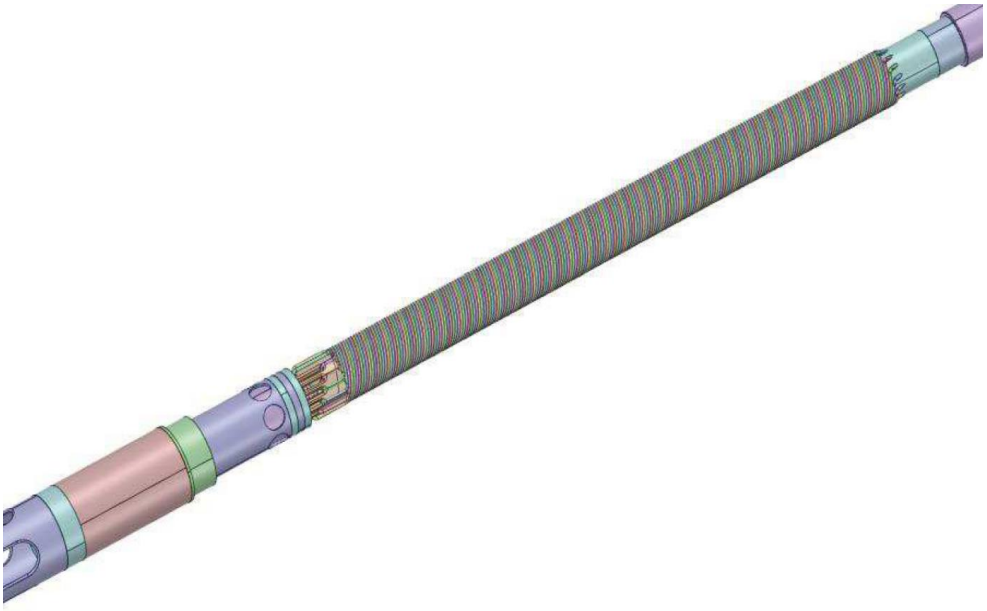

Fig. 3. Inside of the in-core part of the ISHTAR device, heating wires visible.

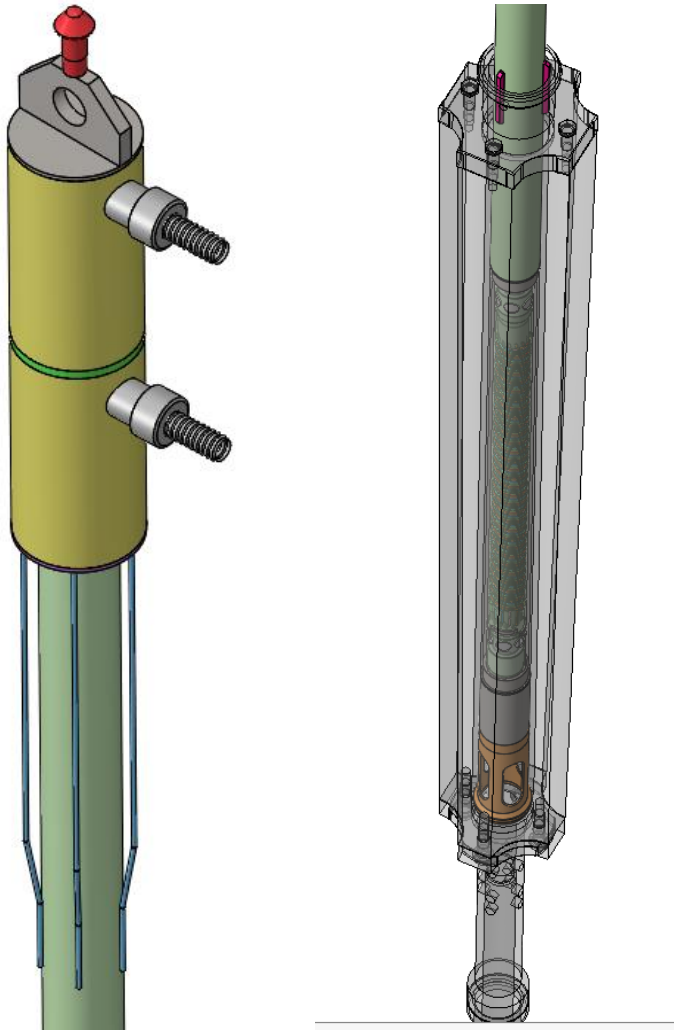

Fig. 4. ISHTAR irradiation device. Left: upper part with junction connectors visible. Right: installation in beryllium block.

4. In-core irradiation of ISHTAR device – thermocouples degradation

Ishtar device have been irradiated in the MARIA reactor in the second half of 2021 for several operational cycles without any major issues. However interesting phenomenon was recorded: with operational time increase electrical heating power, controlled by the logic cabinet, was increasing. Explanation of this occurrence can be, that with the increasing neutron fluence, in high temperature environment, relatively thin 0.5 mm K-type thermocouples are degrading and are not measuring temperature completely correct. Literature studies carried out after the experiment confirmed that such a phenomenon exists, however, the methods of preventing it are not fully known [7]. This effect is presented in the Figure 5, below. Because reactor thermal power (corresponding with the nuclear heating inside the capsule) have not been recorded by the data acquisition system during the experiment, uncoupling of the temperature data is unfortunately not possible. Possible solutions for longer irradiation period in the future shall be evaluated. Either the use of larger diameter thermocouples or the change of the TC type is recommended.

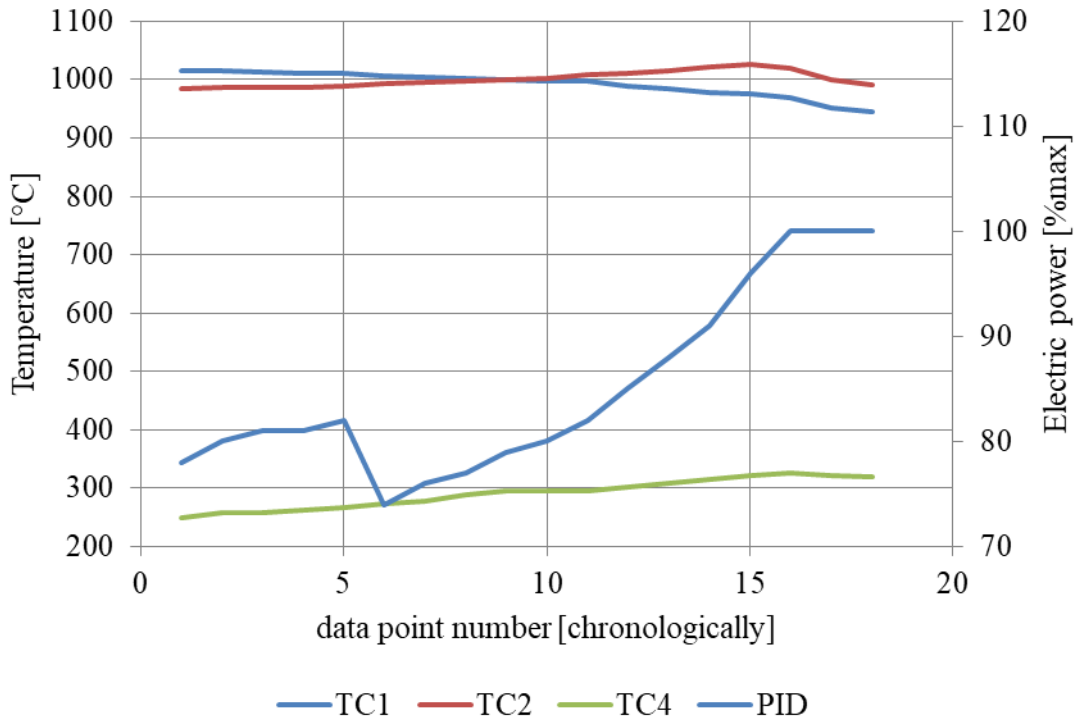

Fig. 5. In-capsule parameters during the irradiation. TC1, TC2 – temperatures in the irradiated sample, TC4 – gas gap temperature, PID – electric heaters power.

5. Dismantling of the ISHTAR device and extracting graphite samples

After completion of the operation in the core and cooling period in the MARIA reactor storage pool, the ISHTAR rig was transported via water route to the hot cell to be dismantled and material samples to be extracted for further testing. This was carried out on February 22, 2022. During the probe dismantling process, some challenges were encountered. In addition to the cuts planned in the disassembly manual, a few additional cuts were required to dismantle the probe. As it turned out, the entire samples train inside the irradiation rig was shifted by approx. 3 to 5 cm towards the upper part of the capsule in relation to the technical drawings. Additionally, the inner tube directly securing the sample holders experienced thermal deformations, which additionally made it difficult to extract the samples from the rig. A cut was made through the central and inner tubes dividing the sample section in half, which enabled the removal of the graphite samples. Apart from minor damage to one of the holders, all samples were preserved in their entirety and were safely transported to the Material Testing Laboratory (part of the National Centre for Nuclear Research) for further strength tests. As a result, the procedure for the next rings assembly was slightly modified to avoid such issues in the future.

6. Conclusions

The design, construction and implementation of the ISHTAR irradiation device was a joint effort of many specialists from the National Centre for Nuclear Research. Thus, the competences lost for almost 40 years of non-existence of such projects in MARIA reactor were brought back.

The design of the ISHTAR thermostatic rig was developed after a series of computational and experimental studies. Measurements of the pressure drop in the irradiation channel filled with the thermostatic device were performed., followed by thermal measurements of the temperature field inside and outside the ISHTAR capsule. The temperature measurement's results proved the adequacy of the computational methods and the design. ISHTAR thermostatic irradiation device can achieve desired parameters, that is, temperature

>1000°C. Capsule started its regular operation in the MARIA core in Q3 2021. It was irradiated for several operational cycles, providing irradiation material samples for generation 4 and fusion reactors research.
The thermocouple-degrading effect needs further studies, both literature and experimental. For that purposes, testing of different thermocouple types, and construction of the Johnson noise thermometer are intended.
Careful planning and preparation for the capsule dismantling enabled successful extraction of material samples from the ISHTAR device.
All in all, the close cooperation of many specialist on the project of designing, constructing and commissioning of ISHTAR thermostatic irradiation device revived competences in building such systems and capabilities of MARIA research reactor in thermostatic, in-core irradiation.

7. Acknowledgement

This work was supported by the National Centre for Research and Development (NCBR) as a part of the GOSPOSTRATEG-HTR programme.

8. References

[1] Bonicki W., Review of existing documentation on probes and material testing carried out in the MARIA test reactor, GOSPOSTRATEG-HTR report, HTR-1/2-D-S-2019, NCBJ.
[2] The Council of Ministers, Strategy for Responsible Development for the period up to 2020 including the perspective up to 2030, Monitor Polski, 2017, item 260.
[3] Ministry of Climate, Polish Nuclear Power Programme – draft, 2020, retrieved from: https://bip.mos.gov.pl/fileadmin/user_upload/bip/prawo/inne_projekty/PPEJ/MK_Energia_jadrowa_200806_pop_1.pdf.
[4] GOSPOSTRATEG-HTR: mission and goals of the project, retrieved from: https://www.gohtr.pl/Misja-i-cele-projektu.html.
[5] Talarowska, A., Lipka, M., Wojtania, G., 2021. Preliminary computational and experimental design studies of the ISHTAR thermostatic rig for the high-temperature reactors materials irradiation. Nukleonika 66, 127–132. https://doi.org/10.2478/nuka-2021-0019.
[6] Lipka M., Talarowska A., Wojtania G., Migdal M., Experimental study of ISHTAR thermostatic irradiation device for the MARIA research reactor, The European Physical Journal Conferences, Volume 253, 2021. https://doi.org/10.1051/epjconf/20212530400.
[7] Palmer, A.J., Skifton, R.S., Scervini, M., Hawkes, G.L., Pham, C.B.T., Checketts, T.L., 2021. Summary of Thermocouple Performance in the Advanced Gas Reactor Experiment AGR-5/6/7 During Irradiation in the Advanced Test Reactor 12

OBSOLESCENCE & SPARE MANAGEMENT PROGRAMS – LONG TERM OPERATIONS OF RESEARCH REACTORS

L. STEFANINI
Maintenance Manager HFR, Nuclear Operations, NRG
stefanini@nrg.eu
Westerduinweg 3, 1755LE, Petten, the Netherlands

D. DI GIROLAMO
Consultancy & Service, NRG
Westerduinweg 3, 1755LE, Petten, the Netherlands

ABSTRACT

The nuclear fleet is ageing. As ageing impairs the systems functions, more and more components need replacement. A component is said to be obsolete when it is not obtainable on the market and/or it is no longer supported by the producer. A preventive approach to obsolescence implies the identification and solution of obsolescence issues before running out of spare parts. The effectivity of the obsolescence management program is strictly related to an efficient spare management program. A spare parts management system guides the activity and decision making throughout the life cycle of the spare parts held in inventory. An advantage is a better control of the spare parts storage areas and of the spare parts obsolescence. Moreover it is necessary that obsolescence issues are discovered while a minimum amount of spares is present on location. This paper presents a concept for spare management and its application to the spare management system for the electrical parts of the HFR.

1. Introduction

The nuclear fleet is ageing. One third of operational nuclear power plants a and more than two thirds of operational research reactors are 35 or more years old. As ageing impairs the systems functions, more and more components need replacement. Technological obsolescence becomes a problem for the older facilities. A component is said to be obsolete when it is not obtainable on the market and/or it is no longer supported by the producer. Technological obsolescence is one of three recognised type of obsolescence together with documentation and standards obsolescence.

A spare parts management system guides the activity and decision making throughout the life cycle of the spare parts held in inventory. The development of policies and processes provides a clear framework for action and decision making. Another advantage is a better control of the spare parts storage areas and of the spare parts obsolescence. Obsolete components are generally identified at the moment of ordering new spare parts to refill the shelves. It is therefore important that the spare parts are managed and inventoried efficiently.

This paper presents pragmatic approaches to the two interrelated subject and their applications to the real case of the High Flux Reactor.

2. Obsolescence

Obsolescence is a form of non-physical ageing. Three types of obsolescence are typically recognized:

- Documentation obsolescence;
- Standards obsolescence;
- Technological obsolescence.

This paper focusses on the last type, the technological obsolescence. It is however necessary to recognize the importance of documentation and standards obsolescence in the nuclear industry. Both documentation and standards may not represent anymore the situation present at installation. This can lead to potentially dangerous situations.
Changes in (e.g. design) standards occur often in light of lessons learned. Failing to review the proposed standards may result in not implementing the necessary corrective action and ultimately it may lead to unsafe situations.
Changes in the installation need to be addressed in the relevant documentation. If this does not happen the documentation becomes obsolete. This might have a broad impact on the decision making process. Decisions taken based on obsolete documentation may have detrimental effects on financial, production and, most importantly, safety aspects of the installation.
In order to keep under control documentation and standards obsolescence the HFR has in place various strategy:

- Periodical review of documentation is required by the current Management System;
- Standards are periodically reviewed in the framework of the policies indicating them as relevant;
- Particularly for ageing management, the figure of the Ageing Management Coordinator carries out independent reviews and supervision on the obsolete status of documentation and standards.

3. Technological Obsolescence Management Program

A technological obsolescence management program for research reactors is foreseen in the international requirements. IAEA defines in the requirement 37 of the Specific Safety Requirements -3 [1] that:

> *The design life of items important to safety at a research reactor facility shall be determined. Appropriate margins shall be provided in the design to take due account of relevant mechanisms of ageing, such as neutron embrittlement and wear-out, and of the potential for age related degradation, to ensure the capability of items important to safety to perform their necessary safety functions in operational states and accident conditions in case of demand throughout their design life. The life cycles of the technology utilized and the possible obsolescence of the technology shall be considered.*

and particularly in:

> *Article 6.112. The design for a research reactor shall take due account of physical ageing, the effects of wear and tear and obsolescence in all operational states for which a component is credited, including testing, maintenance, and operational states during and following a postulated initiating event.*

The presence of a technological obsolescence management program is furtherly stressed out as an integral part of the ageing management program of research reactors. Particularly IAEA Specific Safety Guide-10 [2] prescribes:

> *Article 6.2 Obsolescence of SSCs should be identified, and corrective actions should be taken before the occurrence of any decline in reliability or availability of a research reactor.*
>
> *Article 6.3 Obsolescence of SSCs important to safety should be managed proactively (i.e. with foresight and anticipation) throughout their service life.*
>
> *Article 6.4 The operating organization should establish activities for the management of obsolescence throughout the lifetime of the research reactor.*

For the development of HFR technological obsolescence management program IAEA's and EPRI's standards are used. The IAEA TOP401 [3] gives a general description of a typical Technological Obsolescence Programme. This document is used as technical basis. The EPRI document Proactive Obsolescence Management [4] is used as further supporting basis.
The technological obsolescence management program at HFR follows the following scheme:

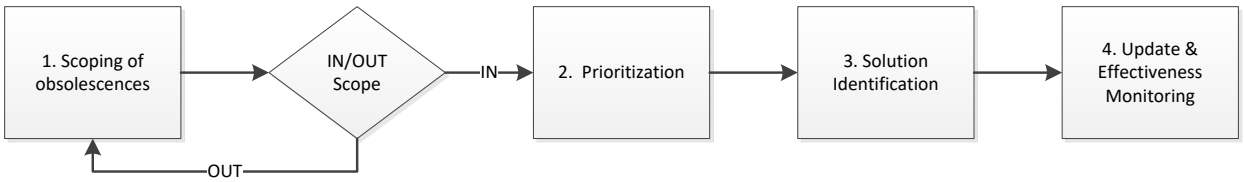

Figure 1 Technological obsolescence management program

The first step that needs to be addressed is the identification of the obsolescence issues. An obsolescence issue is defined at HFR as an item that is not produced anymore or cannot be obtained on the market with the same technical specification. It is not always clear whether a component is still being produced. In case of suspected obsolescence, the item is conservatively considered as an obsolescence issue. A subsequent (optional) step can be taken by checking the obsolescence issue versus the scope of the ageing management program. This step is generally not necessary because most items are used over a wide spectrum of systems within the reactor. As a result, almost all component types are part of the scope of the ageing management program. Once the obsolescence issue is identified it is stored for records in the HFR obsolescence database. The database contains the following information:

- Item identifications (type, brand, specifications);
- Correspondent components in the installation (unique ID);
- Issue priority status;
- Obsolescence team composition and responsible staff;
- Type of proposed solutions;
- Obsolescence issue status.

Once the obsolescence issue is identified a prioritization process take place. Prioritization may not be necessary for newer installations or in the first stages of the technological obsolescence management program implementation. In both cases, the number of obsolescence issues will be limited and manageable without prioritization. However, as the installation ages and the procedure for obsolescence identification becomes transversally used within the installation, the number of obsolescence issues starts to increase. In order to keep the workload bearable and in order to enhance the program effectiveness, the obsolescence issues are therefore prioritized.

There are many possible ways to prioritize the obsolescence issues. Each organization can chose the way that works better in their particular situation. At the HFR the prioritization tool is based on:

- Safety relevance
- Relevance to production continuity
- Current reserve status.

Prioritized items are then analyzed accordingly. The prioritization introduces deadlines that are coherent with the severity of the issue.

Following prioritization a research effort is conducted in order to identify the best possible solution for the obsolescence issue. Five main domains are investigated:

- Consistency of the obsolescence issue: due to scarce knowledge of the obsolete status of most components within the installation also suspected obsolescence issues are reported. A suspected obsolescence issue may be reported by operators spotting a visibly old and degraded component (many components are in service since sixty years). A suspected obsolesce issue may be reported by the engineer who would like to bring potential installation problems to light. Suspected obsolescence issues need to be investigated to confirm the obsolete status of the component(s).
- Existence of market surplus: once the obsolescence issue is verified the first step is to control the presence of a market surplus. If the company that used to produce the component still exists a stock might be present at their location. In other cases third

parties (e.g. warehouses, suppliers) might have the component in stock. In certain instances also privates may deliver private stocks. This option is preferable because it does not require an installation change. However, costs might be high.

- Special manufacturing run: if the company originally producing the component(s) is still active, it might still be in state of resuming production for a special manufacturing run. This option has the advantage that it does not require an installation change. Costs related to special manufacturing runs are often very high and might represent a major drawback to this solution option.
- New manufacturer, same component: in the case that the original component(s) cannot be obtained or in the case that a newer component is desirable, a market research is initiated. The research aim to identify new manufacturers that currently produces similar components with comparable technical specifications. A tender might be initiated together with a variant study. The drawback of this option is that, due to the replacement not being like-to-like, an installation modification procedure needs to be initiated. However, the requirements attached to quasi like-to-like replacement are less stringent than full modification. Major advantages of this solution are to ensure the presence of spare parts in the long term and a to modernize the installation at the same time.
- Scavenging and reverse engineering: in case a reserve of (removed/not working) components is present at the facility reverse engineering and scavenging techniques might be used in order to create a new functioning reserve. This solution is mostly temporary or suitable to components present in few units within the installation. A drawback of this solution is that the new component(s) need to undergo intensive testing before being used within the installation. Moreover, an installation modification procedure might be started and external technical support might not be available.

In order to launch this investigation an obsolescence team is created. Typical obsolescence teams are composed by:

- A chairman responsible and facilitator;
- Maintenance experts;
- Engineering experts;
- Procurement experts;
- Ageing Management experts.

The results of the investigation are discussed within the team and a decision is made on how to proceed to the obsolescence issue solution. In case none of the above mentioned solutions is applicable and/or desirable a project for full installation modification is started.
Two key performance indicators are used to determine the effectiveness of the obsolescence program:
Total amount of obsolescence issues;
Amount of proactively discovered obsolescence issues.
The results of the obsolescence program are furthermore evaluated yearly, during the yearly assessment of the ageing management program and every ten years in the framework of the Periodic Safety Review.

4. Spare Parts Management

Spare parts management and inventory control are an important part of any goods-producing organization. An effective and efficient inventory control has beneficial effect on:

- Financial maintenance aspects;
- Reliability;
- Production continuity;
- Safety.

At a deeper level, a good inventory control saves times to technicians and creates a friendlier environment for commercial and technological activities.
For an installation like the HFR an efficient inventory control is of the outmost importance. Most systems contributes to the continuity of production. The ageing related failure rate (and therefore the replacement rate) steadily increases. An effective inventory control helps the

reactor to maintain a correct stock of spares necessary to production and to identify and correct obsolescence issues.

1.1 Categories

The first step in identifying spare parts is to define a criteria for the categorization of the item that will be stored [5]. Categorization helps the decision making process regarding what needs to be stocked. Different categories of items can be managed in a different manner .
The following categories are relevant for the HFR:

- Ordinary spare parts: these are the spares of components whose failure will not impact safety or production continuity. Unavailability of these items can be tolerated for a defined period of time. These spare parts could also be called as “not critical”.
- Critical spare parts: these are the spares of components whose failures directly impact safety and/or production continuity. Availability of these spares is necessary at any time.

1.2 Spare Parts Identification System

A spare part identification system is a way to differentiate spare parts and their location. Every spare part is identified with code, description, brand, brand code and additional info.
A simple and practical coding has been used at HFR for both spare parts and storage areas. An effective identification systems was developed following the principle that codes need to have a meaning beyond being a simple identifier. For what concern the location, the code is based on an identifier of the storage area name, followed by letters and numbers associated to a cabinet (K), a drawers (L) a shelf and/or a slot (V). For example XXX – K1 – L2 – V3 means that the spare part is in the magazine “XXX”, in the cabinet 1, drawer number 2, slot number 3.
To avoid a lack of standardization every spare part is described according to the following structure:

Noun, qualifier 1, qualifier 2, etc.

The noun gives a general overview of the spare part. The qualifiers are used to described the main features of the spare part. The qualifier gives directly the information needed when a spare part must be replaced with a new one. For a transistor this would translate in:

Transistor, 40V, 600mA, 625 mW, etc.

1.3 Deciding what to stock

Deciding which items to stock can be facilitated by determining the relevance of the items to be stocked in terms of criticality to the safety and production continuity. The next steps can be taken to determine if a spare part is critical or not:

1) Determine whether the part is machine critical. It means that the subsystem in which the part is used cannot operate without this part functioning correctly.
2) Determine the operational criticality of the part. It means that the plant cannot continue production if the part cannot functioning correctly or if the spare part is not available. It’s possible that a part is machine critical but not operational critical. Two different levels of operational criticality have been used for the HFR:
    - Low: the part can be replaced or repaired in an acceptable time frame, or have backup equipment, or maintain production and output until a spare is available.
    - High: unavailability cannot be accepted due to critical relevance to safety and/or production continuity.
3) Apply the criticality matrix:

		Operational criticality	
		Low	**High**
Machine criticality	**No**	Ordinary part Order when needed	Investigate condition monitoring possible? No --> Apply Risk Matrix Yes --> Ordered when needed
	Yes	Go to supplier matrix	

By applying this matrix the following conclusions can be made:

- If an item is not machine critical and its operational criticality is rated as low, then it is *not* a critical spare part and should be ordered only when the need arise.
- If an item is machine critical but has low operational criticality, then apply the supplier matrix (step 4).
- If an item has operational criticality rated as high condition monitoring should be applied (predictive maintenance). If the condition of the part can be monitored, meaning that the supply of the part can be manage in advance, then the part should be ordered when the need arise. If the part cannot be successfully monitored than move to step 5.

4) Apply the supplier matrix:

		Lead time	
		Acceptable	**Unacceptable**
Supplier quantity	**Matches requirements**	Ordered when needed	Investigate condition monitoring No --> Risk matrix Yes --> Ordered when needed
	Don't matches requirements	Create stock Item ROP = 0	

Using this matrix indicates if:

- The supplier can supply the exact quantity required and the lead time (or delivery time of the part), is acceptable, then there is no need to stock the spare part in inventory.
- The lead time is acceptable but the supplier will only supply in quantities that don't match the immediate requirements (or the component is obsolete). For example only 5 spare parts are needed, but the supplier can supply them just in multiple of 10. In this case need to stock the item in the storage areas in order to manage the excess of spares. After the stock level reaches zero, there is no need to reorder until the need arises as the lead time is acceptable.
- The lead time is unacceptable, the opportunity for condition monitoring should be investigated. If it's possible to estimate the operating-life of the part, then the part should be ordered when needed. If the part cannot be successfully condition monitored, then move to the next step.

5) Risk analysis. First determine the consequences of non-availability of the part in different areas, like safety of operations, financial issues and quality of the final product. Then, if the likelihood that the spare part will be used in the short term is high and the consequence of unavailability are high, the spare part should be purchased and stocked.

1.4 Deciding how much to stock

A practical approach has been used in order to define the stock level of the spare parts. The approach is based on the following inventory control settings:

- ROP = reorder point, which is the stock level at which the need to reorder is triggered.
- ROQ = reorder quantity, which is the quantity to be reordered after the ROP is reached.

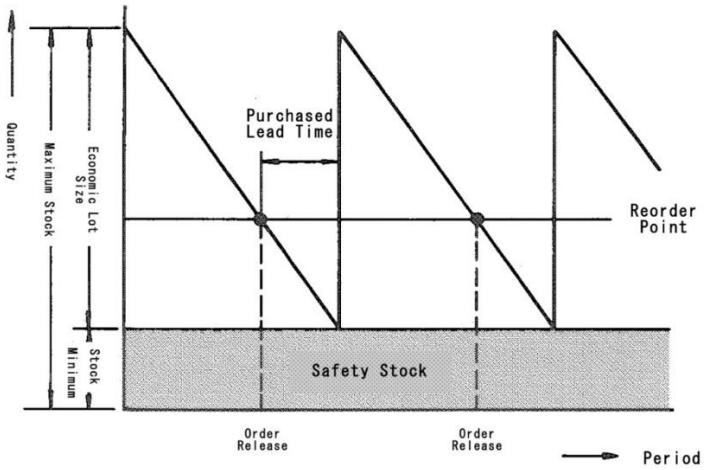

Three values need to be determined:

1) **The cycle stock:** when the available quantity of an item in the inventory reaches its ROP an order is place for refilling the stock. The quantity of parts ordered is called the replacement stock. The cycle stock is the stock that is used during the delivery time. Comparing the lead time (LT) and the demand rate (DR) indicates the stock cycle. The DR is the number of spares used during the time interval. The following rules can be applied:
   - If LT>DR : cycle stock is needed because there is likely to be a demand for the item before the replacement stock arrives.
   - If LT<DR: the cycle stock is not needed, because the delivery of replacement stock is expected before the next demand for the item.
2) **The safety stock:** is the minimum acceptable level of items stored at the facility.
   - If the item is not a critical spare, no safety stock is required.
   - If the item is not a critical spare but delivery times might become a production or safety issue a value of the safety stock is assigned.
   - It the item is a critical spare, then the variations in the delivery time and usage rate should be monitored in order to have the right value of safety stock.
   - If there is a safety stock, check that the safety stock is greater than any expected peak usage demand.
3) **The ROQ**
   - It must be at least equal to the cycle stock.
   - It must be at least equal to the minimum order quantity (MOQ) of the supplier.

1.5 Details of HFR spares management

The above considerations have been applied to the electrical spare parts stored in the HFR.
In order to support spare management 2D and 3D layouts of all storage areas have been created. This allows to have a snapshot of the disposition of the spare parts inside the storage areas.
Subsequently, all the spare parts have been checked. First, the focus has been posed on the criticality of every spare parts. Based on the categories defined above, the information about the most important spare parts for safety and operation have been obtained.
All the information regards the electrical spare parts are stored in a Microsoft Access based database. Embedded in Microsoft Access, a graphical user interface has been developed in order to make the database user friendly. Through the database is possible to:

- Search for a spare part to get all the information (including obsolescence).
- Change the amount of spare parts available in the storage area and have feedback when the amount of a spare part is below the minimal value.
- Have a report of the spare parts that should be bought in order to bring their amount to, at least, their safety stock.
- Perform a periodic cycle count (inventory) of the storage areas

5. Conclusions

This paper gave an overview of two strongly interrelated programs at HFR. The Technological Obsolescence Management Program and the Spare Management. The two processes are strictly related: a correct spare management favours the realization of a proactive obsolescence program and an effective obsolescence program makes sure that spare management can ensure the presence of spare parts at any time.

6. References

[1] IAEA, 'Safety of Research Reactors – Specific Safety Requirements SSR-3', Vienna 2016.

[2] IAEA, 'Ageing Management for Research Reactors – Specific Safety Guide SSG-10', Vienna 2010.

[3] IAEA, IGALL Database, R. Krivanek, 'TOP401-Technological Obsolescence Programme', 19 December 2014.

[4] EPRI-Electrical Power Research Institute, M. Tannenbaum, E. Sisk, 'Plant Support Engineering: Proactive Obsolescence Management – Program Implementation and Lession Learned', December 2009.

[5] Phillip Slater, 'Spare Parts Inventory Management: A Complete Guide to Sparesology', Industrial PR Inc, 25 November 2016.

Double Heterogeneity Effect on Reactivity of U-Mo Research Reactor Fuel

Hironobu Unesaki

Institute for Integrated Nuclear and Radiation Science, Kyoto University (KURNS),

Kumatori-cho, Sennan-gun, Osaka 590-0494, Japan

ABSTRACT

This study focuses on the impact of fuel heterogeneity on neutronics of U-Mo Al dispersion fuel used for research reactor, which is caused by the fine heterogeneity of the U-Mo particles and its stochastic distribution in the aluminum matrix. Such heterogeneity is called as double heterogeneity and impacts the resonance self-shielding of uranium as well as the escape probability of neutrons from the fuel meat. Neutronic calculation is performed using the Monte Carlo code MVP. Results based on representative plate type fuel show that the heterogeneity effect is strongly dependent on the neutron spectrum of the core, and is also a result of compensation of both positive and negative reactivity occurring in different energy regions. The overall reactivity effect is observed to be insignificant for the conventional fuel and reactor design of the U-Mo fuel.

1. Introduction

U-Mo based fuel is widely considered as the candidate of the very high-density LEU fuel required for the conversion of high-performance research reactors. Two types of U-Mo based fuel – monolithic and dispersion - are currently under development for the futhre application in the aforementioned conversion activities. Amongst the U-Mo based fuel, dispersion type fuel, in which the U-Mo particles are dispersed in aluminum matrix, will be used for the LEU conversion of the Dry core of the Kyoto University Critical Assembly (KUCA) of the Institute for Integrated Nuclear and Radiation Science, Kyoto University (KURNS)[1].

In a dispersion fuel, the fuel particles and its random distribution in the matrix material presents a microscopic heterogeneous structure. Such microscopic heterogeneity can significantly affect the neutronic characteristics of the reactor core due to the presence of strong neutron absorber (fuel particles) randomly distributed in weak (or transparent) absorber (aluminum) matrix. Compared to the homogeneous media, neutron absorption (especially the resonance absorption) by the fuel particles and neutron transmission may show different behavior in such heterogeneous media. This microscopic heterogeneity, embedded in the more macroscopic heterogeneity – fuel/moderator structure – as shown in Figure 1 is generally known as “double heterogeneity” and has been studied especially

in the case of particle fuel in high-temperature gas-cooled reactor in regards with the resonance self-shielding effect and spatial homogenization, which are related to cell averaged (homogeneous) cross section evaluation used in the deterministic neutronic calculation.

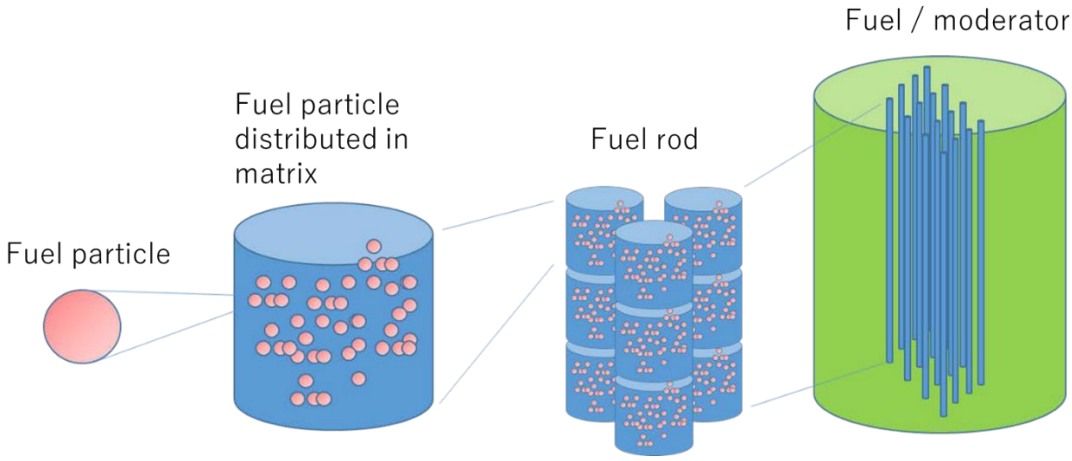

Figure 1. Example of multi-layered heterogeneity in reactor fuel

Such double heterogeneity structure does exist in the U-Mo Al dispersion fuel, where the U-Mo particles are stochastically distributed in the aluminum matrix. The impact of fuel heterogeneity on neutronics of U-Mo Al dispersion fuel has been investigated by the author using a simplified cylindrical fuel cell (pin-type fuel) model, and the results show that. although the heterogeneity effect depends on the U-Mo particle size and the neutron spectrum of the core, the effect is insignificant [2]. However, systematic analysis based on more realistic plate type research reactor fuel model with various fuel cell parameters were noted to be remaining works.

This study extends the previous work by the author, and the double heterogeneity effect on reactivity of a representative plate type U-Mo Al dispersion fuel is investigated.

The methodology and fuel cell model are described in Chapter 2. The results, discussions and observations are summarized in Chapter 3. Conclusions and future works are summarized in Chapter 4.

2. Methodology and fuel cell model used in this study

Analysis of neutronic characteristics was performed using Statistical Geometry Model (SGM) [3] capability of continuous energy Monte Carlo code MVP (version 2.0) [4], together with JENDL-4.0 as neutron cross section library. U-Mo particles are treated as sphere and the location of the particles are randomly generated and sampled probabilistically along the particle flight path from the spatial probability distribution of spherical fuels. The Analytical Nearest Neighbor Distribution, depending on the fuel particle radius and packing fraction as shown in the equation below, is used as the

statistical geometry model in this study.

$$\frac{dF(r)}{dr} = \frac{3}{2} \cdot \frac{f_p}{1 - f_p} exp\left(-\frac{3}{2} \cdot \frac{f_p}{1 - f_p} r \right)$$

Here, $F(r)$ is the distribution probability, f_p is the packing fraction of the spherical fuel particles in the matrix and r is the radius of the spherical fuel particles, respectively.

An infinite array of U-Mo Al dispersion plate type fuel is used in this study (Figure 2). Material composition is based on U-10Mo (density data taken from Ref. [5]) with packing fraction of 0.5 in aluminum matrix, corresponding to 7-8gU/cc loading. The neutron spectrum of the fuel is varied by changing the moderator thickness (fuel pitch) from 2.5mm to 7mm (total of 7 cases) so as to cover the moderator-to-volume ratio (V_m/V_f) from 2.4 to 12.8 as shown in Table 1.

The radius of U-Mo sphere particles was varied as 5, 10, 15, 20, 25, 30, 40, 50, 75, 100 and 150 μm (total of 11 cases) to cover the representative radius distribution of the U-Mo dispersion fuel. The homogenized U-Mo-Al mixture is taken as reference. 54000 particles x 2200 cycles (200 skip cycles) were tracked for each calculation using 12 CPU MPICH parallel processing LINUX PC system, yielding the standard deviation of 0.002% to 0.004%.

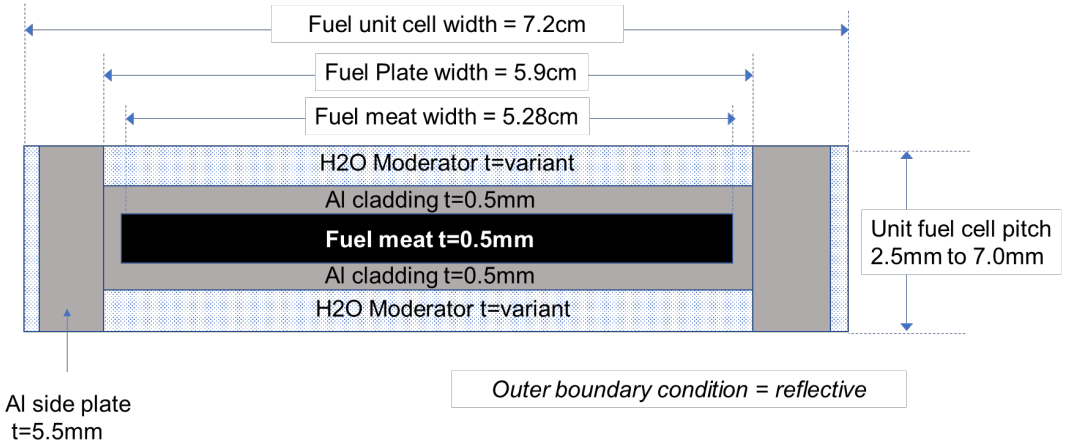

Figure 2. Fuel Cell Model

Table 1. Unit fuel cell pitch and V_m/V_f for each cases

Case ID	Cell pitch (mm)	V_m/V_f
C20	2.5	2.4
C30	3.0	3.6
C35	3.5	4.7
C45	4.5	7.0
C50	5.0	8.2
C60	6.0	10.5
C70	7.0	12.8

3. Results and Discussions

Hereafter, heterogeneity effect is defined as the reactivity difference between heterogeneous model (e.g. considering the U-Mo particle in the mixture) and homogeneous model. Figure 3 shows the heterogeneity effect for each U-Mo particle size and its dependency to V_m/V_f values.

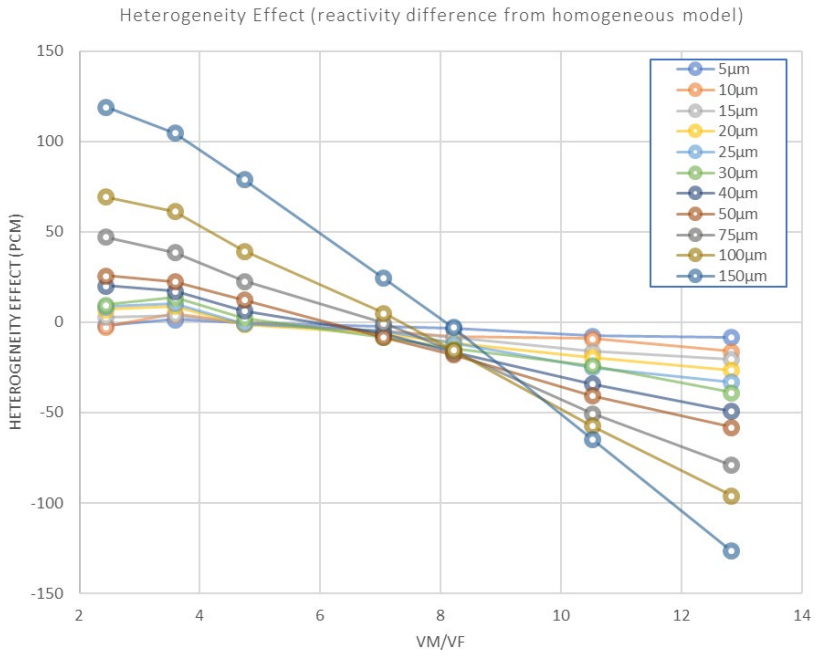

Figure 3. Dependence of Heterogeneous effect to V_m/V_f for each U-Mo particle size

The absolute value heterogeneity effect generally increases with fuel particle size, but its sign (e.g. positive or negative) is dependent on V_m/V_f – or neutron spectrum – of the fuel cell. For all particle size, the heterogeneity effect is positive for small V_m/V_f values (e.g. less thermalized system); the absolute value decreases with increasing V_m/V_f, and are inverted at around V_m/V_f = 8, turn to negative value and the magnitude increases with increasing V_m/V_f. The maximum value of the heterogeneity effect is observed for

particle size 150μm, and is approximately +/- 120pcm at the lower and higher end of the V_m/V_f range.

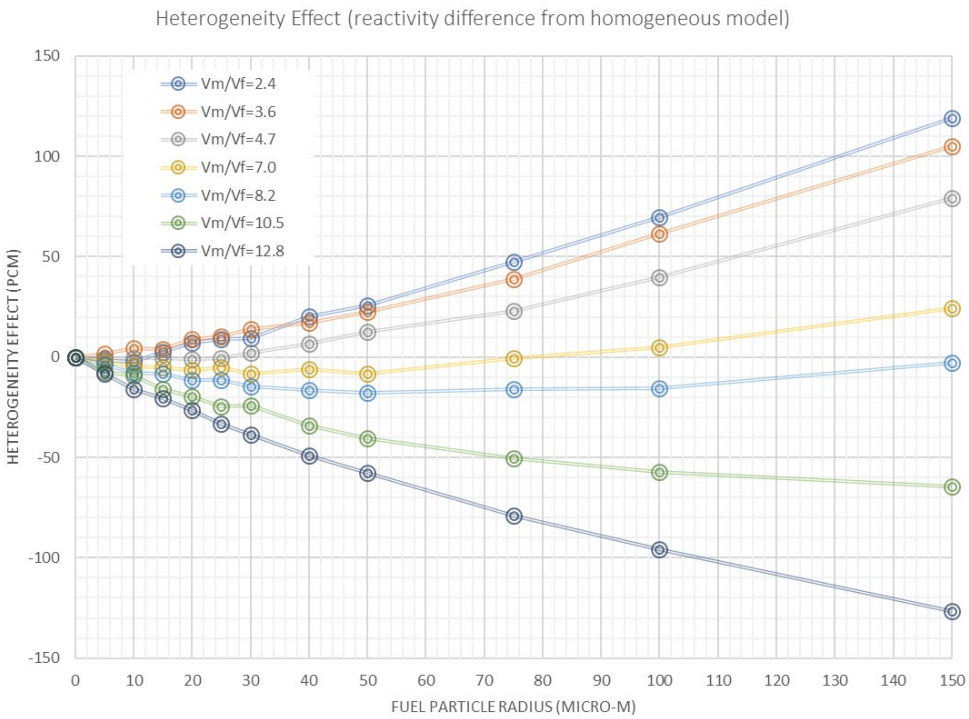

Figure 4. Dependence of Heterogeneous effect on U-Mo particle size for each V_m/V_f

Figure 4 is a different representation of the heterogeneity effect, showing the dependence of heterogeneity effect on U-Mo particle size for each case with different V_m/V_f values. As mentioned before, the absolute value of the heterogeneity effect increases with fuel particle size; for the practical particle size currently being adopted for reactor fuel fabrication (less than 100μm), the heterogeneity effect is approximately in the order of 50 to 70 pcm, which could be considered to be practically negligible compared to other uncertainty factors on reactivity in the reactor core calculation.

The inversed trend for the extremity of the V_m/V_f values – e.g. inversed sign of the reactivity difference – and the practically negligible heterogeneity effect for intermediate V_m/V_f value (at around V_m/V_f =8) with weak dependency on fuel particle size suggests that there should be multiple components constructing the heterogeneous effect, and the sign and magnitude of the components be strongly dependent on fuel particle size and V_m/V_f. This is further investigated by examining the macroscopic reaction rate balance for each case and using the cell averaged macroscopic reaction rate to decompose the reactivity difference into contributing components.

The reactivity difference between arbitrary two cases (in this study, two different cases for identical V_m/V_f fuel cell with different fuel particle size) could be decomposed to relevant components as shown below[6];

$$\Delta\rho = \frac{1}{\overline{k_\infty}} \sum_g \left(\frac{\Delta P^g}{\overline{P}} - \frac{\Delta C^g}{\overline{A}} - \frac{\Delta F^g}{\overline{A}} + \frac{\Delta N^g}{\overline{A}} \right)$$

where $\Delta\rho$ is the reactivity difference, $\overline{k_\infty}$ is the averaged k-infinity value for the two cases, g is the energy group index, *P, C, F* and *N* are macroscopic production (nu-fission), capture, fission and (N, 2N) reaction rate, respectively, A is the macroscopic absorption rate (e.g. C+F-N), and upper bar denotes the averaged macroscopic reaction rate for the two cases. In this study, macroscopic reaction rates were obtained in 4 energy groups, with upper energy of 2.0E+07, 1.68E+04, 1.41E+01 and 1.19E-02 eV, respectively.

The components ("terms") of the reactivity difference is defined as follows;

Production term: $\frac{1}{\overline{k_\infty}} \sum_g \left(\frac{\Delta P^g}{\overline{P}} \right)$

Fission term: $\Delta\rho = \frac{1}{\overline{k_\infty}} \sum_g \left(-\frac{\Delta C^g}{\overline{A}} \right)$

Capture term: $\Delta\rho = \frac{1}{\overline{k_\infty}} \sum_g \left(-\frac{\Delta F^g}{\overline{A}} \right)$

(N,2N) term: $\Delta\rho = \frac{1}{\overline{k_\infty}} \sum_g \left(\frac{\Delta N^g}{\overline{A}} \right)$

The reactivity difference between two cases with fuel particle size of 10μm and 150μm are decomposed using this formula, and the results for the two extreme cases - C25 (V_m/V_f =2.4) and C70 (V_m/V_f =12.8) - are shown in Table 2.

Table 2. Breakdown of reactivity difference between fuel particle size of 10μm and 150μm

1) Case C25 (Vm/Vf=2.4)

Group	Upper energy(eV)	Production Term (pcm)	Fission Term(pcm)	Capture term(pcm)	(N,2N) term(pcm)	Total
1	2.00E+07	9.5	-5.5	-1.0	0.2	3.3
2	1.68E+04	-21.8	14.2	105.2	0.0	97.7
3	1.41E+01	151.7	-98.7	-15.2	0.0	37.8
4	1.19E-02	-23.2	15.1	-8.8	0.0	-16.9
Total		116.2	-74.8	80.2	0.2	121.8

2) Case C70 (Vm/Vf=12.8)

Group	Upper energy(eV)	Production Term (pcm)	Fission Term(pcm)	Capture term(pcm)	(N,2N) term(pcm)	Total
1	2.00E+07	11.3	-6.2	-0.9	0.2	4.4
2	1.68E+04	-9.1	5.7	106.8	0.0	103.4
3	1.41E+01	75.9	-47.3	-146.9	0.0	-118.3
4	1.19E-02	-181.2	112.6	-30.6	0.0	-99.2
Total		-103.2	64.8	-71.5	0.2	-109.7

The different behavior between the two cases are found to be caused by different magnitude and balance of the relevant terms, especially in the 3rd group (main resonance region) and 4th group (thermal region). For well-thermalized C70 (V_m/V_f =12.8) case, increased fuel particle size results to significant decrease of production term in thermal region and increased neutron capture in resonance region (thus resulting to large negative capture term), which results to negative reactivity change. On the other hand, for an under-moderated C25 (V_m/V_f=2.4) case, increased production term overrides the negative capture term in resonance region, and the decrease of production term in thermal region is relatively small, resulting to a positive reactivity change with increased heterogeneity. The heterogeneous effect is a result of such complex compensation of relevant reactivity difference terms in respective energy regions, which strongly depends on the neutron spectrum of the system. Further investigation of the difference of the heterogeneous effect may include detailed analysis of microscopic reaction rate balance, especially for U-235 and U-238 and their resonance self-shielding, as well as the detailed investigation of the escape probability change caused by the heterogeneous structure of the system.

4. Conclusions

The impact of fuel heterogeneity on neutronics of U-Mo Al dispersion fuel used for research reactor, which is caused by the fine heterogeneity of the U-Mo particles and its stochastic distribution in the aluminum matrix, is investigated through systematic neutronic calculation using the Monte Carlo code MVP. Results based on representative plate type fuel show that the heterogeneity effect is strongly dependent on the neutron spectrum of the fuel system. Through the decomposition of reactivity difference based on macroscopic reaction rates, it is found that the heterogeneity effect is also a result of compensation of both positive and negative reactivity terms occurring in different energy regions.

The overall reactivity effect is observed to be in the order of 50 to 70 pcm for the conventional fuel design of the U-Mo fuel and could be considered to be negligibly small.

The results also show that with particle radius of less than 100μm, the U-Mo dispersed mixture could be sufficiently considered as homogeneous media in terms of reactivity, with the magnitude of the reactivity effect caused by the heterogeneous structure of the fuel to be in the order of 50 to 70 pcm.

References

[1] G. Aliberti, J.A. Morman, J.G. Stevens, T. Sano, H. Unesaki, T. Misawa, B. Stepnik, “Update of Neutronic Analysis of KUCA Dry Core using LEU Fuel”, Proc. European Research Reactor Conference RRFM 2018 (2018).

[2] H. Unesaki and T. Sano, “Impact of Fuel Heterogeneity on Neutronic Characteristics of U-Mo Dispersion LEU Fuel”, Proc. RERTR 2017 – 38th International Meeting on Reduced Enrichment for Research and Test Reactors, November 12-15, 2017, Chicago, IL USA (2017).

[3] I. Murata, T. Mori and M. Nakagawa, “Continuous energy Monte Carlo calculations of randomly distributed spherical fuels in high-temperature gas-cooled reactors based on a statistical geometry model”, Nucl. Sci. Eng. 123(1); p. 96-109 (1996).

[4] T. Mori and M. Nakagawa, "MVP-GMVP: General Purpose Monte Carlo Codes for Neutron and Photon Transport Calculation based on Continuous Energy and Multigroup Methods," JAERI-Data/Code 94-007 (1994) (in Japanese).

[5] D. E. Burkes, G. S. Mickum and D. M. Wachs, “Thermophysical Properties of U-10Mo Alloy”, INL/EXT-10-19373, Idaho National Laboratory (2010).

[6] H. Unesaki, S. Shiroya, K. Kanda, S. Cathalau, F.-O. Carré, O. Aizawa, T. Takeda, “Analysis of Differences in Void Coefficient Predictions for Mixed-Oxide-Fueled Tight-Pitch Light Water Reactor Cells”, Nuclear Science and Engineering, 135:1, 1-22, DOI: 10.13182/NSE00-A2120 (2000).

POSSIBILITY OF THE HIGH-PERFORMANCE PLATE-TYPE FUEL IMPLEMENTATION IN MARIA RESEARCH REACTOR

M. Lipka

Nuclear Facilities Operations Department, National Centre for Nuclear Research

ul. Andrzeja Sołtana 7, 05-400 Otwock-Świerk, Poland

Maciej.Lipka@ncbj.gov.pl

ABSTRACT

MARIA is a channels-in-pool type research reactor. Fuel elements are located inside pressurised fuel channels. For over forty years of operation, MARIA has been using fuel elements in the shape of concentric tubes. Their performance is entirely satisfactory; however, implementing plate-type fuel elements is tempting with the development of high-density fuel by multiple vendors. This article presents thermal-hydraulic calculations of various variants of plate fuel that would be in a circular fuel channel during operation. Such hypothetical fuel will enable the significant growth in MARIA's nuclear fuel suppliers, resulting in better protection of its operational needs. Equipment developed for the in-core testing will additionally benefit the international nuclear community.

1. Introduction

Research reactors being the source of neutrons for science and radioactive isotopes production for medicine and industry must have two basic characteristics: high-density neutron flux and low operation temperature. Both of those characteristics are provided, among others, by the nuclear fuel of the certain shape and composition. Traditionally highly enriched uranium (HEU) fuel was used, but for quite some time, due to the international agreements, conversion to low-enriched uranium (<20% ^{235}U) was performed [1]. Recently the term high-assay low-enriched uranium (HALEU) begins to be used for the latter if the enrichment is between 5 and 20% ^{235}U [2], and that term will be used in the next parts of this article.

Conversion to HALEU demanded the increase of uranium density in the fuel meat to compensate the decrease of enrichment. The same principle applies to the molybdenum-99 (^{99}Mo) irradiation targets. Current, commercially available fuels contain up to c.a. 4.8 $g_{U\text{-}235}/cm^3$ and the efforts to increase that number are ongoing. As a rule of thumb, it can be said the higher the density, the higher the neutron flux, but issues with high heat-flux accompany that feature, and they might demand changes of the fuel shapes.

This article presents the possibility of possibility of use the plate-shaped nuclear fuel in MARIA reactor. Additionally, similar shape is currently used for the irradiation of ^{235}U targets for the ^{99}Mo production Supply of both is important as MARIA is currently undergoing major refurbishment that will allow its long-term operation (LTO) to the year 2053.

MARIA, drawing on its experience, it is interested both in expanding the group of suppliers and in helping other reactors to use new types of fuel. The latter is provided, among others, as part of the LEU-FOREvER programme.

2. MARIA currently operated nuclear fuel elements and irradiation targets

MARIA is a channels-in-pool type research reactor, meaning that fuel elements are placed within the pressurised fuel channels that are immersed in the reactor pool. The core, since the beginning of its operation in 1974, underwent several fuel conversions. The initial related to decrease 235U enrichment from 80 to 36%. The recent, which was successfully finished in 2015, decreased the enrichment further, to the levels below 20%. Additionally, since 2017 MARIA uses HALEU irradiation targets for ^{99}Mo production.

Currently MARIA operates on MC-5 (Framatome-CERCA) and MR-6 (TVEL) fuel elements, being one of the few, or the only one at all research reactors with multiple, independent fuel suppliers. The key features of the fuel elements are indicated in the table 1. MC-5 fuel is made out of bended plates, MR-6 is made out of extruded tubes. For the ^{99}Mo production via ^{235}U fission, thin UO_2 targets are used, they are irradiated inside the fuel channels in the same way as fuel elements [3].

Table 1: MARIA reactor fuel elements comparison [4].

Parameter	**Value**	
	MC-5	MR-6
Number of fuel tubes	5	6
Total length [mm]	1315	1380
Fuel meat length [mm]	1000	1000
Fuel meat material	U_3Si_2 dispersed in Al	UO_2 dispersed in Al
Tube thickness [mm]	2	2
Mass of ^{235}U [g]	485 ± 5	485 ± 5
Uranium density [g/cm^3]	4.79	3.59
Total heat transfer area [m^2]	1.29	1.79

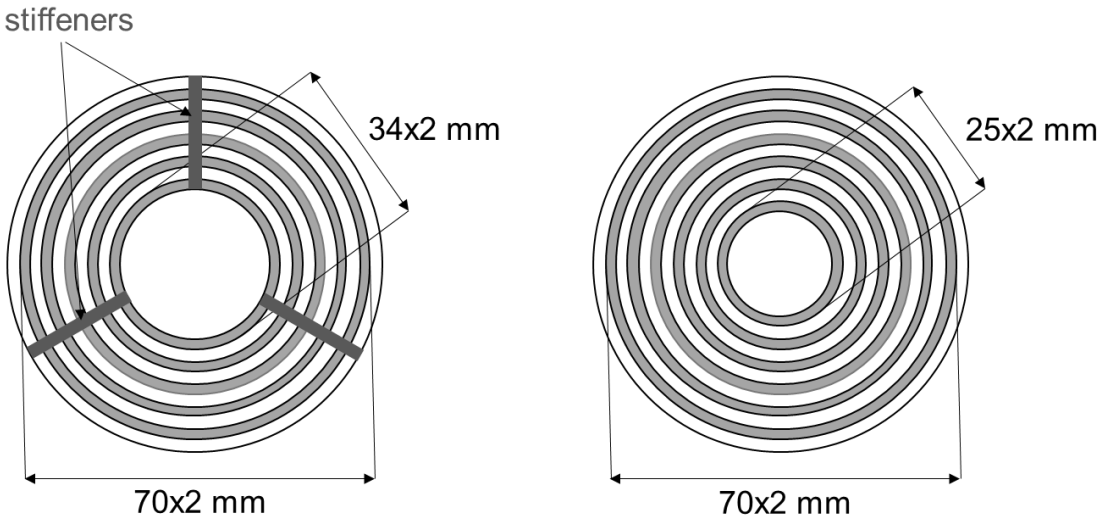

Figure 1: MC-5 (left) and MR-6 (right) fuel elements cross-sections comparison

3. Potential for plate-type fuel elements operation

One of the most important safety features connected to the safe operation of the nuclear fuel is its low temperature both in steady state and transients. It can be achieved by the combination of the high coolant flow and appropriate heat-flux from the fuel element to the coolant. Additionally in MARIA reactor, onset of nucleate boiling ratio (ONBR) is an important safety indicator, as the coolant boiling is not allowed in normal operation state.

As MARIA is using fuel channels with the circular cross-section, special adapter is needed for the plate-type fuel element for the geometry adaptation. The idea of that is given in the figure 2. Fuel elements might contain from six up to ten fuel plates of various thicknesses. Slightly bent plates are also possible.

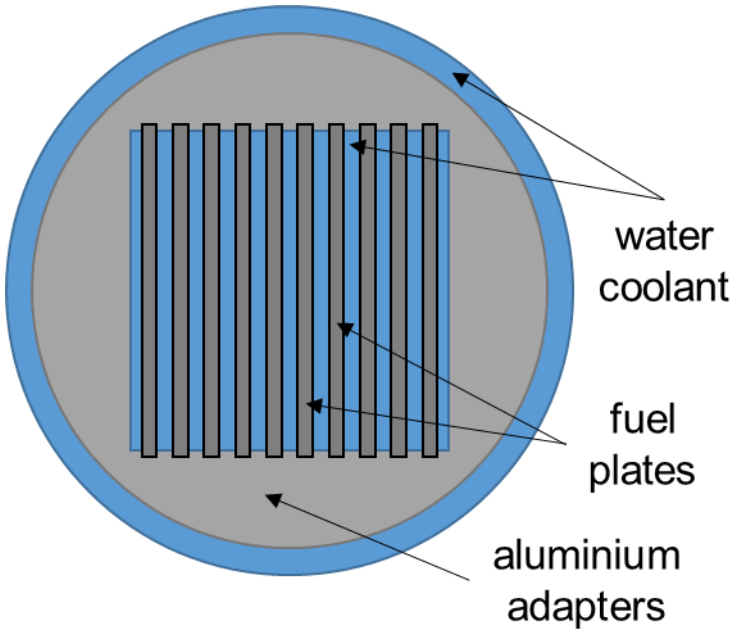

Fig 2: Fuel channel with plate-type fuel element inside,
various number of the plates and their thickness is possible.

For the purposes of this article, several plate configuration have been considered. The constraints for the optimalisation were:

- Minimisation of the heat flux
- Maximisation of the ONBR
- Coolant flow velocity in the fuel channel below 10 m/s

Several fuel plates' number and thicknesses were considered and the optimum, ten plate configuration was selected. Results are presented in the next part of the article, followed by conclusions.

4. Calculation results

Mathematical modelling revealed that when considering plate-type fuel element inside the MARIA reactor fuel channel, the optimum geometry contains 10 fuel plates with the thickness 2 mm each. That configuration enables the efficient heat transient of up to 1.8 MW. All of the assumed safety parameters are fulfilled in that case, i.e.:

- ONBR = 1.201
- Maximum coolant velocity w_{max} = 8.83 m/s
- Maximum heat flux HF_{max} = 3.3 MW/m^2
- Maximum mass of HALEU uranium in the fuel element: 300 g

Cladding and water temperatures are presented in the figures 3 and 4 respectively

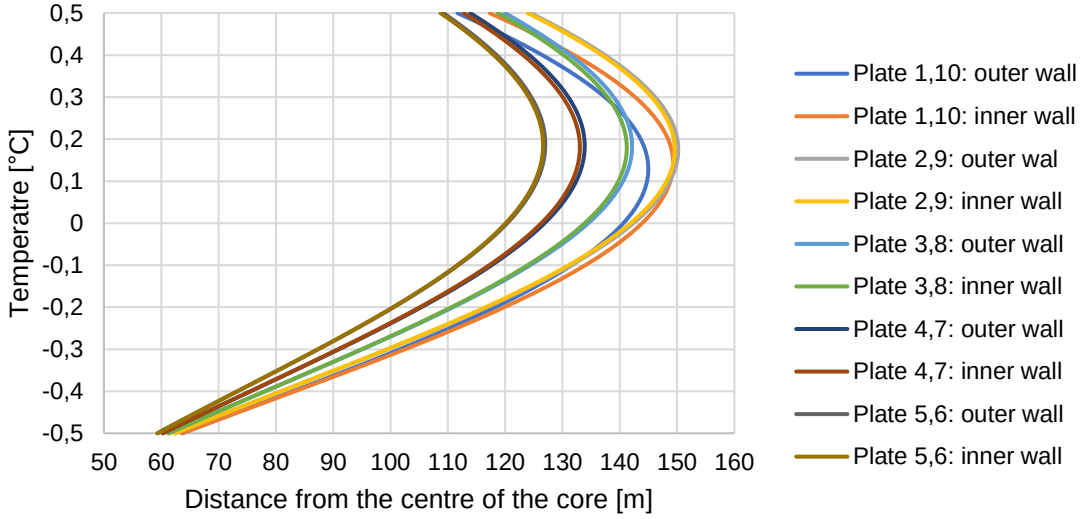

Figure 3: Cladding temperatures

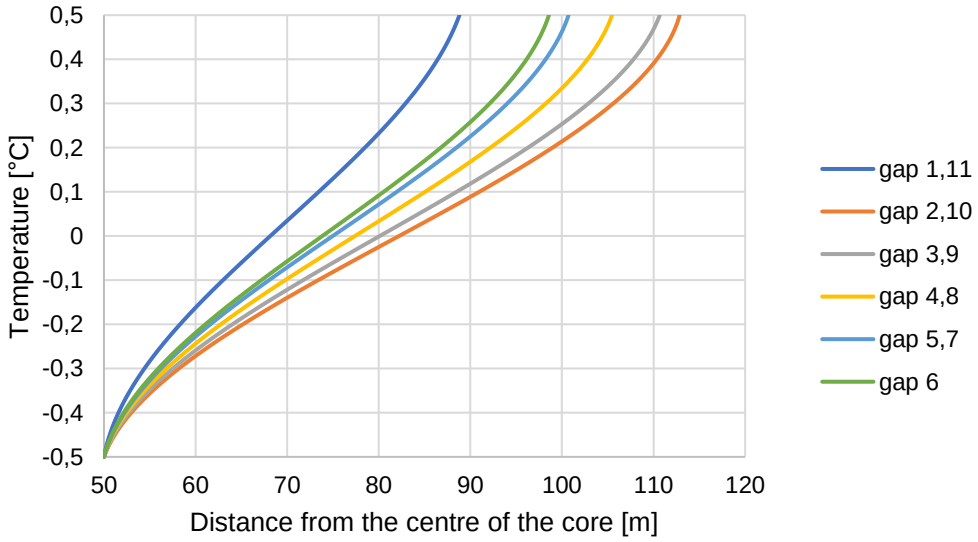

Figure 4: Cooling water temperatures

5. Conclusions

Placing plate-type fuel elements in the circular fuel channel was not the brightest idea. The plate-type fuel element configuration has a significantly lower heat transfer area than the current plate-type fuel elements operated in the MARIA reactor (0.8 vs 1.29–1.70 m2). This unfortunate feature limits the amount of ^{235}U in the fuel element from the currently used 485 g HALEU in the single fuel element to c.a. 300g. This would mean a significant decrease in the neutron flux compared to the fuel elements used. Consequently, plat-type is not the sustainable configuration of the fuel element.

However, calculations and measurements in the MARA core reveal that a single fuel channel with a tubular fuel element can transfer up to 3 MW of the heat, 50% more than the current operational limit of 1.97 MW. This leaves considerable scope for optimizing the uranium content of the fuel element and allowing a significant increase in the MARIA's future neutron flux.

MARIA fuel elements are unique, however almost identical to those operated in BR2 (Belgium) and similar to the VVR-S (and their derivatives) types that are used, i.a., LVR-15 (Czechia) and BRR (Hungary). Nearly the same fuel shape is planned to be used in JHR (France). Additionally, many reactors in the world use slightly bent plates that can be made into tubes, as is known from the current cooperation with CERCA and past cooperation with INVAP.

As MARIA is undergoing LTO modifications and plans for its operation up to the year 2053 are implemented, the situation creates a pretty significant future market for the high-density fuels in the tubular shape.

References

[1] Krzysztoszek G. Maria research reactor conversion to LEU fuel. Available from: https://www-pub.iaea.org/MTCD/publications/PDF/P1360_ICRR_2007_CD/Papers/G.%20Krzysztoszek.pdf

[2] What is High-Assay Low-Enriched Uranium (HALEU)? [Internet]. Energy.gov. [cited 2022 Apr 15]. Available from: https://www.energy.gov/ne/articles/what-high-assay-low-enriched-uranium-haleu

[3] Migdal M, Balcer E, Bartosik Ł, Bąk Ł, Celińska A, Cybowska J, et al. MARIA Reactor Irradiation Technology Capabilities towards Advanced Applications. Energies. 2021 Dec 5;14(23):8153.

[4] Pytel K; Bąk W, Borek-Kruszewska E, Ciborek E, Czarnecki M, Dorosz M, et al. Eksploatacyjny Raport Bezpieczeństwa Reaktora MARIA; National Centre for Nuclear Research: Świerk, Poland, 2015.

Practical issues while restarting the Delft research reactor after an extended shutdown period.

A.WINKELMAN

Reactor Institute Delft/ TUDelft

Mekelweg 15, 2629jb Delft – Netherlands

ABSTRACT

After an extended shutdown period of the reactor from May 2019 to November 2021 to accommodate for various upgrade projects, the HOR research reactor in Delft experienced a smooth restart. Startup required acquiring and use of a neutron start-up source. Operators were trained to perform an approach to critical using the in house simulator. Operations at nominal power required dealing with poisoned Beryllium reflector assemblies. The poisoning of the reflector elements where predicted using Beryl and Serpent calculations and checked by measurements after loading the core. Reload calculation results showed to be accurate. These practical items will be discussed and shared.

1 Recap of Oyster phase 1 modifications to HOR.

From May 2019 a two and a half year shutdown period of HOR, the Delft University of Technology research reactor, allowed for (amongst others)
Renewal of two in-pool beam-tubes to accommodate a cold source,
Renewal of the primary and secondary cooling system,
Installation of new hall penetrations (in preparation for cold source cryogenic feedthrough and new pneumatic rabbit systems).

2 The need for a startup neutron source

Data from the shutdown BER2 (Stefan Welzel) was used to estimate that after the long term shutdown, the gamma radiation driven intrinsic Be (gamma,n) neutron source is too weak to meet the required minimum signal on the start-up channel fission chamber, even when this detector is at optimal position (closest to the core).
A small Cf source, normally used in the subcritical assembly, was used to test the fission chamber signal response and estimate the required neutron source strength. A complicating factor here is the absence of fuel assemblies, which could only be loaded back into the grid after finishing Oyster phase 1. MCNP6 was used to translate testing in the core grid with reflector assemblies only to fuel loaded configurations.
For HOR a 50 MBq Cf source was estimated to be sufficient for startup.
At the time (mid 2021), 252Cf was very scarce and after asking the community, TA (Laurent Manifacier) pointed me to QSA as the JHR supplier. HOR was able to obtain a compact 140 MBq Cf source that fitted in the central Be irradiation facility. Getting the source to the institute in Netherlands proved to be very difficult and required a lot of attention.

3 Be poisoning

Poisoning of irradiated Be after extended shutdown of research reactors is a well-known phenomenon. HOR has operated more than 20 years in its current compact core shape with fixed Be reflector positions. The central hollow Be assembly holding two dry 16 mm diameter irradiation tubes received highest fast neutron fluency (more than 2.5 times the fast n fluency of other reflector assemblies).
For HOR operational history, 6Li was estimated to saturate and should not increase during the shutdown while 3He is steadily produced at impressive (almost) constant rate throughout the complete shutdown period because of abundant 3H present at the end of operation before shutdown.

With a shutdown period of more than 2 years it was estimated by the Beryl method that total Be poisoning would amount to -1200 to -1800 pcm (-1.7 to -2.5 β). The large uncertainty reflects the uncertainty in local reaction-rates for the poison reactions. Later, using full 3d Serpent core burnup modified for control rod position adjustment, calculated Be poisoning showed good agreement of reactivity worth with measured values from swapping experiments.
The poison worth of the central hollow Be assembly alone turned out to be a whopping -1100 pcm. Putting this into perspective: a typical HOR cycle consists of 16 weeks of operation from Monday to Friday and the total reactivity swing BOC-EOC is in the order of 1600 pcm.
First loading the core in the highly poisoned reflector configuration with low excess reactivity showed to be good practice because the configuration reacts quite tame. Since the poison reactivity uncertainty was quite high, critical control rod positions were also uncertain. Thus an approach to critical was executed. This will be mentioned in the next item.
After complete reactivity measurements on this 'tame' core the central hollow Be assembly was swapped with one that received an estimated 4% of the fast n fluency. Again all required reactivity measurements were executed before going to the nominal power range. Downside of this swap needed to reach an acceptable excess reactivity (and core cycle length) is that the highly poisoned assembly now is in a low flux position and will probably not recover from 3He excess.

4 Approach to critical by the inverse multiplication method.
Since the predicted critical control rod positions had relatively high uncertainty, it was decided to use the inverse multiplication method with fixed source to experimentally predict criticality while loading and searching critical control rod positions. MCNP6 was used to predict fission chamber response after various loading steps. HOR must show sub critically at 45% out-of-core bank position so fission chamber response was checked at various loading steps at 45% out. The inverse multiplication clearly predicted sub criticality of the completely loaded core. The expected low excess reactivity was confirmed early during the approach to critical with control bank pulling in steps of 10 % (or less) of the total travel. Already at 30 % out of core position the inverse multiplication method prediction of criticality converged to the critical bank position of 70% out-of-core.

5 Operator training
Before operation, all operators were trained on instrumentation, procedures and used the in house Labview reactor simulator to exercise startup, low and nominal power operation featuring Xe buildup and fuel burnup. Specific exercises were developed to exercise the approach to critical using inverse multiplication and to simulate behavior of the reactor with a fixed source.

6 Power determination

Since HOR power indication is based on N16 gamma measurement along the hot leg of the primary cooling system and both PCS and SCS were completely renewed, there was no calibrated power reading available at startup. N16 power is calibrated against thermal power but this needs averaging over typically one complete week of operation and was of course not available at startup after modification. It was however possible to use an unchanged pool dose-rate channel to indicate power within 10 % error margin by correcting its reading for the moderate influence of control rod bank position taking into account its reading vs control rod bank position during many cycles.

Low power testing was performed to preliminary calibrate N16 power indication referenced to the power indicated by pool dose rate. Also foil activation was performed to match the power indication. Because of the increased power indication uncertainty it was decided to

run the first operational week at 70% of estimated nominal power and check thermal power during this week to set N16 reading to the correct conversion. The second week again ran at 70% of nominal power to be on the safe side and the N16 indicated power was checked again to reflect the thermal power during that week of operation. It was found that power indication was indeed correct, and typical power operation was cleared to go ahead.

7 Conclusions

Restarting the Delft research reactor critically depended on using an external neutron source, on the availability of an unchanged reference channel, on available historic data, on the appreciation of Be poison buildup and on training operators on startup procedures specific to the approach to critical method. Operation at nominal power depended on dealing with negative Be poison reactivity and the ability to calibrate power indication.

High Resolution Power Density Measurement of MTR Fuel Using Gamma Spectroscopy

G. Gabrieli, U. Steinitz, Z. Yungrais, O. Aviv, L. Danon, A. Krakovich, T. Makmal, I. Neder

Soreq Nuclear Research Centre
rd. 4111, Yavne 81800 – Israel

guyga@soreq.gov.il, urist@soreq.gov.il

ABSTRACT

An accurate estimation of the power density distribution is essential in planning, commissioning, and maintaining the operational lifecycle of nuclear reactors. In situations such as in the vicinity of a flux trap, the high local thermal flux significantly increases the power peaking factor (PPF), affecting the core's safety margins. Reliable prediction of this effect is computationally challenging as it strongly depends on local core features such as fuel depletion distribution, precise geometrical modeling and local water-to-fuel ratio and may require high resolution simulations. Thus, experimental validation of computed PPF allows a better estimation of the calculation errors. Here we report high-resolution measurements allowing 2D mapping of the surface power density in MTR fuel assemblies using gamma spectroscopy analysis of fission products. We performed the experiments in the Israeli Research Reactor - 1 (IRR-1), probing a fuel assembly both before and after irradiating it in the reactor at a position adjacent to a flux trap. The measurements revealed a steep power density slope near the flux trap boundary, indicating that a high tally resolution is needed to correctly portray the effect. However, the resulting PPF was in good agreement with a full-core 3D Monte-Carlo simulation of the IRR-1, assuming a homogeneous burnup over the fuel plates' breadth, an assumption that was validated in the experiment as well. Therefore, a high-resolution flux tally is needed to enable a correct prediction of the local PPF. These results augment IRR-1's ongoing IAEA burnup benchmark dataset, which could be beneficial for benchmarking reactor calculations.

1. INTRODUCTION

In a thermal reactor, a volume of a moderator adjacent to a nuclear fuel assembly creates what is known as a ‘flux-trap’, where the fast fission neutrons thermalize, resulting in an increased thermal neutron flux in the moderator region. This thermalized flux increases the fission rate in the fuel assembly near the fuel-moderator interface, creating a peak in the power density and consequently a large power peaking factor (PPF– the safety parameter that represents the maximal power density relative to the average, which is the relevant parameter used in the thermo-hydraulic safety calculations). Flux traps are common in nuclear reactors, either for uses such as irradiation sites in or near the reactor’s core, or as part of the design, for

example, in absorber blade guides which remain filled with water when the blades are retracted. The core of the Australian reactor OPAL features such a built-in flux trap [1] which creates a local power increase.

Computational evaluation of the effect may require a resource-heavy calculation and is highly dependent on the exact geometry and the resolution of the calculation. In [2], it is shown that the sharp ascent in flux and power density occurs within about 1 cm of the fuel, and therefore lower resolution simulations flatten the effect significantly, giving gross underestimations of the PPF. Furthermore, long-term irradiation of fuel assemblies near a flux trap results in highly inhomogeneous fuel depletion. Correctly accounting for the flux trap effect in a high resolution full-core simulation is computationally inefficient and could be impractical.

From a safety perspective, the flux trap effect increases the uncertainty in the PPF of a single fuel assembly (FA), and in the power distribution throughout the core. The uncertainties require increased safety margins, which could lead to decreased operating power. These challenges create the need to experimentally measure the magnitude of this effect and validate the computational models of reactors.

Here, we present the results of measurements of the power distribution within an HEU MTR-type FA irradiated near a flux trap in the Israeli research reactor IRR-1 in Soreq. The local fuel content and power density distributions within the FA were determined by gamma spectroscopy assessing the local unstable fission product abundance. The results help both in validation of our computational models, and in a direct observation and quantification of the flux-trap effect.

The paper is organized as follows: section 2 gives a short description of the experimental setup; section 0 details preliminary considerations regarding the gamma spectroscopy analysis, and full-core simulations of the IRR1, to which the experimental results will be compared. In section 4, the experiments' results are shown and discussed, and conclusions are given in section 5.

2. EXPERIMENTAL DESCRIPTION

Measurements of spatial power distribution are described in several previous works [3] [4]. Here, we used a setup similar to one described previously [5], consisting of a high-purity germanium spectroscopic gamma detector (model Falcon5000, Canberra) aligned with an air-filled collimator, positioned above a fuel assembly lying horizontally. We used a motorized stage to scan the FA, with the fuel plates lying perpendicularly to the collimator (Figure 1). The counts from fission products are proportional to the power density, and hence can be used to measure the power density profile and PPF in a single fuel assembly.

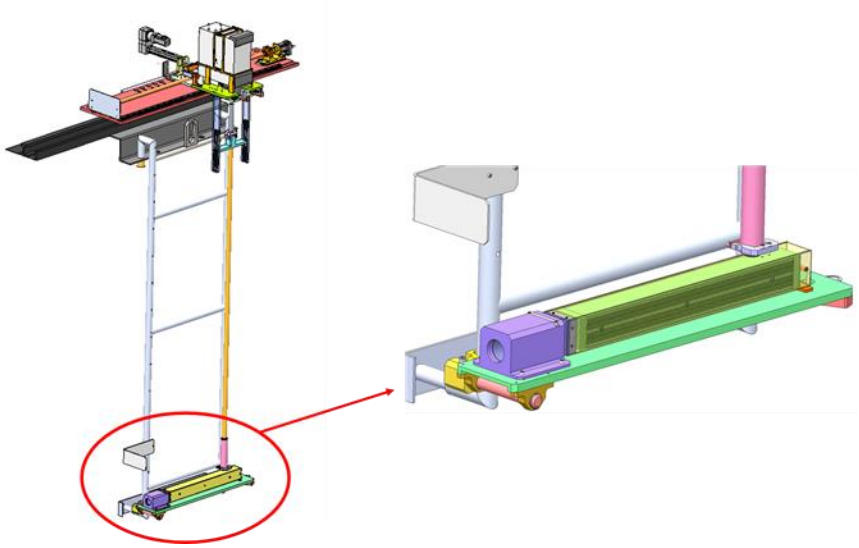

Figure 1. The experimental setup: the fuel assembly lying horizontally, with the fuel plates perpendicular to the collimator. The latter leads to an HPGe detector.

We chose to measure a FA considerably depleted, with local depletion ranging from 20% to 80%, depending on the height [3]. The FA was not used recently, allowing a preliminary measurement to be conducted, where we scanned the FA more than a decade after it was last used or irradiated in the reactor. Analysis of the long-lived fission products (namely Cs-137) provided the power distribution within the fuel plates throughout its 30 years of irradiation history, and consequently the remaining fuel content distribution.

In the main experiment, this same assembly was inserted into the IRR-1 core and irradiated next to a vacant lattice cell in the core filled with water (which acts as the flux trap). The FA was irradiated for 3 hours, with the core operating at 5 MW. This paper presents measurements taken two weeks after the irradiation. In order to measure the effect of a recent, short irradiation of a FA in the core, the analysis is concerned with fission products having short half-lives, ensuring that the only contribution measured is of recent irradiations.

3. PRELIMINARY CONSIDERATIONS AND CALCULATIONS

2.1. Gamma Spectroscopy

The use of gamma spectroscopy in this experiment is similar to that described in [6]. A reliable tool for this purpose is a high-purity germanium detector, which is a semiconductor-based photon radiation detector, characterized by a high energy resolution (~0.1%) of gamma/X-rays, and capable of identifying and quantifying multiple radionuclides simultaneously. These are highly useful features in nuclear fuel assembly measurements, in which a large amount of fission and activation products are present, and emit hundreds of characteristic gamma rays.

The main isotopes to be used in the analysis of this experiment are Cs-137, which has a half-life of $T_{1/2}$ ~30 years and hence is indicative of the whole irradiation history, and isotopes such as I-131, I-132, La-140 and Tc-99, which have short half-lives, and thus their signal could only originate from the irradiation of the fuel assembly next to the flux trap. Information on the relevant isotopes is given in Table I.

Table I. Properties of some fission products used in this experiment

Radionuclide	Emission probability P_g	Energy E $[keV]$	Decay constant λ $[1/sec]$
Cs-137	0.850	662	7.31E-10
Ba/La-140	0.954 0.461	1596 487	6.29E-7
I-131	0.812	364	9.99e-7
Te/I-132	0.987	668	2.48E-6
Mo/Tc-99m	0.896	140	2.92E-6

An estimation of the count rates for these isotopes will now be presented. The activity of a measured isotope is given by [7]:

$$A = \frac{N-B}{t\epsilon P_g f_1} f_2 \ , \tag{1}$$

Here, A is the activity, N the number of counts in the relevant energy peak, B represents the background measurement, t the effective measurement duration (live time), ϵ the detection efficiency ($counts/\gamma$), P_g the emission probability (branching ratio) of the radionuclide, and f_1 and f_2 are the correction factors for decay during measurement, and decay from the end of irradiation to the beginning of measurement, respectively. The correction factors depend on the measurement duration t and the time between irradiation and measurement t', and are given by:

$$f_1 = \frac{\lambda t}{1-\exp(-\lambda t)} \ , f_2 = \exp(-\lambda t') \quad . \tag{2}$$

Using these, the net count rate $n = \frac{N-B}{t}$ is expressed as:

$$n = \frac{A\epsilon P_g f_1}{f_2} \ . \tag{3}$$

An estimate of the activities of the relevant isotopes was obtained using MCNP's CINDER burnup module, and the detector efficiencies for different energies were extracted from the Cs-137 efficiency measured in [3] using experimental calibration curves for a point source positioned 1 meter away from the detector. An estimate for the net count rate is given in **Error! Not a valid bookmark self-reference.**, from which it is relatively straightforward to extrapolate for any irradiation and decay times.

Table II. Estimation of the net count rate resulting from a 1-hour irradiation, measured after 1 week.

Radionuclide	$\boldsymbol{E}$ $[\boldsymbol{keV}]$	$\boldsymbol{\epsilon}$ $\left[\frac{\boldsymbol{counts}}{\boldsymbol{\gamma}}\right]$	Activity $[\boldsymbol{Ci}]$	n [sec^{-1}]
Mo/Tc-99m	140	2.71E-7	9.2	55
I-131	364	1.02E-7	4.9	10
Ba-140	487	6.90E-8	8.7	7
Cs-137	662	6.00E-8	237	499
Te/I-132	668	6.00E-8	4.9	12
La-140	1596	4.00E-8	8.7	8

2.2. Full-Core Simulations

The main computational tool used to model the IRR1 is a burnup-coupled Monte Carlo program called MUTZAV [3]. Based on over 30 years of recorded operations, each core configuration is calculated using MCNP 4b and the fuel assemblies (divided into two side plates and a "bulk" of the middle 21 plates, and 5 axial burnup zones each, for a total of 15 burnup zones) are burned using the DRAGON burnup module. Figure 2 shows the core configuration of the current experiment, where the fuel assembly to be measured (outlined in red) was irradiated next to a flux trap (an empty lattice site in the core filled with moderator – light water).

G	G	G	G	G	G	G	G
G	38%	26%	R	57%	54%	2%	G
G	12%	67%	46%	76%	47%	7%	G
G	22%	39%	53%	50%	55%	11%	G
G	21%	72%	43%	Be	42%	10%	G
G	2%	33%	58%	W	46%	3%	G
G	G	G	G	DFT	G	G	G

Figure 2. Core configuration for the irradiation experiment. The values indicate the average depletion of each fuel assembly. W – water-filled lattice site (flux trap), G – graphite reflector, R – regulating control rod, DFT – irradiation channel, Be – beryllium control assembly with absorber blades. Black outline – control fuel assembly with absorber blades, red outline – fuel assembly to be measured.

The flux trap effect in the fuel assembly in question was simulated using MCNP. For the upper-most burnup zone of the assembly (which is the least depleted zone, and which is the height range in which the measurement of the power distribution was actually performed), the thermal neutron flux along the x direction was calculated using a volume fluence tally. To increase the tally statistics and allow for a high resolution near the edges, the flux was averaged over the volume of the 10 outermost fuel plates. The result is displayed in Figure 3.

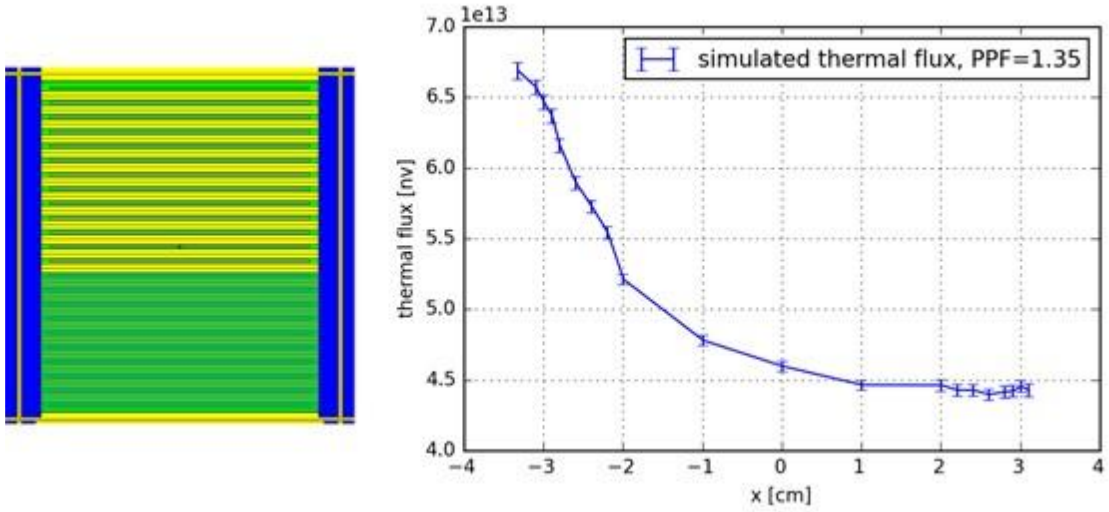

Figure 3. Left: z cross-section of the fuel assembly, the region with a green shadow denotes the tally volume. Right: the thermal neutron flux obtained in a full-core MCNP simulation.

The increased thermal flux near the flux trap boundary is apparent, yielding $PPF = 1.35$. Given the flux along the assembly, and the fact that the fuel density is constant along this direction in the model, the power distribution $P(x)$ is given by:

$$P(x) = \gamma \Sigma_f \Phi(x) \ , \tag{4}$$

Where $\gamma \sim 200\ MeV$ is the average energy released per fission, Σ_f is the macroscopic fission cross-section and $\Phi(x)$ is the local thermal flux.

4. RESULTS AND DISCUSSION

A preliminary measurement was conducted on the chosen fuel assembly that was out of the core for the past decade. These measurements focused on the count rate of the 662 keV emission line of the long-lived Cs-137 along the z axis as well as along the x axis. This allowed for calibration of the experimental setup against previous measurements, and yielded the depletion distribution, as a result of the irradiation history of the assembly. Analysis similar to that presented in [6] shows that the FA self-absorbs 40% of the gamma rays emitted from Cs-137 on average. As a result, the measurement is affected mainly by the three fuel plates nearest to the detector.

The FA was scanned along its x axis in three different positions on the z axis (where $z = 0$ is the bottom of the fuel plate, and $z = 60\ cm$ its top). Another scan was performed with the assembly rotated 180 degrees around its z axis Figure 4, measuring the plates from the opposite side.

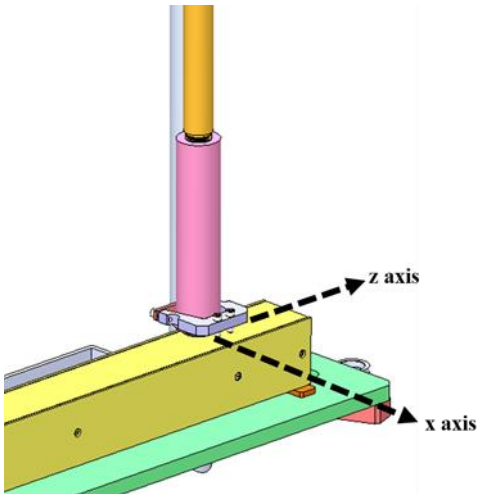

Figure 4. Definition of the z,x axes of the FA.

The results in Figure 5 demonstrate a largely homogeneous depletion inside the plate in the x axis, with max to mean depletion of 1.1 at the most, for the least depleted cross-section $z = 55\ cm$. The depletion is symmetric around the center of the fuel plates and on both sides of the assembly, which was expected since the irradiation of the assembly was generally uniform throughout the history. The power still peaks slightly at the edges of the fuel plates, wherein the aluminum side plates perpendicular to the fuel plates the thermal neutron absorption is considerably lower than in the fuel region, raising the thermal flux at the edge of the fuel plates.

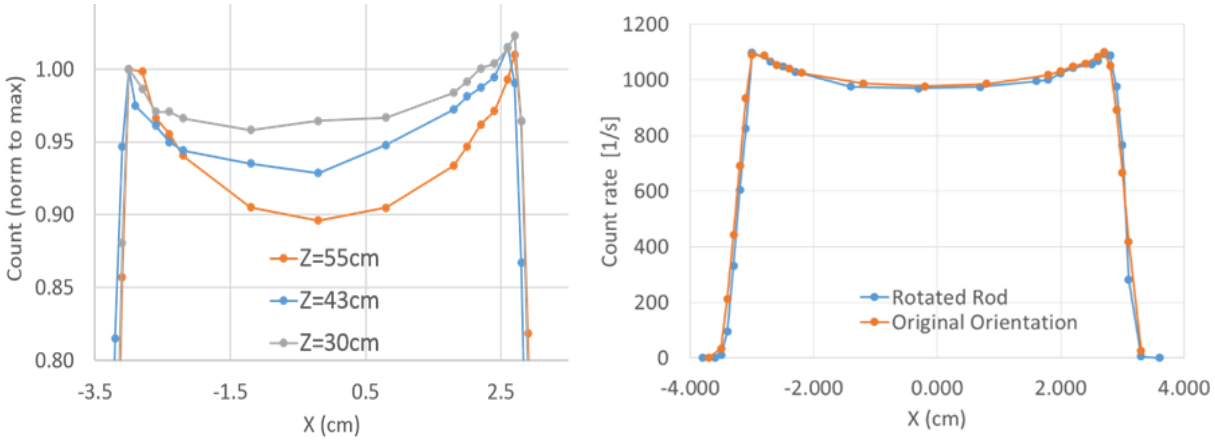

Figure 5. Preliminary measurement results. Left: x scans at various heights along z direction, corresponding to different depletion values. Right: comparison between measurements from opposing sides of the FA, at z=55 cm.

Later, the fuel assembly was irradiated next to the flux trap Figure 6, and a measurement was conducted. The assembly was scanned along the x direction, 5 cm below the top of the fuel plate. The results of the main short-lived isotopes are presented in Figure 7.

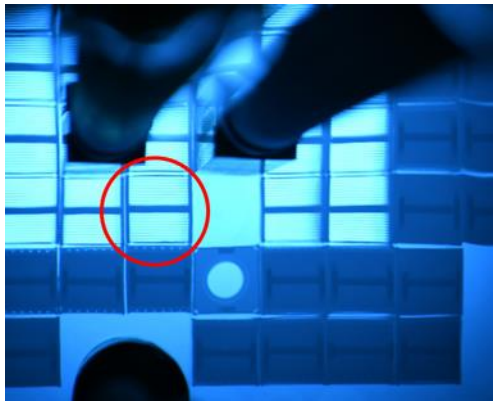

Figure 6. Irradiation of the FA intended for measurement (circled in red) next to a flux trap (lattice space filled with water, to the right of said FA) in the IRR-1 core.

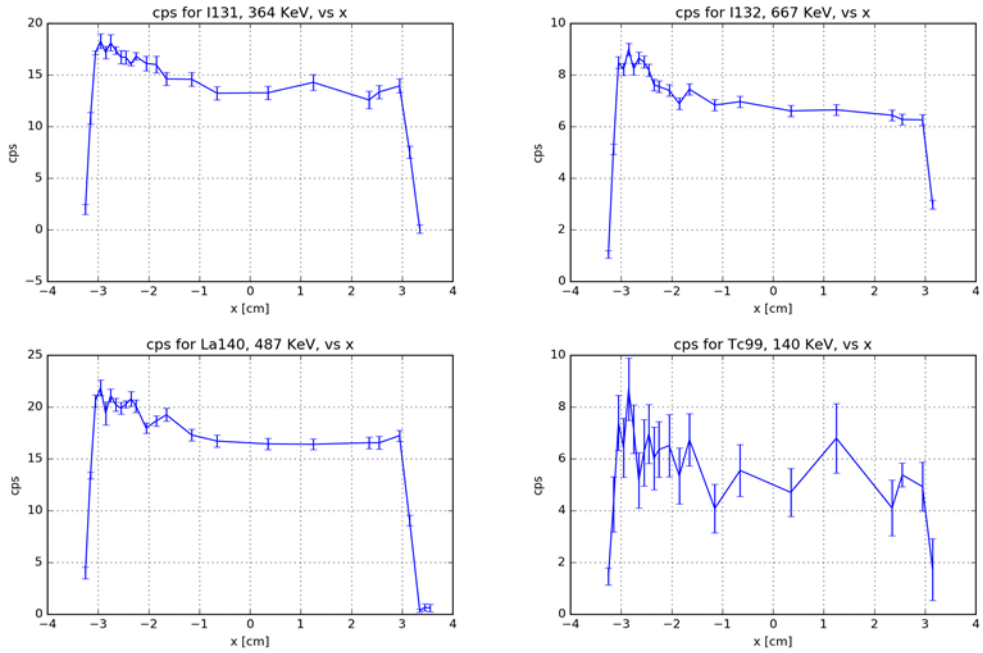

Figure 7. Measurement results for several short-lived isotopes.

These figurers showcase low count rates and relatively large measurement errors, resulting from a long decay time between the irradiation and the measurement. In order to decrease the measurement errors, the results of several isotopes measured at the same x position were combined: Denoting by $\tilde{y}_i(x_j)$ the measurement results of the ith isotope at measurement point x_j normalized by the average over x measurements, the standard deviation $\sigma_i(x_j)$ is calculated by error propagation. We then perform a variance-weighted average over the isotopes to obtain the value $\bar{y}(x_j)$, which has the minimal error.

$$\bar{y}(x_j) = \sum_i \frac{\tilde{y}_i(x_j)}{\sigma_i^2(x_j)} \Big/ \sum_i \frac{1}{\sigma_i^2(x_j)} . \tag{5}$$

This is performed for each measurement position x_j. The result is then compared to the simulation of the thermal flux from chapter 0, normalized to its average and convolved with a window function of width $3\ mm$ to simulate the effect of a collimator. Figure 8 shows the result of the comparison.

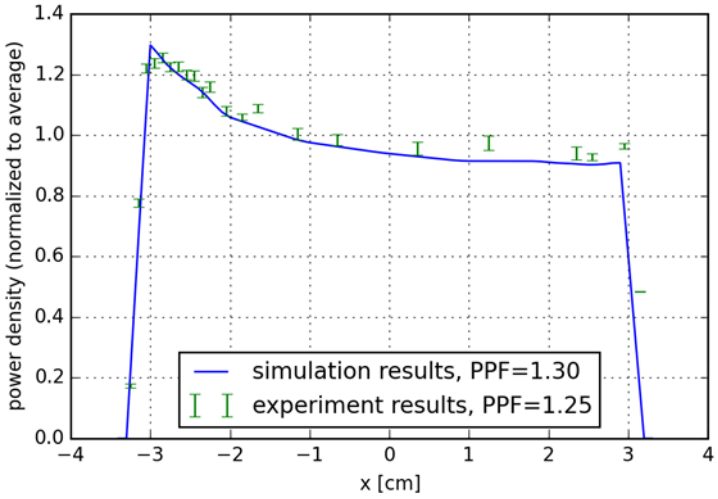

Figure 8. Comparison between the measured power density distribution and the simulated distribution.

It is worthwhile to mention that the simulated PPF is reduced from 1.35 shown in Figure 3 to 1.30 (±0.01), as a result of the convolution with the step function. This is because the convolution averages the peak near the edge and smudges it. The experimental data fits the simulation nicely, yielding a PPF of 1.25 (±0.02).

5. CONCLUSIONS

The results of our experiments validate the computational model of the IRR1. Notice that in Figure 8, the measured power distribution is compared directly to the simulated thermal flux (both normalized to their averages), and the two data sets fit well. This indicates that the fuel depletion distribution is approximately constant throughout the fuel plates' breadth, as it is modelled in MUTZAV. We conclude that our computational model is valid for the IRR-1, but for establishing the correct PPF, it is required to calculate the instantaneous flux in a high resolution. However, the computation of cores which incorporate built-in flux traps (such as OPAL, as discussed in the introduction), the depletion of the fuel assemblies which are adjacent to the water guide for the control blades should be treated more carefully, possibly requiring special calculation schemes [8]. In such cases, our experimental method could be a useful tool to benchmark the calculations.

In future iterations of this experiment, we intend to perform more measurements in various depletion levels (heights), and calibrate the detector efficiency such as to obtain absolute results of activity, rather than power or flux distributions relative to the average. Furthermore, an independent measurement of the thermal flux along the plates (using activation analysis), can be combined with the power distribution measurement to derive the fuel distribution along the fuel plates.

ACKNOWLEDGMENTS

This research was supported by the Pazy Research Foundation.

REFERENCES

[1] E. Villarino and A. Doyal, "Neutronic and Thermalhydraulic Coupled Uncertainties Analysis in a Research Reactor," in *RRFM 2021*, Helsinki, 2021.

[2] I. Neder, U. Steinitz and R. Hayat, "Theoretical Investigation of the Effect of Flux-Trap inside MTR Core on the Power-Peaking Factor and Burnup," in *RRFM 2020,* Helsinki, 2020.

[3] A. Krakovich, I. Neder, U. Steinitz, O. Aviv, L. Danon, K. Ben-Meir and N. Hazenshprung, "Measurements of IRR1 Fuel Depletion Validating Whole-Core Monte-Carlo Simulations of More than Thirty Years of Operation," in *PHYSOR 2018*, Cancun, 2018.

[4] J. Di Salvo, A. Gruel and O. Rivin, "Assembly Power Measurement: Dead Time Study," CEA/Cadarache report DO 79, 2013.

[5] T. Makmal, O. Aviv and E. Gilad, "A simple gamma spectrometry method for evaluating the burnup of MTR-type HEU fuel elements," *Nuclear Instruments and Methods in Physics Research Section A: Accelerators, Spectrometers, Detectors and Associated Equipment,* no. 834, pp. 175-182, 2016.

[6] M. Mora, J. L. C. Palomino, L. A. A. Terremoto and A. Gallardo, "Nondestructive Burnup Measurements by Gamma-Ray Spectroscopy on Spent Fuel Elements of the RP-10 Research Reactor," *Progress in Nuclear Energy 53,* pp. 344-353, 2011.

[7] G. Knoll, Radiation Detection and Measurement 3rd edition, Wiley & Sons, 2010.

[8] Steinitz, U., and I. Neder. "TRIGON: A Monte-Carlo graded composition scheme for multiphysics reactor calculations." *Annals of Nuclear Energy* 173, 109144, 2022

Neutronic Analysis of a Modified MNSR Reactors

R. O. ABDALAZIZ
Radiation and Nuclear Safety Institute, Sudan Atomic Energy Commission
Aljamaa Street, 3001 Khartoum – Sudan

M. THABIT, L. MUZAMIL
Department of Nuclear Engineering, Sudan University of Science and technology
Aljamaa Street, 3001 Khartoum – Sudan

ABSTRACT

In this work a neutronic analysis performed for an MNSR reactor with a modified design of core reflector. The proposed modifications selected to test the impact on the neutron flux distribution among the core and in selected zones. The effective multiplication factor (keff) and the neutron flux distribution for each case were determined. The probabilistic Monte Carlo method was used for the neutronic analysis. The results reflect that; using of reference core configuration with top reflector of water, radial reflector of beryllium and bottom reflector of beryllium is the best choice for MNSR research reactor for the selected plan of operation

1. Introduction

Many of the world's nuclear reactors are used for research, education and training, materials testing, or the production of radioisotopes for medicine and industry. They are basically neutron factories. Research reactors are much smaller than power reactors or those used in propelling ships, many are on university campuses. Approximately there are about 240 such reactors operating, in 56 countries. Some operate with high-enriched uranium fuel, and an international program is working to substitute low-enriched fuel. The primary purpose of research reactors is to provide a neutron source for research and other purposes, their output (neutron beams) can have different characteristics depending on uses on utilization plan. Research reactors fulfill diverse needs, including medical and industrial isotope production, elemental analysis, silicon doping, neutron beam based science and applications, education and training, scientific research, and technology development. MNSR (miniature neutron source reactor) is a compact, thermal and low power research reactor, It adopts tank-in-pool type structure, fuel element of high enriched uranium, and light water as moderator, coolant and shield. The core is surrounded by annulus, bottom and top beryllium reflectors that reduce the critical mass and provide neutron flux peak inside the reflectors where the irradiation sites are situated, it works with a nominal power of 30kW. This type is the topic of our research.

2. MNSR Design Description

The Chinese Miniature Neutron Source Reactor (MNSR) is a low power research reactor with maximum thermal neutron flux of (1×10^{12} n.cm-2.s-1) in one of its inner irradiation channel and thermal power of approximately 30kW. The MNSR is designed based on the Canadian SLOWPOKE reactor and is one of the smallest commercial research reactors presently available in the world. Its commercial versions currently in operation in China, Ghana, Iran, Nigeria, Pakistan and Syria, and is considered as an excellent tool for Neutron Activation Analysis (NAA), training of Scientist, and Engineers in nuclear science and

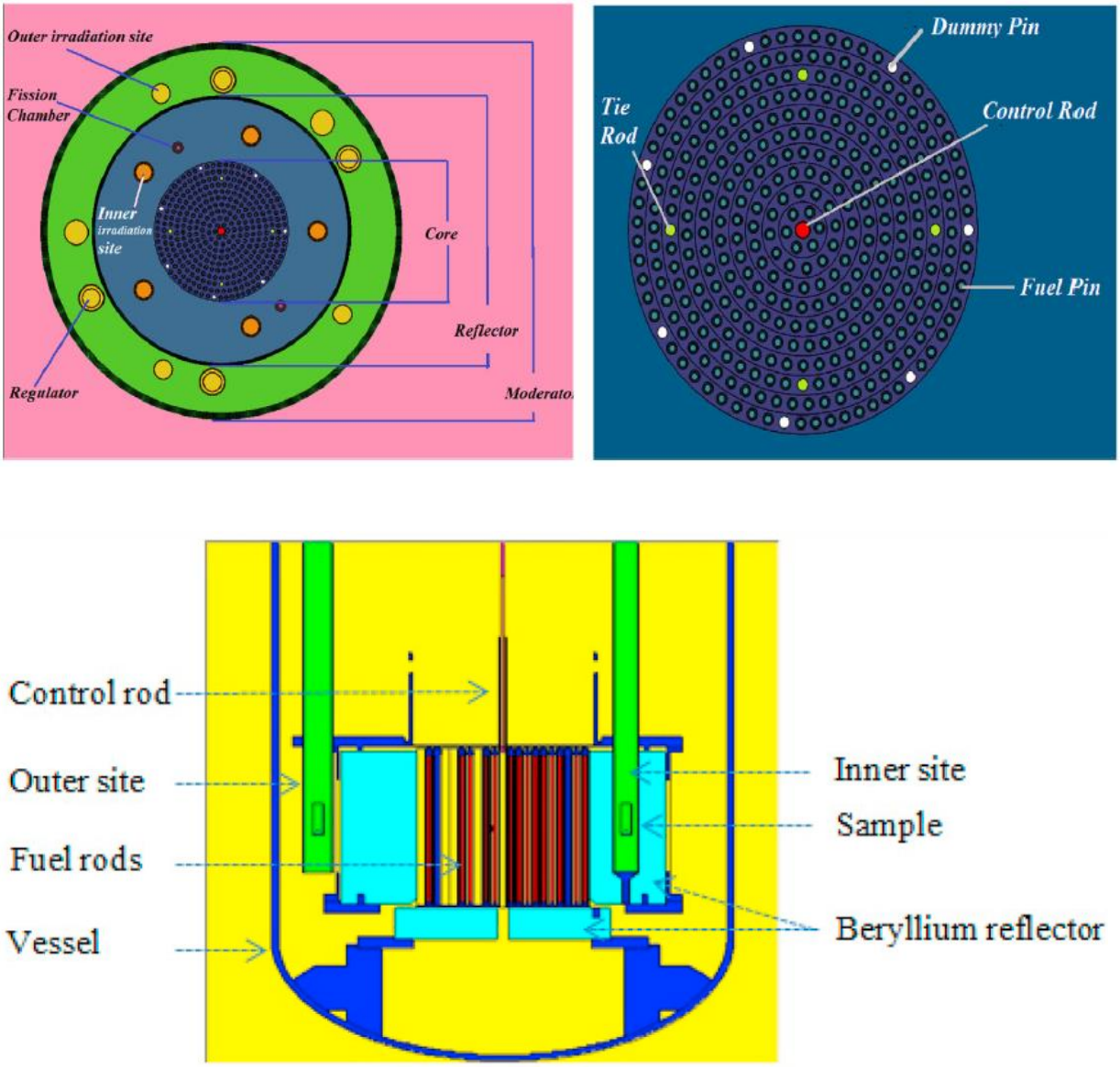

Fig. 1. MNSR Design Mode

MNSR (miniature neutron source reactor) is a compact, thermal and low power research reactor. It adopts tank-in-pool type structure, fuel element of high enriched uranium, and light water as moderator, coolant and shield. The core is surrounded by annulus, bottom and top beryllium reflectors that reduce the critical mass and provide neutron flux peak inside the reflectors where the irradiation sites are situated. The thermal neutron flux achieves, at the nominal power of 30 Kw, A maximum of about 1×1012 neutrons cm−2 s−1 in the inner irradiation channels of the annular reflector .There is only one control rod located at the centre of the core to regulate power, compensate reactivity, and safely shut down the reactor. The core consists of about 350 fuel rods that are cooled by natural convection.

The MNSR core consists of fuel elements that form a fuel cage, which is surrounded by an annular beryllium reflector and rests on a lower beryllium reflector plate. The element cage consists of two grid plates, four tie rods and a guide tube for the control rod. The total number of lattice positions is about 350 and that of fuel elements is 347. The remaining positions are occupied with dummy aluminum elements. The fuel elements are arranged in ten multi-concentric circle layers at a pitch distance varied between 10.58 and 11.47 mm The fuel

element is a rod with 230mm effective height, 5.5mm outer diameter and 4.3mm fuel diameter. The fuel material is UAl4 alloy dispersed in aluminum matrix; the clad is 0.6mm thickness of aluminum. The fission material is uranium 235 with approximately 89.87% enrichment and 27.63% mass fraction of the fuel alloy. The use of HEU allowed reaching the criticality in small amount of uranium, its inventory in MNSR is about 1 kg.
MNSR contains annulus, bottom and top beryllium reflectors. An aluminum tray holds the upper reflector that contains semicircular beryllium shims which are added approximately once a year to compensate for fuel burn-up and samarium poisoning. Beside the main function of reflecting the leaking neutrons out of the core due to its big scattering cross-section, beryllium acts partially as moderator due to its low atomic number. In addition beryllium has the property of producing delayed neutrons. Also, in MNSR the maximum thermal neutron flux is realized in the annulus beryllium, which is utilized for irradiation applications.
In MNSR there are internal and external irradiation sites. In common design, the internal sites exist of five cylindrical holes in the beryllium annulus distributed at one circle with diameter 330 mm. The external sites are five tubes out of annulus reflector. Both the internal and the external irradiation sites are accessible by means of long tubes that penetrate the reactor vessel at the top. The published work reflect that; the maximum neutron fluxes inside the internal and the external irradiation tubes are 10^{12} and 5×10^{11} neutrons cm^{-2} s^{-1} respectfully, with 3% radial and axial non uniformity.

4. Proposed Modifications

In this work the proposed core design modification only concentrate on reflector configuration. The six core reflector configurations proposed was shown below:

1. **Case one**: The reference core (top reflector water, radial reflector is beryllium and the bottom is beryllium)

2. **Case two**: All the reflector sides are beryllium

3. **Case three**: All the reflector sides are graphite

4. **Case four**: All the reflector sides are water

5. **Case five**: Top reflector water, radial reflector is graphite and the bottom is graphite.

6. **Case six**: Top reflector water, radial reflector is graphite and the bottom is beryllium.

5. Analysis Tools

In this work a Monte Carlo code used for the calculation to determine the effective multiplication factor k^{eff} and the neutron fluxes. MCNP is a general-purpose Monte Carlo N-Particle code that can be used for neutron, photon, electron, or coupled neutron/photon/electron transport. It was developed by Los Alamos National Laboratory.

6. Results and Discussion

In this section the results obtained for the effective multiplication factor (k^{eff}) and neutron flux were presented.

6.1 Criticality

In table1, the (k^{eff}) values obtained for the 6 different core reflector configurations of the MNSR reactor was shown. The values reflect the impact of the reflector configuration on the core criticality. We see the obvious decrease in the effective multiplication factor (not achieving criticality) after using cases that include Gr and H2O because they have a lower reflection effect than Be that has the ability to make core critical (case 1 and case 2). The results reflect that k^{eff} is highest in case two which use reflector configuration with all sides from beryllium.

Table 1: The effective multiplication factor for the different core reflector configurations.

Case	keff	Sd
1	1.00770	0.00274
2	1.01369	0.00262
3	0.91931	0.00271
4	0.91908	0.00279
5	0.92687	0.00252
6	0.93365	0.00289

6.2 Neutron Flux

For all cases of the core reflector configurations, the neutron flux was calculated in three positions; cell 3 (central position), cell 939 (in reflector) and 831 (out of reflector). Results was presented in tables and figures bellow.

6.2.1 Neutron Flux in the Central Position

The results illustrated in the bellow figure and tables reflect that, flux starts to increase in case of using Be reflector in place of the top water reflector. And when replace all Be with Graphite the thermal and epithermal decreased while the resonance and fast-g1 increased beside the fast-g2 be at the same level. On the other hand when replace the reflector to water all the neutrons decreased. And with mixing Be and Graphite the neutron flux began to increase again.

Table 5.4: Neutron flux inside cell 3 with the corresponding energies

Energy (MeV)	case 1		case 2		case 3	
	Flux	Sd	Flux	Sd	Flux	Sd
6.25E-07	1.04E+12	0.046	1.11E+12	0.0438	1.06E+12	0.0457
4.00E-06	2.22E+11	0.0755	2.47E+11	0.0727	2.32E+11	0.082
9.12E-03	1.06E+12	0.0414	1.13E+12	0.0407	1.15E+12	0.039
8.21E-01	1.35E+12	0.0372	1.44E+12	0.0355	1.54E+12	0.0343
1.00E+01	1.31E+12	0.036	1.41E+12	0.0357	1.41E+12	0.0357
Total	4.98E+12	0.0206	5.34E+12	0.0201	5.39E+12	0.0199

Table 5.5: Neutron flux inside cell 3 with the corresponding energies

Energy (MeV)	case 4		case 5		case 6	
	Flux	Sd	Flux	Sd	Flux	Sd
6.25E-07	8.87E+11	0.0468	9.84E+11	0.0488	1.08E+12	0.0461
4.00E-06	2.10E+11	0.0851	2.52E+11	0.0718	2.61E+11	0.0728
9.12E-03	1.01E+12	0.0415	1.12E+12	0.0388	1.22E+12	0.0385
8.21E-01	1.41E+12	0.0376	1.46E+12	0.0346	1.61E+12	0.0333
1.00E+01	1.30E+12	0.0352	1.49E+12	0.0342	1.51E+12	0.0341
Total	4.82E+12	0.021	5.31E+12	0.0198	5.68E+12	0.0196

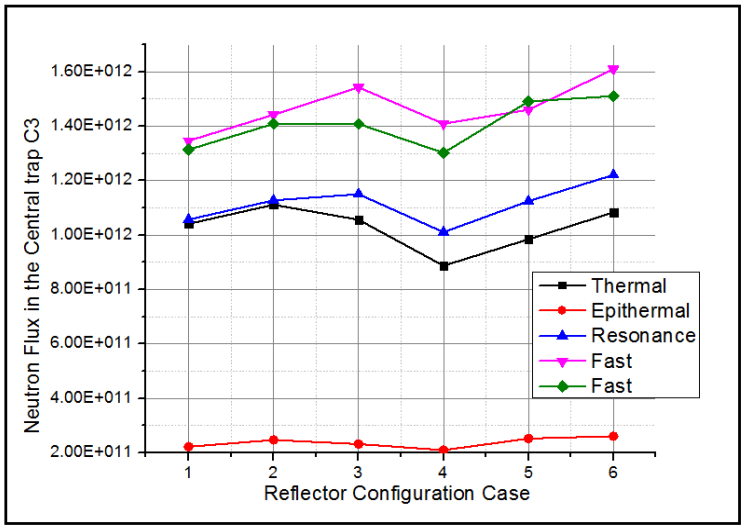

Figure 5.1: Neutron flux variation with reflector configuration

6.2.2 Neutron Flux in the Inner Irradiation Position (Cell 939)

In cell 939 which represent the irradiation site inside the beryllium reflector the values of neutron flux are reduced away from the core center from a value ~ 5*1012 to a value ~ 1.7*1012, with a maximum (~ 2*1012) in the case one (reference core) the neutron flux values in the irradiation site are good for different applications for MNSR reactor.

Table 5.7: Neutron flux inside cell 939 with the corresponding energies

Energy (MeV)	**case1**		**case2**		**case3**	
	Flux	Sd	Flux	Sd	Flux	Sd
6.25E-07	8.15E+11	0.0401	8.57E+11	0.0406	6.41E+11	0.0416
4.00E-06	8.30E+10	0.1131	8.74E+10	0.1059	6.16E+10	0.1297
9.12E-03	4.88E+11	0.055	4.27E+11	0.0562	3.27E+11	0.0595
8.21E-01	4.61E+11	0.0535	4.46E+11	0.0538	4.27E+11	0.0543
1.00E+01	2.08E+11	0.0646	1.97E+11	0.0667	2.71E+11	0.0596
Total	2.05E+12	0.0274	2.01E+12	0.0275	1.73E+12	0.0265

Table 5.8: Neutron flux inside cell 939 with the corresponding energies

Energy (MeV)	**case4**		**case5**		**case6**	
	Flux	Sd	Flux	Sd	Flux	Sd
6.25E-07	8.49E+11	0.0413	6.52E+11	0.0412	6.99E+11	0.0404
4.00E-06	1.92E+10	0.2251	7.57E+10	0.1261	6.79E+10	0.1349
9.12E-03	7.78E+10	0.1091	2.72E+11	0.0654	3.57E+11	0.061
8.21E-01	6.61E+10	0.1095	4.34E+11	0.0524	4.30E+11	0.0556
1.00E+01	7.85E+10	0.0988	2.83E+11	0.0553	2.75E+11	0.0594
Total	1.09E+12	0.0377	1.72E+12	0.0264	1.83E+12	0.0268

6.2.3 Neutron Flux in the Outer Irradiation Position (Cell 831)

In cell 831 which represent the irradiation site inside the coolant the values of neutron flux are reduced away from the core center from a value ~ $5*10^{12}$ to a value ~ $6*10^{10}$. with a maximum (~ $4*10^{11}$) in the case three (all the reflector sides are graphite) since it allows more neuron escape from the core . The neutron flux values in the irradiation site are good for different applications for MNSR reactor.

Table 5.9: Neutron flux inside cell 831 with the corresponding energies

Energy (MeV)	**Case 1**		**case2**		**case3**	
	Flux	Sd	Flux	Sd	Flux	Sd
6.25E-07	2.93E+11	0.0361	2.81E+11	0.0362	2.95E+11	0.0348
4.00E-06	1.27E+10	0.1341	1.14E+10	0.143	1.08E+10	0.1357
9.12E-03	4.81E+10	0.0768	3.78E+10	0.0843	4.97E+10	0.073
8.21E-01	3.16E+10	0.0874	3.08E+10	0.0836	4.55E+10	0.0728
1.00E+01	1.38E+10	0.1183	1.78E+10	0.1059	3.01E+10	0.0829
Total	3.99E+11	0.0319	3.78E+11	0.0318	4.32E+11	0.0293

Table 5.10: Neutron flux inside cell 831 with the corresponding energies

Energy (MeV)	**case 4**		**case 5**		**case 6**	
	Flux	Sd	Flux	Sd	Flux	Sd
6.25E-07	5.71E+10	0.078	2.84E+11	0.0369	2.87E+11	0.0356
4.00E-06	3.17E+08	0.6005	1.23E+10	0.1429	1.93E+10	0.1284
9.12E-03	2.27E+09	0.2873	4.95E+10	0.075	4.64E+10	0.0743
8.21E-01	2.95E+09	0.2852	4.58E+10	0.0745	4.15E+10	0.0809
1.00E+01	3.71E+09	0.2471	3.32E+10	0.0791	2.95E+10	0.0862
Total	6.64E+10	0.072	4.25E+11	0.031	4.24E+11	0.0305

7. Conclusion

From the above results and dissection we conclude that the suitable core reflector configuration, case one (reference core) is better for achieving criticality (keff =1.00770) and getting the maximum neutron flux in the core and the irradiation sites for various applications of MNSR.

7. References

[1] B. Soleimani et all ()

[2] djdjjdjdjjdjjdjjdjdjjhfjkfkfkfklkfllflflflllflfl

[3] djdjjdjdjjdjjdjjdjdjjhfjkfkfkfklkfllflflflllflfl

[4] djdjjdjdjjdjjdjjdjdjjhfjkfkfkfklkfllflflflllflfl

[5] djdjjdjdjjdjjdjjdjdjjhfjkfkfkfklkfllflflflllflfl

CURRENT DEVELOPMENTS ON THE WENRA REFERENCE LEVELS FOR RESEARCH REACTORS

R. KLEIN MEULEKAMP
Chair of Working Group Research Reactors, Western European Nuclear Regulators Association (WENRA, www.wenra.eu)

ABSTRACT

The Western European Nuclear Regulators Association (WENRA) is a group comprising the heads of the regulatory bodies of 18 European countries, together with 14 associated members and observers from Europe and the rest of the world. WENRA's aim is to develop a common approach to nuclear safety, and to allow chief nuclear safety regulators in Europe to exchange experience and discuss significant safety issues. WENRA exists since 1999 and has established several thematic working groups, including in 2017 the Working Group on Research Reactors (WGRR). Since 1999 WENRA has developed sets of Safety Reference Levels for Nuclear Power Plants (NPPs), Radioactive Waste Management and Storage, and Decommissioning. They reflect expected practices agreed by the regulatory authorities to be implemented in the WENRA countries. SRLs are expectations against which each WENRA member country is assessed, and each WENRA member has committed itself to implement actions to ensure the SRLs are met within its national regulatory framework. SRLs build on, and are complementary to, the IAEA's Safety Standards. In 2020, WGRR formalised a set of SRLs for Research Reactors (RRs) that is strongly based on the SRLs for NPPs (issued in 2014). In 2021 WGRR started with the self-assessment of the national regulatory frameworks against the new set of SRLs for research reactors as well as and assessment of the possibility to adapt more recent SRLs for NPP in particular those on internal (issue SV) and external (issue TU) hazards. In addition, WGRR is assessing the existing NPP guides on design extension conditions (issue F) and natural hazards (issue T) for their applicability to research reactors. In 2022 WGRR intends to start with the development of an additional issue on core management. This paper will provide an update of [1] and discuss the ongoing and planned activities by WGRR, discuss in more detail the current set of RLs for research reactors and the first lessons learned from the ongoing self-assessment and provide an outlook for future activities.

1. Introduction

The Western European Nuclear Regulators Association (WENRA) is a group comprising the heads of the regulatory bodies of 18 European countries, together with 14 associated members observers (11 from Europe and 3 from the rest of the world: Canada and Japan). WENRA's mission is working together as regulatory bodies to continuously improve and harmonize nuclear safety to as high as reasonably practicable, and thus protecting the people and the environment. It allows chief nuclear safety regulators in Europe to exchange experience and discuss significant safety issues. WENRA has established several thematic working groups such as the Reactor Harmonisation Working Group (RHWG), the Working Group on Waste and Decommissioning (WGWD), and the Working Group on Research Reactors (WGRR).

To achieve a harmonized approach to nuclear safety of operating Nuclear Power Plants (NPPs) the Reactor Harmonization Working Group (RHWG) was mandated by WENRA to develop Safety Reference Levels (SRLs) for operating nuclear power plants. These SRLs are

agreed by the WENRA members. They reflect expected practices to be implemented in the WENRA countries. Since its establishment, the SRLs for NPPs have been revised several times (2006, 2014 and 2020).

During its 31st meeting the European Nuclear Safety Regulators Group (ENSREG) requested WENRA to develop Safety Reference Levels for Research Reactors (SRLs for RR). Following this request, during its Spring 2016 meeting in Vienna, WENRA decided to develop Safety Reference Levels for Research Reactors through establishment of an ad-hoc working group (WGRR). The WGRR started with 8 participating countries and gradually grew to the current group of 13 countries. In its autumn plenary meeting in 2020 WENRA decided to make the so far ad-hoc WGRR its third permanent working group. The SRLs for Research Reactors that the WGRR developed were adopted by WENRA and published on 18 December 2020.This paper described the current and ongoing work of the WGRR in particular the validation of the implementation of the SRLs.

2. Initiation and development of the WGRR

The concept of the work was to develop SRLs for RR based on the scope of Issues covered by the existing set of SRLs for NPPs, version 2014 [2]. Recent updates [3] of these SRLs were also considered for implementation during the development process. Further Additional inputs from national regulations, IAEA standards for RR, e.g. specifics for experiments were to be considered as well.

3. Developing the SRLs for RR

The WGRR developed the SRLs for research reactor in several steps:

- Select of the reference set of SRLs and assessment of the need for additional issues;
- Assess applicability and need for modification of each reference level;
- Draft reference levels for new issues;
- Review and modify each reference level as needed;
- Seek stakeholder feedback on reference levels;
- Assess stakeholder feedback and modify reference levels as needed.

3.1 Selection of reference and need for additional issues

The RHWG SRLs for existing NPPs, version 2014 [2], was selected as the reference based on which to develop the SRLs for research reactors. It is noted that the RHWG issued a revised set of SRLs for existing NPPs, version 2020 [3] and the WGRR assessed that it was feasible to include the updates of Issues C (Leadership and Management for Safety) and I (Ageing Management) by RHWG in the SRLs for research reactors, but that the inclusion of the updates for Issues SV (internal hazards) and TU (external hazards) would need to be deferred to a future update of the SRLs for RR (see §4).

The SRLs for existing NPPs, version 2014, is a set of 342 SRLs covering 19 Issues. Including Issues C and I from the version 2020 gives a total of 363 SRLs that served as the basis for the SRLs for research reactors. In addition to the 19 RHWG Issues, the WGRR identified that “Experimental Devices and Experiments” and “Core Management” were potential Issues that could be further developed for research reactors. The development of reference levels for Issue X “Experimental Devices and Experiments” was initiated and resulted in 7 additional RLs, whereas the potential development for “Core Management” was deferred to the future activities (see §4). Besides the SRLs for existing NPPs, also IAEA standards and national regulations served as input to the drafting of the SRLs for research reactors.

3.2 Applicability and need for modification

Each of the 363 SRLs was assessed for its applicability to all research reactors and identifying the necessity of grading, for research reactors with a lower risk potential. Each SRL was rated according to a three-level scale:

A – applicable with no or minor change
B – applicable with (significant) modification
C – not applicable.

The preliminary conclusion of this exercise was that about 80% of the reference levels could be applied to all research reactors. The remaining 20% should either be rephrased, graded or removed all together.

3.3 Review and modification

All of the 363 SRLs were subjected to a review of their formulation and the need for minor textual modifications, the focus of this step however was on the 20% of the reference levels that had scored B or C. The process of review and modification, typically take several iterations and many deliberations, resulted in the suppression of about half of the reference levels in question and an important modification of the other half. During this stage also the application of the graded approach was elaborated further and a specific glossary was developed; both texts were added as an annex to the SRLs for research reactors.

3.4 Stakeholder feedback

Early 2019 the set of SRLs for research reactors had sufficiently advanced and matured that the WGRR could start with inviting feedback from stakeholders in line with the WENRA common practice. These stakeholders were all RR licensees of WGRR members and other WENRA- countries with RRs and the IAEA. In addition, some countries asked their Technical Safety Organisations (TSO) to supply comments and, upon their request, also the British regulator ONR (Office for Nuclear Regulation) got the opportunity for providing feedback.

In total 233 comments were received by 27 different entities. The Issues that were most commented upon, were Issue E (design basis), Issue F (design extension conditions) and Issue LM (emergency operating procedures and severe accident management guidelines). About 80% of the comments were accepted. The remaining comments were discussed in detail and ultimately resolved.

3.5 Result

The SRLs for Research Reactors [4] developed by the WENRA WGRR were published on 18 December 2020 and consist of 331 Safety Reference Levels covering 20 Issues. These SRLs are accompanied by annexes on the application of the graded approach and the glossary as well as a guidance on probabilistic safety assessments for research reactors [5].

The scope of application of these SRLs covers all types of research reactors with the exception of critical, sub-critical assemblies, homogeneous zero-power reactors and accelerator driven systems.

4. Current and future activities of the WGRR

A 5-year plan was developed by the WGRR that outlines its activities in the period that focus on three areas: benchmarking the implementation of the SRLs, revising and extending the SRLs and providing additional guidance on the implementation of SRLs.

4.1 Implementation

With the adoption of the SRLs for RR by WENRA the next phase in the harmonization process is the benchmarking of the implementation of the SRLs in the countries. For that, a distinction is made in two phases, being:

1. benchmarking the SRL implementation in the national regulations and
2. benchmarking the SRL implementation in the installations.

The first phase has started in 2021 and is scheduled to continue until 2024. The second phase is currently planned to start in 2025.

The first phase consists of the following steps:

1. self-assessment by each country;
2. (peer)review and validation of the self-assessments;
3. establishment of national action plans and their follow-up.

To proceed efficiently, the SRL Issues have been grouped into sets of 2-4 Issues for which the above steps are carried out by groups consisting typically of 3-4 countries.

During the self-assessment each country assigns a code based on the implementation of each SRL as follows:

A: Yes – already harmonized in substance;

B: No – a difference exists, but can be justified from a safety point of view; or

C: No – a difference exists, and should be addressed for harmonization.

It is expected that the SRLs assessment results coded ‘C’ form the basis of the national action plan.

The results available from the benchmarking that have been performed up to now, show a mixed level of implementation; for some Issues the SRLs have been mostly implemented (A or B) whereas for other Issues more significant gaps are observed (C). Experience of similar benchmarking by the RHWG showed that the actual implementation by the installations exceeded the level of implementation in the national regulations; whether or not this will also apply to research reactors remains to be verified.

4.2 Revision and extension of the SRLs

A revision of the SRLs for RR is scheduled to be published not earlier then 2025. However, work has started to prepare this revision. In particular the updates for Issues SV (internal hazards) and TU (external hazards) of the SRLs for NPP, version 2020, are being assessed for their applicability to research reactors. The results for Issue SV are that most SRLs are applicable with no or minor changes. For Issue TU this assessment has just started and a number of potential items for further discussion were identified.

Besides “Experimental Devices and Experiments” one additional area was identified as potential candidate for extending the SRLs with additional Issues: “Core Management”. In the second half of 2022, the WGRR will start with assessing the need and opportunities for SRLs related to “Core management”.

4.3 Guidance's for the implementation of SRLs

The RHWG issued specific guidance on Issues F ("design extension conditions") and T ("natural hazards") [6] resp. [7], the latter of which has recently been revised in function of the transition from issue T to TU ("external hazards"). Both these guidance's are of relevance to the implementation of the SRLs for research reactors and therefore the WGRR has started to identify their applicability. For the guidance on Issue F this activity has been largely completed and for the guidance on Issue T this activity has recently started. It is expected that this work is finalized and published in the first half of 2023. Recently the WGRR decided that rather than issuing adapted guidance´s, it intends to issue a position paper on the applicability of the existing guidance´s.

5. Highlights of the current SRLs for Research Reactors

The SRLs for Research Reactors are strongly based on the SRLs for NPPs, however, several changes were made to accommodate their application to research reactors. Most notable changes are:

Graded approach:
Given the various types of existing research reactors, and considering that they can represent very different risk potentials, it was realized that there is a need for applying a graded approach in the application of the SRLs, which is stressed in Annex A of the SRLs for RRs. As such it is clarified that all SRLs have to be addressed and applied, but that the way they are applied may be graded (i.e. proportional), as long as sufficient levels of safety are reached. This would for instance allow to grade requirements for DEC- B analysis for low-risk RRs for which it can be shown that severe core degradation can be practically excluded.

Students, scientists and utilization:
Students and scientists have been explicitly included as part of the "site personnel" and are specifically included in a few SRLs, such as C4.3 on the culture for safety. Similarly the use of some research reactors for training and educational purposes has been accommodated explicitly. Utilization of the research reactor was also added as a safety factor of the periodic safety evaluation.

Containment
Although debatable, the term "containment" as used in the SRLs for NPPs is often interpreted to refer only to a particularly strong reinforced concrete outer reactor structure and as such is often seen as not applicable to many research reactors. Therefore the term "means of confinement" is used throughout the SRLs indicating that the release and dispersion of radioactive substances can be prevented or controlled by several different means.

Probabilistic assessment
The use of probabilistic assessments is also for research reactors recognized as a potentially useful complementary tool for the improvement of safety, however it was also realized that given the various, often unique, designs of research reactors as well as their utilization including varying experimental facilities, might complicate a "standard" probabilistic safety assessments (PSA) and limit the benefits that can be gained. Hence Issue O on "probabilistic safety assessment" only features 1 SRL that aims to stimulate the use of probabilistic safety assessments by requiring that consideration is given to carrying out a PSA. A specific guidance [5] was issued that further clarifies the potential benefits of and expectation for a PSA.

Experimental Devices and Experiments
Issue X on "Experimental Devices and Experiments" is an issue that was added and it contains 7 SRLs that cover the design, assessment, authorization and utilization of experimental devices and experiments.

6. Summary

In 2017 the Western European Nuclear Regulators Association (WENRA) established a Working Group on Research Reactors (WGRR) to develop a set of research reactor specific Safety Reference Levels (SRLs) following the already existing SRLs for NPPs. Within three years 331 SRLs for research reactors were developed including a new Issue X covering experiments and experimental devices. The process included a stakeholder consultation of the draft version, the development of an annex on the application of a graded approach and a guidance on Issue O (Probabilistic Safety Assessment of Existing Research Reactors). The final WGRR SRLs were published in December 2020.
Current work of WGRR includes benchmarking the national regulations against the new SRLs for RR and, in a later stage, the implementation of the SRLs at the installations. Further ongoing developments are the assessment and inclusion of recent updates of the SRLs for NPPs, in particular issues SV and TU, and the integration of new topics such as core management. The revised WGRR SRLs are expected to be published in 2025.
In addition, WGRR provides an excellent and unique platform and network opportunity for regulatory experts to exchange on RR specific topics.

7. References

[1] R. Jansen and M. Trapp, “WENRA SAFETY REFERENCE LEVELS FOR RESEARCH REACTORS: DEVELOPMENT AND IMPLEMENTATION”, RRFM October 2021
[2] WENRA RHWG, “Report WENRA Safety Reference Levels for Existing Reactors, Update in Relation to Lessons Learned from Tepco Fukushima Dai-ichi accident”, September 2014.
[3] WENRA RHWG, “Report WENRA Safety Reference Levels for Existing Reactors 2020”, February 2021
[4] WENRA WGRR, “Report WENRA Safety Reference Levels for Existing Research Reactors”, November 2020.
[5] WENRA WGRR, “Guidance Document Issue O: Probabilistic Safety Assessment of Existing Research Reactors, Guidance for the WENRA Safety Reference Levels for existing Research Reactors”, March 2020.
[6] WENRA RHWG, “Guidance Document Issue F: Design Extension of Existing Reactors”, September 2014
[7] WENRA RHWG, “Guidance Document Issue T: Natural Hazards”, April 2015

DEVELOPMENT OF LASER PROCESSES ON U-10Mo MONOLITHIC FUEL FABRICATION PROCESS AT FRAMATOME (CERCA BUSINESS LINE)

K. BUDUCAN[1], S. LORAND, B. BAUMEISTER[1], T. CHEMNITZ[1], W. PETRY[1]
B. STEPNIK[2], C. RONTARD[2], F. GAUCHE[2]

1: Forschungs-Neutronenquelle Heinz Maier-Leibnitz (FRM II)
Technische Universität München, Lichtenbergstr. 1, 85747 Garching – Germany
2: Framatome (CERCA business line)
2 Rue Professeur Jean Bernard, 69007 Lyon - France

ABSTRACT

Within the framework of the conversion of European High Performance Research Reactors (EU-HPRR) from Highly Enriched Uranium (HEU) to lower enriched fuels and in the scope of the European HERACLES initiative, Framatome (CERCA business line) and the Technical University of Munich (TUM) are working together to develop and fabricate U-10Mo monolithic fuel for European research reactors and specifically FRM II (Forschungs-Neutronenquelle Heinz Maier-Leibnitz, Garching, Germany).

Framatome (CERCA business line) has implemented a complete pilot production line, mainly funded by TUM, at their R&D workshop. Aim of this line is the development and optimization of the fabrication process from metal uranium to full-size fuel plates, in depleted uranium (DU) and in Low Enriched Uranium (LEU), while respecting European and French safety rules. The fabrication process includes alloying, casting and canning of U-Mo ingots as well as hot and cold-rolling, cutting and cleaning of full-size U-Mo foils.

Within these developments, innovative processes have been implemented, including laser technology for welding the ingot containers before hot-rolling and for cutting the rolled U-Mo foils. This paper reports on the progress made by Framatome (CERCA business line) and TUM on laser processes development for the U-10Mo fuel fabrication process using inert material and DU. It focuses on the laser technology capability to produce tight and strong welds on the ingot containers and to cut foils with the desired quality. The impact of the cutting on the local U-10Mo microstructure is also evaluated.

1. Purposes

Since 2005, neutrons provided by the Forschungs-Neutronenquelle Heinz Maier-Leibnitz (FRM II, Garching, Germany) are dedicated to fundamental research, material science and the production of radioisotopes for medical applications [1]. In the frame of the European HERACLES initiative, that gather the efforts of CEA, ILL, SCK CEN, TUM and Framatome (CERCA business line) and with other international partners, FRM II works closely with worldwide partners to qualify and extract fuel candidates to convert its reactor with a lower enriched fuel, as an alternative to the current HEU fuel.

To compensate for the loss on the enrichment in fissile material, higher density fuels are needed. Among uranium alloys, one of the most promising candidates is a monolithic uranium-molybdenum alloy fuel (U-10Mo) with a uranium density up to 15.3 $gU.cm^{-3}$ for U10Mo, much higher than classical dispersed U_3Si_2 with 4.8 $gU.cm^{-3}$ [1, 2].

FRM II works with Framatome (CERCA business line) to develop a European manufacturing pilot line for the monolithic U-Mo fuel production (Figure 1). The fuel plate will be composed of a U-Mo foil core coated with few micrometres thick zirconium (Zr) and then cladded in an aluminum frame. The fuel plate manufacturing follows different steps to obtain the desired design and properties. Raw molybdenum and uranium are first alloyed in an arc melting furnace. This step assures the production of the right U-10Mo alloy and the homogenization of the material for further steps. Then, alloy is melted a second time into an induction furnace to cast an ingot according to desired bare foil dimensions. This U-Mo ingot is then encapsulated into a canister welded by laser beam technology. This assembly process is followed by hot rolling to reduce ingot thickness prior to U-Mo bare foil decanning. A step of bare cold rolling is implemented to optimize surface characteristics for following process of Zr-coating and aluminum cladding. Laser cutting process is then implemented to adjust foils geometry according to required dimensions while removing some defects. In summary, laser technology is used two times in the U-Mo monolithic plate manufacturing pilot line: for encapsulating the uranium ingot into canister prior to hot rolling step, and for cutting the uranium foil obtained. This technology constitutes an innovation in the research reactor fuel fabrication.

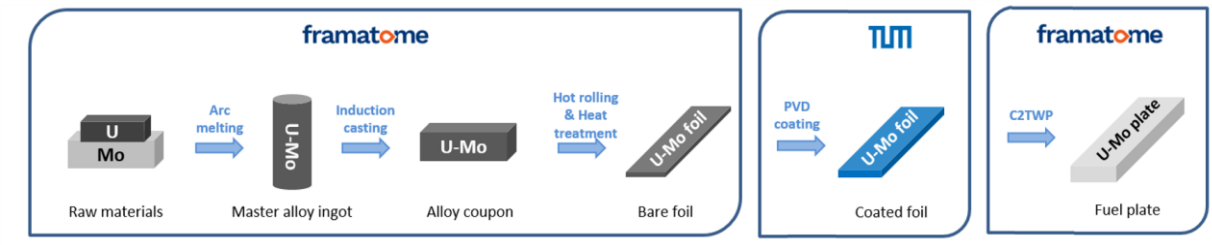

Figure 1: Manufacturing pilot line for U-Mo monolithic fuel

This paper shows uses and developments of laser processes in the U-Mo foil manufacturing project for FRM II conversion. Experiments conducted on parameters influence for both welding and cutting by laser will be presented in order to improve U-Mo manufacturing process.

2. Laser beam welding of stainless steel canister

2.1 Canister design for U-Mo encapsulating

Each welding process corresponds to a way and a specific weld to be done according to its position, the thickness part and material properties. For the development of the monolithic rolling process, a good accuracy to weld the canister is needed to assure mechanical maintain and thigh-leak during hot rolling process of the welded assembly. To ensure this accuracy, laser beam welding (LBW) is used in monolithic fuel development. Laser beam welding is an accurate energy-based process able to weld with good depth penetration and without external metal supply. The absorbed energy locally melts part of the material and then bounds them after cooling. It has numerous advantages compared to conventional welding process: no change in part geometry, high precision with laser beam, no external metal needed, a small Heat Affected Zone (HAZ) and weld length and width reduced [3]. Mainly four parameters have an important influence on welding process, from visual aspect to microstructure: laser power, focal distance between the lens and the part to weld, welding speed and shielding gases. An optimization of parameters is needed to obtain desired sets for welding and avoiding defects as inclusions, thermomechanical cracks, geometric defects, or fusion lacks [4,5,6].

In the U-Mo foil manufacturing development presented in this paper, the U-Mo ingot is encapsulated in a canister and laser welded prior to hot rolling process. The canister is composed with two parts: a housing to insert the coupon and a lid part to enclose the ingot inside (

Figure 2). A part of the lid that will be welded to the canister is thinner than the rest to allow a good penetration of the laser through the lid to the housing and assure mechanical maintain during the hot rolling process. High depth penetration value, at least higher than this part thickness and with a sufficient width to mechanically keep the lid attached to the housing during the process of hot rolling.

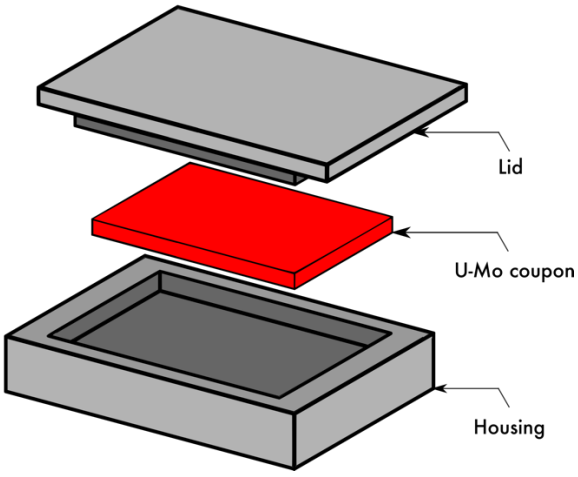

Figure 2: Exploded view of U-Mo assembly with canister

Different materials have been studied for the canister with set of parameters developed for each. The development made on a low carbon stainless-steel material is presented here as comparative baseline of other developments made at Framatome (CERCA business line).

Low carbon stainless steels are usually used for their mechanical and thermal properties as well as their “SCC” resistance (Stress Corrosion Cracking) [7]. Low carbon is further needed to avoid U-Mo contamination by carbon diffusion or particles and to facilitate welding [8].

Understanding of stainless steel LBW is needed to prove feasibility and industrial uses of laser technology for canister welding and U-Mo monolithic manufacturing.

2.2 Experimental setup

2.3 Sample mounting & sample preparation

The experimental machine setup parameter for welding is presented in Table 1. It sums up possible ranges of machine parameters (laser power, laser speed and gas pressure).

	Minimum	Maximum
Laser power (W)	60	1000
Laser speed (mm.min^{-1})	100	10000
Gas pressure (L.min^{-1})	0	18.6
Working distance (mm)	> 0	20

Table 1: Parameters range and controllers of laser beam welding machine

The machine contains a moving table in X & Y direction and a motorized head in Z direction for laser welding process. The laser head is composed of a copper nozzle to canalized an assisting shielding gas flow (Figure 3 – 3) and a vision tool to inspect weld beads after the welding process (Figure 3 – 1).

A machined tool in aluminum alloy (Figure 3 – 2) is placed on the table to mount and maintain the canister. During welding, the lid is also maintained in position by removable clamp (Figure 3 – 4). The mounted canister is welded on concerned areas after detection of two top edges by the vision tool system implemented on the laser equipment and the specific machine program. This detection gives coordinates position for weld beginning. Then, the program interpolates the welding direction and makes appropriate corrections about length & angle welding according to the vision system.

For development, an experimental set-up, composed of two foils assembled and a metallic support (Figure 3 – 4) is used. In this paper, the term “sample” refers to foils and the term “assembly” refers to the addition of the metallic support and the previous sample defined.

For evaluating the correct process parameters for the subsequent canister welding, experimental lines of 70 mm length are welded across the set-up, with 5 mm length distance between each to avoid thermal interaction for further analysis. All available area for welding experiments is used to maximize weld bead number.

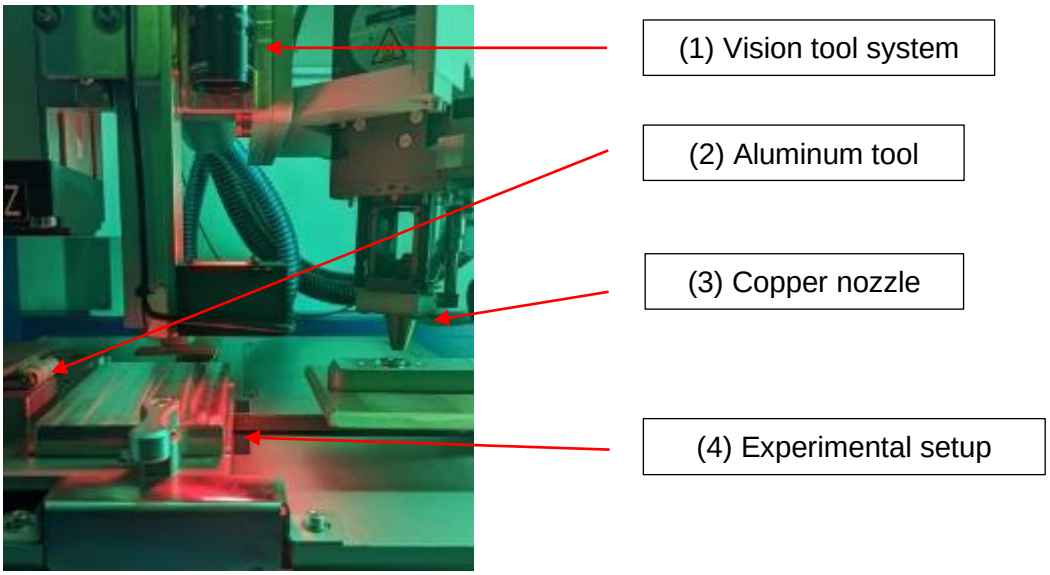

Figure 3: Experimental setup in laser beam machine

Laser beam welding is realized on the sample to weld them together: the top foil reproduces the canister lid, and the bottom foil reproduces the canister housing. To reduce bending due to thermal distortion, the sample is screwed at each 4 corners to a support designed according to canister geometry to fit with existing welding tool. Nuts are placed between the sample and the support before fixing them to physically separate both and avoid welding with the support thanks to laser defocus.

To prepare samples for characterisation after welding, plates are sawed with disk sawing machine in transverse direction to get the profile of each line. These cuts are then embedded and chemically etched with an aqueous solution of HCl and $FeCl_3$ to revealed weld pool. Chemical etching is realized in a range of time between 5 to 30 seconds, according to welding visual aspects.

2.4 Experimental parameters & analysis scope

All experiments detailed in the next section are realized with a laser beam configured in continuous mode, with maximum power supplied directly according to the power value. Assisting gas pressure is not studied in this paper and is set constant according to the standard value of the equipment. Finally, it has been decided in the following experiment plan to keep the focal distance constant to the surface of the material. According to experimental parameters study, experiment batch is realized to extract a set of parameters to weld lid to housing for U-Mo encapsulation. For this experiment, parameters set of power and speed are selected to maintain a constant amount of energy introduced into the material during the experiment. This amount of energy, called heat input, corresponds to the ratio between power supplied by the laser and welding speed value. Experiments with different values are realized to have a range of heat input needed to weld the sample. Depth penetration and weld width are analysed to understand process parameters. Sample is considered welded when the melted area crosses the separation line between both stainless-steel foils (Figure 4). The weld width measured corresponds to the width of welded section on the separation line. The surface width is not relevant in this study due to no mechanical impact for the next manufacturing process, especially hot rolling.

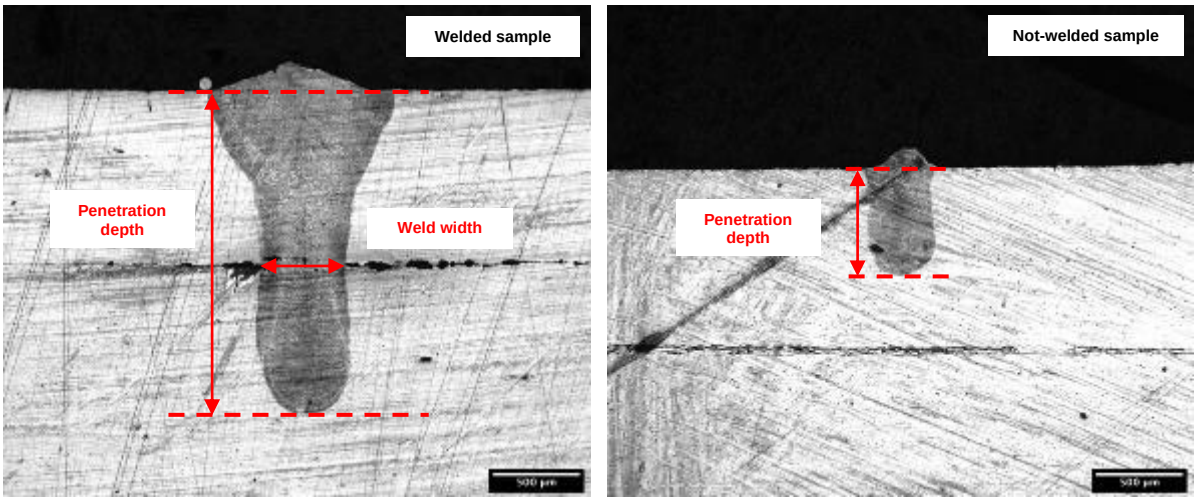

Figure 4: Measurement criteria for weld bead for welded (left) & not-welded sample (right)

2.5 Results

Experiment batch is realised with 6 heat input values numbered from H1 to H6, where H1 corresponds to the lowest heat value used and H6 the highest. Following plots (Figure 5) show depth penetration and weld width values when the sample is welded for different heat input values. A constant power value and variation in welding speed to obtain desired heat input values is used for the left plot while the right plot is realized with a constant speed and variation of power value. For both depth and width, the uncertainty for values is ± 5 µm.

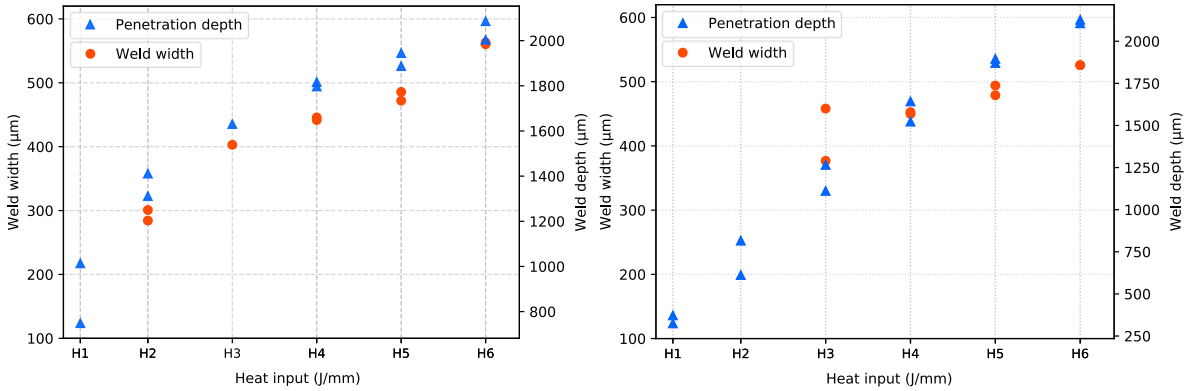

Figure 5: Plots of heat input variation experiments for laser beam welding with constant power (left) and constant speed (right)

As heat input is increasing, weld depth and width weld increase according to plots. The melt pool produced during the process is increasing more in depth and make available a deeper penetration of liquid formed to weld both foils together. These values are mainly affected by thermal properties of the material and then its ability to dissipate heat during the process and its melting temperature to produce the melt pool.

According to results on weld depth, a heat input higher than heat value of H2 seems to be enough to penetrate at least 1 mm into stainless steel. This value of minimal heat input is different depending on power and speed applied. For the same heat input, laser weld with variation of power achieves to weld the sample, while variation in speed does not. The following figure (Figure 6) compare two welds realized with the same H4 heat input value.

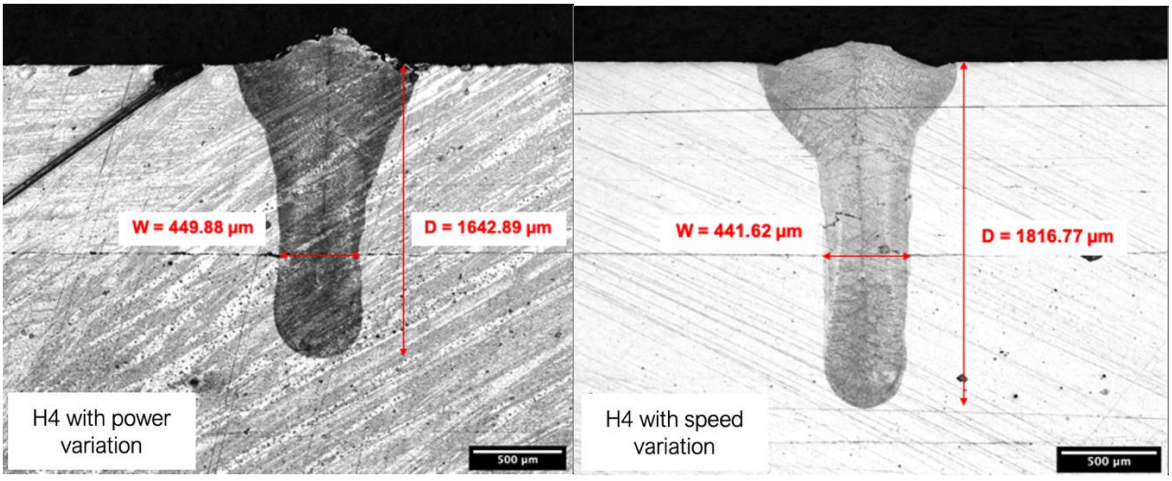

Figure 6: Welding transverse cut of weld bead for H4 with power variation (left) and speed variation (right)

Weld profile on left corresponds to variation in power and the right one a variation of speed. According to these pictures, previous plots and minimal heat input for 1 mm depth penetration, a high value in power leads to a higher value on depth. Among studied parameters, power seems to be the main parameter which affects depth penetration. In addition, melt pool created on the top of the weld is more important for a higher value of power. For weld width, a low value of speed seems to increase weld width: interaction time between the sample and laser could affect this value.

2.6 LBW conclusion

In the case of U-Mo monolithic fuel development, minimizing power is needed here to reduce thermal effect on the sample and keeping good mechanical strength with high depth values. In terms of weld width, increasing of this value is needed to improve mechanical strength for next flat rolling step by increasing mechanical contact between the lid and the housing. Control on power and speed allows a perfect control on depth penetration and width of the weld: high power to increase depth penetration and low speed to increase width weld. This knowledge of stainless steel behaviour under laser beam allows to improve canister design for the lid and thickness for further industrial manufacturing. Mechanical tests will be realized for laser welding to highlight behaviour during hot rolling process. About parameters influence, further comparison for laser beam welding of other material will be conducted to study influence of thermal properties (conductivity, specific heat…) on weld penetration and width measured.

3. Laser beam cutting of uranium foil

3.1 Laser cutting scheme

Laser beam cutting (LBC) process is widely used in many industrial sectors to cut metallic and non-metallic parts with specific geometry and high precision. Many articles and reviews highlight laser cutting for metallic and plastic material with different scopes: industrial production & feasibility, parameters influence, process optimization [9,10] This technology has numerous advantages: edge quality, contactless technology, high level of automation, less consumables needed, good accuracy [11].

As LBW, the work piece is mainly affected by thermal stresses which may affect or make even unusable the part after the process. Both laser process shares similar key parameters: laser power, frequency for pulsed laser, cutting speed and gas pressure. These parameters are essential to control for kerf width, eg. the cut produced by the laser, in entry and exit and heat affected zone around the cut part [7,8]. However, issues and defects which can affect the cutting quality and the final foil are different compared to LBW: local microstructure changes, surface roughness involved, aerosols composition. Kerf width in entry and exit of part is a key parameter for LBC to understand how entry variables influence the process. HAZ locally affects the part from the nearby melting area and thermal diffusion and so affects local microstructure. It increases with power laser and decrease with cutting speed. Seon et al. [12] highlight that a higher power laser increase HAZ during laser cutting, then decrease with a higher cutting speed. Nevertheless, laser technology is not widely used in nuclear sector to cut uranium parts. Studies about laser cutting of uranium and nuclear fuel are difficult to find and concerned mainly uranium pellets or nuclear waste [13,14].

To increase accuracy and quality of the U-Mo monolithic foils, Framatome (CERCA business line) has developed LBC applied to a wide range of materials, including multi-layer materials such as U-Mo foils with Zr coating or U-Mo foils with cladding of aluminium or stainless steel. The using of laser cutting technology for U-Mo bare foil represents a breakthrough technology as it was never used until now for nuclear fuel manufacturing. Understanding of laser cutting of U-Mo is needed to prove feasibility and industrial uses, as well than to improve global quality of U-Mo foil for FRM II conversion

3.2 Experimental setup

The machine setup for cutting is composed of a laser cutting machine implemented in a controlled atmosphere glovebox for the safety of the operator and to preserve quality of the atmosphere during preparation. The Table 2 sums up possible range for machine parameters and controller for each parameter.

	Minimum	Maximum
Laser power (W)	60	1000
Laser speed (mm.min^{-1})	100	10000
Gas pressure (bar)	0	25
Work distance (mm)	> 0	10

Table 2 : Parameters range and controllers of laser cutting machine

The laser machine consists of an immovable table equipped with jagged supports and a motorized head for laser movement (Figure 7 - 2). The laser head is composed of a copper nozzle to canalize an argon assisting gas flow and a vision tool to prepare cutting and to inspect cuts and kerfs during the process (Figure 7 - 3). In addition, an inductive system is implemented in the nozzle to calibrate the Z-axis with the sample to cut before the process.

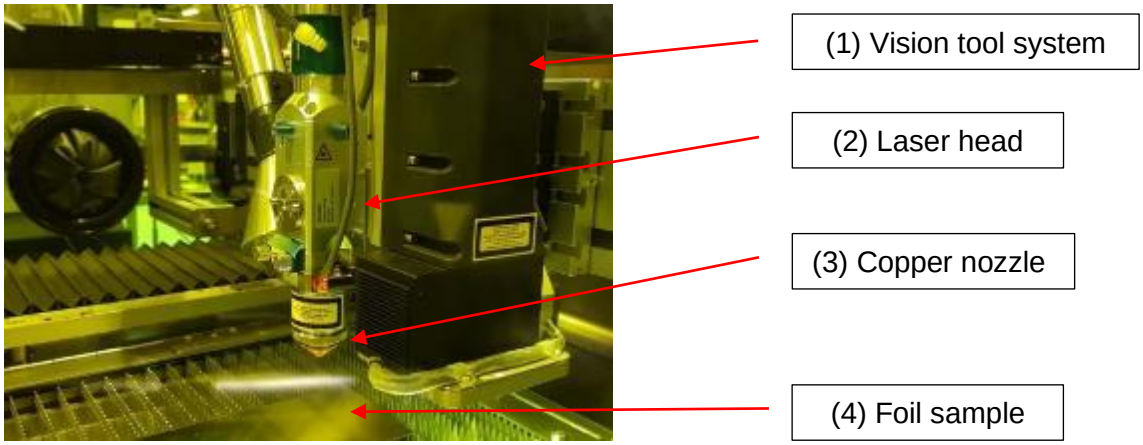

Figure 7: Experimental setup in laser cutting machine

The experimental set-up is composed of the U-Mo foil set on the supporting table (Figure 7 - 4). Each cut is separated by few millimetres to assure thermal diffusion and reducing thermal influence on each other. After the process, kerfs are analysed with microscope to get kerf geometry and apparent defects dross in exit.

Laser cutting kerfs are usually difficult to measure with a high accuracy. Conventional tools and physical instruments typically can not be used for accuracy on values measured of few microns. To improve measurement accuracy, a numerical tool with image processing and automatic kerf detection on microscope pictures is developed via a Python program (Figure 8). This technique gives an accuracy depending on the lens chosen during the picture taking, as well than the threshold technique used for the picture. Results quality depends also on colour and light balance used during image capture which can conduct to potential bias from image processing. After image treatment and numerical measurement, kerf values are summarized, including mean value & kerf extremum, total length measured & uncertainties. Kerf measured alongside is important to assure good parallel parts, tolerances on desired part and kerf thickness repeatability for future manufacturing process.

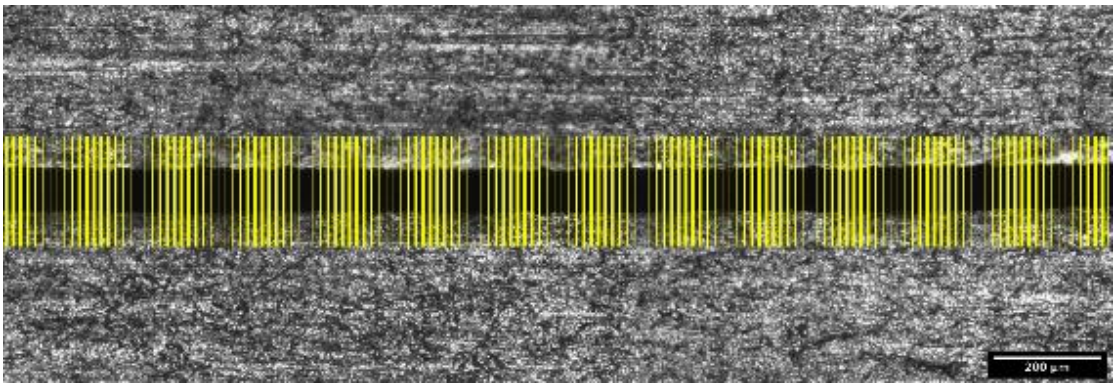

Figure 8: Numerical treating for laser kerf measurement

3.3 Experimental parameters & analysis scope

All experiments are realized with a laser beam configured in pulsed mode, with a pulse duration of 0.3 ms and at maximum frequency available, usually thousands of hertz. Three experiment batches are realized on different thicknesses foils to obtain specific parameters. For the first batch and in the same way than laser welding experiments, set of parameters with power and speed are selected to maintain constant amount of heat input given to the material during the experiment. This experiment is needed to obtain a range of heat input required to cut uranium foil. Among these values, the best one in term of kerf width and dross quantity is selected for the two other batches with variation of pressure for the first one and focal length variation for the second. Kerf measurements is studied among these experiments to understand influence of pressure and focal length on kerf width and global cut quality. Figure 9 shows cut and uncut parts of U-Mo by laser: cut part produced a complete penetration of kerf, uncut part looks like a welded sample.

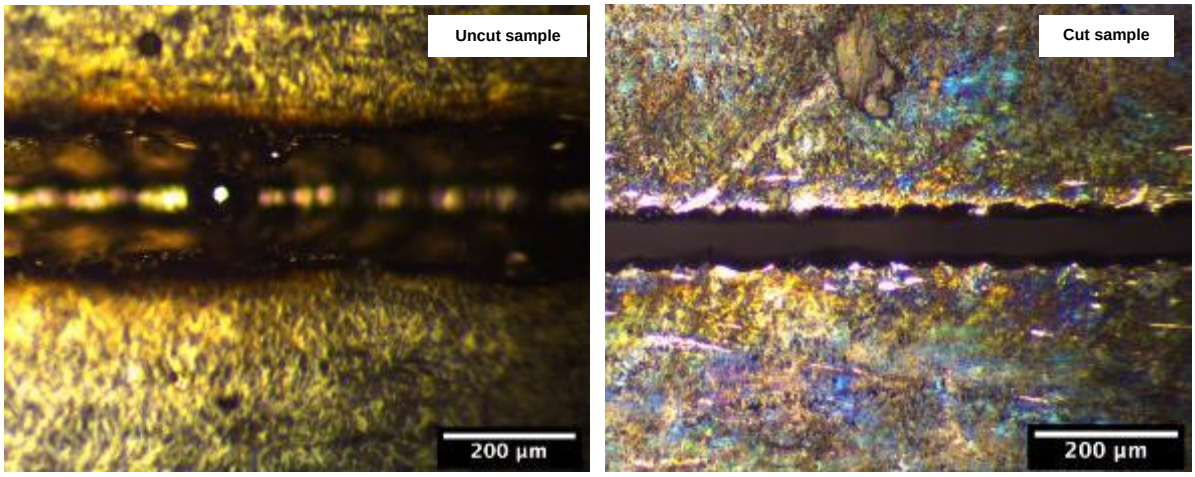

Figure 9: Kerf pictures on U-Mo with uncut (left) & cut parts (right)

3.4 Results

3.4.1 Heat input variation with various power & speed

In the same way than laser beam welding, a first batch of laser cut is realized with 6 heat input values numbered from H1 to H6, where H1 corresponds to the lowest heat value used and H6 the highest. Laser cuts are realized on U-10Mo foils of 0.3 to 0.4 mm thickness. Figure 10 summarizes experiments results for kerf width for different heat values and respectively with constant power and constant speed. Measurements were realized on three different spots of the kerf (beginning, middle and end) to have a representative view of kerf width.

The left plot is realized with constant power value and variation in cutting speed to obtain desired heat input values. The right plot is realized with constant speed and variation in power. Uncertainty for values is given to ± 7 µm.

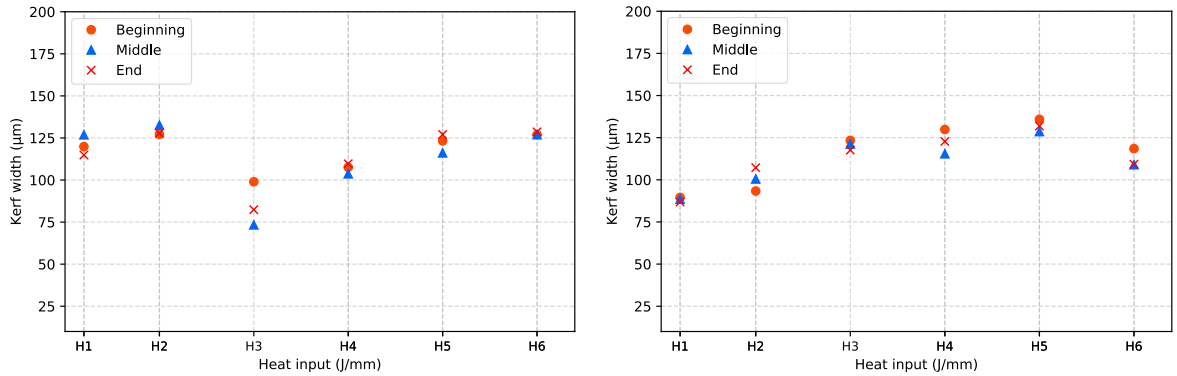

Figure 10: Plot of heat input variation experiments for laser beam cutting with constant power (left) and constant speed (right)

For constant power on left plot from Figure 10, kerf width is not mainly affected, with a constant kerf width when speed increases. An exception for H3 and H4 heat input value is visible. This low value of kerf width could be explained by a local variation of U-Mo thickness on this side, and values extracted from beginning, middle and end seem to confirm this, with a high standard deviation. Kerf widths measured on these different areas for other values does not highlight a difference through kerf with speed or power variation.

On experiment with constant speed value, kerf width is increasing when power increases. Similar to the phenomena observed on laser welding, high power values increase melt pool created on the top and so kerf width. Optimizing by minimizing power is needed here to reduce thermal effects on the sample and reduce the melt pool produce on the top for a low kerf width. Figure 11 shows laser kerfs produced with H4 heat input value, on left with variation of power and on right with variation of speed. Similar to the previous test H3 with constant power, the value of H6 may be discussed and required other tests at this heat input or higher ton confirm the value or another phenomenon.

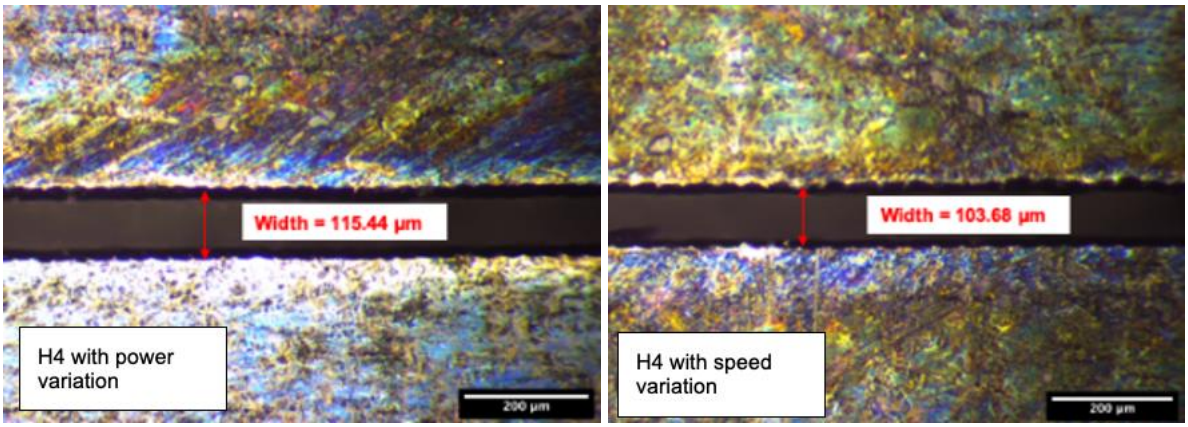

Figure 11: Laser cut of U-Mo with H4 heat input value

Low power with high speed seems to be efficient to reduce kerf width, where a difference of 13 µm could be sawn between both pictures. However, minimizing power is important to reduce quantity of heat into the material, and then reducing HAZ area around the kerf created.

These experiments with variation of power and speed seems to highlight same phenomena than laser beam welding. A high power value for laser cutting increases the kerf width due to a larger melt pool created. In addition, reducing the power decreases amount of thermal energy added to the material and then reduce any modification in material structure. Finally, cutting speed and so interaction time with U-Mo seems to affect kerf width. A high value of speed could reduce the kerf produced by laser cutting. By taking these aspects in consideration, parameter set chosen for pression and focal length variation is speed and power to have H1 heat input value from power variation.

3.4.2 Gas pressure and focal length variation

Laser cut for second and third batches is realized with variation of pression of inert shielding gas, from P1 to P5, where P1 corresponds to the lowest pressure value and P5 the highest. The third batch is realized with variation of work distance between the copper nozzle and the foil surface, from F1 to F9 distance values, where F1 corresponds to the closest distance between the nozzle and the foil, and F9 the highest. In this configuration, F7 is considered as work distance where the lens focal with laser peak power is located on the top surface of the foil. Figure 12 summarizes results obtained for these two experiments.

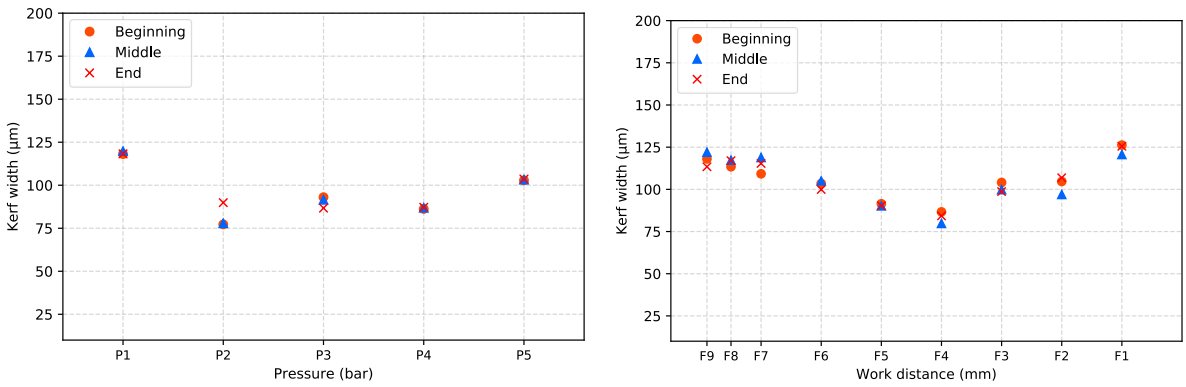

Figure 12: Plots of pressure variation (left) and focal length variation (right) for laser beam cutting of U-Mo

About pressure experiment and its influence on kerf, width values do not have a significant variation from P2 to P5 in pressure values. For a pressure lower than P2, kerf width seems to increase. With a total absence of gas or low gas pressure, the molten material produced during the process cannot be ejected from the kerf: this condition of laser cutting lead to a welding process. Quantity of dross in kerf exit, which are not measured here and difficult to quantify, are present in higher quantity for lower gas pressure.

The variation of working distance parameter has a significant impact on kerf measured as shown in the right plot. The optimal work distance for U-Mo cutting, with thickness here between 0.3 to 0.4 mm, is for F4 value of work distance. The power peak must be, according to plots, inside the matter to reduce kerf width during the process for F7 value higher than F4. Melt pool located in the material looks like to produce a thinner kerf. This value would be dependent on foil thickness, according to the material used.

3.5 Laser beam conclusion

According to plots and experiments conducted with variation of pressure and work distance, these parameters allow a control on kerf obtain for laser cutting of U-Mo. Inert gas flow allows to the molten pool formed during the cutting to go through the kerf. A high gas pressure reduces dross number on exit kerf with a low influence on the kerf width. About work distance, having peak energy power inside the foil produces a low kerf width compared to a peak on the top surface or below the foil to be cut. Analysis of local microstructure and with different surface conditions will be realized to improve laser cutting of U-Mo foil as well than for multi-layer material, especially for U-Mo foil decanning after hot rolling process.

Conclusion & outlook

Goals of using laser technology for monolithic U-Mo fuel for FRM II conversion are to improve quality of U-Mo bare foil compared to conventional process using TIG welding for canister or shearing for foil cutting.

For the LBW, experiments with variation of power and speed were conducted to highlight impact of these parameters on depth penetration and width weld. These results are important to assure mechanical maintain of canister during the entire hot rolling process. Mechanical tests with parameters study from this paper will be conducted to highlight mechanical behaviour of welds under high strength value of hot flat rolling process.

For laser cutting, similar experiments were conducted with in addition experiments with gas pressure and work distance variation. Gas pressure is necessary during the entire process to cut the foil. Kerf width can be optimized by parameters sets choice and with work distance according to thickness to cut. A particular attention must be done on foil waviness to keep the same focal length during all the process, to assure repeatability on laser cutting of U-Mo foils.

Experiments about HAZ variation with parameters for both process, aerosol composition and dross characterization for laser cutting or mechanical experiments for laser welds will be realized to improve the control on laser technology process for U-Mo monolithic bare foil manufacturing.

Acknowledgement

This work was supported by the European Commission in the framework of HORIZON 2020 through Grant Agreement 945009 in the EU-QUALIFY project.

References

[1] FRM II - Forschungs-Neutronenquelle Heinz Maier-Leibnitz: https://www.frm2.tum.de/frm2/startseite/

[2] Daniel M. Wachs, Curtis R. Clark, Randall J. Dunavant, 2008. CONCEPTUAL PROCESS DESCRIPTION FOR THE MANUFACTURE OF LOW-ENRICHED URANIUM-MOLYBDENUM FUEL (No. INL/EXT-08-13840, 935449). https://doi.org/10.2172/935449

[3] D. Cosme, "Choisir la soudure par laser," *Techniques de l'ingénieur,* 2013.

[4] Jiang, P., Wang, C., Zhou, Q., Shao, X., Shu, L., Li, X., 2016. Optimization of laser welding process parameters of stainless steel 316L using FEM, Kriging and NSGA-II. Advances in Engineering Software 99, 147–160. https://doi.org/10.1016/j.advengsoft.2016.06.006

[5] Kawahito, Y., Matsumoto, N., Abe, Y., Katayama, S., 2011. Relationship of laser absorption to keyhole behavior in high power fiber laser welding of stainless steel and aluminum alloy. Journal of Materials Processing Technology 211, 1563–1568. https://doi.org/10.1016/j.jmatprotec.2011.04.002

[6] Williams, S., Suder, W., 2011. USE OF FUNDAMENTAL LASER MATERIAL INTERACTION PARAMETERS IN LASER WELDING, in: CLEO:2011 - Laser Applications to Photonic Applications. Presented at the CLEO: Applications and Technology, OSA, Baltimore, Maryland, p. AMA1. https://doi.org/10.1364/CLEO_AT.2011.AMA1

[7] SASSDA, "The welding of stainless steel :an overview of the basic principles," 2016, pp. 1-6.

[8] "La soudabilité des aciers," *Techniques de l'ingénieur,* 2004.

[9] A. Q. F. B. M. D. V. J. C. R. L. F. P. J. Riveiro, "Laser Cutting: A Review on the Influence of Assist Gas," *Materials,* no. 12, p. 157, 2019.

[10]V. Senthilkumar, "Laser cutting process – A Review," 2014.

[11] P. Y. Y. Di Pietro, "An investigation into characterizing and optimizing laser cutting quality - A review," *International Journal of Machine Tools and Manufacture,* no. 34, pp. 225-243, 1994.

[12] Seon, S., Shin, J.S., Oh, S.Y., Park, H., Chung, C.-M., Kim, T.-S., Lee, L., Lee, J., 2018. Improvement of cutting performance for thick stainless steel plates by step-like cutting speed increase in high-power fiber laser cutting. Optics & Laser Technology 103, 311–317. https://doi.org/10.1016/j.optlastec.2018.01.054

[13] Chang, S., Yan, T., Zheng, W., Li, G., Zou, S., Wang, Xinlin, Wang, Xiangjiang, Tang, D., Xiao, W., 2020. Microstructure and dissolution of UO2 pellet after cutting by fiber laser. Optics & Laser Technology 132, 106493. https://doi.org/10.1016/j.optlastec.2020.106493

[14] Journeau, C., Monerris, J., Tormos, B., Brissonneau, L., Excoffier, E., Testud, V., Chagnot, C., Roulet, D., 2017. Fabricating Fukushima Daiichi in-vessel and ex-vessel fuel debris simulants for the development and qualification of laser cutting technique 12.

SAFETY ANALYSES OF THE BEAM SHUTTER FOR THE HORIZONTAL BEAM EXPERIMENTAL FACILITY IN MARIA RESEARCH REACTOR

A. TALAROWSKA, G. MADEJOWSKI, R. PROKOPOWICZ, G. WOJTANIA, K. TYMIŃSKA, E. MICHAŚ
Nuclear Facilities Operations Department, National Centre for Nuclear Research
Sołtana 7, 05-400 Otwock - Poland

ABSTRACT

In National Centre for Nuclear Research in Poland a new neutron beam tube facility with a neutron research laboratory is being constructed at the MARIA research reactor. The beam consists mainly of the thermal neutrons and gamma radiation. Anticipated thermal neutron flux ranges 8.9E+8 to 1.5E+9 [cm−2s−1]. The beam enables irradiation of the objects outside the reactor core, especially large material samples and biological specimens. Currently, deterministic safety analyses, considering ten initiating events are being performed in the process of an internal review. The beam shutter is to be installed in autumn 2022. The beam shutter was designed to maximise the passive safety level ensuring beam shutdown in case of a station blackout event. This paper presents the highlights of the safety analyses and the potential of the facility for further development.

1. Introduction

1.1. MARIA Research Reactor

MARIA Research Reactor is a multi-purpose channel reactor with an open pool, originally designed as material testing reactor suitable for attaching test loops.. Fuel elements consist of assemblies of six concentric tubes containing enriched (20%) uranium. MARIA is a high flux reactor of 30MW nominal power. It is moderated with light water and beryllium. The thermal and fast neutron flux density may reach $3 \cdot 10^{14}$(n/cm^{2}s) and $2 \cdot 10^{14}$(n/cm^{2}s) respectively. The reactor has been designed with a high degree of application flexibility. Fuel channels are situated in beryllium matrix enclosed by lateral reflector made of aluminium canned graphite blocks. MARIA is equipped with vertical channels for irradiation target materials, accessible via pool at any time. A hydraulic rabbit system for precise irradiations enables controlling irradiation time with a single second resolution while monitoring neutron fluence online. Eight horizontal channels (beam tubes) named H1 to H8 enable to lead the neutron beam outside the biological shield of the reactor. The MARIA Research reactor is a convenient and powerful neutron source for irradiation of target materials for medicine and industry: radioisotopes production, Mo-99 production, neutron modification of minerals and silicon doping. Recently the capability of irradiating small samples in elevated temperature (up to 1000^{O}C has been restored. It is anticipated that MARIA will be able to operate until 2050 after several modernisation take place.

1.2. H2 experimental facility

The so-called H2 experimental facility is being designed at utilising of the H2 horizontal neutron beam channel of MARIA reactor (Fig. 1). The main investigation directions are as follows:

- radiobiological research on boron carriers used in boron-neutron capture therapy;
- radiobiological studies on the influence of mixed radiation (n + γ) and neutron field on selected cell lines;
- research on the methods of determining the dose components in boron-neutron capture therapy;
- development of the detectors and mixed radiation dosimetry methods. Development of the dosimetry techniques based on the phenomenon of local recombination of ions in the gas;
- research on neutron spectrometry systems for beam and environmental applications;
- irradiation of large components and entire devices with simultaneous tracking of the reversible changes in the operating parameters of devices in the radiation field, as well as irreversible changes resulting from radiation damage.

The beam of H2 irradiation facility will offer relatively high neutron flux density of 10^8 (n/cm^{2}s). The beam footprint will have a diameter of 150 mm. The design philosophy was to ensure flexibility of the beam forming allowing installation of irradiation filters made of various materials. The beam shutter in the closed position ensures that the safety requirements are met and the irradiation room is accessible while the reactor remains operational.

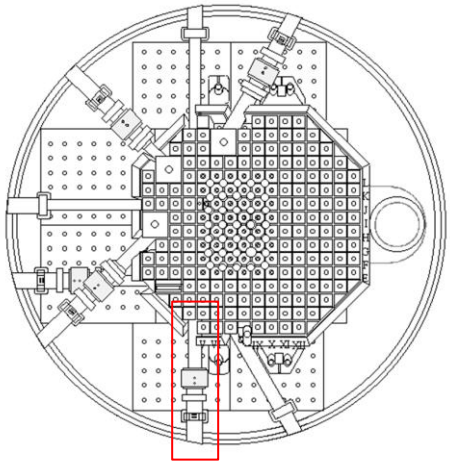

Fig. 1.: Horizontal cross-section of the MARIA reactor core with horizontal channels from H1 (lower right corner) to H8 (upper right corner) visible. The H2 beam tube is marked red.

The vertical cross-section along the installation in the H2 channel is presented in Figure 2.

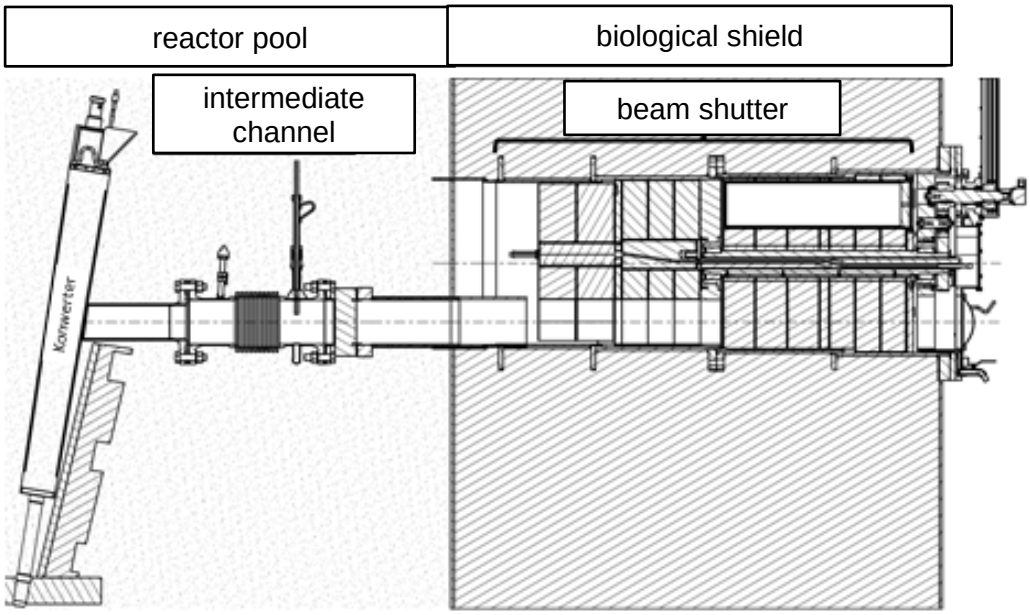

Fig. 2:. The vertical cross-section along the installation

2. Normal operation working conditions analysis

The beam shutter is a drum which can rotate. The beam goes parallel below the drum axis, so that it may pass along one of the parallel cylinders or holes put eccentrically in the drum body. There are three operational states of the beam shutter:

- Closed state; the beam passes through the lead drum body, the cylinders are above the beam. The drum is in the stable equilibrium in that position
- Open state; one of the cylinders is in the lowest position, the beam passes through it. The drum must be kept in this position by the electromagnetic clutch
- Transition state; any state between open and closed, the drum is in motion.

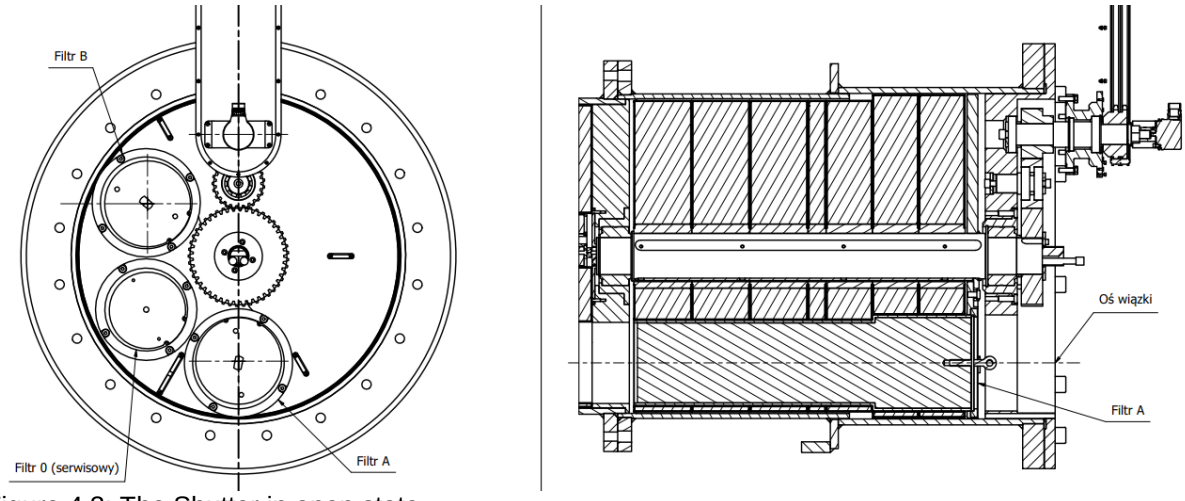

Figure 4.3: The Shutter in open state.

The beam shutter in its closed state functions as a biological shield. By means of an electric drive the movable section (drum) of the shutter is rotated and set in the open position. The hollow cylinder in its lowest position enables the beam to be led out of the reactor core. In the open position the drum with its hollow opening without additional filters acts as a beam collimator.
Additionally, the service mode is distinguished, in which all the circles of the rotating part are placed in such a way that one of the holes with a diameter of 150 mm is placed in the lowest position. The position of the closing rings is mechanically locked against rotation with a safety wedge. The use of the service mode is allowed only when the MARIA reactor is turned off and the intermediate channel is filled with water the drum may be mechanically fixed in the open position with a safety wedge so that service operations behind the drum may be carried out.

2.1. Shielding calculations

The Monte Carlo calculations for the MARIA reactor core model with the MCNP6 code were carried out[1] for two configurations - with the intermediate channel closed and with the intermediate channel open, when the neutrons hitting the H2 channel have energies in the thermal range. The results show that the neutron beam consists mainly of thermal neutrons whereas the gamma beam covers wide spectrum of energies.

2.2. Shutter shielding calculations for a closed intermediate channel

The MCNP calculations for the shielding show that the dominant component of the radiation dose rate downstream of the shutter is primary gamma radiation (<100 μSv / h). The neutron radiation dose is approximately two orders of magnitude lower, and the dose of secondary gamma radiation lower by another two orders of magnitude. The calculated dose rate equivalent was below 1 μSv / h [2] at a distance of 3 meters along the beam axis. The effectiveness of the labyrinth locks used was proven as no increased values of the dose rate were observed in the meshes corresponding to the edges of the structure elements.
On order to assess the clearances width influence on the shielding effectiveness, an additional calculations were made. The modelled clearances were significantly enlarged - up to a width of 5 mm, while the maximum real width predicted basing of the bearing documentation is up to 2 mm. The model calculations do not show an increase in radiation along the edge of the structure in that conservative case.

2.3. Measurements of the radiological situation in the irradiation room with the opened shutter and the intermediate channel

The typical operational state of the facility will be reached when both beam shutter and intermediate channel will be open, releasing the full potential of the beam as well as creating the most challenging radiological hazard. To assess the radiological situation in the irradiation room, we measured the absorbed dose rate equivalent prior to the shutter installation with the opened intermediate channel during the reactor operation. The measured absorbed dose rate equivalent H* on the cover of the cavity of the H2 channel in the beam footprint was 5.7 ±1.8 Sv / h at 5 MW of the reactor thermal power, thus at full power (30 MW) one may expect 34.3 ±12 Sv / h [2]. Although the additional shielding of the facility will be designed, the entry to the irradiation room will be restricted during irradiation by the operations licence.

2.4. Heat calculations

The heat transfer calculations of the closed shutter were conducted using ANSYS Fluent software, whereas the nuclear heat generation originates from the MCNP calculations. The energy deposited in the first ring of the shutter when the intermediate channel is filled with water has a negligible effect on the temperature of the first rotating disc of the shutter, i.e. below 1° C. In the case of an open intermediate channel, the energy deposited in the first rotary ring of the closure is 0.08 W and causes the temperature of the first coil to increase by about 14° C above the ambient air temperature.

3. Analysis of potential failure events, risk assessment and effects of failure

The mechanical elements of the shutter have been designed with significant safety margins ensuring their reliability during normal operation. However, there is always a possibility that some of the elements will be flawed. For each of the identified malfunctions, the initiating events or their sequences leading to their occurrence were defined.

3.1. Malfunction of the slide bearings of shutters shaft

The malfunction of the beam shutter bearings may result in the immobilisation of the shutters disks. Excessive abrasion or seizure of bearings may occur in the case of inaccurate inspection and late replacement of elements. The assumed operating period of the bearings is 20 years. The occurrence of failure of slide bearings with the shutter closed does not affect radiological safety in the room. The occurrence of a malfunction with the shutter open makes it impossible to enter the room while the reactor is operating. None of the above-mentioned events requires intervention within the meaning of the Atomic Law [3]. It is unacceptable to attempt to open the malfunctioning beam shutter. A malfunction of plain bearings is an anticipated operating event.

3.2. Chain or gear malfunction

Chain transmission failure may occur due to the break of chain or damage of the gear sprocket. This situation may occur as a result of improper use or servicing of the installation. Both the broken chain and the damage to the gear wheel do not lead to a radiological hazard, because as soon as transmission breaks down, the beam shutter passively returns to the closed position. After 20 - 30 seconds the beam is closed and after no longer than 60 seconds the system reaches stable equilibrium. Such an event should be included in the anticipated operational events. Its occurrence does not require the introduction of intervention measures.

3.3. Engine malfunction

The occurrence of engine malfunction may be caused by the degradation of the device's components as a result of working in the radiation field. The result of a malfunction will be the inability to open the neutron beam until the repair or purchase of a new engine. If the failure occurs when the door shutter is in the open state, then the disengagement of the drive system causes the door shutter to return to the closed position by gravity. The occurrence of engine failure does not lead to a radiological hazard. The event should be included in the anticipated operational events.

3.4. Electro - clutch malfunction

Electro-clutch malfunction results with blocking the clutch in its rest position. The occurrence of an event may be caused by improper maintenance or improper use, i.e. a short circuit. In the case of the failure of the electro-coupling, it is not possible to open the beam closing device. A malfunction in any other position causes passive shutter closing. The occurrence of an electro-coupling failure does not lead to a radiological hazard. The event should be considered as an anticipated operational event.

3.5. Ventilation failure in the irradiation room

Ventilation of laboratory rooms is connected with the ventilation system of the reactor. In the event of ventilation failure, it is necessary to leave the premises immediately.

3.6. Shutter immobilisation in open position

The coincidence of bearing failure and engine failure may lead to shutters immobilisation in open position with no possibility of intervention until reactor shutdown. That kind of event leads no other threats than radiological hazard in the irradiation room. The room would be inaccessible until the reactor cycle end. The coincidence of bearing failure and engine failure is a design failure.

3.7. Power failure

In the case of a power failure, the electro-clutch will disengage and the closure rings will automatically return to the closed position. Power failure does not lead to a radiological hazard. The event should be included in the anticipated operational events.

3.8. Incorrect control system indications

The access to the irradiation room will be forbidden when the shutter opening system will not confirm its closed position. The malfunction of this system might cause a misleading indication. The redundancy have been provided by displaying the output of the irradiation room dosimetric system in the vestibule, at the door leading to the irradiation room.

4. Future upgrades

The possibility of affecting spectrum of beams neutrons would make the beam much more useful. The roadmap for the facility development identifies two future actions leading to that goal:

- Installing a neutron converter, which would produce fast neutrons consuming thermal neutrons instead,
- Installing a set of neutron filters, allowing for partial thermalisation of fission neutrons and cutting out thermal neutrons leading to the gain of epithermal neutrons share.

5. References

1. Goorley, T., 2012. Initial MCNP6 release overview. Nucl. Technol. 180, 298–315. https://doi.org/10.13182/NT11-135.K.
2. K. Tymińska, M. Araszkiewicz, G. Madejowski, Obliczenia osłonności zamykacza wiązki na kanale H2 – modelowanie Monte Carlo, Raport wewnętrzny NCBJ nr B-9 2021
3. Norma PN-EN 206+A1:2016-12: „Beton. Wymagania, właściwości, produkcja i zgodność”

The Panel Discussion "*Medical Isotopes - Challenges and opportunities for a sustainable supply*", which took place at the European Research Reactor Conference 2022 in Budapest, has been a profitable exchange of inspiring ideas and experiences on this key topic.

The high-level speakers from irradiating reactors, other isotope producers and direct users, highlighted the **crucial role medical radioisotopes play in beating cancer** and stressed on the **necessity to secure a reliable, stable production and supply chain for the future.** Indeed, the challenges of technologies and increasing demands rise at the same pace as the importance of the sector.

Europe plays an essential role in the production of medical radioisotopes. Just consider that 4 neutron irradiation services suppliers on 6 and the 2 largest separation facilities for ^{99}Mo are located on our continent, where more than 1,500 nuclear medicine centres deliver about 10 million procedures to patients each year. At the European level, the Euratom Supply Agency (ESA) is co-chairing the European Observatory on the Supply of Medical Radioisotopes, which plays an important role in monitoring all the aspects related to this field.

Medical progress and innovation lead the radioisotopes market to a continuous evolution. Currently, promising therapeutic medical radioisotopes like lutetium-177 (^{177}Lu) or actinium-225 (^{225}Ac) are gaining their place in this market and others like terbium-161 (^{161}Tb) or copper-64 (^{64}Cu) are gaining attention. Therapies based on the use of these radioisotopes are recording positive results, saving thousands of lives with a limited number of non-invasive applications and a low level of toxicity.

The global demand of these and other radioisotopes is expected to increase dramatically in the coming years. The current European Research Reactor fleet is not sufficient to meet the future increasing demand for those radiopharmaceuticals requiring neutron irradiation for their production. This is certainly the case if some of the existing reactors would reach their end of life, so new and different facilities are necessary to avoid any shortages.

The successful cooperation between research reactors in Europe has already prevented the radioisotopes shortage on several occasions. The last one happened at the beginning of 2022 when a rescheduling of work at the MARIA research reactor in Poland and extending operating cycle of the BR-2 research reactor in Belgium prevented temporary shortages of medical molybdenum-99 (^{99}Mo) due to the temporary shutdown of HFR reactor in The Netherlands for one cycle. Panelists discussed the possibility of making up for the lack of research reactors in Eastern Europe by supporting the younger MARIA reactor (operating since 1974) to become a regional cooperation center. The development and building-up of the medical isotope production at traditionally beam-line type research reactors like FRM II in Germany and ILL in France is helpful to avoid such critical shortages in the future and to improve the European capacities.

Cyclotrons and other particle accelerators established themselves as part of the dynamic developments. In combination with Research Reactors and novel neutron sources, they can support the supply of medical isotopes for a part of the growing market. Such complementarity requires a strong cooperation between the different communities, as well as mutual, positive communication and efforts. Still, as clearly confirmed by the recently published SAMIRA and SMER reports, a stable supply of the full portfolio of medical isotopes will continue to also depend on the availability of Research Reactors – which will undoubtedly face significant challenges in keeping up with the dynamics.

An increasing number of **standards and regulations adopted in research reactors from nuclear power plants are rarely easily implemented in existing installations**,

causing the increase of the resources needed for justification of continued operation. And while life-time management operations currently allow for keeping up the lifesaving production of medical isotopes, the gap will inevitably increase if major isotope producing European research reactors shut down without available replacement. **A long-term strategy is urgently needed to prevent a critical shortage of research and production capacities.**

Many of the novel isotopes are based on irradiations of isotopically pure powders of non-radioactive material, a resource which is relatively rare for some of these. The stable isotopes supply situation depends on the production methods for each one individually, with some of the more crucial ones currently supplied by a single source. **As the development of additional production infrastructures is a capital-intensive endeavor, the business case tends to be unfavorable as long as the market forecasts are unclear. Oppositely, the successful development of new radio-pharmaceutical products will only be sponsored if there is a stable supply chain available**, which includes a reliable, diverse, and sustained supply of precursor material. **An issue where the supply of the precursor material would threaten the deployment of new radiopharmaceuticals, which has occurred in the past, should be avoided**, and fortunately current projections estimate that new players are expected to emerge in the stable isotope supply field over the coming years, as long as the positive forecasts for the development of the radiopharma field continue to be realised**. It remains to be seen to what extent some of these new players will be in Europe, which threatens the independency of the European isotope production chain.**

It is therefore clear that a sustainable framework for the European supply of medical isotopes will need to consider the entire chain of production, including the availability of suitable source materials, which also means the fissile materials required for isotope production routes relying on fission, either as a target or as a fuel for the neutron source in which they are produced. With finite resources of Highly Enriched Uranium (HEU) used for down-blending to High Assay Low Enriched Uranium (HA-LEU), a similar issue as with the isotope precursor materials will arise if action is not taken. Currently, no HA-LEU can be sourced anywhere in Europe and all non-European actors benefit from very strong political and financial government support in their own country. Equally, diversification of fuel element manufacturing is recommendable, and the qualification of suppliers should be supported. Although the

ESA is preparing some activities needed to resolve these problems[1], **the sector would benefit from innovations and commitments for the security of fuel supply.**

For the production of radioisotopes based on research reactor irradiations to be sustainable, it is required that reactors can recover their costs directly and indirectly linked to the production activities and generate a margin capable of managing their dismantling provisions, as well as the preparation of a construction of a replacement reactor. Historically, this sustainability was never created as isotope production was a small by-product of research reactors and pricing was never adopted to secure sustainability as public funding was flowing thanks to the other missions of those research reactors. Alternative missions of the existing research reactors are often less and less supported by the countries in which they operate and cannot be commercially offered at prices which cover the costs, let alone to allow margins to be created. At the same time, projected dismantling costs continue to rise, all of which reduces the support to use public funding supplied by the taxpayers of those host countries to continue to operate the reactors. Because the production of the radio-isotope is at the beginning of the value chain, it requires an evolution throughout the value chain to allow it to increase. For pharmaceutical products, this is further complicated by the reimbursement policies in healthcare. **It is vital for Europe to consider decoupling the reimbursement of the radioisotope from the rest of the reimbursement of the nuclear medicine procedure, as is already the case in Belgium and a few other member states. In that way, these tariffs can be individually managed and evolve with the true evolution of the production cost. The impact on the healthcare budgets of individual member states is minute, while the impact on the sustainability of the reactors in the host countries and therefore of the radioisotope supply chain, is a game changer.**

All experts welcomed the **European Radioisotope Valley Initiative (ERVI)**, planned under the European Commission's SAMIRA Action Plan[2], as a first step into the right direction. **Expectations are for a framework that stimulates much needed policy changes, as well as investments in new research reactors, novel neutron sources, accelerators and stable isotopes enrichment centers**. The COVID pandemic and the Russian invasion on Ukraine have shown the risks of a dependence on outside suppliers and the US is strongly investing in indigenous supply of different medical radioisotopes. This indicates the necessity to retain and develop the skills and the

[1] https://euratom-supply.ec.europa.eu/document/download/f639d7d8-1447-4834-bf27-861b860662c1_en?filename=HALEU%20report%20May%202022%20print.pdf

[2] https://energy.ec.europa.eu/topics/nuclear-energy/radiological-and-nuclear-technology-health/samira-action-plan_en

facilities for supporting the whole chain domestically in Europe as well. It would reduce the dependency and allow Europe to remain a global leader in nuclear medicine.

All speakers recognised the global good situation regarding the technology aspects and the partnership in international scale, but further efforts in terms of harmonization of both medical procedures' requirements and the transport of radioactive materials are always desirable.

The European Research Reactor Conference (RRFM) is the annual gathering of the Research Reactor Community. It regularly brings together more than 200 experts from over 40 countries worldwide. At this years' edition, a Panel of experts from irradiating reactors and other isotope producers as well as direct users discussed the situation and prospects for the security of supply of medical isotopes.

Participants: Mr Jean Bonnet (IRE, Belgium – attended online), Dr Sven Van Den Berghe (SCK CEN – BR2, Belgium), Dr Frodo Klaasen (NRG - HFR Petten and Pallas, The Netherlands), Mr Maciej Lipka (National Centre for Nuclear Research – MARIA Research Reactor, Poland), Dr Richard Henkelmann (ITM Isotope Technologies Munich SE, Germany), Mr Harrie Buurlage (ShineMED, The Netherlands/USA), Mr Laurent Bigot (Orano, France), Dr Gilles Bignan (CEA – JHR, France).

Moderators: Remigiusz Barańczyk, Euratom Supply Agency (ESA), and Steven Van Dyck (SCK CEN)